Universidade do Minho
Escola de Engenharia

Antonio Murano

Out-of-plane behaviour of masonry walls: Structural assessment and strengthening

Dezembro 2024

Out-of-plane behaviour of masonry walls: Structural assessment and strengthening
Antonio Murano
UMinho | 2024

Fundação para a Ciência e a Tecnologia
REPÚBLICA PORTUGUESA
NORTE2020 PROGRAMA OPERACIONAL REGIONAL DO NORTE
PORTUGAL 2020
UNIÃO EUROPEIA Fundo Social Europeu

Universidade do Minho
Escola de Engenharia

Antonio Murano

Out-of-plane behaviour of masonry walls: Structural assessment and strengthening

Tese de Doutoramento
Doutoramento Engenharia Civil

Trabalho efetuado sob a orientação de
Professora Graça Vasconcelos
Professor Hugo Rodrigues
Doutor Javier Ortega

Dezembro 2024

DIREITOS DE AUTOR E CONDIÇÕES DE UTILIZAÇÃO DO TRABALHO POR TERCEIROS

Este é um trabalho académico que pode ser utilizado por terceiros desde que respeitadas as regras e boas práticas internacionalmente aceites, no que concerne aos direitos de autor e direitos conexos.

Assim, o presente trabalho pode ser utilizado nos termos previstos na licença abaixo indicada.

Caso o utilizador necessite de permissão para poder fazer um uso do trabalho em condições não previstas no licenciamento indicado, deverá contactar o autor, através do RepositóriUM da Universidade do Minho.

Licença concedida aos utilizadores deste trabalho



Atribuição-NãoComercial-CompartilhaIgual
CC BY-NC-SA

https://creativecommons.org/licenses/by-nc-sa/4.0

ACKNOWLEDGEMENTS

This is probably the hardest part of the thesis I had to write. There is always a way out when it comes to justifying a bad result (poorly recorded data, poorly calibrated instruments, new/old racket, new/old shoes, etc.) but, in this case, I am really risking forgetting people and their role in this lifechanging experience. So, let's drop here a preliminary apology in case you, my dear reader, are not able to find your name.

This PhD thesis is financially supported by the Portuguese Foundation for Science and Technology (FCT) through the individual PhD Scholarship SFRH/BD/147708/2019.

I would like to thank my supervisors Prof. Graça Vasconcelos, Prof. Hugo Rodrigues and Dr. Javier Ortega.

Thanks to Prof. Paulo B. Lourenço who gave me the chance to attend SAHC master program, which represented a milestone event in my life. In case the results of the work I am presenting will be used to destroy our civilization, my future reader, if you have access to advanced technology that allows you to time travel around, you know WHEN to go (September 2017 btw).

The experimental work presented would not have been completed without the support of Mr. Matos and Dr. Alberto Barontini. Thanks from the bottom of my heart. I would also like to acknowledge Fassa Bortolo Portugal for providing the strengthening solution and the technical support for its application during the experimental campaign.

I want to thank Anjali Mehrotra, for her kindness and for her invaluable help with 3DEC software. To Elesban and Abide, with whom I shared several existential crises in my doctoral journey. Thank you, guys. Elesban, I guess we have to reschedule our collaboration for the next PhD. Thanks to Eduarda who decided to start a PhD just to keep me company in the last months of my academic experience.

To Gigi and Carla, thanks for all the padel we shared. You have always made me feel like M1 and, why not even F1 sometimes. Thanks to Robertino, who proved to me that long-distance relationships may actually work. Thanks to Paula, Claudia and Vinicius, with whom I always felt at home.

To all those whom I let down. I am sorry from the bottom of my heart; it wasn't really my intention.

To my parents Giuseppe and Eva, and to my brothers Matteo and Alessandro, and to my aunt Diana thank you for your endless support and affection even though you were not fully grasping what I was doing. Don't worry guys, I proceeded blindfolded most of the time. Thank you to all the loved ones who are not with us anymore. Finally, Jacopo and Nicoletta, YOU ARE WELCOME. I know you consider it a privilege to have such a charismatic and amazing person like me in your life. Guys, it is finally over and...WE WON (someone more than others, but still).

STATEMENT OF INTEGRITY

I hereby declare having conducted this academic work with integrity. I confirm that I have not used plagiarism or any form of undue use of information or falsification of results along the process leading to its elaboration. I further declare that I have fully acknowledged the Code of Ethical Conduct of the University of Minho.



Comportamento fora do plano de paredes de alvenaria: avaliação estrutural e reforço

RESUMO: As estruturas de alvenaria constituem uma parte significativa do parque edificado existente. A avaliação do comportamento estrutural dos edifícios em alvenaria requer normalmente uma abordagem multidisciplinar. Assim, este trabalho de investigação aborda o estudo do comportamento mecânico para fora do plano em paredes de alvenaria de dois panos através de abordagens experimentais e numéricas.

O trabalho numérico centra-se nos seguintes aspetos: (i) comparação de diferentes abordagens numéricas, nomeadamente modelação com base em elementos finitos (FE) (escala macro e micro) e modelação com base em elementos discretos (DE); (ii) estudo paramétrico envolvendo (a) propriedades mecânicas dos materiais a partir de uma base de dados previamente desenvolvida; (b) características geométricas (disposição das juntas verticais e horizontais, disposição das pedras de ligação entre panos de alvenaria, arranjo do aparelho dos panos de alvenaria e travamento dos cantos).

O estudo paramétrico foi realizado em escala reduzida e em escala real. O modelo em escala reduzida consistiu numa parede em U testada experimentalmente sob carga aplicada fora do plano cujos resultados foram utilizados na calibração dos modelos numéricos seguindo diferentes abordagens.

O estudo paramétrico em modelos em escala real combina macro e micro-modelação e dois métodos numéricos diferentes, nomeadamente elementos finitos (FE) e elementos discretos (DE), para obter uma compreensão mais detalhada sobre a influência dos parâmetros geométricos e mecânicos no comportamento para fora do plano das paredes de alvenaria de dois panos.

O trabalho experimental foi realizado em duas paredes de alvenaria de tijolo de dois panos para avaliar o desempenho de uma solução de reboco armado (argamassa reforçada com malhas de fibras têxteis -TRM).

A partir da análise numérica foi possível definir: (i) expressões empíricas para uma avaliação preliminar da capacidade resistente para fora do plano em paredes de alvenaria; (ii) um conjunto de expressões empíricas para estimar parâmetros necessários nas análises numéricas (abordagem FE e DE). O trabalho experimental forneceu dados sobre a eficácia da solução de reforço na melhoria do desempenho de paredes de dois panos sob carga fora do plano em diferentes condições.

Considera-se que os resultados apresentados podem representar uma base sólida para o desenvolvimento de análises mais detalhadas sobre o tópico em análise. Além disso, o conhecimento obtido pode servir de referência para profissionais envolvidos em atividades de engenharia destinadas à avaliação estrutural de edifícios existentes.

Palavras-chave: Base dados sobre propriedades mecânicas, teste de airbag fora do plano, simulações numéricas FEM/DEM, soluções de reforço, paredes de alvenaria em duas folhas.

Out-of-plane behavior of masonry walls: structural assessment and strengthening

Abstract: Masonry structures are a significant part of the existing building stock. As a result of seismic events, they often experience in-plane or out-of-plane failure mechanisms. The assessment of masonry buildings' structural behaviour usually requires a multidisciplinary approach. Therefore, this research project addresses the study of the out-of-plane behaviour in two-leaf masonry walls encompassing both experimental and numerical approaches. The numerical work is focused on the analysis of the out-of-plane behaviour of stone masonry walls: (i) comparison of different numerical approaches, namely macro and micro finite element (FE) modeling and discrete element modeling (DE); (ii) parametric study involving (a) material mechanical properties from a database previously defined; (b) geometrical features characterising the masonry bonds (arrangement of vertical and horizontal joints, layout of the connection leaf stones, masonry bond leaves and corner interlocking). The parametric study was carried out at different scales, namely reduced and full scale. The reduced scale model was a U shape wall experimentally tested under out-of-plane load whose results were used in the calibration of the numerical models based on different numerical approaches. The parametric study on full-scale models combines macro/micro modeling, and two different numerical methods, namely finite element (FE) and distinct element (DE), to gather a deeper insight regarding the influence of geometrical and mechanical parameters on the out-of-plane performance of two-leaf masonry walls. The experimental work was conducted on two brick masonry walls in undamaged and damaged conditions to assess the reliability of a textile-reinforced mortar (TRM) strengthening solution in enhancing their out-of-plane capacity. The results of the numerical analysis were statistically analyzed, and regression models were used to better comprehend the influence of material and geometrical parameters on the out-of-plane capacity of masonry walls.

The experimental work provided an insight regarding the effectiveness of the TRM strengthening solution in improving the out-of-plane performance of two-leaf walls under out-of-plane load in damaged and undamaged conditions.

To conclude, the results provided may represent a valuable starting point for the development of further in-depth analyses on the subject. Furthermore, the insights gathered may represent a valuable support for all those professionals involved in practice-oriented engineering activities aimed at the structural assessment of existing buildings.

Keywords: database mechanical properties, out-of-plane airbag test, FEM/DEM numerical simulations, strengthening solutions, two-leaf masonry walls.

Table of contents

Direitos de autor e condições de utilização do trabalho por terceiros ii

Acknowledgements iii

Statement of integrity iv

Table of contents vii

List of figures xii

List of tables xix

1 Introduction 1

1.1 Background and Motivation 1

1.2 Thesis objectives 3

1.3 Research Methodology 4

1.4 Outline and organization of the thesis 10

2 Database of mechanical properties for 2-leaf masonry walls 13

2.1 Introduction 13

2.2 Bayesian inference in existing structures assessment and uncertainty reduction 14

2.3 Database definition: Adopted criteria 17

2.3.1 Masonry Quality Index (MQI) 19

2.3.2 Sonic Testing (ST) 20

2.3.3 Flat-jacks test (FJ) 20

2.3.4 Compression test (CT) 21

2.3.5 Diagonal-compression test (DC) 22

2.3.6 Shear-compression test (SC) 22

2.3.7 Final Database 23

2.4 Data fusion for the update of masonry mechanical properties 26

2.4.1 Reference update 30

2.4.2 Updating procedure A (only Italian Data) 35

2.4.3 Updating procedure B (only Portuguese Data) 39

2.4.4 Data fusion results vs technical standards reference values 42

2.5 Final remarks 47

3 Numerical modelling approaches for the out-of-plane behaviour assessment in 2-leaf masonry walls 49

3.1 Introduction 49

3.2 Description of the reduced scale masonry walls 52

3.3 Finite Elements macro and micro-modelling: Brief Overview 56

3.3.1 Description of the Finite Elements macro-models 57

3.3.2 Description of the Finite Elements micro-models 59

3.4 Distinct Elements Method (DEM): Brief Overview 60

3.4.1 Distinct Elements Method: 3DEC Software 61

3.4.2 Description of the Distinct Elements micro-models 63

3.5 Mechanical properties in Finite Elements (FE) and Distinct Elements (DE) models 64

3.6 Calibration of numerical models and results 70

3.6.1 Drystone wall (DS) 71

3.6.2 Regular stone masonry wall (REGW) 81

3.6.3 Assessment of the onset out-of-plane load via updated analytical formulation 87

3.7 Final remarks 92

4 Numerical parametric study on reduced scale models 95

4.1 Introduction 95

4.2 Numerical parametric study on material properties 96

4.2.1 Drystone masonry wall (DS) main outcomes 99

4.2.2 Regular stone masonry wall (REGW) main outcomes 102

4.2.3 Main conclusions 106

4.3 Parametric study on geometrical characteristics 107

4.3.1 Definition of geometrical variations 108

4.3.2 Analysis of results 111

4.3.3 Discussion on the out-of-plane load capacity 133

4.3.4 Discussion on the on recurring collapse mechanisms 135

4.4 Final remarks 141

5 Numerical parametric study on full-scale models of two-leaf masonry walls 143

5.1 Introduction 143

5.2 Numerical parametric study on material properties 145

5.2.1 Empirical expressions derived from the parametric study (Limit States) 149

5.2.2 Empirical expressions for the estimation of mechanical parameters in different numerical modelling approaches: FEM vs DEM 155

5.3 Numerical parametric study on geometrical characteristics of masonry walls 158

5.3.1 Outcomes of the parametric study on geometrical features and masonry bond characteristics in two-leaf masonry walls 162

5.3.2 Analysis of the masonry bond configuration: recurring trends and main outcomes 166

5.3.3 Empirical expressions for the out-of-plane load estimation based on reference geometrical parameters 173

5.3.4 Prediction of the load multiplier (λ) based on geometrical parameters 177

5.4 Final remarks 184

6 Experimental out-of-plane behaviour in strengthened and unreinforced 2-leaf masonry walls 187

6.1 Introduction 187

6.2 Experimental characterization of masonry walls under out-of-plane load 188

6.3 Strengthening techniques for the improvement of the out-of-plane performance 191

6.3.1 Techniques for the improvement of masonry quality 192

6.3.2 Techniques for the improvement of wall-to-wall connections 194

6.3.3 Innovative techniques for the improvement of wall-to-wall connections 197

6.4 Description of the experimental campaign 199

6.4.1 Construction of the reduced scale U-shaped walls 200

6.4.2 Test setup 201

6.5 Material characterization 204
6.5.1 Sonic tests 204
6.5.2 Dynamic identification 207
6.6 Experimental behaviour of the U-shaped brick walls 210
6.6.1 Damage patterns 212
6.6.2 Evaluation of the seismic response 218
6.6.3 Limit states 219
6.6.4 Post damage dynamic identification 220
6.7 Final Remarks 223
7 Conclusions and future works 225
7.1 Database of Masonry mechanical properties 225
7.2 Study of numerical modelling strategies comparison 226
7.3 Parametric study on reduced scale models 227
7.4 Parametric study on full scale models 228
7.5 Experimental test on retrofitted 2-leaf brick masonry walls 231
Annex 1 – Probability Density Functions (PDFs) for representative masonry typologies 233
Annex 1.1 – Reference Update 233
Annex 1.2 – Italian Data 239
Annex 1.3 – Portuguese Data 243
Annex 2 – Geometrical parametric study on reduced scale numerical models of 2-leaf stone masonry walls 247
Annex 2.1 – Set 1 3D Models 247
Annex 2.2 – Set 2 3D Models 249
Annex 2.3 – Set 3 3D Models 251
Annex 2.4 – Set 4 3D Models 253
Annex 2.5 – Load Capacity comparison 255
2.5.1 Set 1 vs Set 2 and Set 3 vs Set 4 255

2.5.2 Set 1 vs Set 3 and Set 2 vs Set 4 256

Annex 3 – Numerical parametric study on full-scale models of 2-leaf stone masonry walls . 257

Annex 3.1 – Table of mechanical properties for FE-based analyses 257

Annex 3.2 – Limit States summary finite element macro models 260

Annex 3.3 – Summary load levels for each limit state 263

Annex 3.4 – Summary displacement levels for each limit state 266

Annex 3.5 – Dataset correlation Young Modulus vs interface properties 269

Annex 3.6 – Table of interface properties for DE-based analyses 272

Annex 3.7 – Set 1 3D Models (good corner interlock) 275

Annex 3.8 – Set 2 3D Models (ineffective corner interlock) 281

Annex 3.9 – Dataset empirical expression for the out-of-plane capacity estimation based on geometrical parameter 287

Annex 3.10 – Capacity curves and collapse mechanisms Set 1 full-scale models (C1 corner configuration) 292

Annex 3.11 – Capacity curves and collapse mechanisms Set 2 full-scale models (C2 corner configuration) 298

Annex 3.12 – Dataset empirical expression for the out-of-plane load multiplier estimation based on geometrical parameter 304

References 309

List of figures

Figure 1.1 - Typical seismic induced damage in structural walls [5]. 2
Figure 1.2 - Annual rates of earthquake deaths since 1900 by decade [6]. 2
Figure 1.3 - Task 1 Workflow..... 6
Figure 1.4 - Task 2 Workflow..... 7
Figure 1.5 - Task 3 Workflow..... 8
Figure 1.6 - Task 4 Workflow..... 9
Figure 1.7 - Task 5 Workflow..... 10
Figure 2.1 - Selected masonry types. 18
Figure 2.2 - (a) Testing procedure results distribution; (b) Testing procedure results classified by masonry typologies. 24
Figure 2.3 - (a) Testing procedure results classified by country of origin; (b) Data distribution (in-situ/laboratory experimental campaigns). 25
Figure 2.4 - Definition of outliers within the Young's Modulus dataset obtained from Compression Tests. . 26
Figure 2.5 - Young's Modulus (a) and Compression strength (b) updating process flowchart. 29
Figure 2.6 - Shear Modulus and shear strength updating process flowchart. 29
Figure 2.7 - Probability Density Function (PDF) updated values Young modulus (a), Compression strength (b), Shear modulus (c), Shear strength (d)..... 34
Figure 2.8 - Probability Density Function (PDF) updated values Italian masonry panels Young modulus (a), Compression strength (b), Shear modulus (c), Shear strength (d). 39
Figure 2.9 - Probability Density Function (PDF) updated values Portuguese masonry panels Young modulus (a), Compression strength (b), Shear modulus (c), Shear strength (d). 42
Figure 3.1 - Modelling strategies for masonry structures: (a) macro-modelling; (b) simplified micro-modelling; (c) detailed micro-modelling (adapted from [75]). 50
Figure 3.2 - Plan configuration tested specimens (a); front view drystone masonry wall (DS); (c) front view regular stone masonry wall (REGW)..... 53
Figure 3.3 - Load configuration and test setup configuration adopted for the OOP test..... 54
Figure 3.4 - Experimental force-displacement diagrams drystone wall (a) regular stone masonry wall (b). . 54
Figure 3.5 - Experimental damage pattern drystone wall (DS). 55

Figure 3.6 - Experimental damage pattern regular stone masonry wall (REGW). 56
Figure 3.7 - Geometrical 3D model for finite element based macro-modelling application (a) and final macro model (b). 58
Figure 3.8 - Geometrical 3D model for simplified finite element based micro-modelling drystone masonry wall (a); Drystone masonry wall (DS) final finite element micro model (b); Geometrical 3D model for simplified finite element based micro-modelling regular stone masonry wall (c); Regular stone masonry wall (REGW) final finite element micro model (d). 59
Figure 3.9 - Contact between two blocks. 61
Figure 3.10 - Mechanical behaviour of interfaces: (a) Mohr-Coulomb slip model; (b) bilinear dilatant model; (c) behaviour under uniaxial loading 61
Figure 3.11 - Geometrical 3D model for simplified finite element based micro-modelling drystone masonry wall (a); Drystone masonry wall (DS) final distinct element micro model (b); Geometrical 3D model for simplified distinct element based micro-modelling regular stone masonry wall (c); Regular stone masonry wall (REGW) final distinct element micro model (d). 64
Figure 3.12 - Workflow calibration procedure. 71
Figure 3.13 - Drystone masonry wall (DS) calibration procedure DS_Micro_DEM_Step 1 (a) and DS_Micro_DEM_Step 2 (b). 71
Figure 3.14 - Drystone masonry wall preliminary analyses macro-model (DS_Macro_FEM_Step 1) vs DE-based simplified micro-model (DS_Micro_DEM_Step 2). 74
Figure 3.15 - DE micro-model drystone masonry wall Mode 1 (a), Mode 2 (b) and Mode 3 (c); FE macro-model drystone masonry wall Mode 1 (d), Mode 2 (d) and Mode 3 (c). 75
Figure 3.16 - Mode shapes and frequencies for all the modelling approaches considered (DS). 78
Figure 3.17 - Experimental and numerical Load vs Displacement curves drystone masonry wall (DS). 79
Figure 3.18 - Numerical and experimental damage pattern drystone masonry wall. 80
Figure 3.19 - Regular masonry wall (REGW) calibration procedure step 1 (a) and step 2 (b). 81
Figure 3.20 - Mode shapes and frequencies for all the modelling approaches considered (REGW). 84
Figure 3.21 - Experimental and numerical Load vs Displacement curves regular masonry wall (REGW). ... 85
Figure 3.22 - Experimental and numerical damage pattern regular masonry wall (REGW). 86

Figure 3.23 - Scheme of internal and external actions in simple rocking (a), compound rocking (b) and horizontal flexure mechanism(c); 3D schematic view of simple rocking (d), compound rocking (e) and horizontal flexure (e) mechanism. 88
Figure 4.1 – Normal stiffness variation drystone masonry wall (DS). 99
Figure 4.2 – Shear stiffness variation drystone masonry wall (DS). 100
Figure 4.3 – Cohesion variation drystone masonry wall (DS). 101
Figure 4.4 – Tensile strength variation drystone masonry wall (DS). 101
Figure 4.5 – Friction angle variation drystone masonry wall (DS). 102
Figure 4.6 – Normal stiffness variation regular stone masonry wall (REGW). 103
Figure 4.7 – Shear stiffness variation regular stone masonry wall (REGW). 104
Figure 4.8 – Cohesion variation regular stone masonry wall (REGW). 104
Figure 4.9 – Tensile strength variation regular stone masonry wall (REGW). 105
Figure 4.10 – Friction angle variation regular stone masonry wall (REGW). 106
Figure 4.11 – Variation of the masonry bond based on WC parameter (through-stones marked in grey). 108
Figure 4.12 – Masonry bond definition for HJ parameter. 109
Figure 4.13 – Masonry bond configuration for VJ parameter. 109
Figure 4.14 – Different corner configuration: C1 front view (a) and rear view (b), C2 front view (c) and rear view (d). 110
Figure 4.15 – Reference models 3D views for Set 1 (a), Set 2 (b), Set 3 (c) and Set 4 (d); reference models plan view for Set 1 (e), Set 2 (f), Set 3 (g), Set 4 (h). 111
Figure 4.16 – Geometrical parametric study final load-displacement curves in Set 1 (a), Set 2 (b), Set 3 (c) and Set 4 (d). 112
Figure 4.17 – Set 1 variation in vertical joints (VJ) configuration. 114
Figure 4.18 – Set 1 variation in horizontal joints (HJ) configuration. 116
Figure 4.19 – Set 1 variation in wall connection (WC) configuration. 118
Figure 4.20 – Set 2 variation in vertical joints (VJ) configuration. 120
Figure 4.21 – Set 2 variation in horizontal joints (HJ) configuration. 122
Figure 4.22 – Set 2 variation in wall connection (WC) configuration. 123
Figure 4.23 – Set 3 variation in vertical joints (VJ) configuration. 125
Figure 4.24 – Set 3 variation in horizontal joints (HJ) configuration. 126

Figure 4.25 – Set 3 variation in wall connection (WC) configuration. 128
Figure 4.26 – Set 4 variation in vertical joints (VJ) configuration. 129
Figure 4.27 – Set 4 variation in horizontal joints (HJ) configuration. 131
Figure 4.28 – Set 4 variation in wall connection (WC) configuration. 132
Figure 4.29 – Set 1 vs Set 2 load capacity comparison (a); Set 3 vs Set 4 load capacity comparison (b). 134
Figure 4.30 – Set 1 vs Set 3 load capacity comparison (a); Set 2 vs Set 4 load capacity comparison (b). 135
Figure 4.31 – Recurring collapse mechanisms: FM1 (a), FM2 (b), FM3 (c), FM4 (d). 136
Figure 4.32 – Failure modes frequency rate. 136
Figure 4.33 – Abacus of failure modes (M1 to M9) for the whole dataset (Set 1, 2, 3 and 4) of the geometrical parametric study. 138
Figure 4.34 – Abacus of failure modes (M10 to M18) for the whole dataset (Set 1, 2, 3 and 4) of the geometrical parametric study. 139
Figure 4.35 – Abacus of failure modes (M19 to M27) for the whole dataset (Set 1, 2, 3 and 4) of the geometrical parametric study. 140
Figure 5.1 – Model's reference geometry. 143
Figure 5.2 – Reference FE-Based macro model 3D view (a) and plan configuration (b). 145
Figure 5.3 – Workflow parametric study on material properties. 146
Figure 5.4 – Macro models Load vs Displacement curves (a); Limit States identification (b); reference model maximum principal strain distribution LS1 (c), LS2 (d), LS3 (e) and LS4(f). 147
Figure 5.5 – Reference DE model (a) and 3D CAD view (b) 148
Figure 5.6 – Limit States three-linear curves (a); Pushover curves DE-based micro models (b) 149
Figure 5.7 – Scatter plot load levels limit states LS1 (a), LS2 (b), LS3 (c), LS4 (d) 154
Figure 5.8 – Scatter plot displacement levels limit states LS1 (a), LS2 (b), LS3 (c), LS4 (d) 155
Figure 5.9 – Scatter plot load Interface Properties Normal stiffness (a), Shear stiffness (b), Tensile strength (c), Cohesion (d) 157
Figure 5.10 – Geometrical configuration 3D models parametric study. 160
Figure 5.11 – Average Limit States curves for the calibration of the reference DE-based model (a); final mechanical properties DE-based reference model (b) 161
Figure 5.12 – Influence of slenderness in models with 60 cm thickness (a) and 40 cm thickness (b) considering height variation. 163

Figure 5.13 – Influence of slenderness in models with 60 cm thickness (a) and 40 cm thickness (b) considering span variation. 163
Figure 5.14 – Influence of height to span ratio in C1 sets of models (a) and C2 sets of models (b)..... 164
Figure 5.15 – Influence of thickness to span ratio in 60 cm thickness sets of models (a) and 40 cm thickness sets of models (b)..... 165
Figure 5.16 – Geometrical parametric study REF set models (a) and REF_TH1 set models (b)..... 167
Figure 5.17 – Geometrical parametric study H1 set models (a) and H1_TH1 set models (b)..... 168
Figure 5.18 – Geometrical parametric study H2 set models (a) and H2_TH1 set models (b)..... 169
Figure 5.19 – Geometrical parametric study H3 set models (a) and H3_TH1 set models (b)..... 170
Figure 5.20 – Geometrical parametric study SP1 set models (a) and SP1_TH1 set models (b) 171
Figure 5.21 – Geometrical parametric study SP2 set models (a) and SP2_TH1 set models (b) 172
Figure 5.22 – Scatter plot out-of-plane load capacity predicted vs actual values. 176
Figure 5.23 – Classification of collapse mechanisms in 2-leaf masonry walls full-scale models..... 177
Figure 5.24 – Failure modes frequency rate..... 178
Figure 5.25 – Capacity curves and collapse mechanism in REF_C1 wall and REF_C1_TH1 models..... 179
Figure 5.26 – Structural scheme collapse mechanisms identified..... 180
Figure 5.27 – Scatter plot out-of-plane load multiplier predicted vs analytical values..... 183
Figure 6.1 – Assessment techniques for the out-of-plane behaviour of masonry walls [3]. 188
Figure 6.2 – Behaviour of stone units with rounded surfaces subject to self-weight, adapted from [140]. 189
Figure 6.3 – Grout injection technique (a), jacketing (b), textile reinforced mortar (c)..... 193
Figure 6.4 – Standard repointing (a) and Reinforced repointing (b), FRP application..... 194
Figure 6.5 – Detail of anchoring and connection ties (a); Strengthening of existing timber floor (b). 195
Figure 6.6 – Stiffness improvement for timber floors (a) [5]; Only wood technique proposed by Modena; Stiffness improvement of timber floor with FRP materials (b). 196
Figure 6.7 – Example of strengthening with CAM system..... 197
Figure 6.8 – Shape memory effect (a); Super-elasticity (b)..... 198
Figure 6.9 – SMADs applications in Assisi (a), Foligno (b) and Montegranaro..... 199
Figure 6.10 – U-shaped masonry wall plan view (a) and axonometric view (b); U-shaped unreinforced masonry wall (c). 200

Figure 6.11 – Axonometric view of the TRM solution (a), installation stages of the strengthening solution (b, c, d), detail of the anchoring system (e). 201
Figure 6.12 – Load configuration out-of-plane test setup. 202
Figure 6.13 – Displacement-time law history (a); airbag test setup (b). 203
Figure 6.14 – LVDTs location. 203
Figure 6.15 – Compression test (a), diagonal compression test (b), flexural test (c). 204
Figure 6.16 – Direct sonic test: reference grid and contour plot of the P wave velocity (m/s) in UMW (a) and RMW (b). 205
Figure 6.17 – Dynamic identification accelerometers location. 207
Figure 6.18 – Main mode shapes and frequency of vibration in UMW, RMW and RMW_UND before the out-of-plane airbag test. 208
Figure 6.19 – Load-displacement diagram at measurement point C1 (a); envelope curve (b). 210
Figure 6.20 – Load-displacement diagram up to 10 mm at measurement point C1 (a); envelope curve up to 10 mm at the same location (b). 211
Figure 6.21 – Secant stiffness variation. 211
Figure 6.22 – Post airbag test damage pattern in UMW lateral right wall (a), façade (b), lateral left wall (c); Post airbag test damage pattern in RMW right side (c) and left side (d); Post damage pattern in RMW_UND right side (e) and left side (f). 213
Figure 6.23 – Damage pattern in UMW right lateral wall (a), façade (b), left lateral wall (c): Damage pattern in RMW right lateral wall (d), façade (e), left lateral wall (f); Damage pattern in RMW_UND right lateral wall (g), façade (h), left lateral wall (i). 214
Figure 6.24 – Contour map in UMW right lateral wall (a), façade (b) left lateral wall (c); Contour map in RMW right lateral wall (d), façade (e), left lateral wall (f), Contour map in RMW_UND right lateral wall (g), façade (h), left lateral wall (i). 215
Figure 6.25 – Maximum horizontal displacement profiles façade bottom (a), middle (c), upper (e); Maximum vertical displacement profiles façade left side (b), central (d), right side (f). 217
Figure 6.26 – Base Shear Coefficient (a) and Energy dissipation capacity (b) of the masonry walls for each testing condition. 218
Figure 6.27 – Limit states identification in UMW, RMW and RMW_UND. 219

Figure 6.28 – Main mode shapes and frequency of vibration in UMW, RMW and RMW_UND after the out-of-plane airbag test. 221

List of tables

Table 2.1 - Prior knowledge and new information summary for Masonry Type 1 (overall data). 30
Table 2.2 - Prior knowledge and new information summary for Masonry Type 2 (overall data). 31
Table 2.3 - Prior knowledge and new information summary for Masonry Type 3 (overall data). 31
Table 2.4 - Prior knowledge and new information summary for Masonry Type 4 (overall data). 32
Table 2.5 - Prior knowledge and new information summary for Masonry Type 5 (overall data). 32
Table 2.6 - Prior knowledge and new information summary for Masonry Type (overall data). 33
Table 2.7 - Prior knowledge and new information summary for Masonry Type 1 (Italian data). 35
Table 2.8 - Prior knowledge and new information summary for Masonry Type 2 (Italian data). 36
Table 2.9 - Prior knowledge and new information summary for Masonry Type 3 (Italian data). 36
Table 2.10 - Prior knowledge and new information summary for Masonry Type 4 (Italian data). 37
Table 2.11 - Prior knowledge and new information summary for Masonry Type 5 (Italian data). 37
Table 2.12 - Prior knowledge and new information summary for Masonry Type 6 (Italian data). 38
Table 2.13 - Prior knowledge and new information summary for Masonry Type 1 (Portuguese data). 40
Table 2.14 - Prior knowledge and new information summary for Masonry Type 2 (Portuguese data). 40
Table 2.15 - Prior knowledge and new information summary for Masonry Type 3 (Portuguese data). 41
Table 2.16 - Prior knowledge and new information summary for Masonry Type 6 (Portuguese data). 41
Table 2.17 - Bayesian update results versus Eurocode [47] and Italian standards [26]. 45
Table 2.18 - Bayesian update results versus Italian Research Council recommendations [15]. 46
Table 3.1 - Summary of the main parameters needed for macro-modelling and simplified micro-modelling (adapted from [113]). 65
Table 3.2 - Summary of interface properties for drystone masonry. 68
Table 3.3 - Summary of interface properties for masonry with mortar joints. 69
Table 3.4 - Mechanical parameters to the simplified micro-model (DS). 72
Table 3.5 - Estimation of the Equivalent Young's Modulus (DS). 73
Table 3.6 - Initial (DS_Macro_FEM_Step 1) and final (DS_Macro_FEM_Step 2) properties macro-model drystone masonry wall. 75
Table 3.7 - Mechanical parameters simplified micro-model (REGW). 82
Table 3.8 - Equivalent Young's Modulus values (REGW). 82

Table 3.9 - Mechanical parameters macro-modelling approach (REGW). 83
Table 3.10 - Onset load for the out-of-plane mechanism estimated based on experimental, analytical, and numerical results. 91
Table 4.1 – Reference mechanical properties and set of values parametric study in Drystone masonry wall (DS) and Regular stone masonry wall (REGW) 98
Table 4.2 – Masonry Quality Index coefficients for out-of-plane actions (adapted from [41]). 110
Table 5.1 – List of P-values for equations 44 to 51 152
Table 5.2 – List of standardized beta coefficients (β) for equations 44 to 51 152
Table 5.3 – Summary of RMSE and MAE measurements 153
Table 5.4 – Summary of RMSE and MAE measurements 156
Table 5.5 – Reference combinations masonry bond configuration 159
Table 5.6 – Statistical indicators for continuous variables geometrical parametric study 174
Table 5.7 – List of P-values and standardized coefficients (β) related to equation 56. 176
Table 5.8 – Summary of RMSE and MAE measurements 176
Table 5.9 – List of P-values and standardized coefficients related to equation 56 183
Table 5.10 – Summary of RMSE and MAE measurements 184
Table 6.1 – Direct sonic test: average velocity in m/s and coefficient of variation between brackets in UMW (a) and RMW (b). 206
Table 6.2 – Dynamic identification in UMW before the airbag test: comparison between frequencies f, damping ratios ξ and mode shapes in terms of MAC. 209
Table 6.3 – Dynamic identification in RMW before the airbag test: comparison between frequencies f, damping ratios ξ and mode shapes in terms of MAC. 209
Table 6.4 – Dynamic identification in RMW before the airbag test: comparison between frequencies f, damping ratios ξ and mode shapes in terms of MAC. 209
Table 6.5 – Lateral drifts and corresponding limit states. 220
Table 6.6 – Dynamic identification in UMW after the airbag test: comparison between frequencies f, damping ratios ξ and mode shapes in terms of MAC. 222
Table 6.7 – Dynamic identification in RMW after the airbag test: comparison between frequencies f, damping ratios ξ and mode shapes in terms of MAC. 222

Table 6.8 – Dynamic identification in RMW_UND after the airbag test: comparison between frequencies f, damping ratios ξ and mode shapes in terms of MAC. 222
Table 6.9 – Comparison of natural frequency variation before and after the out-of-plane airbag test. 223

This page is intentionally left blank

1 Introduction

1.1 Background and Motivation

Masonry is a traditional construction material widely used in building practice throughout history. Historical masonry buildings have considerable resistance to static vertical loads. Nevertheless, earthquakes and induced horizontal loads represent one of the major threats to these structures. Common construction details typically observed in this type of structures (e.g. high percentage of voids and lack of connecting stones between masonry leaves, lack of effective connections among structural components, irregular arrangement of the masonry units, low quality materials) can affect the seismic behaviour of stone masonry constructions and eventually lead to out-of-plane failures in the event of an earthquake.

Despite the research interest concerning the study of the out–of–plane behaviour of stone masonry walls in recent years, there is still a limited understanding of this phenomenon due to its complexity.

Masonry walls are often labelled depending on the characteristics of their components' assemblages [1]. Old masonry constructions are often the product of non-engineered processes based on three main structural criteria: (1) Strength, meaning that the structure must be strong enough to carry any kind of load imposed, including its self-weight; (2) Stiffness, meaning that the structures should exhibit a reduced deflection rate; (3) Stability, meaning that only negligible displacement levels can be developed within the structure.

The application of the aforementioned criteria, combined with rules of geometry and proportion, often resulted in the construction of oversized structural components, mainly due to the necessity of effectively dealing with seismic events [1] [2].

The seismic behaviour of masonry constructions highly depends on constructive details such as the morphology of load-bearing walls (masonry units, mortar, interlocking of units, regularity of courses, etc.), slenderness of the walls, quality of the connection among the walls and between walls and horizontal structures, or the presence of adequately rigid floor diaphragms [3]. Poor detailing can lead to premature out–of–plane failure, which consists of the complete or partial overturning of the masonry walls orthogonally oriented with respect to the seismic wave, ideally assumed acting only in one direction [2] [4], see Figure 1.1.

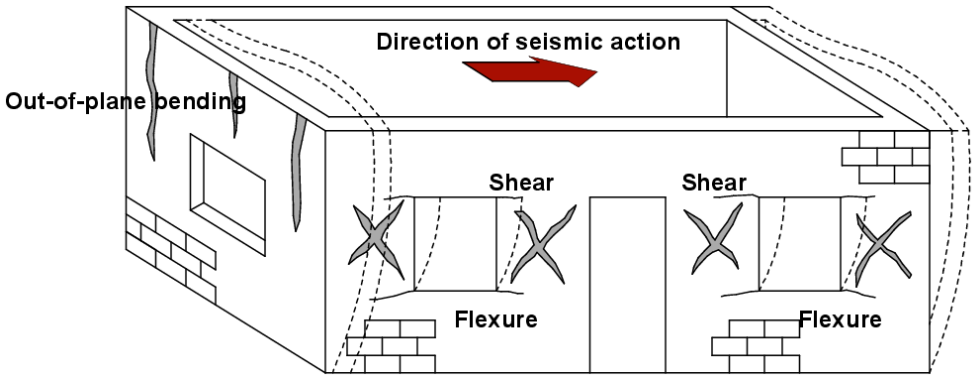


Figure 1.1 - Typical seismic induced damage in structural walls [5].

Throughout history, earthquakes have caused significant damage in terms of both economic, human losses and homeless people. Unfortunately, the technological advances and the increasing awareness concerning this phenomenon didn't result in considerable mitigation of seismic risks. In fact, according to the CREED database held at the University of Louvain (see Figure 1.2), in the first half of the 20th century (considering the decades from 1900 to 1960), an average of 19600 lives were lost as a result of earthquakes each year [6].

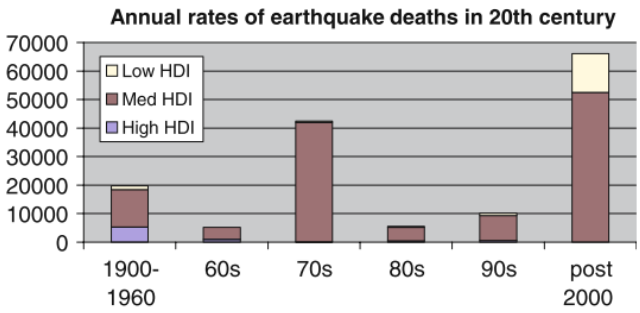


Figure 1.2 - Annual rates of earthquake deaths since 1900 by decade [6].

It is common to detect the presence of earthquake resistant techniques developed in highly seismic prone areas. Due to the long-term exposure to earthquake hazard, the local populations were forced to adapt and protect their built environment by means of traditional earthquake resistant techniques [7]. These techniques usually consist of the use of locally available materials (e.g. timber), which are embedded in the masonry structural components, aiming at the enhancement of the overall seismic performance of the building [8] [9] [10]. However, there are numerous stone masonry buildings in medium/high seismic prone areas where this

construction culture did not exist and strengthening techniques need to be used to improve their seismic resilience. The strengthening techniques commonly used in the building practice are based on identical structural principles. Indeed, they aim to improve the wall connections and the box behaviour of the building in which they are installed. Furthermore, when it comes to strategic buildings (e.g. heritage constructions), reversibility and reduced invasiveness of the interventions should be prioritized. Among the techniques and strengthening solutions commonly used in the building practice, textile-reinforced mortars (TRM) seem to comply with the characteristics previously identified in terms of intervention's compatibility with existing structural/material components. For this reason, a TRM solution based on a glass fiber mesh embedded in the mortar layer has been selected in this study and experimentally tested in order to gather insight regarding its effectiveness in improving the out-of-plane performance of masonry walls in different conditions, namely damaged and undamaged.

The present research work focuses (1) on the study (numerical and experimental) of the structural behaviour of masonry walls under out-of-plane load induced by earthquakes; (2) on the identification of the most influential geometrical and mechanical key-parameters affecting the out-of-plane performance of masonry walls; (3) on the use linear regression analysis to quantify the influence of key-parameters on the out-of-plane capacity in masonry walls and (4) on the assessment of specific strengthening solutions to improve their seismic performance.

The outcomes of this work are intended to represent a contribution to the preservation of the traditional masonry heritage by enhancing our understanding of their seismic behaviour. In particular, the work aims to contribute to the better understanding of the out-of-plane performance of masonry constructions, as well as assessing the efficiency of using textile reinforced mortar as a strengthening technique to improve it.

The investigation is also expected to provide efficient and expedited methods to assess the seismic behaviour of masonry structures, which is key for the conservation of a built heritage that is widespread throughout many regions in the world.

1.2 Thesis objectives

Masonry walls constitute the main structural system of many traditional and historical buildings located in seismic prone regions, acting mostly in shear. However, as aforementioned, if connection among the structural elements is not ensured (walls to walls, walls to floors), premature out-of-plane of the walls can occur. The high vulnerability of masonry walls under out-of-pane loading, revealed after past seismic events,

makes it mandatory to understand better their mechanical behaviour and to improve their out-of-plane load capacity in order to increase the structural stability of masonry constructions. A gap in knowledge still exists regarding the out-of-plane behaviour of these types of structural elements and, above all, a better insight is required about the most efficient techniques to reduce their seismic vulnerability. This is particularly relevant in the case of multiple leaf masonry walls, due to the reduced previous numerical and experimental works carried out. An additional issue tackled by the present research is related to the role of uncertainties regarding the material properties, boundary conditions and geometry, on the assessment of the out-of-plane behaviour of masonry walls, and how they need to be considered when numerical or design strengthening solutions are required.

Therefore, the present research aims to:

Objective 1: gather insight on the influence of key factors in the out-of-plane behaviour of multiple-leaf masonry walls. It is also intended to account for the uncertainty of the key factors, such as material properties, boundary conditions or connection level.

Objective 2: propose some simplified tools (e.g. empirical expressions) to quantify the influence of different key-parameters on the out-of-plane strength of masonry walls.

Objective 3: assess the effectiveness of strengthening solutions to reduce seismic vulnerability.

Research goals are in line with point 11.4 of the 2030 Agenda for Sustainable Development: “Strengthening efforts to protect and safeguard the world’s cultural and natural heritage”. Furthermore, the results of the research could be applied both in Portugal and in other countries with medium/high seismic hazard and masonry construction.

1.3 Research Methodology

To accomplish the research objectives, experimental, numerical, statistical, and analytical analyses were combined, namely (1) identification of the main key parameters influencing the out-of-plane behaviour of 2-leaf masonry walls (boundary conditions, material properties and geometry) through parametric studies taking into account the uncertainty of the mechanical properties, connections and boundary conditions; (2) construction of a database of mechanical properties for 2-leaf masonry walls updated by means of Bayesian inference; (3) identification of appropriate numerical modeling strategies for masonry walls under out-of-plane loading and calibration of numerical models based on experimental results; (4) numerical parametric study on both geometrical and material level in order to gather insight on the most influential parameters affecting

the out-of-plane behaviour of masonry walls; (5) experimental testing on plain 2-leaf masonry walls under out-of-plane loading; (6) experimental testing of strengthening solutions aiming at improving the out-of-plane behaviour.

A key-aspect of this work is the contribution regarding the development of simplified tools and methodologies for the assessment of the influence of specific mechanical and geometrical parameters on out-of-plane performance in 2-leaf masonry walls. This goal was achieved using statistical simulations relying on data collected from literature review and from numerical parametric studies.

The numerical analysis included: (a) the assessment of different numerical approaches to the out-of-plane analysis of stone masonry walls; (b) calibration of numerical models based on experimental results; (c) parametric study to obtain better insight on the man parameters affecting the out-of-plane performance of masonry walls, considering material (mechanical properties) and structural uncertainties (masonry bond configuration, connections' effectiveness). Experimental activities provided a better insight regarding the actual behaviour of reduced-scale masonry prototypes under the combined effect of axial load and out-of-plane action. Hence, the specific following tasks have been developed considering the objectives:

- Task 1: Literature review.
- Task 2: Database on masonry walls mechanical properties.
- Task 3: Numerical modelling.
- Task 4: Experimental characterization of the out-of-plane behaviour of plain and strengthened or retrofitted two-leaf stone masonry walls.
- Task 5: Numerical parametric study and out-of-plane performance evaluation.

Task 1: Literature review

This task includes a systematic state of the art on the out-of-plane behaviour of stone masonry walls and on the experimental and numerical work carried out in the past in similar subjects. In detail, an overview of the existing knowledge will be presented regarding the: (1) typology of 2-leaf masonry walls, considering the geometry, materials, masonry bonds and boundary conditions (see Chapter 2); (2) non-destructive, minor-destructive and destructive testing procedures for the assessment of masonry mechanical properties (see Chapter 2); (3) statistical models, based on the Bayes Theorem, applied in order to update reference mechanical properties characterising the structural performance of 2-leaf masonry walls (see Chapter 2); (4) numerical approaches used to analyze the of out-of-plane behaviour of masonry walls (see Chapter 3); (5)

experimental characterization of masonry walls under out-of-plane loading (see Chapter 6); (6) strengthening techniques that can be used to improve the out-of-plane behaviour of stone masonry walls (see Chapter 6). The main outcomes of this task were the preliminary characterization of the most relevant data about masonry walls in terms of typology (Outcome 1), quantitative factors such as mechanical properties and qualitative factors such as connections and characteristics of the masonry bond (Outcome 2), experimental techniques for the characterization of the out-of-plane behaviour in masonry walls (outcome 3) and strengthening techniques for the improvement of the out-of-plane capacity in masonry walls (Outcome 4), see Figure 1.3.

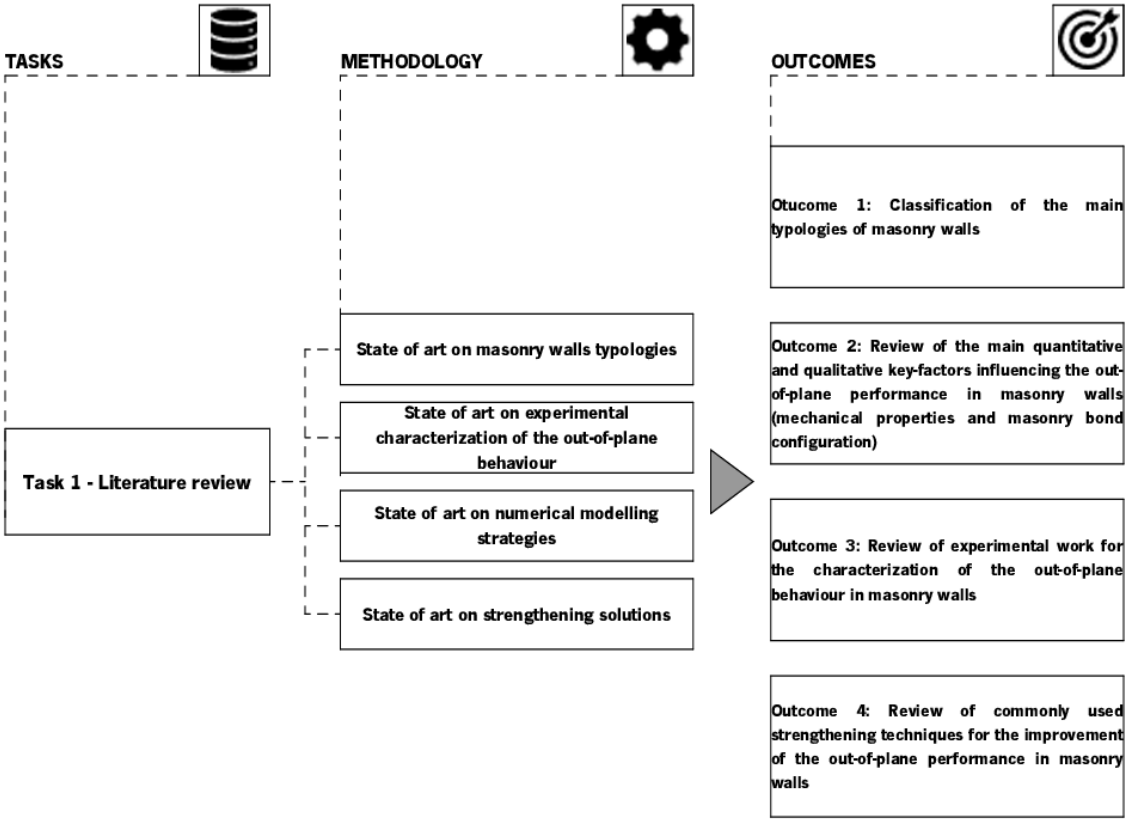


Figure 1.3 - Task 1 Workflow.

It must be noted that a chapter specifically presenting the information gathered through the literature review is not provided in the document. The structure of the documents is characterized by an introduction in each chapter where an overview and background information are provided regarding the topic addressed in the chapter itself. Hence the results of the literature review are interspersed throughout the document.

Task 2: Database on masonry walls mechanical properties

This task aimed at the development of a database, presented in Chapter 2, containing information about (1) masonry walls, namely at the level of geometry, masonry bonds, materials, connections to other structural elements and boundary conditions; (2) the key factors mostly influencing the seismic vulnerability of stone masonry walls; (3) the characterization of the key parameters in terms of features (qualitative information) and range variations (quantitative information) aiming at enabling the analysis of uncertainties in the mechanical out-of-plane behaviour of the stone masonry walls.

At the materials level, it was intended to define starting ranges for the key mechanical properties (modulus of elasticity, compression strength, shear strength, tensile strength, etc.), based on literature review and seismic standard guidelines (Outcome 5). It is intended to update the materials properties through additional data coming from literature sources regarding the characterization of masonry mechanical properties with different assessment techniques (non-destructive, minor-destructive, and destructive procedures). It is also intended to gather detailed information about geometry (height to length ratios, arrangement of cross sections) and connections with transversal walls and other boundary conditions.

Qualitative and quantitative information were integrated in the Database to enhance its accuracy and completeness. Moreover, statistical models based on the Bayes Theorem and on data fusion procedure were applied to update the reference range of values previously defined by means of literature review (Outcome 6), see Figure 1.4. This task provided an updated range of reference values to be used in numerical parametric studies concerning the analysis of uncertainty of the key parameters in the out-of-plane behaviour of the stone masonry walls (see also Task 4).

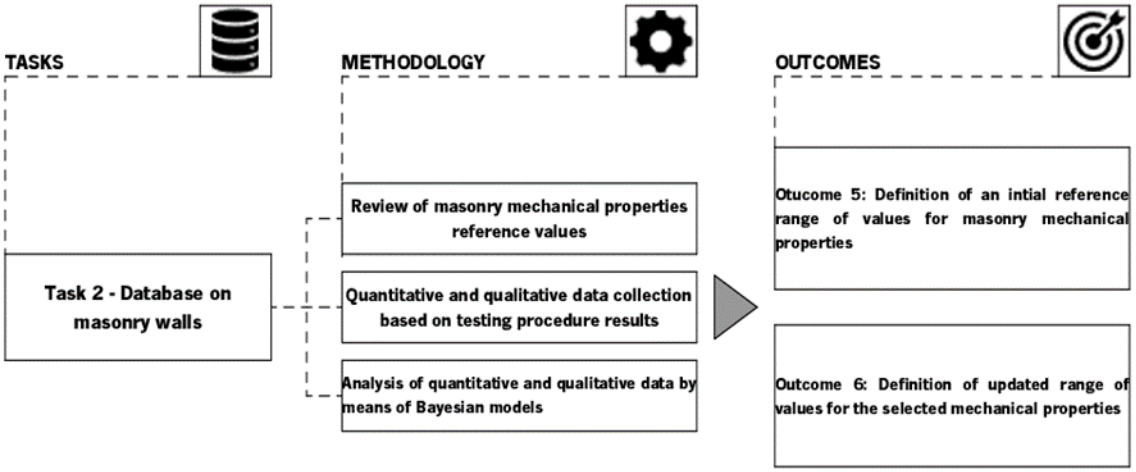


Figure 1.4 - Task 2 Workflow.

Task 3: Evaluation of different numerical modelling approaches

This task aimed at assessing the most appropriate numerical approach to simulate the behaviour of two-leaf masonry walls under out-of-plane loading. To this end, finite element (FE) models and discrete element models (DE) were analyzed. The calibration of the non-linear properties may be carried out based on the results of previous laboratory experimental campaigns dealing with the experimental characterization of the out-of-plane behaviour of masonry walls.

A comparison between experimental and numerical results is performed in terms of pushover curves deformation, and damage patterns (Outcome 7). Finally, a comparison between the different modelling strategies was carried out in terms of accuracy and computational effort (Outcome 8) so that the most appropriate approach could be used in the parametric studies carried out in the following tasks (Task 4), see Figure 1.5.

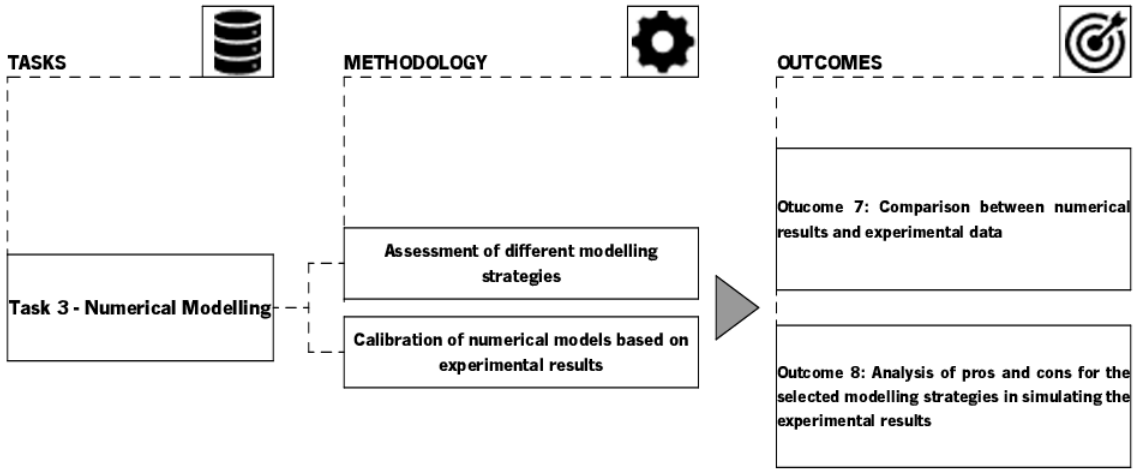


Figure 1.5 - Task 3 Workflow.

Task 4: Numerical parametric study and out-of-plane performance evaluation

This task aims at assessing the out-of-plane performance of two-leaf masonry walls by means of a probabilistic approach based on the numerical strategy revealed as the more appropriate and selected considering the result obtained in Task 3. To this end, a numerical parametric study will be implemented considering the key parameters characterising the geometry of stone masonry walls and the range of values defined in Task 2.

In addition to the evaluation of the key parameters' variation, the parametric study made it possible to identify their influence on the out-of-plane behaviour of the walls when a combination of different parameters is considered (Outcome 9). Statistical simulations were applied to analyze raw data and extract information to

correlate the variation (uncertainty) of a set of selected parameters (mechanical and geometrical), to the out-of-plane failure (Figure 1.6).

It is intended to:

- Derive a set of empirical expressions to quantify the individual influence of material and geometrical parameters on the out-of-plane performance in masonry walls based on different parameters such as strength and deformation for the limit states (Outcome 10).
- Propose guidelines that contribute effectively for the reduction of seismic vulnerability of stone masonry walls (Outcome 11).

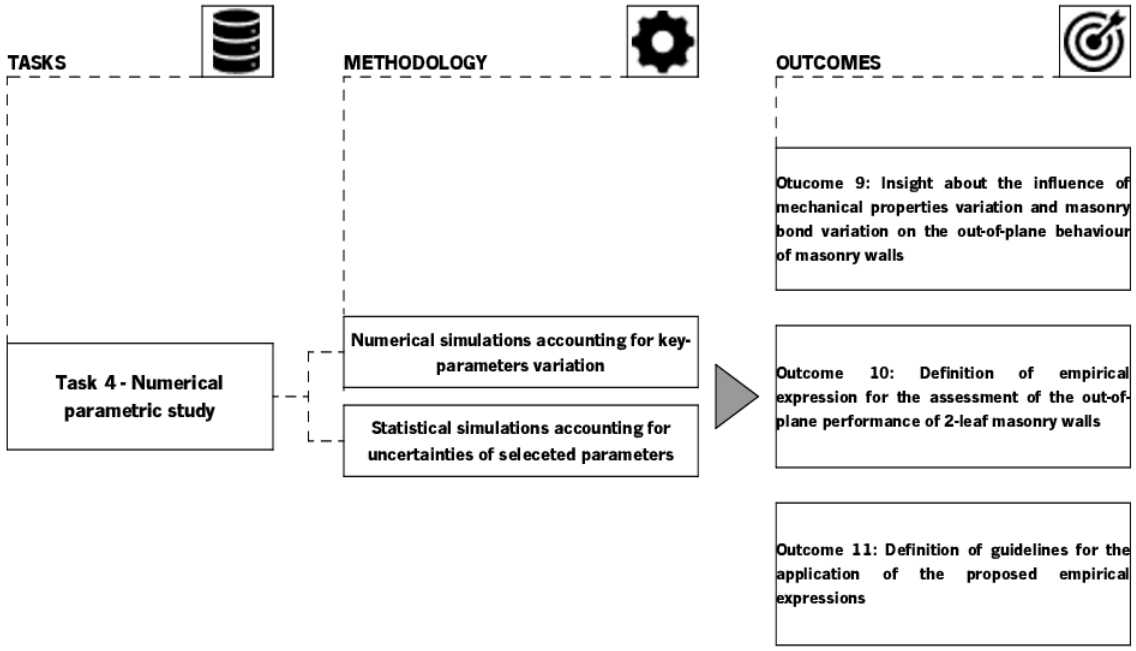


Figure 1.6 - Task 4 Workflow.

Task 5: Experimental out-of-plane behaviour of masonry walls

The main aims of this task are: (1) the experimental evaluation of out-of-plane behaviour of two-leaf masonry walls; (2) evaluation of the effectiveness of the combination of strengthening techniques to reduce the out-of-plane vulnerability of masonry walls.

A 2-phase work was considered: (1) characterization of masonry raw materials and strengthening materials; (2) out-of-plane tests on plain and strengthened U-shaped two-leaf masonry walls accounting for the combined effect of axial load and out-of-plane action (Figure 1.7). Unreinforced and strengthened walls were tested until

failure to define damage pattern and damage limit states and in order to assess the effectiveness of the proposed strengthening solutions.

The out-of-plane tests were performed under displacement control and the out-of-plane loading was simulated by means of an airbag, applied on rear surface of a U-shaped wall. Non-destructive procedures (e.g. dynamic identification tests) were carried out to obtain data for the mechanical characterization of the specimens.

To summarize, the main outcomes of this task are: (1) characterization of the out-of-plane behaviour of masonry walls through the definition of force-displacement pushover curves, dissipation energy capacities, crack/damage patterns and limit states characterized by a deformation and damage level (Outcome 12); (2) evaluation of the effectiveness of the different strengthening techniques and definition of guidelines for their application (Outcome 13), see Figure 1.7.

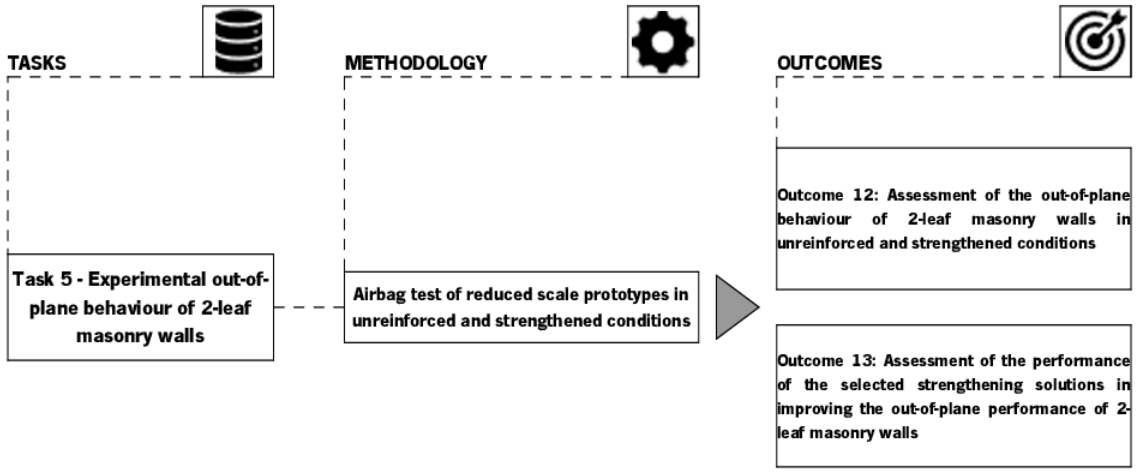


Figure 1.7 - Task 5 Workflow.

1.4 Outline and organization of the thesis

This document consists of seven chapters. Chapter 1 addresses, on one hand, the background, motivations, objectives, and research methodology of the research work presented, on the other, it provides a brief description of the structure of the thesis.

Chapter 2 presents a comprehensive review of non-destructive tests (sonic tests), minor-destructive tests (flat jacks) and destructive tests (diagonal-compression, shear-compression, and compression tests), as well as hybrid (qualitative and quantitative) procedures for the evaluation of masonry mechanical properties (Masonry Quality Index). A database of masonry mechanical properties has been defined based on the gathered data. Successively, statistical simulations based on the Bayes Theorem have been applied to a set of selected key

parameters in order to update the range of values of mechanical properties in reference masonry typologies provided by the technical guidelines commonly used in the building practice.

Chapter 3 presents a review and a comparison of modelling strategies for the simulation of the out-of-plane behaviour of 2-leaf masonry walls. The main outcome of the chapter is to highlight pros and cons of the selected modelling strategies accounting for results' accuracy and computational effort. The insight gathered regarding the performance of different modelling approaches will be later applied in the parametric studies presented in Chapter 4 and 5 respectively.

Chapter 4 outcomes refer to a parametric study on reduced scale numerical models. The parametric studies carried out aim to provide insight on the influence of mechanical parameters and geometrical configuration of the masonry bond of the selected wall typology.

In Chapter 5, the parametric study is applied to full-scale models, and it aims at the definition of empirical expressions for the assessment of the influence of a set of mechanical and geometrical reference parameters on the out-of-plane performance in 2-leaf masonry walls. Moreover, additional empirical expressions are provided regarding the estimation of recurring input parameters required to perform numerical simulations.

Chapter 6 presents the results of experimental out-of-plane tests carried out on two U-shape reduced scale masonry walls enabling the assessment of the out-of-plane performance in unreinforced and strengthened conditions. The strengthening solution consists of a textile testing forced mortar applied to the external surface of the frontal wall. A comparative analysis between plane and strengthened masonry is carried out to highlight the effectiveness of the strengthening performance.

To conclude, Chapter 7 presents a summary of the research activities performed and the main conclusions drawn based on the obtained results and possible future research works.

This page is intentionally left blank

2 Database of mechanical properties for 2-leaf masonry walls

2.1 Introduction

Traditional engineering models based on a deterministic approach have been widely applied over the last decades in professional practice. These models usually consist of simplified rules deduced accordingly to the available experimental data. Despite their effectiveness in terms of cost reduction and overall improvement of structural performance in engineering systems, these approaches only partially account for uncertainty affecting physical quantities (e.g. materials' mechanical properties) by means of conservative values and/or safety factors [11].

Uncertainty may play a considerable role in the assessment of existing buildings such as masonry heritage constructions, due to a significantly greater variability observed in the description of geometry, materials, and acting loads.

When dealing with historical constructions and monuments, a specific assessment procedure is considered effective if it combines a significant level of knowledge with minimum invasiveness of interventions, thus aiming at the conservation of the cultural asset [12]. To tackle this issue, Italian and European guidelines (NTC 2008, Eurocode 8 - Part 3) [13] have traditionally relied on a semi-probabilistic framework that defines Knowledge Levels (KLs). Different KLs are achievable once a defined amount of geometrical, architectonic, constructive, and mechanical data is gathered. The achieved *Knowledge Level* corresponds to a *Confidence Factor (CF)* that, once applied to a specific parameter provided by the code, results in a reduction of its value in order to compensate for a biased knowledge of the structure [13] [14].

In recent years, there has been a progressive rise of awareness on how to consider variability and uncertainty in the material, geometric and construction characteristics related to the structural assessment procedures of existing buildings, which has led to a relevant upgrade of the standard deterministic method, particularly in the field of seismic safety assessment procedures.

A methodology for the probabilistic assessment of existing building has been proposed by the National Research Council of Italy (CNR) [15]. It models uncertainties based on the classification of three types of variables, namely deterministic (characterized by a negligible margin of uncertainty), random (related to the intrinsic variability of the properties of the structure) and epistemic (related to the lack of knowledge of the structure in terms of mechanical properties) [15].

A significant aspect concerning the application of probabilistic approaches in the construction industry is the acquisition of suitable data and information for the reduction of the global uncertainty characterising the entire process.

Within this framework, non-destructive techniques and expedited assessment methods based on visual inspections are highly valuable tools for existing buildings' material characterization. They are complementary to minor-destructive and destructive procedures that are not always applicable or advisable (e.g. lack of minimum intervention criterion applied to conservation of heritage constructions).

Hence, recent upgrades in technical guidelines acknowledged the relevance of collecting data from different sources (e.g. non-destructive, minor-destructive, and destructive testing procedures). The guidelines envisage the possibility to combine this information by means of advanced statistical techniques, in order to estimate mechanical parameters [16].

To this end, Bayesian inference has been generally adopted due to its effectiveness in reducing uncertainties. It allows, on one hand, to fuse together various types of data and, on the other hand, to further upgrade a given parameter when new information is available [15] [16].

Based on the previous considerations, this chapter presents the research activity carried out to collect data from non-destructive, minor-destructive, and destructive testing procedures by means of literature review. The data was assembled into a large database of mechanical properties related to different historical two-leaf stone masonry types. Successively, using the collected information, Bayesian inference has been applied to obtain range of variation for different mechanical properties of two-leaf stone masonry types. Lastly, the ranges obtained are compared with the ranges proposed in current standards. The outcomes herein presented can provide a valuable support for practice-oriented engineering activities addressing the assessment of existing buildings.

2.2 Bayesian inference in existing structures assessment and uncertainty reduction

Classic statistic methods are based on a frequentist interpretation of probability according to which frequencies are used as a measure of uncertainties. Conversely, Bayes' theorem is a proposition about conditional probabilities. A probability distribution function describes an unknown parameter, hence the probability itself to provide an estimation of uncertainty.

According to this approach, an initial distribution of data based on a priori information can be updated, obtaining a posterior distribution, when new observations are available [17]. If a value X = x is observed, and h(θ) is the prior distribution, the Bayes theorem is translated as follows:

$$h(\theta|x) = \frac{h(\theta)f(x|\theta)}{\int_{\theta} h(\theta)f(x|\theta)d\theta} \quad (1)$$

where h(θ|x) is the posterior distribution of θ after observing X = x. The initial information is characterized by h(θ) and modified with the observed data by being updated to h(θ|x); f(x) is the prior predictive distribution for X; that is for an observation of X whatever value of θ.

Bayes theorem weighs the prior information with the evidence provided by the new data. The posterior distribution is a compromise with reduced uncertainty between the prior information and the one contained in the new data [18].

The prior distribution should include all plausible values of a certain variable and its parameters can be estimated based on known initial observations (e.g. literature review) and/or subjective knowledge (e.g. personal judgment). It is possible to choose a prior distribution with small standard deviation (good prior knowledge), large standard deviation (limited knowledge) or it is also possible to choose a prior distribution, which reflects a range of situations from no knowledge. Prior distribution and posterior distribution follow the same parametric form (conjugacy property). Therefore, if prior and likelihood functions are normally distributed, the posterior function will be normally distributed as well [18].

The joint probability distribution of the data and the parameter (likelihood) is given by h(θ|x) according to the expression:

$$h(\theta|x) = L(\theta) = \prod_{i} h(x_i|\theta) \quad (2)$$

where i is the number of outcomes of the new data.

The Bayes theorem allows to estimate the density function of the posterior distribution by multiplying the likelihood function and the density function of the prior distribution with subsequent normalization [19].

The posterior density expresses the fusion between prior observation and new data, and it provides a basis for posterior inference regarding θ.

Bayesian inference versatility allowed this method to address different engineering applications, ranging from structural performance assessment to estimation of materials' mechanical properties. In its early stage, research activities involving Bayesian methods mainly dealt with the definition of probabilistic frameworks aimed at the updating of structural models based on dynamic test data [20] [21] [22].

Further contributions, concerning the development of a methodology combining Bayesian inference and data obtained from dynamic identification tests, were used to update the probability density function (PDF) of the elasticity modulus in masonry towers [23] [24] [25].

Aiming at the definition of capacity models for reinforced concrete components (e.g. bridge columns), Gardoni [26] estimated fragility curves under cyclic load by means of Bayesian update. Successively, research activities based on Bayesian frameworks applied to reinforced concrete structures mainly addressed the reduction of uncertainties in estimating mechanical properties. To this end, the Bayesian method has been applied to combine experimental data and reference values provided by standards and guidelines (e.g. Eurocode and Italian Standards), to overcome the limitations affecting the use of *Confidence* Factors in reducing the mechanical properties depending on the achieved *Knowledge Level*. This code-based approach, in fact, is unable to account for the reliability of information gathered by means of different testing procedures [27] [28] [29].

Similarly, advanced statistical methodologies (Bayesian inference and Monte Carlo simulation) have been integrated in code-based assessment procedures for existing masonry buildings to reduce different sources of epistemic uncertainty (e.g. selection of the *Knowledge Level*, selection of location, and results of in-situ tests) [30] [31].

Additional contributions addressing the application of Bayesian methods for masonry structures were reported in Campostrini [32]. In this study, the authors developed a probabilistic methodology for the seismic vulnerability assessment at urban scale. Moreover, Beconcini [33] and Conde [34] proposed two different methodologies based on a Bayesian framework for the assessment of ancient constructions, applying their findings to a historical aqueduct and to a masonry arch bridge respectively.

A data fusion procedure, based on the Bayesian framework presented in Miranda [35] for the update of geomechanical parameters, was applied by Ramos [36] to a real case study (St. Torcato Church in Guimarães, Portugal). The goal of the study was to reduce the uncertainties in the estimation of the Young's modulus of the granite stone that compose the masonry walls of the church. The proposed methodology aims to overcome difficulties in selecting the right value for a certain parameter, which is crucial to perform

subsequent structural assessment. This data fusion technique has been taken as a reference approach to obtain updated values of historical masonry mechanical properties using a large set of experimental data.

2.3 Database definition: Adopted criteria

The work herein presented consists of a systematic review of experimental campaigns addressing the assessment of two-leaf masonry walls' mechanical properties. This wall morphology, highly widespread in Portugal, Italy, and other European countries, has been selected since it represents a construction technology typically applied in a considerable number of historical buildings [37].

It is noted that the work presented intends to be an exemplary application of the methodology proposed and it can be carried out for other masonry typologies typically observed in historical and regular constructions, such as one-leaf and three-leaf masonry walls.

Based on the guidelines provided by Eurocode 8 - part 3 [13] and Italian Code (Table C8.5.1, Circolare n. 7 - 21/01/2019) [38], six different stone masonry types have been considered to build the final database (Figure 2.1), namely:

- Masonry Type 1 (Irregular stone masonry) - Neither artificial nor handmade techniques have been applied to modify the stone units in terms of shape and/or geometric characteristics. The masonry bond is irregular and significantly chaotic;
- Masonry Type 2 (Roughly cut stones with wythes of irregular thickness) - Masonry wall constructed using slightly cut stone units having roughly defined shapes. Despite stone units may vary from each other both in terms of shape and size, the masonry bond often presents a regular texture and a good overall arrangement;
- Masonry Type 3 (Uncut stonework with good texture) - Masonry wall constructed using regular-shaped stone units. Stone units may vary from each other both in terms of shape and size. Additionally, they do not have experienced any kind of handmade or artificial working process. The masonry bond is considerably regular. Moreover, it can be detected the presence of horizontal bed joints;
- Masonry Type 4 (Masonry of irregular soft stone blocks) - This category proposes a classification mostly based on a specific material. Masonry units related to this wall typology can be made of roughly cut volcanic rocks (tuff) or sedimentary rocks (tufa) [39]. Throughout history, tuff has been often used in heritage constructions because it is a light and easily workable material;

- Masonry Type 5 (Regular masonry of soft stone blocks) - Similarly to the previously listed typology (Masonry Type 4), this category refers to masonry walls built with volcanic and sedimentary rocks and with masonry units that can be defined as "dressed stones", meaning that they have been worked and assembled together resulting in a masonry bond embodying the main criteria of the "rules of the art";
- Masonry Type 6 (Squared stone masonry) - Masonry wall constructed using stone units that can be found in quarries. Stone units may differ in terms of size, but they have been shaped to be as much regular as possible. The masonry bond is characterized by vertical and horizontal bed joints uniformly distributed throughout the entire masonry wall.

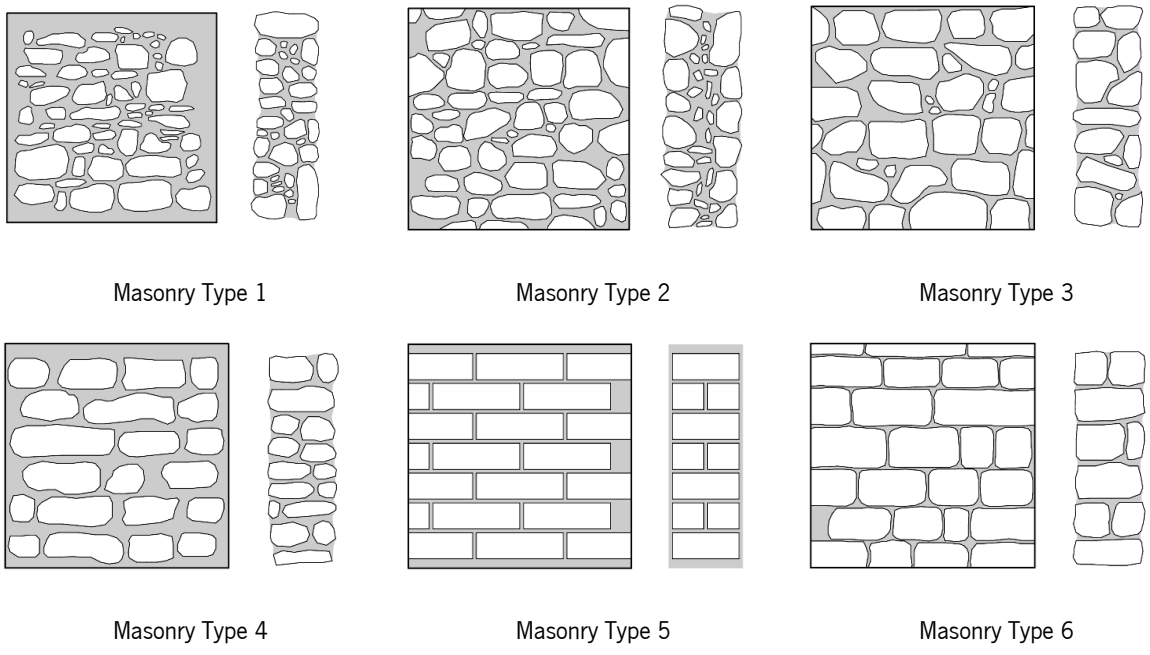


Figure 2.1 - Selected masonry types.

Experimental data collected for the construction of the database refers to the following mechanical parameters: Young's Modulus (E), Shear Modulus (G), Compressive Strength (f_m) and Shear Strength (τ_0). The testing procedures considered are: Sonic Testing (ST), Flat-Jacks Tests (FJ), Compression Tests (CT), Diagonal-Compression (DC) and Shear-Compression Tests (SC).

The comprehensive literature search was carried out on 5 electronic indexing databases: Scopus, Science Direct (SCD), Web of Knowledge (WOK), Civil Engineering Database (ASCE), and MADA RELUIS Database [40].

In addition to the collected papers, other relevant documents were considered, such as Ph.D. thesis and technical reports of Integrated Projects (SA7) carried out within the framework of the Advanced Masters in Structural Analysis of Monuments and Historical Constructions (SAHC). These additional documents provided highly valuable information in order to fill the gap regarding the availability of experimental data from Sonic Testing procedures applied to historical masonry.

Papers whose titles were not about two-leaf masonry walls tested by means of the non-destructive, minor-destructive, and destructive procedures selected for this study were excluded. On the other hand, those papers complying with the established criteria were included in the final set of data, and they were carefully screened to avoid any possible repetition. A detailed list with the final set of papers and reports, collected to extract experimental data for the present work, is provided in *http://dx.doi.org/10.17632/mprjsnr6mp.1*.

Lastly, once completed the screening process, every masonry panel described in the final set of documents was evaluated by means of the Masonry Quality Index (MQI) method [41] [42] in order to obtain an empirical initial estimation of the reference mechanical parameters (E, G, f_m, τ_0). The following sections present a brief overview of the assessment methods and techniques considered to gather the information later adopted to build the database.

2.3.1 Masonry Quality Index (MQI)

Masonry Quality Index (MQI) correlates mechanical properties and masonry bond characteristics. MQI has been developed to assess masonry walls, considering the traditional technical guidelines applied to build workmanlike constructions.

This method is mainly based on a qualitative criterion, which consists in evaluating the presence (Fulfilled - F), the partial presence (Partially Fulfilled - PF) or the absence (Not Fulfilled - NF) of certain parameters which contribute to define the "rules of the art" for an ideal masonry wall, namely (1) conservation state of the stone units – SM, (2) stones' dimension – SD, (3) stones' shape (SS), (4) characteristics of the wall section – WC, (5) characteristics of horizontal joints – HJ, (6) characteristics of vertical joints – VJ, (7) quality of the mortar – MM. Moreover, stone units' interlock (WC) can be quantitatively determined using the concept of the minimum trace length (MTL), which is defined as the minimum length of an ideal line passing through mortar joints and connecting two vertically aligned points mutually spaced 1 meter [41] [42].

MQI application results in the definition of three indexes related to the vertical loads (MQI_v), to the in-plane load (MQI_i) and to the out-of-plane load (MQI_o). Once a MQI value for a loading condition is known, using

specific correlation curves, it is possible to calculate the main mechanical parameters, namely compressive strength, shear strength, Young's Modulus and Shear Modulus. According to the studies present in the literature, the correlation curves related to the vertical load index are the most effective in predicting Young's modulus and compressive strength, whereas the empirical equations based on the in-plane load index proved to be more reliable in estimating shear strength and shear Modulus [43].

2.3.2 Sonic Testing (ST)

The sonic test method is one of the most widely used non-destructive procedures. This technique is based on the generation of sonic or ultrasonic impulses by means of a transmitter (e.g. percussion or electrodynamics/pneumatic devices). The resulting elastic wave propagates through the material and is collected by a receiver. Data post processing measures the time that an impulse takes to cover the distance between the transmitter and the receiver, which can be placed in various positions throughout the structure. As a result, the sonic tests allow estimating the primary waves velocity (V_P) and the surface or Rayleigh waves (V_R), which are related to the mechanical properties of materials according to the following equations [44] [45]:

$$\frac{V_P}{V_R} = \sqrt{\frac{2 \cdot (1-\nu) \cdot (1-\nu)^2}{(1-2\nu) \cdot (0.87+1.12\nu)^2}} \tag{3}$$

$$V_P = \sqrt{\frac{E}{\rho} \cdot \frac{(1-\nu)}{(1+\nu) \cdot (1-2\nu)}} \tag{4}$$

Where E is the deformation modulus, ν is the Poisson's ratio and ρ is the material density.

Since their early application for the inspection of historical constructions, sonic testing procedures proved to be a reliable tool in providing qualitative information regarding the internal structure of masonry elements (e.g. the identification of voids and constructive flaws) [46] [47], as well as the monitoring of the effectiveness of repairing solutions for damaged masonry (e.g. grout injections) [48].

2.3.3 Flat-jacks test (FJ)

The flat-jack tests provide information about the compressive stress level and the deformability properties of the masonry. The test consists of performing two parallel plane cuts perpendicular to the masonry surface. The flat jacks can then be introduced in the slots and loaded progressively, applying uniaxial compressive

stress to the portion of the wall delimited by the cuts, which allows estimating the Young's modulus and compressive strength.

This technique is classified as minor-destructive because the damage caused to the structure can be repaired once the test is concluded [49]. The flat-jack testing protocol is defined by the American Society for Testing Materials [50] [51] and by the Reunion International des Laboratoires et des Materiaux, Systemes de Construction et Ouvrages (RILEM) [52].

This method is based on the following assumptions, namely (1) masonry surrounding the slot is homogenous, (2) the stress applied to the masonry by the flat jacks is uniform, (3) the state of stress in the tested portion of the wall is uniaxial and, therefore, lateral constraining effects of adjacent masonry can be neglected [37]. Initially, this technique was applied in the field of rock mechanics. Early stage applications of flat-jacks test to stone masonry constructions can be found in Binda [53] and Lourenço [54]. The results obtained in a considerable number of experimental campaigns showed a significant scattering rate, proving that the procedure must be adjusted according to a case-by-case approach based on preliminary evaluations of test location, materials, and local construction techniques.

2.3.4 Compression test (CT)

Compression tests are usually carried out to estimate the modulus of elasticity E and the compressive strength of masonry f_m, which are key parameters for the assessment of structural performances in existing buildings.

In-situ compression tests are carried out based on the guidelines provided in [50] [51] [52] and following the procedure related to the double flat jack test. The maximum pressure of the test is used to estimate the compressive strength of the masonry, while the normal elastic modulus E and the Poisson ratio (ν), derived from the measured displacement, allow to estimate the shear modulus G through equation 5:

$$G = \frac{E}{2(1+\nu)} \tag{5}$$

If the magnitude of horizontal displacements is too small, it can be difficult obtaining reliable measurements of the Poisson ratio and, consequently, an accurate estimation of the shear modulus [55].

Laboratory compression tests are carried out using specific equipment, often consisting of supporting metallic frames equipped with actuators [56]. Once the specimen is in position, metallic rigid plates can be applied in order to uniformly distributing the load on its upper surface. Vertical displacements are measured using

Linear Variable Displacements Transducers (LVDTs) that can be placed on the sides of the masonry prism to be tested.

Both monotonic and cyclic compressive tests can be performed on the same specimen. The monotonic test enables the determination of the value of the maximum compressive strength, which can be later used to define the procedure for the cyclic tests [56] [57]. Loading and unloading cycles can be performed reaching a maximum compressive strength level corresponding to a share (e.g. 25%, 50%) of the value detected during the monotonic test. The mechanical properties are then calculated based on the stress-strain curves resulted from the testing procedure.

2.3.5 Diagonal-compression test (DC)

Diagonal-compression test is carried out to evaluate the shear behaviour of masonry panels. It can be performed both in-situ and in laboratory. During the in-situ test, 4 cuts are realized in the masonry wall to isolate the tested panel. The lower part of the masonry remains attached to the wall wing. A jack, placed on one of the two corners of the masonry panel, exerts the compressive diagonal force. In the regular test procedure, loading/unloading cycles, with a constant increment after each step, are applied until failure. The shear strength τ_k^{diag} is evaluated using the following equation:

$$\tau_k^{diag} = \frac{\sqrt{2}}{2}\frac{P_{max}}{A_n} \tag{6}$$

where P_{max} is the maximum load applied by the jack during the test and A_n is the net area of the panel as defined in ASTM guidelines, which also provide the specifications to perform the laboratory test procedure [58].

2.3.6 Shear-compression test (SC)

Shear-compression in-situ testing procedure is based on the work carried out by Sheppard [59]. It consists of separating the tested masonry panel from the wall by means of vertical lateral cuts and a top horizontal cut. The "isolated" specimen (recommended dimensions 0.90 X 1,80 m²) is then subjected to a vertical compressive stress, which is kept constant by means of a suitable system of steel plates, steel rods and jacks. During the test, a hydraulic jack exerts an increasing horizontal force to the centre of the panel. Thus, shear stresses are distributed over the whole thickness of the panel.

Panel's bottom and top are fixed to a steel structure by means of a suitable device. Hence, the specimen is ideally divided into two square specimens, subject to different shear forces [55]. The shear strength of the masonry is estimated using equation 7 [60]:

$$\tau_{max} = \tau_k^{sc} \sqrt{1 + \frac{\sigma_0}{1.5\tau_k^{sc}}} \quad (7)$$

where σ_0 is the vertical compression stress (recommended value 0.30 MPa), τ_k^{sc} the shear strength of the masonry, whereas τ_{max} is the maximum shear stress defined as:

$$\tau_{max} = \frac{T_{max}}{A} \quad (8)$$

being T_{max} the maximum shear load in the lower half of the panel and A the horizontal cross-section of the panel. If the test is performed in laboratory, the masonry panels must be fixed at both upper and lower extremities and subjected to constant vertical load, applying increasing lateral forces on one of the two ends.

2.3.7 Final Database

The online research on electronic indexing databases resulted in the identification of 4239 documents. The most considerable contributions are represented by the results obtained from SCOPUS and Web of Knowledge databases, with 1840 and 1738 documents, respectively.

In each database consulted, the distribution of results clearly shows the prevalence of compression tests data, which account for more than 50% of the total, followed by diagonal-compression tests. Non-destructive testing data could be obtained from all the consulted databases except for ASCE and MADA Reluis database [40]. After the removal of duplicates, 124 documents were accurately examined, leading to a final number of suitable results equal to 678. The final complete database with detailed information on the documents analysed has been published in http://dx.doi.org/10.17632/mprjsnr6mp.1. The highest number of observations refers to diagonal-compression tests (195), followed by compression tests (169). The lowest number of observations registered is 97 (shear-compression tests), whereas almost the same amount of data is available for sonic test and flat-jacks test, with 110 and 107 observations, respectively (Figure 2.2a).

Looking at the distribution of experimental outcomes for each masonry type (Figure 2.2b), it is possible to observe that Masonry Types 1, 2 and 3 have been widely investigated through all the testing procedures considered in this study. On the other hand, only compression test, diagonal-compression test and shear-

compression test results are available for Masonry Type 4 and 5. Overall, experimental results related to the first three masonry types are the majority for all the testing procedures considered.

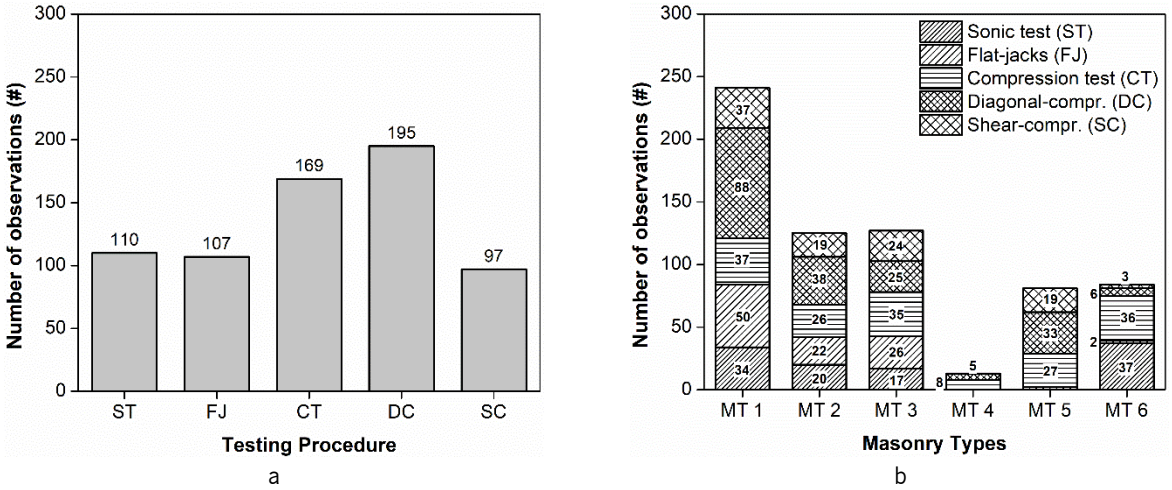


Figure 2.2 - (a) Testing procedure results distribution; (b) Testing procedure results classified by masonry typologies.

Further data analyses have been carried out to classify the collected information depending on the country where the experimental campaign was carried out (Figure 2.3a). Overall, the highest number of observations refers to Mediterranean countries, where stone is a locally available material that has been commonly used throughout history in the building practice.

Portugal and Italy account for more than 50% of the total number of results in both non-destructive and destructive testing procedures. It is also worth pointing out that most of the data obtained from diagonal-compression and shear-compression testing procedures belongs to Italian experimental campaigns.

The total number of observations is almost equally distributed between in-situ testing campaigns and laboratory testing campaigns, with 336 and 342 results respectively (see Figure 2.3b).

A detailed survey of the collected information clearly highlights that no data is available related to flat-jacks tests carried out in the laboratory. Additionally, the final database includes a low number of sonic tests data related to laboratory campaigns. This trend is clearly due to the characteristics of these testing procedures, which are mainly used in on-site campaigns.

On the other hand, destructive testing procedures have been widely applied in laboratory experimental campaigns. They require, in fact, highly complex setups and instrumentations, which are often difficult to install in non-controlled environments (in-situ conditions). Moreover, the invasiveness of these procedures (compression, diagonal-compression, and shear compression tests) must not be overlooked. In order to test

a masonry wall on-site, it must be isolated from the rest of the building, leading to an irreversible change in terms of the overall structural behaviour. Therefore, this aspect makes the aforementioned procedure not suitable for the assessment of existing constructions especially if they have a cultural value.

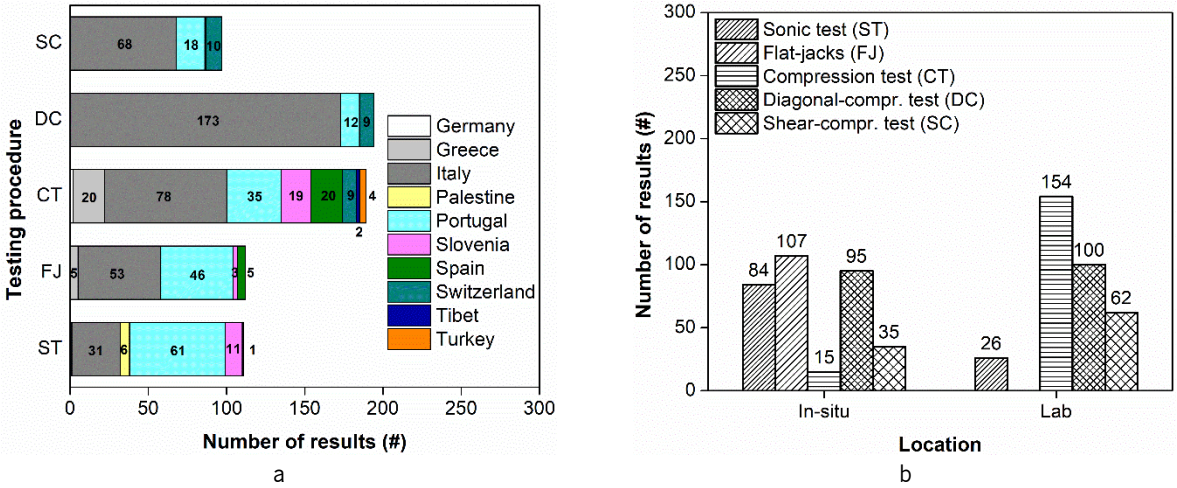


Figure 2.3 - (a) Testing procedure results classified by country of origin; (b) Data distribution (in-situ/laboratory experimental campaigns).

2.4 Data fusion for the update of masonry mechanical properties

Data collected to build the database have been further examined to filter any possible outliers that could affect the Bayesian updating process. Hence, the dispersion of the whole dataset has been assessed. The interquartile range (IQR) of data distributions has been calculated as the difference between the 75th (Q3) and the 25th (Q1) percentile (IQR = Q3 – Q1). All those observations below the limit Q1 - 1.5*IQR and above the limit Q3 + 1.5*IQR have been considered as outliers, hence not statistically valid for the purpose of this study [61]. The filtering procedure has been carried out for all the selected masonry types, mechanical parameters, and testing procedures. As an example, Figure 2.4 depicts the boxplot related to the identification of outliers within the Young's Modulus data distribution.

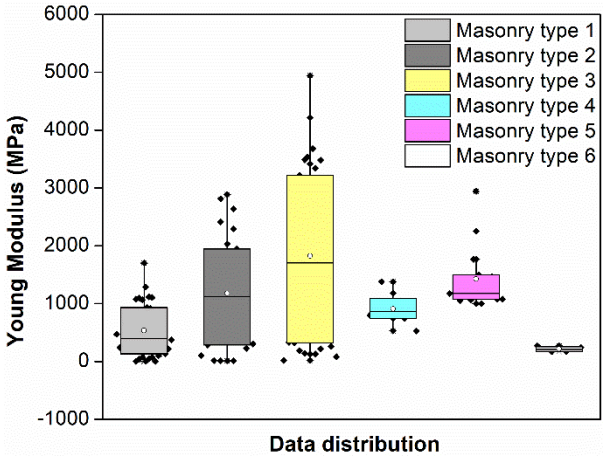


Figure 2.4 - Definition of outliers within the Young's Modulus dataset obtained from Compression Tests.

The Bayesian methodology applied in this study refers to a theoretical framework proposed by Ramos [36]. A key aspect characterising the updating procedure is the definition of a prior knowledge, which represents the starting point of the whole data fusion technique based on Bayesian inference. As mentioned in Section 2.3, all masonry panels considered in the final database have been examined by means of Masonry Quality Index (MQI). This visual assessment method allowed to estimate the reference mechanical parameters considered in this study (E, G, f_m, τ_0), using the empirical equations provided in the literature [41] [42]. The evaluation of all masonry specimens belonging to each masonry type using the MQI method resulted in a probabilistic distribution for each parameter, defined by a mean value and a standard deviation. These distributions were adopted as prior knowledge for the Bayesian updating process.

As presented in Ramos [36] mean (μ) and variance (σ2) are considered random variable; their joint distribution is expressed by:

$$h(\mu|\theta) \propto \left(\frac{n_0}{\sigma^2}\right)^{1/2} exp\left[-\frac{n_0}{2\sigma_0}(-\mu_0)^2\right] \times \left(\frac{1}{\sigma^2}\right)^{\frac{\nu_0}{2}+1} exp\left[\frac{S_0}{2\sigma^2}\right] \quad (9)$$

Where n_0 is the size of the initial sample, S_0 is the initial sum of squared differences between the values and their mean, μ_0 and σ_0 are the initial mean and initial standard deviation.

Prior and posterior distribution belong to the same family (conjugate distribution). Hence, the prior for μ conditional on σ2 is a normal with mean μ_0 and variance $\sigma 2/n_0$:

$$\mu|\sigma^2 \sim N\left(\mu_0, \frac{\sigma^2}{n_0}\right) \quad (10)$$

The prior for the precision $(1/\sigma^2)$ is a gamma distribution with hyperparameters $\nu_0/2$ and $S_0/2$:

$$\frac{1}{\sigma^2} \sim gamma\left(\frac{\nu_0}{2}, \frac{S_0}{2}\right) \quad (11)$$

The conditional posterior density of μ, given σ^2 is given by:

$$\mu|\sigma^2, x \sim N\left(\mu_1, \frac{\sigma^2}{n_1}\right) \quad (12)$$

In the data fusion model, mean (μ) and variance (σ^2) are updated as new information is gathered, resulting in the definition of a final values with reduced uncertainty. The posterior mean and the posterior sum of squared differences, which is the sum of the square of variation defined as the spread between each individual value and the mean, are expressed by equation 13 and 14 respectively:

$$\mu_1 = \frac{n_0}{n_0 + n} \cdot \mu_0 + \frac{n}{n_0 + n} \cdot x \quad (13)$$

$$S_1 = S_0 + (n-1) \cdot s^2 + \frac{n_0 \cdot n}{n_0 + n} \cdot (x - \mu_0)^2 \quad (14)$$

Where μ_0 is the prior mean (prior knowledge), μ_1 is the posterior mean, n_0 is the size of the initial sample, n is the size of the new data sample (new observations), x is the mean of the new data sample, S_0 is the prior sum of squared differences (to be computed for every single observation), and s is the standard deviation of

the new observed data. The updated standard deviation (σ_1) can be computed as the square root of the ratio between S_1 and the total number of considered observations (n_0 + n).

The marginal posterior density of $1/\sigma_2$ is gamma:

$$\frac{1}{\sigma^2}|x \sim gamma\left(\frac{\nu_1}{2}, \frac{S_1}{2}\right) \tag{15}$$

where

$$\nu_1 = \nu_0 + n \tag{16}$$

Once the posterior distribution has been defined, its characteristics, namely update mean and updated standard deviation, can be estimated through numerical simulations. Markov Chain Monte Carlo (MCMC) is one of the most popular and widely used method. A sequence of random variables Xn ≥ 0 is a Markov chain if for any n, given the current value, Xn, the past Xj, j ≤ n-1 and the future Xj: j ≥ n+1 is independent [36]. Moreover, the Gibbs algorithm has been selected to carry out the sampling process related to the posterior distribution.

The adopted data fusion technique combines two sources of information at a time, resulting in a posterior distribution (updated mean value and updated standard deviation) that can be used as a prior distribution for the following update. The reference sequence followed in order to carry out the whole procedure is based on the approach suggested by technical guidelines [13] [16] in order to assess the performance of existing buildings. Therefore, the updating process simulates a scenario in which data collected by means of visual inspections (MQI) experiences a stepwise upgrade once new pieces of information, experimentally collected through non-destructive and destructive techniques, are available.

For all the masonry types selected, mechanical properties have been updated depending on the output obtained from each testing procedure. Therefore, in order to calculate the final value of the Young's modulus (E), data from sonic tests (ST), flat-jacks (FJ) tests and compression tests (CT) have been used, whereas the final value for the compression strength (f_m) has been updated using flat-jacks (FT) test and compression test (CT) results (Figure 2.5). Lastly, diagonal-compression tests (DC) and shear-compression test results (SC) have been considered in the updating process of both shear modulus (G) and shear strength ($\tau 0$), see Figure 2.6.

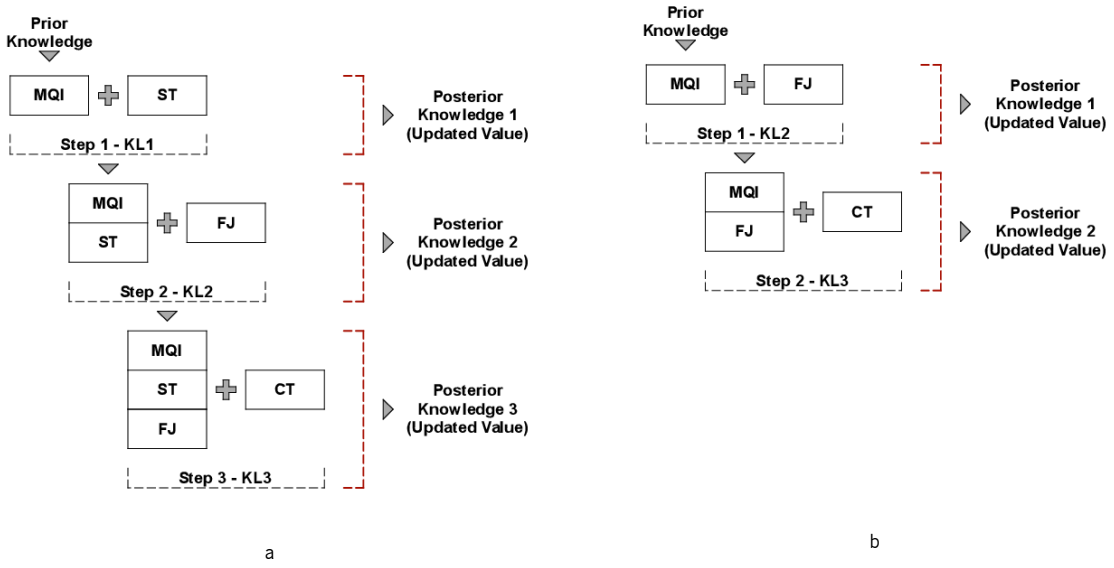


Figure 2.5 - Young's Modulus (a) and Compression strength (b) updating process flowchart.

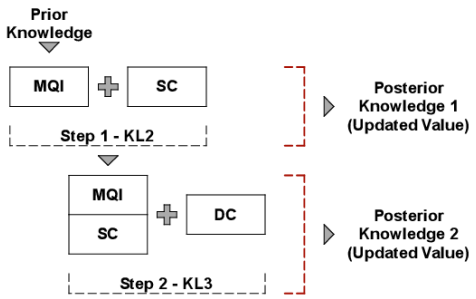


Figure 2.6 - Shear Modulus and shear strength updating process flowchart.

Therefore, only values directly provided by the specific testing procedures were considered and computed according to the standards mentioned in Section 2.3. Moreover, it should be noted that, regarding the sonic tests results, based on equations 3 and 4, the dynamic elastic modulus was estimated assuming a mean value of Poisson ratio (ν) equal to 0.25 and an average density (ρ) estimated on the basis of the ranges proposed in [13] and [16]. These ranges of values were adopted to build normal probability distribution functions and, by means of Monte Carlo simulation method 1000 draws of each distribution were sampled and applied in equation 2 and 3 to provide a fist estimation of the dynamic modulus of elasticity.

As noted in several studies [62] [63], an inequality exists between static and dynamic modulus of elasticity of masonry. Therefore, taking into consideration this aspect, the empirical equation proposed by Makoond

[64] has been used in order to estimate the static modulus of elasticity (E_{st}) starting from the dynamic one (E_{dy}) resulted from sonic tests. The proposed equation reads:

$$E_{st} = 0.87E_{dy} \tag{17}$$

In order to progressively increase the accuracy of the process, data related to the testing techniques considered to be the most reliable is used in the last steps of the updating procedure. Additionally, following the code-based approach, a different *Knowledge Level* has been attributed to each testing method.

2.4.1 Reference update

A reference updating procedure has been carried out using all the experimental results stored in the final database. The data fusion procedure followed all the stages previously described in terms of outliers' removal and sequence of updates (see Figure 2.5 and Figure 2.6). Moreover, equation 13 and 14 have been applied to calculate the final updated values of mean (μ) and standard deviation (σ) respectively. If no data was available for a specific testing technique, the data fusion procedure was carried out according to the reference sequence, discarding the step characterized by a lack of information.

Table 2.1 to Table 2.6 present mean value, standard deviation, and number of observations, related to each testing procedure, and classified according to a specific masonry type.

Table 2.1 - Prior knowledge and new information summary for Masonry Type 1 (overall data).

	Prior Knowledge			**New Information**			**New Information**			**New Information**		
MT1	**Masonry Quality Index**			**Sonic Test**			**Flat-jacks Test**			**Compression Test**		
	Mean	**St. Dev.**	**#**	**Mean**	**St. Dev.**	**#**	**Mean**	**St. Dev.**	**#**	**Mean**	**St. Dev.**	**#**
	Young Mod. - E (MPa)			**Young Mod. - E (MPa)**			**Young Mod. – E (MPa)**			**Young Mod. – E (MPa)**		
	1015.33	166.54	205	1135.12	662.80	9	1086.23	766.15	38	708.64	429.90	22
	Compr. Str. - f_m (MPa)			**Compr. Str. - f_m (MPa)**			**Compr. Str. - f_m (MPa)**			**Compr. Str. - f_m (MPa)**		
	2.16	0.44	205	NA	NA	NA	1.34	0.74	34	0.92	0.67	30
	Masonry Quality Index			**Shear-Compr. Test**			**Diag. Compr- Test**					
	Shear Mod. – G (MPa)			**Shear Mod. – G (MPa)**			**Shear Mod. – G (MPa)**					
	350.29	52.46	205	177.97	97.43	26	141.02	121.16	57			
	Shear Str. – τ_o (MPa)			**Shear Str. – τ_o (MPa)**			**Shear Str. – τ_o (MPa)**					
	0.04	0.008	205	0.162	0.096	20	0.05	0.03	62			

Table 2.2 - Prior knowledge and new information summary for Masonry Type 2 (overall data).

	Prior Knowledge			New Information			New Information			New Information		
	Masonry Quality Index			**Sonic Test**			**Flat-jacks Test**			**Compression Test**		
	Mean	**St. Dev.**	**#**	**Mean**	**St. Dev.**	**#**	**Mean**	**St. Dev.**	**#**	**Mean**	**St. Dev.**	**#**
	Young Mod. - E (MPa)			**Young Mod. - E (MPa)**			**Young Mod. – E (MPa)**			**Young Mod. – E (MPa)**		
	1249.20	133.69	102	1270.42	525.74	6	1182.17	610.70	12	1759.69	737.92	16
	Compr. Str. - f_m (MPa)			**Compr. Str. - f_m (MPa)**			**Compr. Str. - f_m (MPa)**			**Compr. Str. - f_m (MPa)**		
MT2	2.79	0.37	102	NA	NA	NA	1.45	0.72	16	1.72	0.96	18
	Masonry Quality Index			**Shear-Compr. Test**			**Diag. Compr- Test**					
	Shear Mod. – G (MPa)			**Shear Mod. – G (MPa)**			**Shear Mod. – G (MPa)**					
	406.15	32.28	102	268.53	162.02	26	198.08	95.26	5			
	Shear Str. – τ_o (MPa)			**Shear Str. – τ_o (MPa)**			**Shear Str. – τ_o (MPa)**					
	0.048	0.005	102	0.187	0.057	20	0.054	0.035	10			

Table 2.3 - Prior knowledge and new information summary for Masonry Type 3 (overall data).

	Prior Knowledge			New Information			New Information			New Information		
	Masonry Quality Index			**Sonic Test**			**Flat-jacks Test**			**Compression Test**		
	Mean	**St. Dev.**	**#**	**Mean**	**St. Dev.**	**#**	**Mean**	**St. Dev.**	**#**	**Mean**	**St. Dev.**	**#**
	Young Mod. - E (MPa)			**Young Mod. - E (MPa)**			**Young Mod. – E (MPa)**			**Young Mod. – E (MPa)**		
	1798.13	258.77	83	1986.70	452.80	6	2385.15	492.02	19	2202.05	767.31	19
	Compr. Str. - f_m (MPa)			**Compr. Str. - f_m (MPa)**			**Compr. Str. - f_m (MPa)**			**Compr. Str. - f_m (MPa)**		
MT3	4.38	0.78	83	NA	NA	NA	2.02	0.85	15	4.06	2.20	21
	Masonry Quality Index			**Shear-Compr. Test**			**Diag. Compr- Test**					
	Shear Mod. – G (MPa)			**Shear Mod. – G (MPa)**			**Shear Mod. – G (MPa)**					
	558.55	79.49	83	297.20	96.44	5	444.20	268.73	10			
	Shear Str. – τ_o (MPa)			**Shear Str. – τ_o (MPa)**			**Shear Str. – τ_o (MPa)**					
	0.073	0.013	83	0.137	0.083	16	0.114	0.086	24			

Table 2.4 - Prior knowledge and new information summary for Masonry Type 4 (overall data).

	Prior Knowledge			New Information			New Information			New Information		
	Masonry Quality Index			**Sonic Test**			**Flat-jacks Test**			**Compression Test**		
	Mean	**St. Dev.**	**#**	**Mean**	**St. Dev.**	**#**	**Mean**	**St. Dev.**	**#**	**Mean**	**St. Dev.**	**#**
	Young Mod. - E (MPa)			**Young Mod. - E (MPa)**			**Young Mod. – E (MPa)**			**Young Mod. – E (MPa)**		
	1234.13	72.69	12	NA	NA	NA	NA	NA	NA	913	270.97	8
	Compr. Str. - f_m (MPa)			**Compr. Str. - f_m (MPa)**			**Compr. Str. - f_m (MPa)**			**Compr. Str. - f_m (MPa)**		
MT4	2.74	0.20	12	NA	NA	NA	NA	NA	NA	2.20	1.30	8
	Masonry Quality Index			**Shear-Compr. Test**			**Diag. Compr- Test**					
	Shear Mod. – G (MPa)			**Shear Mod. – G (MPa)**			**Shear Mod. – G (MPa)**					
	416.27	20.74	12	NA	NA	NA	394.67	102.04	3			
	Shear Str. – τ_0 (MPa)			**Shear Str. – τ_0 (MPa)**			**Shear Str. – τ_0 (MPa)**					
	0.05	0.003	12	NA	NA	NA	0.051	0.012	5			

Table 2.5 - Prior knowledge and new information summary for Masonry Type 5 (overall data).

	Prior Knowledge			New Information			New Information			New Information		
	Masonry Quality Index			**Sonic Test**			**Flat-jacks Test**			**Compression Test**		
	Mean	**St. Dev.**	**#**	**Mean**	**St. Dev.**	**#**	**Mean**	**St. Dev.**	**#**	**Mean**	**St. Dev.**	**#**
	Young Mod. - E (MPa)			**Young Mod. - E (MPa)**			**Young Mod. – E (MPa)**			**Young Mod. – E (MPa)**		
	1548.98	94.33	42	NA	NA	NA	NA	NA	NA	1248.54	227.78	13
	Compr. Str. - f_m (MPa)			**Compr. Str. - f_m (MPa)**			**Compr. Str. - f_m (MPa)**			**Compr. Str. - f_m (MPa)**		
MT5	3.63	0.27	42	NA	NA	NA	NA	NA	NA	1.87	0.67	15
	Masonry Quality Index			**Shear-Compr. Test**			**Diag. Compr- Test**					
	Shear Mod. – G (MPa)			**Shear Mod. – G (MPa)**			**Shear Mod. – G (MPa)**					
	499.73	40.31	42	NA	NA	NA	411.60	188.31	5			
	Shear Str. – τ_0 (MPa)			**Shear Str. – τ_0 (MPa)**			**Shear Str. – τ_0 (MPa)**					
	0.063	0.007	42	0.067	0.048	18	0.186	0.096	10			

Table 2.6 - Prior knowledge and new information summary for Masonry Type (overall data).

	Prior Knowledge			New Information			New Information			New Information		
MT6	Masonry Quality Index			Sonic Test			Flat-jacks Test			Compression Test		
	Mean	St. Dev.	#	Mean	St. Dev.	#	Mean	St. Dev.	#	Mean	St. Dev.	#
	Young Mod. - E (MPa)			Young Mod. - E (MPa)			Young Mod. – E (MPa)			Young Mod. – E (MPa)		
	2614.14	312.57	70	2512.66	935.48	21	2445.50	1738.98	4	3374.67	1735.19	15
	Compr. Str. - f_m (MPa)			Compr. Str. - f_m (MPa)			Compr. Str. - f_m (MPa)			Compr. Str. - f_m (MPa)		
	6.94	1.03	70	NA	NA	NA	3.21	1.01	4	6.14	2.76	20
	Masonry Quality Index			Shear-Compr. Test			Diag. Compr- Test					
	Shear Mod. – G (MPa)			Shear Mod. – G (MPa)			Shear Mod. – G (MPa)					
	795.94	63.33	70	NA	NA	NA	842.67	138.23	6			
	Shear Str. – τ_0 (MPa)			Shear Str. – τ_0 (MPa)			Shear Str. – τ_0 (MPa)					
	0.114	0.012	70	NA	NA	NA	0.197	0.043	6			

It should be noted that data estimated through the MQI method highlights a considerable uniform distribution, resulting in low scattering rate and low standard deviation values. Experimental results show a different trend, their variability in terms of mean and standard deviation much higher if compared to the qualitative assessment results. This was expected given the simplifications assumed in the MQI method, which considers a set of parameters that are similar within each masonry type. This pattern can be also related to the fact that the experimental dataset encompasses both laboratory and in-situ testing campaigns, characterized by different environmental and boundary conditions, which leads to a significant variability in the results.

The final values of mean and standard deviation, calculated for each reference mechanical parameter and for all the selected masonry types, have been used to define Probability Density Functions (PDF) highlighting the evolution that characterizes the application of the proposed data fusion method after each stage of the updating process. The lognormal distribution was selected to represent the PDFs of the mechanical parameters since it leads only to positive values. For the sake of brevity, only the results related to Masonry Type 1 are presented in detail (Figure 2.7). The reader is referred to Annex 1 – Probability Density Functions (PDFs) for representative masonry typologies for the PDFs related to all Masonry Typologies considered.

Looking at the graphs, it can be inferred that, even though the standard deviation values related to the experimental results used as new information are significantly higher than the standard deviation characterising the Prior Knowledge (see Table 2.1), the final standard deviation related to the considered

parameters is reduced. The standard deviation related to the last updating stage is slightly higher than the one resulted from MQI assessment (Prior Knowledge).

Moreover, the updated mean values appear to be closer to the Prior Knowledge data. In fact, the higher number of observations related to MQI accounts for a more significant contribution in the overall estimation of the updated mean values.

For instance, Table 2.1 shows that the updating process related to the Young modulus begins with a mean and a standard deviation equal to 1015 MPa and 166 MPa, respectively (Prior Knowledge). Similar mean values are provided by sonic and flat-jacks tests new information (1135 MPa and 1086 MPa, respectively), whereas the standard deviation is around 660 MPa (sonic tests) and 760 MPa (flat-jacks test), hence much higher than the Prior Knowledge standard deviation.

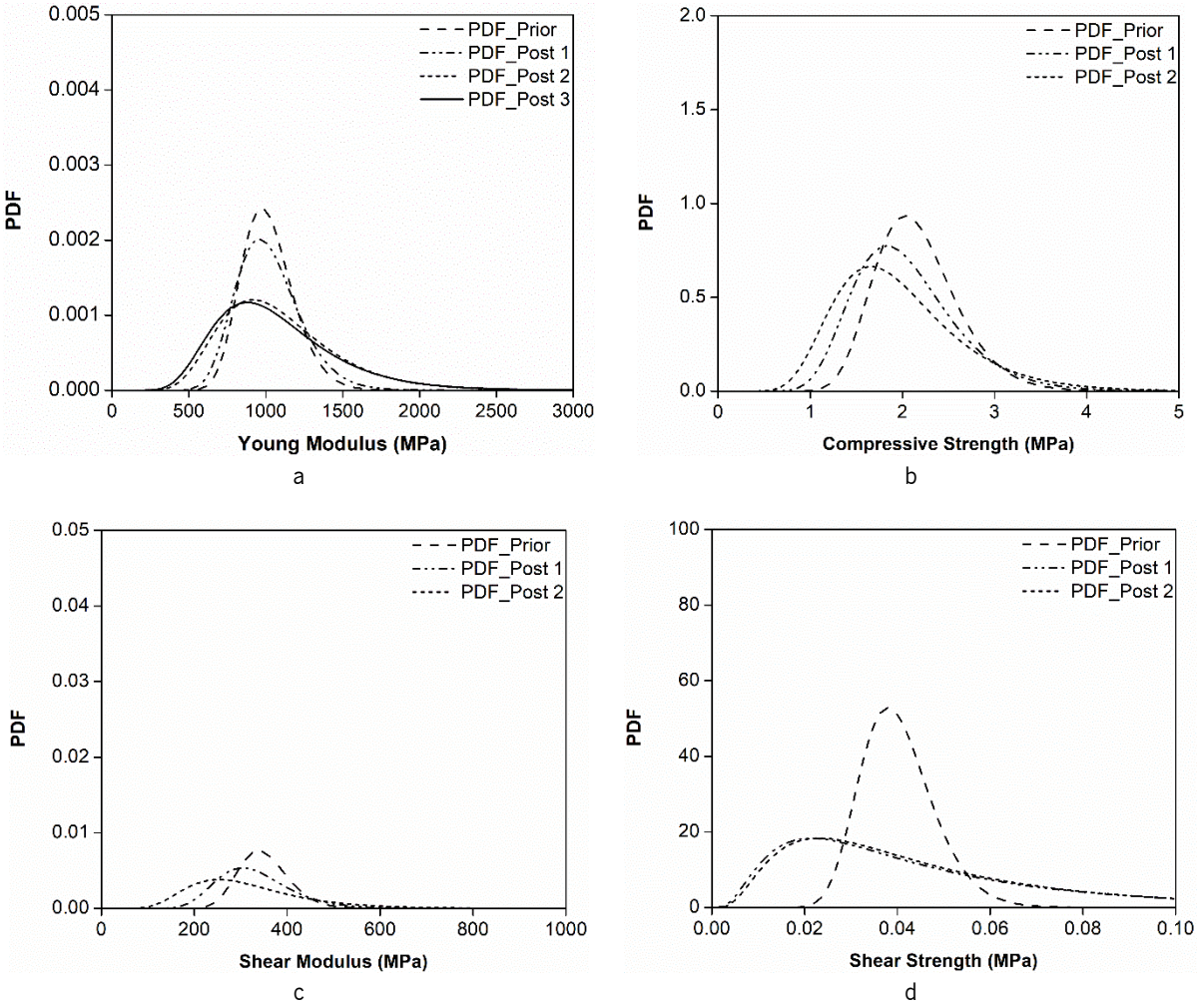


Figure 2.7 - Probability Density Function (PDF) updated values Young modulus (a), Compression strength (b), Shear modulus (c), Shear strength (d).

Lastly, the contribution of compressive test data consists of a mean and a standard deviation equal to 708 MPa and 429 MPa respectively. The data fusion procedure led to a final mean value and a final standard deviation equal to 1004 MPa and 376 MPa respectively, determining an overall reduction of initial standard deviation related to the experimental data. However, the final mean value resulted in being closer to the Prior Knowledge. This trend is similar in all the distributions considered.

2.4.2 Updating procedure A (only Italian Data)

This section summarizes the outcomes related to the application of the data fusion procedure considering only the results of Italian two-leaf stone masonry walls. Once defined the final set of information for each testing procedure according to a specific masonry type, the updating procedure has been applied following the same steps described in the previous sections. Data related to Prior Knowledge and New Information is summarized in Table 2.7 to Table 2.12.

Table 2.7 - Prior knowledge and new information summary for Masonry Type 1 (Italian data).

	Prior Knowledge			**New Information**			**New Information**			**New Information**		
	Masonry Quality Index			**Sonic Test**			**Flat-jacks Test**			**Compression Test**		
	Mean	**St. Dev.**	**#**	**Mean**	**St. Dev.**	**#**	**Mean**	**St. Dev.**	**#**	**Mean**	**St. Dev.**	**#**
	Young Mod. - E (MPa)			**Young Mod. - E (MPa)**			**Young Mod. – E (MPa)**			**Young Mod. – E (MPa)**		
	1061.76	181.75	128	1003	415.62	3	1102.88	406.28	8	832	330.20	5
	Compr. Str. - f_m (MPa)			**Compr. Str. - f_m (MPa)**			**Compr. Str. - f_m (MPa)**			**Compr. Str. - f_m (MPa)**		
MT1	2.29	0.48	128	NA	NA	NA	2.04	0.67	12	0.45	0.30	3
	Masonry Quality Index			**Shear-Compr. Test**			**Diag. Compr- Test**					
	Shear Mod. – G (MPa)			**Shear Mod. – G (MPa)**			**Shear Mod. – G (MPa)**					
	367.69	52.86	128	211.48	67.70	12	225.24	113.92	26			
	Shear Str. – τ_0 (MPa)			**Shear Str. – τ_0 (MPa)**			**Shear Str. – τ_0 (MPa)**					
	0.043	0.008	128	0.181	0.055	13	0.049	0.028	66			

Table 2.8 - Prior knowledge and new information summary for Masonry Type 2 (Italian data).

	Prior Knowledge			New Information			New Information			New Information		
	Masonry Quality Index			**Sonic Test**			**Flat-jacks Test**			**Compression Test**		
	Mean	**St. Dev.**	**#**	**Mean**	**St. Dev.**	**#**	**Mean**	**St. Dev.**	**#**	**Mean**	**St. Dev.**	**#**
	Young Mod. - E (MPa)			**Young Mod. - E (MPa)**			**Young Mod. – E (MPa)**			**Young Mod. – E (MPa)**		
	1250.47	133.51	71	1611.52	416.34	3	1138.50	422.77	6	1703.33	360.40	9
	Compr. Str. - f_m (MPa)			**Compr. Str. - f_m (MPa)**			**Compr. Str. - f_m (MPa)**			**Compr. Str. - f_m (MPa)**		
MT2	2.79	0.37	71	NA	NA	NA	2.11	0.69	4	2.36	0.45	13
	Masonry Quality Index			**Shear-Compr. Test**			**Diag. Compr- Test**					
	Shear Mod. – G (MPa)			**Shear Mod. – G (MPa)**			**Shear Mod. – G (MPa)**					
	405.10	30.56	71	352.68	127.61	10	165.64	78.93	11			
	Shear Str. – τ_0 (MPa)			**Shear Str. – τ_0 (MPa)**			**Shear Str. – τ_0 (MPa)**					
	0.048	0.005	71	0.188	0.059	16	0.060	0.035	28			

Table 2.9 - Prior knowledge and new information summary for Masonry Type 3 (Italian data).

	Prior Knowledge			New Information			New Information			New Information		
	Masonry Quality Index			**Sonic Test**			**Flat-jacks Test**			**Compression Test**		
	Mean	**St. Dev.**	**#**	**Mean**	**St. Dev.**	**#**	**Mean**	**St. Dev.**	**#**	**Mean**	**St. Dev.**	**#**
	Young Mod. - E (MPa)			**Young Mod. - E (MPa)**			**Young Mod. – E (MPa)**			**Young Mod. – E (MPa)**		
	1770.54	230.43	46	NA	NA	NA	2091.40	575.15	10	1840.08	391.11	13
	Compr. Str. - f_m (MPa)			**Compr. Str. - f_m (MPa)**			**Compr. Str. - f_m (MPa)**			**Compr. Str. - f_m (MPa)**		
MT3	4.29	0.69	46	NA	NA	NA	2.15	0.56	8	4.29	2.36	9
	Masonry Quality Index			**Shear-Compr. Test**			**Diag. Compr- Test**					
	Shear Mod. – G (MPa)			**Shear Mod. – G (MPa)**			**Shear Mod. – G (MPa)**					
	551.77	54.05	46	297.20	96.44	5	479.14	254.46	7			
	Shear Str. – τ_0 (MPa)			**Shear Str. – τ_0 (MPa)**			**Shear Str. – τ_0 (MPa)**					
	0.072	0.009	46	0.104	0.065	9	0.073	0.053	18			

Table 2.10 - Prior knowledge and new information summary for Masonry Type 4 (Italian data).

	Prior Knowledge			New Information			New Information			New Information		
	Masonry Quality Index			**Sonic Test**			**Flat-jacks Test**			**Compression Test**		
	Mean	**St. Dev.**	**#**	**Mean**	**St. Dev.**	**#**	**Mean**	**St. Dev.**	**#**	**Mean**	**St. Dev.**	**#**
	Young Mod. - E (MPa)			**Young Mod. - E (MPa)**			**Young Mod. – E (MPa)**			**Young Mod. – E (MPa)**		
	1234.13	72.69	12	NA	NA	NA	NA	NA	NA	913	270.97	8
	Compr. Str. - f_m (MPa)			**Compr. Str. - f_m (MPa)**			**Compr. Str. - f_m (MPa)**			**Compr. Str. - f_m (MPa)**		
MT4	2.74	0.20	12	NA	NA	NA	NA	NA	NA	2.20	1.30	8
	Masonry Quality Index			**Shear-Compr. Test**			**Diag. Compr- Test**					
	Shear Mod. – G (MPa)			**Shear Mod. – G (MPa)**			**Shear Mod. – G (MPa)**					
	416.27	20.74	12	NA	NA	NA	394.67	102.04	3			
	Shear Str. – τ_0 (MPa)			**Shear Str. – τ_0 (MPa)**			**Shear Str. – τ_0 (MPa)**					
	0.05	0.003	12	NA	NA	NA	0.051	0.012	5			

Table 2.11 - Prior knowledge and new information summary for Masonry Type 5 (Italian data).

	Prior Knowledge			New Information			New Information			New Information		
	Masonry Quality Index			**Sonic Test**			**Flat-jacks Test**			**Compression Test**		
	Mean	**St. Dev.**	**#**	**Mean**	**St. Dev.**	**#**	**Mean**	**St. Dev.**	**#**	**Mean**	**St. Dev.**	**#**
	Young Mod. - E (MPa)			**Young Mod. - E (MPa)**			**Young Mod. – E (MPa)**			**Young Mod. – E (MPa)**		
	1536.57	85.95	39	NA	NA	NA	NA	NA	NA	1229.10	325.38	10
	Compr. Str. - f_m (MPa)			**Compr. Str. - f_m (MPa)**			**Compr. Str. - f_m (MPa)**			**Compr. Str. - f_m (MPa)**		
MT5	3.60	0.25	39	NA	NA	NA	NA	NA	NA	1.85	0.74	12
	Masonry Quality Index			**Shear-Compr. Test**			**Diag. Compr- Test**					
	Shear Mod. – G (MPa)			**Shear Mod. – G (MPa)**			**Shear Mod. – G (MPa)**					
	491.93	29.67	39	NA	NA	NA	411.60	188.31	5			
	Shear Str. – τ_0 (MPa)			**Shear Str. – τ_0 (MPa)**			**Shear Str. – τ_0 (MPa)**					
	0.062	0.005	39	0.067	0.048	18	0.186	0.096	10			

Table 2.12 - Prior knowledge and new information summary for Masonry Type 6 (Italian data).

	Prior Knowledge			New Information			New Information			New Information		
MT6	Masonry Quality Index			Sonic Test			Flat-jacks Test			Compression Test		
	Mean	St. Dev.	#	Mean	St. Dev.	#	Mean	St. Dev.	#	Mean	St. Dev.	#
	Young Mod. - E (MPa)			Young Mod. - E (MPa)			Young Mod. – E (MPa)			Young Mod. – E (MPa)		
	2434.75	326.90	16	NA	NA	NA	NA	NA	NA	2394.38	418.48	8
	Compr. Str. - f_m (MPa)			Compr. Str. - f_m (MPa)			Compr. Str. - f_m (MPa)			Compr. Str. - f_m (MPa)		
	6.36	1.08	16	NA	NA	NA	NA	NA	NA	3.98	1.33	8
	Masonry Quality Index			Shear-Compr. Test			Diag. Compr- Test					
	Shear Mod. – G (MPa)			Shear Mod. – G (MPa)			Shear Mod. – G (MPa)					
	811.04	50.81	16	NA	NA	NA	842.67	138.23	6			
	Shear Str. – τ_0 (MPa)			Shear Str. – τ_0 (MPa)			Shear Str. – τ_0 (MPa)					
	0.117	0.009	16	NA	NA	NA	0.197	0.043	6			

Overall, the reduced number of observations resulted in a decrease of experimental data mainly related to Masonry Type 4, 5 and 6, whereas the data filtering process based on the origin country resulted in a data sample able to ensure information related to all the testing procedures addressing the assessment of masonry walls classified as type 1, 2, and 3.

As highlighted in Section 2.4.1 regarding the trends characterising the final results of the data fusion process, the reduction of standard deviation for all the selected mechanical parameters consists of significantly lower values than the standard deviations related to the single experimental results and slightly higher values than the standard deviations related to the Prior Knowledge, whereas updated means are closer to the outcomes provided by the MQI method (Prior Knowledge), see Figure 2.8.

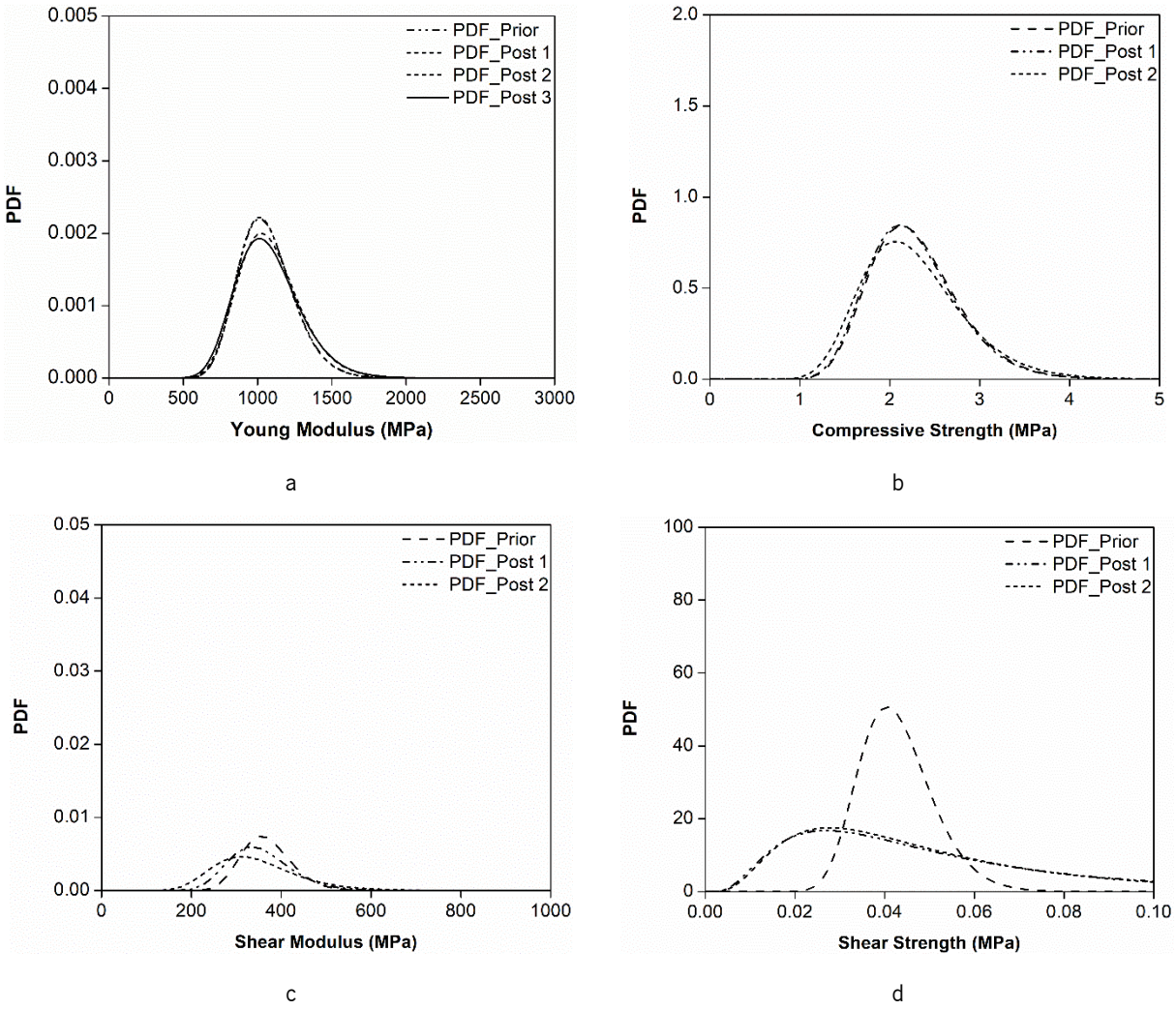


Figure 2.8 - Probability Density Function (PDF) updated values Italian masonry panels Young modulus (a), Compression strength (b), Shear modulus (c), Shear strength (d).

2.4.3 Updating procedure B (only Portuguese Data)

Results related to Portuguese masonry walls are herein presented (Table 2.13 to Table 2.16). The reduction of suitable information to carry out the data fusion procedure resulted in a complete application of the proposed methodology only for masonry types 1, 2, and 3. Note that Masonry type 4 and 5 data refer exclusively to Italian experimental campaigns. Moreover, despite the significant number of sonic test results related to masonry type 6, only 2 compression test observations have been considered, whereas no information could be gathered for flat-jacks, shear-compression, and diagonal-compression testing procedures.

Table 2.13 - Prior knowledge and new information summary for Masonry Type 1 (Portuguese data).

	Prior Knowledge			New Information			New Information			New Information		
	Masonry Quality Index			**Sonic Test**			**Flat-jacks Test**			**Compression Test**		
	Mean	**St. Dev.**	**#**	**Mean**	**St. Dev.**	**#**	**Mean**	**St. Dev.**	**#**	**Mean**	**St. Dev.**	**#**
	Young Mod. – E (Mpa)			**Young Mod. – E (Mpa)**			**Young Mod. – E (Mpa)**			**Young Mod. – E (Mpa)**		
	963.91	139.02	50	1185.98	692.39	5	880.95	383.75	16	1031.20	468.93	5
	Compr. Str. – f_m (Mpa)			**Compr. Str. – f_m (Mpa)**			**Compr. Str. – f_m (Mpa)**			**Compr. Str. – f_m (Mpa)**		
MT1	2.03	0.36	50	NA	NA	NA	0.93	0.41	21	1.13	0.66	10
	Masonry Quality Index			**Shear-Compr. Test**			**Diag. Compr- Test**					
	Shear Mod. – G (Mpa)			**Shear Mod. – G (Mpa)**			**Shear Mod. – G (Mpa)**					
	336.09	43.72	50	NA	NA	NA	198	152.78	4			
	Shear Str. – τ_o (Mpa)			**Shear Str. – τ_o (Mpa)**			**Shear Str. – τ_o (Mpa)**					
	0.038	0.006	50	NA	NA	NA	0.140	0.09	4			

Table 2.14 - Prior knowledge and new information summary for Masonry Type 2 (Portuguese data).

	Prior Knowledge			New Information			New Information			New Information		
	Masonry Quality Index			**Sonic Test**			**Flat-jacks Test**			**Compression Test**		
	Mean	**St. Dev.**	**#**	**Mean**	**St. Dev.**	**#**	**Mean**	**St. Dev.**	**#**	**Mean**	**St. Dev.**	**#**
	Young Mod. – E (Mpa)			**Young Mod. – E (Mpa)**			**Young Mod. – E (Mpa)**			**Young Mod. – E (Mpa)**		
	1191.81	89.69	17	1243.54	461.25	4	877.01	530.38	6	NA	NA	NA
	Compr. Str. – f_m (Mpa)			**Compr. Str. – f_m (Mpa)**			**Compr. Str. – f_m (Mpa)**			**Compr. Str. – f_m (Mpa)**		
MT2	2.63	0.25	17	NA	NA	NA	1.09	0.22	10	NA	NA	NA
	Masonry Quality Index			**Shear-Compr. Test**			**Diag. Compr- Test**					
	Shear Mod. – G (Mpa)			**Shear Mod. – G (Mpa)**			**Shear Mod. – G (Mpa)**					
	391.15	19.03	17	NA	NA	NA	320.50	96.87	2			
	Shear Str. – τ_o (Mpa)			**Shear Str. – τ_o (Mpa)**			**Shear Str. – τ_o (Mpa)**					
	0.046	0.003	17	0.175	0.007	2	0.244	0.033	2			

Table 2.15 - Prior knowledge and new information summary for Masonry Type 3 (Portuguese data).

	Prior Knowledge			New Information			New Information			New Information		
	Masonry Quality Index			**Sonic Test**			**Flat-jacks Test**			**Compression Test**		
	Mean	**St. Dev.**	**#**	**Mean**	**St. Dev.**	**#**	**Mean**	**St. Dev.**	**#**	**Mean**	**St. Dev.**	**#**
	Young Mod. – E (Mpa)			**Young Mod. – E (Mpa)**			**Young Mod. – E (Mpa)**			**Young Mod. – E (Mpa)**		
	1905.41	306.30	23	2283.57	520.46	6	2161.80	421.13	6	NA	NA	NA
	Compr. Str. – f_m (Mpa)			**Compr. Str. – f_m (Mpa)**			**Compr. Str. – f_m (Mpa)**			**Compr. Str. – f_m (Mpa)**		
MT3	4.70	0.94	23	NA	NA	NA	2.05	1.12	6	3.27	1.33	7
	Masonry Quality Index			**Shear-Compr. Test**			**Diag. Compr- Test**					
	Shear Mod. – G (Mpa)			**Shear Mod. – G (Mpa)**			**Shear Mod. – G (Mpa)**					
	582.87	123.89	23	NA	NA	NA	NA	NA	NA			
	Shear Str. – τ_o (Mpa)			**Shear Str. – τ_o (Mpa)**			**Shear Str. – τ_o (Mpa)**					
	0.077	0.021	23	NA	NA	NA	NA	NA	NA			

Table 2.16 - Prior knowledge and new information summary for Masonry Type 6 (Portuguese data).

	Prior Knowledge			New Information			New Information			New Information		
	Masonry Quality Index			**Sonic Test**			**Flat-jacks Test**			**Compression Test**		
	Mean	**St. Dev.**	**#**	**Mean**	**St. Dev.**	**#**	**Mean**	**St. Dev.**	**#**	**Mean**	**St. Dev.**	**#**
	Young Mod. – E (Mpa)			**Young Mod. – E (Mpa)**			**Young Mod. – E (Mpa)**			**Young Mod. – E (Mpa)**		
	2610.85	314.95	23	2602.21	665.07	13	NA	NA	NA	NA	NA	NA
	Compr. Str. – f_m (Mpa)			**Compr. Str. – f_m (Mpa)**			**Compr. Str. – f_m (Mpa)**			**Compr. Str. – f_m (Mpa)**		
MT6	6.93	1.02	23	NA	NA	NA	4.02	0.65	2	NA	NA	NA
	Masonry Quality Index			**Shear-Compr. Test**			**Diag. Compr- Test**					
	Shear Mod. – G (Mpa)			**Shear Mod. – G (Mpa)**			**Shear Mod. – G (Mpa)**					
	801.50	78.02	23	NA	NA	NA	NA	NA	NA			
	Shear Str. – τ_o (Mpa)			**Shear Str. – τ_o (Mpa)**			**Shear Str. – τ_o (Mpa)**					
	0.115	0.014	23	NA	NA	NA	NA	NA	NA			

Probability density functions (PDFs) related to the updated mechanical properties in masonry type 1 show the same pattern highlighted in the previous application of the data fusion method carried out using the whole data sample and only Italian data respectively, namely overall reduction of standard deviation and mean values close to the MQI estimation (Figure 2.9).

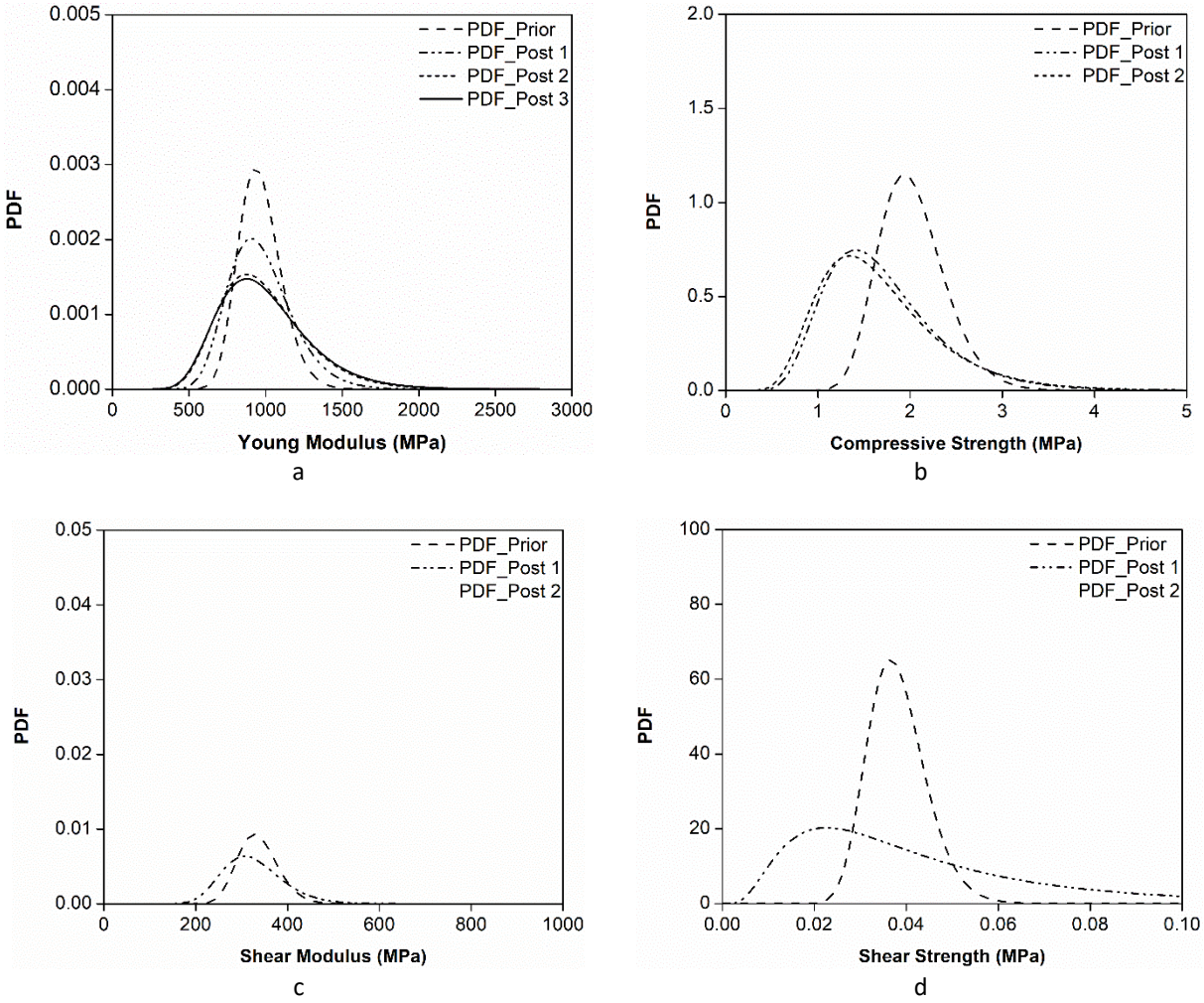


Figure 2.9 - Probability Density Function (PDF) updated values Portuguese masonry panels Young modulus (a), Compression strength (b), Shear modulus (c), Shear strength (d).

2.4.4 Data fusion results vs technical standards reference values

This section presents the overall outcomes of the data fusion procedure applied to update the mechanical properties of the selected masonry types. Moreover, the final results have been compared to the range of values proposed in Eurocode 8 (Part 3 – Annex C) [13], Italian standards (Table C8.5.I – Circolare 21/01/2019) [38] and CNR-DT 212/2013 recommendations [15].

Table 2.17 shows the range of values proposed by the codes and those ones obtained through the Bayesian updating procedure. Results calculated using all the data of the final database (Bayesian Update_ALL) are reported together with updated values related to Italian (Bayesian Update_ITA) and Portuguese (Bayesian Update_POR) masonry walls. They are classified depending on the reference mechanical property and the specific masonry typology. The ranges of the mechanical properties have been defined by subtracting (lower bound) and adding (upper bound) the corresponding standard deviation to the mean value (bracketed values reported in Table 2.17).

Overall, the ranges obtained utilizing the Bayesian updating procedure appear to be consistent with the values recommended by Eurocode and Italian standards. Young's modulus, Shear modulus, and compression strength results show lower bound limits close to those suggested in Italian standards, whereas upper bound values are slightly higher. Eurocode's mechanical properties mean values shown in Table 2.17 are lower than the corresponding values resulted from the different updating scenarios considered, namely Bayesian Update_ALL, ITA, and POR. Moreover, the estimation of shear strength is characterized by significant variability, which yields high standard deviation values and growth of the reference properties' ranges mainly for Masonry Type 1 and 2. On the other hand, Masonry Type 4 and 5 results appear to be highly consistent with the Italian standard. To this end, it is interesting to point out that data related to these masonry types only derives from Italian experimental campaigns.

It is also noted that the variability expressed by the updating process involving the whole dataset is slightly higher than the variability related to the updating procedure carried out only relying on data classified based on the country of origin. Therefore, based also on the evidence related to Masonry Type 4 and 5, it is possible to say that the characteristics of construction materials as well as environmental and boundary conditions in which the testing procedure is carried out significantly affect the homogeneity of the data sample. Hence, an increase in uncertainty reflects low homogeneity of the data sample. Conversely, high homogeneity corresponds to reduced uncertainty levels.

A similar pattern is highlighted in Table 2.18, which compares the values provided in CNR – DT 212/2013 [15], in terms of mean values and standard deviation of the natural logarithm to the updated results. In this case, an overall increase in terms of mean and standard deviation mostly affects results related to the reference Bayesian updating procedure (Bayesian Update_ALL). Furthermore, Portuguese (Bayesian Update_POR) data presents a slight variation, whereas Italian results (Bayesian Update_ITA) often highlight a significant consistency with the code values.

An additional aspect arisen from this study concerns the overestimation of the Bayesian results mean values. To this end, it must not be overlooked that codes suggest mechanical properties that refer to low-quality masonry walls built without following the practice-oriented set of rules (rules of the art). Conversely, data used to construct the final database involves masonry walls characterized by better mechanical properties and higher workmanship average quality compared to a reference masonry panel considered in technical standards.

Table 2.17 - Bayesian update results versus Eurocode [47] and Italian standards [26].

		Young Mod. - E (MPa)	**Comp. Str. - f_m (MPa)**	**Shear Mod. - G (MPa)**	**Shear Str. - τ_0 (MPa)**
MT1	Eurocode 8 [13] [65]	900	1.10 - 1.90	300	0.03 - 0.055
	NTC 2018 [38]	690 - 1050	1.00 - 2.00	230 - 350	0.018 - 0.032
	Bayesian Update_ALL	1004 (376) 634 - 1386	1.92 (0.68) 1.24 - 2.60	293 (117) 176 - 410	0.051 (0.045) 0.006 – 0.096
	Bayesian Update_POR	955 (289) 677 - 1255	1.63 (0.65) 0.98 - 2.28	326 (66) 260 - 392	0.046 (0.036) 0.004 – 0.082
	Bayesian Update_ITA	1054 (213) 845 - 1271	2.23 (0.56) 1.67 – 2.79	334 (90) 244 - 424	0.053 (0.039) 0.014 – 0.092
MT2	Eurocode 8	1200	2.00 - 3.00	400	0.05 - 0.08
	NTC 2018	1020 - 1440	2	340 - 480	0.035 - 0.051
	Bayesian Update_ALL	1304 (383) 930 - 1694	2.49 (0.74) 1.75 - 3.23	371 (97) 274 - 468	0.066 (0.051) 0.015 - 0.117
	Bayesian Update_POR	1105 (310) 815 - 1445	2.06 (0.78) 1.28 – 2.84	384 (36) 348 - 420	0.077 (0.066) 0.011 - 0.143
	Bayesian Update_ITA	1300 (268) 1042 - 1576	2.70 (0.44) 2.26 – 3.14	371 (95) 276 - 466	0.070 (0.055) 0.015 – 0.125
MT3	Eurocode 8	1700	2.60 - 3.80	600	0.08 - 0.11
	NTC 2018	1500 - 1980	2.60 - 3.80	500 - 660	0.056 - 0.074
	Bayesian Update_ALL	1955 (480) 1490 - 2448	4.03 (1.38) 2.65 – 5.41	533 (128) 405 - 661	0.089 (0.054) 0.035 - 0.14
	Bayesian Update_POR	1963 (392) 1631 - 2397	3.98 (1.43) 2.55 - 5.41	Not Available	Not Available
	Bayesian Update_ITA	1830 (342) 1448 - 2172	4.02 (1.26) 2.76 - 5.28	521 (122) 399 - 643	0.076 (0.036) 0.037 - 0.112
MT4	Eurocode 8	1100	1.40 - 2.20	400	0.05 - 0.06
	NTC 2018	900 - 1260	1.40 - 2.20	300 - 420	0.028 - 0.042
	Bayesian Update_ALL	1106 (231) 875 - 1337	2.53 (0.83) 1.70 – 3.36	412 (42) 370 - 454	0.05 (0.006) 0.044 - 0.056
	Bayesian Update_POR	Not Available	Not Available	Not Available	Not Available
	Bayesian Update_ITA	1106 (231) 875 - 1337	2.53 (0.83) 1.70 – 3.36	412 (42) 370 - 454	0.05 (0.006) 0.044 - 0.056
MT5	Eurocode 8	1400	2.00 - 3.20	500	0.10 - 0.19
	NTC 2018	1200 - 1620	2.00 - 3.20	400 - 500	0.09 - 0.12
	Bayesian Update_ALL	1478 (185) 1293 - 1663	3.17 (0.88) 2.29 - 4.05	490 (72) 418 - 562	0.088 (0.061) 0.027 - 0.149
	Bayesian Update_POR	Not Available	Not Available	Not Available	Not Available
	Bayesian Update_ITA	1474 (174) 1300 - 1648	3.19 (0.85) 2.34 - 4.04	483 (68) 415 - 551	0.088 (0.062) 0.026 - 0.15
MT6	Eurocode 8	2800	6.00 - 8.00	900	0.19 - 0.25
	NTC 2018	2400 - 3200	5.00 - 8.00	800 - 1100	0.09 - 0.12
	Bayesian Update_ALL	2692 (910) 1865 - 3663	6.61 (1.72) 4.89 - 8.33	799 (71) 728 - 870	0.121 (0.027) 0.094 - 0.148
	Bayesian Update_POR	2485 (447) 2152 - 3064	6.70 (1.25) 5.45 - 7.95	799 (71) 728 - 870	0.121 (0.027) 0.094 - 0.148
	Bayesian Update_ITA	2421 (344) 2077 - 2765	5.57 (1.58) 3.99 - 7.15	820 (79) 741 - 899	0.14 (0.04) 0.10 - 0.144

Table 2.18 - Bayesian update results versus Italian Research Council recommendations [15].

		Young Mod. - E (MPa)	**Comp. Str. - f_m (MPa)**	**Shear Mod. - G (MPa)**	**Shear Str. - τ_o (MPa)**
MT1	CNR-DT 212/2013 [15]	870 (σ_{ln} = 0.21)	1.40 (σ_{ln} = 0.29)	290 (σ_{ln} = 0.21)	0.026 (σ_{ln} = 0.24)
	Bayesian Update_ALL	1004 (376) (σ_{ln} = 0.36)	1.92 (0.68) (σ_{ln} = 0.34)	293 (117) (σ_{ln} = 0.38)	0.051 (0.045) (σ_{ln} = 0.72)
	Bayesian Update_POR	955 (289) (σ_{ln} = 0.30)	1.63 (0.65) (σ_{ln} = 0.39)	326 (66) (σ_{ln} = 0.20)	0.046 (0.036) (σ_{ln} = 0.69)
	Bayesian Update_ITA	1054 (213) (σ_{ln} = 0.20)	2.23 (0.56) (σ_{ln} = 0.25)	334 (90) (σ_{ln} = 0.27)	0.053 (0.039) (σ_{ln} = 0.66)
MT2	CNR-DT 2012/2013	1230 (σ_{ln} = 0.17)	2.50 (σ_{ln} = 0.20)	410 (σ_{ln} = 0.17)	0.043 (σ_{ln} = 0.19)
	Bayesian Update_ALL	1304 (383) (σ_{ln} = 0.29)	2.49 (0.74) (σ_{ln} = 0.26)	371 (97) (σ_{ln} = 0.26)	0.066 (0.051) (σ_{ln} = 0.68)
	Bayesian Update_POR	1105 (310) (σ_{ln} = 0.28)	2.06 (0.78) (σ_{ln} = 0.37)	384 (36) (σ_{ln} = 0.09)	0.077 (0.066) (σ_{ln} = 0.55)
	Bayesian Update_ITA	1300 (268) (σ_{ln} = 0.20)	2.70 (0.44) (σ_{ln} = 0.16)	371 (95) (σ_{ln} = 0.25)	0.070 (0.055) (σ_{ln} = 0.69)
MT3	CNR-DT 2012/2013	1740 (σ_{ln} = 0.14)	3.20 (σ_{ln} = 0.19)	580 (σ_{ln} = 0.14)	0.065 (σ_{ln} = 0.14)
	Bayesian Update_ALL	1955 (480) (σ_{ln} = 0.24)	4.03 (1.38) (σ_{ln} = 0.33)	533 (128) (σ_{ln} = 0.24)	0.089 (0.054) (σ_{ln} = 0.56)
	Bayesian Update_POR	1963 (392) (σ_{ln} = 0.20)	3.98 (1.43) (σ_{ln} = 0.35)	Not Available	Not Available
	Bayesian Update_ITA	1830 (342) (σ_{ln} = 0.19)	4.02 (1.26) (σ_{ln} = 0.31)	521 (122) (σ_{ln} = 0.23)	0.076 (0.036) (σ_{ln} = 0.45)
MT4	CNR-DT 2012/2013	1080 (σ_{ln} = 0.17)	1.90 (σ_{ln} = 0.27)	360 (σ_{ln} = 0.17)	0.035 (σ_{ln} = 0.20)
	Bayesian Update_ALL	1106 (231) (σ_{ln} = 0.21)	2.53 (0.83) (σ_{ln} = 0.32)	412 (42) (σ_{ln} = 0.10)	0.05 (0.006) (σ_{ln} = 0.12)
	Bayesian Update_POR	Not Available	Not Available	Not Available	Not Available
	Bayesian Update_ITA	1106 (231) (σ_{ln} = 0.21)	2.53 (0.83) (σ_{ln} = 0.32)	412 (42) (σ_{ln} = 0.10)	0.05 (0.006) (σ_{ln} = 0.12)
MT5	CNR-DT 2012/2013	1080 (σ_{ln} = 0.17)	1.90 (σ_{ln} = 0.27)	360 (σ_{ln} = 0.17)	0.035 (σ_{ln} = 0.20)
	Bayesian Update_ALL	1478 (185) (σ_{ln} = 0.12)	3.17 (0.88) (σ_{ln} = 0.27)	490 (72) (σ_{ln} = 0.15	0.088 (0.061) (σ_{ln} = 0.39)
	Bayesian Update_POR	Not Available	Not Available	Not Available	Not Available
	Bayesian Update_ITA	1474 (174) (σ_{ln} = 0.12)	3.19 (0.85) (σ_{ln} = 0.26)	483 (68) (σ_{ln} = 0.14)	0.088 (0.062) (σ_{ln} = 0.40)
MT6	CNR-DT 2012/2013	2800 (σ_{ln} = 0.14)	7.00 (σ_{ln} = 0.14)	860 (σ_{ln} = 0.09)	0.105 (σ_{ln} = 0.14)
	Bayesian Update_ALL	2692 (910) (σ_{ln} = 0.33)	6.61 (1.72) (σ_{ln} = 0.26)	799 (71) (σ_{ln} = 0.09)	0.121 (0.027) (σ_{ln} = 0.22)
	Bayesian Update_POR	2485 (447) (σ_{ln} = 0.18)	6.70 (1.25) (σ_{ln} = 0.18)	Not Available	0.121 (0.027) (σ_{ln} = 0.22)
	Bayesian Update_ITA	2421 (344) (σ_{ln} = 0.14)	5.57 (1.58) (σ_{ln} = 0.28)	820 (79) (σ_{ln} = 0.10)	0.14 (0.04) (σ_{ln} = 0.29)

2.5 Final remarks

A systematic review of experimental (in situ and laboratory) tests is herein presented, aiming at the definition of a database of mechanical properties of two-leaf stone masonry panels. Five electronic indexing databases have been accessed, namely Scopus, Science Direct, Web of Knowledge, Civil Engineering Database (ASCE), and MADA RELUIS Database [40], collecting data concerning the estimation of the following reference mechanical properties: (1) Young's modulus, (2) compression strength, (3) shear modulus, and (4) shear strength.

Additionally, six different stone masonry types, recurring in traditional constructions, have been identified based on the recommendation provided by Eurocode [13] and Italian standards [38]. Data from non-destructive (sonic tests), minor-destructive (flat-jacks tests), and destructive testing procedures (compression, shear-compression and diagonal-compression tests) have been considered as a source of information. Once the database was completed, the information gathered has been used to carry out an updating procedure based on Bayesian inference.

The procedure complies with the latest recommendation of technical guidelines, and it is intended to simulate a scenario in which raw information related to the assessment of existing masonry buildings is progressively refined when new experimental evidence is available. Three different updates have been carried out using (1) the whole dataset, (2) only the data related to Italian experimental campaigns, and (3) only the data related to Portuguese experimental campaigns.

The comparison between updated results (Bayesian data fusion outcomes) and values provided in the codes (Eurocode and Italian standards) showed good consistency in all the reference mechanical parameters selected for each masonry type.

Overall, the standard deviation characterising the experimental results experienced a reduction once the data fusion process was concluded but, at the same time, updated mean values have been found slightly higher than the mean values suggested by the codes.

This can be explained, on one hand, taking into account the homogeneity of the data sample, which affects the estimation of standard deviation and, on the other considering that the overall quality of the tested masonry panels can yield to an overestimation of their mechanical properties, especially if these results are compared to the values suggested in [13] and [38], which refer to low-quality masonry panels.

The outcomes of the applied data fusion procedure represent a valuable contribution in complementing the existing literature with an updated range of values potentially applicable in practice-oriented engineering activities, both in a general European context and in more specific geographical areas (Portugal and Italy).

Moreover, it must not be overlooked that the proposed values can be used, on one hand, as a reference mechanical parameter and on the other, they can be considered as a starting point of an ongoing process consisting of further updating a specific mechanical parameter if new experimental observations are available.

In conclusion, this study presents a methodology to update a set of selected mechanical properties of two-leaf stone masonry walls, by means of Bayesian inference. The proposed methodology is consistent with the guidelines provided by the Eurocode and Italian standards concerning the assessment of existing buildings.

Although this work exclusively addresses two-leaf masonry walls, nevertheless the proposed methodology is highly versatile and applicable to others masonry types and to any kind of building regardless of its construction system.

The methodology presented in this work can represent a valuable tool for professionals involved in practice-oriented engineering activities addressing the estimation of mechanical parameters using different types of experimental data.

3 Numerical modelling approaches for the out-of-plane behaviour assessment in 2-leaf masonry walls

3.1 Introduction

Masonry is a composite material made of units (natural or manmade) arranged in space usually following a regular pattern characterized by a succession of horizontal overlapping layers which are staggered to avoid the formation of continuous vertical joints. Ideally, the presence of mortar (made of fine aggregate, sand, water, air and/or hydraulic lime binders) should ensure masonry structures with a monolithic behaviour. In the case of dry-stone masonry, no mortar is present, and the units are stacked on top of each other trying to achieve a good interlock to provide an effective structural stability. A significant part of the existing worldwide building stock consists of ordinary and historical masonry buildings (churches, temples, fortresses, etc.) [66]. Indeed, historical masonry buildings are often the result of a non-engineered building practice rooted in practical expertise developed by craftsmen over the centuries and successively codified as rules of thumb, which are essentially an array of techniques consistently detected in historical constructions.

Therefore, when it comes to assessing the structural performance of historical masonry buildings, there are some key aspects that need to be considered, such as the geometrical configuration of masonry bond and the uncertainty related to the estimation of mechanical properties. Inevitably, qualitative, and quantitative features of masonry constructions need to be examined in order to provide an accurate estimation of the overall structural behaviour [67].

The study of qualitative aspects concerning masonry constructions often deals with the analysis and classification of collapse mechanisms caused by seismic action, to which masonry structures are particularly vulnerable. In this regard, on-field observation carried out during post-earthquake damage assessments led to the classification of recurring damage patterns and the definition of analytical expressions, based on the application of the principle of virtual work and on newly upgraded formulation [68] [69], able to estimate a collapse multiplier (load factor) for each recurring and codified damage mechanism [70] [71].

Among the recurring collapse mechanisms, the overturning of the buildings' external walls (first damage mode or out-of-plane failure) represents the most severe condition of vulnerability in masonry buildings, and it is highly dependent on the lack of connection between perimeter and internal load bearing walls [2].

Therefore, starting from the contribution of historical essays describing the main characteristics of a traditional construction [72] [4], further studies have been carried out aiming at correlating reference mechanical

properties (e.g. Young's modulus, shear modulus, compressive strength, and shear strength) to a set of selected key-parameters (e.g. vertical joints configuration, horizontal joints configuration, etc.), resulting in the definition of the so-called Masonry Quality Index method (MQI) [41].

With regard to the structural analysis of masonry buildings, several modelling approaches, ranging from highly simplified to highly advanced, have been developed to numerically simulate the behaviour of masonry structures [73].

Each of these approaches has pros and cons in terms of accuracy and computational effort. Moreover, the derivation/estimation of input parameters (from empirical formulas or experimental data) has a great influence on the final output, affecting the reliability of the numerical simulations.

Even though the array of numerical strategies used for both academic purposes and professional practice is extremely wide, a categorization of these procedures can be provided considering the level of refinement achieved once the numerical model is built [74] [75] [73].

In macro-modelling approaches (1), masonry can be modelled as one-phase material, where units, mortar and units-mortar interfaces are smeared out in a homogeneous continuum (Figure 3.1a). Simplified micro-modelling approaches (2), on the other hand, rely on the definition of "expanded" masonry units combined with zero-thickness interface elements to simulate mortar joints behaviour (Figure 3.1b). Conversely, in a detailed micro-modelling approach (3) masonry is represented as a three-phase material (Figure 3.1c) implying that masonry units and mortar joints are represented by continuum elements whereas the unit–mortar interface is represented by discontinuous elements.

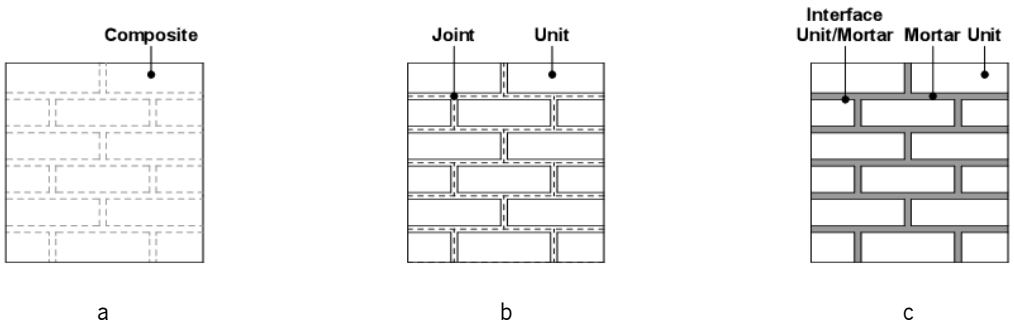


Figure 3.1 - Modelling strategies for masonry structures: (a) macro-modelling; (b) simplified micro-modelling; (c) detailed micro-modelling (adapted from [75]).

Macro-modelling has typically been the preferred approach for modelling complex historical masonry buildings (e.g. churches, towers, fortresses) [73] [23] [76] [77] or complex structural systems such as

building aggregates [78] [79] [80] because it represents a good compromise between results' reliability and computational effort, especially when the buildings to be analyzed are considerably large. Indeed, the computational effort of FE macro-model analyses is considerably lower than comparable analyses conducted using detailed and simplified FE micro-modelling [81] [82]. Moreover, in the literature, FE micro-modelling has mainly been applied to the structural analysis of constructions comprising single-leaf regular masonry walls [83] [84] [85] [86]. These types of masonry constructions are easier to analyse using this approach due to the reduced complexity of the system in comparison with other masonry morphologies, e.g. three-leaf walls, or irregular ones.

Over the last two decades, the discrete element method (DEM) has become an effective alternative modelling approach for simulating the behaviour of masonry structural systems. DEM is particularly suited for detailed models used in research and interpretation of experimental results. Moreover this method allows to model block systems undergoing large motions and, from a computational standpoint, the use of explicit time-stepping algorithms in DE codes results in a smaller run time per step if compared to codes based on implicit algorithm methods [87].

DEM early-stage applications to masonry structures involved the simulation of the behaviour of curved structural systems, as well as the study of masonry constructions characterized by easily replicable and recurring geometrical patterns (e.g. obelisks, aqueducts, Greek temples) [88] [89].

Many literature contributions also address the analysis of single-leaf masonry panels studied both under in-plane and out-plane loading conditions [90] [91], while also investigating the influence of mechanical parameters on the overall structural performance of the selected case study [92] [93] [94].

Although some comparative studies addressing the performance of different modelling approaches in simulating the behaviour of masonry structures can be found in the literature [95] [96], however, for both FE and DE-based modelling approaches, the body of knowledge related to the analysis of the out-of-plane failure mechanisms of two-leaf masonry walls, could be further expanded.

Several aspects, ranging from the interaction between the different leaves constituting the whole masonry panel to the study of the influence of mechanical properties and geometrical characteristics (e.g. masonry bond configuration), demand further attention due to their tendency to significantly influence on the seismic behaviour of masonry structures.

Despite the significant level of advanced numerical modelling techniques nowadays available to analyze the structural behaviour of unreinforced masonry walls, the definition of standardized and sound rules accounting for the aforementioned epistemic uncertainties (geometrical and mechanical) is strongly needed [97].

Additionally, due to the high level of expertise required to properly define and calibrate refined models, the proposal of guidelines and recommendations to effectively support engineers and practitioners represent a significant open issue to be addressed [97].

This chapter presents a comparison among different numerical modelling strategies to simulate the out-of-plane behaviour of two-leaf stone masonry walls. The different strategies adopted are: (a) FE macro-model and a simplified micro-model approach by means of the FE software DIANA FEA [98]; and (b) simplified micro-modelling approach using the distinct element software 3DEC [99].

The experimental data adopted for the calibration of the models and the comparison of the results refers to an out-of-plane test carried out by means of an airbag on two different reduced scale (1:2) U-shaped stone masonry walls, namely an irregular dry-stone wall (DS) [100] and a masonry wall with regular stone units and mortar joints (REGW) [101].

Based on the aforementioned premises, it is intended: (1) to present a systematic overview of the literature sources; (2) to provide a set of reference values and empirical formulation; (3) to define the main mechanical input parameters to characterize the mechanical behaviour of the models depending on the adopted modelling strategy; (4) to assess the reliability of different modelling approaches and commercial software packages in simulating the out-of-plane behaviour of unreinforced masonry walls with complex geometry, namely two-leaf stone masonry walls with different bonds, since few studies in the literature analyzed from a numerical standpoint these masonry typologies; (5) to highlight pros and cons of the selected modelling strategies accounting for results' accuracy and computational effort; (6) to provide insight to be used as a support/guidelines in practice-oriented engineering activities.

3.2 Description of the reduced scale masonry walls

The double-leaf stone masonry walls analyzed in this work replicate the main characteristics of stone masonry walls commonly found in vernacular buildings in the northern region of Portugal [101], but similar morphologies can be found in other regions in Portugal, and other Mediterranean countries. In order to study experimentally their out-of-plane behaviour, reduced scale (1:2) masonry walls specimens with U-shaped plan configuration were adopted. The final wall specimens present a span of 2.25 m, a height of 1.35 m and a

thickness of 0.30 m. In the experimental work two different types of masonry walls were considered, namely dry-stone wall (DS) [100] with roughly cut stone units and a regular stone masonry wall (REGW) [101] with mortared joints. In both specimens, through-stones (headers) were also used to ensure an adequate connection between the wall leaves; headers were distributed throughout the area of the walls, as shown in Figure 3.2, where they have been highlighted in grey. Further details about the geometrical configuration of the reference stone masonry walls can be found in Martins [100] (drystone masonry wall) and Maccarini [101] (regular stone masonry wall with mortar joints). Moreover, raw experimental data as well as CAD 3D models of both walls are available in an online repository (DOI: 10.17632/pngbt7f4pv.1).

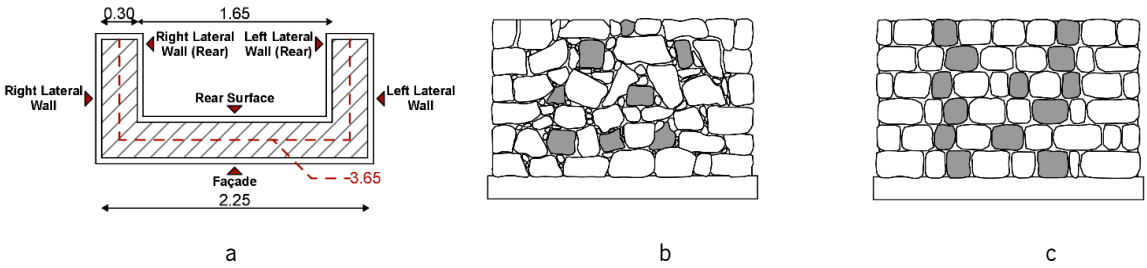


Figure 3.2 - Plan configuration tested specimens (a); front view drystone masonry wall (DS) [100]; (c) front view regular stone masonry wall (REGW) [101].

The experimental setup was identical for both walls and the seismic action was simulated by means of an airbag (area of 1.65×1.35 m^2), exerting a uniformly distributed load on the rear surface of the wall's façade. Additionally, a vertical load was also applied to the transversal walls to simulate the self-weight of a timber roof. A supporting steel frame was placed between the reinforced concrete reaction wall of the laboratory and the airbag. Four load cells, placed between the steel profiles and the reaction wall, recorded the load applied by the airbag to the wall. The out-of-plane test was carried out under displacement control, with the control point located at the top of the frontal wall at mid-span, which is where the highest displacement was expected (Figure 3.3).

The monitoring of the displacements of the frontal wall during the out-of-plane test was carried out using linear variable differential transducers (LVDTs), further details about the testing setup can be found in Martins [100], Maccarini [101] and Murano [102].

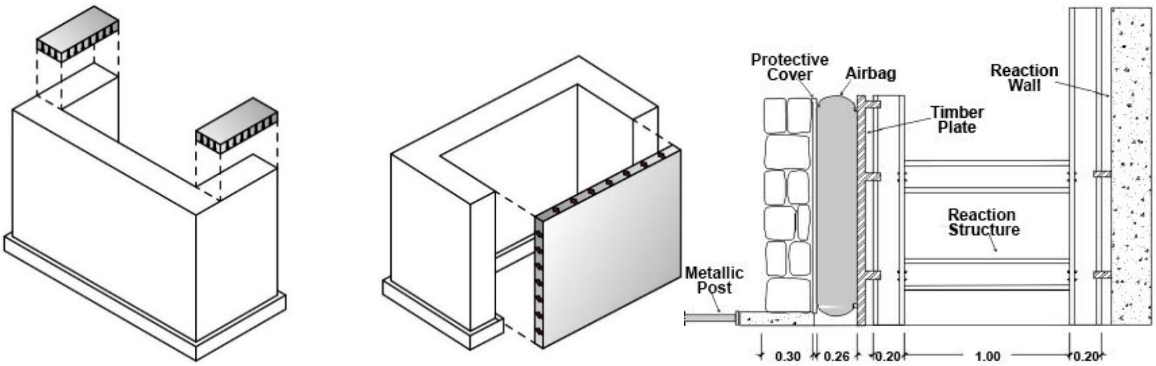
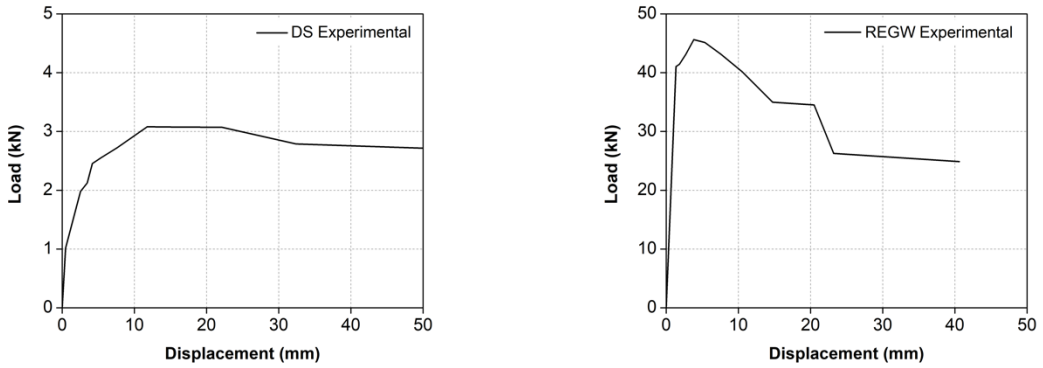


Figure 3.3 - Load configuration and test setup configuration adopted for the OOP test [100] [101] [102].

The force-displacement diagram obtained from the out-of- plane tests of the drystone (DS) and regular stone masonry wall (REGW) is shown in Figure 3.4a and Figure 3.4b respectively. The force represents the sum of the forces recorded by the four load cells. The displacement is measured by the control LVDT (located at the top mid span of the wall).



a b

Figure 3.4 - Experimental force-displacement diagrams drystone wall (a) and regular stone masonry wall (b).

Regarding the drystone wall (DS), the force-displacement diagram highlights a relatively low resistance but a reasonable deformation capacity (approximately 70 mm). The wall shows increasing plastic deformations due to the small percentage of the deformation recovered during the unloading cycles of the test. This deformation pattern indicates that the displacement of the wall is caused by a progressively increasing sliding movement of the stones due to the absence of mortar joints able to limit this phenomenon.

This aspect can also explain the marked non-linearity in the pre-peak regime up to the maximum force (approximately 2.5 kN). Low levels of resistance are expected since the interlock between external and internal

leaf is just provided by the presence of through-stones. Additionally, it is observed that the lack of connections in the corners affects the deformation of the wall, resulting in an asymmetric damage pattern.

Overall, the façade shows a cracking pattern governed by an out-of-plane movement. The opening of three vertical cracks was observed along the joints of the stones: (1) at the top mid-span of the wall along the through-stones (Figure 3.5b and Figure 3.5e); (2) at the intersection between façade and transversal walls (Figure 3.5a-c-d-e-f). The most significant cracks arose in the left half of the wall (see convention adopted in Figure 3.2). Small stone fragments filling the joints, and some stones from the outer surface ended up falling, creating voids in the wall in the final phase of the test. The effectiveness of the connection and of the interlock among stone units significantly affected the final damage pattern. In fact, on the right transverse wall the damage is barely visible, with only two small vertical cracks being observed, proving a better quality of the masonry bond (Figure 3.5a and Figure 3.5d).

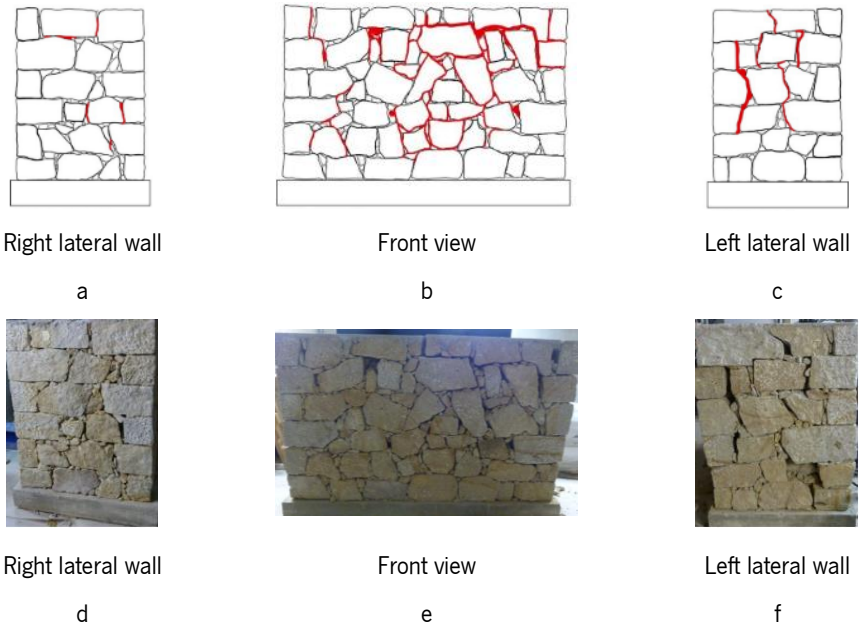


Figure 3.5 - Experimental damage pattern drystone wall (DS) [100].

The response of the regular wall (REGW) is characterized by a linear elastic regime approximately up to the peak load. The initial stiffness exhibits a reduction when approaching a load level around 40 Kn. After the maximum resisting load of 47.8 kN the wall shows a notably higher deformation rate (Figure 3.4). The post-peak behaviour is characterized by a relatively smooth softening branch corresponding to the decrease of the force for increasing lateral displacements. The test was stopped (due to safety reasons) after reaching an out-of-plane displacement of approximately 40 mm.

The final cracking pattern of the regular wall (REGW) shows a diagonal crack in the external surface of the frontal wall arising from the mid-span at the top towards the left bottom corner (see convention adopted in Figure 3.2), characteristic of the out-of-plane bending failure mode (Figure 3.6b and Figure 3.6a). In addition, a vertical crack also developed at the right transversal wall, adjacent to the connection to the frontal wall (Figure 3.6a and Figure 3.6d). At the back surface of the U-shaped wall, a significant horizontal crack developed in the frontal wall along the second bed joint from the bottom base, showing the formation of a clear overturning mechanism (Figure 3.6d and Figure 3.6f).

It should be noted that the crack at the left corner passes through the whole thickness of the wall, contrarily to the crack that developed at the right corner, which is only visible at the back surface. The development of this crack explains the lack of symmetry in the diagonal crack pattern at the front wall, also depending on the small irregularities in the construction process.

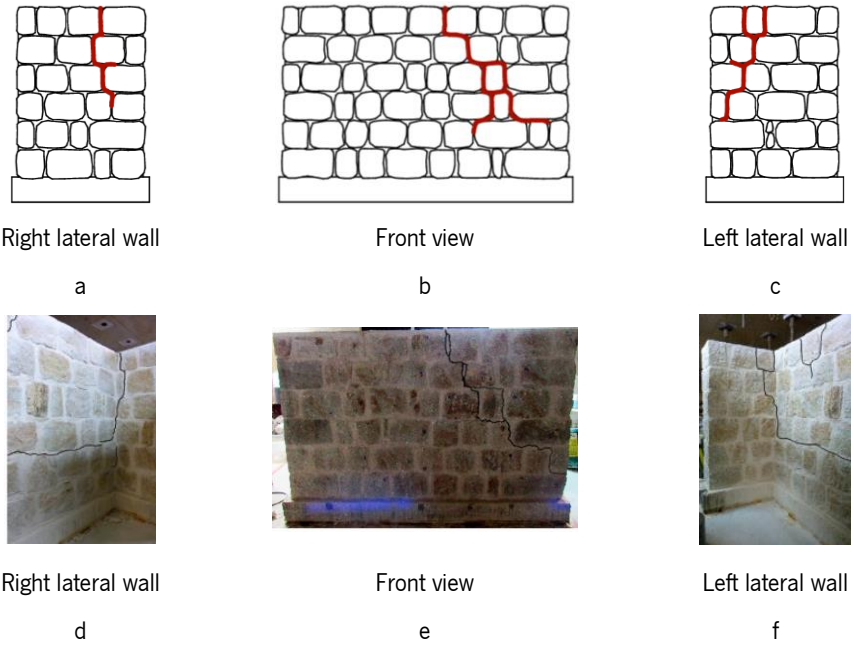


Figure 3.6 - Experimental damage pattern regular stone masonry wall (REGW) [101].

3.3 Finite Elements macro and micro-modelling: Brief Overview

Macro-modelling is an extremely effective approach due to its lower calculation demands. In practice-oriented analyses on large structural members or full structures, a detailed description of the interaction between units and mortar may not be necessary. Hence, macro-modelling approximates masonry as a homogeneous

isotropic continuum material. The practical advantage of this approach relies on the use of simpler finite element (FE) meshes since there is no need of accurately simulating masonry components [75].

One of the most challenging tasks related to the use of macro-models is the formulation of adequate homogeneous constitutive laws able to simulate the mechanical features of masonry (e.g. anisotropy in the elastic regime, different compressive and tensile behaviour, post peak response). Constitutive laws for masonry could be described based on experimental results (direct approach) or deduced using homogenization techniques, which link the structural-scale model to a material-scale model of a representative volume element (RVE) of the structure [73]. Damages are described as a smeared property spreading over a large volume of the structure, which is an approximation that may lead to some inaccuracy because actual cracks in masonry structures usually arise in concentrated or isolated locations [103].

The detailed micro-modelling approach considers independently masonry units, mortar joints and mortar-unit interfaces. It is an extremely accurate method although it is highly time-consuming. Therefore, it is mainly applied to study limited portion of structures or to analyse elastic and inelastic properties of units and mortar since their mutual interaction can be realistically described.

Simplified micro-models overcome the computational drawbacks of the standard micro-modelling technique. In this approach, a sort of "average interface" merges together each mortar joint and two adjacent unit-mortar interfaces, whereas the units are expanded to keep constant the overall geometrical configuration. Thus, expanded units represented by continuum elements are used to model both units and mortar material, whereas the behaviour of the mortar joints and unit-mortar interfaces is lumped to the discontinuous elements [104].

Macro and micro-models have been extensively used to analyse the seismic response of a wide range of masonry structures characterized by different boundary and load conditions [105] [106] [107]. Despite the limitations mentioned above, both approaches have proved their reliability in capturing the out-of-plane behaviour of masonry structures, showing a good agreement with the experimental results presented in research works available in the literature [81] [108].

3.3.1 Description of the Finite Elements macro-models

The numerical macro-model of the walls was defined with DIANA software using twenty-node tetrahedron solid 3D elements (CHX60). Each isoparametric solid element has 60 degrees of freedom and it is based on quadratic interpolation and Gauss integration [98]. Since the model is intended to simulate the experimental test, the concrete base was also included in the numerical model using the same solid 3D elements. Full

connection was considered between the wall and the concrete base (translations and rotations fully constrained), assumed to exhibit a linear elastic behaviour.

The material model adopted to represent the non-linear behaviour of the stone masonry is a standard isotropic Total Strain Rotating Crack Model (TSRM). The model describes the tensile and compressive behaviour of the material with one stress-strain relationship and assumes that the crack direction rotates with the principal strain axes [98]. An exponential softening function simulates the non-linear behaviour of the material in tension, whereas a parabolic function was adopted to describe the crushing behaviour in compression [98]. From a geometrical standpoint, both drystone (DS) and regular stone masonry wall (REGW) macro-models are the same, whereas they differ for the mechanical properties assigned (see Figure 3.7). The overall size of the finite elements mesh is equal to 0.10 m.

The vertical loads acting on the model are the self-weight and a uniformly distributed load on each lateral wall equal to a resulting force of 10 kN (simulating the weight of structural elements such as the roof acting on the top of the structure).

The structural response of all the macro-models considered (both for the drystone and the regular wall) is described by a capacity pushover curve, which represent the horizontal load versus the displacement at the control point taken at the same position where the control LVDT was placed in the experimental test (top mid-span of the frontal wall).

The pushover analysis is based on the incremental application of a uniformly distributed horizontal load in the rear surface of the frontal wall (simulating the action exerted by the airbag); the analysis is considered completed when approaching the displacement level attained in the experimental test (assumed as a conventional state of collapse of the tested wall).

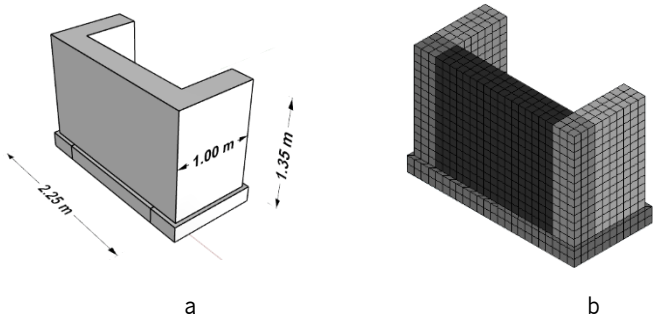


Figure 3.7 - Geometrical 3D model for finite element based macro-modelling application (a) and final macro model (b).

3.3.2 Description of the Finite Elements micro-models

The finite element based micro-model has been constructed starting from a 3D CAD file imported into DIANA software. To this end, it is important to point out that the overall geometry has been simplified and regularized by removing from the final 3D model all those stones with a reduced sized used to fill the joints of the wall. Once imported the geometric characterization of the model was concluded, the next task consisted in the application of interface elements connecting the stone units. A 3D interface available in DIANA for the connection of solid elements has been applied (CT361, 6 nodes triangular interface). Coulomb friction constitutive model has been assigned to the interface elements, implying that cracks occur at the masonry joints, whether they are dry or mortar joints [98].

Hence, the nonlinearities characterising the mechanical behaviour of the wall are concentrated in the joints, whereas stone units (modelled using solid 3D elements, CHX60) are assumed to have linear elastic behaviour. The final geometrical and finite element models for both walls are presented in Figure 3.8.

In order to have a good representation of the strain and stress distribution, the average size of the finite elements mesh considered for the stone units and their interfaces is equal to 0.05 m.

The vertical loads acting on the model are the same considered for the finite element based macro-model (self-weight and a distributed load of 10 kN for each lateral wall). The base of the model is fully constrained and assumed to have linear elastic behaviour. In order to define the structural response of the micro-models, a pushover analysis has been carried out following the same procedure applied for the macro-models (see Section 3.3.1).

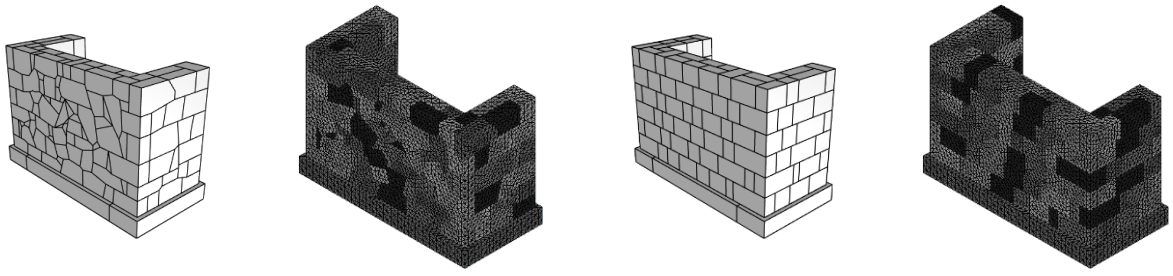


Figure 3.8 - Geometrical 3D model for simplified finite element based micro-modelling drystone masonry wall (a); Drystone masonry wall (DS) final finite element micro model (b); Geometrical 3D model for simplified finite element based micro-modelling regular stone masonry wall (c); Regular stone masonry wall (REGW) final finite element micro model (d).

3.4 Distinct Elements Method (DEM): Brief Overview

The "distinct element method" (DEM) was proposed by Cundall in 1971. Its theoretical assumptions are rooted in the field of rock mechanics and slope analysis, for which the conceptual model of a jointed rock mass as an assembly of rigid blocks was common in the 1960s.

In many DE models the interaction between blocks is represented by a set of contact points. Each contact force is a function of the relative block displacement at a specific point. In 2D models, a length is assigned to each contact point, whereas in three dimensions an area is assigned.

Thus, stresses are calculated according to the joint constitutive models typically formulated in terms of stresses and relative displacements. This approach makes it possible to handle different types of geometric interaction and large block movements [87].

The mechanical behaviour of contacts in DE models can be represented using two models: 1) the hard contact model, which envisages the condition of no overlap between blocks and 2) the soft contact model, in which contact stiffness is defined in the normal and shear directions and a small overlap occurs when the contact is in compression; the latter hypothesis is usually preferred in most DE formulations.

In the shear direction, Coulomb friction is the most widely accepted model for masonry joints. Hence, in DE codes that assume deformable contacts and the point contact approach, the normal contact force (ΔF_n) and shear contact force (ΔF_s) increments are calculated from the increments of relative displacement between blocks in the normal direction (Δu_n) and shear directions (Δu_s) as [87]:

$$\Delta F_s = k_s \, A_c \, \Delta u_s \tag{18}$$

$$\Delta F_n = k_n \, A_c \, \Delta u_n \tag{19}$$

where the k_n and k_s are the normal joint stiffness and shear joint stiffness and A_c denotes the contact area.

From a mechanical standpoint, blocks are assumed to have a rigid behaviour. This option (present in all DE codes) is highly suitable for all those practical problems in which failure via specific collapse mechanisms is common (e.g. assessment of the collapse loads in stone masonry construction). For such problems, the structural deformation can be concentrated in the elastic contacts (deformable contact models) or assumed to be negligible (hard contact models).

The basic assumptions related to a computer-based discrete element modelling approach are [87]: (1) development of finite displacements and rotations of discrete bodies (blocks), including the complete detachment; (2) automatic recognition of new contacts between blocks as the calculation progresses.

3.4.1 Distinct Elements Method: 3DEC Software

In 3DEC, the software developed by Itasca that is used in this work [99], masonry is represented as an assemblage of discrete blocks (rigid or deformable) connected by zero thickness interfaces representing mortar joints. Deformable blocks are internally discretized into a finite number of constant strain tetrahedral elements. Nonetheless, as opposed to FEM, in DEM, a compatible finite element mesh between the blocks and the joints is not required [90].

Rigid blocks are suitable to simulate the behaviour of a structural system that is governed by the joints characteristics. Blocks are connected to each other by a sets of point contacts, located at the outer perimeter of the blocks themselves. For each contact point, there are two spring connections (Figure 3.9), transferring either a normal force or a shear force from one block to another [87] [90].

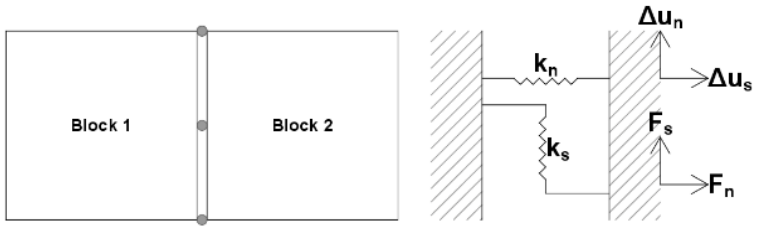


Figure 3.9 - Contact between two blocks [99].

A zero-thickness interface between adjacent blocks simulates the joints behaviour by means of a Mohr-Coulomb model with a tension cut-off, which considers both shear and tensile failure (Figure 3.10).

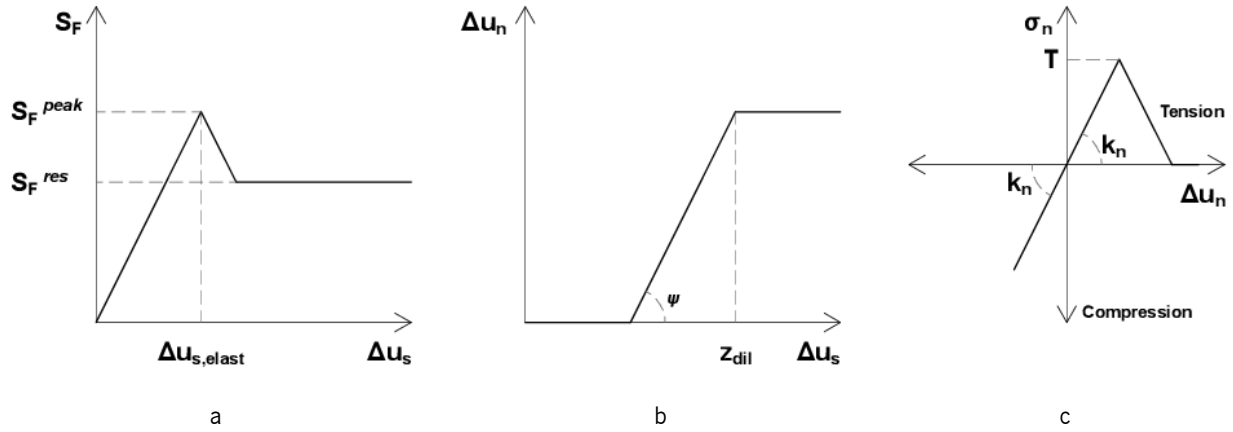


Figure 3.10 - Mechanical behaviour of interfaces: (a) Mohr-Coulomb slip model; (b) bilinear dilatant model; (c) behaviour under uniaxial loading [90].

In the elastic range, the incremental normal and shear stresses on a joint are computed by multiplying normal and shear displacements by normal (k_n) and shear stiffness (k_s) [99]:

$$\Delta\sigma_s = k_s \Delta u_s \tag{20}$$

$$\Delta\sigma_n = k_n \Delta u_n \tag{21}$$

where $\Delta\sigma_n$ and $\Delta\sigma_s$ are the incremental normal and shear stress respectively, whereas u is the normal displacement and u_s is the shear displacement. The maximum shear stress allowed is given by [99]:

$$S_F^{peak} = c + \sigma_{n,max} \cdot \tan\phi \tag{22}$$

where c is the cohesion, σ_n is the normal stress and ϕ is the friction angle. After the peak strength has been reached, shear strength drops until a residual strength stress calculated as (Figure 3.10a):

$$S_F^{res} = c_{res} + \sigma_n \cdot \tan\phi_{res} \tag{23}$$

where c_{res} is the residual cohesion, and ϕ_{res} is the residual friction angle.

After the shear strength has been exceeded, it is possible for the zero-thickness interfaces to dilate with continued shearing (e.g. mortar fails in shear), see Figure 3.10b. The normal displacement, corresponding to the opening of the joint in the normal direction during shear loading, can be expressed as [99]:

$$\Delta u_{n,dil} = \Delta u_s \cdot \tan\psi \tag{24}$$

where ψ is the dilatancy angle and Δu_n is the normal displacement. The equation for normal stress can be adjusted considering the effect of dilation as follows:

$$\sigma_{n,tot} = \sigma_{n,elast} + \sigma_{n,dil} = k_n \Delta u_n + k_n \Delta u_{n,dil} = k_n \Delta u_n + k_n \cdot \Delta u_s \tan\psi \tag{25}$$

When dilation is present, the shear displacement is in the plastic phase ($\Delta u_s > \Delta u_{s,elas}$), see Figure 3.10a. The normal displacement is assumed to be linear until z_{dil} (Figure 3.10b). Dilation increases if the increment of shear displacement runs in the same direction as the total shear displacement. The extension occurs until the limiting shear displacement (z_{dil}) is reached. Under axial loads, elastic behaviour is assumed in the interfaces until tensile failure occurs (Figure 3.10c).

Mechanical damping is used in the distinct element method to solve two general classes of problems, namely static (non-inertial) and dynamic solutions. The damping models available in 3DEC are: (1) adaptive global

damping and (2) local damping [99]. Itasca's 3DEC manual recommends the use of local damping for static analyses since it allows to minimize oscillations that may arise when abrupt failure occurs in the model.

Over the past two decades, 3DEC has proved to be quite versatile in modelling the behaviour of different types of structural systems, such as masonry wall panels [90] [91], reduced scale mock-ups of masonry structures, historical stone masonry structures with irregular masonry bond geometrical configuration [87], stone masonry arches and aqueducts [87] [109] [110] and column-architrave structures under seismic action [111] [112] [89].

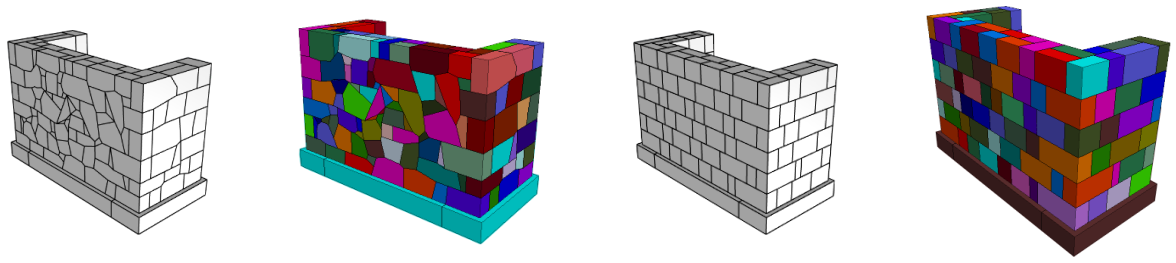
3.4.2 Description of the Distinct Elements micro-models

The simplified micro-models built using 3DEC software envisages the use of rigid blocks (undeformable) to simulate masonry stone units both in drystone wall (DS) and in regular stone masonry wall (REGW), whereas the nonlinear behaviour is simulated by means of interface contact points based on a Mohr-Coulomb constitutive model, which have been used to simulate the joints behaviour in both models (DS and REGW) [99].

Figure 3.11 presents the final geometrical and distinct element models for both walls. Despite the fact that the 3D models imported in 3DEC software are the same used in DIANA, the definition of the contact interfaces among stone units has been significantly faster. Stone units are assumed to have a linear elastic behaviour, as well as the concrete base of the wall that is fully constrained.

The input parameters required to characterize the mechanical behaviour of the interface are normal/shear stiffness, cohesion, tensile strength, dilatancy and friction angle. Dilatancy has been assumed equal to zero in both models (DS and REGW). Damping models and default values suggested in 3DEC manual have been considered [99]. Cohesion and tensile strength have been assumed equal to zero to simulate the same physical configuration of the drystone wall. Conversely, in the regular stone masonry wall (REGW), the presence of mortar joints required a calibration of these values, which has been carried out starting from values collected from sources available in the literature. Average values proposed in the literature have been also considered for friction angle and stiffness properties. Further details about parameters estimation and calibration procedures of both walls are presented in Section 3.5 and 3.6 respectively.

The vertical loads acting on both drystone and regular wall models are the self-weight and the distributed load of 10 kN acting on each lateral wall. The structural response of the model has been evaluated by means of pushover analyses (following the same criteria) as mentioned in Section 3.3.1 and Section 3.3.2 and regarding the finite element based macro and micro models.



a b c d

Figure 3.11 - Geometrical 3D model for simplified finite element based micro-modelling drystone masonry wall (a); Drystone masonry wall (DS) final distinct element micro model (b); Geometrical 3D model for simplified distinct element based micro-modelling regular stone masonry wall (c); Regular stone masonry wall (REGW) final distinct element micro model (d).

3.5 Mechanical properties in Finite Elements (FE) and Distinct Elements (DE) models

As aforementioned, the modelling approaches considered in this study are: (1) macro-modelling and (2) simplified micro-modelling. The macro-modelling analyses will be carried out using a FE-based commercial software (DIANA [98]), whereas for the simplified micro-modelling, two different software, namely DIANA [98] and the DEM-based software 3DEC by Itasca [99], will be used.

The main challenges regarding the development of a numerical model are, on one hand, the definition of a geometrical model that accurately replicates the reference structure without being excessively detailed and on the other hand, the effective estimation of the mechanical properties that characterize the materials' behaviour.

Hence, as highlighted in Section 3.2, macro-modelling approaches consider masonry as an isotropic continuum material having linear and non-linear properties. Conversely, in a simplified micro-model it is assumed that the non-linear properties of masonry are concentrated on the interface connecting the units (see Table 3.1). Hence, the input parameters required to carry out the numerical analysis may vary according to the modelling approach adopted and the software characteristics, with the latter factor depending also on the constitutive model selected to simulate the behaviour of a certain structural system.

Table 3.1 - Summary of the main parameters needed for macro-modelling and simplified micro-modelling (adapted from [113]).

	ELEMENTS	**LINEAR PARAMETERS**	**NONLINEAR PARAMETERS**
Macro-modelling	Homogeneous continuum (units and joints): Isotropic	Young's Modulus Poisson ratio Density	Tensile and Compressive strength Fracture Energy in tension and in compression
Simplified Micro-modelling	Expanded units: assumed isotropic	Normal and Shear Stiffness	None (All the nonlinearities are lumped at the interfaces, i.e., Masonry joints and potential cracks in the units)
	Joints (bed and head): Interface elements	Normal and Shear Stiffness	Bond tensile strength; Cohesion; Friction Angle; Dilatancy; Mode I and Mode II fracture energy

The estimation of the mechanical properties related to the macro-modelling approach is typically based on the recommendations provided by Lourenço [75], consisting of a set of empirical expressions which link the macro-model's mechanical properties to a reference parameter, namely the Young's Modulus of masonry, usually determined by means of experimental testing procedures. The equations used to estimate macro-model mechanical properties in this study are:

$$f_c = \frac{E}{\alpha} \tag{26}$$

$$f_t = \frac{1}{10} f_c \tag{27}$$

$$G_{fc} = d_{u,c} \cdot f_c \tag{28}$$

$$G_{f1} = 12\ N/m \tag{29}$$

Where E is the Young's Modulus, f_c is the compressive strength, α is a coefficient assumed to be equal to 1000, f_t is the tensile strength, G_{fc} is the compressive fracture energy, $d_{u,c}$ is the ductility index in compression assumed equal to 1.60 mm and G_{f1} is the Mode I fracture energy [75]. It must be noted that the values of α, $d_{u,c}$ and G_{f1} have been set based on the same set of recommendations, as already proposed in other works concerning the macro-modelling of masonry structures [114] [108].

An important aspect related to the comparison of the modelling strategies presented in this study involves the use of suitable equations enabling the transition from one modelling approach to another depending on the input data available (e.g. estimation of Young's Modulus starting from joints' normal stiffness and vice

versa). In fact, the calculation of interface stiffness is a crucial aspect for the application of simplified micro-modelling approaches both for FE-based software and for DE-based software. Therefore, providing reference values for interface elements can represent a good starting point in the calibration procedure characterising any numerical simulation, especially when initial information is limited and/or few experimental data is available. According to Itasca manual [99], the relation between Young's Modulus and normal and shear stiffness can be expressed as:

$$\frac{1}{E_m} = \frac{1}{E_{m,u}} + \frac{1}{k_n \cdot s} \tag{30}$$

$$k_n = \frac{E_m \cdot E_{m,u}}{s \cdot (E_{m,u} - E_m)} \tag{31}$$

$$k_s = \frac{k_n}{2 \cdot (1 + \upsilon)} \tag{32}$$

Since 3DEC's initial field of application was geotechnical engineering, these equations originally referred to uniaxial loading of rock containing a single set of uniformly spaced joints oriented normal to the direction of loading. The equations have been adjusted in order to be applied to masonry structures, hence E_m is the masonry equivalent modulus (formerly rock mass Young's modulus); $E_{m,u}$ is the block Young's Modulus (formerly intact rock mass Young's modulus), k_n is the joint normal stiffness, k_s is the joint shear stiffness, s is the thickness of the mortar joints (formerly joint spacing), which for the purpose of this study is assumed equal to 1 cm.

Sarhosis and Sheng [93] investigated the parameter prediction problem for masonry constitutive micro-models, proposing a methodology based on an optimization technique to minimize the differences between results obtained experimentally and computationally. Once bricks and mortar properties are known, the first estimation of normal and shear stiffness is obtained using the following equations:

$$Jk_n = \frac{E_b \cdot E_m}{h_m \cdot (E_b - E_m)} \tag{33}$$

$$Jk_s = \frac{G_b \cdot G_m}{h_m \cdot (E_b - E_m)} \tag{34}$$

$$G = \frac{E}{2 \cdot (1 + \upsilon)} \tag{35}$$

Where E_b is the blocks Young's Modulus; E_m is the mortar Young's Modulus; G_b is the blocks Shear Modulus (estimated using equation 35); G_m is the mortar Shear Modulus (estimated using equation 35); h_m is the

thickness of the mortar joints; ν is the Poisson ratio = 0.2 (assumed value); Jk_n is the joint normal stiffness; Jk_s is the joint shear stiffness.

Other relations to predict the normal and shear stiffness of masonry joints were provided by Bui et al [90], who studied in-plane and out-of-plane behaviour of masonry walls by comparing numerical simulations and experimental results. Masonry panels or masonry mock-ups were made with brick (simulated by means of rigid elements) and dry joints (simulated by means of zero-thickness interface elements). The elastic stiffness properties for interface elements have been obtained using the following equations:

$$k_n = \frac{E_b \cdot E_m}{h_b \cdot (E_b - E_m)} \tag{36}$$

$$k_s = \frac{k_n}{2 \cdot (1 + \upsilon)} \tag{37}$$

Where E_m is the masonry equivalent modulus assumed; E_b is the block Young's Modulus; k_n is the joint normal stiffness; k_s is the joint shear stiffness; h_b is the height of the masonry unit.

Similarly, Gonen et al analysed the seismic capacity of a stone masonry Roman aqueduct (Valens Aqueduct), constructed in the 4th century A.D. in Istanbul (Turkey), using the discrete element method (DEM) [110]. The modelling approach comprises distinct rigid blocks interacting along their boundaries based on the point-contact hypothesis. The normal stiffness (k_n) was predicted based on the ratio between masonry elastic modulus (E) and horizontal joint spacing (h), which includes one brick plus the mortar joint thickness (Equation 38). The shear stiffness (k_s) was calculated through the theory of elasticity (Equation 39):

$$k_n = \frac{E}{h} \tag{38}$$

$$k_s = \frac{k_n}{2 \cdot (1 + \upsilon)} \tag{39}$$

In addition to the expressions previously presented, data collected referring to interface properties in masonry structural systems (e.g. complex buildings, laboratory mock-ups, ancient aqueducts, column-architrave classical structures) with dry joints and mortar joints, is presented in Table 3.2 and Table 3.3 and respectively. Besides normal stiffness (kn) and shear stiffness (ks), information is also included regarding joint tensile strength (ft), cohesion (c) and friction angle (fr). It must be noted that, in all the works examined, the dilatancy (dl) value is assumed to be zero.

Table 3.2 - Summary of interface properties for drystone masonry.

Reference	**Normal Stiffness - k_n (N/m³)**	**Shear Stiffness - k_s (N/m³)**	**Tensile Strength - f_t (N/m²)**	**Cohesion – c (N/m²)**	**Friction Angle – fr (°)**
Sincraian [115]	1.00E+11	1.00E+11	2.00E+6	0 - 7.00E+6	40
Drei [116]	0	1.00E+11	0	0 - 5.00E+5	25 – 30
Mirabella [117]	5.00E+10	2.00E+10	NA	0	30
Papantonopoulos [111]	1 - 2.00E+9	1.00E+9	0	0	35 – 37
Psycharis [112]	1.00E+9	1.00E+9	0	0	37
Psycharis [88]	1.00E+9	1.00E+9	0	0	43 – 66
Oliveira [118]	3.49E+9	1.75E+9	2.00E+6	0	35
Rouxinol [119]	1.00E+9	4.00E+8	0	0	36
Lemos [120]	4.00E+9	2.00E+9	NA	0	25 – 40
Sarhosis [89]	4.00E+12	2.00E+12	0	0	14 – 36.80
Bui [90]	1.96E+9	8.20E+08	NA	0	38
Bui [90]	5.87E+9	2.45E+9	NA	0	35.50
Bui [90]	8.08E+9	3.37E+9	NA	0	35.50
Bui [90]	1.14E+11	4.73E+9	NA	0	35.50
Bui [90]	1.30E+11	5.43E+9	NA	0	35.50
Bui [90]	5.87E+9	2.45E+9	NA	0	30.40
Moranova [109]	3.53E+9	1.48E+9	NA	0	25 – 35
Mordanova [109]	2.90E+9	1.23E+9	NA	0	26 – 35
Pulatsu [121]	4.39E+10	1.83E+10	2.67E+4	4.00E+4	35
Pulatsu [122]	5.00E+9	2.50E+9	0	0	35
Average	2.43E+11	1.13E+11	4.03E+5	2.22E3	34.74

Table 3.3 - Summary of interface properties for masonry with mortar joints.

Reference	**Normal Stiffness - k_n (N/m³)**	**Shear Stiffness - k_s (N/m³)**	**Tensile Strength - f_t (N/m²)**	**Cohesion – c (N/m²)**	**Friction Angle – fr (°)**
Oliveira [123]	1.00E+9	4.00E+8	0	5.00E+5	35
Oliveira [123]	1.00E+9	4.00E+8	0	0	45
Oliveira [123]	1.00E+9	4.00E+8	0	7.50E+5	30
Oliveira [123]	1.00E+9	4.00E+8	0	7.50E+5	30
Schlegel[124]	7.64E+11	2.47E+11	4.00E+5	5.00E+5	30 – 39
Alexandris [125]	3.00E+10	3.00E+10	1.25E+5	1.00E+6	30
Alexandris [125]	3.00E+10	3.00E+10	1.25E+5	1.00E+6	30
De Felice [125]	3.00E+10	3.00E+10	1.25E+5	1.00E+6	30
De Felice [126]	1.88E+9	7.53E+9	0	0	30
Sarhosis [127]	7.64E+9	1.79E+9	1.00E+5	1.00E+5	35
Lemos [87]	3.00E+9	1.50E+9	1.60E+5	3.20E+5	35
Gonen [110]	1.67E+13	7.20E+12	1.00E+5	2.50E+5	35
Gonen [110]	1.00E+13	4.20E+12	2.50E+5	1.25E+5	35
Average	2.00E+12	9.00E+11	1.07E+5	4.80E+5	32.73

The values related to the mechanical properties reported in Table 3.2 and Table 3.3 resulted from specific experimental campaigns (e.g. dynamic identification tests) or reference values provided in the literature.

However, it must be noted that in all the consulted documents, the initial mechanical properties, whether they were defined using experimental data or mathematical expressions, required further adjustments to fit the experimental data (if available) and/or to define a DE model able to accurately replicate the actual behaviour of the analyzed structural system.

Overall, based on the information gathered, in both drystone masonry and masonry with mortar joints, the ratio between normal and shear stiffness ranges from 2 to 2.4 (k_n = 2 - 2.4 k_s) and the cohesion to tensile strength ratio ranges from 1.25 and 1.5 (c = 1.25 – 1.50 f_t). The friction angle values range from 30° to 40° and from 30° to 45° for drystone masonry and masonry with mortar joints respectively.

In the present study, the normal stiffness was assumed as $k_n = 2k_s$ and the cohesion was estimated as 1.25 ft, following a more conservative estimation since no experimental data regarding the mechanical characterization of stone and mortar was available. Any variation characterising the calibration procedure has been carried out keeping these ratios constant. To conclude, Table 3.2 and Table 3.3 presents also the average values related to the joints' mechanical properties for dry stone masonry walls and mortared masonry walls respectively. The average parameters will be used as a starting point for the calibration procedure addressed in Section 3.6.

3.6 Calibration of numerical models and results

The calibration procedure, applied for both walls (DS and REGW), consists of the following steps: (1) preliminary analysis carried out using the simplified micro-model built with 3DEC software (DE-based software) since it allows to obtain an initial estimation of the model's structural behaviour with a smaller computation effort compared to the others modelling approach considered in this study, namely FE macro-modelling and FE-based micro-modelling. The starting mechanical properties used to characterize the behaviour of the interface elements have been set equal to the average values proposed in Table 3.2 and Table 3.3, resulting from the literature review previously presented in Section 3.5; the second step involves the adjustment of the preliminary numerical load-displacement pushover curve to fit the experimental results. The fitting process consisted in different pushover analyses (trial/error approach) carried out modifying the mechanical inputs of the model in terms of stiffness (keeping the ratio $k_n = 2k_s$ as mentioned in Section 3.5 and maximum load capacity (keeping the ratio $c = 1.25\ f_t$, as mentioned in Section 3.5).

In REGW, friction angle value has been kept constant and assumed as the average of the values proposed in the literature for this specific masonry typology (see Table 3.3), whereas in the drystone masonry wall , the friction angle was reduced since the average value computed based on the sources gathered in the literature, resulted slightly higher for this specific masonry typology; the normal stiffness value (k_n) obtained at the end of the tuning process carried out in the previous step is used to: (1) estimate a corresponding value of Young's Modulus in order to define the corresponding properties to be used in the macro-model (see equations 26, 27, 28); and (2) to provide a first estimation of the shear stiffness (k_s), based on the ratio $k_n = 2k_s$ presented in Section 3.5; once the macro-model's mechanical properties have been defined, a modal analysis was carried out to compare numerical mode shapes and natural frequencies of vibration for all the considered modelling approaches (FE macro and micro-models, DE-based micro-model), to have a first insight regarding

the effectiveness of the parameters' estimation procedure and the consistency of the behaviour of the models. An overview of the workflow is shown in Figure 3.12.

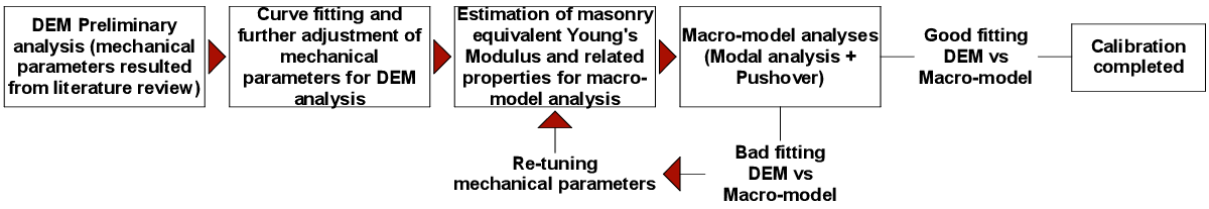


Figure 3.12 - Workflow calibration procedure.

3.6.1 Drystone wall (DS)

The load-displacements curves of dry stone wall obtained in the early stage of the calibration procedure (DS_Micro_DEM_Step 1) and after the iterative fitting process carried out in order to match numerical and experimental data (DS_Micro_DEM_Step 2) are presented in Figure 3.13a and Figure 3.13b respectively.

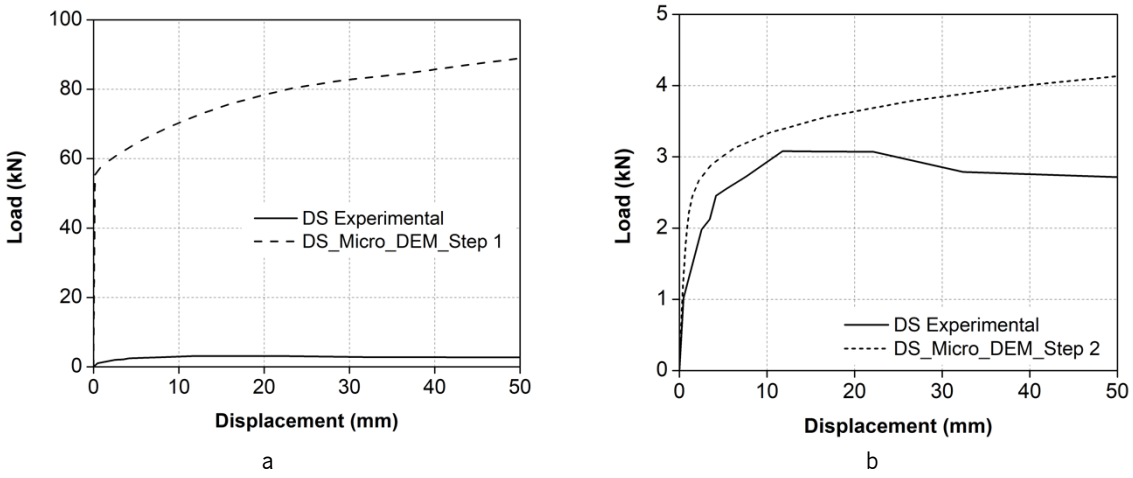


Figure 3.13 - Drystone masonry wall (DS) calibration procedure DS_Micro_DEM_Step 1 (a) and DS_Micro_DEM_Step 2 (b).

The first trial analysis (DS_Micro_DEM_Step 1) carried out with a DE simplified micro-model shows a considerable overestimation both in terms of initial stiffness and in terms of peak value attained. Looking at the graph in Figure 3.13a, it is possible to highlight a significant rigid behaviour of the model until reaching a load level of approximately 60 kN. Subsequently, the numerical curve displays a progressively increasing load level up to 80 kN, which leads to the out-of-plane failure of the wall. Once exceeded this threshold (80 kN),

the curve is characterized by a plateau-like trend displaying slightly increasing load levels corresponding to a progressively increasing displacement level.

Conversely, Figure 3.13b displays a better consistency between numerical and experimental outcomes. Initially, numerical, and experimental curves show a similar behaviour at least up to the load level of 1 kN. After that, the experimental curve shows more accentuated non-linear behaviour and a gradual loss of stiffness up to approximately 3 kN, which corresponds to the appearance of severe damage at the wall. The experimental plateau is characterized by slightly decreasing loading levels corresponding to increasing displacements levels. Regarding this latter aspect, DS_Micro_DEM_Step 2 curve displays a gradually increasing trend both for load and displacement levels. On the other hand, the behaviour of the wall until the development of significant damage levels appears to be satisfactorily captured.

As previously stated for the drystone masonry wall, the first analysis has been carried out using the reference average values presented in Table 3.2, whereas the final input parameters are reported in Table 3.3. The significant inconsistency between the experimental outcome and the numerical curve DS_Micro_DEM_Step 1, could be partly explained considering the heterogeneity of the data collected regarding drystone structural systems. The stiffness parameters used in the first trial analysis are, in fact, 66 times and 78 times higher than the final values adopted for normal and shear stiffness respectively. Additionally, in the second trial carried out using adjusted parameters, tensile strength and cohesion values were set equal to zero to better match the experimental and numerical outcomes.

The final parameters characterising the interface properties are presented in Table 3.4; it must be noted that the values in brackets refer to the input parameters used in the first trial of the calibration procedure reported in Table 3.2.

Table 3.4 - Mechanical parameters to the simplified micro-model (DS).

Normal Stiffness (k_n)	2.00E+9 N/m^3 (2.40E+11 N/m^3)
Shear Stiffness (k_s)	1.00E+9 N/m^3 (1.13E+11 N/m^3)
Tensile Strength (f_t)	0 N/m^2 (4.03E+5 N/m^2)
Cohesion (c)	0 N/m^2 (2.22E+3 N/m^2)
Dilatancy (dl)	0 N/m^2
Friction Angle (fr)	10° (34°)

Once the final mechanical properties for the DE-based simplified micro-model have been adjusted, the following step involved the estimation of a Young's Modulus to be used for the calculation of the remaining input parameters needed for the macro-model developed for the drystone wall.

To this end, starting from the value of normal stiffness k_n presented in Table 3.2, a first estimation of the Young's Modulus has been carried out based on the expressions provided in the literature (see Section 3.5, equations 31, 33, 36 and 38). The main assumptions adopted to estimate an equivalent Young's Modulus of masonry for the drystone wall were: (1) the average height of stone units has been set equal to 0,20 m (20 cm); (2) if requested by a specific equation, mortar Young's Modulus and joints' thickness have been considered extremely low (values close to zero), since no mortar joints are present in the drystone wall examined.

The results obtained using the different formulations are summarized in Table 3.5. The average value for the Young's Modulus of the drystone wall stands at 3.98 E+8 N/m^2 (400 MPa).

It must be noted that, due to the characteristics of the formulation proposed by Sarhosis [93] which considers Young's Modulus for both stone units and mortar, it has not been possible to estimate a value of equivalent Young's Modulus suitable for the purpose of this study.

Table 3.5 - Estimation of the Equivalent Young's Modulus (DS).

Itasca Manual [99]	**Sarhosis** [93]	**Bui** [90]	**Gonen** [110]
4.00E+8 N/m^2	Not Available	3.93E+8 N/m^2	4.00E+8 N/m^2

Overall, the application of the inverse formulations yielded similar results confirming the consistency of the expression adopted, regardless of the initial assumptions applied to comply with the characteristics of the structural system analyzed (drystone masonry wall).

Macro-model parameters related to the initial stage of the calibration procedure (DS_Macro_FEM_Step 1) have been estimated starting a Young's Modulus value of 398 MPa (3.98E+8 N/m^2), resulted from the average of the results presented in Table 3.5.

According to the empirical equation proposed in Section 3.5, macro-model properties have been estimated and used as input parameters (see Table 3.6) to run a preliminary modal analysis and pushover analysis later compared to the results obtained by means of DE method. The initial results showed a significant overestimation of the Load-Displacement macro-model curve if compared to both numerical results (3DEC software simplified micro-modelling) and experimental results (Figure 3.14).

As mentioned above, DS_Macro_FEM_Step 1 curve has been obtained using the parameters reported in Table 3.6 (see column Step 1), resulted from the application of equations 26, 27, 28 and 29 reported in Section 3.5. It must be noted that these equations provide an estimation of compressive strength, tensile strength and compressive fracture energy based on the value of the Young's Modulus. Therefore, these parameters are linked to each other, except for the Mode I fracture energy which is set equal to 12 N/m as suggested in the literature [75].

Looking at Figure 3.14, it is clearly visible a significant inconsistency of the macro-model curve (DS_Macro_FEM_Step 1) if compared to experimental and numerical results obtained by means of DEM (DS_Micro_DEM_Step 2). The initial behaviour of the drystone wall analyzed by means of the macro-model approach shows a considerably higher initial stiffness. The peak load is slightly higher than 20 kN, which is around 7 times higher than the corresponding peak loads (approximately 3 kN) detected both in the experimental curve and DE pushover analysis (curve DS_Micro_DEM_Step 2).

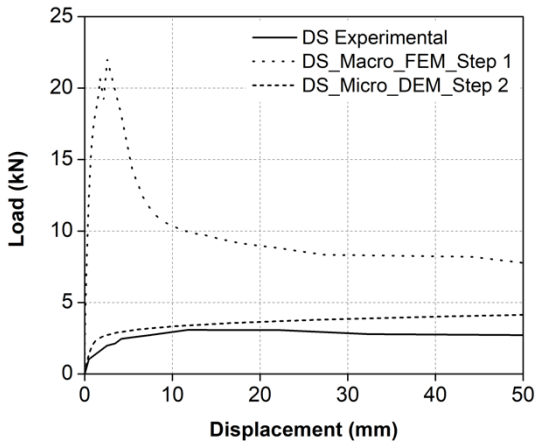


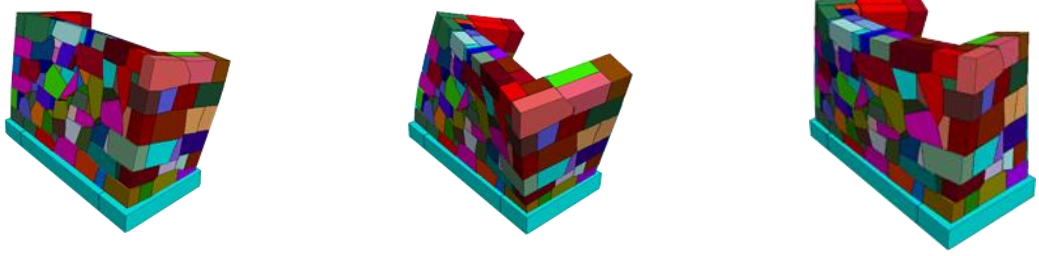
Figure 3.14 - Drystone masonry wall preliminary analyses macro-model (DS_Macro_FEM_Step 1) vs DE-based simplified micro-model (DS_Micro_DEM_Step 2).

Table 3.6 - Initial (DS_Macro_FEM_Step 1) and final (DS_Macro_FEM_Step 2) properties macro-model drystone masonry wall.

Parameter	DS_Macro_FEM_Step 1	DS_Macro_FEM_Step 2
Young's Modulus (E)	3.98E+08 N/m^2	2.95E+08 N/m^2
Poisson ratio (ν)	0.20	0.20
Density	2450 kg/m^3	2450 kg/m^3
Tensile strength (f_t)	39800 N/m^2	934.20 N/m^2
Mode I Fracture Energy (Gf1)	12 N/m	0.04 N/m
Compressive Strength (f_c)	398000 N/m^2	93416.70 N/m^2
Compr. Fracture Energy (Gfc)	637 N/m	149.47 N/m

The comparison between frequencies of vibration and mode shapes obtained from modal analysis carried out with macro and micro-modelling approaches also revealed an overestimation of natural frequencies of vibration in the macro-model (DIANA) with respect to the simplified micro-modelling approach in 3DEC (around 20% higher for the first 2 modes of vibration and 3% for the third one). On the other hand, no differences were detected in the mode shapes (Figure 3.15). In addition, it should be stressed that no experimental data was available regarding the dynamic identification of the drystone masonry wall, hence, the results presented refer only to numerical simulations.

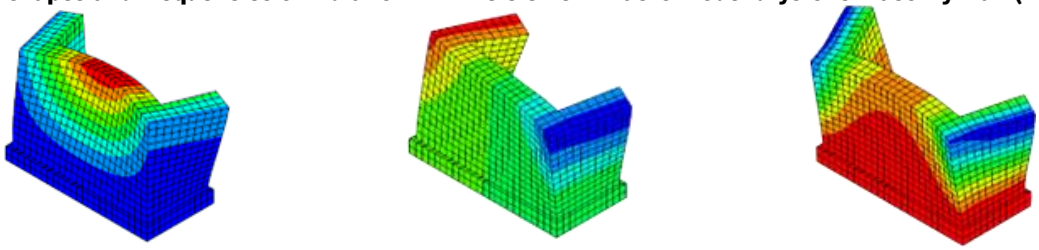
Mode shapes and frequencies of vibration in simplified micro-model drystone masonry wall (3DEC)



Mode 1 - 17.60 Hz) | Mode 2 - 19.67 Hz) | Mode 3 - 24.77 Hz

a | b | c

Mode shapes and frequencies of vibration in finite element macro-model drystone masonry wall (DIANA)



Mode 1 - 20.19 Hz (18%) | Mode 2 - 22.99 Hz (17%) | Mode 3 - 25.58 Hz (3%)

d | e | f

Figure 3.15 - DE micro-model drystone masonry wall Mode 1 (a), Mode 2 (b) and Mode 3 (c); FE macro-model drystone masonry wall Mode 1 (d), Mode 2 (d) and Mode 3 (c).

Taking into account the outcomes of the analyses regarding the parameters estimation in Step 1 of the calibration process, further adjustments on the mechanical properties related to the macro-model approach have been carried out to reach an acceptable consistency of the results (see Table 3.6, column Step 2).

In the DE analyses, the zero cohesion and zero tension assumptions result in a significant decrease in terms of stiffness and peak load as soon as the contact between two stone units weakens. This physical condition cannot be replicated in the macro-model because from a geometrical point of view, the model itself assumes a continuous configuration, which does not allow simulation of contact opening between the stones. Furthermore, from a computational standpoint, convergence problems occurred in DIANA whenever tensile strength, compressive strength, compressive fracture energy and mode I fracture energy values approached zero.

For this reason, in order to obtain a macro-model able to replicate the same assumptions characterising the DE model, namely no tension and no cohesion at the level of dry joints, the values of the input mechanical parameters, such as compressive fracture energy and Mode I fracture energy, have been set equal and with extremely low values (Table 3.6, column Step 2), ignoring the dependency of parameters such as tensile/compressive strength and compressive fracture energy from the masonry Young's Modulus.

Once the mechanical parameters have been modified, it was observed that natural frequencies of vibration obtained in the macro-model reduced and approximate the values obtained in the micro-modelling approach. The vibration modes resulting from numerical analyses have been qualitatively compared taking as a reference modes shapes and vibration frequencies those obtained via simplified DE-based micro-modeling. Successively, a quantitative evaluation of the level of correlation among vibration modes has been carried out by means of Modal Assurance Criterion (MAC), calculated using the following expression [128]:

$$MAC_{ij} = \frac{(\varphi_i^{num} \times \varphi_j^{num})^2}{\left(\varphi_i^{num} \times \varphi_j^{num}\right)\left(\varphi_i^{exp} \times \varphi_j^{exp}\right)}; i = 1,2,\dots,n^{num}; j = 1,2,\dots,n^{exp} \quad (40)$$

where $\varphi_{i\ num}$ and $\varphi_{j\ exp}$ are the vectors of the modal components numerically and experimentally identified for n^{num} and n^{exp} modes, respectively.

Due to the lack of experimental data and being the main goal of this study to get an insight into the effectiveness of the modeling strategies adopted the input data referred to the experimental components has been obtained by simulating a dynamic identification test in 3DEC. Hence, a history of velocities of about 100

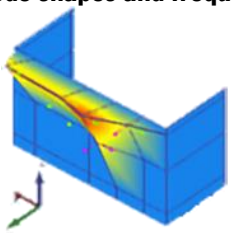
s corresponding to a white noise (frequency contents between 0 and 30 Hz) was applied at the base of the DE-base model [128].

The modal components obtained in 3DEC and post-processed in ARTeMIS software, have been used to assess the correspondence between DE-based models and FE-based models results in terms of mode shapes and frequencies of vibration. The peak values of frequency were selected using Frequency Domain Decomposition (FDD) and Subspace Identification-Unweighted Principal Components (SSI-UPC) technique.

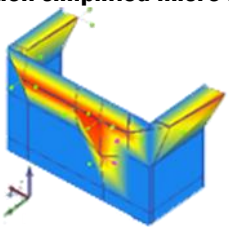
In the numerical macro-model, the third natural frequency is 11% lower than the corresponding value obtained in the micro-model (DE model), whereas the first and second frequency of vibration have approximately the same value in both numerical models (Figure 3.16).

Figure 3.16 also shows the results of the natural frequencies and modes of vibration obtained for the micro-model prepared in DIANA. It should be stressed that the same mechanical properties used for the DE model have been adopted for the interface elements in the DIANA micro-model (Table 3.4), also considering the Mohr-Coulomb interface model. A good agreement can be also observed between DIANA and 3DEC simplified micro-models.

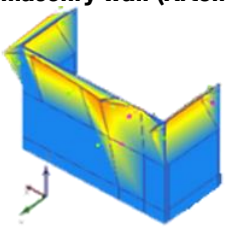
Mode shapes and frequencies of vibration simplified micro-model drystone masonry wall (Artemis)



Mode 1 - 17.60 Hz
a

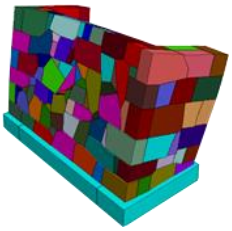


Mode 2 – 19.67 Hz
b

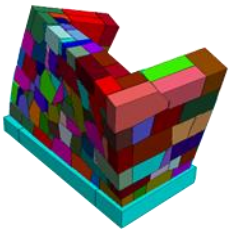


Mode 3 – 24.77 Hz
c

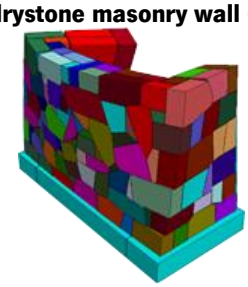
Mode shapes and frequencies of vibration simplified micro-model (3DEC) drystone masonry wall (DS)



Mode 1 - 17.60 Hz
d

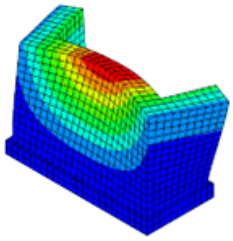


Mode 2 - 19.67 Hz
e

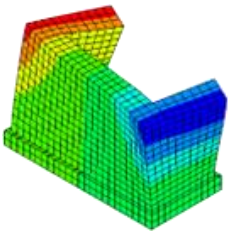


Mode 3 - 24.77 Hz
f

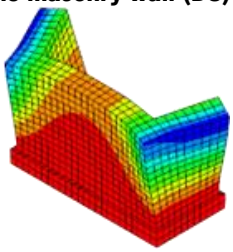
Mode shapes and frequencies of vibration macro-model (DIANA) drystone masonry wall (DS)



Mode 1 – 17.50 Hz (2%)
MAC – 0.93
g

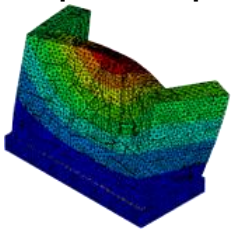


Mode 2 – 19.20 Hz (1%)
MAC – 0.83
h

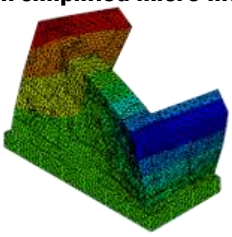


Mode 3 – 22.99 Hz (-11%)
MAC – 0.85
i

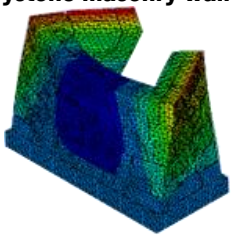
Mode shapes and frequencies of vibration simplified micro-model (DIANA) drystone masonry wall (DS)



Mode 1 – 18.90 Hz (10%)
MAC – 0.87
l



Mode 2 – 20.80 Hz (6%)
MAC – 0.85
m



Mode 3 - 25.09 Hz (1%)
MAC – 0.78
n

Figure 3.16 - Mode shapes and frequencies of vibration for all the modelling approaches considered (DS).

From Figure 3.17, it is possible to analyse the force-displacement curves (control point) obtained from the calibrated macro-model (FEM) and micro-models (DEM and FEM) and compare them with the experimental results. It is observed that at this stage, there is a good consistency between macro-modelling and simplified

micro-modelling. However, simplified micro-modelling curves tend to overestimate the experimental peak load, whereas the peak load obtained from the macro-model is slightly lower than the experimental maximum resisting force. The macro-model appears to properly capture the behaviour of the wall up to the end of the elastic regime. The post-peak behaviour shows a plateau in the FE simplified micro-model analysis, whereas as previously stated, DE-based micro-model curve shows a plateau-like trend displaying slightly increasing load levels corresponding to a progressively increasing displacement level.

In the case of the macro-model, there is a slight decrease of the resistance, which is in more accordance with the experimental result. Additionally, the post-peak branch in the macro-model simulation has a decreasing trend more similar to the experimental results. Overall, it appears that the stiffness in the numerical models is higher than the experimental test, which highlights a substantial loss of stiffness in the early stage of the test (for load level corresponding to approximately 1 kN).

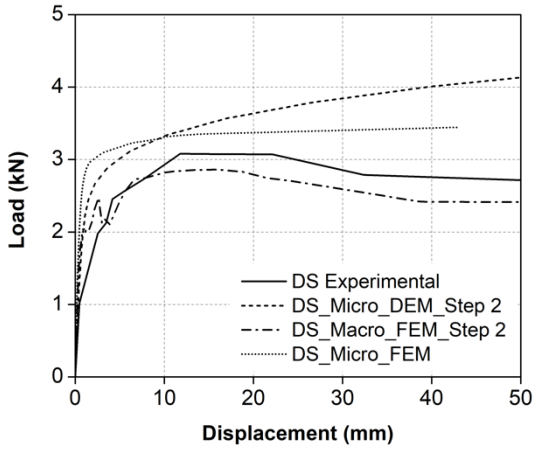


Figure 3.17 - Experimental and numerical Load vs Displacement curves drystone masonry wall (DS).

Looking at the damage pattern corresponding to a displacement of 40 mm measured at the top mid span of the wall, it is possible to observe a good agreement between the simplified micro-model results (DIANA and 3DEC) and the experimental damage pattern. During the experimental out-of-plane test, the upper left portion of the façade wall (see Figure 3.2 for reference) experienced a significant crack opening (Figure 3.18a-b-c). The opening of this crack occurs at end of the linear behaviour of the wall, and it determines a progressive detachment of the façade from the left lateral wall.

This phenomenon has been captured in 3DEC (Figure 3.18d-e-f) and the DIANA micro-models (Figure 3.18l-m-n). It is also interesting to notice that the micro-models are very sensitive to the critical points related to the lack of interlocking of vertical joints, as both micro-models can capture the localized cracks at the main

façade. Due to its intrinsic features, the macro-model is not able to capture this crack pattern related to the geometrical configuration of the stones. Despite this expected limitation, the macro-model is able to simulate the detachment phenomenon of the façade with respect to the lateral walls (Figure 3.18g-h), revealed by the strain concentration at the connection between main façade and transversal walls.

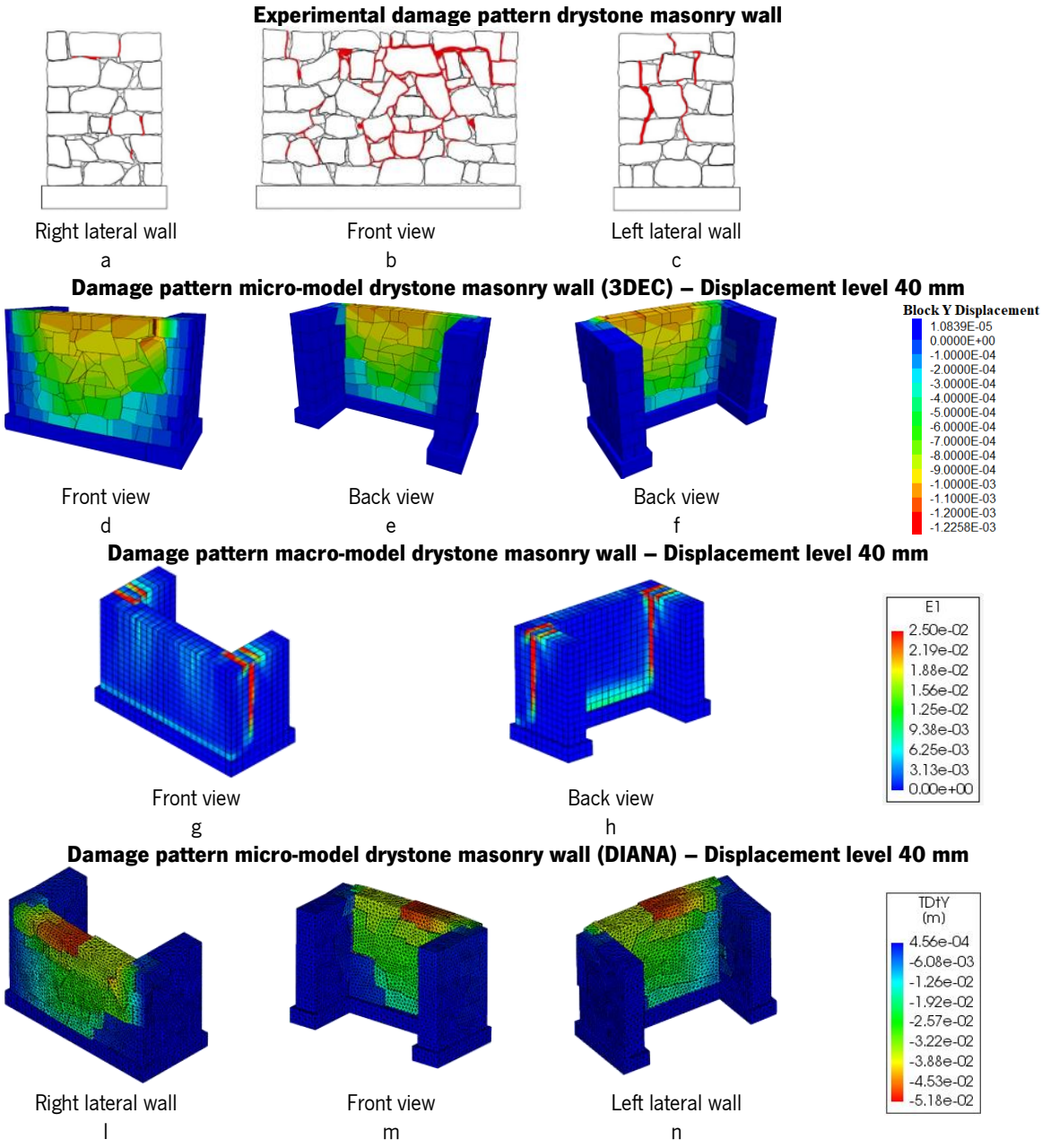


Figure 3.18 - Numerical and experimental damage pattern drystone masonry wall.

3.6.2 Regular stone masonry wall (REGW)

Similar to what was carried out for the drystone masonry walls and following the steps from the calibration procedure summarized in Figure 3.12, a preliminary analysis of the regular walls with mortar joints was carried out using 3DEC (e.g. the DE-based software). The initial mechanical properties adopted to characterize the interface elements of the DE models were previously defined and presented in Table 3.3 (see average values). As aforementioned, this table summarizes the outcomes of the literature review carried out to gather reference values for the mechanical properties of the interface elements representing mortar joints.

Figure 3.19 provides a comparison between the experimental load-displacement curve obtained in the out-of-plane test with numerical response of the wall corresponding to first stage of the calibration procedure (REGW_Micro_DEM_Step 1). It is also possible to compare it with the load-displacement diagram resulting from the iterative fitting process carried out in order to match the numerical and experimental data (REGW_Micro_DEM_Step 2).

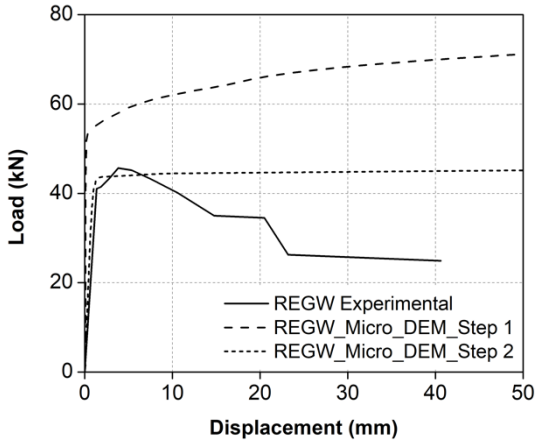


Figure 3.19 - Regular masonry wall (REGW) calibration procedure step 1 (a) and step 2 (b).

The first trial of the calibration analysis showed an overestimation in terms of peak load attained (approximately 60 kN). Similarly, the stiffness of the numerical model appears to be significantly higher when compared to the experimental result (see Figure 3.19, REGW_Micro_DEM_Step 1 curve).

Hence, a refinement of the model's mechanical properties was carried out by adjusting stiffness parameters (assuming $k_n = 2k_s$ as mentioned in Section 3.4) and tensile parameters assuming the cohesion equal to 1.5 ft (tensile strength), as mentioned in Section 3.5. The final parameters characterising the interface properties are presented in Table 3.7; it must be noted that the values in brackets refer to the input parameters used in the first trial of the calibration procedure reported in Table 3.3, Section 3.5.

As previously stated regarding the drystone wall, both simplified micro-models (DE-based and FE-based model) have the same properties since both use a similar constitutive model for the interface elements (Mohr-Coulomb).

Table 3.7 - Mechanical parameters simplified micro-model (REGW).

Normal Stiffness (k_n)	4.20E+9 N/m³ (2E+12 N/m³)
Shear Stiffness (k_s)	2.10E+9 N/m³ (9E+11 N/m³)
Tensile Strength (f_t)	1.50E+5 N/m² (1.10E+5 N/m³)
Cohesion (c)	1.90E+5 N/m² (4.85E+5 N/m³)
Dilatancy (dl)	0 N/m²
Friction Angle (fr)	33°

Once, the final values of normal and shear stiffness were correctly set, the updated normal stiffness was used to estimate the equivalent Young's Modulus of masonry to calculate other mechanical parameters as material input parameters for the macro-model analysis (using equations 31, 33, 36 and 38). The values for the Young's Modulus of the drystone wall, calculated based on the different formulations are summarized in Table 3.8, and the average value stands at 8.47E+8 N/m² (847 MPa). Also for this type of masonry, it was not possible to use the formulation proposed by Sarhosis [93] due to the absence of reference values related to the Young's modulus of mortar.

Table 3.8 - Equivalent Young's Modulus values (REGW).

Equivalent Young's Modulus estimation (Regular Masonry Wall with mortar joints – REGW)			
Itasca Manual [99]	**Sarhosis** [93]	**Bui** [90]	**Gonen** [110]
8.20E+8 N/m²	Not Available	8.20E+8 N/m²	9.00E+8 N/m²

Table 3.9 presents the final values adopted for the macro-modelling approach, estimated using equations from 26 to 29 and based on the average equivalent Young's Modulus value (8.47E+8 N/m²). The consistency of the properties, estimated for each modelling approach, has been assessed by means of a modal analysis to compare mode shapes and natural frequencies of vibration.

The numerical results have been also compared to the experimental data obtained from the dynamic identification test performed on the masonry wall (REGW).

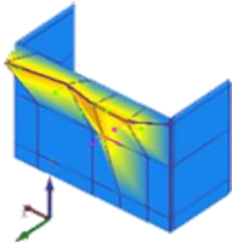
Table 3.9 - Mechanical parameters macro-modelling approach (REGW).

Young's Modulus (E)	8.47E+8 N/m^2
Poisson ratio (ν)	0.39
Density	2495 kg/m^3
Tensile strength (f_t)	8.47E+4 N/m^2
Mode I Fracture Energy (Gf1)	12 N/m^2
Compressive Strength (f_c)	8.47E+5 N/m^2
Compr. Fracture Energy (Gfc)	1355 N/m

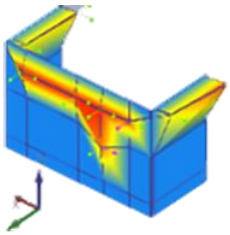
As Figure 3.20 illustrates, good consistency can also be observed in terms of natural frequencies of vibration and mode shapes. The assessment of the correspondence among modal components has been carried out similarly to what mentioned in Section 3.6.1 regarding the drystone wall (DS), hence applying the Modal Assurance Criterion, taking as a reference the results obtained after simulating an dynamic identification test on the regular wall (REGW) in 3DEC.

In the simplified DE-based micro-model, the first frequency of vibration is 6% higher than the corresponding experimental value (Figure 3.20d) and conversely, the second frequency of vibration is 7% lower than the corresponding experimental value (Figure 3.20e). A similar trend was found for both the macro-model analysis and FE micro-model analysis. The macro-model presents natural frequencies values 5% higher and 8% lower than the experimental data for the first and second frequencies respectively (Figure 3.20g and Figure 3.20h), whereas the FE-based micro-model shows an increase equal to 5% for the first natural frequency and a decrease equal to 12% for the second frequency when compared to the experimental results (Figure 3.20l and Figure 3.20m).

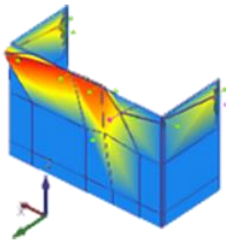
Mode shapes and frequencies of vibration simplified micro-model regular masonry wall (Artemis)



Mode 1 – 28.35 Hz
a

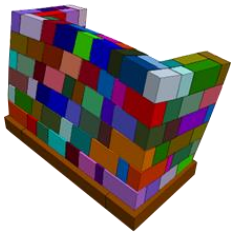


Mode 2 – 32.45 Hz
b

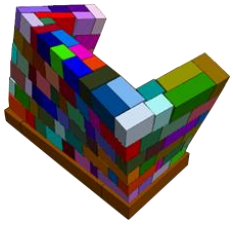


Mode 3 – 36.15 Hz
c

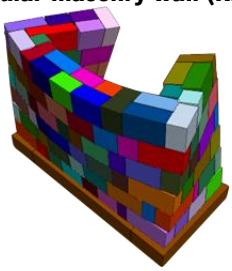
Mode shapes and frequencies of vibration simplified micro-model (3DEC) regular masonry wall (REGW)



Mode 1 – 28.35 Hz (6%)
d

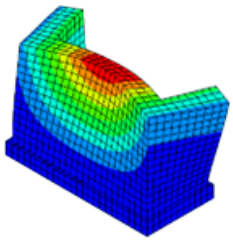


Mode 2 – 32.45 Hz (-7%)
e

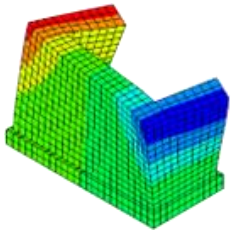


Mode 3 – 36.15 Hz
f

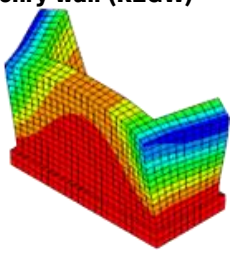
Mode shapes and frequencies of vibration macro-model regular masonry wall (REGW)



Mode 1 – 28.03 Hz (5%)
MAC – 0.91
g

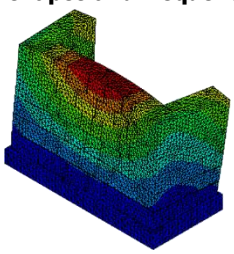


Mode 2 – 32.06 Hz (-8%)
MAC – 0.84
h

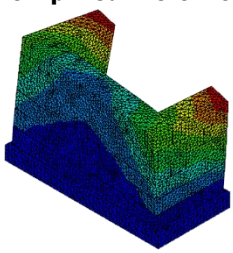


Mode 3 – 35.71 Hz
MAC – 0.79
i

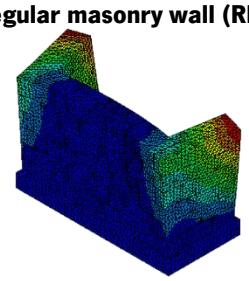
Mode shapes and frequencies of vibration simplified micro-model (DIANA) regular masonry wall (REGW)



Mode 1 – 28.01 Hz (5%)
MAC – 0.88
l



Mode 2 – 30.73 Hz (-12%)
MAC – 0.83
m



Mode 3 – 36.52 Hz
MAC – 0.81
n

Figure 3.20 - Mode shapes and frequencies of vibration for all the modelling approaches considered (REGW).

Figure 3.21 presents the load-displacement diagrams resulting from the pushover analyses performed using the different calibrated modelling approaches. All the considered modelling approaches yielded similar results in terms of initial stiffness.

The FE-based micromodel led to a peak load of approximately 40 kN, which is slightly lower in comparison to the peak load achieved in the analysis carried out with DE-based simplified micro-model (peak load around 43 kN). In both cases the value is very close to the experimental peak load of 43.50 kN.

A higher difference in terms of peak load was found for the macro-model. In this case, the peak load is around 15% lower than the experimental peak load. The post-peak behaviour in both simplified micro-modelling approaches (DE-based and FE-based) shows a plateau characterized by almost no increasing load for increasing lateral displacements. On the other hand, the macro-model load-displacement curve is characterized by an abrupt decrease of the lateral resistance of the wall after reaching the peak load.

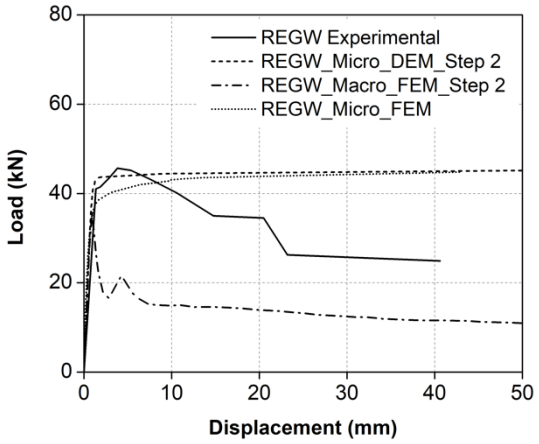


Figure 3.21 - Experimental and numerical Load vs Displacement curves regular masonry wall (REGW).

The damage pattern in the DE and FE simplified micromodels (corresponding to a displacement level equal to 40 mm) is also similar. Diagonal cracks open in the façade wall resulting in a progressive increase of the detachment between the façade and the lateral walls (Figure 3.22d-e-f and Figure 3.22l-m-n). For a higher level of displacement, it is possible to observe a gradual sliding phenomenon affecting the top masonry horizontal layer.

Looking at the macro-model strain concentration (corresponding to a displacement level equal to 40 mm), it is possible to conclude that damage mostly affects the connection between lateral walls and façade, as well as the upper central part of the main façade. It is possible to observe that the strain concentration coincides with the diagonal cracks that developed in both simplified micro-models (Figure 3.22g-h). Moreover, the highest strain concentration in the upper part of the façade shows a good consistency with the outcome related to the micro-model-based analyses, which show higher displacements of the upper masonry layers.

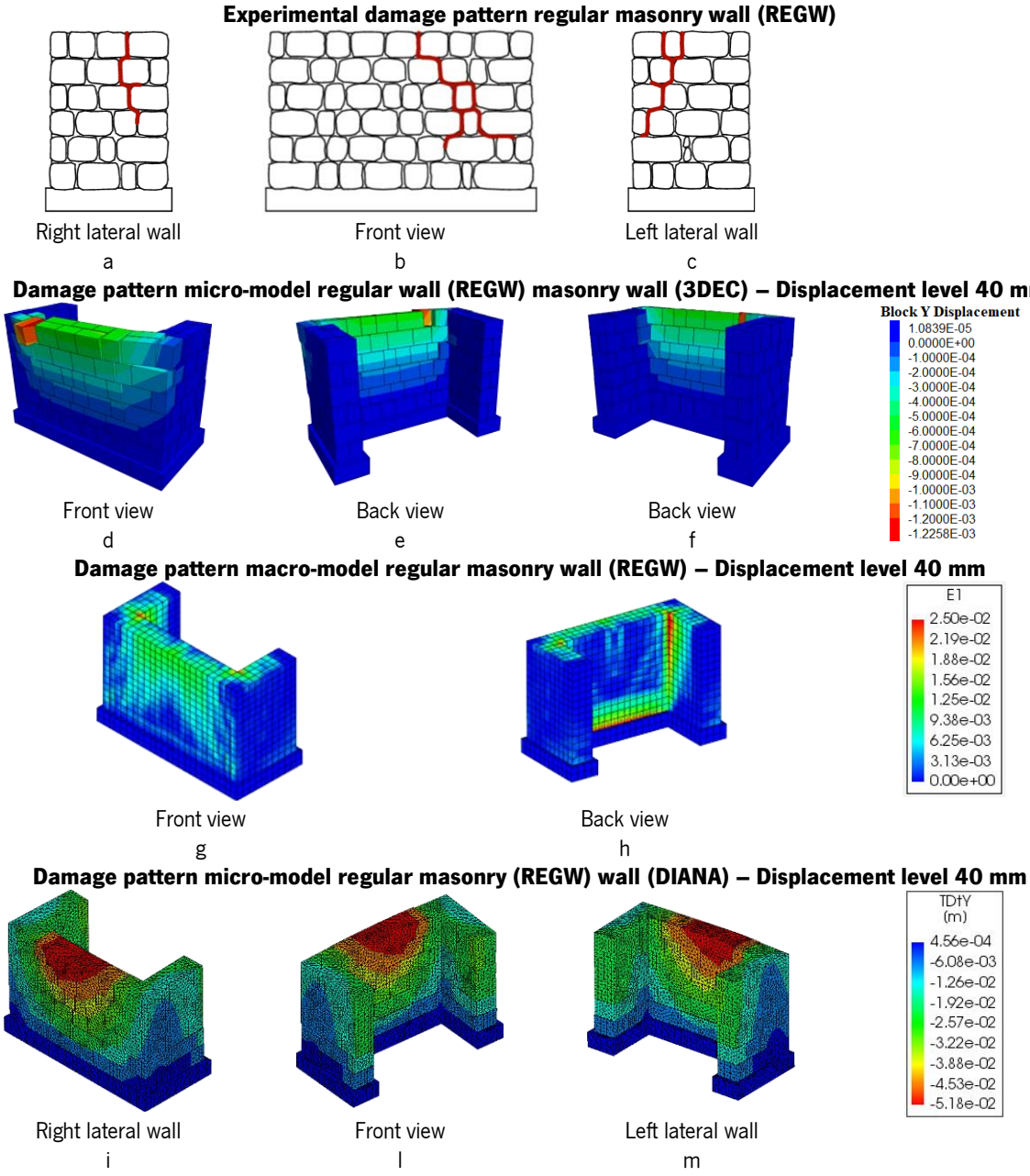


Figure 3.22 - Experimental and numerical damage pattern regular masonry wall (REGW).

Regarding the experimental damage pattern (Figure 3.22a-b-c), the numerical models are also roughly able to represent the damage, even if the crack asymmetry could not be captured by DE-based simplified micro-model and FE-based macro-model. On the other hand, in the FE-based simplified micro-model the occurrence of an asymmetrical damage pattern was slightly captured (Figure 3.22i-l-m).

Therefore, it is possible to state that the selected numerical approaches proved to be reliable in assessing the out-of-plane performance of the selected experimental reference. In particular, the micro-model

approaches (DE-based and FE-based) provided a good estimation of the out-of-plane performance of the regular wall (REGW) both in terms of peak load attained and initial stiffness. The post peak branch, however, is characterised by a plateau (Figure 3.21REGW_Micro_DEM_Step 2 curve and REGW_Micro_FEM curve) which overestimates the displacement capacity of the walls, when compared with the experimental results. Nevertheless, the main advantage of both micro-model analyses lies in the considerable accuracy in simulating the final damage pattern.

On the other hand, the macro-model analysis showed an expected lack of accuracy in simulating asymmetrical damage patterns. This is essentially due to the specific characteristic of the modelling approach which represents complex geometries in a simplified configuration. Therefore, since acting loads and boundary conditions are symmetrically applied to the model the corresponding displacements and deformations will spread symmetrically as well.

Obviously, depending on the aim of a specific study and depending on the extent of the structure to be analyzed, one procedure can be preferred to another. Overall, the macro-model and DE-based micro-model approaches provided good results with an effective balance between accuracy and computational effort. In particular, the DE-based analysis provided a better approximation of the damage pattern and a considerably smaller computational demand if compared to FE-based micro-model, which in any case, provided similar results. However, the preparation of the 3D geometry of DE-based models is significantly more time consuming than FE-based macro-models.

To summarize, macro-model is the most suitable option for practice-oriented engineering activities involving the analysis of large structures. A viable alternative could be DE-based analyses whenever a better understanding of specific damage mechanisms is required, and the morphology of the wall is simple to model and/or the model can accept simplifications of the morphology of the masonry bond and geometry. FE-based micro-model analyses, which have a higher computational demand, remain a good option to model smaller portions of structures or to simulate experimental testing procedures involving reduced-sized specimens.

3.6.3 Assessment of the onset out-of-plane load via updated analytical formulation

Starting from the experimentally observed damage patterns, a limit analysis based on an updated formulation proposed in Casapulla [68] has been carried out in order to estimate the load level that activates the failure mechanism in both drystone (DS) and regular stone masonry wall (REG).

DS and REGW damage mechanisms involve the overturning of a portion of the façade combined to the detachment of the façade itself from the lateral walls. Three possible failures modes have been considered

namely, a simple rocking (Mechanism A), a compound rocking (Mechanism B) and a horizontal flexure (Mechanism D), see also Table 1, Mechanism A, B and D reported in [68]. Figure 3.23a, b and c show the scheme of external and internal actions in all the mechanisms considered in the limit analysis procedure as well as a 3D schematic view (Figure 3.23d, e and f).

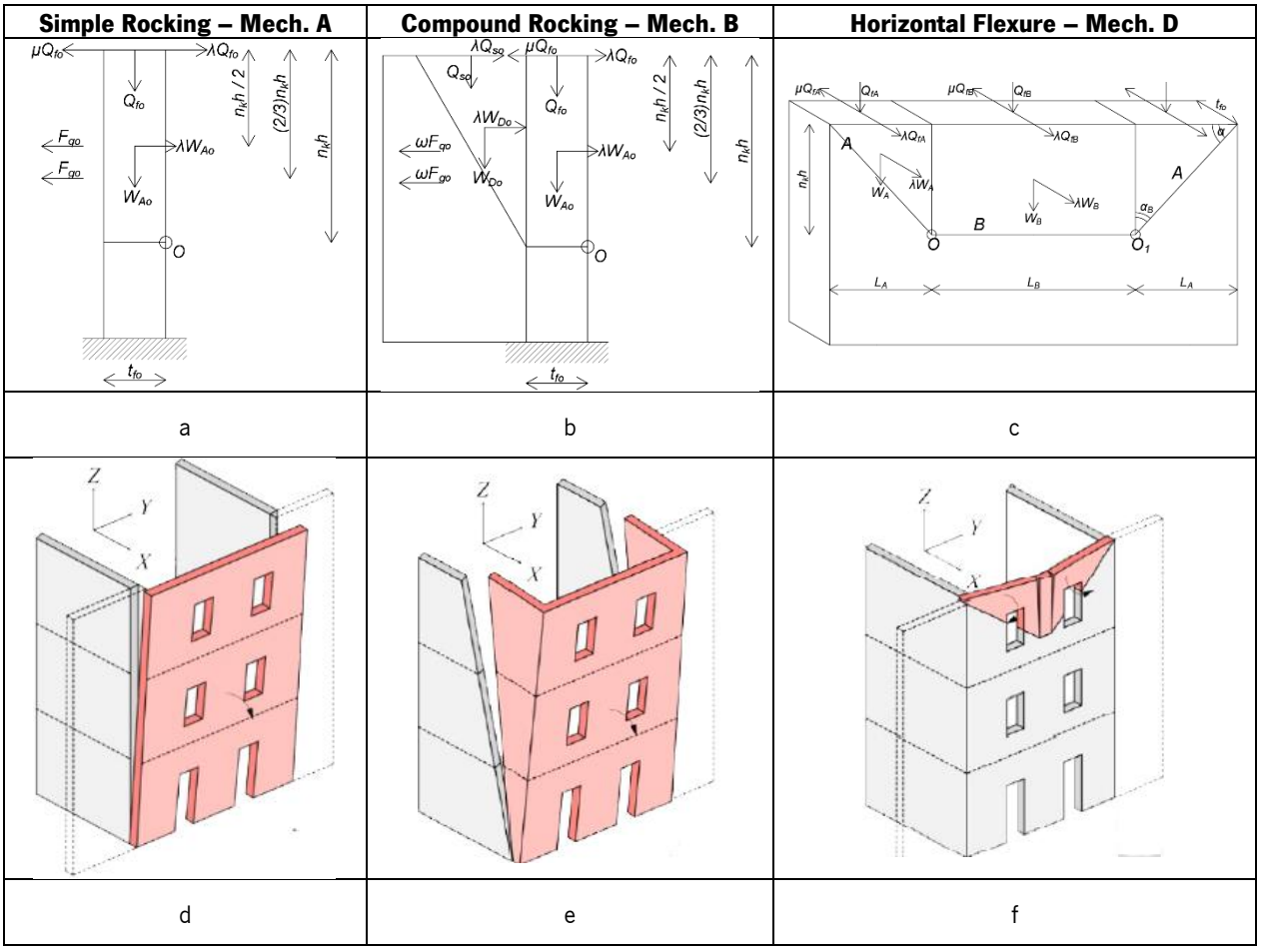


Figure 3.23 - Scheme of internal and external actions in simple rocking (a), compound rocking (b) and horizontal flexure mechanism(c); 3D schematic view of simple rocking (d), compound rocking (e) and horizontal flexure (e) mechanism, adapted from [68].

It is noteworthy to point out that the notation and the nomenclature adopted for the input parameters used in the limit analysis are the same of those proposed in Casapulla [68]. Additionally, the basic assumptions considered to obtain a structural scheme as close as possible to the load configuration and the experimental setup of the out-of-plane test are the following: (a) The restraining action due to beam connection (μQ_{fo}) is neglected since this type of load is not present in the experimental configuration. A uniformly distributed load equal to 5.48 kN/m has been considered acting on top of each tested wall. This value resulted from the ratio

between the total external vertical load acting on the top of the tested walls (20 kN in both DS and REGW) and the extension of the centroidal axis of the plan view of the wall (equal to 3.65 m, see Figure 3.2a).

(b) The number of masonry courses in REGW is 6, whereas the number of courses between the top of the wall and the hinge O (n_k) is set equal to 4. In Mechanism B, the number of courses crossed by the crack at the i^{th} storey (n_c) is set equal to 4.

(c) The average height of stone units is set equal to 0.225 m, the thickness is set equal to 0.15 m considering a two-leaf wall with total thickness of 0.30 m, and the average length of stone units is set equal to 0.29 m. The resulting staggering ratio (ν) is 0.144 m. Based on these assumptions, the estimated maximum admissible crack angle (α_b) in compliance with the staggering ratio is approximately 26°. In Mechanism B, a value of 13° has been set for the crack inclination angle (α_c), hence considering an average contribution of the frictional forces to the failure mechanism.

(d) To overcome issues related to the irregular geometrical configuration in DS, the same assumptions related to stone units' dimensions and staggering ratio have been adopted.

(e) The friction coefficients (μ) have been computed starting from the friction angle values presented in Table 3.4 and Table 3.7 for the drystone wall (DS) and regular stone masonry wall (REGW) respectively. The load factor corresponding to the selected failure mechanism can be estimated as follows for DS and REGW [68]:

$$\lambda_{r,o_A} = \frac{W_{Ai}X_{Ai} + \mu Q_{fi}Z_{Q_{fi}} + Q_{fi}X_{Q_{fi}}}{W_{Ai}Z_{W_{Ai}} + Q_{fi}Z_{Q_{fi}}} + \frac{n_s(F_{gi}Z_{F_{gi}} + F_{qi}Z_{F_{qi}})}{W_{Ai}Z_{W_{Ai}} + Q_{fi}Z_{Q_{fi}}} \quad (41)$$

$$\lambda_{r,o_B} = \frac{W_{Ai}X_{Ai} + \mu Q_{fi}Z_{Q_{fi}} + Q_{fi}X_{Q_{fi}} + n_s(W_{Di}X_{W_{Di}} + \omega(F_{ji} + Q_{si}X_{Q_{si}}))}{W_{Ai}Z_{W_{Ai}} + Q_{fi}Z_{Q_{fi}} + n_s(W_{Di}Z_{W_{Di}} + Q_{si}Z_{Q_{si}})} \quad (42)$$

$$\lambda_{1,r,o_D} = \frac{2\left(W_AZ_{W_A} + \mu Q_{f_A}Z_{Q_{f_A}}\right) + (W_BZ_{W_B}) + (\mu Q_{f_B}Z_{Q_{f_B}}) + 4k(T_{o_g} + T_{o_q})}{2\left(W_AY_{W_A} + Q_{f_A}Y_{Q_{f_A}}\right) + \left(W_BZ_{W_B} + Q_{f_B}Y_{Q_{f_B}}\right) + 2kd_0(W_A + W_B + Q_{f_A} + Q_{f_B})} \quad (43)$$

For the sake of brevity, the reader is referred to Casapulla [68], for a more detailed definition of the variables common to the selected mechanisms. These formulations refer to N-storey buildings, considering the storeys indexed by the variable i = 1, 2, 3, ...N, from the top to the ground storeys. Since the structural scheme considered for both walls has just 1 floor, i is equal to o (i=o).

W_{Ai} (external action due to self-weight), $Q_{fi/si}$ (overload on the façade/lateral walls), F_{gi} (maximum frictional resistance due to the contribution of the self-weight) and F_{qi} (maximum frictional resistance due to the

contribution of the overload) together with their lever arms (X, Y and Z) are calculated according to the equations proposed in [68] (see Table 3, 4 and 6 for Mechanism A, B and D respectively).

S_{oj} and T_o are the shear and torsion contributions, respectively, which characterize Mechanism D [68], computed taking into account a reduction of contact interfaces corresponding to a corrective coefficient k set equal to 0.5.

Finally, due to the absence of specific information regarding the tested drystone wall (DS), the same density value as the REGW has been assigned. It must not be overlooked that the actual density value for this type of masonry is lower than that considered, hence, leading to an analytical value closer to those related to experimental, FE-macro model and DE-model results.

The load factor and its corresponding load are reported in Table 3.10 for both DS and REGW. The table reports the percentage difference between the Light Damage Load and the Limit Analysis Load for each mechanism considered, this value is presented in round brackets while the letter A, B and D refer to the mechanism considered (see column Light Damage Load in Table 3.10).

The analytically estimated load has been compared to the Light Damage Load which corresponds to the load level in the so-called Light Damage limit state, according to the definition proposed in [129], which correlates the beginning of cracking phenomena in masonry structures to a reduction of 2% of the initial stiffness.

Moreover, Load Factor and Limit Analysis Load analytically computed are shown in the last 2 columns. The onset load (Limit Analysis Load) is computed by multiplying the load factor derived from the limit analysis procedure (λ), by the mass of the macro-element related to the mechanism selected and by the gravitational acceleration (≈10 m/s^2).

Table 3.10 - Onset load for the out-of-plane mechanism estimated based on experimental, analytical, and numerical results.

	Initial Stiffness (kN/mm)	Initial Displ. (mm)	Prevalent Collapse Mech. Observed	Light Damage Load (kN)	Load Factor (λ)	Limit Analysis Load (kN)
DS Experimental	2.15	0.47	Compound Rocking - B	0.99 (50%) – A 0.99 (71%) – B 0.99 (2%) – D	Mech. A = 0.09 Mech. B = 0.302 Mech. D = 0.083	Mech. A = 2.01 Mech. B = 3.38 Mech. D = 0.97
DS_Micro_ DEM_Step 2	2.80	0.48	Horizontal Flexure - D	1.31 (35%) – A 1.31 (61%) – B 1.31 (26%) – D		
DS_Macro_ FEM_Step 2	3.10	0.57	Simple Rocking - A	0.83 (59%) – A 0.83 (75%) – B 0.83 (14%) – D		
DS_Micro_ FEM	4.18	0.50	Horizontal Flexure - D	2.05 (2%) – A 2.05 (39%) – B 2.05 (53%) – D		
REGW Experimental	29.80	0.33	Compound Rocking - B	9.63 (46%) – A 9.63 (23%) – B 9.63 (73%) – D	Mech. A = 0.231 Mech. B = 0.391 Mech. D = 0.270	Mech. A = 5.16 Mech. B = 7.46 Mech. D = 1.45
REGW_Micro _DEM_Step 2	46.09	0.22	Horizontal Flexure - D	9.93 (48%) – A 9.93 (25%) – B 9.93 (74%) – D		
REGW_Macro _FEM_Step 2	46.42	0.24	Simple Rocking - A	10.91 (53%) – A 10.91 (32%) – B 10.91 (76%) – D		
REGW_Micro _FEM	43.08	0.23	Horizontal Flexure - D	9.71 (47%) – A 9.71 (23%) – B 9.71 (73%) – D		

In DS wall, despite Mechanism B is the prevailing failure mode experimentally observed, the onset load related to the horizontal flexure (Mechanism D) is closer to the experimental outcome. On the other hand, DE-base micro-model results show a good consistency between the observed failure mode, namely horizontal flexure (Mechanism D) and the loads numerically and analytically computed, with a percentage difference of 26% (the lowest among the collapse mechanisms considered), see Table 3.10.

FE-based micro-model is characterized by a horizontal flexure prevailing failure mode. However, a better agreement in terms of load level is shown when considering a simple rocking mechanism (Mechanism A).

Fe-based macro-model presents a simple rocking failure, but in terms of load level the lowest difference between numerical and analytical results is detectable when Mechanism D is considered (14%).

In REGW, experimental and analytical results show a good agreement both in terms of collapse mechanism detected (Mechanism B) and in terms of load levels attained (lowest percentage difference among the mechanisms considered, approximately 23%), see Table 3.10.

DE-based micro-model results highlight a good consistency between load levels attained when Mechanism B is considered, even though the observed failure mode is a horizontal flexure. A similar trend is detectable looking at the result of the FE-based micro-model.

However, in FE-based macro-model the percentage difference between the onset load related to Mechanism A is 53% if compared to the numerically estimated load. In this case, despite being simple rocking the observed failure mode, from a load level standpoint the best approximation of the numerical results is provided by the limit analysis carried out assuming a collapse due to a compound rocking behaviour.

Overall, in the case of the regular wall (REGW), the mechanism experimentally observed (Mechanism B, compound rocking) is consistent with the results obtained by means of limit analysis. Analytical results obtained by assuming a compound rocking failure mechanism proved to be sufficiently accurate when compared to the numerical results, although some discrepancies between observed and assumed failure modes can be detected.

On the other hand, DS wall's results display more heterogeneity. The experimentally observed failure mode is compound rocking (Mechanism B), but the value of onset load closer to the Light Damage State load refers to the limit analysis carried out assuming a horizontal flexural failure. Among the numerical methods considered, FE-based micro-model provided a good fitting of the analytical results. Indeed the intrinsic complexity of the physical phenomena involved in the simulation of the behaviour of the drystone masonry wall (mostly frictional action influenced by the geometrical configuration of the masonry bond), makes it difficult to obtain a perfect fitting among experimental, numerical, and analytical results.

3.7 Final remarks

This chapter presents a comparison among different numerical modelling approaches applied for the simulation of the out-of-plane behaviour of two-leaf stone masonry walls, namely finite element-based macro/micro modelling and distinct element based micro modelling.

The numerical results were compared with experimental results from out-of-plane tests previously carried out. The walls have different masonry bonds and constructive systems, namely one wall is a drystone masonry wall (DS), and the other is a roughly regular masonry bond wall with mortar joins (REGW). The main aspects arising from this study are: (1) the calibration procedure of the models, carried out based on reference values of mechanical properties and empirical equations available in the literature, highlighted a lack of consistency in estimating the mechanical properties of the drystone wall (DS) mainly when a finite element based macro

modelling approach is considered, whereas a better agreement between empirical expression and final mechanical properties has been obtained in the regular wall with mortar joints (REGW). The empirical expressions found in the literature are, in fact, mainly targeted for masonry walls with mortar joints, hence, further analyses could be carried out to fill this gap related to the parameter estimation of drystone masonry.
(2) The masonry bond geometrical configuration strongly influenced the overall out-of-plane response of the selected walls. The regular wall with mortar joints (REGW) showed a higher strength capacity and a higher stiffness level compared to the drystone wall (DS), due to, among other aspects, a better interlock among stone masonry units.
(3) Despite its intrinsic limitations (e.g. inability in simulating asymmetrical crack patterns and inability to fully capture the frictional phenomena characterising the drystone masonry wall), finite element-based macro modelling approach proved to be reliable in identifying the areas of the walls which may be display higher level of damages. On the other hand, both finite element-based, and distinct element-based micro modelling approaches provided a more accurate estimation of the crack patterns of the walls under study.
(4) Taking into account the aforementioned considerations the choice of a specific modelling approach should take into account the computational effort and the time required to build the geometrical model to be used in the software package selected to carry out the numerical simulation. To this end, it is worth to mention that a finite element based micro-model pushover analysis required a run time higher than 7 days, whereas the run time for a distinct element-based pushover analysis required less than 30 minutes; a is similar computational effort (average of 30 minutes) characterized the finite element based macro-model analyses carried out.
Additionally, one of the most time-consuming tasks for the finite element based micro-model is the contact detection and the application of interface elements in DIANA software. This task had to be carried out manually for all the masonry units (overall duration ranging from 5 to 10 hours). Conversely, in 3DEC (DE-based software), the detection and the definition of the interface elements is a semi-automatic procedure (overall duration less than 15 min depending on the geometrical complexity of the model), carried out by means of specific code-based inputs that considers the configuration of the CAD 3D model.
In conclusion, among the finite element-based modelling approaches considered in this study, macro-modelling represents the best solution for practice-oriented engineering activities since it provides a good compromise between accuracy and computational effort. On the other hand, finite element based micro-modelling provided accurate results but with considerable computational effort. Overall, this approach is a

viable choice whenever experimental tests on small-scale specimens need to be simulated, but it is not an effective option when it comes to analysing particularly large models. On the other hand, distinct element based micro modelling proved to be effective in simulating the overall behaviour of both drystone (DS) and regular wall (REGW) with a reasonable run time for all the analyses performed, hence representing a viable alternative to both FE-based modelling approaches.

4 Numerical parametric study on reduced scale models

4.1 Introduction

As discussed in the previous chapter, the structural performance of masonry walls is dependent on two pivotal aspects, namely mechanical properties, and geometrical configuration of stone/masonry units. This chapter investigates the aforementioned aspects in an effort to obtain a deeper insight regarding the influence of key parameters in the out-of-plane behaviour of masonry walls, both from a mechanical and a geometrical standpoint, using a comprehensive numerical parametric study.

Chapter 3 provided an insight regarding the calibration procedures and the array of modelling approaches nowadays available to simulate the out-of-plane behaviour of 2-leaf masonry walls. A significant aspect arisen from the results obtained consists in the advantages, in terms of computational effort, related to the use of Discrete Element Method (DEM) in performing numerical simulations using simplified micro-models.

Despite several scientific works addressing the numerical modelling of masonry structures by means of DE-based models, there is still a gap in the literature related to the assessment of the influence of mechanical properties' variation in the out-of-plane behaviour of masonry structures and, more specifically, 2-leaf masonry walls [130] [112] [92] [122] [91].

Moreover, as highlighted in historical treaties, masonry bond configuration plays a key role in the overall structural performance of masonry subject to seismic actions. Indeed, ancient building practice was predominantly based on empirical know-how, often leading to the construction of oversized buildings. The so-called "rule of thumb" was the compass of every single craftsman involved in the building process [2].

The awareness of the scientific community towards the stereotomy applied in historical constructions has progressively grown over time. Previous studies [67] evaluated how the presence or absence of diatones (through-stones) influences the collapse of masonry piers. More recently hybrid quantitative and qualitative methods have been defined in order to correlate the characteristics of the masonry bond and its constructive quality to the mechanical properties [41].

Almeida refined the MQI application integrating a shape factor that accounts for the regularity or irregularity of the masonry units (e.g. roughly cut stones vs regular stones) [131].

Numerical studies have been conducted to assess the influence of the spatial configuration of stone-units in the overall performance of masonry walls [132]. However, one of the main hurdles related to the implementation of numerical parametric studies aimed at the evaluation of the geometrical features in

masonry constructions, is the limitation of generating random geometrical configurations of the masonry panels. In this regard, some authors already proposed advanced tools for the automatic generation of random masonry bonds, even though the models were mostly single-leaf panels with reduced dimensions [133].

Starting from these premises, the objective of the parametric study herein presented is two-fold: (1) to investigate the influence of the mechanical properties variation in the out-of-plane performance of 2-leaf masonry walls; and (2) assess the influence of geometrical parameters such as horizontal/vertical joints configurations, presence/absence of diatones (through stones) on the out-of-plane behaviour of 2-leaf masonry walls.

The reference models considered in this study are those already calibrated in Chapter 3, namely the drystone wall (DS) and the regular stone masonry wall (REGW). The models keep the reduced scale (1:2) and the same load and boundary conditions.

It is worth pointing out that the study of material properties involves both DS and REGW walls. The properties analyzed are normal (k_n) and shear stiffness (k_s), cohesion (c), joints tensile strength (f_t), and friction angle (fr). These are the input parameters of the contact interfaces to characterize linear and nonlinear behaviour of the simplified DE micro-models.

Conversely, the geometrical parametric study only refers to the regular stone masonry wall (REGW), since it is easier to have control over the geometrical parameters' variation for that specific masonry type.

Finally, it was deemed more significant to carry out the study exclusively with the 3DEC software, due to the reduced number of similar studies available in scientific literature [90] [122] [132].

4.2 Numerical parametric study on material properties

The first part of the numerical parametric study addresses the variation of material properties and their influence on the out-of-plane performance of the selected masonry walls, namely drystone wall (DS) and regular stone masonry wall (REGW). The reference mechanical material properties both from a geometrical and a numerical point of view, have been already presented in Chapter 3 (Table 3.4 and Table 3.7). The numerical analyses carried out using 3DEC software consists in the incremental application of a uniformly distributed horizontal load in the rear surface of the frontal wall (pushover) and it is considered completed when approaching the displacement level attained in the experimental test (assumed as a conventional state of collapse of the tested wall) as stated in Chapter 3.

As aforementioned, the main goal of the study is to provide an insight regarding the following parameters: normal (k_n)/shear stiffness (k_s), cohesion (c), joints tensile strength (f_t) and friction angle (fr). These are the input parameters required to numerically simulate the linear and nonlinear behaviour of DS and REGW according to the Coulomb Friction Material Law, which is the material model behaviour selected in the 3DEC software.

Besides the reference mechanical property, 4 values more have been considered in the material parametric analysis. Concerning the drystone masonry wall (DS), the criterion to vary the normal and shear stiffness consisted of multiplying the reference value by a factor equal to 0.25 (-75%), 0.50 (-50%), 2 (+100%) and 3 (+200%) to obtain incremented values.

The reference values of tensile strength and cohesion resulting from the calibration of the drystone masonry wall numerical model are equal to zero. Therefore, a different approach has been applied in this case. Starting from an initial value of cohesion equal to 0.26 MPa, a progressive increase of 0.50 MPa has been considered up to 1.76 MPa, aiming at covering the range of variation for this mechanical property resulting from the literature review (see Table 4.1).

Similarly, the initial value of tensile strength has been set equal to 0.30 MPa, and a progressive increase of 0.50 MPa has been considered up to 1.8 MPa, aiming at providing a significant range of variation for this mechanical parameter, based on the values observed from literature review proposed in Section 3 (see Table 3.2). Finally, the friction angle varied from 15° to 30°, considering a progressive increment equal to 5°.

Concerning the regular stone masonry wall (REGW), reduction of 50% and 75% was considered, and an increase of 100% and 200% of the reference value were adopted (see Table 4.1). In this case, friction angle ranges from 23° to 43°, considering a 5° increase for each analysis performed.

In each numerical analysis, the model presents the reference mechanical parameters (resulting from the calibration procedure carried out in Chapter 3) whereas the parameter to be assessed is the only one that varies. Therefore, the results of 4 models were used to compare with the reference wall. The total number of numerical models (including the reference ones) generated is 40 (20 for each masonry wall). Table 4.1 presents an overview of the mechanical properties' values considered in the parametric study.

Table 4.1 – Reference mechanical properties and set of values parametric study in Drystone masonry wall (DS) and Regular stone masonry wall (REGW)

DS_Reference				
kn = 2E+9 N/m³	0.25 kn = 5E+8 N/m³	0.50 kn = 1E+9 N/m³	2 kn = 4E+9 N/m³	3 kn = 6E+9 N/m³
ks = 1E+9 N/m³	0.25 ks = 2.5E+8 N/m³	0.50 ks = 5E+8 N/m³	2 ks = 2E+9 N/m³	3 ks = 3E+9 N/m³
c = 0	c = 2.6E+5 N/m²	c = 7.6E+5 N/m²	c = 1.26E+6 N/m²	c = 1.76E+6 N/m²
ft = 0	ft = 3E+5 N/m²	ft = 8E+5 N/m²	ft = 1.3E+6 N/m²	ft = 1.8E+6 N/m²
fr = 10°	fr = 15°	fr = 20°	fr = 25°	fr = 30°
REGW_Reference				
kn = 4.2E+9 N/m³	0.25 kn = 1.05E+9 N/m³	0.50 kn = 2.1E+9 N/m³	2 kn = 8.4E+9 N/m³	3 kn = 1.26E+10 N/m³
ks = 2.1E+9 N/m³	0.25 ks = 5.25E+8 N/m³	0.50 ks = 1.05E+9 N/m³	2 ks = 4.2E+9 N/m³	3 ks = 6.3E+9 N/m³
c = 1.5E+5 N/m²	0.25 c = 5.625E+4 N/m²	0.50 c = 1.125E+5 N/m²	2 c = 4.5E+5 N/m²	3 c = 6.75E+5 N/m²
ft = 1.9E+5 N/m²	0.25 ft = 3.75E+4 N/m²	0.50 ft = 7.5E+4 N/m²	2 ft = 3E+5 N/m²	3 ft = 4.5E+5 N/m²
fr = 33°	fr = 23°	fr = 28°	fr = 38°	fr = 43°

The following sections present an overview of the results related to the material parametric study in drystone masonry wall and regular stone masonry wall. For each mechanical property variation, a graph is reported that compares the load-displacement curves resulted from the numerical simulations. Additionally, the results are also assessed in terms of damage patterns. To this end, it is important to point out that all the images showing damage patterns refer to the same displacement level (40 mm), which has been assumed as a reasonable threshold for the collapse of the walls, according also to the outcomes in terms of limit states definition proposed in experimental out-of-plane tests on similar wall typologies [101].

The load-displacement curves herein presented are characterized by a linear elastic behaviour up to the peak load, after which the displacement level increases significantly even for lower load levels. After reaching the maximum out-of-plane capacity, the wall shows a residual structural strength up to the threshold previously mentioned (40 mm).

Once exceeded the threshold, the physical meaning of the information associated to the capacity curves is no longer reliable since it is mostly the representation of the behaviour of the centroid of the stone unit considered as a control point in the pushover analysis. Hence, the global behaviour of the walls is difficult to capture.

In general, it is possible to identify a first change of inclination in the elastic branch corresponding to the end of the linear behaviour also associated to the occurrence of the first crack in the wall.

With regard to the peak load, it has been assumed as the point corresponding to a second change of the slope in the pushover curves usually corresponding to the beginning of the branch showing a trend closer to a plateau-like behaviour.

4.2.1 Drystone masonry wall (DS) main outcomes

The main outcomes regarding the numerical parametric study on material properties variation in the drystone masonry wall (DS) are shown from Figure 4.1 to Figure 4.5.

Figure 4.1 shows the results regarding joint normal stiffness variation. Lower joint normal stiffness values (0.2kn and 0.5kn) led to Load-Displacement curves with an evident decreasing trend in terms of maximum out-of-plane capacity. Conversely, the increase of normal stiffness results in a growth of the peak load.

Curves obtained with the highest values of joint normal stiffness, namely 2kn and 3kn, show higher global stiffness (steeper slope), while the opposite trend is visible for curves obtained with the lowest values, namely 0.25kn and 0.5kn.

Moreover, the percentage variation in terms of peak load is higher when 3kn curve is compared to the reference curve (2.7 kN vs 3.2 kN), corresponding to 17% variation. When the joint normal stiffness value is twice the reference normal stiffness, the variation of peak load is lower (2.7 kN vs 3kN), corresponding to a variation of 11%. The damage pattern is similar in all the models, with higher displacement values concentrated where the bond pattern is more irregular, hence providing a poor interlock.

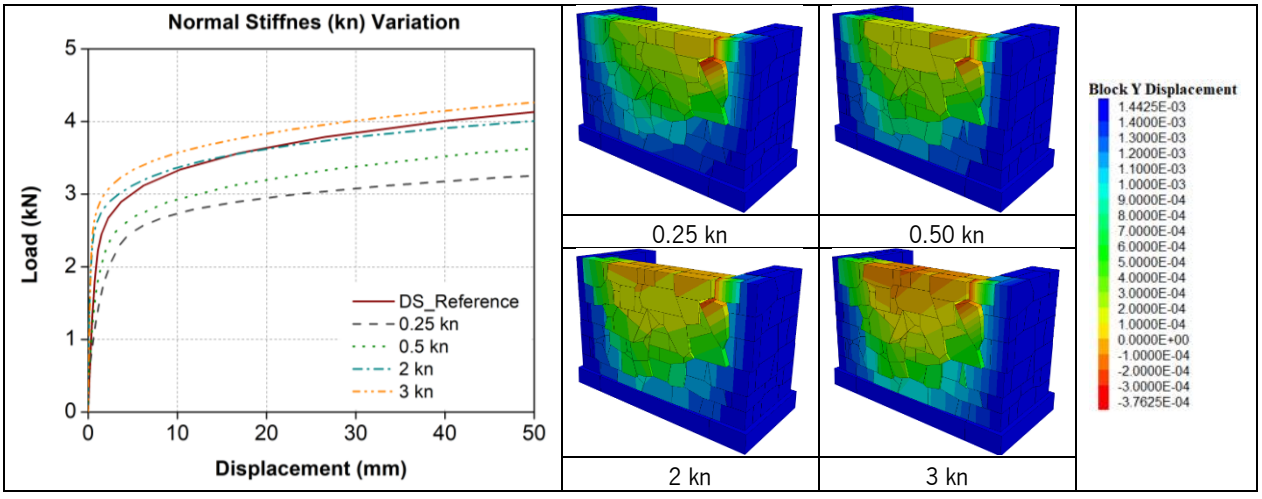


Figure 4.1 – Normal stiffness variation drystone masonry wall (DS).

The variation of joint shear stiffness does not affect the initial slope of the elastic branch, see Figure 4.2. The peak loads in all the curves appear to be slightly lower than the reference curve. However, it is clearly visible that any changes in ks values do not significantly affect the overall load capacity. From a strictly numerical standpoint, a possible explanation can be related to the formulation of the Mohr-Coulomb model applied to simulate the contact surfaces among stone units, which estimates the peak strength in the joint based on the contribution of cohesion, normal stress, and friction angle (see also equation 22 in Chapter 3). The final damage patterns appear to be similar in all the models considered.

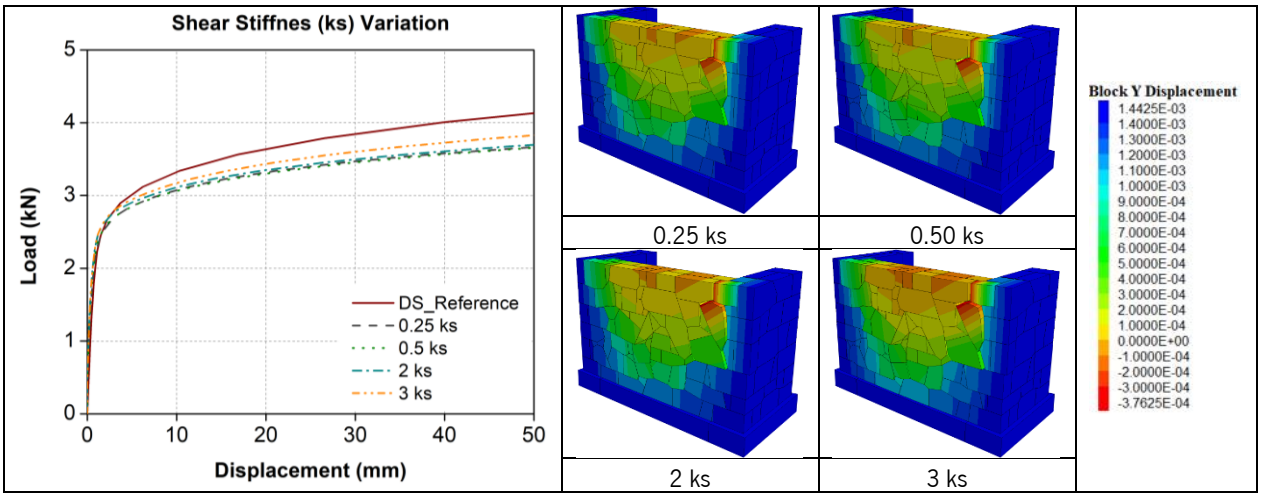


Figure 4.2 – Shear stiffness variation drystone masonry wall (DS).

Increasing the joint shear cohesion results in a significant increase of the peak load. In all the models considered, the damage pattern consists in an overturning of the façade. For lower values of cohesion, the overturning mostly affects the upper part of the façade, whereas when the cohesion increases (c = 1.26 MPa and c = 1.76 MPa), the damage mechanism appears to be more extended and the monolithic behaviour more evident, gradually involving more the transversal walls.

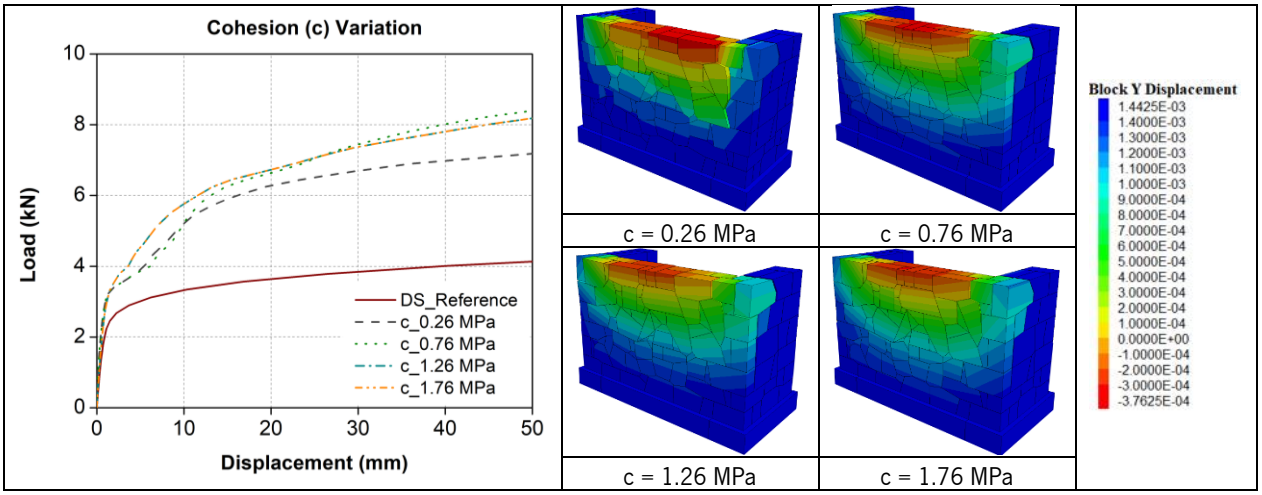


Figure 4.3 – Cohesion variation drystone masonry wall (DS).

Adding tensile strength to the joints results in a slight decrease of the post-peak branch, whereas the elastic behaviour up to the peak load appears to be substantially unaltered for all the set of models. The collapse mechanism consisting in an overturning of the façade is essentially similar in all the models.

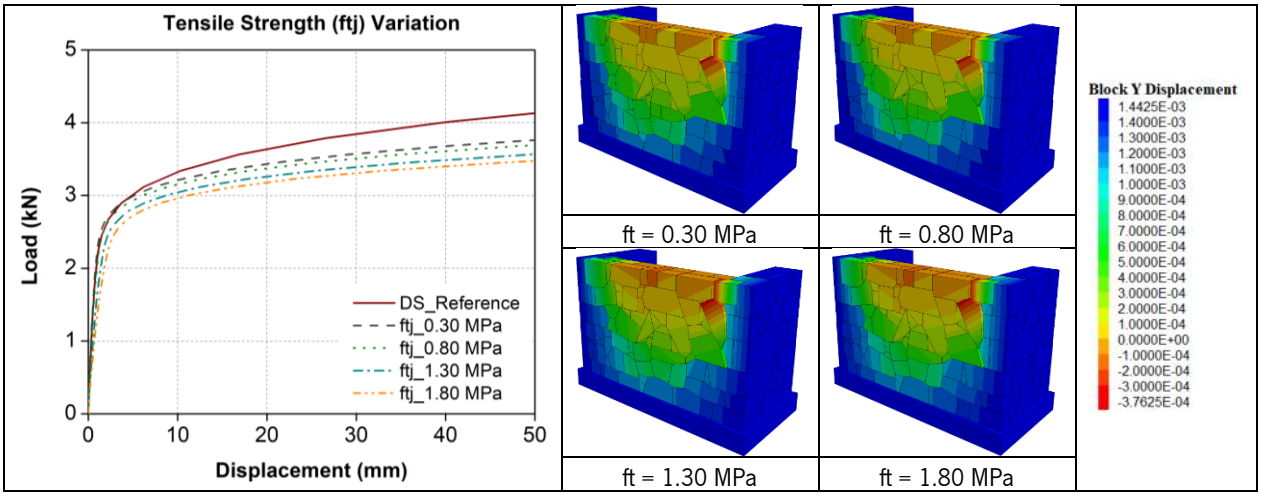


Figure 4.4 – Tensile strength variation drystone masonry wall (DS).

The friction angle significantly affects both the out-of-plane resistance of the wall and the overall damage mechanism. This trend is in agreement with the formulation proposed in 3DEC for the resistance of the joints, as the peak load depends on cohesion, normal tension, and friction angle (see equation 22 in Chapter 3). The prevailing collapse mechanism is the overturning of the façade, which appears to be concentrated in the upper part of the wall for higher friction angle values (25° and 30°). In all cases, increasing friction angle

improves the monolithic behaviour of the wall by involving the transversal wall (particularly the right wall). The irregularity of the masonry bond may affect the distribution of the load applied to the lateral walls resulting in asymmetric displacement maps.

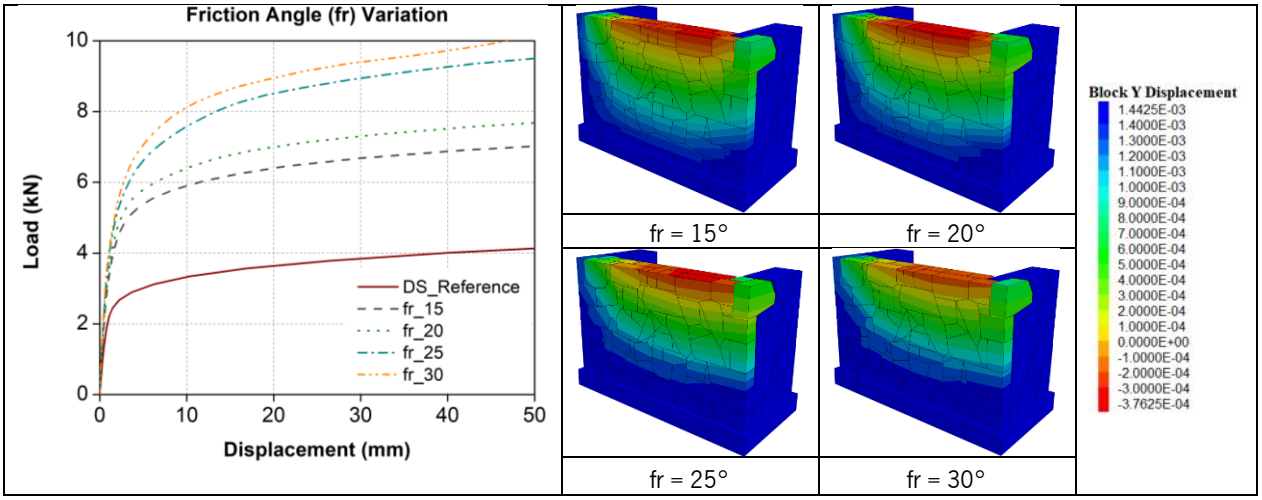


Figure 4.5 – Friction angle variation drystone masonry wall (DS).

4.2.2 Regular stone masonry wall (REGW) main outcomes

The main outcomes regarding the numerical parametric study involving material properties variation in the regular stone masonry wall (REGW) are highlighted from Figure 4.6 to Figure 4.10.

The highest values of joint normal stiffness correspond to an increase of the inclination of the slope in the elastic branch of the force-displacement curve ranging from 5 to 10% when compared with the reference model. Regarding the peak load, the prevailing trend shows higher loads for lower joint normal stiffness, namely 0.25kn and 0.5kn curves. Overall, the peak load values experience a gradual reduction corresponding to progressively increasing kn values. Indeed, the force-displacement curves obtained in the models 2kn and 3kn show the lowest peak load, 39.76 kN and 38.98 kN respectively corresponding to a 10% and a 12% reduction compared to the reference model (peak load equal to 43.66 kN).

Numerically speaking the normal stiffness contribution for the peak load lies in the computation of the normal stress, given by the product of joint normal stiffness and normal displacements (equation 21, Chapter 3). Lower values of joint normal stiffness results in higher levels of displacement. Conversely, in the case of stiffer models, the displacement capability is constrained and the normal stress contribution to the final peak load may be consequently reduced. The overturning of the façade is the prevailing failure mechanism. It is

observed that the wall models having higher values of normal stiffness present a failure mechanism involving the simultaneous collapse/overturning of the façade and of a portion of lateral wall.

For lower joint normal stiffness values, the prevailing mechanism is a simple overturning of the upper part of the façade. Overall, it appears that for higher joint normal stiffness values the damage pattern affects smaller portions of the wall, this phenomenon may affect the final peak load attained in the stiffer models.

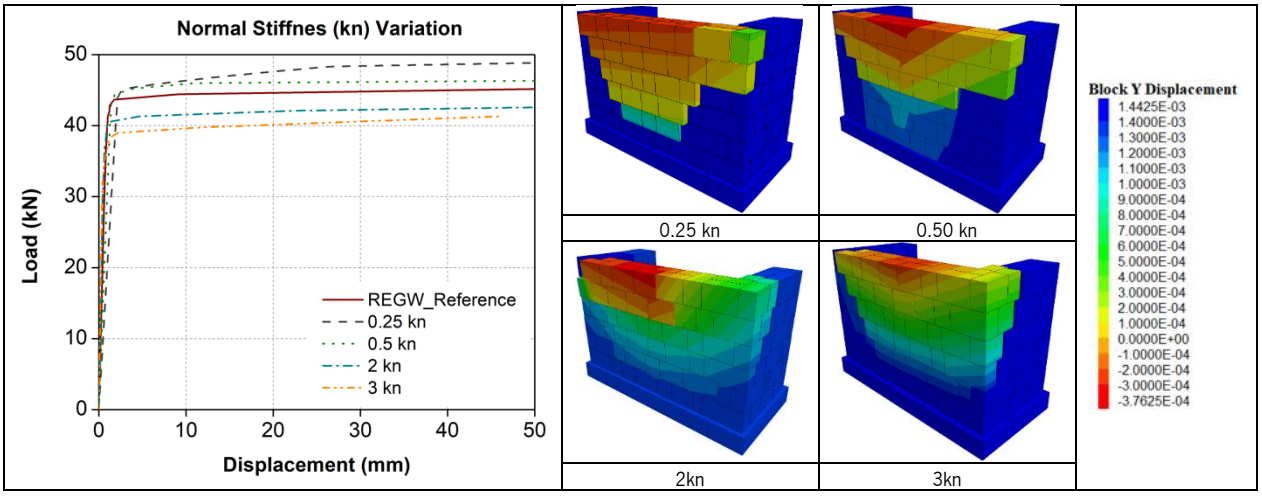


Figure 4.6 – Normal stiffness variation regular stone masonry wall (REGW).

Lower values of joint shear strength are associated with lower peak loads. Shear strength in regular walls models shows a more important contribution also in terms of damage pattern which seems to be more significantly affected by the stiffness variation compared to the drystone wall models. Similarities can be found in the damage pattern, which is mostly governed by the overturning of larger portions of the façade for progressively increasing shear stiffness. For lower joint shear stiffness values, the damage mechanism is quite extended and also involves the lateral walls. in case of the wall model corresponding to 0.5ks, the mechanism is not only overturning, but also flexural failure also develops in the central part of the façade.

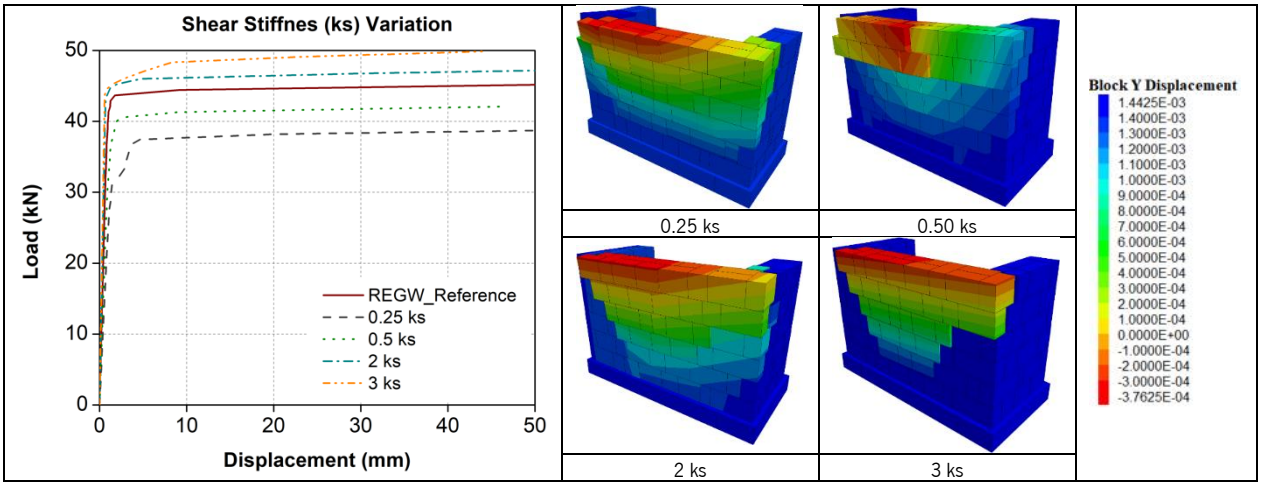


Figure 4.7 – Shear stiffness variation regular stone masonry wall (REGW).

Variations on the cohesion appear to have a significant influence on the post-peak behaviour. Low values of cohesion lead to a significant decrease of the peak load, namely by 70% (13.03 kN) and 34% (29.06 kN) in models 0.25c curve and 0.5c respectively, when compared to the reference model (43.66 kN).

The collapse mechanism is common for all models and consists of the overturning of the façade combined with a flexural failure (horizontal bending). Low values of cohesion correspond to a more extended portion of the façade involved in the overturning mechanism. The contribution of the transversal walls for the failure pattern increases and the cohesion increases and the 3c model displays a rocking behaviour of the whole wall.

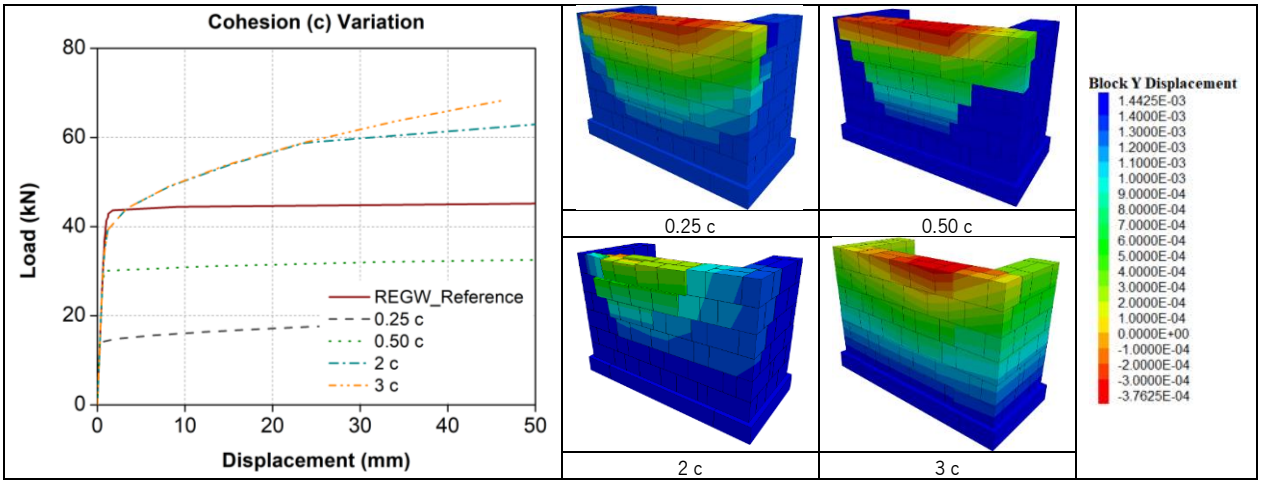


Figure 4.8 – Cohesion variation regular stone masonry wall (REGW).

In 3DEC software, the tensile strength sets the threshold after which the elastic behaviour ends, and the tensile failure occurs. Therefore, it is expected that higher values of tensile strength lead to higher out-of-plane loads. The load-displacement curves obtained for the highest tensile strength do not show any significant difference both in terms of elastic behaviour and post-peak behaviour. The peak load attained is similar (approximately 55 kN) and is about 21% higher with respect to the reference value (43.66 kN).

On the other hand, values of the tensile strength lower than the reference value results in a decrease of about 81% (0.25ft) and a 36% decrease (0.5ft) of peak load compared to the reference peak load (43.66 kN). The collapse mechanism is similar for all models (overturning of a portion of façade). In this case, the overturning of the façade is mainly concentrated in its upper part, whereas the opposite trend is detectable when the tensile strength value increases. The asymmetry characterising the displacement distribution may be connected to the arrangement of the stone units in the areas or portion of lateral walls where the vertical load is applied.

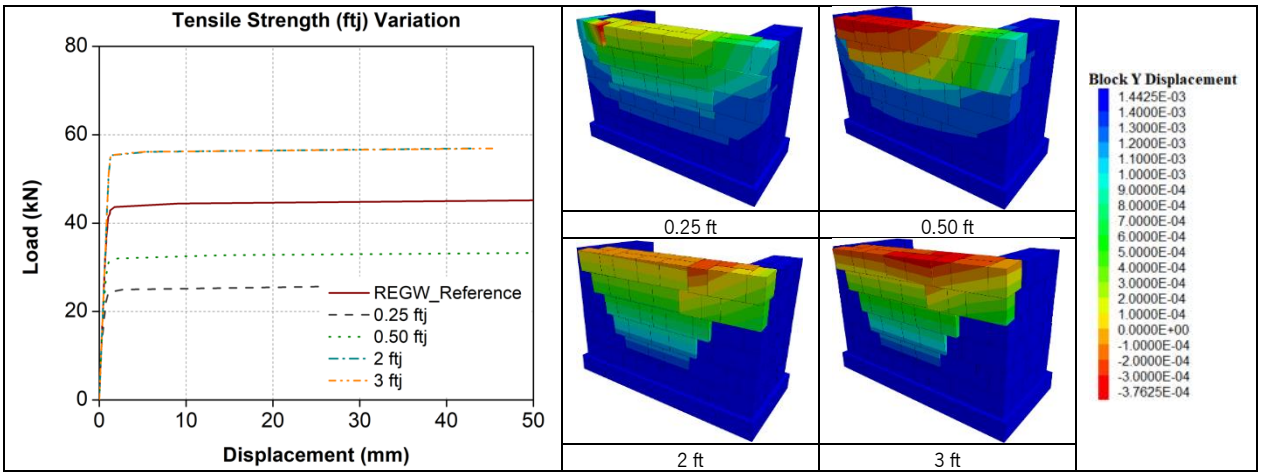


Figure 4.9 – Tensile strength variation regular stone masonry wall (REGW).

The variation of friction angle values does not result in a significant change in terms of elastic behaviour, peak-load attained and post-peak behaviour. This trend is opposite in the drystone wall in which friction angle variation is highly influential due to the null contribution of cohesion and tensile strength implying that the behaviour of the models is strongly governed by the sole mechanical parameter different from zero. Looking at the mathematical formulation to calculate the peak load in 3DEC software summarized in Chapter 3 (e.g. equation 22), it is clear that the friction angle value predominantly affects the capacity of a model in which cohesion and tensile strength are set equal to zero.

On the other hand, differences are noteworthy in terms of damage patterns. The models having friction angle equal to 23° and 28° showed a similar asymmetric collapse mechanism characterized by the sliding of the upper right portion of the façade. For higher friction angle values, namely 38° and 43°, the collapse mechanism is characterized by an overturning of the façade and of a portion of lateral wall.

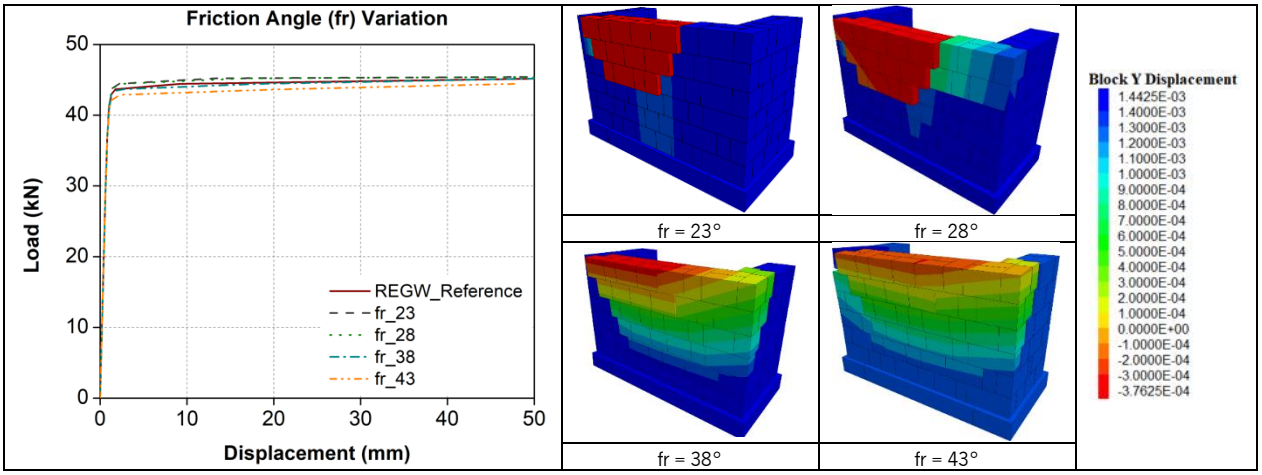


Figure 4.10 – Friction angle variation regular stone masonry wall (REGW).

4.2.3 Main conclusions

The following conclusions can be withdrawn from the material parametric analysis of the drystone wall (DS):

- The overall stiffness of the model is strongly influenced by the variation in the joint normal Stiffness (k_n), whereas joint shear stiffness (k_s) appears to have less influence on the overall behaviour of the wall. Higher normal stiffness leads to a higher peak-load. When k_n decreases, the peak-load and the slope of the elastic branch in the load-displacement curves decrease accordingly. This trend is in agreement with the formulation proposed in 3DEC software since peak load estimation depends on cohesion, normal stress and friction angle contribution (equation 22, Chapter 3). For the same reason, cohesion and friction angle increments lead to higher peak-loads. Tensile strength and shear stiffness mostly affect the post-peak behaviour of the models. Their influence on the initial stiffness and on the peak-load is negligible. This trend is also related to the specific formulation used in 3DEC software and briefly summarized in Section 3.4.
- The governing collapse mechanism is the overturning of the façade. Changes may occur in the portion of the façade affected by the mechanism itself. The parameters that have the most significant influence on the final mechanism are cohesion and friction angle. Their increase resulted in a

progressively better connection between façade wall and perpendicular walls, contributing to the monolithic behaviour of the model. Conversely, low values of cohesion and friction angle generate overturning mechanisms involving a reduced portion of façade (mostly in the upper part).

With respect to regular wall (REGW), it is possible to conclude:

- Firstly, progressively increasing values of the joint normal stiffness corresponds to a gradual decrease in the peak load attained by the models, which is the opposite of what is observed in the drystone (DS) masonry wall. Peak load in 3DEC is estimated based on joints cohesion, friction angle, and normal stress values. In the DS wall, the contribution of cohesion was null (cohesion equal to zero) and consequently, normal stress had a predominant role in peak load computation. On the other hand, in REGW wall, the combination of increased stiffness and low displacement levels attained due to stiffer interfaces may have led to a reduction of the maximum load capacity. Regarding joint shear stiffness variation, it is observed a reduction of peak load for lower values of joint shear stiffness ks.
- In terms of peak load, cohesion and tensile strength proved to have the most significant influence on the out-of-plane load capacity. Conversely, the variation of friction angle did not significantly affect the maximum load of the REGW models.
- The prevailing collapse mechanism in REGW consists in an overturning of the façade. This mechanism involves a reduced portion of façade when lower values of normal/shear stiffness, cohesion and friction angle have been adopted, whereas the monolithic behaviour of the wall turned out to be more evident for higher values of the parameters considered, especially when the increment was applied to cohesion and friction angle values.

4.3 Parametric study on geometrical characteristics

The second part of the parametric study carried out focuses on the assessment of the influence of a selected set of geometrical parameters in the out-of-plane performance of 2-leaf stone masonry walls. The reference wall considered in this study is the regular stone masonry wall (REGW) calibrated in Chapter 3. Due to the characteristics of its masonry bond (regular stone units), it was deemed easier to define different geometrical 3D models having at the same time, the possibility to optimize the masonry bond generation.

All the models have been generated by means of a 3D CAD software (Rhinoceros), later imported in 3DEC software, which is the software selected to carry out the parametric study. The numerical analyses performed

present the same settings and characteristics of the analyses carried out in Section 3.2 for the parametric study on mechanical properties in both drystone (DS) and regular stone masonry wall (REGW).

Once again, a series of pushover analyses have been performed with incremental application of a uniformly distributed horizontal load in the rear surface of the frontal wall. Each analysis is considered completed when approaching the displacement level attained in the experimental test (assumed as a conventional state of collapse of the tested wall, see Chapter 3). From a mechanical standpoint, all the models present the same mechanical properties, which are those resulted from the calibration procedure described in Chapter 3 (Table 3.7). The unique difference among the models is represented by the variation on bond configurations.

4.3.1 Definition of geometrical variations

The criterion applied in the variation of the masonry bond features is based on the guidelines of the Masonry Quality Index (MQ). This method enables to estimate the mechanical properties of masonry panels based on a hybrid approach, considering qualitative and quantitative geometric parameters characterising the masonry bond pattern [41]. The estimation of the MQI consists of assigning specific values to a selected set of parameters based on the presence or absence of certain conditions. The parameters considered in the study are the following: (1) wall connection (WC); (2) horizontal joints configuration (HJ); and (3) vertical joints configuration (VJ). These parameters may satisfy or not the requirement listed in MQI application guidelines, being its variation associated to different masonry bonds. Based on these assumptions, different models have been generated based on these assumptions. For WC parameter, the fulfilled (F) condition is reached when 2 through-stone for each masonry course are present in the wall. In the partially fulfilled condition (PF) the number of through stones is reduced by 50%. When WC is not fulfilled no through-stones exist in the wall (see Figure 4.11 in which the through-stones are higlited in grey colour).

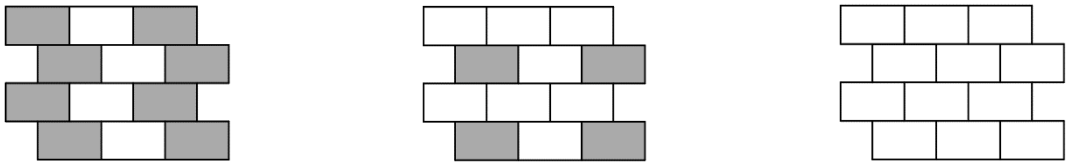


Figure 4.11 – Variation of the masonry bond based on WC parameter (through-stones marked in grey).

According to MQI guidelines, horizontal joint configuration (HJ) is fulfilled (F) when the joints are perfectly aligned showing continuity throughout the whole masonry panel. Starting from this assumption, the partially

fulfilled condition (PF) has been simulated by interrupting the continuity of the joints in 50% of the masonry courses present in the masonry wall, whereas the non-fulfilled (NF) condition consists in the absence of continuity in all the horizontal joints (Figure 4.12).

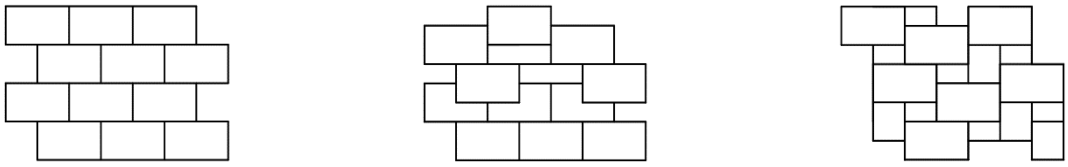


Figure 4.12 – Masonry bond definition for HJ parameter.

The vertical joint configuration (VJ) parameter is fulfilled (F) when vertical joints are perfectly staggered, improving the interlocking of the masonry panel. The partially fulfilled condition (PF), foresee the presence of aligned vertical joints for 50% of the masonry courses present in the masonry; the non-fulfilled condition (NF) is characterized by fully aligned vertical joints with no interlock throughout the masonry panel (Figure 4.13).

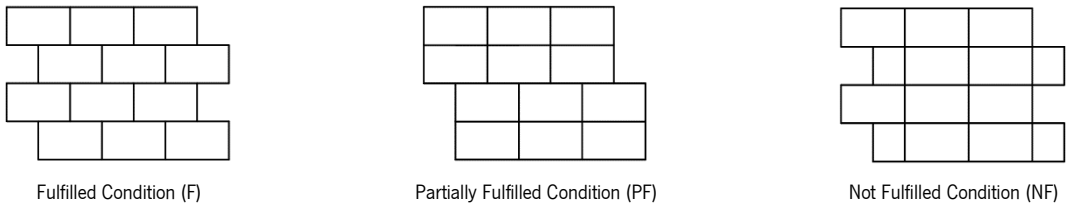


Figure 4.13 – Masonry bond configuration for VJ parameter.

Each 3D model used in this study presents a MQI value which has been determined based on the coefficients provided in the literature (see Table 4.2). The red bold parameters have been varied in order to perform the parametric study, whereas the remaining parameters have been assumed to be constant and associated to a fulfilled condition.

Table 4.2 – Masonry Quality Index coefficients for out-of-plane actions (adapted from [41]).

	NF	PF	F
SM	0.5	0.7	1
SD	0	0.5	1
SS	0	1	2
WC	**0**	**1.5**	**3**
HJ	**0**	**1**	**2**
VJ	**0**	**0.5**	**1**
MM	0	0.5	1

It is worth pointing out that this study only aims to estimate the influence of the masonry bond geometrical configuration in the out-of-plane behaviour of 2-leaf stone masonry walls with regularly cut masonry units. Therefore, the parameters associated to the conservation state of masonry units (SM), to the masonry units' shape (SS) and to the dimensions (SD), as well as the mortar mechanical properties (MM), are considered to be fulfilled for all models [41].

Additionally, the corner configuration has been also considered in the study. For this, two different scenarios (C1 and C2) have been analyzed replicating a good corner interlock (Figure 4.14a and b) and an ineffective corner interlock (Figure 4.14c and d).

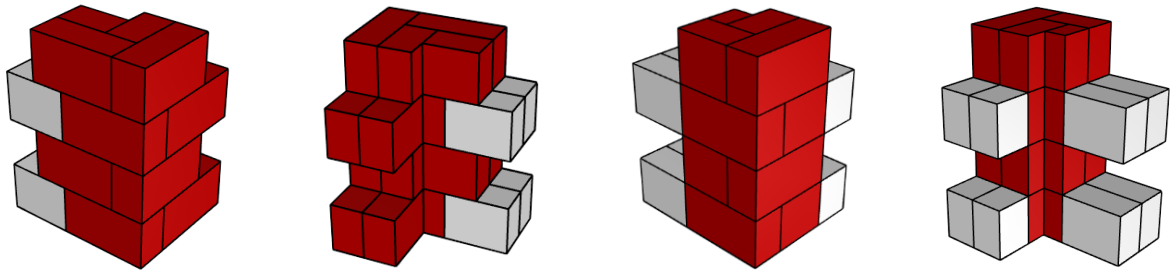


Figure 4.14 – Different corner configuration: C1 front view (a) and rear view (b), C2 front view (c) and rear view (d).

Finally, the latter aspect to be assessed is the leaves' configuration and how their interaction affects the out-of-plane performance of the models. In this case, models have been generated with: (a) two perfectly overlapped leaves; and (b) two staggered leaves. The application of the aforementioned masonry bond variations led to the definition of 108 models divided into 4 sets of 27 models each (Figure 4.15):

- Set 1 (S1), models with good corner interlock and perfectly overlapped leaves.

- Set 2 (S2), models with good corner interlock and staggered leaves.
- Set 3 (S3), models with ineffective corner interlock and perfectly overlapped leaves.
- Set 4 (S4), models with ineffective corner interlock and staggered leaves.

For the sake of conciseness, Figure 4.15 shows the characteristics of the reference model for each of the sets considered, namely through a plan and a 3D view. Corner stones are highlighted with red colour, through-stones are highlighted in green colour. Finally, a complete list of the models in a 3D configuration is presented in Annex 2 – Geometrical parametric study on reduced scale numerical models of 2-leaf stone masonry walls together with the corresponding Masonry Quality Index and geometric parameters defining the masonry bond variation.

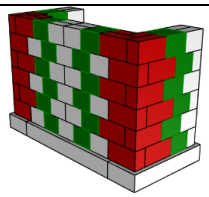
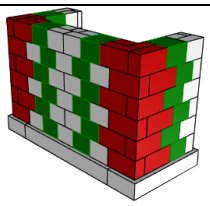
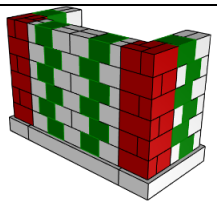
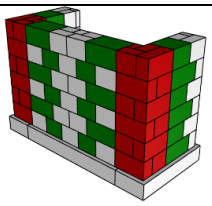
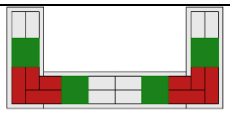
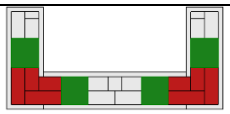
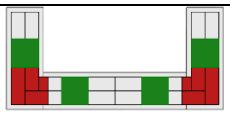
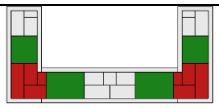
S1 Reference Model	**S2 Reference Model**	**S3 Reference Model**	**S4 Reference Model**
			
a	b	c	d
			
e	f	g	h

Figure 4.15 – Reference models 3D views for Set 1 (a), Set 2 (b), Set 3 (c) and Set 4 (d); reference models plan view for Set 1 (e), Set 2 (f), Set 3 (g), Set 4 (h).

4.3.2 Analysis of results

Figure 4.16 shows the force-displacement diagrams obtained from the parametric study for each set of models under analysis. Overall, Set 1 and Set 2 models highlight a better performance compared to Set 3 and Set 4 numerical models. The variation of corner configuration plays a key role in the out-of-plane capacity of the models. In general, a better corner interlock corresponds to higher peak loads and this aspect seems to have higher influence on the final performance of the wall than the leaf configuration (staggered vs overlapped leaves).

Looking at the groups of graphs (Set 1 and Set 2) with similar corner configurations (good interlocking) and different leaf configurations, it appears that the overall out-of-plane capacity in terms of peak load is not significantly affected by the presence or absence of staggered leaves. Moreover, although staggered leaves

may result in a more effective monolithic behaviour of the models, the final damage pattern does not seem to be significantly affected by this aspect.

Conversely, in the condition of ineffective corner interlock, the staggered leave configuration enhances the out-of-plane capacity, with an increasing trend in terms of peak (comparison between Set 3 and Set 4). However, as it will be pointed out in the following sections the staggered configuration of the leaves does not significantly govern the final damage pattern resulting from the analysis of the models in all the Sets of models considered.

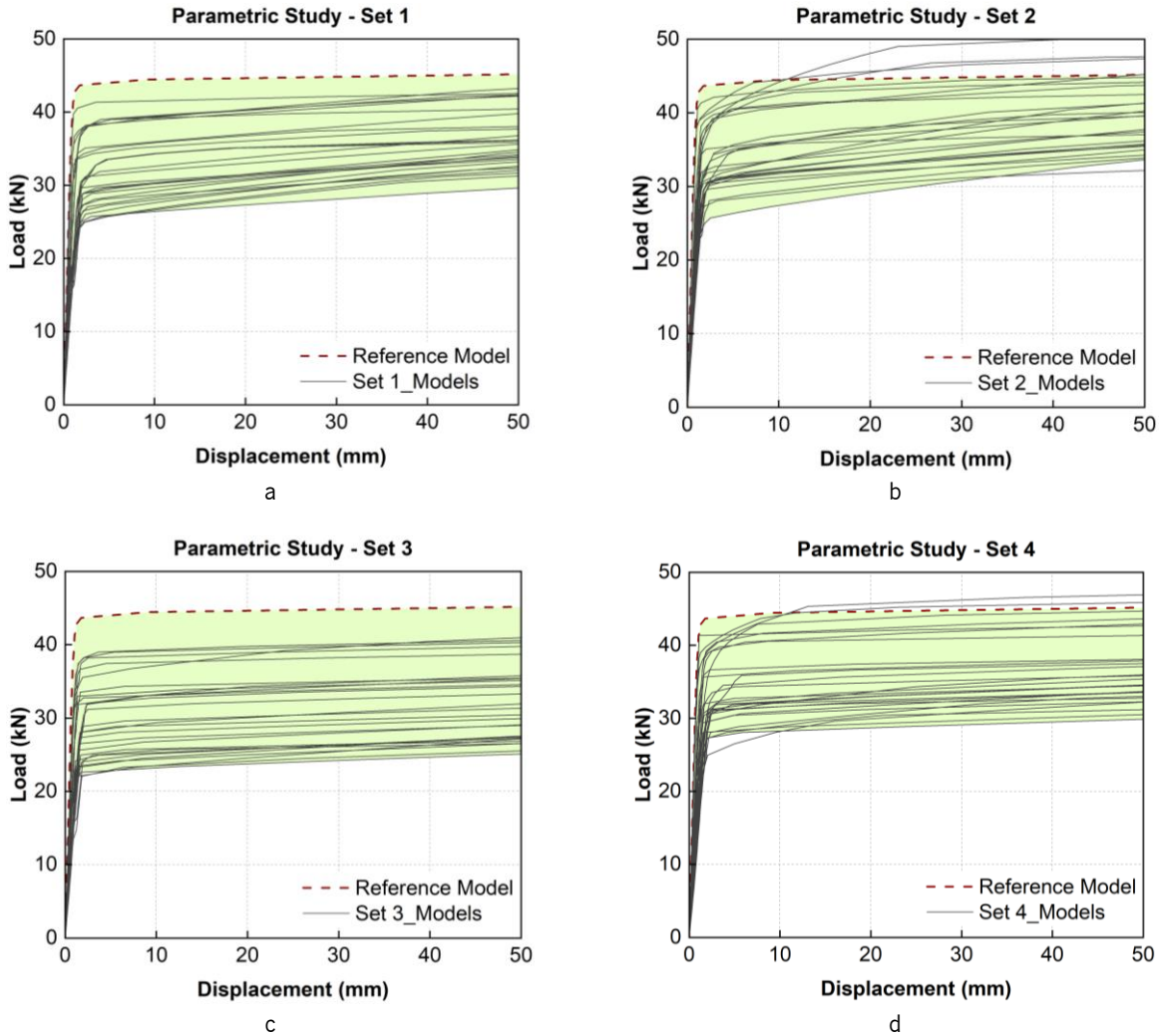


Figure 4.16 – Geometrical parametric study final load-displacement curves in Set 1 (a), Set 2 (b), Set 3 (c) and Set 4 (d).

Additional considerations regarding the main outcomes of the parametric study are presented in the following sections. In order to facilitate a clear interpretation of the results, grasping the most significant trends arisen from the study, the load-displacement curves of each set of models will be presented in smaller groups in

order to enable a focus on the analysis of one parameter at a time, among those selected as the most influential for the definition of out-of-plane capacity in stone masonry walls.

Taking into account that the masonry bond mostly depends on wall connection (WC), horizontal joints configuration (HJ), and vertical joints configuration (VJ), the criterion applied to effectively represent the results envisages the use of graphs in which two of the parameters are constant in their condition, namely fulfilled (F), partially fulfilled (PF) or not fulfilled (NF), whereas just one of them varies from a fulfilled condition to a not fulfilled condition. In all the graphs presented, the curves are reported using different colours following a decreasing order based on the MQI values, ranging from a grey dashed line (higher value) to a pink dashed line (lower value).

This strategy is applied in each set of models ensuring the control of the corner and leaves configuration, keeping them constant according to the features of the set of models analyzed.

Finally, each figure will present 4 load-displacement curves, one of them will always refer to the regular stone masonry wall (REGW) calibrated in Chapter 3, whereas the remaining curves refer to the numerical models of the geometrical study classified following the criteria mentioned before.

4.3.2.1 Analysis of Set 1

Figure 4.17 shows the variation of the structural behaviour in terms of force-displacement diagrams and displacement field for the models with different configuration of vertical joint parameter (VJ), when the wall connection and horizontal joint parameters are kept fulfilled (Figure 4.17a), partially fulfilled (Figure 4.17e) and not fulfilled (Figure 4.17i).

When VJ is fulfilled (Figure 4.17b - M1) or partially fulfilled (Figure 4.17c - M2) the collapse of the wall consists in an overturning of the upper part of the façade. Conversely, when VJ is not fulfilled (Figure 4.17d - M3) the overturning occurs from a central crack along the vertical plane developed due to the lack of a staggered alignment and effective interlock among the vertical joints. Peak loads decrease according to the reduction of MQI and with the presence or absence of properly arranged vertical joints (Figure 4.17a). However, the lowest load is attained in M2, in which the vertical arrangement is partially fulfilled. This vertical arrangement condition may probably lead to the definition of a weaker masonry bond despite in this case the MQI index is higher than the one obtained in M3 model. Indeed, this is one of the main drawbacks detected during the 3D generation of masonry bonds for the study carried out.

Figure 4.17e shows a similar trend for the reduction of the out-of-plane peak load with the decrease of the MQI reflecting the progressive condition of parameters partially fulfilled and not fulfilled, namely by the

presence or absence of properly arranged vertical joints. Collapse mechanisms mainly consist of the overturning of the upper part of the façade (Figure 4.17f-g) and, when VJ is not fulfilled, a greater portion of the main façade, as well as part of the lateral walls are also involved (Figure 4.17h).

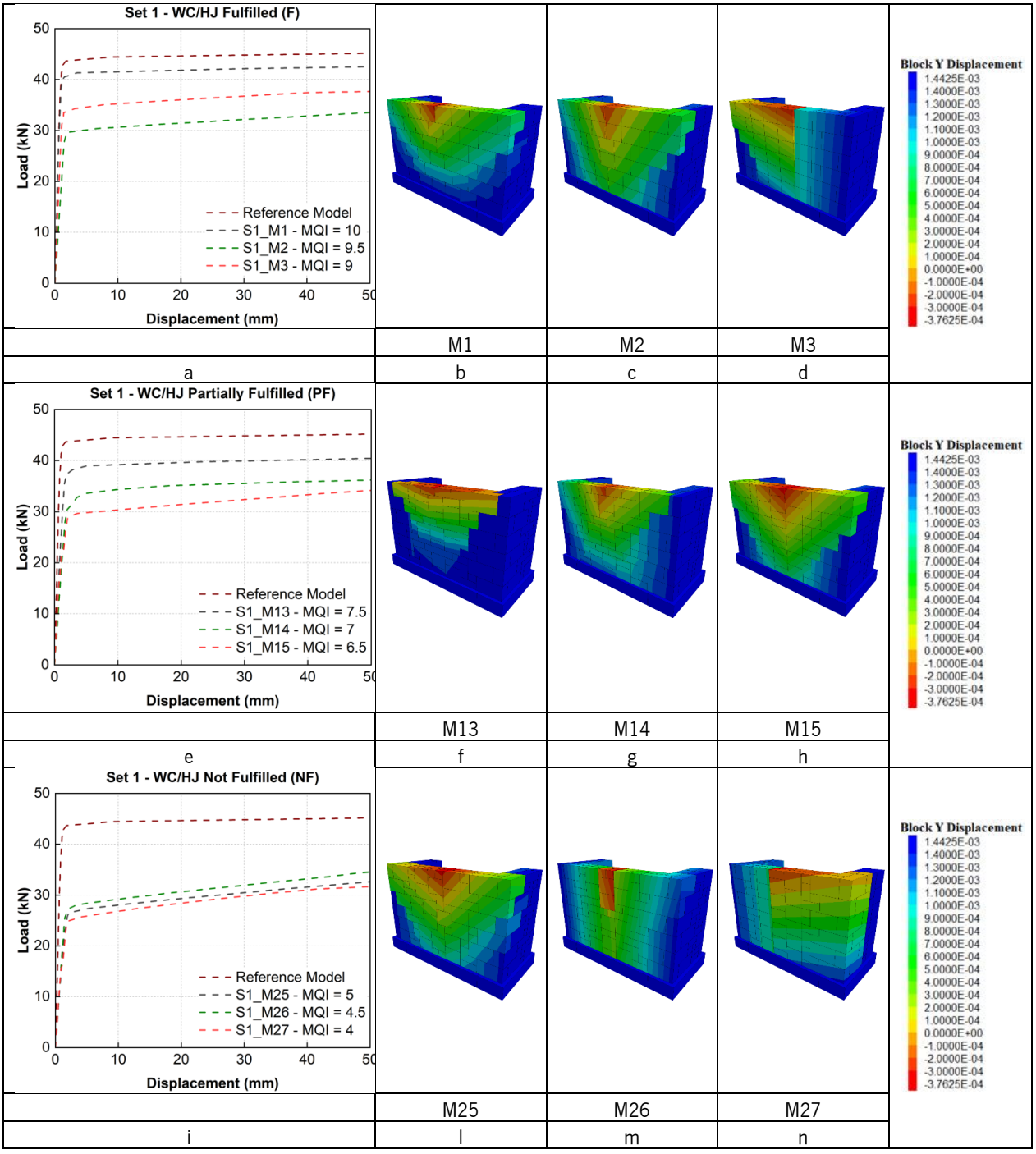


Figure 4.17 – Set 1 variation in vertical joints (VJ) configuration.

It is interesting to notice that the influence of the different levels of fulfilment of the arrangement of vertical joints in the peak load is lower in case of non-fulfillment of the other geometric parameters (wall leave connection and horizontal joints), see Figure 4.17i. The lowest load is attained in the model M27 (Figure 4.17n), which is the model with the lowest MQI (see Figure 4.17e). The models M25 and M26 have similar curves (Figure 4.17i) and, despite M25 having an MQI higher than M26 (MQI = 5 and MQI = 4.5 respectively), the peak load is slightly higher in the latter. The gradual change in terms of vertical joint configuration results in an evolution of the collapse mechanism which consists in an overturning of the upper façade in M25 (Figure 4.17). But when VJ criterion is partially fulfilled the overturning is combined with the development of a vertical crack along the plane resulting from the lack of staggered arrangement in the vertical joint (Figure 4.17m). Finally, when VJ is not fulfilled a central vertical crack occurs from the top to the bottom of the façade defining a significant portion of the façade itself overturning together with portion of lateral walls (Figure 4.17n).

Figure 4.18 shows the variation of the structural behaviour in the models for different configuration of horizontal joint parameter (HJ) when wall connection (WC) and vertical joint (VJ) parameters varied from fulfilled (Figure 4.18a), partially fulfilled (Figure 4.18e) and not fulfilled arrangement (Figure 4.18i).

When WC and VJ are simultaneously fulfilled (Figure 4.18a-b-c-d), the models highlight similar collapse mechanism (overturning of the upper part of the façade). The difference in terms of peak load in the model M7 compared to the others may be due to the presence of discontinuous horizontal joints that partially affects the vertical joints alignment. Hence, M7 masonry bond presents a lack of vertical joints interlock resulting in a weakening of the wall (Figure 4.18a and Figure 4.18d).

In Figure 4.18e, the parameters WC and VJ are simultaneously partially fulfilled (PF). The model M11 has higher MQI but a slightly lower peak load than the model M14 (see Figure 4.18f and Figure 4.18g respectively). The combination of partially fulfilled condition (PF) in both vertical and horizontal joint configuration appears to generate weaker areas. Indeed, masonry bond in the model M11 is characterized by portion of the façade with aligned vertical joints.

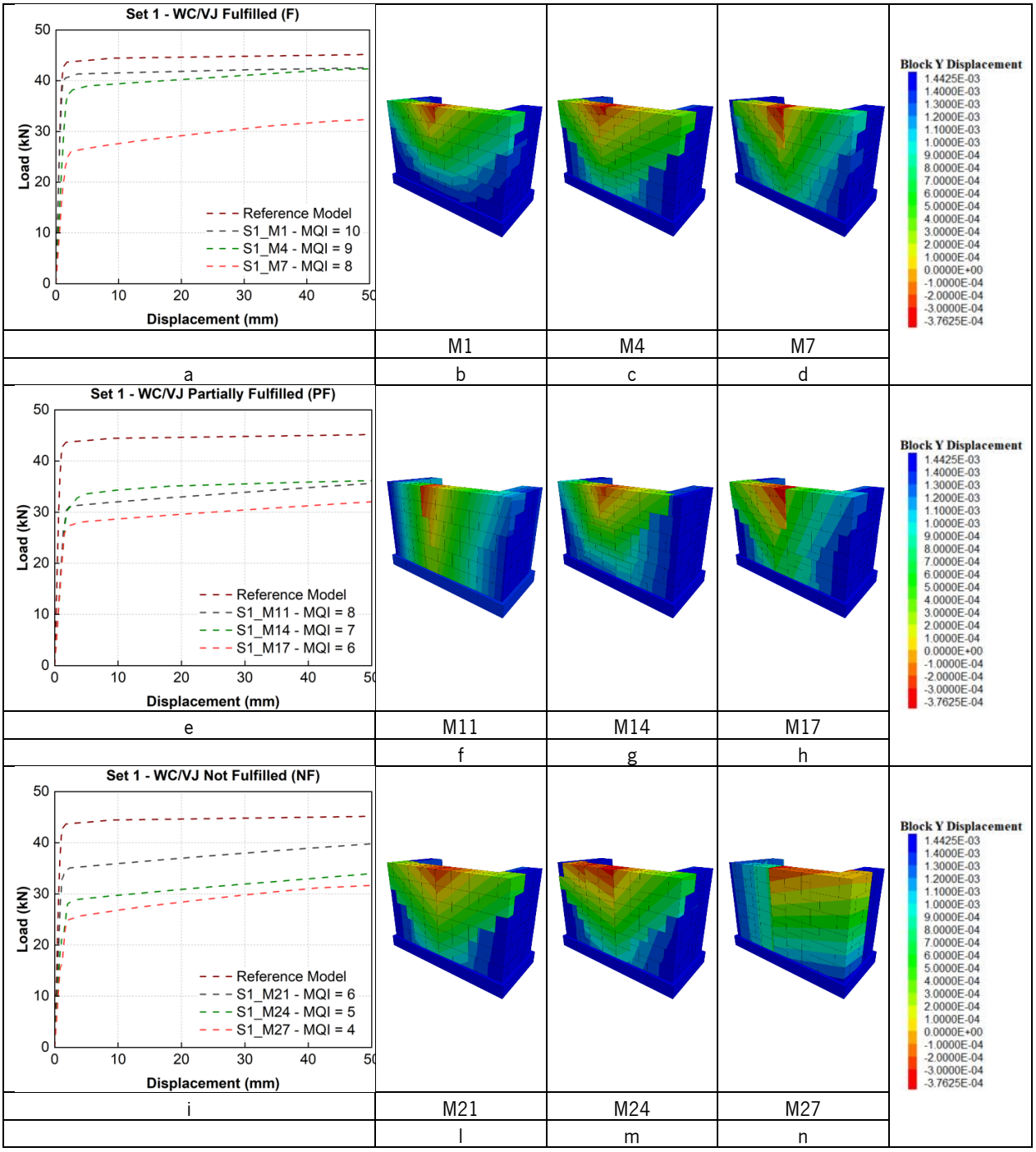


Figure 4.18 – Set 1 variation in horizontal joints (HJ) configuration.

Therefore, the resisting portion of the wall bearing the horizontal out-of-plane load seems to be reduced. In fact, the highest level of displacement in the model M11 is concentrated in the upper part of the façade (last two masonry courses from the top of the wall, see Figure 4.18f). Even if both models M11 and M14 have WC and VJ partially fulfilled, in the model M14 the condition of horizontal joints (HJ) partially fulfilled (PF)

resulted in a sort of interlock effect which improved the performance of the wall (Figure 4.18e and Figure 4.18g). In the model M17 this phenomenon is less evident due to the significant effect that the not fulfillment of VJ (NF) has on the overall performance of the wall (trend already highlighted in the previous models), see Figure 4.18h.

The models M21 and M24 have similar collapse mechanisms, even though the model M24 displays a more evident vertical crack due to the absence of an effective VJ staggered configuration (Figure 4.18l and Figure 4.18m respectively). The crack is much more evident in the model M27 when VJ is not fulfilled (NF), see Figure 4.18n. This configuration results in a different collapse of the wall consisting in an overturning of a portion of façade together with a portion of lateral wall (Figure 4.18n), which is a similar mechanism resulted in other models where VJ is not fulfilled (e.g. Figure 4.17n). Overall, in this group of models, the peak loads decrease according to the reduction of MQI.

Figure 4.19 shows the variation of the structural behaviour in the models for different configuration of wall connection parameter (WC) when horizontal joints (HJ) and vertical joint (VJ) geometric criteria varied from fulfilled (Figure 4.19a), partially fulfilled (Figure 4.19e) and not fulfilled (Figure 4.19i).

Overall, the WC parameter appears not to have a significant influence on the overall performance of the walls, namely when it is partially fulfilled (PF) and not fulfilled (NF), see Figure 4.19b-d. This may be related to the configuration of the leaves of the models, which overlap. Probably, in this scenario the presence of through-stone does not provide a bond between the leaves, it may represent indeed an element of discontinuity in the overall masonry bond arrangement. Peak loads decrease according to the MQI reduction.

Figure 4.19e presents overlapped load-displacement curves for the different WC arrangements with no changes in terms of peak load and damage mechanisms (overturning of the façade, see Figure 4.19f-h). This trend confirms that WC parameter does not significantly affect the performance of the walls either in terms of damage mechanism or in terms of peak load reached. Despite the lowest MQI value, model M23 presents similar performances when compared with model M9 (MQI = 7) and model M18 (MQI = 5.5). From a theoretical point of view models M9, M18 and M27 have different MQI values and it would be expected that they behaved in a different manner, but perfectly overlapping of leaves makes these models essentially equivalent to each other, at least from a numerical point of view (Figure 4.19i).

To this end, it must be mentioned that 3DEC software automatically detects and generates contact interfaces among stone units (blocks), hence also between the leaves, and this could partly justify the better or

equivalent performance of models whit similar masonry bonds differing just for the presence/absence of through-stones.

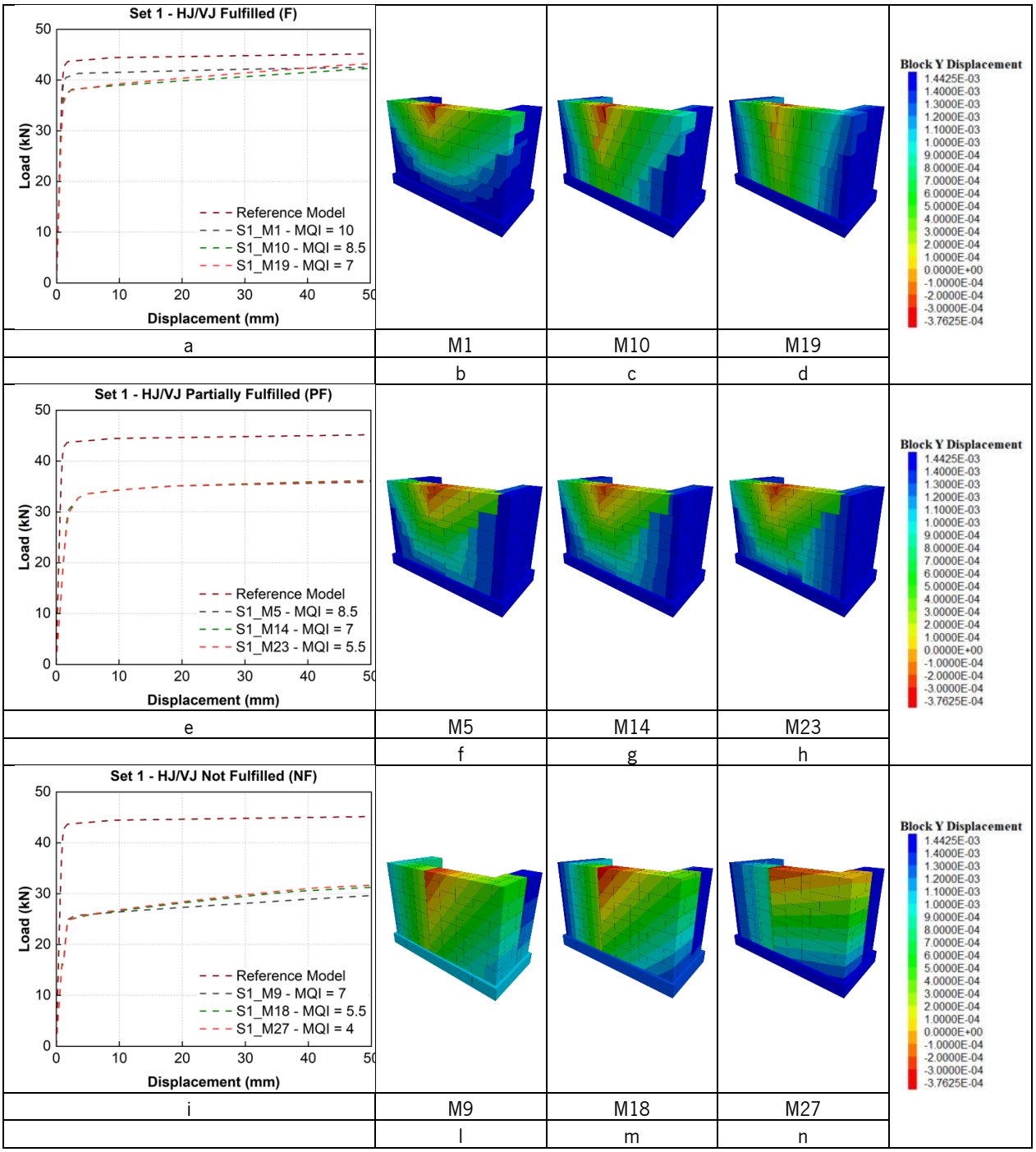


Figure 4.19 – Set 1 variation in wall connection (WC) configuration.

Figure 4.19i shows almost perfectly overlapped load-displacement curves confirming the trend already pointed out. The models have a similar load-displacement curve and damage mechanisms (overturning of

the façade with portion of lateral walls detaching along the fracture plane generated by the presence of aligned vertical joints).

For the types of analyses performed and the initial assumptions considered in this study for the generation of the 3D models of the walls, it was found that the presence or absence of through stones does not significantly affect the peak load and the collapse pattern. In general, horizontal joints (HJ) and vertical joints (VJ) configuration play a more relevant role in the final out-of-plane performance of the models considered, with the latter showing the most significant influence both in term of load capacity and in term of damage mechanisms.

4.3.2.2 Analysis of Set 2

Figure 4.20 shows the variation of the structural behaviour in the models with good corner connections and staggered wall leaves for different configuration of vertical joints configuration (VJ) when according to the MQI calculations, the wall connection (WC) and horizontal joints (HJ) parameters are fulfilled (Figure 4.20a), partially fulfilled (Figure 4.20e) and not fulfilled (Figure 4.20i).

Looking at the first group of models (Figure 4.20a-b-c-d), it is clearly visible that model M1 (VJ fulfilled) attains the highest peak load. Model M3 (Figure 4.20d) has higher peak load than M2 (Figure 4.20c) despite VJ is not fulfilled. This trend may be related to the effectiveness of the staggered leaves configuration obtained in M3 masonry bond. Indeed, M3 has fully aligned vertical joints but the overall structural behaviour benefits from the staggered configuration of external and inner leaves (Figure 4.20d). Conversely, model M2 (Figure 4.20c) shows more discontinuity in the masonry bond due to the presence of masonry units with different sizes and more unevenly arranged. The collapse mechanism consists of an overturning of the upper façade in all three models (Figure 4.20b-d). Additionally, in model M3, when VJ is not fulfilled, a central vertical crack occurs along the separation plane of masonry units (Figure 4.20d).

When HJ and WC are simultaneously partially fulfilled (PF) (Figure 4.20e), the peak load of the models decreases according to the reduction of MQI. The collapse mechanism mainly involves the overturning of the upper part of the façade in both models M13 and M14 (Figure 4.20f - g), whereas in model M15 (VJ not fulfilled) it is possible to notice a vertical crack developing along the façade. The model M13 (with highest MQI) attains the highest peak load (Figure 4.20e - f), whereas models M14 and M15 have almost similar peak loads (Figure 4.20e).

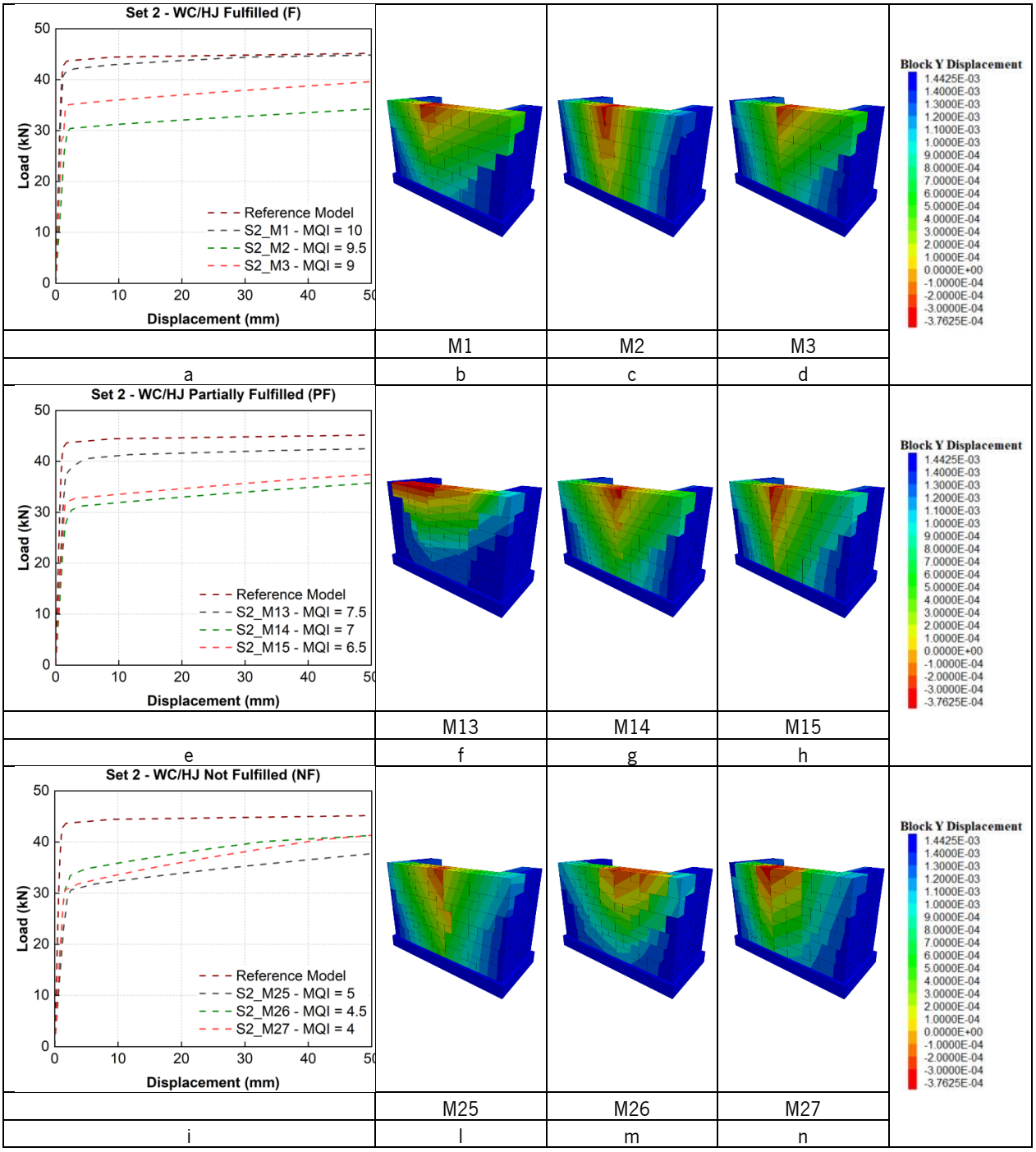


Figure 4.20 – Set 2 variation in vertical joints (VJ) configuration.

Figure 4.20i shows that no considerable differences in terms of peak load were found among the models analyzed (Figure 4.20l - m - n). However, M25 does not present the higher load attained despite having the highest MQI. This can be explained by the localization of a vertical crack at the mid span of the wall.

Models M26 and M27 display a close load-displacement curve (Figure 4.20i). The damage mechanisms are influenced by the configuration of VJ parameter. In the models M25 and M26, the overturning appears to govern the out-of-plane behaviour of the façade (Figure 4.20l and Figure 4.20m respectively). In the model M27, where VJ is not fulfilled (Figure 4.20n), it is possible to notice the development of a local overturning mechanism involving only a portion of façade delimited by the separation planes of the aligned vertical joints (VJ) arranged in order to simulate a not fulfilled condition (NF).

Figure 4.21 shows the variation of the structural behaviour in the models for different configuration of horizontal joint parameter (HJ) when wall connection (WC) and vertical joint (VJ) parameters are fulfilled (Figure 4.21a), partially fulfilled (Figure 4.21e) and not fulfilled (Figure 4.21i). The prevailing collapse mechanism is the overturning of the upper part of the façade. Peak load variation follows the variation of MQI values; hence the highest load corresponds to the highest MQI value (Figure 4.21b - c – d).

In models where the wall connection (WC) and vertical joint (VJ) parameters are partially fulfilled, the peak load is obtained in the model M17, corresponding to the lowest MQI and when HJ is not fulfilled. When HJ is fully and partially fulfilled (Figure 4.21e-h), corresponding to models M11 and M14 respectively, the peak load is very close. The model M11 displays some weaker plans due to its horizontal joints configuration, because in spite of HJ is fulfilled according to the MQI criteria, the combination with WC and VJ partially fulfilled results in a model offering lower performances compared to M17. Having HJ not fulfilled allows to create a bond having a more effective interlocking, resulting in the improvement of the performance of the wall. Models M11 (Figure 4.21f) and M17 (Figure 4.21g) seem to develop some local collapse mechanism, whereas M14 (Figure 4.21h) displays a global overturning of the façade.

Figure 4.21i compares the load-displacement curves of models with VJ and WC not fulfilled (NF). In the case where WC and VJ are not fulfilled, the highest MQI corresponds to the highest load observed (Figure 4.21i). The damage mechanism is similar in M24 and M27 (Figure 4.21m - n), which also have a similar load-displacement curve. The damage pattern is characterized by the overturning of the façade combined with the detachment of a portion delimited by the separation plan defined by aligned vertical joints. M21 shows a more global behaviour consisting in the overturning of the façade (Figure 4.21l).

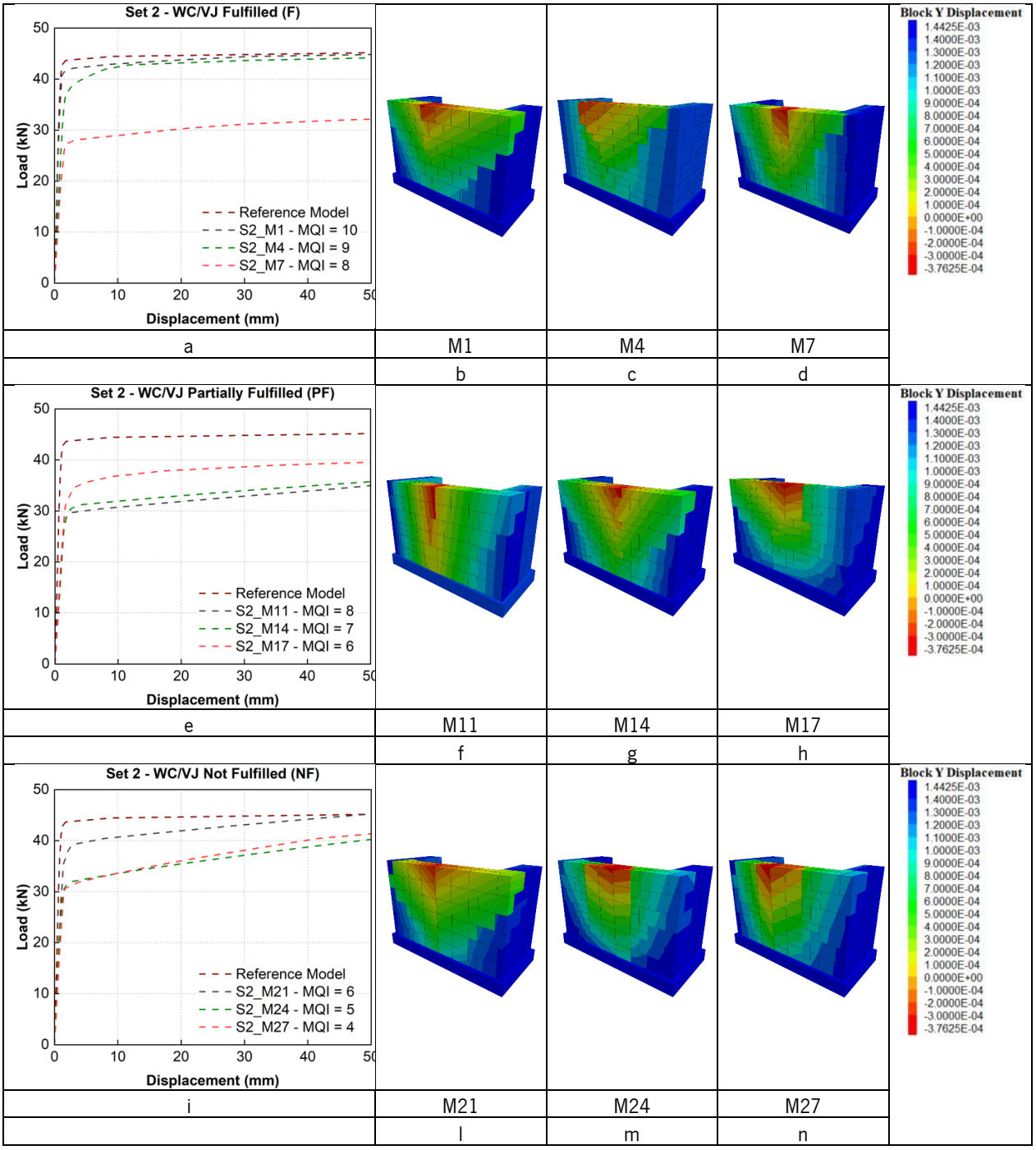


Figure 4.21 – Set 2 variation in horizontal joints (HJ) configuration.

Figure 4.22 shows the trends in the out-of-plane behaviour obtained by varying the fulfillment level of WC for variable HJ and VJ arrangement conditions. It is observed that in case of all parameters are fulfilled, the models display similar peak load and collapse mechanisms, see Figure 4.22b-d.

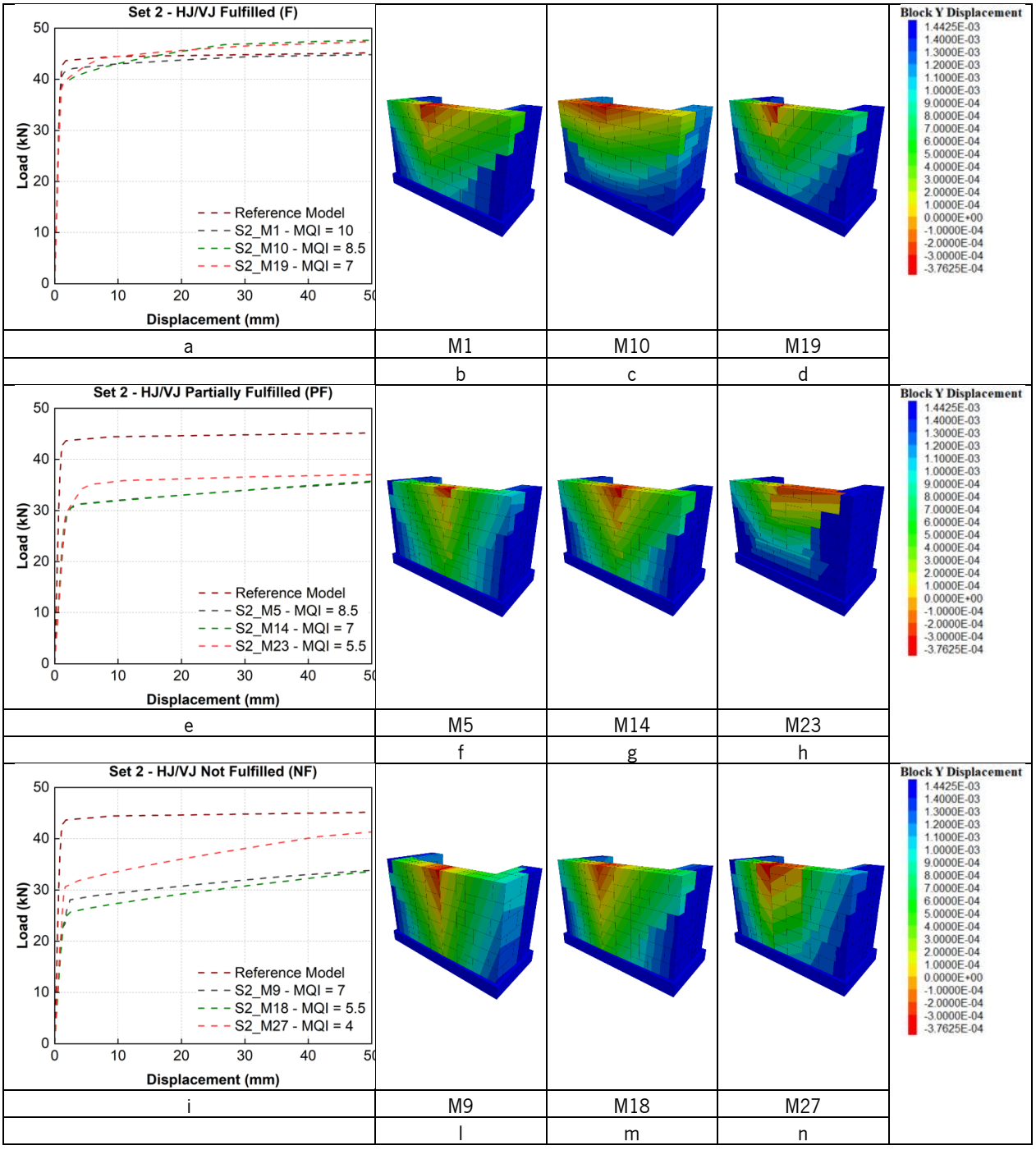


Figure 4.22 – Set 2 variation in wall connection (WC) configuration.

It is reasonable to state that the role of through-stone is not so relevant both in terms of peak load and in terms on the damage patterns (Figure 4.22b - c - d).

Looking at the force-displacement curves obtained for HJ and VJ partially fulfilled (Figure 4.22e), it appears that models M5 and M14 have similar peak load and damage mechanisms (Figure 4.22f - g). M23 has a

lower MQI but shows a slightly higher peak load (Figure 4.22h). Apparently, the absence of through-stones (WC not fulfilled) resulted in a definition of a masonry bond with better interlock properties and in general, a better load capacity (even though not significantly higher) if compared to the other models.

When HJ and VJ are not fulfilled, models M9 and M18 have a similar load-displacement curve (Figure 4.22i). Overall, the damage mechanisms are similar in all the models (Figure 4.22l - m - n). The highest load refers to the model having the lowest MQI, but this trend is also detected in other models displaying a similar feature related to the possibility given by the lack of through-stone to create a more uniform and less discontinuous masonry bond. This trend, which is not expected to occur, may be a result of the limitations related to the boundary conditions and to the geometrical definition of the models used in this study.

4.3.2.3 Analysis of Set 3

From Figure 4.23, it is possible to analyze the variation of the structural behaviour in the models with poor corner connections and for different configuration of vertical joints (VJ) when wall connection (WC) and horizontal joints (HJ) parameters fulfilled (Figure 4.23a), partially fulfilled (Figure 4.23e) and not fulfilled (Figure 4.23i).

When WC and HJ are fulfilled, model M1 (VJ fulfilled) shows the highest peak load (Figure 4.23a). Despite M3 being modelled with VJ parameter not fulfilled, it presents higher peak load than model M2, which has VJ partially fulfilled. The aligned vertical joints configuration in model M3 results in the development of local mechanisms consisting in the overturning of a corner of the façade which weakens the global response of the wall itself (Figure 4.23d).

Regarding the partially fulfillment of WC and HJ parameters, it is possible to say that the load capacity displays a reduction consistent to the gradual decrease of the MQI values (Figure 4.23e). Similar collapse mechanisms are detected in all the 3 models considered (detachment of the façade from the lateral walls and consequent overturning of the façade itself), see Figure 4.23f - g - h.

When WC and HJ are in a not fulfilled condition, models M25 and M27 display a similar peak load (Figure 4.23i). On the other hand, model M26 has the highest load capacity, which may be due to the combination of the conditions related to HJ not fulfilled and VJ partially fulfilled, leading to a more effective interlock when compared to the other models, namely models M25 and M27.

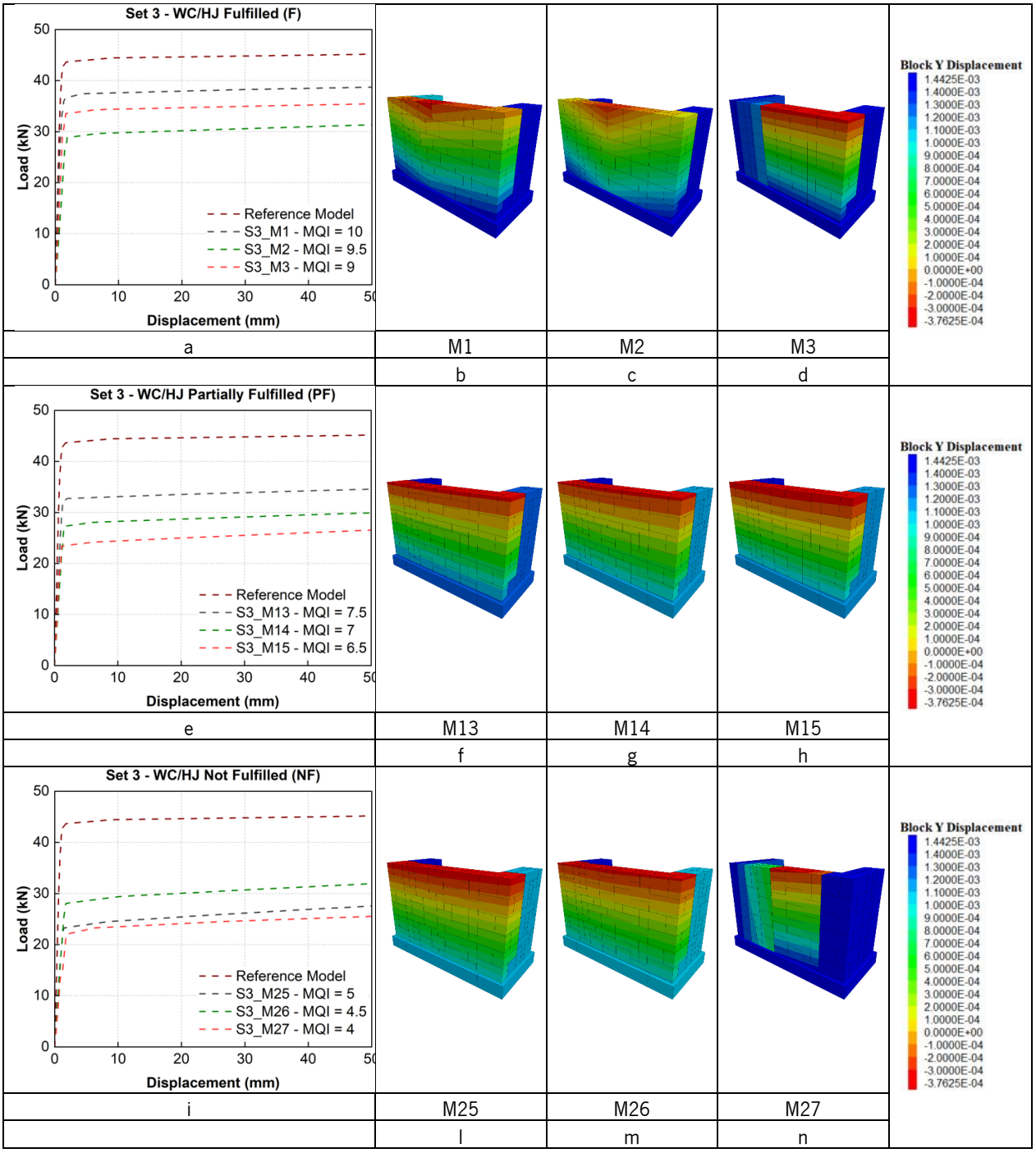


Figure 4.23 – Set 3 variation in vertical joints (VJ) configuration.

Similar collapse mechanisms are detected in models M25 and M26 (overturning of the façade), see Figure 4.23l - m. A slightly different mechanism is observed model M27, being governed by the overturning of the central part of the façade not involving the corner stones, which is clearly the result of the fully aligned vertical joints corresponding the not fulfilled condition (NF), see Figure 4.23n.

The structural behaviour of models with varying HJ arrangement conditions are shown in Figure 4.24.

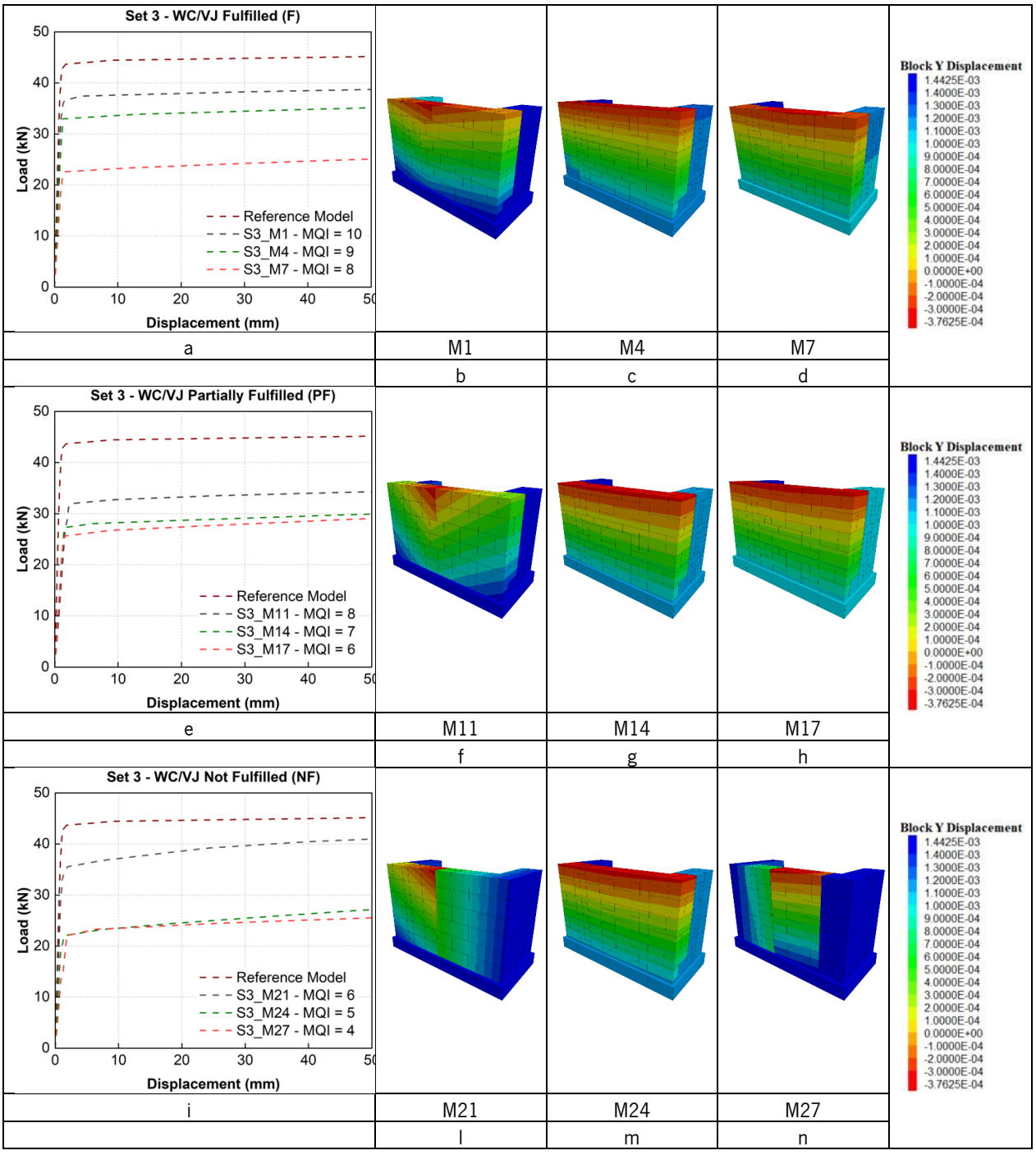


Figure 4.24 – Set 3 variation in horizontal joints (HJ) configuration.

Models with WC and VJ fulfilled (Figure 4.24a-d) and partially fulfilled (Figure 4.24e-h), show similar damage patterns and collapse mechanisms (overturning of the façade with the detachment from the lateral walls).

Moreover, the load capacity seems to be directly correlated with the MQI values, hence the highest MQI values correspond to the highest peak load and, conversely, a reduction of MQI results in decrease of the load capacity of the model.

When WC and VJ are not fulfilled, model M21 has the highest peak load and the highest MQI (HJ parameter fulfilled). In case of HJ is partially and not fulfilled, any significant increase or decrease of peak load was attained (Figure 4.24i). The collapse mechanism is characterized by the overturning of the façade (Figure 4.24m) or an overturning of a reduced portion of the façade itself due to the formation of vertical cracks in the central part of the façade (Figure 4.24l - n).

The main conclusion arisen from the analysis of the group of models related to the combination HJ and VJ fulfilled (F) is that the presence or absence of through-stone does not significantly affect the load capacity of the models and the final damage pattern (Figure 4.25a - b, c - d).

Looking at the models having HJ and VJ parameter fulfilled (Figure 4.25e), it is clearly visible that models M5 and M14 have similar peak load and damage mechanisms (Figure 4.25f - g). On the other hand, model M23 has a lower MQI but shows a slightly higher load capacity (Figure 4.25e). In model M23, the condition of not fulfillment of WC parameter probably results in the definition of a masonry bond with better interlock, leading to a better load capacity (even though not significantly higher), when compared to the other models. No significant difference is detectable in the damage mechanism of the 3 models which consists of the overturning of the façade (Figure 4.25f -g - h).

Figure 4.25i - l - m - n show similar load-displacement curves for all models with not fulfilled HJ and VJ. The highest out-of-plane capacity corresponds to the highest MQI value. In addition, damage patterns show no relevant difference among the models analyzed (Figure 4.25l-n). The damage pattern is characterized by an overturning of a portion of façade, which is a trend clearly influenced by the presence of aligned vertical joints, corresponding to the VJ not fulfilled (NF).

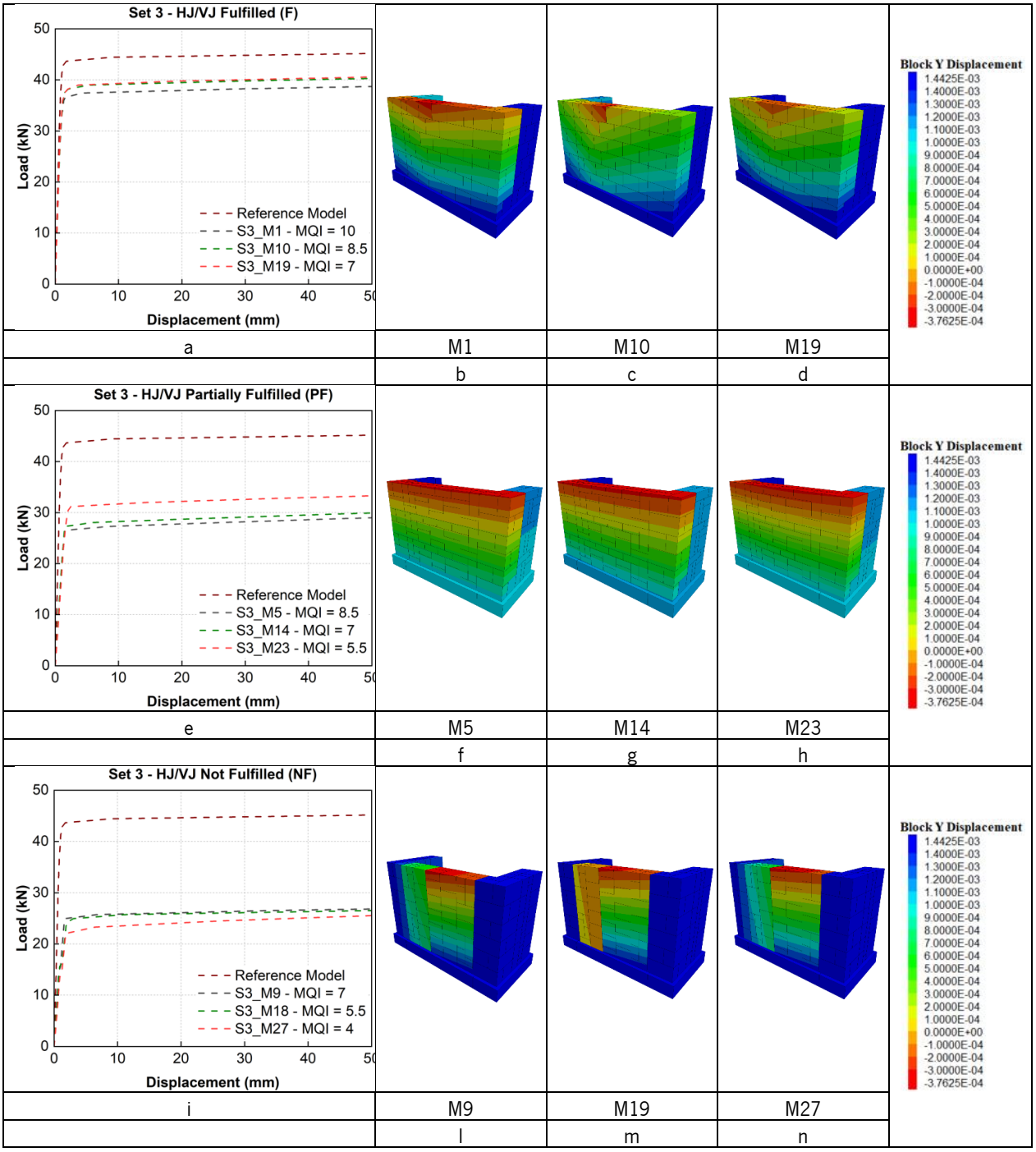


Figure 4.25 – Set 3 variation in wall connection (WC) configuration.

4.3.2.4 Analysis of Set 4

Figure 4.26 shows the variation of the structural behaviour in the models for different configuration of vertical joints configuration (VJ) when wall connection (WC) and horizontal joints (HJ) parameters fulfilled (Figure

4.26a), partially fulfilled (Figure 4.26e) and not fulfilled (Figure 4.26i). All models have poor corners connections and staggered leaves.

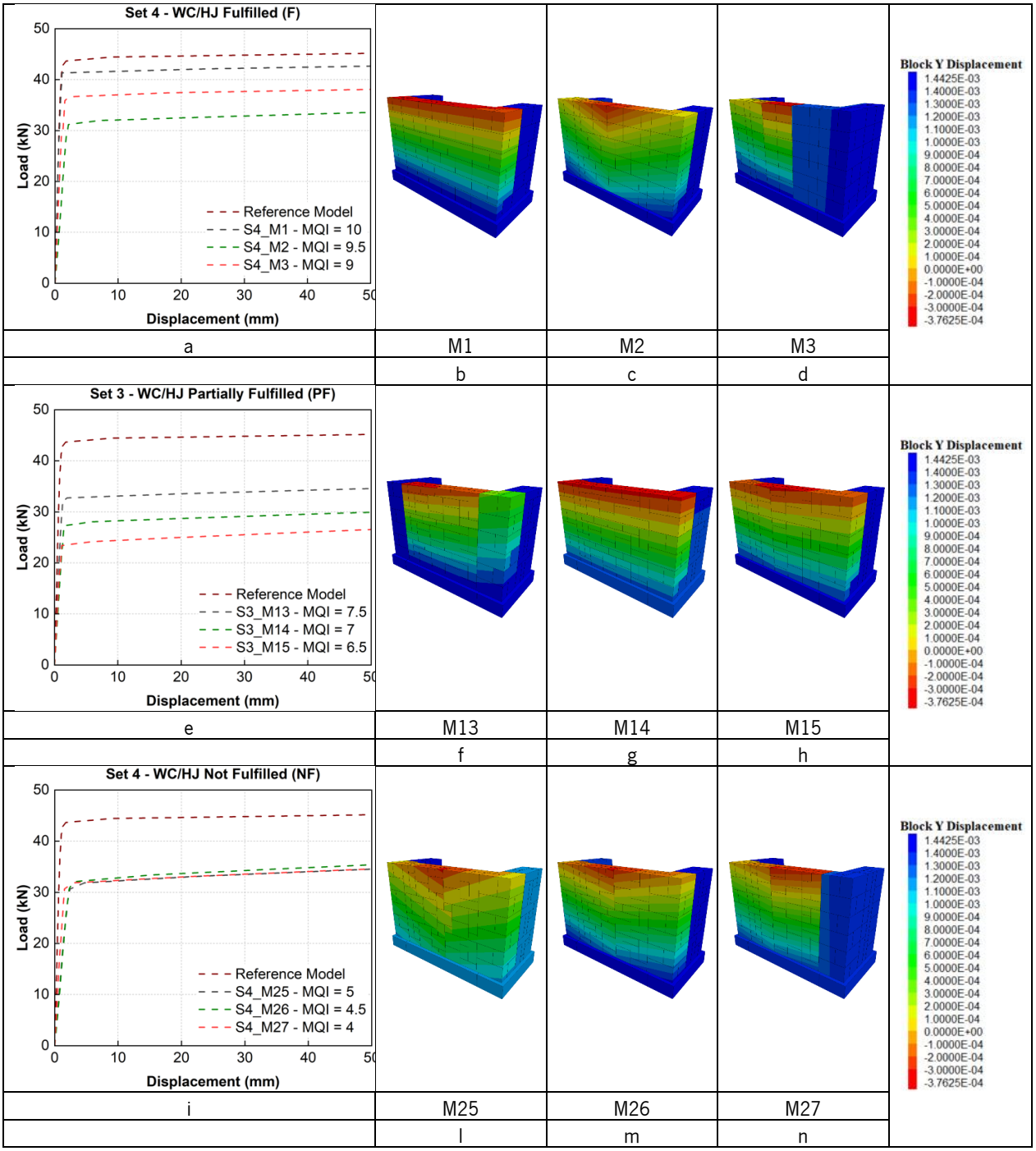


Figure 4.26 – Set 4 variation in vertical joints (VJ) configuration.

Figure 4.26a shows that the highest peak load is attained in model M1 (VJ fulfilled). Moreover, in model M3, whose VJ is not fulfilled, the peak load is higher than the one found in model M2. The configuration of the masonry bond in model M3 makes it easier to stagger the leaf of the wall. This may result in a better performance of model M3 compared to M2, which is characterized by higher discontinuity in of the masonry bond (e.g., stone units with different sizes and more irregular masonry bond configuration compared to M3). The collapse mechanism mainly consists of an overturning of the façade (Figure 4.26b-d). Additionally, in model M3 (with VJ not fulfilled), there is the development of a central vertical crack along the sliding plan of stone units, which is directly connected to the presence of aligned vertical joins typical (Figure 4.26d).

When WC and HJ are partially fulfilled (Figure 4.26e), the load level decreases according to the reduction of MQI and to the presence or absence of properly arranged vertical joints. Collapse mechanisms in models M13, M14 and M15 are similar (Figure 4.26f - g - h), consisting of the overturning of the façade. When VJ is fulfilled (M13) the overturning mainly involves the central part of the façade itself, excluding the corner stones, at least for lower displacement levels.

The models with WC and HJ not fulfilled are characterized by having no considerable differences in terms of peak load (Figure 4.26i). The models where VJ is fulfilled and partially fulfilled do not exhibit considerable difference in terms of damage patterns (Figure 4.26l - m), whereas when VJ is not fulfilled, the overturning of the façade is combined with the development of a lateral and a central crack (Figure 4.26n).

In the models where fulfillment of HJ is analyzed, and when WC and VJ are fulfilled, the models M1, M4 and M7 show collapse mechanisms characterized by a combination of overturing and sliding of the façade (or a portion of façade), see Figure 4.27b - c - d). The load capacity of the models increases according to the MQI values (higher load corresponds to higher MQI), see Figure 4.27a. Indeed, HJ variation leads to results consistent to what can be expected when MQI decreases.

When WC and VJ are partially fulfilled (PF), the highest peak load refers to the model with lowest MQI, which is probably due to the definition of a masonry bond having a better interlock hence providing a better performance (Figure 4.27e).

The last group of models refers to the ones where WC and VJ are not fulfilled (Figure 4.27i). In this case, the highest MQI corresponds to the highest load detected. The damage mechanism is similar in models M21 and M24 (Figure 4.27l - m), consisting of the simple overturning of the façade. However, in model M27 (all parameters not fulfilled), the damage pattern combines the overturning of the façade combined with the

asymmetrical detachment of a portion of the façade along a separation plan defined by aligned vertical joints (Figure 4.27n).

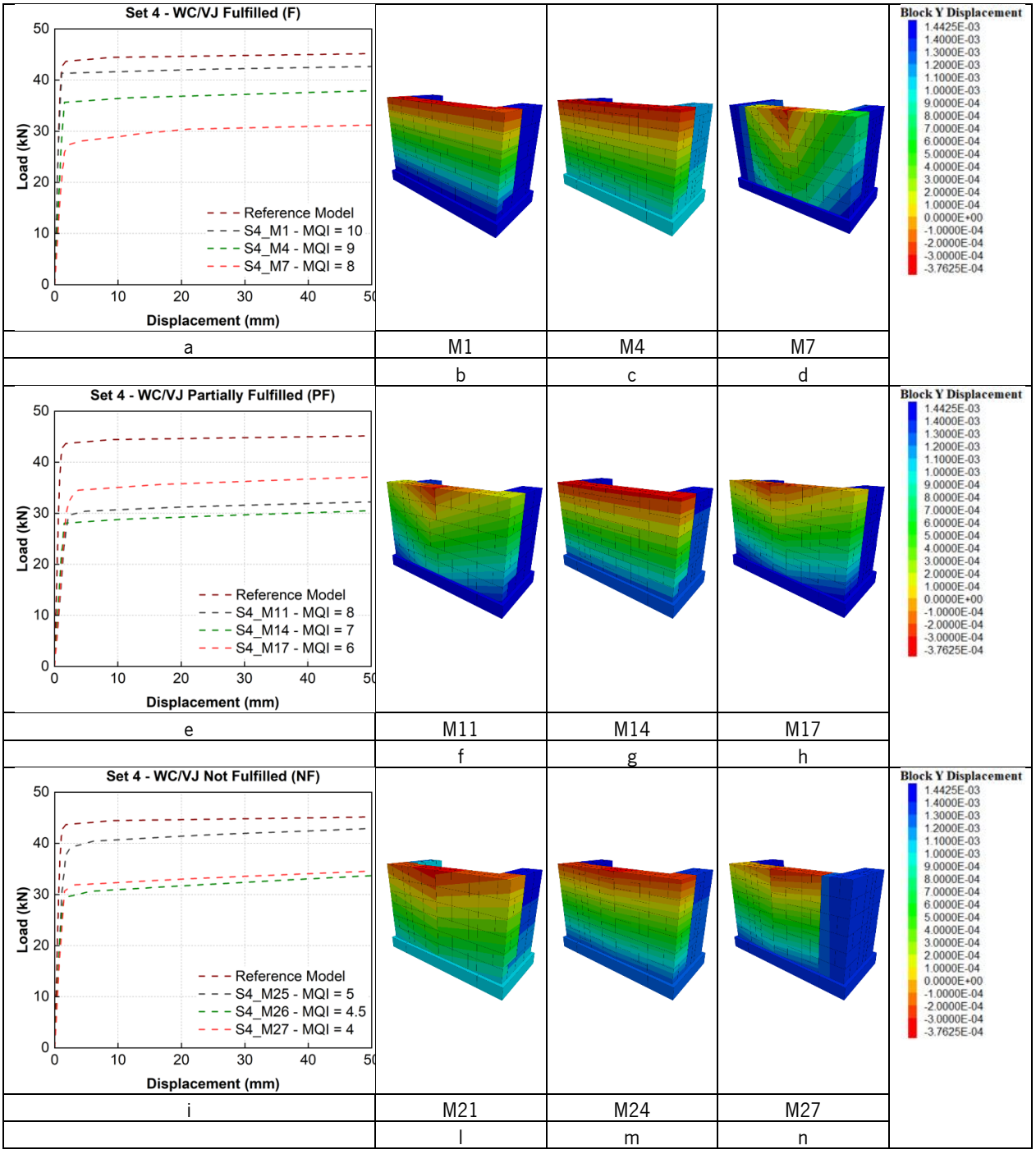


Figure 4.27 – Set 4 variation in horizontal joints (HJ) configuration.

The analysis of the compliance of WC criterion, together with the variation of the fulfillment level of VJ and HJ criteria, can be carried out based on the results shown in Figure 4.28.

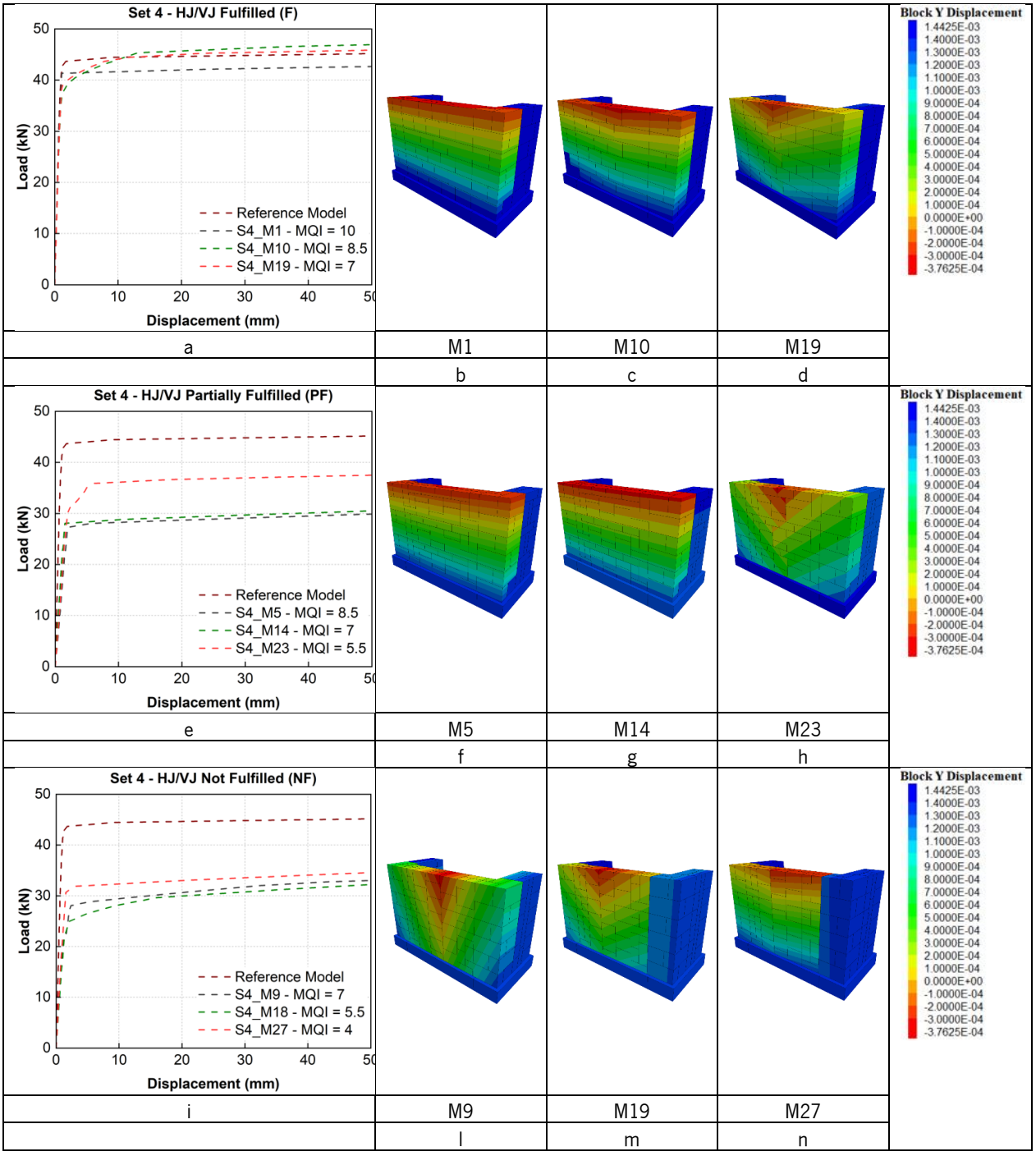


Figure 4.28 – Set 4 variation in wall connection (WC) configuration.

The force-displacements displayed in Figure 4.28a clearly shows that the role of through-stone is not so relevant both in terms of maximum load and of damage patterns (Figure 4.28b - c - d), when HJ and VJ are both fulfilled.

When HJ and VJ are partially fulfilled (Figure 4.28e), it is possible to see that models M5 and M14 have similar peak load. Conversely, model M23 has the lowest MQI in this group of models but shows a higher peak load. In model M23, WC is not fulfilled and probably this characteristic resulted in a definition of a masonry bond with better interlock and in general, a better load capacity (even though not significantly higher), when compared to the other models. This trend may be related to the limitation of the 3D generation of the models proposed in this study. Damage patterns are similar in all the models (M5, M14, M23), see Figure 4.28f - g - h.

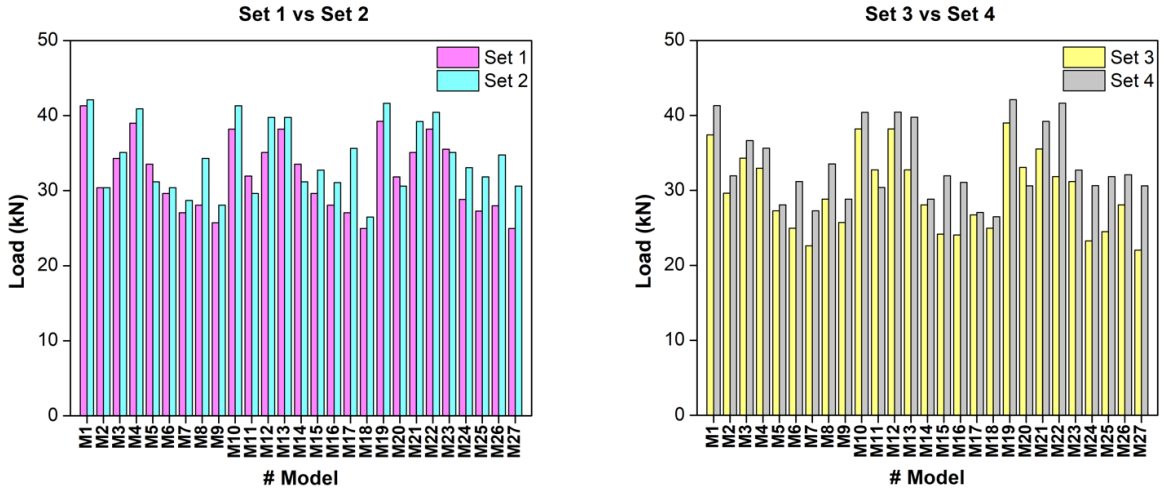
Figure 4.28i shows the results of the group of models having HJ and VJ not fulfilled. In this case, the highest load refers to the model having the lowest MQI, which is a trend previously detected in other groups of models in similar conditions. In this case, the absence of through-stones may result in a more regular masonry bond with no discontinuity and a more effective monolithic behaviour of the model, resulting in a better out-of-plane performance.

4.3.3 Discussion on the out-of-plane load capacity

The results of the geometrical parametric study are herein summarized, taking into consideration the out-of-plane resistance reached by the models in each of the sets analyzed. This section's primary goal is to provide a summary of the findings so that readers can more easily understand the trend that emerged from the investigation while accounting for the significance of the different parameters when assessing the walls' overall structural performance, namely cornerstone configuration, leaves masonry bond, vertical joints configuration (VJ), horizontal joint configuration (HJ) and wall connection (WC).

A comparison between the 4 sets of models has been conducted, taking into consideration their features: (i) comparison between Set 1 and Set 2 and between Set 3 and Set 4 with similar corner arrangement. Set 1 and 2 have identical cornerstone configurations but distinct leaf arrangements (perfectly overlapped vs staggered leaves in Set 1 and Set 2 respectively). Set 3 and Set 4 will be compared since they share the same cornerstone configuration (poor interlock), whilst having different leaves arrangement: (ii) comparison among the models having the same leaf arrangement. Hence, Set 1 and Set 3 are compared to each other as well as Set 2 and Set 4. It must be noted that the present section shows bar graphs to visualize the results

of the analyses carried out on the four sets of models. For the sake of conciseness, the reader is referred to Annex 2.5 – Load Capacity comparison where the numerical data regarding the 4 sets of models is reported. Figure 4.29a shows that Set 2 models exhibit higher peak loads, which may be attributed to the staggered leaf layout that provides a more monolithic wall behaviour. Only 4 models in Set 2 have lower load capacity than the corresponding models in Set 1 (M5, M11, M14 and M20). Their common feature is that the VJ parameter is partially fulfilled.



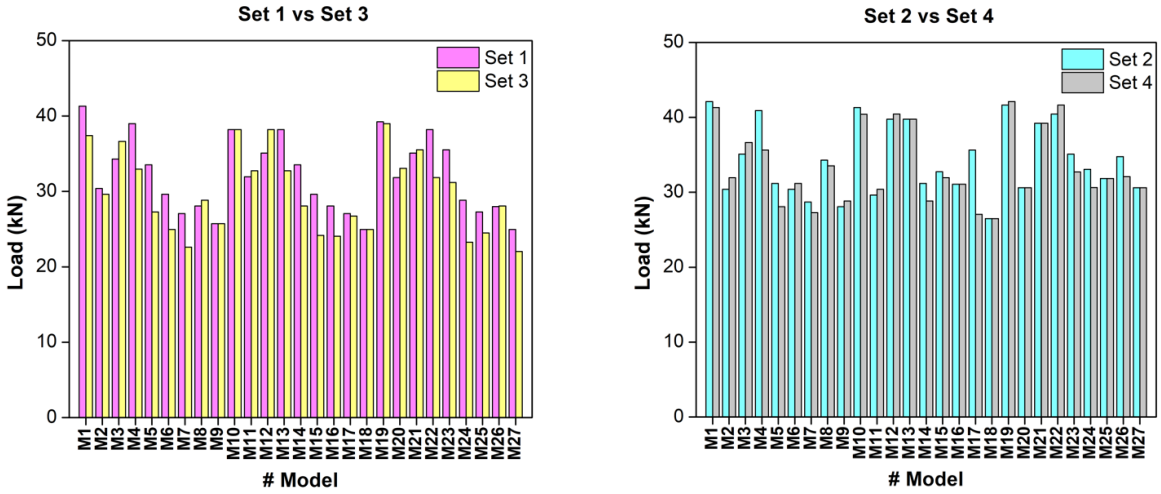
a b

Figure 4.29 – Set 1 vs Set 2 load capacity comparison (a); Set 3 vs Set 4 load capacity comparison (b).

Models in Set 3 and Set 4 have cornerstone configuration which does not provide any interlock between façade and lateral walls. In fact, the difference between the two sets of models is the leaves arrangement which are perfectly overlapped (Set 3) and staggered (Set 4). The interlock provided by staggered leaves in Set 4 models resulted in higher peak loads compared to the corresponding models in Set 3 and the percentage variation confirms this trend (Figure 4.29b). Two exceptions are detected, namely M11 and M20. These cases are characterized by partially fulfilled condition of vertical joints and the presence of 2 perfectly overlapped leaves resulted in a better structural performance of the models. In fact, the need to have staggered leaves led, in some cases, to the use of smaller stone units which probably affected the effectiveness of the final masonry bond.

Set 1 and Set 3 models are built considering perfectly overlapped leaves. The only difference is represented by the cornerstone configurations, which provide a good interlock in Set 1 and a poor interlock in Set 3. As expected, this characteristic led to a decrease in terms of peak load as it is clearly detectable when the

percentage variation of both sets is compared. The reduction ranges from 10 to 20% approximately (Figure 4.30a).



a b

Figure 4.30 – Set 1 vs Set 3 load capacity comparison (a); Set 2 vs Set 4 load capacity comparison (b).

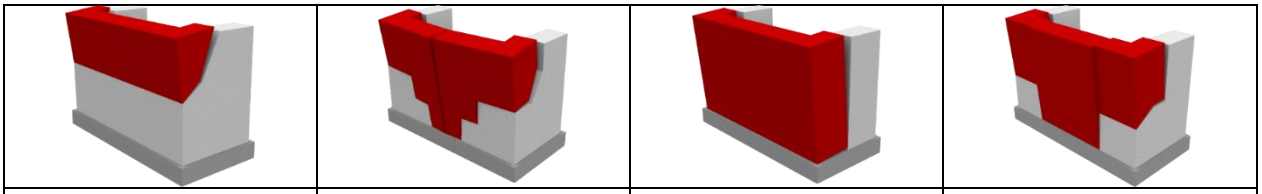
The trends previously highlighted are once again confirmed, especially regarding the role of the WC parameter, looking for instance at the results of model M1 (all parameters fulfilled) and model M19 (all parameters fulfilled except WC). In both sets, the difference in terms of load capacity in presence or absence of through-stones is subtle (4% approximately), confirming that at least for the types of analyses and boundary conditions considered in this study and, for the masonry bond characteristics used to build the 3D models of the walls analyzed, vertical/horizontal joints configuration (VJ/HJ) and cornerstones configuration have a more significant influence on the structural performance of the models. Looking at Figure 4.30b, as it is reasonable to expect, the corners configuration affects the load capacity. In most cases, peak loads detected in Set 4 are lower compared to those in Set 3. However, the presence of staggered leaves reduces the percentage variation between the 2 sets of models.

4.3.4 Discussion on the recurring collapse mechanisms

There are essentially four types of collapse mechanisms characterising the failure of the models analyzed in the geometrical parametric study. They can be summarized as follows:

- Failure Mode 1 (FM1) is an overturning of the upper part of the façade with the consequent detachment of a portion lateral walls (Figure 4.31a);

- Failure Mode 2 (FM2) is a mixed failure mode characterized by an overturning of the façade together with the onset of a central crack identifying two portions of masonry wall rotating with respect to the corners (Figure 4.31b);
- Failure Mode 3 (FM3) consists in a complete overturning of the façade and a detachment of the lateral walls (Figure 4.31c);
- Failure Mode 4 (FM4) is characterized by a complete overturning of the central part of the façade and opening of 2 vertical cracks delimiting the detached portion of masonry wall, together with the overturning of reduced portion of lateral walls (Figure 4.31d).



FM1	FM2	FM3	FM4
a	b	c	d

Figure 4.31 – Recurring collapse mechanisms: FM1 (a), FM2 (b), FM3 (c), FM4 (d).

Overall, failure modes FM1 and FM3 are the failure modes most frequently detected. In Set 1 and Set 2, the failure mode FM1 develops in approximately 74% of the models. The models from Set 3 and Set 4 show a similar trend concerning FM3; around 70% of the models in these groups experienced this type of damage mechanism mainly due to the cornerstone configuration with poor interlock. Failure modes FM2 and FM4 frequency rates are lower when compared to the other failure modes. If the total number of models is considered, FM 2 accounts for 6.5%, whereas FM4 accounts for 14% approximately. These are more complex damage mechanisms often occurred in those models characterized by partially fulfilled conditions.

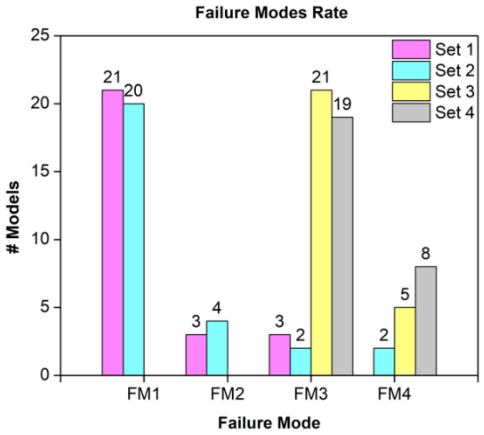


Figure 4.32 – Failure modes frequency rate.

Most of the models in Set 1 and Set 2 have an FM1 type of failure. In these models, the corner configuration provides an effective interlocking between façade and lateral walls. Models M3, M6, M12 in Set 1 and Set 2 exhibit the failure mode type 2 (FM2) due to the configuration of vertical joints not fulfilled (the crack arises along the vertical plane delimited by aligned stone units), see from Figure 4.33 to Figure 4.35.

The models M9, M18 and M27 from Set 1 show a failure mode type 3 (FM3), due to the simultaneous absence of a good vertical and horizontal joints configuration (VJ and HJ are not fulfilled). The collapse mechanism does not seem to be significantly affected by the presence or absence of through-stones. Model M9 from Set 2 has a similar behaviour (FM1). Conversely, M18 and M27 are characterized by failure mode type 2 (FM2) and type 4 (FM4) respectively. These collapse patterns are typical of the models having poor vertical joints configurations, see Figure 4.33, Figure 4.34 and Figure 4.35.

An additional consideration related to the models from Set 1 and Set 2 is that the configuration of the leaves (perfectly overlapped in Set 1 or staggered in Set 2) does not significantly affect the final collapse mechanism. Conversely, the staggered configuration of the leaves has a beneficial effect on the peak load attained during the analysis (Figure 4.33, Figure 4.34, Figure 4.35). Most models in Set 3 and Set 4 show failure mode type 3 (FM3). This trend is related to their corner configuration which does not provide any interlock between façade and lateral walls. The models M9, M18, M20, M26 and M27 in Set 3 have a failure mode type 4 (FM4) which often occurs when vertical joints configuration is not fulfilled (NF). The same happens in models M3, M6, M10, M13, M18, M22, M26 and M27 in Set 4, in which the lack of good vertical joints combined with the corner configuration results in the collapse of the central part of the façade, even if in some cases a good horizontal joints configuration and a good number of through-stones are present (Figure 4.33, Figure 4.34, Figure 4.35).

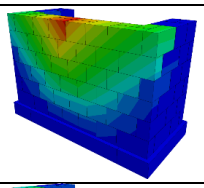
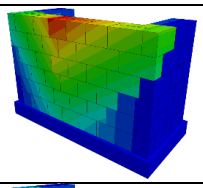
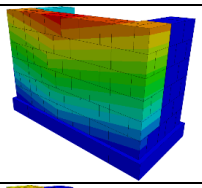
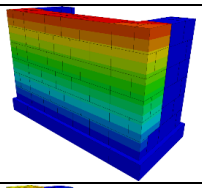
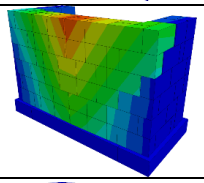
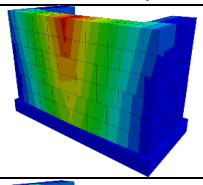
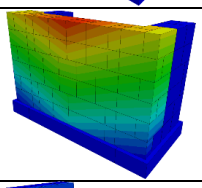
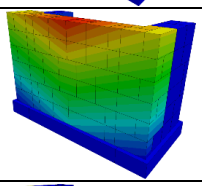
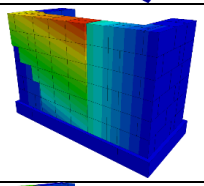
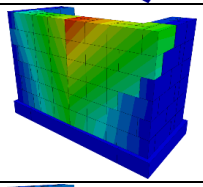
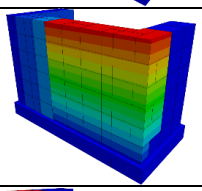
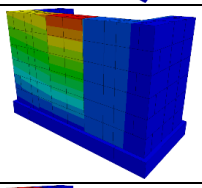
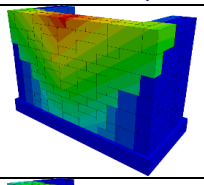
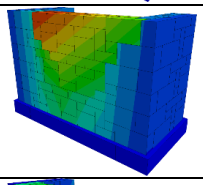
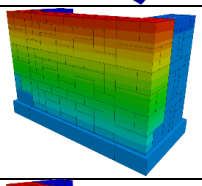
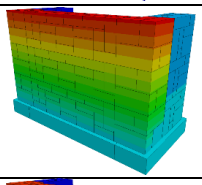
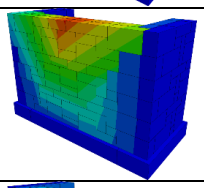
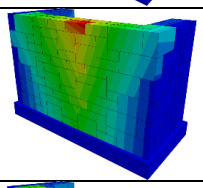
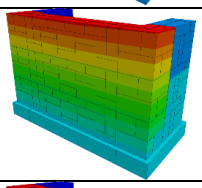
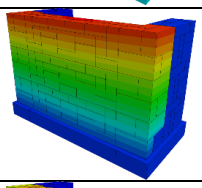
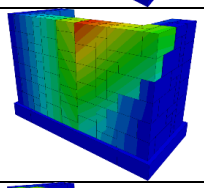
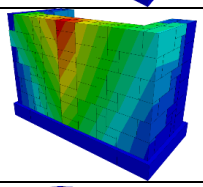
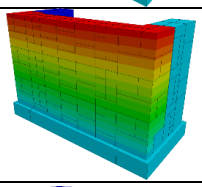
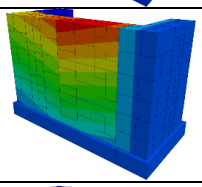
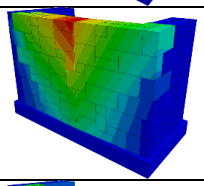
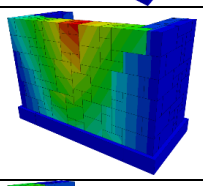
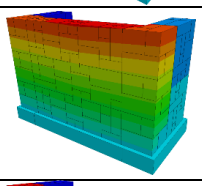
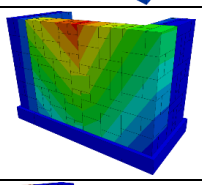
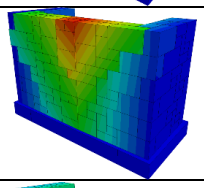
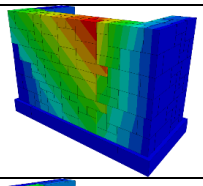
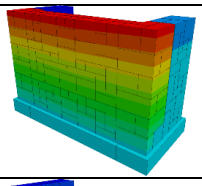
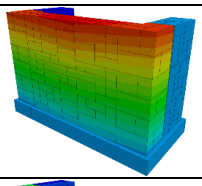
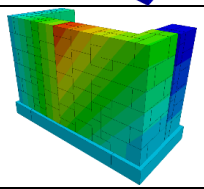
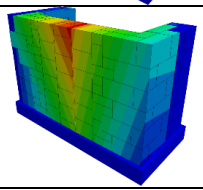
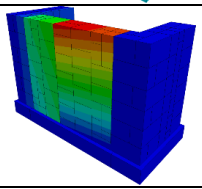
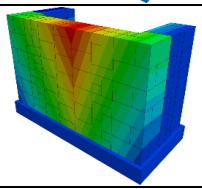
# Model	Set 1	Set 2	Set 3	Set 4
M1 WC - F HJ - F VJ - F				
M2 WC - F HJ - F VJ - PF				
M3 WC - F HJ - F VJ - NF				
M4 WC - F HJ - PF VJ - F				
M5 WC - F HJ - PF VJ - PF				
M6 WC - F HJ - PF VJ - NF				
M7 WC - F HJ - NF VJ - F				
M8 WC - F HJ - NF VJ - PF				
M9 WC - F HJ - NF VJ - NF				

Figure 4.33 – Abacus of failure modes (M1 to M9) for the whole dataset (Set 1, 2, 3 and 4) of the geometrical parametric study.

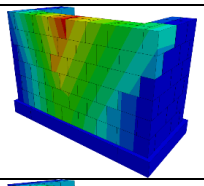
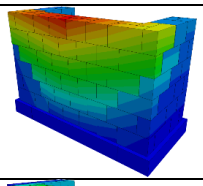
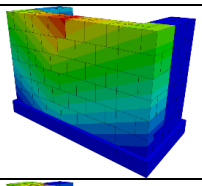
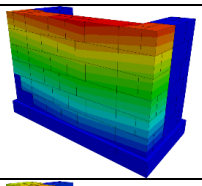
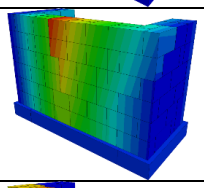
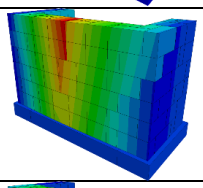
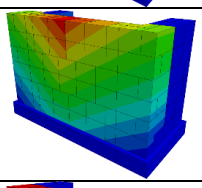
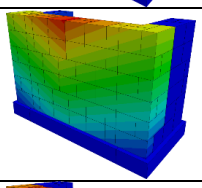
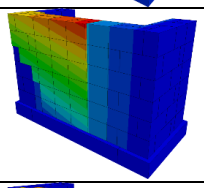
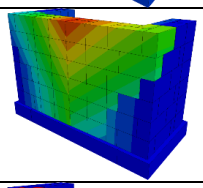
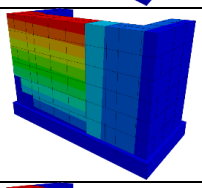
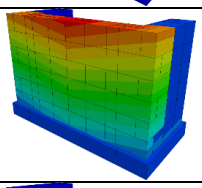
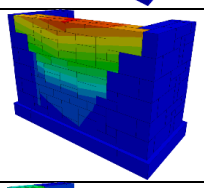
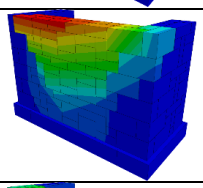
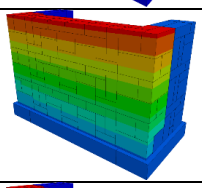
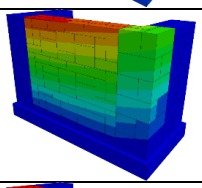
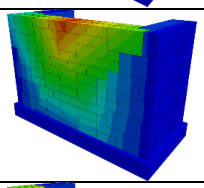
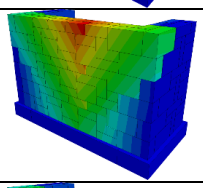
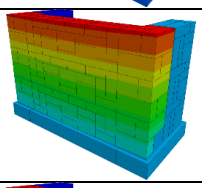
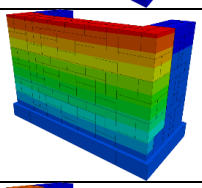
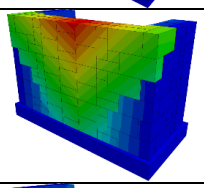
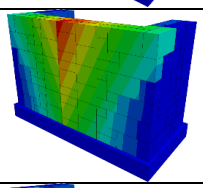
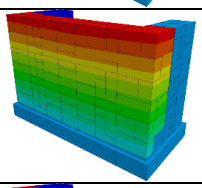
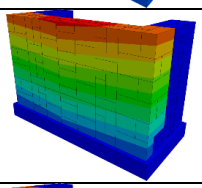
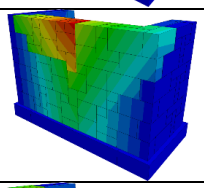
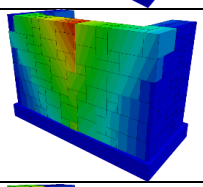
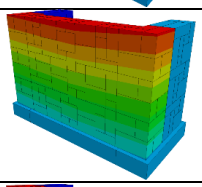
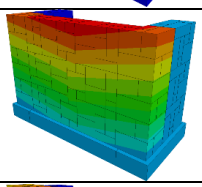
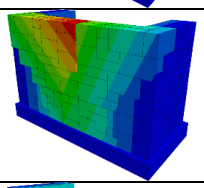
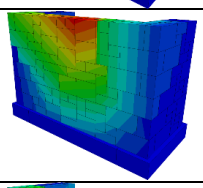
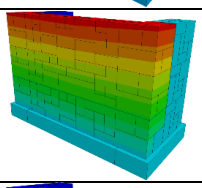
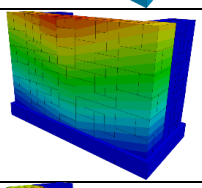
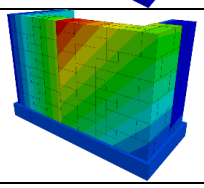
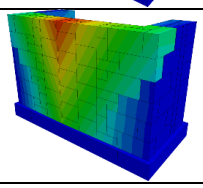
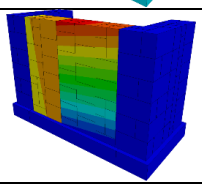
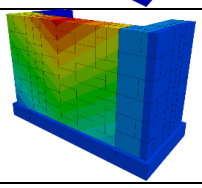
# Model	Set 1	Set 2	Set 3	Set 4
M10 WC - PF HJ - F VJ - F				
M11 WC - PF HJ - F VJ - PF				
M12 WC - PF HJ - F VJ - NF				
M13 WC - PF HJ - PF VJ - F				
M14 WC - PF HJ - PF VJ - PF				
M15 WC - PF HJ - PF VJ - NF				
M16 WC - PF HJ - NF VJ - F				
M17 WC - PF HJ - NF VJ - PF				
M18 WC - PF HJ - NF VJ - NF				

Figure 4.34 – Abacus of failure modes (M10 to M18) for the whole dataset (Set 1, 2, 3 and 4) of the geometrical parametric study.

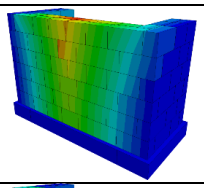
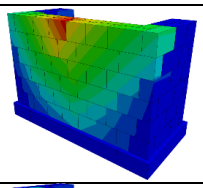
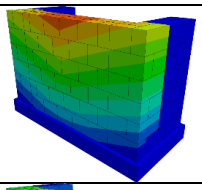
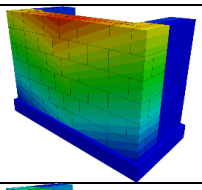
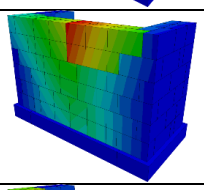
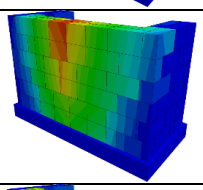
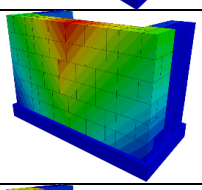
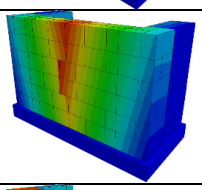
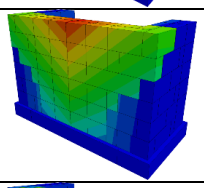
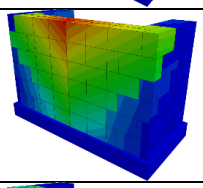
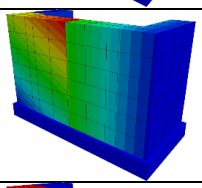
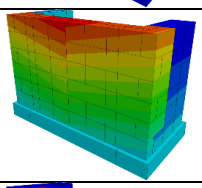
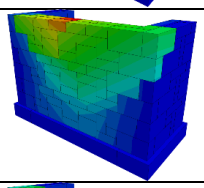
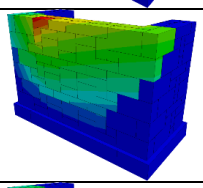
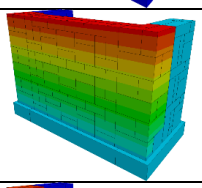
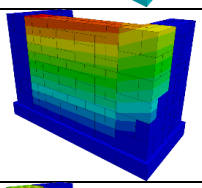
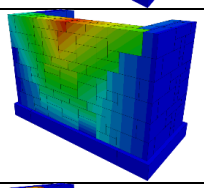
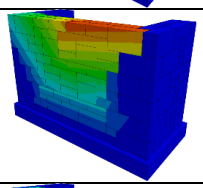
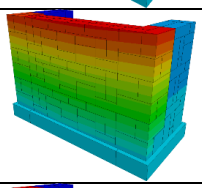
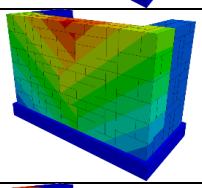
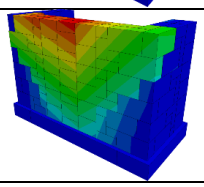
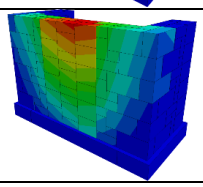
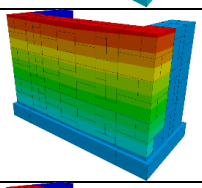
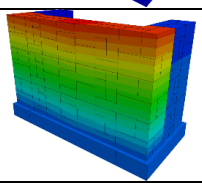
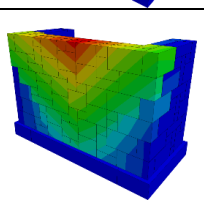
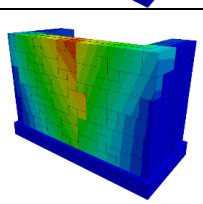
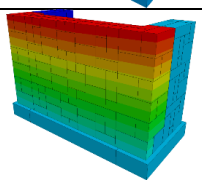
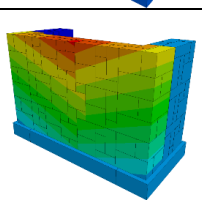
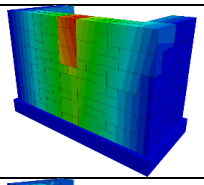
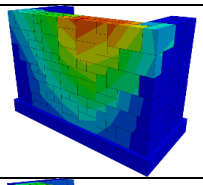
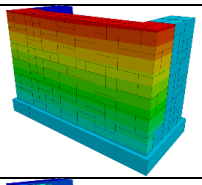
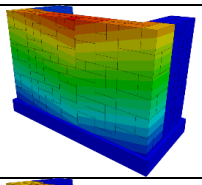
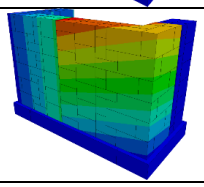
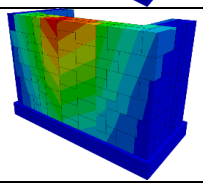
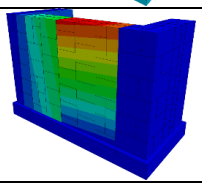
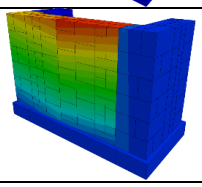
# Model	Set 1	Set 2	Set 3	Set 4
M19 WC - NF HJ - F VJ - F				
M20 WC - F HJ - F VJ - PF				
M21 WC - NF HJ - F VJ - NF				
M22 WC - NF HJ - PF VJ - F				
M23 WC - NF HJ - PF VJ - PF				
M24 WC - NF HJ - PF VJ - NF				
M25 WC - NF HJ - NF VJ - F				
M26 WC - NF HJ - NF VJ - PF				
M27 WC - NF HJ - NF VJ - NF				

Figure 4.35 – Abacus of failure modes (M19 to M27) for the whole dataset (Set 1, 2, 3 and 4) of the geometrical parametric study.

4.4 Final remarks

This chapter presents two different parametric studies addressing, on one hand, the influence of material properties and, on the other, the influence of a set of geometrical parameters on the out-of-plane behaviour of 2-leaf stone masonry walls.

The first part of the chapter focuses on a series of analyses conducted on numerical models previously calibrated using a distinct element (DE) based software (3DEC by Itasca). This numerical method has been selected to carry out the parametric studies (material and geometry) since few examples are provided in the literature addressing these aspects via the distinct elements method. Additionally, the DE-based software selected offers a good balance between accuracy and computational effort. The numerical simulations carried out aimed at the evaluation of the influence of mechanical parameters on the overall performance of a drystone (DS) and of a regular stone masonry wall (REGW).

In both cases, normal stiffness variation (k_n) significantly affected the elastic behaviour of the walls (initial stiffness) and, to a lesser extent, the load capacity of the models. On the other hand, cohesion and friction angle variation significantly affected both the final load capacity and the failure mechanism of DS and REGW.

The geometrical parametric study has been carried out on a set of 108 models divided into 4 groups (Set 1, Set 2, Set 3 and Set 4) according to different cornerstones configuration (effective vs poor interlock) and leaves arrangement (perfectly overlapped vs staggered). In all models, the influence of the arrangement of vertical and horizontal joints, as well as of the through-stones are analyzed.

The main conclusion arising from the geometrical parametric study is that horizontal joint (HJ) and vertical joints (VJ) configurations have the most relevant role on the overall structural behaviour of the walls. In particular, peak load and failure modes are significantly influenced by these parameters.

A significant aspect arisen from the study of whole set of models (all 4 Sets), concerns the role of through-stones. As mentioned above, for the type of analyses performed and the initial assumptions of the parametric study, the presence (WC fulfilled) or absence (WC not fulfilled) of through-stones does not necessarily correspond to an improved models' structural performance. However, this characteristic may also be related to two main aspects, namely 1) the size of the walls considered, which are, in this case reduced scale (1:2) models and the 2) wall typology considered (regular stone masonry wall). Indeed, the presence of through-stones has a beneficial effect on irregular stones arrangements [134].

A good corner configuration improves the load capacity of the walls, affecting at the same time the failure modes, which are often characterized by an overturning of the façade together with a portion of lateral walls

when the corners offer an effective interlock. Conversely, the absence of an effective corner configuration results, most of the time, in a simple overturning of the central part of the façade delimited by the separation plan defined by the aligned vertical joints.

The leaves staggered configuration seems to have a beneficial effect on the overall performance of the wall solely in those models with poor corner interlock. Apart from this, no significant changes have been detected when models have different leaf arrangements.

It must be pointed out that the models have been manually generated using CAD software and following the MQI guidelines to simulate the variation of geometrical parameters and their combinations for the masonry bond in each model. The partially fulfilled condition appeared to be difficult to replicate in particular if combined with other parameters configuration. This "modeling or geometrical ambiguity" led, in fact, to the definition of models that despite a lower MQI value had better performances than models with higher MQI values. To conclude, it is worth highlighting the fact that this study was conducted on reduced scale models, hence the findings herein present could be further expanded taking into account full-scale walls exploring the possibility of varying not only HJ, VJ, WC but also other dimensional characteristics such as height, span, and thickness, to further investigate the role of the masonry bond features and to further validate the trends herein presented and analyzed. All these aspects will be further analyzed in Chapter 5.

5 Numerical parametric study on full-scale models of two-leaf masonry walls

5.1 Introduction

This section presents an extension of the work carried out in Chapter 3 and 4. It builds on the main conclusions from the comparison of different modelling strategies for the simulation of the out-of-plane behaviour in 2-leaf masonry walls (Chapter 3), as well as on the main trends and patterns characterising the geometrical parametric study on reduced scale masonry walls numerical models (Chapter 4). Among the main conclusions derived from the numerical work carried out, it is worth mentioning the difficulties in estimating mechanical input parameters when shifting from two different modeling approaches. For instance, the correlation between finite elements-based macro model input parameters and micro models (both finite element-based and distinct element-based) was not straightforward. In addition, from a geometrical standpoint, it has been observed that the presence/absence of through-stones and the staggered configuration of the masonry leaves are not as influential as expected on the out-of-plane performance of the selected masonry walls.

Therefore, the work presented herein considers two different parametric studies concerning both material and geometrical characteristics. The parametric studies will be carried out on full-scale models with the same plan configuration of the walls analyzed in the previous chapters, namely a U-shaped plan configuration consisting of a façade and two lateral walls. The reference model's geometry adopted in the study is presented in Figure 5.1.

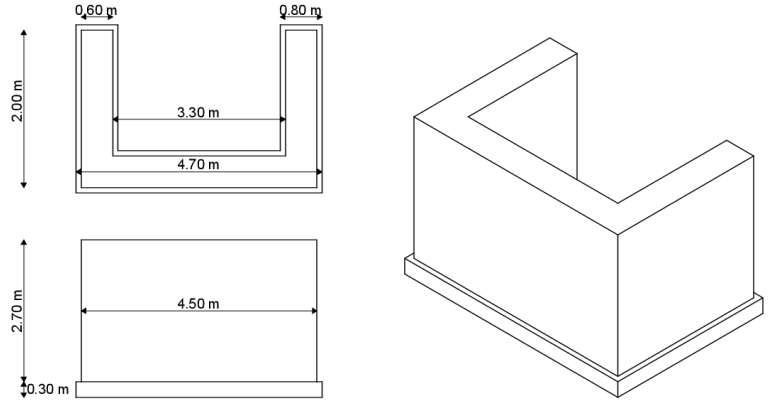


Figure 5.1 – Model's reference geometry.

The masonry typology selected is Masonry Typology 6, according to the classification proposed in Chapter 2. This masonry type is characterized by regularly cut stone units and mortar joints. Similar to what already discussed regarding the parametric study on reduced-scale models, the choice of this masonry typology lies in the possibility of generating different masonry bond configurations in a 3D CAD environment relying on repetitive and regular patterns/arrangements of the stone units. It is also intended to reduce as much as possible the presence of any possible ambiguity in the model generation that may lead to unclear or misleading results interpretation.

The parametric studies carried out aim to investigate the influence of an array of specific parameters on the out-of-plane performance of 2-leaf stone masonry walls corresponding to the reference typology above mentioned (Masonry Typology 6).

Since the out-of-plane behaviour of masonry walls is a complex phenomenon from a mechanical and a geometrical point of view, the work presented in this chapter is two-fold. On one hand, mechanical properties will be analyzed to gain an insight into the global behaviour of the walls on a macro-scale. On the other hand, the out-of-plane behaviour will be analyzed on a micro-scale level considering the variation of specific geometrical parameters often used as a reference to describe/assess the masonry bond quality (e.g. wall connection, vertical joints configuration, horizontal joints configuration, etc.).

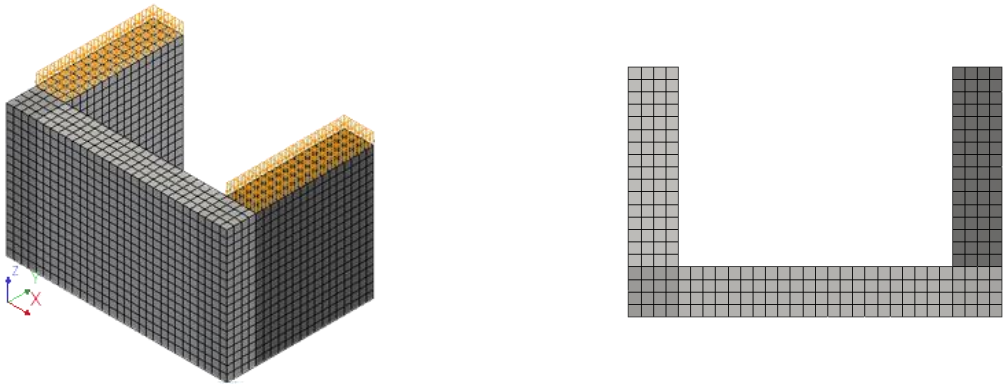
The results of the numerical parametric studies (mechanical and geometrical) will be compared and cross-referenced to have a better understanding of the role of the parameters identified as the most influential on the out-of-plane performance of masonry walls singularly taken or combined.

A set of empirical expressions will be defined and calibrated based on the results of the parametric studies carried out. These expressions will address the above-mentioned open challenges, namely the estimation of input parameters in macro/micro model analyses and the assessment of the out-of-plane capacity of two-leaf stone masonry walls.

Although they are a tool for an expedited estimation of the out-of-plane performance, they serve a broader purpose. Indeed, they must be primarily intended as a synthesis of the findings of the parametric studies which “translates” in the form of an equation the relationship between the variables considered and their influence on the walls’ performance on both a mechanical and a geometrical level. In fact, the main purpose of the parametric studies presented is the estimation of the individual influence of mechanical and geometrical key-parameters on the out-of-plane performance in 2-leaf masonry walls.

5.2 Numerical parametric study on material properties

In order to analyze the influence of material properties on the out-of-plane performance of full-scale masonry walls, a set of 100 models has been built. It must be mentioned that the material properties variation has been studied using finite element (FE) macro-models. The reference geometry is the same for all the models (see Figure 5.1 and Figure 5.2), whereas the input parameters used to characterize the mechanical behaviour have been varied in each analysis performed.



a b

Figure 5.2 – Reference FE-Based macro model 3D view (a) and plan configuration (b).

Since the masonry typology selected for the study is Masonry Typology 6 (see Figure 2.1 in Chapter 2), the reference mechanical values considered are the same resulted from the Bayesian updating procedure described in Chapter 2, reported in Table 2.17 and Table 2.18. A set of 100 values has been generated using a Monte Carlo simulation and a Gibbs sampling algorithm, similarly to what described in Chapter 2. All the mechanical parameters have been considered lognormally distributed.

Once defined the set of mechanical properties, 100 pushover analyses have been performed using DIANA FEA software [98]. The pushover analyses consisted in an incrementally increasing load, proportional to the mass of the wall, applied to the whole model. In all the analyzed models, the base has been considered fully constrained and a vertical load equal to 20 kN has been applied to each lateral wall.

The numerical analyses carried out (100 pushover curves) have been used to identify the upper and lower bound pushover curve describing the structural performance for the set of models considered in the parametric study.

The reference range of load-capacity curves resulting from the FE-based study has been used to calibrate the mechanical properties of the simplified micro-models analyzed via distinct element (DE) method and to obtain matching DE-based pushover curves able to fit the results obtained using FE macro-models.

The main goal of the parametric study on the mechanical material properties is to have an insight regarding the link between reference mechanical properties used as input parameters in FE-based analyses and those used in DE-based simplified micro-models previously analyzed in Chapter 4 (e.g. normal/shear stiffness, cohesion, tensile strength, friction angle).

The overall workflow of the parametric study is described in Figure 5.3. Moreover, for the sake of conciseness, the mechanical properties resulting from the Monte Carlo simulation are presented in Annex 3.1 – Table of mechanical properties for FE-based analyses.

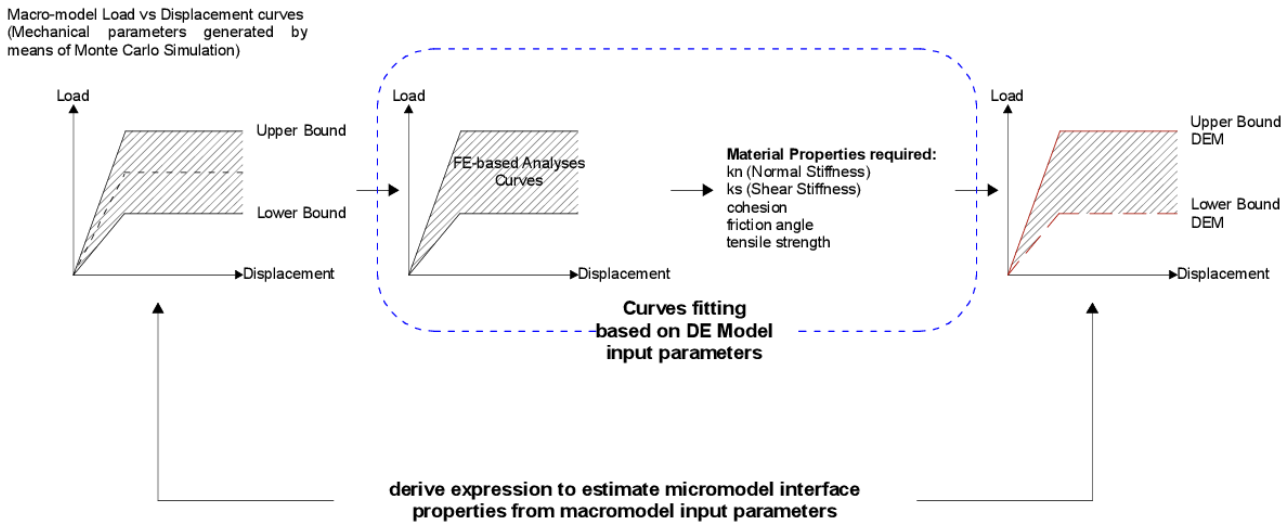


Figure 5.3 – Workflow parametric study on material properties.

The results of the pushover analyses made it possible to obtain recurring trends/patterns in terms of load and displacement levels which have been analyzed and associated with the structural performance of the models and a set of limit states.

Figure 5.4a shows the load-displacement curves related to the FE-based study on the variation of material properties. Overall, the curves present a linear behaviour up to the peak load. Immediately after the attainment of the maximum out-of-plane capacity, a significant reduction in terms of load levels is clearly visible. The softening behaviour of the models is then characterized by the presence of a plateau-like branch highlighting gradually increasing displacement levels corresponding to a slight variation in terms of load levels.

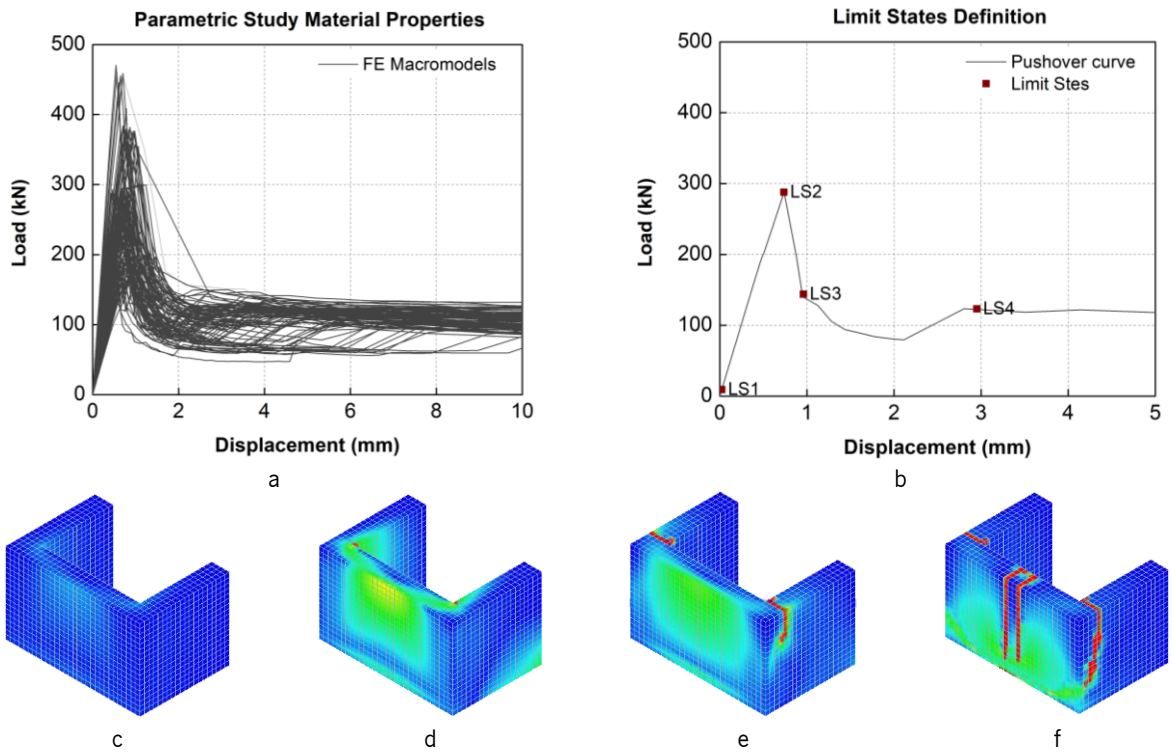


Figure 5.4 – Macro models Load vs Displacement curves (a); Limit States identification (b); reference model maximum principal strain distribution LS1 (c), LS2 (d), LS3 (e) and LS4(f).

Based on qualitative and quantitative observation regarding the behaviour of the models used in the parametric study, the following limit states were defined:

- LS1, corresponds to a reduction of stiffness of approximately 2%, similarly to what proposed also in other studies [129]. This limit state can be associated to the occurrence of the first crack (Figure 5.4b and Figure 5.4c) and it can be considered equivalent to a damage limitation state (DL) as it is defined in the Eurocode 8 [13].
- LS2, is identified as the maximum load capacity attained by the model and the corresponding displacement (Figure 5.4b and Figure 5.4d). It can be considered equivalent to significant damage state (SD) [13].
- LS3, is associated to the drop in terms of load levels, which has been estimated as a 40 to 60% reduction of the maximum load capacity, based on the analysis of the results. From a physical point of view, this limit state corresponds to the stage in which the first separation between façade and lateral walls occurs

(Figure 5.4b and Figure 5.4e) [135]. It represents an intermediate stage between the significant damage and near collapse state of the structure.

- LS4 defines the beginning of the plateau-like behaviour; it corresponds to the complete detachment between façade and lateral walls, hence the load level is the same as LS3, whereas the displacement has been estimated to be 3 times higher than the value identified in LS2 (Figure 5.4b and Figure 5.4f). It corresponds to the near collapse state (NC) as it is defined in the Eurocode 8 [13].

A table summarizing the quantitative analyses carried out to identify the main trends and patterns arisen from the macro-model parametric study is reported in Annex 3.2 – Limit States summary finite element macro models. The identification of the limit states based on the load-displacement curves, associated to the set of macro-models of the material parametric study, resulted in the definition of equivalent three-linear curves more easily comparable to the pushover curves obtained from distinct elements (DE) analyses, since they provide an approximation of the post-peak branch closer to a plateau-like behaviour.

Every single three-linear curve has been used in a calibration procedure involving a reference DE model having the same plan configuration adopted for the FE-based macro-models. Additionally, no geometrical variations in the masonry bond are considered for the DE-based analyses. All the geometrical parameters have been assumed in a standard and properly arranged configuration as shown in Figure 5.5.

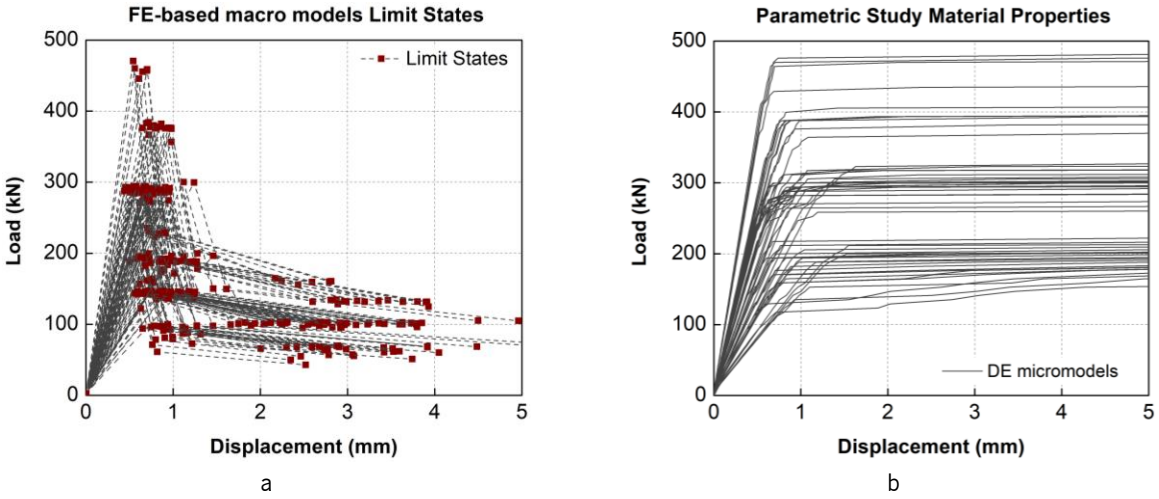


a b

Figure 5.5 – Reference DE model (a) and 3D CAD view (b)

The final stage of the study involves the calibration of the reference DE-model previously built in order to define a set of mechanical input parameters to use in DE-based micro modelling approaches in order to obtain 100 pushover curves equivalent to those already resulted from the FE-based macro model study initially carried out. Therefore, 100 pushover curves have been obtained using DE method, resulting in a set of 100 different combination of interface material properties for the reference DE model. Each DE-based

micromodel pushover curve matches the three-linear pushover curve obtained from the FE-based macro model parametric study (Figure 5.6). The fitting process between pushover curves and trilinear curves is based on a trial-error procedure. Normal and shear stiffness have been progressively adjusted in order to match the linear elastic behaviour of the reference three-linear curve resulted from FE-based macro model analyses, whereas the load capacity has been modified acting on tensile strength and cohesion.



a b

Figure 5.6 – Limit States three-linear curves (a); Pushover curves DE-based micro models (b)

Finally, both set of mechanical parameters (FE-based and DE-based modelling approach) will be analyzed by means of linear regression in order to identify a correlation among the input parameters used in the adopted modelling strategies, namely FE-based macro modelling approach and DE-based micro modeling approach. The tables with the final values of the mechanical properties found for both FE-based and DE-based analyses are reported in Annex 3.1 – Table of mechanical properties for FE-based analyses.

5.2.1 Empirical expressions derived from the parametric study (Limit States)

This section presents the empirical expressions derived from a multiple linear regression analysis performed to identify a correlation between the set of input material parameters used in the FE macro-model analyses and the limit states associated to the models' structural performance.

The linear regression performed combines quantitative continuous data information related to the parameters needed in a FE macro-model analysis. Furthermore, statistical measurements of the material properties used as independent variables in the regression analysis can be found in Table 2.6 (Chapter 2, Section 2.4.1). The

reference table used to carry out the multiple linear regressions is shown in Annex 3.3 – Summary load levels for each limit state and Annex 3.4 – Summary displacement levels for each limit state.

It must be noted that the expressions resulting from the multiple linear regression are calibrated considering the reference mechanical properties characterising Masonry Type 6 (see Table 2.6). Hence, the models used in the numerical parametric study have a Young Modulus ranging approximately from 1800 to 3600 MPa, thickness equal to 60 cm, slenderness ratio equal to 4.5.

The expression resulting from the multiple linear regression are presented below:

LS1	
$\mathrm{F} = -0.34 + (1.80 \cdot 10^{-6})A - (1.03 \cdot 10^{-4})B + 0.01C - 0.03D - 195E$	(44)
$\mathrm{G} = 3.62 \cdot 10^{-11}\mathrm{A} + 7.45 \cdot 10^{-11}B - 2.21 \cdot 10^{-9}\mathrm{C} + 6.29 \cdot 10^{-7}\mathrm{D} - 5.46 \cdot 10^{-6}\mathrm{E}$	(45)

LS2	
$\mathrm{F} = 2.51 + (4.46 \cdot 10^{-5})A - (1.10 \cdot 10^{-3})B + 0.14C + 0.48D + 5173E$	(46)
$\mathrm{G} = 0.001 + 1.24 \cdot 10^{-10}\mathrm{A} - 2.18 \cdot 10^{-9}B + 2.23 \cdot 10^{-8}\mathrm{C} + 8 \cdot 10^{-7}\mathrm{D} + 1.87 \cdot 10^{-4}\mathrm{E}$	(47)

LS3	
$\mathrm{F} = 1.26 + (2.23 \cdot 10^{-5})A - (5.53 \cdot 10^{-4})B + 0.07C + 0.24D + 2587E$	(48)
$\mathrm{G} = 0.0028 + (1 \cdot 10^{-10})A + (1.64 \cdot 10^{-9})B - (5.73 \cdot 10^{-8})C - (7.78 \cdot 10^{-7})D + (5 \cdot 10^{-4})E$	(49)

LS4	
$\mathrm{F} = -17.80 + (1.54 \cdot 10^{-5})A - (5 \cdot 10^{-4})B + 0.05C - 0.25D - 3473E$	(50)
$\mathrm{G} = 0.00683 + (1.35 \cdot 10^{-10})A + (1.36 \cdot 10^{-9})B - (7 \cdot 10^{-8})C - (5 \cdot 10^{-7})D - (1.23 \cdot 10^{-3})E$	(51)

Where:

A is the masonry Young Modulus (E) expressed in $\mathrm{kN/m^2}$.

B is the masonry compressive strength (f_c) expressed in $\mathrm{kN/m^2}$.

C is the masonry tensile strength (f_t) expressed in $\mathrm{kN/m^2}$.

D is the masonry compressive fracture energy (Gfc) expressed in kN/m.

E is the masonry tensile fracture energy (Gf1) expressed in kN/m.

F is the load associated to a specific limit state expressed in kN.

G is the displacement associated to a specific limit state expressed in m.

Variables from A to C are reported in Table 2.6 resulting from the updating process for Masonry Typology 6 carried out based on Bayesian inference.

Tensile fracture energy (Gf1) and Compressive fracture energy (Gfc) are essentially depending on the Young modulus value based on the expressions proposed in Section 3.5 (see equation from 26 to 29). This set of parameters have been selected since they represent the input data used to characterize the mechanical behaviour of the FE-based macro models used in this study.

Once the expressions are applied to estimate a specific load and displacement level, the variables must be expressed in the same units listed before. The estimated results, namely load and displacement levels, will be expressed in kN and m respectively.

Table 5.1 and Table 5.2 present the P-values and the standardized beta coefficients (β) resulting from the dataset processing.

P-values are used to assess the significance of each independent variable's contribution to the overall model. A P-value lower than 0.05, which is commonly assumed as a reference significance level) suggests that the variable is significantly contributing to the model's ability to predict the dependent variable. Conversely, a high P-value indicates that the variable does not provide a significant contribution to the model's prediction, hence it could be potentially removed without affecting the model's reliability/effectiveness. Based on the considerations highlighted regarding the P-values displayed in Table 5.1, it is worth mentioning that variables with P-values higher than 0.05 could be removed from the final expressions provided.

This is also confirmed by the corresponding value of the standardized beta coefficient (Table 5.2). Beta coefficients result from a multiple linear regression analysis in which the variables have been standardized, namely transformed so that each variable has a mean of zero and a standard deviation of one. The primary purpose of standardized beta coefficients is to allow for the comparison of the relative importance of each predictor variable in the regression model.

The absolute value (magnitude) of a standardized beta coefficient reflects the relative importance of the predictor variable. Hence, smaller absolute values indicate a weaker effect on the dependent variable.

A positive sign, in a beta coefficient, means that as the predictor variable increases, the dependent variable also increases, and vice versa. Finally, since all variables are on the same scale (after their standardization), it is possible to directly compare the magnitudes of standardized beta coefficients to assess which predictors have more significant effects.

The P-values reported in Table 5.1 confirm that, for all the limit states defined, the displacement estimation is strongly governed by the Young Modulus (A variable), whereas the remaining parameters considered in the multiple linear regression have a reduced influence. On the other hand, the load capacity is highly influenced by variable A, C and E (Young modulus, tensile strength and tensile fracture energy). Indeed, these parameters strongly affect the final load capacity.

Table 5.1 – List of P-values for equations 44 to 51

P-VALUES	**LS1**		**LS2**		**LS3**		**LS4**	
VARIABLE	**Load (F)**	**Displ. (G)**	**Load (F)**	**Displ. (G)**	**Load (F)**	**Displ. (G)**	**Load (F)**	**Displ. (G)**
A	3.972e-09	7.24e-45	2.58e-13	8.74e-48	2.581e-13	6.414e-31	7.912e-15	1.54e-41
B	0.53	0.928	0.723	0.404	0.723	0.646	0.613	0.689
C	0.000359	0.778	7.781e-06	0.368	7.78·e-6	0.0924	8.026e-08	0.0283
D	0.646	0.072	0.715	0.465	0.715	0.602	0.550	0.723
E	5.53e-06	0.979	1.14e-09	0.770	1.139e-09	0.584	9.064e-14	0.369

Table 5.2 confirms the trend previously described. Moreover, beta coefficients provide insight regarding the relationship between dependent and independent variables. Looking at the values of beta coefficients for displacement estimation, it is clear that the Young Modulus is the most influential variable (highest beta coefficient). With regard to the displacement estimation, higher Young Modulus corresponds to lower displacement levels attained in those limit states associated to the linear behaviour of the models up to the peak load, LS1 and LS2 respectively.

Table 5.2 – List of standardized beta coefficients (β) for equations 44 to 51

β	**LS1**		**LS2**		**LS3**		**LS4**	
VARIABLE	**Load (F)**	**Displ. (G)**	**Load (F)**	**Displ. (G)**	**Load (F)**	**Displ. (G)**	**Load (F)**	**Displ. (G)**
A	0.586	-0.923	0.571	-0.973	0.571	0.970	0.561	0.984
B	-0.1106	-0.00625	-0.0465	-0.0562	-0.0465	0.0505	-0.06	0.0324
C	0.386	-0.0116	0.367	0.0360	0.367	-0.110	0.411	-0.107
D	-0.0576	0.0891	0.0341	0.0349	0.034	-0.0406	-0.0514	0.0208
E	0.301	-0.00066	0.314	0.00696	0.314	0.0214	0.387	-0.0273

Conversely, higher Young Modulus corresponds to higher displacement level attained in those limit states associated to the nonlinear behaviour of the models (LS3 and LS4). The remaining parameters appear to be negligible in the displacement estimation.

On the other hand, looking at the beta coefficient related to the load estimation it is possible to notice that, in general, the load capacity is governed by Young Modulus (A), tensile strength (C) and tensile fracture energy (E). An increase in these variables corresponds to an increase in the load capacity.

Table 5.3 summarizes the root mean square error (RMSE) and the mean absolute error (MAE) resulted from the multiple linear regression performed. Low values of both RMSE and MAE prove that the model is associated with a good performance. Therefore the predictions are consistently aligned with the actual values. Moreover, the small difference between RMSE and MAE suggests a lack of significant outliers in the data in both load estimation and displacement estimation.

Table 5.3 – Summary of RMSE and MAE measurements

	LS1		**LS2**		**LS3**		**LS4**	
	Load (F)	**Displ. (G)**	**Load (F)**	**Displ. (G)**	**Load (F)**	**Displ. (G)**	**Load (F)**	**Displ. (G)**
RMSE	1.88	9.38·e-6	35.48	2.96·e-5	17.74	4.05·e-5	11.25	3.85·e-5
MAE	1.51	7.61·e-6	28.19	2.36·e-5	14.09	3.26·e-5	8.89	3.08·e-5

Figure 5.7 shows the correlation between computed numerical load and predicted values for each limit state resulted from the application of the regression model. The correlation appears to be fairly accurate looking at the R-squared coefficient in LS2, LS3 and LS4 model (Figure 5.7b-c-d), whereas a slightly lower value is associated to the load levels in LS1 (Figure 5.7a).

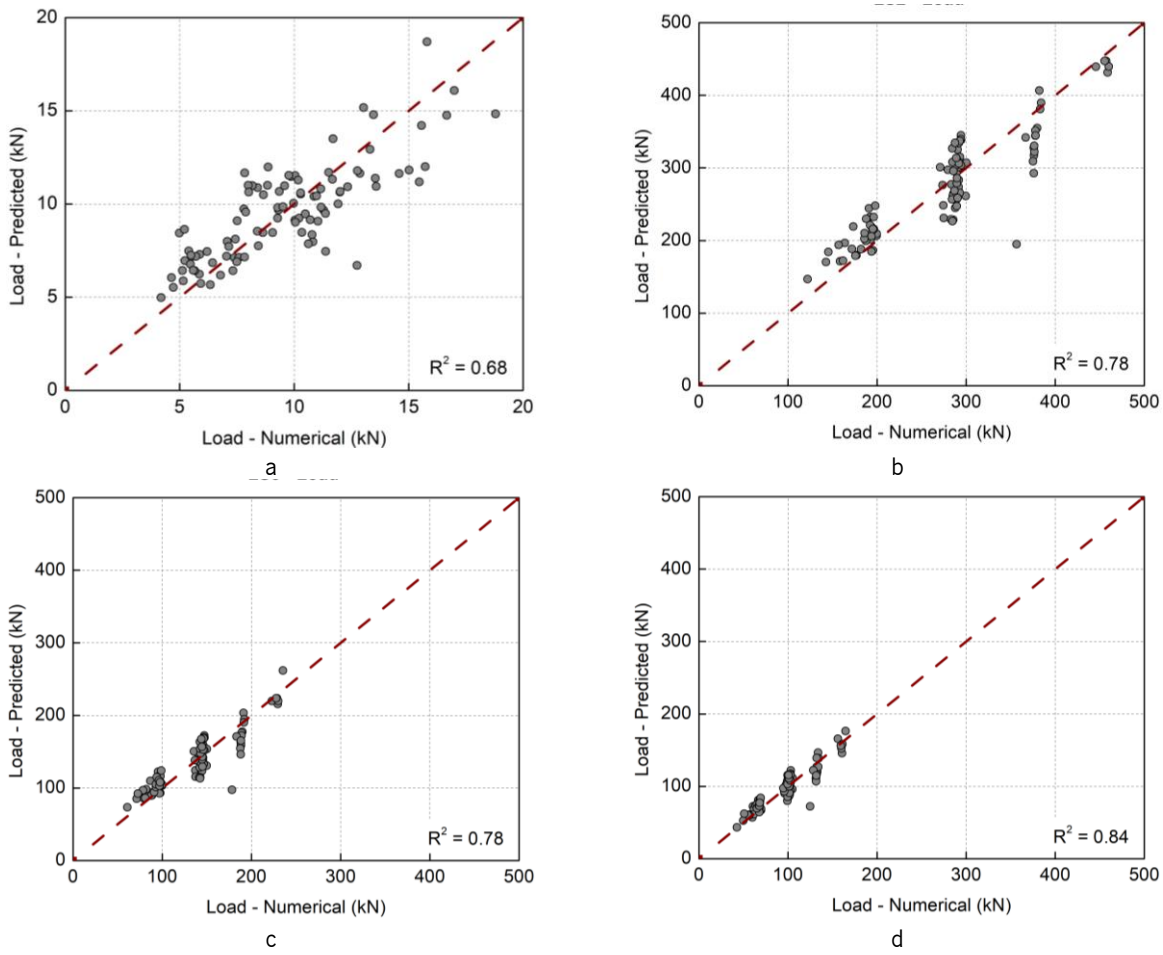


Figure 5.7 – Scatter plot load levels limit states LS1 (a), LS2 (b), LS3 (c), LS4 (d)

The high R-squared value suggests that the independent variables selected for the model are good predictors of the dependent variable. Additionally, it is also possible to infer that a large proportion of the variance in the dependent variable is explained by the independent variables.

The scatter plots related to the displacement levels associated to each limit states (Figure 5.8) show a good effectiveness of the predictive models also corroborated by high values of the R-squared coefficients, ranging from 0.86 to 0.95. This trend can be also due to the reduced variation characterising the dependent variable considered in the predictive model.

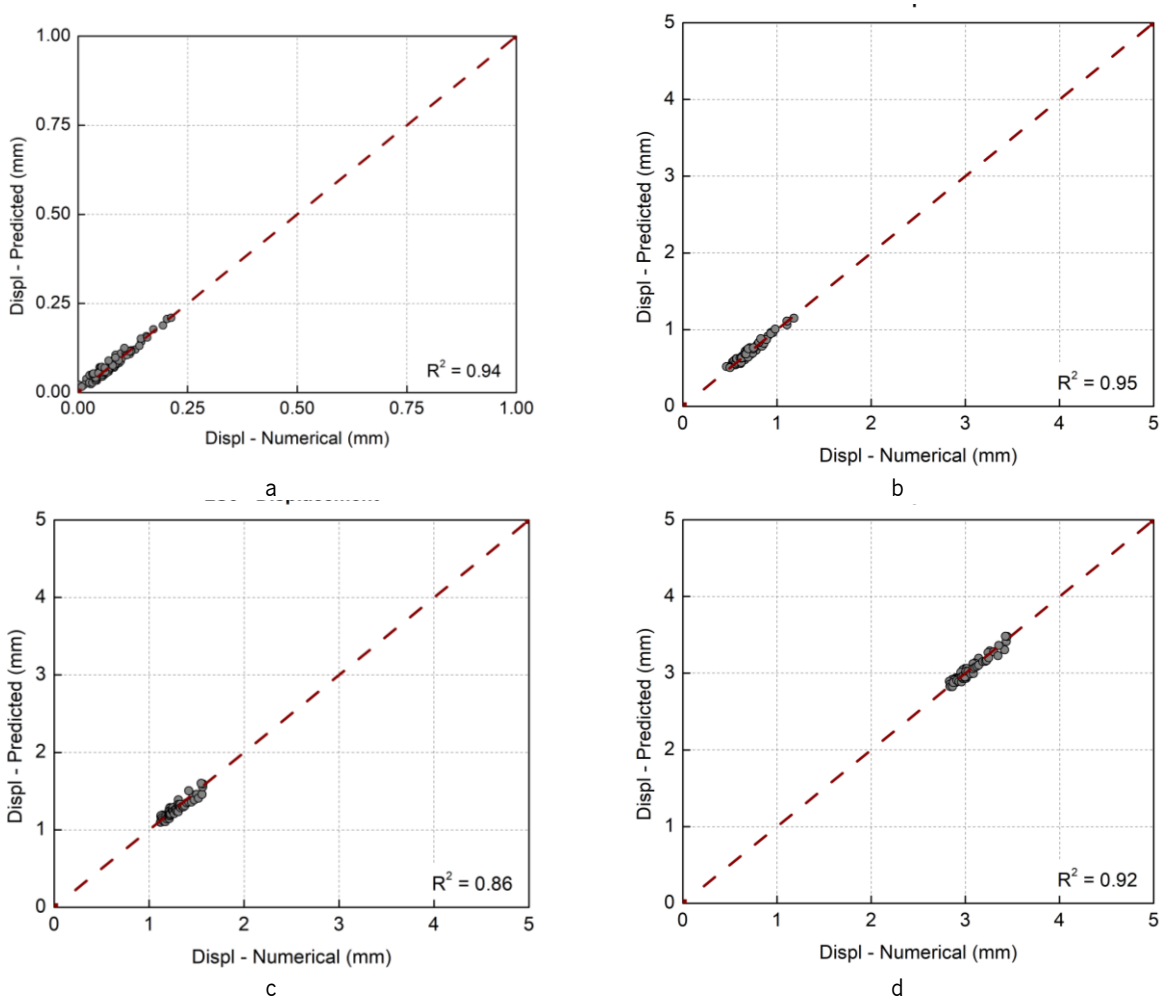


Figure 5.8 – Scatter plot displacement levels limit states LS1 (a), LS2 (b), LS3 (c), LS4 (d)

5.2.2 Empirical expressions for the estimation of mechanical parameters in different numerical modelling approaches: FEM vs DEM

As highlighted in the previous sections, shifting from FEM to DEM modelling approach has been identified as one of the open issues related to the calibration of numerical models. In this regard, an attempt has been made to define a set of empirical expressions for the estimation of input mechanical parameters in both finite element (FE) macro-models and distinct element (DE) simplified micro-models.

The load-displacements curves obtained by mean of FE analyses have been matched to load-displacement curves resulted from pushover analyses performed using the distinct element method. The dataset resulting from this operation (see Annex 3.6 – Table of interface properties for DE-based analyses) correlates the input

parameters commonly used in a FE macro-modelling approach to the interface properties needed to characterize the mechanical behaviour in distinct element models.

Once the dataset was defined (see Annex 3.6 – Table of interface properties for DE-based analyses), multiple linear regression analyses were carried out to define a correlation between the masonry Young's Modulus and the interface properties, namely normal stiffness, shear stiffness, cohesion, and tensile strength. The Young's Modulus has been selected as a reference parameter since on one hand the input parameters considered in the FE macro-models analyzed in this study derive from equations depending on the Young's Modulus values and, on the other hand, Young's Modulus is deemed to be the most straightforward mechanical parameter to assess by means of in-situ experimental tests, e.g., sonic, or flat-jack tests. The expressions resulting from the multiple linear regression are presented below:

$\mathrm{B} = -64338 + 1.11\mathrm{A}$	(52)
$\mathrm{C} = -32169 + 0.55\mathrm{A}$	(53)
$\mathrm{D} = -10.39 + 4\mathrm{e}^{-5}\mathrm{A}$	(54)
$\mathrm{E} = -12.85 + 4.5\mathrm{e}^{-5}\mathrm{A}$	(55)

Where:

A is the masonry Young's Modulus (E) expressed in kN/m^2.

B is the masonry Normal Stiffness expressed in kN/m^3.

C is the masonry Shear Stiffness expressed in kN/m^3.

D is the masonry Tensile Strength expressed in kN/m^2.

E is the masonry Cohesion expressed in kN/m^2.

Table 5.4 summarizes the root mean square error (RMSE) and the mean absolute error (MAE) resulted from the multiple linear regression performed. The variables considered show similar values of RMSE and MAE indicating a balanced errors distribution with no significant outliers.

Table 5.4 – Summary of RMSE and MAE measurements

	Normal Stiffness	**Shear Stiffness**	**Tensile Strength**	**Cohesion**
	B	**C**	**D**	**E**
RMSE	516471	258235	29.49	36.82
MAE	387996	193998	22.82	28.44

Figure 5.9 shows the correlation among the numerical and predicted values related to the interface properties, namely normal stiffness (Figure 5.9a), shear stiffness (Figure 5.9b), tensile strength (Figure 5.9c) and cohesion (Figure 5.9d).

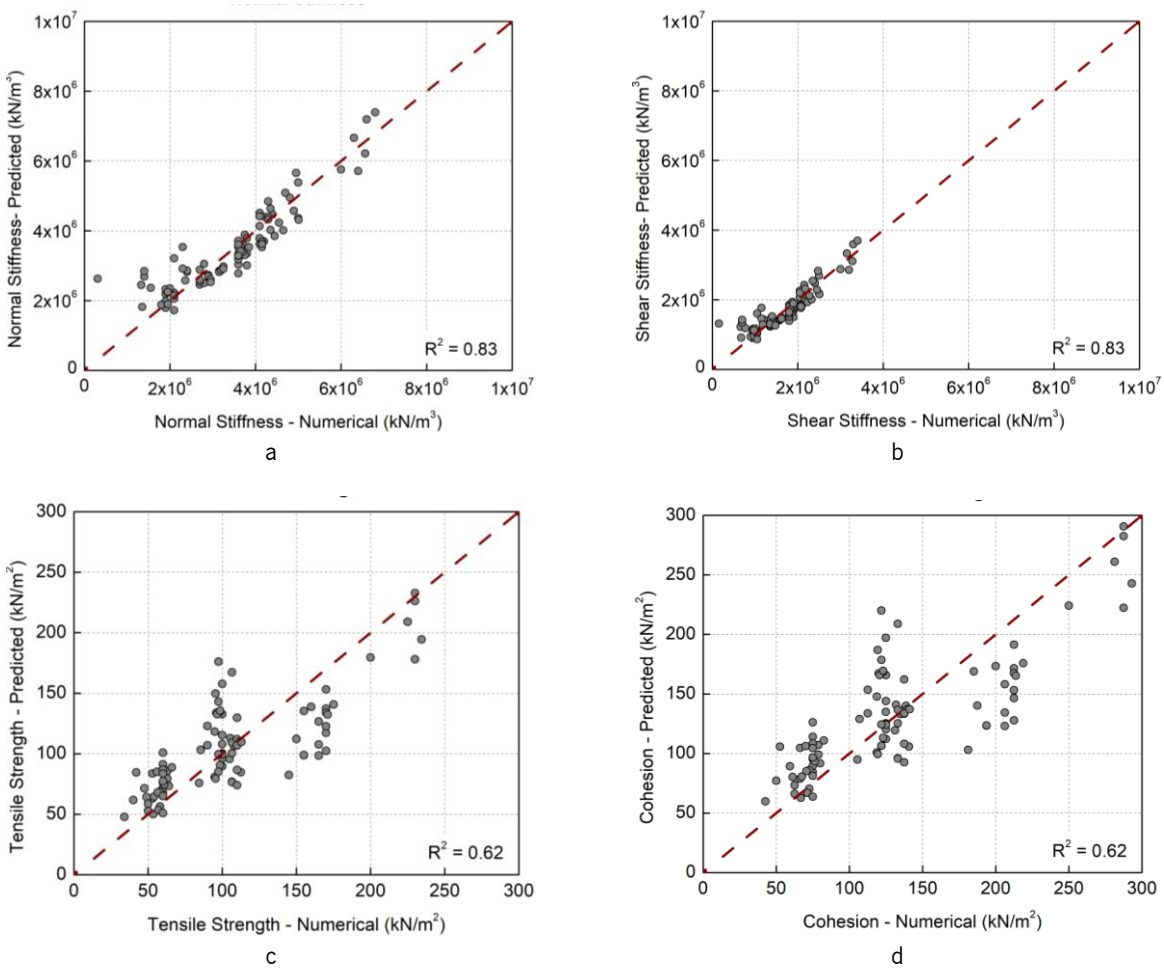


Figure 5.9 – Scatter plot load Interface Properties Normal stiffness (a), Shear stiffness (b), Tensile strength (c), Cohesion (d)

The correlation between Young's Modulus and Stiffness (both normal and shear) is fairly accurate, as it is confirmed by the R-squared coefficient equal to 0.83. A lower R-squared value, associated to the expression related to tensile strength and cohesion (0.62), may suggest that the relationship between these variables is not linear.

Young's Modulus and stiffness parameters are intended to estimate the physical behaviour of masonry in the elastic regime, hence also from a physical standpoint, even if used in different modeling approaches, these parameters describe the same masonry feature.

On the other hand, tensile strength and cohesion strongly influence the load capacity and the masonry walls' nonlinear behaviour. This aspect may explain the lower R-squared coefficient compared to the R-squared coefficient obtained for parameters such as normal/shear stiffness, which mostly governs the models' elastic behaviour, hence having a more substantial linear relation.

5.3 Numerical parametric study on geometrical characteristics of masonry walls

The parametric study addressing the variation of masonry bond geometrical characteristics has been defined considering the insights gathered in Chapter 4 regarding the work carried out on reduced scale models. Overall, it was detected that through-stones did not have a significant influence on the out-of-plane static cyclic performance. Moreover, no significant differences were visible in the models with staggered leaves and perfectly overlapped leaves configuration. Finally, the partially fulfilled condition of masonry bond parameters proved to be difficult to simulate and, in general, the analyses of models presenting partially fulfilled geometrical features yield unexpected or misleading results consisting in a better performance compared to models with masonry bond parameters in fulfilled configurations.

Based on these premises, the dataset for the geometrical parametric study has been built considering models that simulate full-scale walls with regular masonry units and mortar joints (Masonry Type 6, see Figure 2.1 in Chapter 2). It is expected that the use of full-scale models will enable to have a deeper understanding of the through-stones actual role in improving the out-of-plane performance of the walls.

Moreover, it has been decided to disregard models with staggered leaves configuration since this parameter does not represent a source of significant variation in the out-of-plane response of the walls as highlighted in the previous study. Conversely, two different corner configurations have been modelled, namely good corner interlock and ineffective corner interlock (see also Figure 4.14 in Chapter 4).

In order to avoid misleading results and ambiguity in model generation, only parameters in fulfilled (F) or not fulfilled (NF) configuration have been considered for the definition of the masonry bonds. Therefore, since the parameters' variation involves vertical joints configuration (VJ), horizontal joints configuration (HJ) and wall connection (WC), the total number of masonry bond configuration is equal to 8 as it is summarized in Table 5.5.

Table 5.5 – Reference combinations masonry bond configuration

Comb_#	WC	HJ	VJ
1	F	F	F
2	F	F	NF
3	F	NF	F
4	F	NF	NF
5	NF	F	F
6	NF	F	NF
7	NF	NF	F
8	NF	NF	NF

Additional geometrical features such as height variation, span variation and thickness variation were analyzed in the study. The geometrical configuration of the reference wall (see Figure 5.1) has been modified in order to generate 3 more models with increased height (4.05 m, 5.40 m and 6.75 m respectively) and two more models with increased span (6.75 m and 9 m respectively). Two different thicknesses have been also considered, namely 60 cm and 40 cm. The slenderness of the models ranges from 4 to 16.875, whereas the thickness to span ratio ranges from 0.04 to 0.13.

The masonry bond configurations previously defined and based on MQI guidelines (Table 5.5) have been applied to all the models. Therefore, the final number of models built following the aforementioned criteria is 96 for each corner configuration (good/bad interlock), hence 192 models were prepared in total. Figure 5.10 summarizes the geometrical configuration of the models built to perform the parametric study.

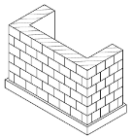
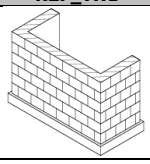
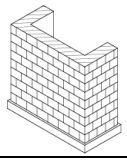
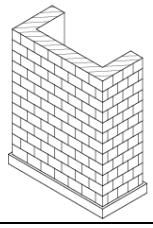
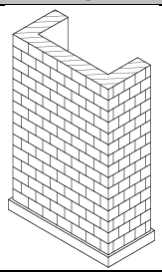
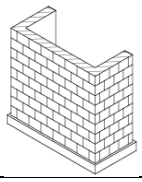
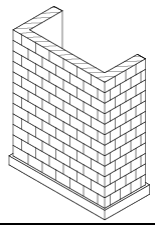
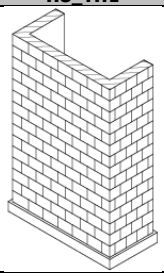
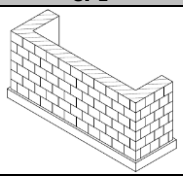
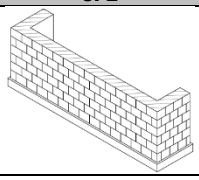
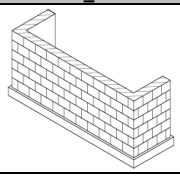
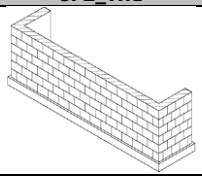
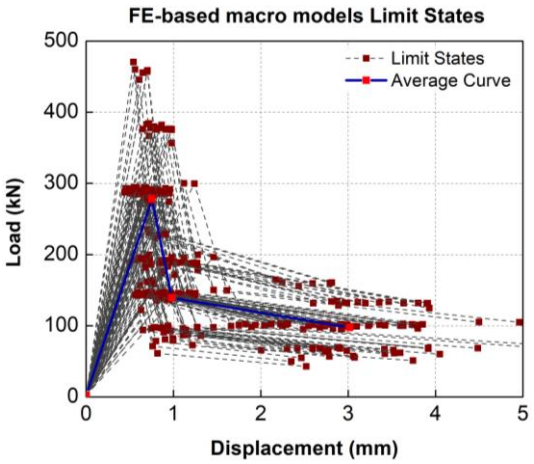
REF	REF_TH1	
		
Span = 4.50 m Height = 2.70 m Thickness = 0.60 m Slenderness = 4.5	Span = 4.50 m Height = 2.7 m Thickness = 0.40 m Slenderness = 11.25	
H1	**H2**	**H3**
		
Span = 4.50 m Height = 4.05 m Thickness = 0.60 m Slenderness = 4.5	Span = 4.50 m Height = 5.4 m Thickness = 0.60 m Slenderness = 9	Span = 4.50 m Height = 6.75 m Thickness = 0.60 m Slenderness = 11.25
H1_TH1	**H2_TH1**	**H3_TH1**
		
Span = 4.50 m Height = 4.05 m Thickness = 0.40 m Slenderness = 10.125	Span = 4.50 m Height = 5.4 m Thickness = 0.40 m Slenderness = 13.5	Span = 4.50 m Height = 6.75 m Thickness = 0.40 m Slenderness = 16.875
SP1	**SP2**	
		
Span = 6.75 m Height = 2.70 m Thickness = 0.60 m Slenderness = 4.5	Span = 9 m Height = 2.70 m Thickness = 0.60 m Slenderness = 4.5	
SP1_TH1	**SP2_TH1**	
		
Span = 6.75 m Height = 2.75 m Thickness = 0.40 m Slenderness = 6.75	Span = 9 m Height = 2.7 m Thickness = 0.40 m Slenderness = 6.75	

Figure 5.10 – Geometrical configuration 3D models parametric study.

For the sake of conciseness, a summary of all the 3D models generated for this study, together with their masonry bond parameter configuration, is reported in Annex 3.7 – Set 1 3D Models (good corner interlock) and Annex 3.8 – Set 2 3D Models (ineffective corner interlock).

The pushover analyses consist in the incremental application of a load proportional to the mass of the model in the out-of-plane direction. The boundary conditions are the same adopted for the macro model parametric study, therefore the base of the models has been considered fully constrained and a distributed vertical load equal to 10 kN has been applied to each lateral wall. The final dataset presents 192 load-displacement curves, obtained by means of DE-based pushover analyses.

All the models have the same mechanical properties, estimated based on the average three-linear curve resulted from the limit states definition carried out after the macro model parametric study (Figure 5.11a). A fitting procedure (trial/error approach) has been conducted considering the reference DE model in order to fit the average three-linear curve and to define a set of reference interface properties to use in the parametric study. The final interface properties used for the DE-based models are shown in Figure 5.11b.



a

Normal Stiffness (k_n)	3.00E+9 N/m³
Shear Stiffness (k_s)	1.50E+9 N/m³
Tensile Strength (f_t)	1.00E+5 N/m²
Cohesion (c)	1.25E+5 N/m²
Dilatancy (dl)	0 N/m²
Friction Angle (fr)	33°

b

Figure 5.11 – Average Limit States curves for the calibration of the reference DE-based model (a); final mechanical properties DE-based reference model (b)

5.3.1 Outcomes of the parametric study on geometrical features and masonry bond characteristics in two-leaf masonry walls

This section aims to grasp the recurring trends and patterns arisen from the analysis of geometrical parameters, such as slenderness, height to span ratio, and thickness to span ratio, in both sets of models examined. Finally, a comparison of the out-of-plane load capacity will also be presented in correlation with the masonry bond configuration.

In order to assess the influence of the aforementioned geometrical characteristics on the out-of-plane performance of the full-scale models built for the study, the data resulting from the numerical analyses performed is presented in terms of box plots. When the influence of the slenderness is considered, the graphs have been divided into 2 groups, namely 60 cm thickness and 40 cm thickness set of models. Each box plot presents the results of models belonging to the same series, for instance REF_C1 box plot refers to walls having the reference geometry shown in Figure 5.10 with 8 different masonry bond configurations defined according to Table 5.5.

Additionally, the series of models differing only in their corner configuration have been represented using the same colour. The box plots related to the models with good corner interlock (C1 configuration) are represented in solid colour, whereas box plots related to an ineffective corner configuration (C2 configuration) have an additional crossed lines pattern.

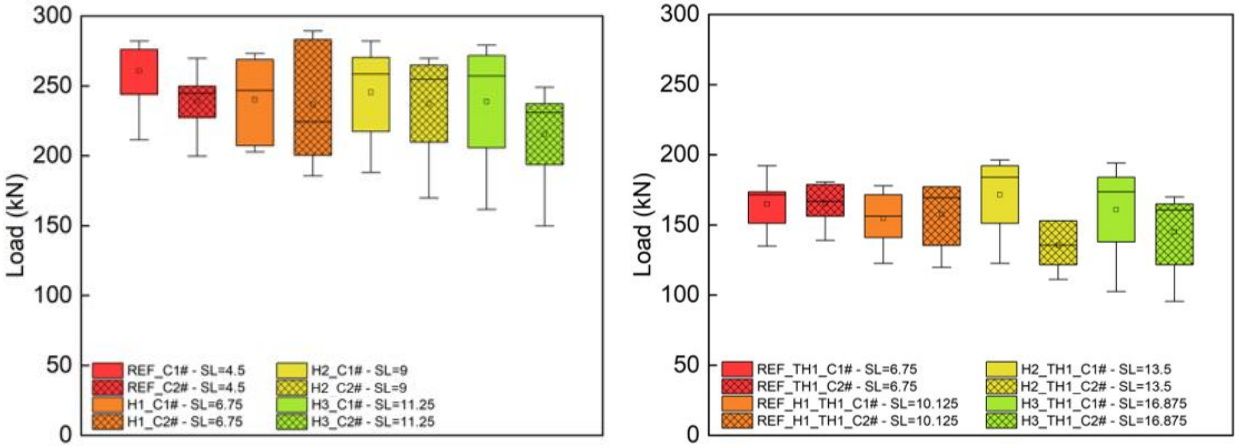
Finally, in order to have a meaningful and clear insight about the data gathered, the graphs presented have been also divided based on the span variation of the models in the dataset.

The models can be classified according to their slenderness into 7 groups:

- Group 1 – Slenderness = 4.5
- Group 2 – Slenderness = 6.75
- Group 3 – Slenderness = 9
- Group 4 – Slenderness = 10.125
- Group 5 – Slenderness = 11.25
- Group 6 – Slenderness = 13.5
- Group 7 – Slenderness = 16.875

Figure 5.12a shows that the models with higher thickness (60 cm) display higher peak load than those with a reduced thickness (Figure 5.12b). In both cases, the increasing slenderness results in a reduction of the

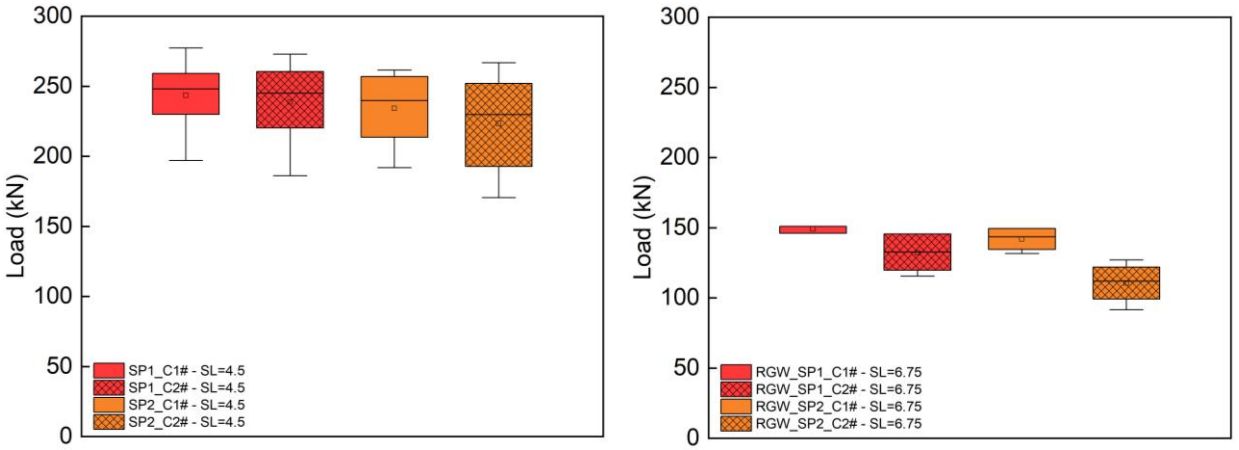
load capacity. Moreover, models with bad corner interlock (C2 configuration) reached lower load levels than the corresponding models with good corner interlock (C1 configuration).



a b

Figure 5.12 – Influence of slenderness in models with 60 cm thickness (a) and 40 cm thickness (b) considering height variation.

Looking at the boxplots related to the models with increased span (Figure 5.14a-b), it appears that the difference in terms of performance is mainly due to the presence or absence of a good corner interlock. Indeed, the peak loads attained in the models with the same characteristics display a reduced variability. However, a span increment combined with a reduced thickness of the models leads to lower out-of-plane capacity as visible in Figure 5.14b.



a b

Figure 5.13 – Influence of slenderness in models with 60 cm thickness (a) and 40 cm thickness (b) considering span variation.

Moreover, both Figure 5.12 and Figure 5.13 show that the series of models with C2 corner configuration (ineffective interlock) yield results affected by a more significant variability than the models characterized by good corner interlock (C1 configuration). This trend is also confirmed by looking at the interval ranging from the first to the third quartile in the box plots with crossed line patterns related to C2 corner configuration models which are more extended than the corresponding box plots referring to the C1 configuration set of models. Here, it is also possible to observe the influence of the slenderness ratio. The increase of slenderness from 4.5 to 6.75 results in a considerable reduction in the out-of-plane peak load.

The models can be classified according to their height to span ratio into 6 groups (Figure 5.14):

- Group 1 – H/Span = 0.3
- Group 2 – H/Span = 0.4
- Group 3 – H/Span = 0.6
- Group 4 – H/Span = 0.9
- Group 5 – H/Span = 1.2
- Group 6 – H/Span = 1.5

Results are analyzed according to the corner configuration of the models, namely C1 (Figure 5.14a) and C2 (Figure 5.14b).

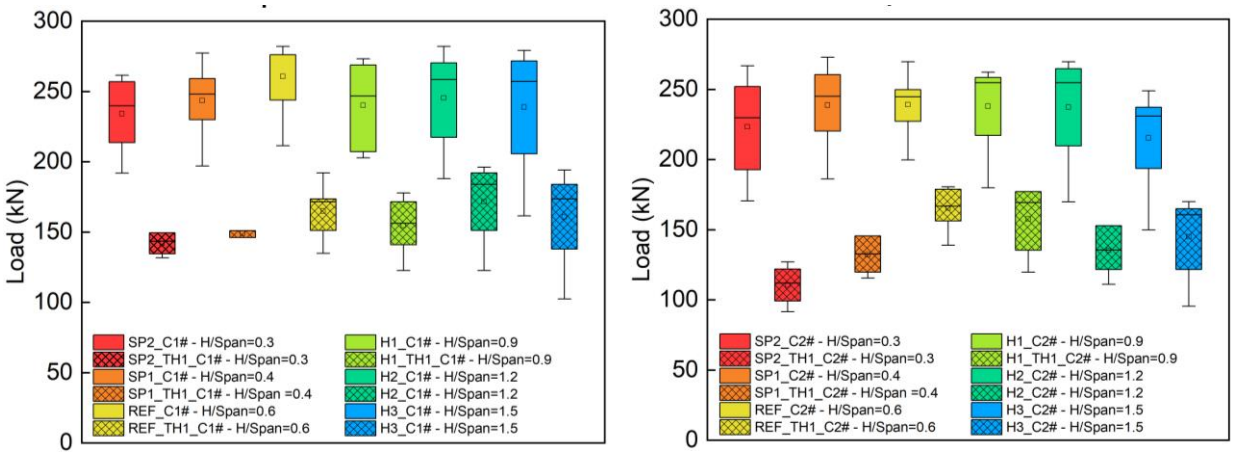


Figure 5.14 – Influence of height to span ratio in C1 sets of models (a) and C2 sets of models (b)

Models having the same height and span are represented using the same colour. The difference between solid-coloured box plots and box plots with crossed line patterns is that the former refers to 60 cm thickness models, whereas the latter refers to 40 cm thickness models. Higher height-to-span ratio corresponds to higher load. Overall, models with good corner interlock C1 performed better and displayed a higher load capacity than the corresponding models in C2 configuration (poor corner interlock).

Models with reduced thickness show less out-of-plane capacity than models with thickness equal to 60 cm. Out-of-plane capacity increases according to the rise in Height Span ratio. The increasing trend is stabilized for higher height-to-span ratios (H/Span > 1.2).

The models can be classified according to their thickness/span ratio, resulting into 5 groups:

- Group 1 – Thickness/Span = 0.04
- Group 2 – Thickness/Span = 0.06
- Group 3 – Thickness/Span = 0.07
- Group 4 – Thickness/Span = 0.09
- Group 5 – Thickness/Span = 0.13

Figure 5.15 shows a comparison among models with a progressively increasing thickness to span ratio. The box plots are divided based on the thickness of the models, namely 60 cm and 40 cm.

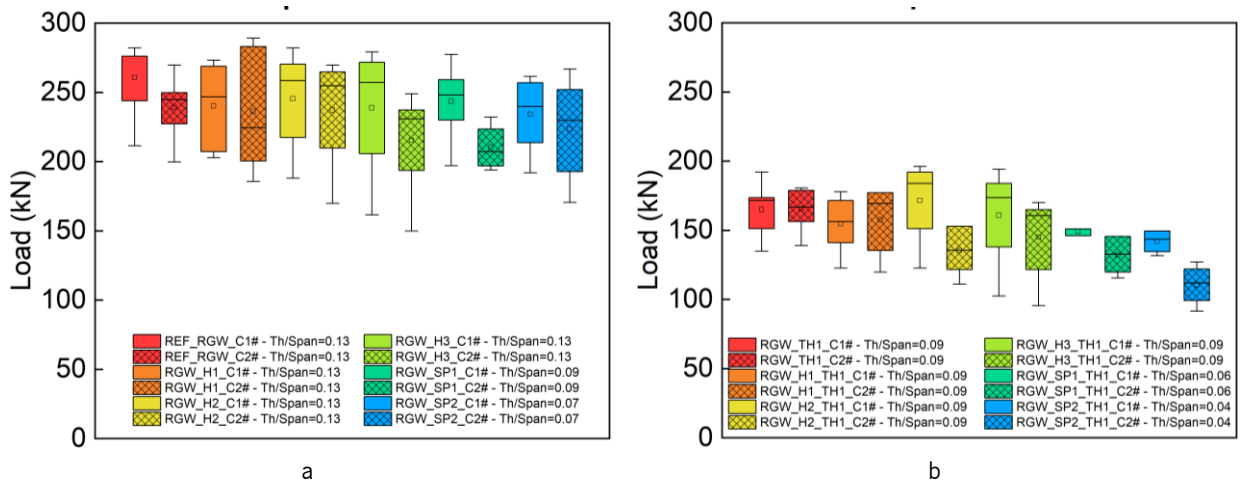


Figure 5.15 – Influence of thickness to span ratio in 60 cm thickness sets of models (a) and 40 cm thickness sets of models (b)

The box plots related to the models with good corner interlock (C1 configuration) are represented in solid colour, whereas box plots related to an ineffective corner configuration (C2 configuration) have an additional crossed lines pattern. Overall, the group of models with higher thickness (60 cm) attained load levels higher than the set of models with reduced thickness (40 cm). Additionally, a progressively decreasing thickness/span ratio results in a lower peak load. In the majority of cases, models with poor corner interlock display worse performances compared to the models with good corner configuration.

5.3.2 Analysis of the masonry bond configuration: recurring trends and main outcomes

The results of the geometrical parametric study are herein analyzed considering the main characteristics of the masonry bond configuration defined for each set of models, according to the combinations based on the Masonry Quality Index summarized in Table 5.5. Moreover, the results are divided based on the corner configuration and the thickness of the models. Finally it is worth mentioning that the legend provided in each figure, regarding the status of masonry bond parameters in fulfilled (F) or not fulfilled (NF) conditions, follows the same sequence reported in Table 5.5, hence the first parameter is wall connection (WC), followed by horizontal joints (HJ) and vertical joints (VJ) configuration.

Figure 5.16a shows the results of the models having the reference geometrical configuration. The highest load has been detected for fulfilled conditions in WC, HJ and VJ (282 kN). The lowest load characterizes the model with not fulfilled conditions in WC, HJ and VJ (212 kN).

Taking as a reference the maximum load, it is possible to say that when WC is not fulfilled the variation is 2.08%, when HJ is not fulfilled the variation is 4.17%, when VJ is not fulfilled the variation is 2.09%. In spite of the low differences, it appears that the parameter most affecting the peak load is HJ. The simultaneous unfulfilled condition of WC, HJ and VJ results in a 25.01% reduction of peak load.

Looking at the set of models with reduced thickness equal to 40 cm (Figure 5.16b) it is possible to say that when HJ is not fulfilled the variation from the maximum load (192 kN) is around 11% (172 kN), similarly to what occurs when VJ is not fulfilled. Hence, taken singularly, VJ HJ and WC equally affect the peak load since the out-of-plane capacity detected when WC is not fulfilled is 172 kN. The simultaneous unfulfilled condition of WC, HJ and VJ results in a 30% reduction of peak load (135 kN). Moreover, it is possible to say that the reduction of thickness results in a reduction of peak load ranging from 30 to 40%. The reduction of initial stiffness ranges from 50 to 60%.

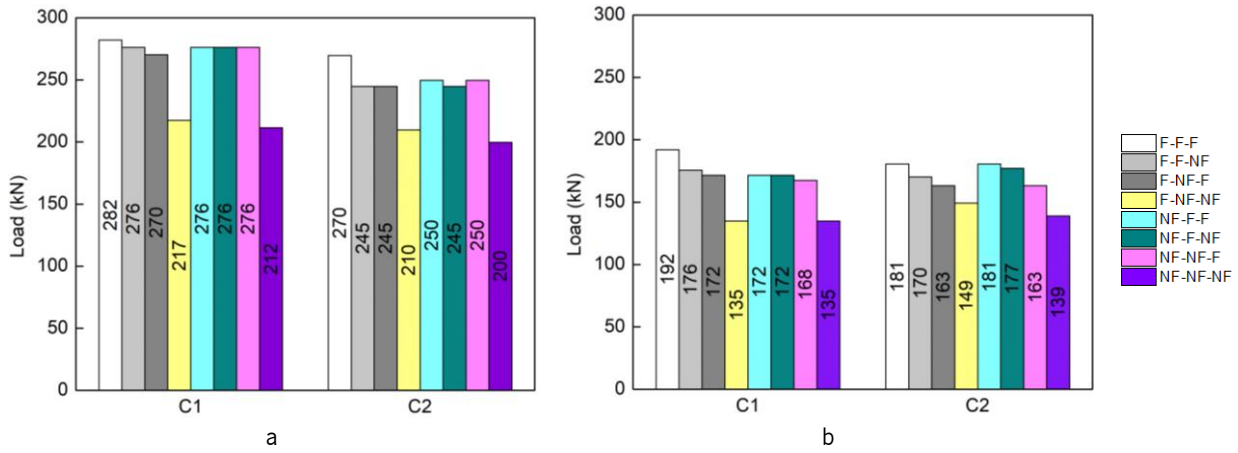


Figure 5.16 – Geometrical parametric study REF set models (a) and REF_TH1 set models (b)

In the models with bad corner interlock (C2 configuration) and standard thickness (60 cm), the highest load has been detected for fulfilled conditions in WC, HJ and VJ (269.7 kN). The lowest load is obtained for the model with not fulfilled conditions in WC, HJ and VJ (199.8 kN), see Figure 5.16a.

Taking as a reference the maximum load, it is possible to observe that when WC is not fulfilled the variation is 7.5% (270 kN vs 250 kN), when HJ and VJ are not fulfilled the variation is 9.26%. Hence taken singularly, the parameter most affecting the peak load are VJ and HJ. When all the geometric parameters (WC, HJ and VJ) are not fulfilled, a 26% reduction of peak load (270 kN vs 200 kN) has been detected, see Figure 5.15a.

Looking at the set of models with reduced thickness and poor corner interlock (C2) in Figure 5.16b, it is possible to say that when WC is not fulfilled the variation from the maximum out-of-plane capacity is null, whereas when HJ is not fulfilled the variation is approximately 10%, when VJ is not fulfilled the variation is 5.76%. The reduction of the peak load is about 23% when all parameters are not fulfilled.

Overall, for the models with C2 corner configuration the reduction of thickness results in a reduction of peak load ranging from 30 to 35%. The reduction of initial stiffness ranges from 35 to 55%.

Figure 5.17 show the results of models with increased height equal to 4.05 m. In the set of models with standard thickness equal to 60 cm (Figure 5.17a) and C1 corner configuration, the highest load has been detected for fulfilled conditions in WC, HJ and VJ (273 kN). The lowest load characterizes the model with not fulfilled conditions in WC, HJ and VJ (203 kN).

When WC is not fulfilled, no variation has been detected in the out-of-plane capacity compared to the maximum load characterising the model in fulfilled conditions. Hence taken singularly, the parameter most

affecting the peak load is HJ. The contemporary unfulfilled condition of WC, HJ and VJ results in a 25.78% reduction of peak load (273 kN vs 203 kN).

Looking at the walls with reduced thickness (40 cm) and C1 corner configuration (Figure 5.17b), it is possible to say that when WC is not fulfilled the variation is almost null, when HJ is not fulfilled the variation is 13.8%, when VJ is not fulfilled the variation is 6.9%. Hence taken singularly, the parameters most affecting the peak load are HJ and VJ. The contemporary unfulfilled condition of WC, HJ and VJ results in a 31% reduction of peak load.

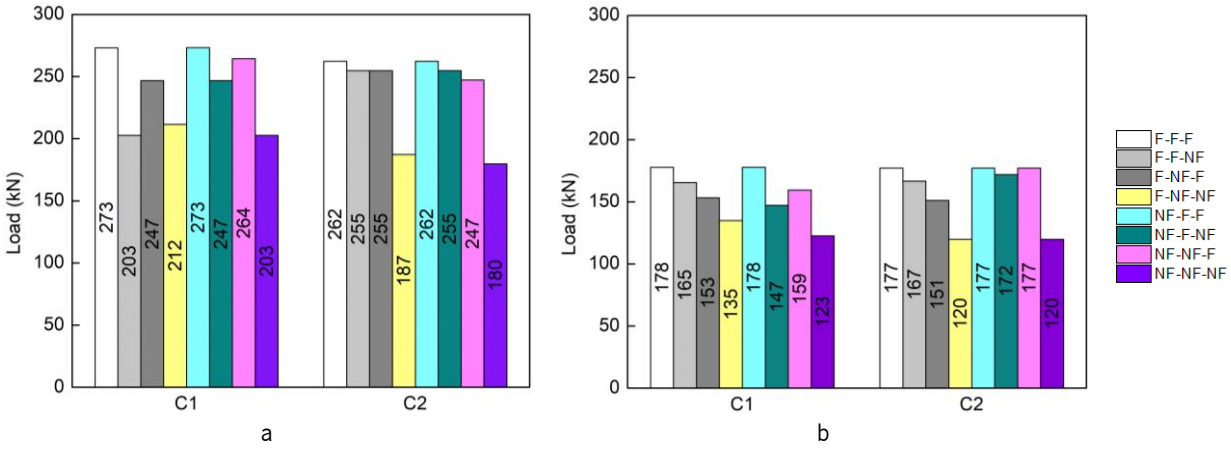


Figure 5.17 – Geometrical parametric study H1 set models (a) and H1_TH1 set models (b)

In the set of models with poor corner interlock (C2 configuration) and 60 cm thickness, the highest load has been detected for fulfilled conditions in WC, HJ and VJ (262 kN). The lowest load characterizes the model with not fulfilled conditions in WC, HJ and VJ (180 kN), see Figure 5.17a.

In the set of models with reduced thickness and C2 corner configuration (Figure 5.17b) it is possible to say that when WC is not fulfilled no variation is detectable in the maximum out-of-plane capacity (177 kN), whereas, when HJ is not fulfilled the variation is 14.7% (177 kN vs 151 kN) and, when VJ is not fulfilled the variation is 5.88% (177 kN vs 167 kN). Also for these models, the peak load reduction is significant when all the geometrical parameters are in a not fulfilled condition (32% reduction).

Figure 5.18 shows the results of models with increased height equal to 5.4 m. In the set of models with 60 cm thickness (Figure 5.18a), the highest load has been detected for fulfilled conditions in WC, HJ and VJ (282 kN). The lowest load characterizes the model with not fulfilled conditions in WC, HJ and VJ (188 kN).

When WC parameter is not fulfilled, the variation in terms of peak load is almost null, whereas if HJ and VJ is not fulfilled the variation is 8.33%. The simultaneous unfulfilled condition of WC, HJ and VJ results in a 33.34% reduction of peak load.

In the set of models with reduced thickness (Figure 5.18b), when WC is not fulfilled the variation of load capacity is negligible, when HJ is not fulfilled the variation is 12.5%, when VJ is not fulfilled the variation is 4.17%. Also in this case, the parameters most affecting the peak load are HJ and VJ. The contemporary unfulfilled condition of WC, HJ and VJ results in a 37.5% reduction of peak load. Moreover, thickness reduction results in a decrease of peak load ranging from 20 to 35%.

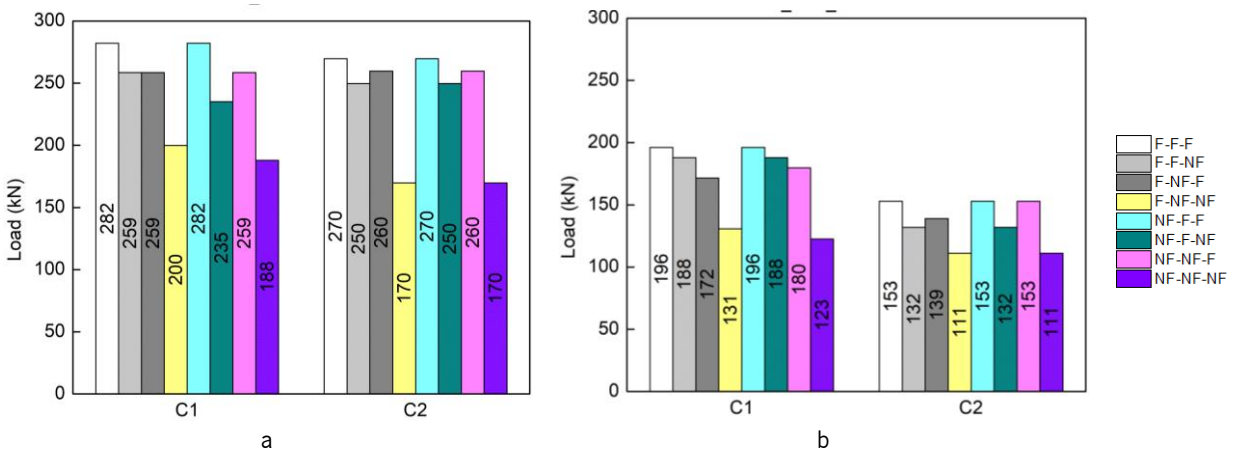


Figure 5.18 – Geometrical parametric study H2 set models (a) and H2_TH1 set models (b)

In the set of models with C2 corner configuration (Figure 5.18), the highest load has been detected for fulfilled conditions in WC, HJ and VJ (269.7 kN). The lowest load characterizes the model with not fulfilled conditions in WC, HJ and VJ (169.81 kN).

When WC is not fulfilled the peak load variation is almost null, when HJ is not fulfilled the variation is 3.7%, when VJ is not fulfilled the variation is 7.4%. The simultaneous unfulfilled condition of WC, HJ and VJ results in a 37% reduction of peak load.

In the set of models with reduced thickness (Figure 5.18b), when WC is not fulfilled the variation is negligible, when HJ and VJ are not fulfilled the variation is 9.08% and 13.63% respectively. A 27.3% drop of peak load has been detected in the model with WC, HJ and VJ not fulfilled. In this case, the reduction of thickness results in a reduction of peak load ranging from 35 to 45%.

Similarly to what detected and described above H3 set of models in both C1 and C2 configurations and for both thicknesses considered (60 cm and 40 cm) show a negligible influence of the WC parameter on the out-of-plane capacity of the models, which is, on the other hand, significantly influenced by the presence/absence of vertical and horizontal joints properly arranged. As it is expected, overall, models with poor corner interlock display lower capacity than the models with C1 corner configurations, see Figure 5.19.

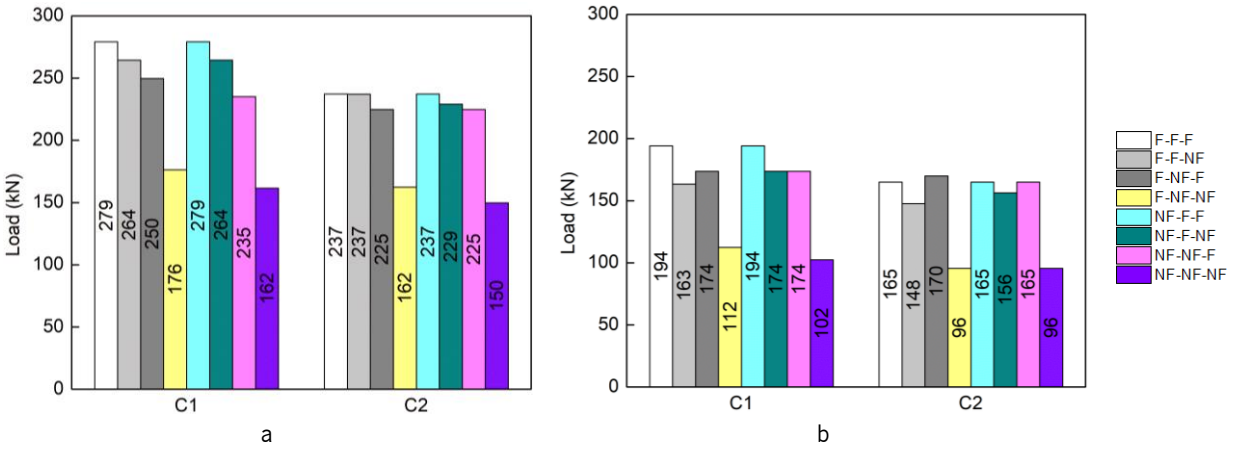


Figure 5.19 – Geometrical parametric study H3 set models (a) and H3_TH1 set models (b)

Figure 5.20 shows the results of the parametric study for those models with increased span equal to 6.75 m. In the set of models with standard thickness (60 cm) and C1 corner configuration, the highest load has been detected for fulfilled conditions in WC, HJ and VJ (277 kN). The lowest load characterizes the model having not fulfilled conditions in WC, HJ and VJ (197 kN), see Figure 5.20a.

In terms of load capacity, the most influential parameters are WC and HJ. In fact, when WC and HJ are not fulfilled the peak load variation is 10.53% compared to the reference maximum load (277 kN), on the other hand, if VJ is not fulfilled the variation is 5.27%. A 29% drop of peak load has been detected when all the geometrical parameters (WC, HJ and VJ) are not fulfilled.

Looking at the set of models with reduced thickness in both C1 and C2 corner configuration (Figure 5.20b), it is possible to say that a trend detected in the previous analyses regarding the role of WC parameter is confirmed. It appears that WC presence or absence is not so influential or beneficial for the out-of-plane capacity of the models considered. Of course, this is a pattern characterising the present study and related to aspects such as type of analyses performed, initial assumptions adopted to build the 3D geometrical models and boundary conditions considered in the numerical simulations. Overall, models with good corner interlock show higher out-of-plane capacity than models having C2 corner configuration. Furthermore, the

unfulfilled conditions in WC, HJ and VJ correspond to the lowest peak load detected in the set of models considered.

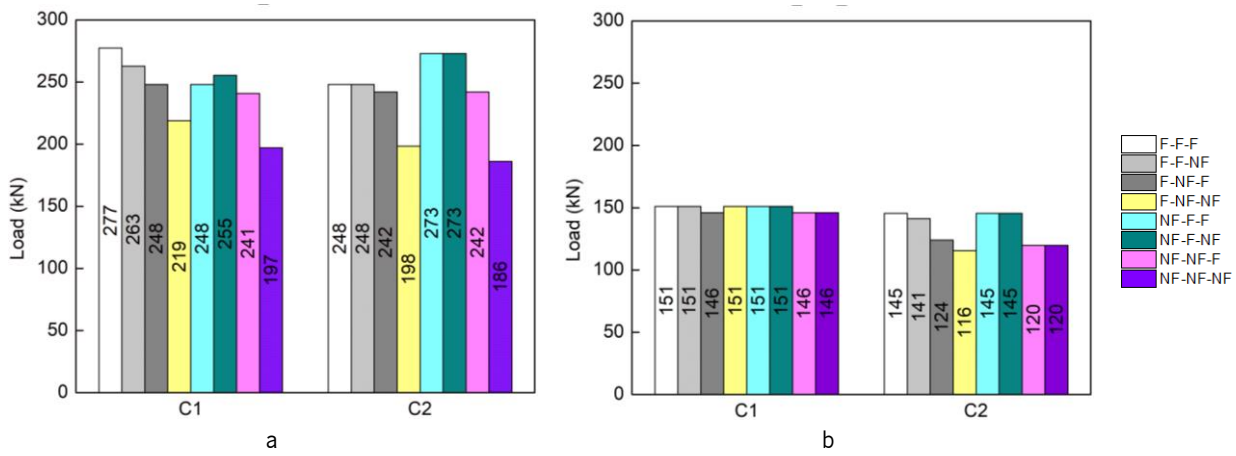


Figure 5.20 – Geometrical parametric study SP1 set models (a) and SP1_TH1 set models (b)

In the set of models with increased span equal to 9 m, 60 cm thickness and C1 corner configuration, the highest load has been detected for fulfilled conditions in WC, HJ and VJ (261.6 kN). The lowest load characterizes the model with not fulfilled conditions in WC, HJ and VJ (192 kN), see Figure 5.21a.

The variation of peak load is approximately 10 % when WC is not fulfilled, when HJ is not fulfilled the variation is 6.7%, whereas if VJ is not fulfilled the variation is 3.33%. The simultaneous unfulfilled condition of WC, HJ and VJ results in a 26.66% reduction of peak load, see Figure 5.21a.

In the set of models with ineffective corner interlock (C2), the highest load (267 kN) has been detected for fulfilled conditions just in the horizontal joints configuration (HJ). This result differs from all the outcomes previously detected and it is highly dependent on the geometrical configuration of the masonry bond, which apparently resulted in being more effective than models with WC, VJ and HJ in fulfilled conditions. Indeed, the generation of 3D models based on the Masonry Quality Index guidelines, has been a challenging task limited also by a process which was carried out manually.

Regarding the set of models with reduced thickness (Figure 5.21b), it is possible to say that WC and VJ do not significantly affect the out-of-plane capacity in both C1 and C2 corner configuration. However, the contemporary unfulfilled condition of WC, HJ and VJ always corresponds to the lowest peak load attained, namely 132 kN and 92 kN in C1 and C2 set of models respectively (see Figure 5.21b).

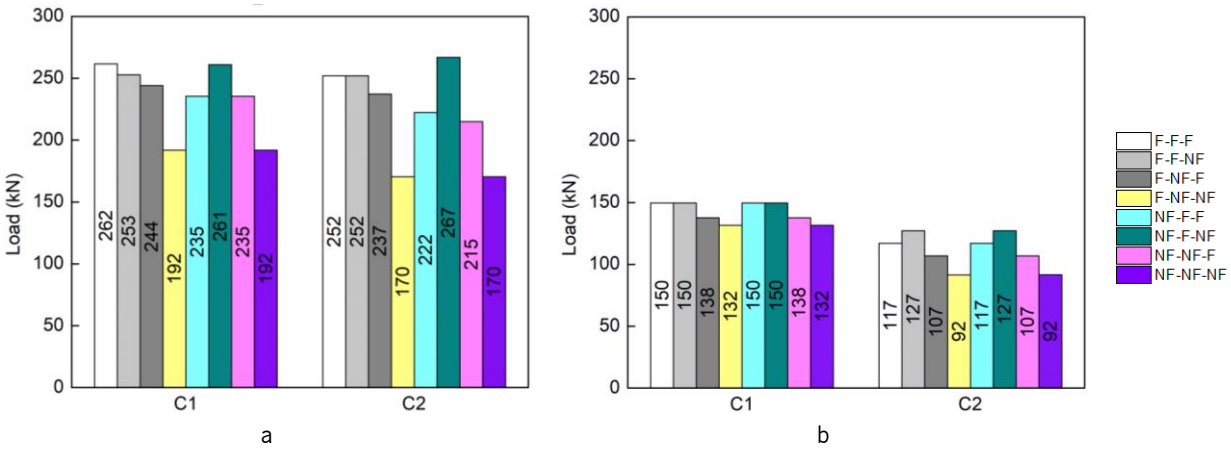


Figure 5.21 – Geometrical parametric study SP2 set models (a) and SP2_TH1 set models (b)

This section presents the results of the geometrical parametric study carried out considering a set of simplified DE-based micro-models. Their out-of-plane performance have been investigated by means of pushover analyses. From a mechanical standpoint, the models have the same interface properties, calibrated starting from the average three-linear curve results from the FE-based parametric study described in section 5.2.

In order to assess the influence of the masonry bond configuration on the structural performance of the models, 8 different stone units' arrangements have been built based on the variation of a set of reference parameters, namely wall connection (WC), horizontal joints configuration (HJ) and vertical joints configuration (VJ), see Table 5.5.

The models have been also modified considering parameters such as slenderness, thickness and span. To this end, it must be noted that two different thicknesses have been selected for the DE-based models, namely 60 cm (reference thickness) and 40 cm (reduced thickness indicated also as TH1). Moreover, the heights of the models range from 2.7 m to 6.75 m and the span variation ranges from 4.5 m to 9 m (see also Figure 5.10). Additionally, two corner configurations have been considered for all the models, corresponding to a good corner interlock (C1) and to a poor corner interlock (C2).

Overall, models in C1 set performed better than the corresponding models with poor corner interlock (C2 configuration). Models with reduced thickness (40 cm) displayed a load capacity lower than models with thickness equal to 60 cm.

The influence of slenderness and thickness on the out-of-plane capacity of the models is relevant. On one hand, higher slenderness values correspond to a drop in terms of peak-load. Conversely, models with higher thickness values displayed an enhanced out-of-plane capacity.

Span increase is associated to a loss of load capacity especially when it is combined with reduced thicknesses. Furthermore, an increase of the height values in large spanning walls resulted in a loss of out-of-plane capacity of the models analyzed.

In both C1 and C2 sets of models the lowest load always refers to the models with VJ, HJ and WC in unfulfilled conditions. To this end, it is important to point out an interesting trend arising from the study carried out which is related to the role of the wall connection parameter (WC) on the out-of-plane performance of the models. As opposed to what expected, WC did not show a significant influence on the load capacity of the models. Frequently, the lack of wall connection (WC not fulfilled) resulted in a null variation of peak load compared to those models having WC in fulfilled conditions.

This trend can be related to the intrinsic characteristics and assumptions of this study. The masonry typology considered (Masonry Type 6, see Chapter 2, Figure 2.1) relies on regularly cut stone units and, from a modelling standpoint, the models have been built considering no gaps between leaves (fully overlapped leaves). These factors may lead to a loss of significance in the role of WC as a key parameter for the definition of an effective masonry bond configuration.

Conversely, horizontal joints configuration (HJ) and vertical joins configuration (VJ) showed a significant influence on the out-of-plane performance of the wall and, especially when VJ has been singularly analyzed, it has been evident how the vertical joints configuration can strongly affect the failure mode of the walls under out-of-plane load. A similar conclusion can be drawn by looking at the outcomes of the corner configuration parameters (C1 and C2), which showed a predominant role in affecting peak load capacity and recurring failure mechanisms.

5.3.3 Empirical expressions for the out-of-plane load estimation based on reference geometrical parameters

This section presents the result of a multiple linear regression performed in order to define an empirical expression for the estimation of the out-of-plane capacity of 2-leaf masonry walls. The independent variables considered for the definition of the final mathematical expression are the reference parameters already selected and analyzed in the geometrical parametric study, namely through-stones configuration (WC), horizontal (HJ) and vertical joints (VJ) configuration, corner configuration (C1 or C2), slenderness, height to span ratio, and thickness to span ratio.

The linear regression performed merges together qualitative (categorical) and quantitative (continuous) data. In fact, WC, HJ and VJ parameters have been evaluated following the Masonry Quality Index guidelines [41],

hence the fulfilled condition, which is considered as the presence of a certain characteristic, is associated to the value 1, whereas the unfulfilled, which is considered as the absence of a certain characteristic, is associated to 0.

On the other hand, the remaining parameters (slenderness, height to span ratio, thickness to span ratio) have been treated as continuous variables with their actual numerical value. The reference database used to carry out the multiple linear regression is shown in Annex 3.12 – Dataset empirical expression for the out-of-plane load multiplier estimation based on geometrical parameter

Table 5.6 summarizes the value of mean, standard deviation and coefficient of variation related to continuous variables, namely slenderness, height to span ratio, thickness to span ratio, out-of-plane load capacity, and the load multiplier (see section 5.3.4).

Table 5.6 – Statistical indicators for continuous variables geometrical parametric study

	Slenderness	H/Span	Thick/Span	Load (kN)	Load Multiplier
MEAN	8.44	0.82	0.10	193.49	0.18
ST DEV	3.73	0.43	0.03	53.61	0.08
COV	44%	53%	30%	28%	46%

The expression resulted from the multiple linear regression to estimate the out-of-plane load capacity in 2-leaf stone masonry walls based on a set of geometrical parameters is presented below (equation 56).

$$H = 141 + 1.65A + 32.34B + 26.85C + 14.04D - 13.20E + 76.20F + 671G \quad (56)$$

Where:

A is the WC parameter assumed to be 0 (not fulfilled) or 1 (fulfilled).

B is the HJ parameter assumed to be 0 (not fulfilled) or 1 (fulfilled).

C is the VJ parameter assumed to be 0 (not fulfilled) or 1 (fulfilled).

D is the corner configuration parameter (CN) equal to 0 (poor interlock) or 1 (good interlock).

E is the Slenderness.

F is the Height to Span ratio.

G is the Thickness to Span ratio.

H is the out-of-plane load capacity.

All the variables in equation 56 are dimensionless, except for the H variable (out-of-plane load capacity) which is expressed in kN. Table 5.7 presents the P-values and the standardized coefficients resulted from the dataset processing. As above mentioned, P-values are used to assess the significance of each independent variable's contribution to the overall model. A low P-value (lower than 0.05 which is the value commonly assumed as a reference significance level) suggests that the variable is significantly contributing to the model's ability to predict the dependent variable. Looking at the P-values reported in Table 5.7, it is clear that all the variables considered in the predictive model have a high significance, except for the parameter A (wall connection WC). It is interesting to point out that the P-values are consistent to the recurring trends detected in section 5.3.2, hence WC does not have a considerable influence on the estimation of the out-of-plane load capacity of the walls analyzed.

Beta coefficients (Table 5.7) provide further validation of the trends identified. In fact, the lowest beta coefficient is associated with variable A (WC), confirming the lack of relevance of this parameter in the estimation of the out-of-plane load. Conversely, higher beta coefficients refer to the remaining variables. The highest absolute value (0.917) refers to the parameter E (slenderness), the presence of the minus sign implies that an increase of slenderness results in a drop of load capacity as shown by the main outcomes related to the geometrical parametric study carried out (see section 5.3.2).

Variables B (HJ), C (VJ) and D (CN) show positive beta coefficients suggesting that whenever their value increases, the load capacity increases accordingly. This trend is consistent with the approach followed to define the masonry bond configurations adopted in this study based on the Masonry Quality Index. In fact, a good masonry bond is associated to higher values of HJ, VJ and CN and it is expected to perform better than masonry wall with poor vertical/horizontal joints arrangement and ineffective corner interlock.

Beta coefficients related to F and G variables confirm the influence of the heigh and the thickness on the out-of-plane performance of two-leaf masonry walls. Overall, higher thickness values result in an enhancement of the out-of-plane capacity of the walls. If the height of the model is kept constant, a span variation associated to a height-to-span ratio reduction, results in a loss of load capacity of the walls, as it can be inferred from the beta coefficient associate to the variable F in Table 5.7 (0.612).

Furthermore, if the thickness of the models is kept constant, a span increase results in a loss of out-of-plane load capacity, hence if the thickness-to-span ratio increases, load capacity increases accordingly, as it is confirmed by the beta coefficient associated to the variable G in Table 5.7 (0.360).

Table 5.7 – List of P-values and standardized coefficients (β) related to equation 56

VARIABLE	P-VALUES	β
A	0.673	0.015
B	2.31·e-14	0.302
C	8.85·e-11	0.251
D	0.0004	0.131
E	2.21·e-6	-0.917
F	0.0083	0.612
G	0.0033	0.360

The scatter plot in Figure 5.22 shows the correlation between actual values and predicted values results from the application of the regression model defined. Moreover, a summary of RMSE (Root Mean Square Error) and MAE (Mean Absolute Error) estimation for the variables considered in presented in Table 5.8.

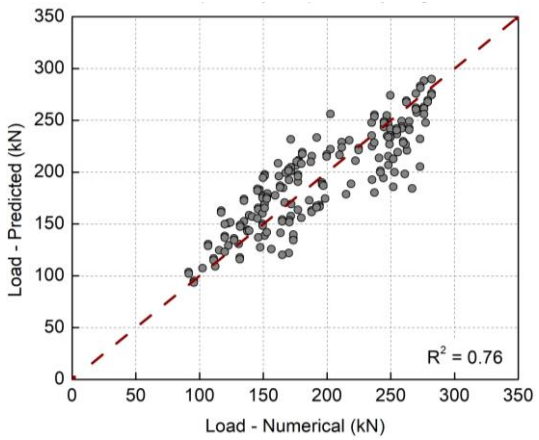


Figure 5.22 – Scatter plot out-of-plane load capacity predicted vs actual values.

Overall, the correlation among the load values is acceptable with an R-squared coefficient equal to 0.76 and the reduced differences between RMSE and MAE metrics suggest the presence of a linear relationship among the variables considered to build the model.

Table 5.8 – Summary of RMSE and MAE measurements

	WC	HJ	VJ	CN	Slenderness	H/Span	Th/Span
	A	**B**	**C**	**D**	**E**	**F**	**G**
RMSE	53.46	50.96	51.75	53.00	49.86	53.42	41.62
MAE	47.06	45.38	45.68	46.77	43.13	47.12	32.77

5.3.4 Prediction of the load multiplier (λ) based on geometrical parameters

The outcomes of the geometrical parametric study have been also analyzed in terms of damage patterns and recurring collapse mechanisms characterising the out of-plane performance of the full-scale models in both Set 1 (C1 corner configuration) and Set 2 (C2 corner configuration). The failures modes detected in the study have been summarized and classified as shown in Figure 5.23.

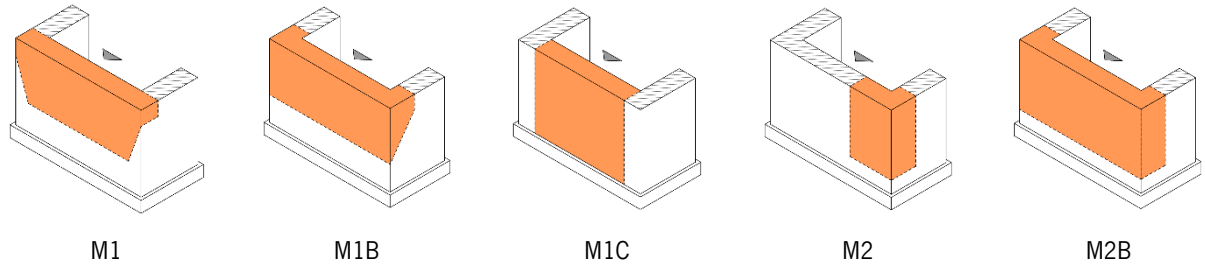


Figure 5.23 – Classification of collapse mechanisms in 2-leaf masonry walls full-scale models.

Looking at Figure 5.23, it is possible to identify 2 main groups of failure modes: (1) M1, characterized by an overturning of the façade; and (2) M2, which mainly involves a detachment between façade and lateral walls. More specifically the collapse mechanisms classified are the following:

- M1 consists in an overturning of the upper part of the façade together with a reduced portion of lateral wall, mostly extended solely in the upper corner area.
- M1B consists in an overturning of the façade combined with a detachment of a significant portion of lateral walls.
- M1C is characterized by a complete overturning of the façade which does not affect the lateral walls, in fact, the detachment plan is concentrated along the corners' bed joints. This mechanism is also characterized by a sliding movement of the façade. This failure mode mostly occurs in walls with an improper vertical joint arrangement.
- M2 consists in an overturning of a portion of wall concentrated in the intersection area between façade and lateral walls.
- M2B consists of a detachment between the whole façade and the lateral walls along the bed joints and in this case, the mechanism mainly occurs whenever the vertical joints are poorly arranged, and it can be also combined with sliding phenomena.

Figure 5.24 shows that the mechanism involving an overturning of the façade together with a portion of lateral walls (M1B) occurs with higher frequency when the walls have a good corner interlock (C1 configuration). On the other hand, the lack of proper corner interlock combined with the absence of proper vertical joints arrangement results in an overturning of the façade along a detachment plan corresponding to the joints between front and transversal walls (M1C).

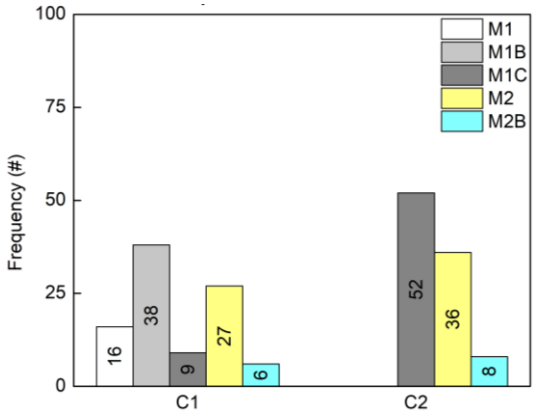
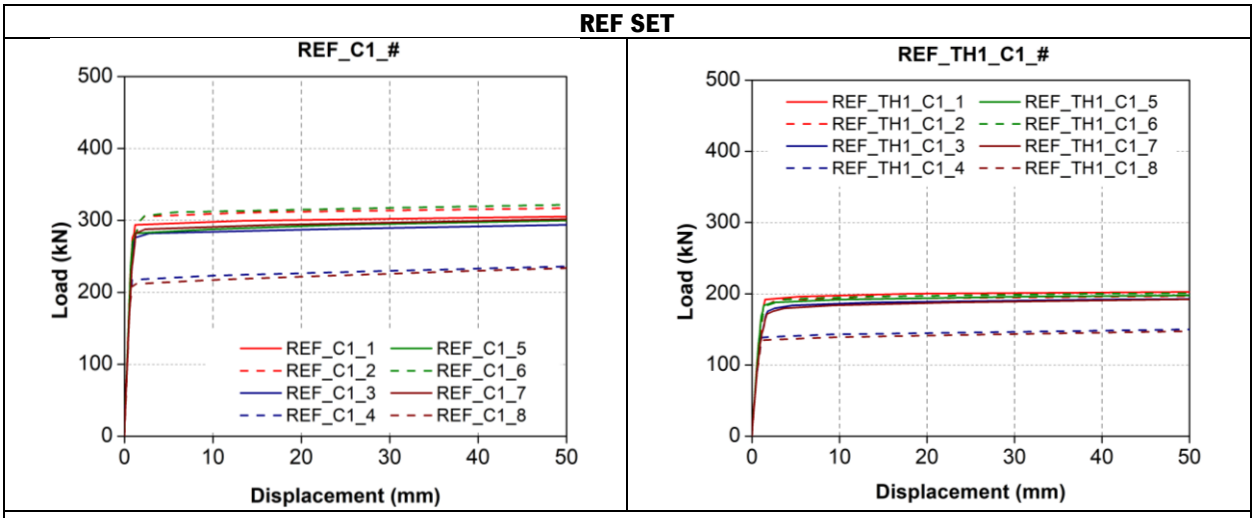


Figure 5.24 – Failure modes frequency rate

As an example, Figure 5.25 shows the results in terms of load-displacement curves and collapse mechanisms related to the reference model with good corner interlock (C1) for all the masonry bond configurations (8 combinations depending on the fulfilled/not fulfilled condition in WC, HJ and VJ) analyzed for the parametric study and for both thicknesses, namely 60 cm and 40 cm (TH1 series).

Overall, models with effective masonry bond configuration show better performance than the models having geometrical parameters in not fulfilled conditions. Indeed, in both sets of models (REF_C1 and REF_C1_TH1), the lower out-of-plane load capacity is shown by the models with WC, HJ and VJ in not fulfilled conditions (masonry bond combination 8). As already mentioned, the recurring failure modes in walls with good corner interlock is M1B, whereas the lack of vertical joints proper arrangement often leads to M1C, M2 or M2B collapse mechanisms (Figure 5.25).



REF_C1 MODELS

REF_C1_1	REF_C1_2	REF_C1_3	REF_C1_4
Failure mode - M1	Failure mode – M1	Failure mode – M1	Failure mode – M2
REF_C1_5	REF_C1_6	REF_C1_7	REF_C1_8
Failure mode - M1	Failure mode - M1	Failure mode - M1	Failure mode – M2

REF_TH1_C1 MODELS

REF_TH1_C1_1	REF_TH1_C1_2	REF_TH1_C1_3	REF_TH1_C1_4
Failure mode - M1B	Failure mode – M2	Failure mode - M1B	Failure mode - M1B
REF_TH1_C1_5	REF_TH1_C1_6	REF_TH1_C1_7	REF_TH1_C1_8
Failure mode - M1B	Failure mode – M2	Failure mode - M1B	Failure mode – M2

Figure 5.25 – Capacity curves and collapse mechanism in REF_C1 wall and REF_C1_TH1 models.

For the sake of brevity, capacity curves and failures modes related to the whole dataset of full-scale models are reported in Annex 3.10 – Capacity curves and collapse mechanisms Set 1 full-scale models (C1 corner configuration) and Annex 3.11 – Capacity curves and collapse mechanisms Set 2 full-scale models (C2 corner configuration) for C1 series and C2 series respectively.

In order to define an empirical expression for the estimation of the load multiplier that triggers the collapse mechanisms identified based on the results of the parametric study, the following structural schemes have been considered (Figure 5.26). It is worth mentioning that the main assumptions regarding the limit analysis performed are the same mentioned in Chapter 3, section 3.6.3, as well as the nomenclature applied to the variables/parameters considered.

More specifically, λ stands for the load multiplier to be estimated, W_{A0} is the contribution of the self-weight of the elements involved in the kinematic mechanism identified and Q represents the contribution of the overload acting on façade (Q_{f0}) and side walls respectively (Q_{s0}).

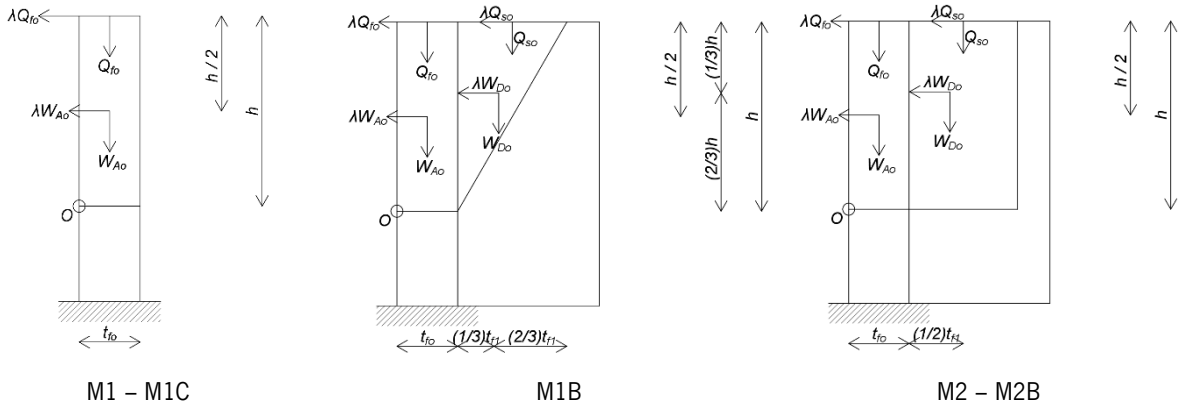


Figure 5.26 – Structural scheme collapse mechanisms identified

As it is clearly noticeable from Figure 5.26, M1 and M1C share a similar structural scheme as well as M2 and M2B failure modes, the difference lies in the dimension (height and thickness) of the macro-element related to the kinematic mechanism analytically analyzed.

Therefore, the expressions referred to the estimation of the load multiplier for these mechanisms consider the same parameters adjusted according to the dimensions and the geometrical features of the elements considered in the kinematic analysis.

$$\lambda_{M1_M1C} = \frac{W_{Ai}\frac{t_{f0}}{2} + Q_{fi}h}{W_{Ai}\frac{h}{2} + Q_{fi}h} \quad (57)$$

$$\lambda_{M1B} = \frac{W_{Ai}\frac{t_{f0}}{2} + W_{Di}\left(\frac{t_{f1}}{3} + t_{f0}\right) + Q_{fi}\frac{t_{f0}}{2} + Q_{si}\left(\frac{t_{f1}}{3} + t_{f0}\right)}{W_{Ai}\frac{h}{2} + W_{Di}\frac{2h}{3} + Q_{fi}h + Q_{si}h} \quad (58)$$

$$\lambda_{M2_M2B} = \frac{W_{Ai}\frac{t_{f0}}{2} + W_{Di}\left(\frac{t_{f1}}{2} + t_{f0}\right) + Q_{fi}\frac{t_{f0}}{2} + Q_{si}\left(\frac{t_{f1}}{2} + t_{f0}\right)}{W_{Ai}\frac{h}{2} + W_{Di}\frac{h}{2} + Q_{fi}h + Q_{si}h} \quad (59)$$

For all the models in Set 1 and Set 2, the load multiplier (λ) that triggers the collapse mechanism has been estimated using equations 57, 58 and 59. In all the equations the load multiplier is calculated as a ratio between the forces triggering the failure mechanism and those forces counteracting it, namely the self-weight of the element (W_i) and the overloads (Q_i) that have a stabilizing effect whenever they can contribute to the attainment of a good box behaviour in the whole structural system.

The forces are multiplied by their respective lever considering the hinge O as the reference point in which the rotation of the assumed mechanism occurs.

A multiple linear regression was performed to define an expression for the estimation of the load multiplier based solely on the geometric parameters analyzed in this study.

The dataset used in the multiple linear regression correlates the geometrical features of the masonry bond previously discussed, namely wall connection (WC), horizontal/vertical joints configuration (HJ/VJ), corner configuration (CN), slenderness, height to span ratio and thickness to span ratio to the load multiplier λ. The linear regression performed merges together qualitative (categorical) and quantitative (continuous) information following the same approach discussed in section 5.3.3.

The expression resulted from the multiple linear regression for the estimation of the load multiplier is presented below (equation 60).

$$H = 0.14 + 0.01A - 0.01B + 0.05C + 0.07D - 0.01E - 0.09F + 1.28G \quad (60)$$

Where:

A is the WC parameter assumed to be 0 (not fulfilled) or 1 (fulfilled).

B is the HJ parameter assumed to be 0 (not fulfilled) or 1 (fulfilled).

C is the VJ parameter assumed to be 0 (not fulfilled) or 1 (fulfilled).

D is the corner configuration parameter (CN) equal to 0 (poor interlock) or 1 (good interlock).

E is the Slenderness.

F is the Height to Span ratio.

G is the Thickness to Span ratio.

H is the load multiplier

All the variables in equation 60 are dimensionless, including the H variable (load multiplier). Table 5.9 presents the P-values and standardized coefficients resulted from the linear regression and describing the influence of the independent variables on the estimation of the target parameter H (load multiplier).

Based on the P-values reported in Table 5.9, it is possible to say that the most influential variables related to the load multiplier estimation are C (vertical joints configuration), D (corner configuration) and G (thickness/span ratio). Indeed, these parameters strongly affect the final configuration of the macro-element identified in the kinematic analysis carried out to analytically estimate the load multiplier. A good vertical joints configuration and an effective corner connection are usually associated to an overturning of limited portion of the façade (mechanism M1 or M1B in Figure 5.23). Conversely a poor corner interlock or a lack of vertical joint proper alignment leads to a detachment of bigger portion of the façade, (e.g. mechanism M1C in Figure 5.23), hence triggering the failure of the wall for lower load levels.

The beta coefficient corresponding to VJ and CN confirm this trend (Table 5.9), they have a significant weight on the overall estimation of the triggering load and, their positive values imply that once VJ and CN increase the load multiplier increases accordingly. Therefore, whenever VJ and CN are closer to the fulfilled condition (VJ = 1 and CN = 1) the load multiplier increases, proving that a good quality of the masonry bond configuration corresponds to a better performance of the wall.

An interesting aspect to point out refers to A and B parameters, wall connection (WC) and horizontal joints (HJ) configuration respectively. They do not have a significant role in the estimation of the load multiplier, as it is possible to infer looking at their P-values and beta coefficients (see Table 5.9). This is a trend previously detected for the WC parameter, which did not result as an influential variable in the peak load estimation. In

terms of absolute value, A and B display similar beta coefficients. This aspect may be explained by the method (kinematic analysis) used to analytically estimate the load multiplier during the construction of the initial database used in the linear egression. Indeed, the kinematic approach does not really consider in its formulation masonry bond characteristics such as WC or HJ.

This consideration does not apply to the VJ parameter due to its strong influence on the definition of the final portion of wall experiencing the kinematic mechanism. Hence, it is almost as if it were indirectly assessed by the analytical formulation adopted.

Slenderness (E) and thickness-to-span ratio (F) have high negative beta coefficients. On one hand, their weight on the load multiplier estimation is relevant. On the other, their increase corresponds to a reduced load multiplier. Indeed, it is more likely for walls with considerable slenderness and/or span to experience failures at an early stage (low load multiplier) compared to masonry walls having reduced values of these parameters.

Table 5.9 – List of P-values and standardized coefficients related to equation 56

VARIABLE	P-VALUES	β
A	0.112	0.074
B	0.137	-0.069
C	5.02·e-10	0.312
D	1.21·e-14	0.402
E	0.261	-0.284
F	0.126	-0.470
G	0.006	0.444

The scatter plot in Figure 5.27 shows the correlation between actual (analytical) values and predicted values results from the application of the regression model defined.

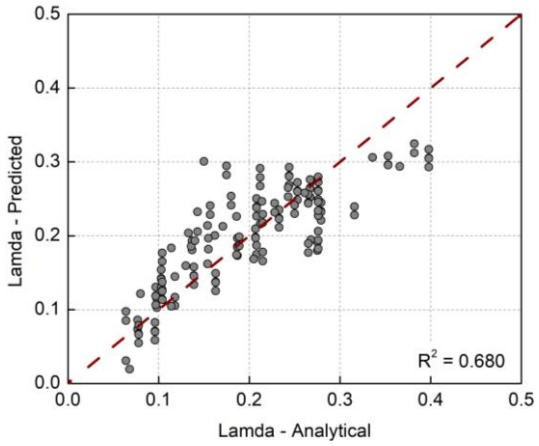


Figure 5.27 – Scatter plot out-of-plane load multiplier predicted vs analytical values.

The R-squared coefficient describing the effectiveness of the predictive model is equal to 0.68 indicating that a significant proportion of the variance in the dependent variable is explained by the independent variables. Hower, the slight difference between RMSE (Root Mean Square Error) and MAE (Mean Absolute Error) metrics for the variables considered may suggest the presence of a linear relationship among dependent and independent variables (Table 5.10).

Table 5.10 – Summary of RMSE and MAE measurements

	WC	HJ	VJ	CN	Slenderness	H/Span	Th/Span
	A	B	C	D	E	F	G
RMSE	0.046	0.045	0.047	0.044	0.046	0.047	0.044
MAE	0.036	0.035	0.033	0.032	0.036	0.036	0.035

5.4 Final remarks

The results of the parametric analyses conducted on 2-leaf masonry walls full-scale models have been described and summarized in this chapter. The work carried out is two-fold and its focus is the study of the out-of-plane performance in two-leaf stone masonry walls (regularly cut stone units).

On one hand, the influence of a set of reference mechanical parameters on the out-of-plane performance of two-leaf masonry walls has been investigated. On the other hand, an attempt has been made to find a correlation among different mechanical properties often used as input parameters in numerical simulations based on different approaches, namely finite element (FE) and distinct element (DE) method.

On a material level, 100 FE-based macro-models have been analyzed by means of pushover analyses in order to assess the influence of reference mechanical properties on their out-of-plane performance.

As a result, specific limit states have been defined to describe the evolution of structural response of the numerical models under out-of-plane load. At the same time, a set of empirical expressions associated to each limit state have been calibrated based on the results of the parametric study carried out.

To this end, it must be noted that all the empirical expressions provided in this study have been defined by means of multiple linear regression analysis. This approach can be considered appropriate to gather information and to identify recurring trends characterising the data distribution as well as the influence of the selected independent variables on the final estimation of the target variable.

The analysis conducted on the variables considered to build the predictive model showed that Young Modulus has the highest influence in the definition of the displacement capacity of the walls, whereas the load capacity is strongly influenced also by tensile strength and tensile fracture energy.

The second part of the parametric study described in the chapter addresses the influence of a set of geometrical parameters on the out-of-plane performance of two-leaf stone masonry walls. In this case, a different modelling approach has been adopted to simulate the variation of masonry bond configuration, namely a DE-based simplified micro-modelling. The models have been analyzed by means of pushover analyses.

The main trends arisen from the geometrical parametric study refer to the influence of vertical joints (VJ) and corner configuration (CN) on the out-of-plan capacity of the walls. It is possible to say the same regarding slenderness and wall thickness.

Moreover, vertical joints configuration (VJ) and corner configuration (CN) strongly affect the recurring failure mechanism of the walls under out-of-plane load.

It is interesting to note that, contrarily to what expected, wall connection parameter (WC) did not show a considerable relevance in the out-of-plane capacity of the models analyzed. This trend may be related to aspects of the study carried out such as masonry typology selected and modelling assumption (perfectly overlapped leaves). A set of empirical expressions for the estimation of the out-of-plane capacity in two-leaf stone masonry walls has been defined and calibrated based on the results of the geometrical parametric study carried out.

The analyses of the variables used to build the predictive model confirmed the trends previously described as it is possible to infer looking at the P-values and beta coefficients related to WC (high P-values, low beta coefficient, not relevant), VJ (low P-values, high beta coefficient, relevant) and CN (low P-values, high beta coefficient, relevant).

Slenderness and thickness are also highly influential parameters in the definition of the load capacity. Higher slenderness values correspond to a reduction of peak load attained and vice versa. Conversely, thickness increase results in an enhancement of the load capacity of the walls.

The dataset built based on the geometrical parametric study has been also used as a starting point to analyze the role of the reference geometrical parameters selected in the definition of the load multiplier triggering a specific failure mode.

To this end, based on the outcomes of the geometrical parametric study, 5 recurring collapse mechanisms have been identified in order to analytically estimate the corresponding load multiplier. The results of the multiple linear regression carried out showed a lack of significance of the WC parameter and HJ parameter in the load multiplier estimation. The lack of significance of the WC parameter is confirmed also in this study

by the high P-values and low beta coefficients. Among the possible causes explaining this trend (characteristics of the masonry typology and modelling assumptions), it must also be noted that the analytical method adopted does not consider in its formulation an explicit contribution associated to wall connection (WC). It is possible to say the same for the horizontal joints configuration (HJ).

Conversely, since VJ and corner interlock (CN) strongly affect the final macro-element configuration used to estimate the kinematic mechanism, their contribution is "indirectly" assessed by the analytical methodology applied.

The study related to the load multiplier estimation confirmed the role of slenderness and thickness as influential variables for the assessment of masonry wall out-of-plane performance. Higher slenderness values correspond to low load multipliers; hence the failure of the wall occurs even for lower load levels. On the other hand, higher thickness results in a better structural performance and higher load multipliers, which means failure mechanisms triggered for higher load levels.

Even if the empirical expressions provided (based on mechanical and geometrical parametric studies) may represent a valuable support for an expeditive assessment of the structural performance in 2-leaf masonry walls, they must be also seen as a tool to understand the main trends and patterns characterising the numerical parametric study carried out.

In this perspective, the goal of the parametric studies was clearly stated at the beginning of this section, namely identify a set of reference mechanical and geometrical parameters in order to assess their influence on the out-of-plane behaviour of a specific masonry typology (2-leaf stone masonry walls with regularly cut stone units).

Finally, it must be pointed out that the work opens a path of investigation to use these expressions for a simplified assessment of the out-of-plane performance of masonry walls, but the database would need to be enlarged and further validated with experimental data available in the literature addressing the out-of-plane performance of masonry wall typology similar to those selected in this study.

In addition, applications to real case studies are required to obtain a deeper assessment of the expressions' effectiveness and, at the same time, specific experimental campaigns could be designed in order to perform out-of-plane tests on masonry walls replicating those used to run the numerical simulation and to build the database later processed by means of multiple linear regression analysis. Moreover, additional simulations may be carried out in the future to enhance the robustness of the datasets built so far aiming at a more effective refinement of the equations provided.

6 Experimental out-of-plane behaviour in strengthened and unreinforced 2-leaf masonry walls

6.1 Introduction

The results of an experimental campaign aimed at the assessment of the out-of-plane performance of 2-leaf brick masonry walls in different conditions, namely unreinforced and strengthened configurations, are herein presented. Two reduced-scale brick masonry walls have been experimentally tested by means of an airbag simulating the horizontal load in the out-of-plane direction.

This experimental campaign represents an extension of the study carried out in the previous chapters since it provides further insight regarding the out-of-plane behaviour of a masonry typology different from those already analyzed, namely stone masonry walls.

Moreover, this work can also constitute a valuable database for the validation of numerical models addressing the analysis of the structural behaviour of 'placa' buildings, a typical Portuguese building typology, commonly adopted during the period 1930-1960 [136].

Once tested, the unreinforced masonry wall (UMW) was repaired (RMW) and tested again. Successively, the results obtained from the first two tests have been compared to the outcomes of an additional airbag out-of-plane test performed on a newly built wall strengthened in undamaged conditions (RMW_UND). The main goal of the experimental campaign is the assessment of the selected strengthening solution's ability to enhance the out-of-plane capacity of the selected masonry typology.

Firstly, a summary of relevant background information is provided regarding the experimental activities carried out to characterize the out-of-plane behaviour of masonry walls, as well as an overview of typical currently available strengthening techniques applied to enhance wall-to-wall connections and to improve the out-of-plane capacity of masonry structural systems.

Finally, the main outcomes of the experimental campaign are presented with emphasis on the following aspects: (i) masonry material characterization with sonic tests; (ii) characterization of the dynamic behaviour; (iii) analysis of the cyclic response of the tested masonry walls; and (iv) comparison of the out-of-plane performance of masonry walls, in terms of damage patterns, load, and displacement capacity, under different initial conditions, namely unreinforced (UMW), repaired (RMW) and reinforced (RMW_UND).

6.2 Experimental characterization of masonry walls under out-of-plane load

Laboratory and in-situ experimental campaigns have been extensively used to characterize the performance of masonry walls. On one hand, laboratory tests deal with some limitations, such as the correct simulation of the existing materials' mechanical performance and the actual state of conservation of the original elements, as well as their boundary conditions. On the other hand, in-situ tests are performed in a non-monitored environment which increases the inherent uncertainty characterising the physical phenomenon object of the study. A significant aspect that must not be overlooked is laboratory space limitations. In fact, the majority of the dynamic (e.g. shaking table tests) or quasi-static tests (e.g. airbag tests) on masonry structures are performed on reduced-scale specimens. Thus, the scaling procedures might affect the material physical properties [137] [138].

In-situ testing procedures offer the possibility to investigate full-scale structures and their actual boundary conditions (material properties, acting loads, etc.), but they do not entirely allow to overcome the uncertainties characterising a non-controlled testing environment. Figure 6.1 shows a possible classification of testing procedures commonly adopted to assess the out-of-plane behaviour of masonry structural systems divided based on the technique and the device used [3].

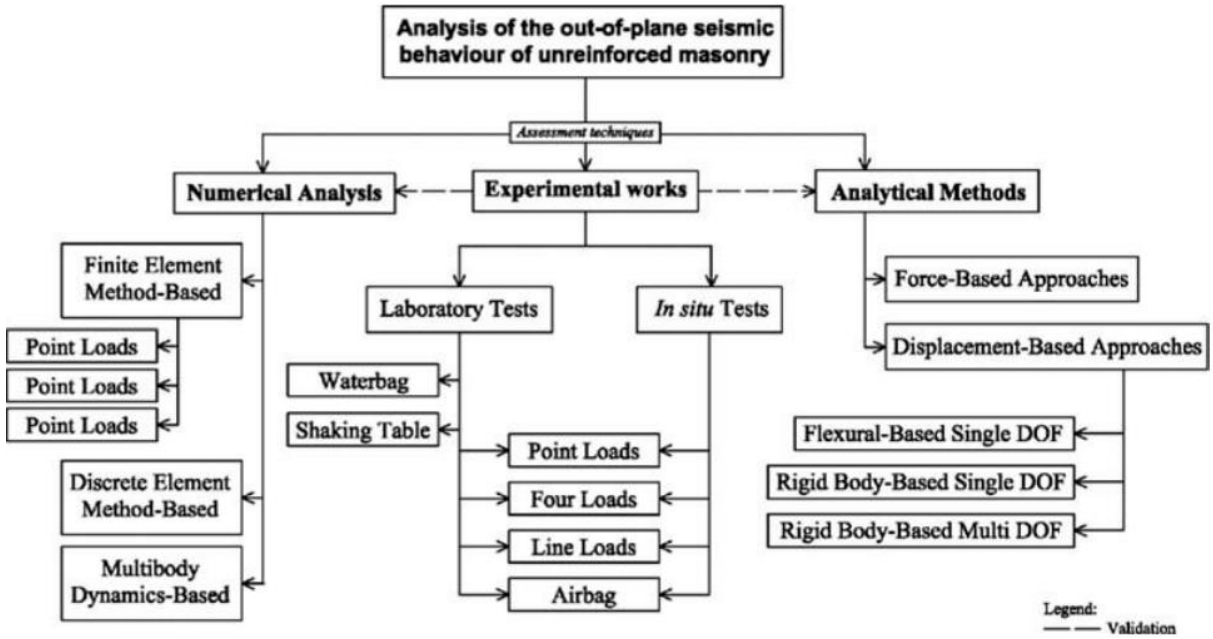


Figure 6.1 – Assessment techniques for the out-of-plane behaviour of masonry walls [3].

Due to the complexity of the phenomenon and to the limitations previously highlighted, most of the experimental campaigns, addressing the out-of-plane failure of masonry walls available in the literature, have been oriented to establish the displacement and load capacity of simple mechanisms often relying on reduced size walls mock-ups and simplified testing setups [3]. The present section provides a brief overview of significant laboratory and in-situ experimental works addressing this topic.

In the 80s, experimental activities addressing the study of the out-of-plane behaviour of masonry walls focused on the analysis of the dynamic response of unreinforced structural system aiming at the definition of a methodology for the mitigation of seismic hazard in existing buildings. Experimental results proved that the dynamic stability of the walls was strongly affected by geometrical parameters such as height/thickness ratio [139].

In its early stages, the study of the out-of-plane behaviour of masonry structural systems addressed the correlation between out-of-plane capacity and masonry bond characteristics. Indeed, geometrical parameters configuration is a key-aspect when it comes to the study of the out-of-plane response of masonry walls, especially when heritage buildings are considered.

Tilting tests on 2-leaf and 3-leaf masonry walls built with the same number of masonry units and the same material properties, but differently arranged masonry bonds, proved that even if the number of through-stones in a wall is not particularly high, the structural performances benefits from their presence and their proper positioning [67] [140]. To this end, it is also worth mentioning that the morphological features of stone units play an important role in the overall structural performance of masonry walls. It has been observed that masonry walls experience some deformations when the self-weight horizontal component increases. This phenomenon is due to the coarseness of the contact surfaces among masonry units [140]. Hence, a physical model was proposed approximating masonry units as a solid with rounded boundary surfaces instead of a perfectly shaped parallelepiped (Figure 6.2).

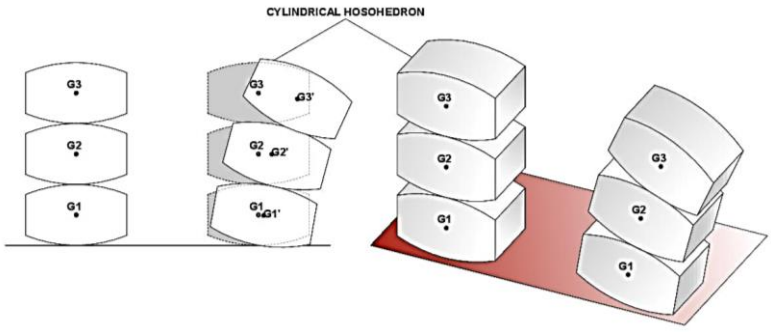


Figure 6.2 – Behaviour of stone units with rounded surfaces subject to self-weight, adapted from [140].

More recently, the use of advanced testing setups allowed the scientific community to further investigate the out-of-plane collapse mechanism collecting data regarding the dynamic aspects characterising rocking phenomena, without overlooking the link between load capacity and architectural features of masonry structural systems.

Shaking table tests allowed to investigate how different dynamic inputs may affect the out-of-plane responses. Indeed, the possibility to assemble larger specimens provided a comprehensive insight into the role of architectural components in the final response of a building [141] [142] [143] [144] [145].

Several experimental campaigns demonstrated how the presence or absence of gables, openings configuration and position, and leaves configuration may significantly affect the out-of-plane behaviour of masonry structures and the final damage pattern. Moreover, on a microscopic level of detail, it is worth pointing out that even the masonry unit typology (stone units vs masonry brick) strongly affects the final out-of-plane failure and the consequent damage pattern [146].

Other than that, static or pseudo-dynamic setups (e.g. airbags and/or hydraulic actuators) have been often used to assess how higher or lower levels of pre-compression stress in masonry walls may result in an increase or decrease of the out-of-plane capacity [147] [146]. More specifically, the application of significant vertical pre-compression loads in unreinforced masonry walls may result in an enhancement of the ductile behaviour, due to the capability of experiencing considerable out-of-plane displacements without collapsing [147].

To summarize, it is possible to say that laboratory tests provide important information, representing a fundamental starting point to evaluate the reliability of different numerical and analytical methods. The intensive use of these tools (e. g. shaking table tests), is limited by complexity, cost, and time efforts, whereas static or pseudo-dynamic setups allow us to carry out simpler investigations. In both cases, it must not be overlooked that the structural models built in the laboratory, even if full-scale prototypes, differ from actual structures in terms of size, geometry, materials, and accuracy.

In-situ experimental works investigating the out-of-plane seismic behaviour of unreinforced masonry walls are less in number if compared to laboratory experimental campaigns. On one hand, in-situ tests can provide a more reliable insight regarding the overall performances of a certain structural system since the presence of controlled boundary and environmental conditions could result in an overestimation of specimens' performance. On the other hand, field activities are affected by some drawbacks mainly related to the lack of ease which frequently characterizes the testing setup layout [148][149][150].

6.3 Strengthening techniques for the improvement of the out-of-plane performance

Nowadays, the techniques for the improvement of the structural performance of masonry buildings can be classified in two main categories, namely rehabilitation and retrofitting. Rehabilitation uses materials and construction techniques with characteristics similar to the original ones in order to maintain and preserve the its historical and architectural significance of a building [151], whereas retrofitting is based on the application of modern techniques and innovative materials to improve the seismic performance of the building in order to meet modern standards especially in terms of structural safety.

A strengthening intervention that leads to an acceptable level of safety in damaged structures can be defined as retrofitting. Retrofitting measures can be applied to undamaged constructions when an accurate evaluation of their structural performance demonstrates their inability to withstand external actions (e.g. earthquakes) with acceptable reliability [152].

Strengthening/retrofitting solutions aim to reduce the risk of economic and human losses by improving the overall quality, equilibrium, and stability of masonry components. To this extent, it is possible to identify a common root underlying modern strengthening solutions and traditional earthquake-resistant techniques. The latter are the result of practical expertise and non-engineered processes aiming to mitigate seismic hazard [153]. They have been developed throughout history in highly seismic prone areas of Europe (e.g. Greece [9], Italy [154], Portugal [154], Turkey [155]), Asia [155] and Central America [155], among others.

A significant aspect related to the application of strengthening/retrofitting techniques to existing buildings concerns the conservation of cultural heritage constructions. Increasing awareness regarding this topic resulted in the definition of ICOMOS [156] [157] and ISCARSAH [158] guidelines. They are based on principles that comply with both ethics and technical aspects concerning the safeguard of cultural heritage, namely (1) the respect of original materials and construction techniques (authenticity), (2) the need to pursue compatibility and durability of new materials applied in conservations works, (3) the need of assuring a reduced invasiveness of the intervention (minimum intervention), (4) the possibility to apply reversible solutions (reversibility).

This section briefly summarizes the main strengthening/retrofitting techniques commonly applied in current building practice, identifying the following categories of interventions:

- Techniques for the improvement of masonry quality;
- Techniques for the improvement of the walls' connections;

- Innovative strengthening solutions.

6.3.1 Techniques for the improvement of masonry quality

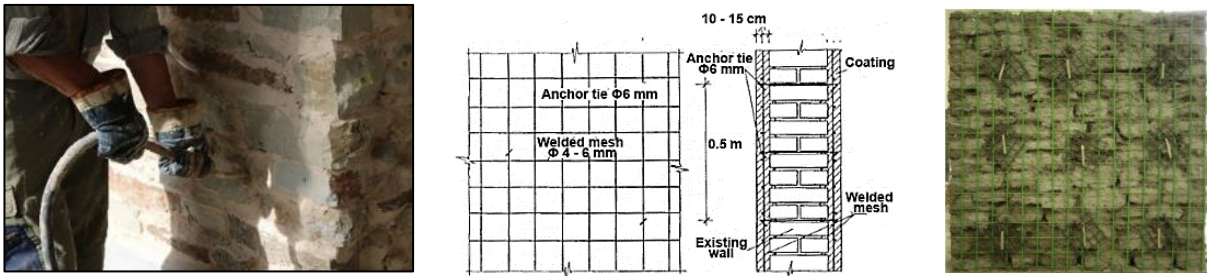
The improvement of the masonry quality is often a consequence of local damage repairing such as cracks and/or local discontinuities. However, long-term lack of maintenance or general poor conditions of masonry components may require this type of intervention. The repair technique should be chosen according to the criteria proposed in standards and guidelines commonly adopted in the building practice [156] [158]. Hereinafter a brief overview of the most recurring repairing techniques applied to masonry structures is proposed.

Stone masonry grouting applications have been largely used on historic buildings and dwellings in the 70s and 80s. The popularity of this technique increased after Friuli and Irpinia earthquakes occurred in Italy in 1976 and 1980 respectively (Figure 6.3a). This intervention consists of injecting grout mixtures of different types into the masonry in order to (1) reconstitute the structural continuity of the masonry; (2) increase the masonry homogeneity, filling voids; (3) enhance masonry strength [159]. Irreversibility, durability and compatibility issues are the main drawbacks of this technique.

Reinforced coatings (jacketing) aim to improve the lateral resistance and energy dissipation capacity of the masonry structural component (Figure 6.3b). This method is easy to apply and, at the same time, has a good efficiency, for this reason it has been widely used to strengthen masonry walls in different countries all over the world [5]. The technique consists of positioning a reinforcing net on both faces of a wall, connecting the two nets with steel anchors and applying on the two faces a cement mortar-based coating layer. The masonry panel acquires high strength and stiffness, which is not always a positive aspect considering the overall behaviour of masonry buildings [159]. Despite its extensive diffusion, the execution of this technique can result in local failures of the reinforced components due to poor connection between masonry and coating system. Moreover, durability issues may arise in buildings with significant capillarity phenomena and high moisture levels since often the reinforced concrete jacketing acts as a sort of barrier for the evaporation.

In the last decade, several efforts have been made to address the compatibility issues characterising outdated jacketing approaches aiming also at the development of a more efficient technical solution also from a structural standpoint. To this end, it is worth mentioning some recent advances related to the application of textile-reinforced mortars (TRM), which is a modern and compatible strengthening strategy for the seismic protection of existing masonry buildings (Figure 6.3c). Similarly to what described above for a standard

jacketing solution, TRM consists of plastering the walls by means of mortar layers and embedded grids of textiles made of long fibers such as glass, carbon, or basalt fibers [160].



a b c

Figure 6.3 – Grout injection technique (a), jacketing (b), textile reinforced mortar (c), adapted from [161].

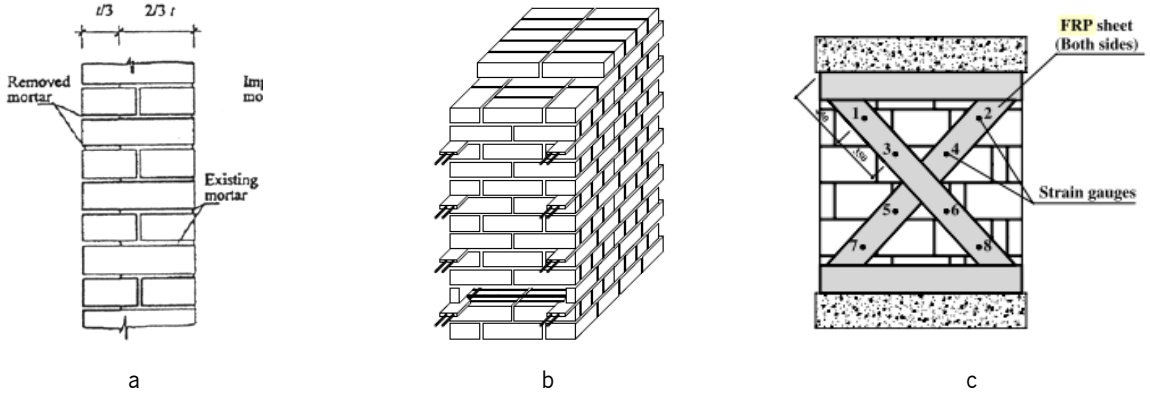
Deep repointing involves the partial replacement of the mortar joints with better quality mortar in order to improve masonry mechanical characteristics [159]. Repointing increases masonry resistance to both vertical and horizontal loads (Figure 6.4a). However, the best results are related to a significant deformations reduction due to the confinement effect exerted by the joints' new configuration. A modern application of this technique is based on the insertion of steel rods or reinforced polymer plates on one or both sides of the wall, eventually connected in the transverse direction (Figure 6.4b).

Overall, repointing can be considered a partially reversible technique (if the new mortar can still be removed from the joints). Durability and compatibility aspects are mainly related to the choice of an adequate mortar to substitute the original one. Usually, cement-based mortars may trigger unwanted chemical reactions in the masonry.

The so-called "engineered materials" such as FRP (Fiber Reinforced Polymers), SRP (Steel Reinforced Polymers) and SRG (Steel Reinforced Grout) are extensively applied for the restoration of vertical and horizontal structural elements as well as isolated monuments (Figure 6.4c). This strengthening technique is based on different types of fibers (e.g. glass, carbon) impregnated in a polymeric matrix [162]. Due to high strength and stiffness-to-weight ratio, fatigue and corrosion resistance, and their exceptional capacity to be tailored according to specific needs, along with decreasing raw materials and production costs, advanced composites have progressively extended their initial fields of applicability.

Their flexibility and somewhat easy application allow a wide range of intervention scenarios for existing structures, characterized by different conditions. A drawback related to the application of these techniques is

represented by the damage in masonry components due to salt crystallization and spalling of treated superficial layers [159]. Other major limits concern the application procedure, which requires smooth surfaces and the removal of the ancient plaster.



a b c

Figure 6.4 – Standard repointing (a) and Reinforced repointing (b) adapted from [159], FRP application adapted from [163].

6.3.2 Techniques for the improvement of wall-to-wall connections

A major cause of damages in masonry building can be attributed to insufficient load-bearing capacity of the walls and/or inadequate connection (e.g. wall-to-wall, wall-to-floor, wall-to roof) [5].

The lack of connection in masonry buildings results in uncoupled vibration that can lead to out-of-plane collapse. Old masonry structures often have poor box-behaviour. The application of tying systems based on the use of different materials has been commonly applied in the building practice in order to strengthen/retrofit existing masonry buildings.

Reinforced concrete ring beams were extensively used as means to reinforce masonry structures by providing continuity and connection at the top of the walls and support the roof/floor structure [162]. Mostly, they are positioned along the four sides of the structure to connect load bearing and shear walls in order to prevent out-of-plane failures. Despite the widespread use of these techniques, in the last decades, many retrofitting design solutions have been directed toward methods that are less invasive. To this end, retrofitting measures based on the use of timber bond beams have been applied and investigated in terms of compatibility, durability and structural performance [159].

Steel bars, anchored with plates or other devices, have been successfully used in the past to improve the overall behaviour by ensuring an adequate wall-to-wall connection. Tie bars are less invasive and can be easily removed in the future. They provide an efficient and durable tying action once the anchorages are maintained in good condition [5]. Steel ties have a reduced mass and increased flexibility if compared to

strengthening/retrofitting solutions such as reinforced concrete tie beams (Figure 6.5a). Experience of past earthquakes proved that high stiffness levels attainable when reinforced concrete beams are applied to masonry constructions can cause unexpected and dangerous mechanisms such as beam slipping and hammering [159].

The effectiveness of the horizontal diaphragm action of floor and roof, as well as a good connection between floor beams and masonry walls, allow to distribute shear forces, preventing possible overturning and out-of-plane collapse of the walls (Figure 6.5b). Conversely, if the timber floor is retained, wooden joists are anchored to the wall with steel connectors. Additionally, when large spanning timber floors need to be preserved due to their historical value, diagonal ties are not effective enough to prevent possible out-of-plane phenomena, horizontal metallic or timber trusses can be placed above the joists. As previously mentioned, this type of intervention presents several drawbacks in terms of durability and reversibility, and it also results in an excessive stiffness increase.

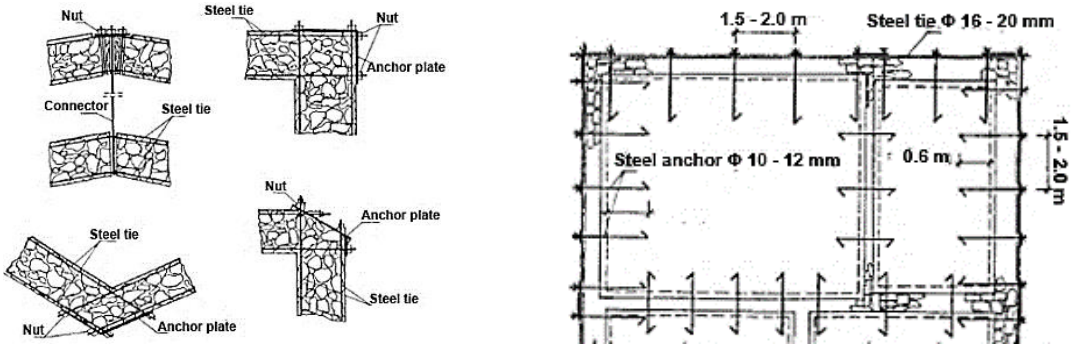


Figure 6.5 – Detail of anchoring and connection ties (a); Strengthening of existing timber floor (b) [5].

New trends in strengthening/retrofitting practice envisage the use of timber or FRP materials in order to reduce the deformability of floor structures and in order to obtain less invasive interventions fulfilling, at the same time, the need for compatibility and the partial or total reversibility of the strengthening/retrofitting measures. Moreover, the use of wood elements can also provide effective solutions for the strengthening of horizontal (slabs, floors) and vertical (walls) structural components [164] [165]. For instance, wooden floor stiffness can be increased by means of timber planks perpendicularly nailed to the existing flooring board in such a way that no differential motions can occur. Moreover, diagonally placed planks can enhance the lateral resistance and rigidity of the strengthened floor structure (Figure 6.6a).

Highly compatible and reversible strengthening techniques involve the application of a new board connected by means of dowels above each beam of the existing frame (Figure 6.6b). The dowels are driven into the dry boards without any material to improve adhesion inside the hole ("only wood" technique [159]).

If the strengthening system is realized using innovative materials (FRP), the principles to be followed are the same highlighted when the enhancement of the floors overall stiffness is achieved with the superimposition of new wooden planks on the existing structure (Figure 6.6c).



a b c

Figure 6.6 – Stiffness improvement for timber floors (a) [5]; Only wood technique proposed by Modena [159]; Stiffness improvement of timber floor with FRP materials (b), adapted from [162].

6.3.3 Innovative techniques for the improvement of wall-to-wall connections

Innovative methods of structural reinforcement can be classified as passive or active approaches. In passive reinforcements, the strengthening elements receive loads only from the structural element, whereas active reinforcements have a pre-load counteracting the deformation of the structural element starting from the moment of its installation. One of the first example of active retrofitting is the so-called CAM (Active Confinement of Masonry), which is based on the use of a continuous three-dimensional system of pre-tensioned ties able to "pack" the masonry structure, hence providing a state of tri-axial compression [151]. CAM system does not use bars to create ties. It consists of steel ribbons that form horizontal and vertical loops, passing through transverse holes; it is quickly applicable and sufficiently reversible (Figure 6.7).

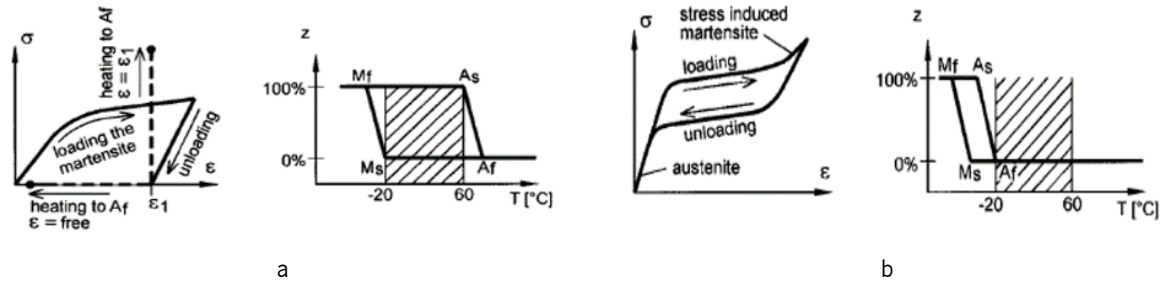


Figure 6.7 – Example of strengthening with CAM system (adapted from [151]).

In current building practice, steel elements (wires, rods) and fiber-reinforced composites are commonly considered reliable and cost-effective solutions in dealing with strengthening interventions. Lately, the use of smart materials, namely shape memory alloys (SMA), is gaining an increasing interest in civil engineering applications, due to properties such as shape memory effect and super-elasticity, which make them extremely suitable in enhancing buildings' structural performances [166].

The shape memory effect in SMA (Shape Memory Alloy) materials is ability to revert to their initial shape upon heating until reaching their high temperature phase after undergoing a certain level of deformation in the low temperature phase (Figure 6.8a). Super-elasticity is a transformation from austenitic to martensitic phase

that occurs just by increasing the external stress without changing the temperature (Figure 6.8b). The alloy undergoes the retransformation to the austenitic state automatically by unloading the stress. The stress-strain curve for the super-elasticity shows a distinctive plateau and a hysteresis [167].



a b

Figure 6.8 – Shape memory effect (a); Super-elasticity (b) [167].

Several studies investigated different types of SMAs; among the others it is worth to mention the MANSIDE project (Memory Alloys for New Seismic Isolation Devices), which aimed at exploiting the potential of Shape Memory Alloys in the field of earthquake engineering. The experimental and theoretical outcomes of the project proved that Nitinol (Nickel-Titanium alloy) is the most appropriate shape memory alloy for engineering purposes due to its high super-elasticity, large recoverable strains, and corrosion resistance. Moreover, it has a relatively affordable cost when compared to other types of shape memory alloys [166] [167]. Despite research is in its early stages, experimental outcomes related to the use of shape memory alloys are promising. Examples can be found in the literature concerning SMA composites (wires embedded in a resin matrix) [168] [169] or near-surface mounted SMA strips applied to improve the flexural behaviour of RC beams [170] [171].

Within the framework of the ISTECH Project, for the first time, shape memory alloy devices were used for the seismic protection of heritage buildings [172]. The super-elastic effect resulting in the absence of sensible residual deformations allowed the creation of SMA devices (SMAD) that exhibit almost zero residual displacements, as opposed to what occurs using traditional devices such as steel ties that need to be removed once they reach their yield limit.

Within the ISTECH project, SMADs have been applied to enhance roof-to-wall and floor-to wall connections highlighting some remarkable engineering features, namely (1) self-balanced behaviour under service loading conditions, (2) under high-intensity loads, they make it possible for the masonry components to dissipate part

of the seismic energy transmitted by earthquakes, (3) under severe horizontal loads, SMADs' stiffness increases, reducing considerably the increasing displacement levels.

In order to eliminate some of the drawbacks related to the use of traditional devices (e.g. steel ties) for the seismic upgrading, SMADs have been applied to some Italian churches (e.g. Basilica of St. Francis in Assisi, San Feliciano Cathedral façade in Foligno, and San Serafino Church at Montegranaro), severely damaged by the Umbria-Marche earthquake (1997/1998), see Figure 6.9.



a b c

Figure 6.9 – SMADs applications in Assisi (a), Foligno (b) and Montegranaro [172].

The main results of these works proved that SMAD ties increased the resistance against out-of-plane seismic vibrations of masonry walls (50% in terms of maximum PGA bearable without damages).

Further experimental campaigns assessing the influence of strengthening solutions, such as SMA tying systems and repointing grids on the out-of-plane performances of masonry constructions, could provide a valuable contribution in bridging an existing scientific gap.

6.4 Description of the experimental campaign

The experimental campaign conducted consisted of out-of-plane quasi-static loading tests by means of an airbag. The specimens, described in the following section, replicates a façade wall of the so-called 'placa building', a typical Portuguese building typology, commonly adopted between 1930 and 1960, characterized by unreinforced brick masonry walls and reinforced concrete (RC) slabs [173]. These mixed masonry-reinforced concrete structures present a significant vulnerability to seismic action due to the increase of inertia load compared to traditional timber floors, the early use of concrete technology and the weak connections among vertical and horizontal structural components. Moreover, their seismic behaviour is still largely unknown, and more research is needed [174]. Indeed, this work is a necessary stage towards a thorough

investigation of such a typology that represents about 22% of the building stock in a seismic area like the region of Lisbon and 33% of the building stock in Continental Portugal [175].

Two wall specimens were built and experimentally tested under different conditions. Initially, a U-shaped Unreinforced Masonry Wall (UMW) was tested using an airbag exerting a horizontal load that simulates seismic action. Successively, the same wall was Repaired (RMW) and further tested using the same protocol and setup. Finally, a second wall with identical geometrical and mechanical features was reinforced (RMW_UND) in undamaged condition and then tested. The strengthening solution applied to the specimens is the same in all the configurations considered in the experimental campaign. The solution was provided by Fassa Bortolo and consists in a textile reinforced mortar (TRM) with glass fibers internal mesh.

The mechanical properties of the U-shaped walls were characterized by means of non-destructive and destructive tests. The structural performance of the tested walls was compared in terms of cyclic response and damage patterns in order to gather data regarding the effectiveness of the proposed strengthening solution in improving the out-of-plane capacity of the selected masonry typology.

6.4.1 Construction of the reduced scale U-shaped walls

The U-shaped specimen reference geometrical configuration consists of a front wall (2.85 m long 1.40 m high, 0.25 m thick) and two transverse walls (1.55 m long, 1.40 m high, 0.25 m thick), with solid clay bricks (0.25 X 0.12 X 0.06 m^3). Flemish bond pattern is used, paying specific attention to the corners, where the regular bricks are cut and carefully placed to provide a good connection between the front and the transverse walls. Horizontal bed joints and staggered vertical joints (10 mm thickness) are made of a class M5 pre-mixed cement-based mortar, mixed with water according to the manufacturer recommendations. The specimen is built on top of a concrete base (0.20 m high and 0.30 m thick), see Figure 6.10.

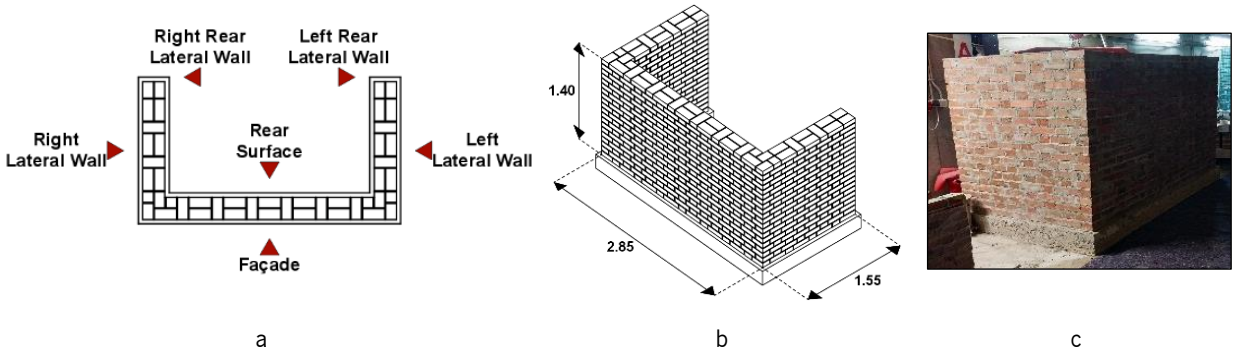


Figure 6.10 – U-shaped masonry wall plan view (a) and axonometric view (b); U-shaped unreinforced masonry wall (c).

The strengthening solution was provided by Fassa Bortolo and is based on a combination between a hydraulic lime mortar (NHL777) and a glass fiber mesh (Fassanet ARG Plus). The mesh was initially applied to the first layer of fresh mortar (Figure 6.11b). In the wall's corners, an additional layer of glass fiber mesh was installed considering an overlapping length of 20 cm for each side. The glass fiber mesh was then connected to the masonry wall by means of glass anchors (Fassa Eliwall, 10 mm diameter, see Figure 6.11e) and steel ties diagonally drilled between façade and lateral walls (45° approximately). Finally, the second mortar layer was applied to complete the installation, see Figure 6.11.

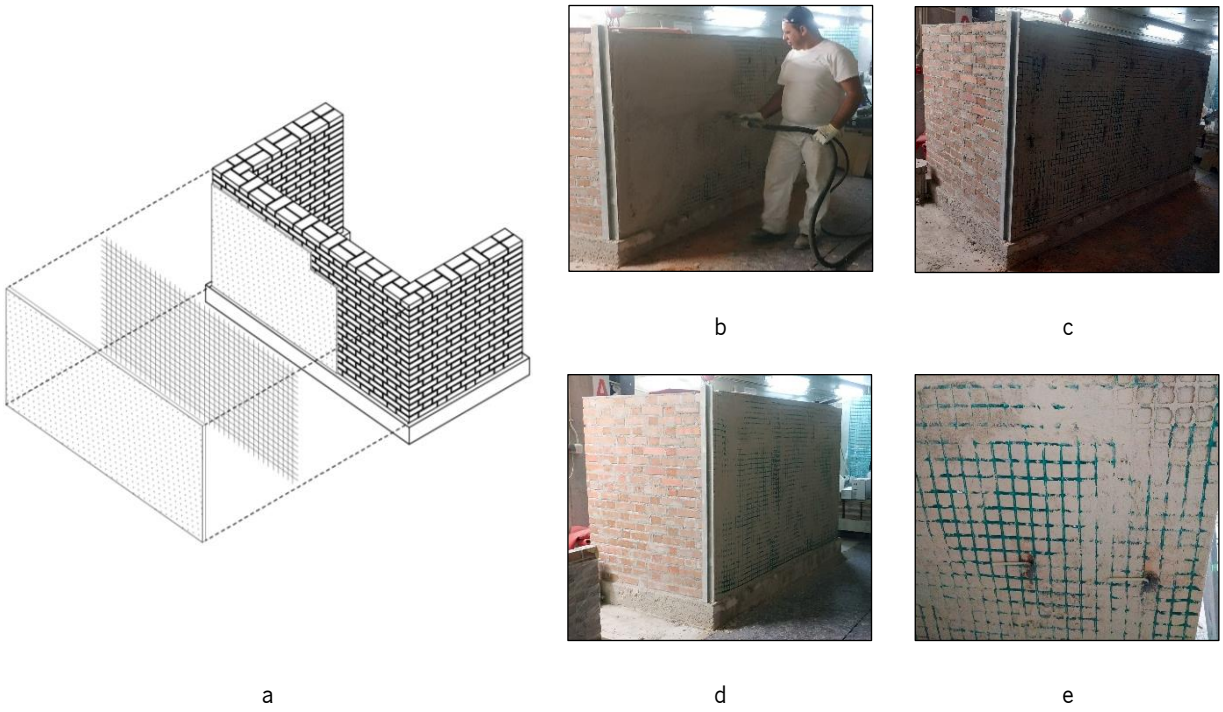


Figure 6.11 – Axonometric view of the TRM solution (a), installation stages of the strengthening solution (b, c, d), detail of the anchoring system (e).

6.4.2 Test setup

The setup configuration used in the out-of-plane test involves an airbag with an area of 1.65×1.35 m^2 that intends to apply a uniform horizontal load to the back of the frontal wall simulating the out-of-plane seismic load. Additionally, a vertical load was also applied to the transversal walls to simulate the self-weight of the upper structural components (e.g. slabs, roof structure). A supporting steel frame was placed between the reinforced concrete reaction wall of the laboratory and the airbag. Wooden planks were attached to the steel supporting structure in order to create a smooth contact surface where the airbag can be placed, avoiding

any possible damage. Four load cells were placed between the steel profiles and the reaction wall at the level of the horizontal steel profiles. These cells allowed the recording of the load applied by the airbag to the wall, overcoming the issue related to the calculation of the contact area between the airbag and the prototype, which may vary throughout the test due to the deformation of the wall. At the top surface of the transversal walls, two steel profiles were placed in order to even the vertical load applied through two vertical hydraulic actuators. The actuators were placed between the steel profiles and the reaction slab. A vertical load corresponding to a normal compressive load of approximately 0.10 MPa, was applied in each transversal wall. Two steel posts were placed at the back of the transversal walls between the concrete base and the reaction slab to avoid a possible overturning of the concrete base (Figure 6.12).

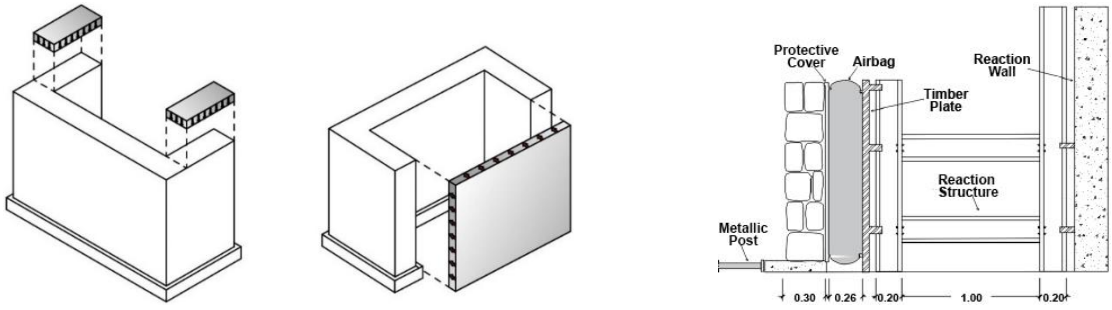
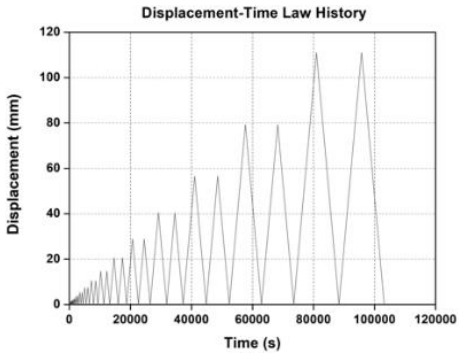


Figure 6.12 – Load configuration out-of-plane test setup.

In order to avoid any possible sliding displacements, six steel posts were also placed between the concrete base of the prototype and the laboratory reaction wall. The horizontal load was applied at the frontal wall after the stabilization of the vertical load. The out-of-plane test was carried out under displacement control, being the control point located at the top of the frontal wall at mid-span, where the highest displacement was expected. The procedure applied during the test consists of imposing positive incremental displacements repeated two times in order to detect possible stiffness and strength degradation after reaching the peak load. At the end of each series, an increment equal to 1.4 times the latest displacement is applied to define the new displacement threshold of the following cycle.



a



b

Figure 6.13 – Displacement-time law history (a); airbag test setup (b).

The pressurization and depressurization of the airbag was carried out in a controlled way using LabView software based on the displacement-time history defined for the out-of-plane test. The airbag has two pressure valves, which allow to inflate the airbag until a certain level of pressure that is enough to attain the imposed lateral displacement. Once the control displacement is reached, the air in the airbag is released until zero displacement in the early stages of the out-of-plane testing. When the non-linear response of the wall is activated, the unloading is only possible up to a residual displacement associated to the permanent deformation of the wall.

The monitoring of the displacements of the frontal wall during the out-of-plane test was carried out using linear variable differential transducers (LVDTs). Figure 6.14 shows the LVDTs setup of the walls for all testing procedures performed.

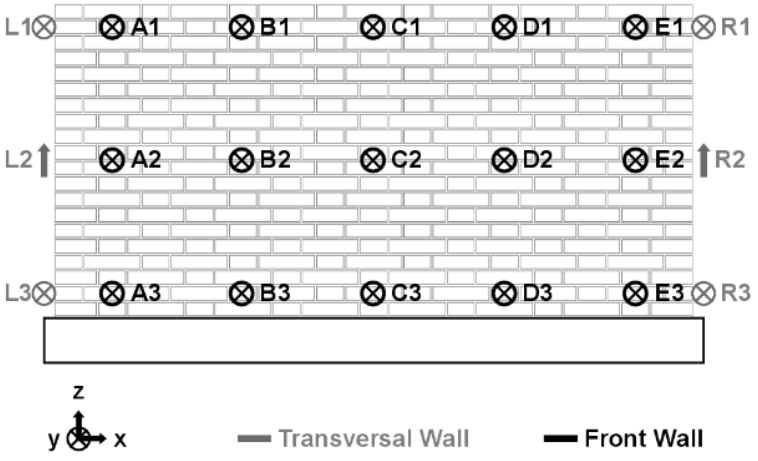


Figure 6.14 – LVDTs location.

6.5 Material characterization

Brick and mortar units have been tested in order to characterize their physical and mechanical properties. A series of mortar specimens were cast, and 3 wallets were built to perform destructive tests on the masonry assemblage and its components.

For the sake of conciseness, the main outcomes regarding the destructive tests are hereinafter summarized. Further details can be found in the study published by Barontini and co-workers [176].

Compressive ($f_{b,c}$) and flexural ($f_{b,f}$) strength of the mortar are determined according to the EN 1015-11 standard [177]. The values for $f_{b,c}$ and $f_{b,f}$ are 3.6 and 1.5 N/mm2, respectively. Masonry wallets have been used to carry out compression tests, diagonal compression tests and flexural tests. Compression tests (Figure 6.15a) were performed according to the guidelines provided in UNI EN 1052-1 [178], which allowed to estimate the average compression strength (7.3 N/mm2), the average Young's modulus (1800 N/mm2) and the Poisson's ratio (0.12).

Shear strength and shear modulus have been estimated by means of uniaxial diagonal compression tests (Figure 6.15b), according to the ASTME E519 standard [179]. The resulting average are 0.120 N/mm2 and 300 N/mm2, respectively. Finally, four point loading flexural tests (Figure 6.15c) allowed to estimate the characteristic flexural strength for the selected masonry typology, which is equal to 0.04 N/mm2 (average value) [180].



a b c

Figure 6.15 – Compression test (a), diagonal compression test (b), flexural test (c).

6.5.1 Sonic tests

Sonic pulse velocity test is a common non-destructive method based on the transmission of mechanical wave in the sonic range (20-20000 Hz). The investigated specimen is hit by an instrumented hammer which

generates a wave pulse that propagates in the specimen and is received and recorded by a sensor placed onto the specimen on the same face (indirect test configuration) or on the opposite face (direct test configuration). Assuming that the medium is elastic, isotropic, homogeneous, and nondispersive, equations 3 and 4 (reported in Section 2.3.2) can be used to relate the velocity of the mechanical wave (VP) with the dynamic modulus of elasticity, the Poisson's ratio and the density of the material.

Direct sonic tests were carried out on the frontal wall UMW and RMW. Tests were carried out using an instrumented impact hammer (PCB Model 086D05) with a measurement range of ±22,240 Npk and an accelerometer (PCB model 352B) with a measurement range of ±5 g and 1000 mV/g sensitivity. The Data Acquisition System adopted allows a high sampling rate (up to 100,000 Hz) required for such typology of tests. Direct sonic test is carried out on a 1×1 m^2 squared area, with measurement points every 25 cm. The points are selected to test the mortar joint, the stretcher, and the header blocks.

It is worth noting that, in the case of the header, the pulse wave travels only within the brick, whereas, in the case of the stretcher, the wave travels through two blocks and the mortar layer in between. In each measurement point, an average of 10 sonic pulses are emitted to estimate the variability. Figure 6.16 shows the reference grid for the direct tests and the contour plot of the pulse velocity.

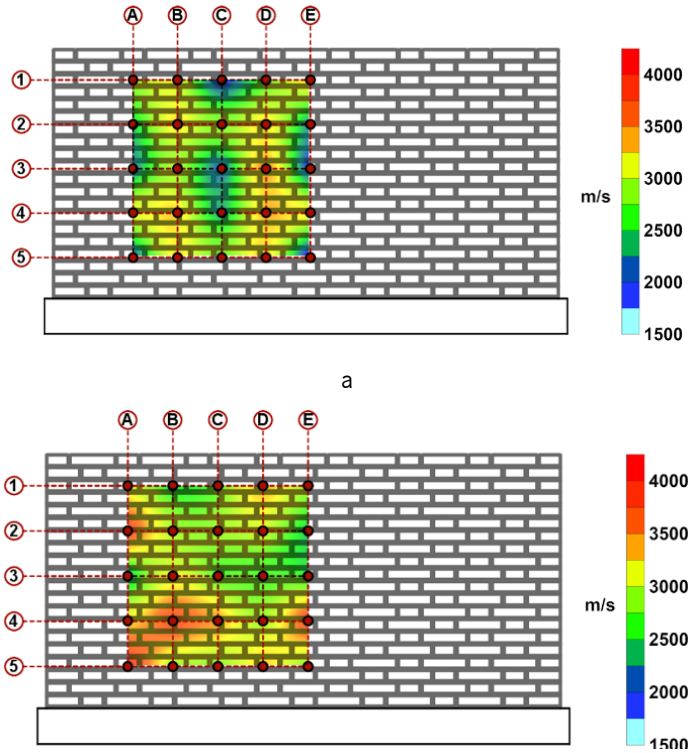


Figure 6.16 – Direct sonic test: reference grid and contour plot of the P wave velocity (m/s) in UMW (a) and RMW (b).

In UMW, the contour map appears to be characterized by slightly less uniformity in terms of velocity distribution (Figure 6.16a). The presence of areas with lower values of sonic pulse velocity correspond to irregularities in the masonry bond configuration (e.g. voids/construction defects). On the other hand, RMW contour map shows a trend characterized by reduced differences among the sonic pulse velocity values detected (Figure 6.16b). This is clearly due to the presence of the TRM solution applied to the façade of the wall. Table 6.1 shows the values of velocity corresponding to the reference grid in UMW and RMW, together with the corresponding coefficient of variation. The values highlighted in red refer to the acquisition points corresponding to the headers of the walls. In both cases, the trend highlighted by the contour map is confirmed.

Table 6.1 – Direct sonic test: average velocity in m/s and coefficient of variation between brackets in UMW (a) and RMW (b).

	A	B	C	D	E
1	2693 (14.1%)	2283 (19.1%)	1995 (13.3%)	3027 (13.3%)	1909 (11%)
2	3020 (11%)	3213 (8.7%)	2833 (7.4%)	3233 (15.3%)	3178 (17.9%)
3	1670 (10.1%)	2730 (11.1%)	1885 (8.4%)	2122 (17.6%)	2595 (10.8%)
4	2568 (24%)	3219 (14.1%)	3464 (9.7%)	3289 (11.6%)	3253 (15.9%)
5	3137 (14.2%)	2118 (14.4%)	1716 (9.2%)	3039 (16.7%)	1698 (7%)

a

	A	B	C	D	E
1	2947 (13%)	3750 (8.6%)	2226 (7%)	3098 (15.6%)	3893 (12.5%)
2	2356 (8.9%)	2818 (8.3%)	3000 (7.1%)	3750 (5.4%)	2727 (14.7%)
3	2553 (11.2%)	2795 (10.6%)	2500 (5.7%)	3333 (7.6%)	2670 (9.5%)
4	3333 (7.9%)	2945 (10.8%)	2500 (5.9%)	2727 (5.3%)	3200 (10.9%)
5	2727 (5.3%)	2280 (16.3%)	2403 (6.5%)	3750 (8.5%)	2636 (7.2%)

b

The average velocity detected in UMW is 2708 m/s, whereas in RMW the average velocity is equal to 2916 m/s. CoVs show a reduced difference (approximately 23%) in both experimental scenarios (UMW and RMW), with a CoV equal to 21% and 17% in UMW and RMW respectively.

However, values related to RMW show more homogeneity in terms of magnitude and a more regular distribution along the points of the reference grid used to perform the sonic tests. Moreover, it is possible to say that the values of velocity estimated, ranging from 1000 to 3000 m/s, are consistent with those found in the literature for the similar masonry typologies [48]. Based on the results obtained, the estimation of masonry dynamic Elastic modulus in UMW led to a value of 5950 N/mm^2 (assuming ρ = 18kN/m^3 and ν = 0.25).

6.5.2 Dynamic identification

Dynamic characterization tests allow to estimate the dynamic characteristics of a structure in terms of natural frequencies and vibration modes. The dynamic characterization tests were carried out, in both walls and in all testing conditions (UMW, RMW, RMW_UND), before the out-of-plane test (undamaged condition) and after the out-of-plane test (damaged near-collapse condition). The results of the dynamic identification tests can also be used as a measure to correlate damage as this causes a variation of the natural frequencies and stiffness reduction [30,31]. The dynamic tests were carried out using uniaxial accelerometers placed in 14 different predefined points within different test setups for each wall. For each setup, a fifteen-minute reading was acquired using a sample frequency rate of 200 samples/s with ambient vibration. The sensor layout related to the tested prototypes is presented in Figure 6.18.

Accelerations were measured in both directions at some locations in order to detect both possible in-plane and out-of-plane mode shapes. The equipment used included accelerometers (PCB model 393B12) with a measurement range of ±0.5 g and 10,000 mV/g, a personal computer, cables, and a data acquisition system. The mode shapes were calculated and drawn in ARTEMIS [181] using linear interpolation, starting from data recorded in discrete sensors locations (Figure 6.17).

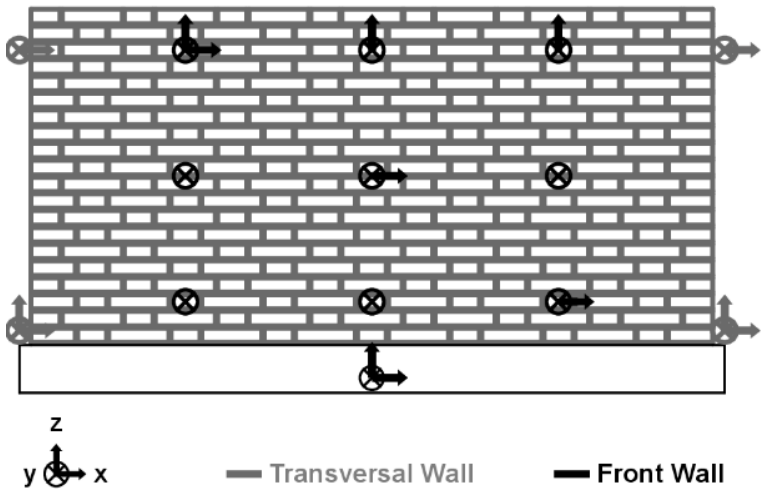


Figure 6.17 – Dynamic identification accelerometers location.

The peak values of frequency were selected using Enhanced Frequency Domain Decomposition (EFDD) and Subspace Identification-Unweighted Principal Components (SSI-UPCX) technique. The results of the analyses have been compared using the Modal Assurance Criterion before and after the out-of-plane airbag test.

Figure 6.18 shows the first three identified mode shapes and natural frequencies for UMW, RMW and RMW_UND before the out-of-plane airbag test.

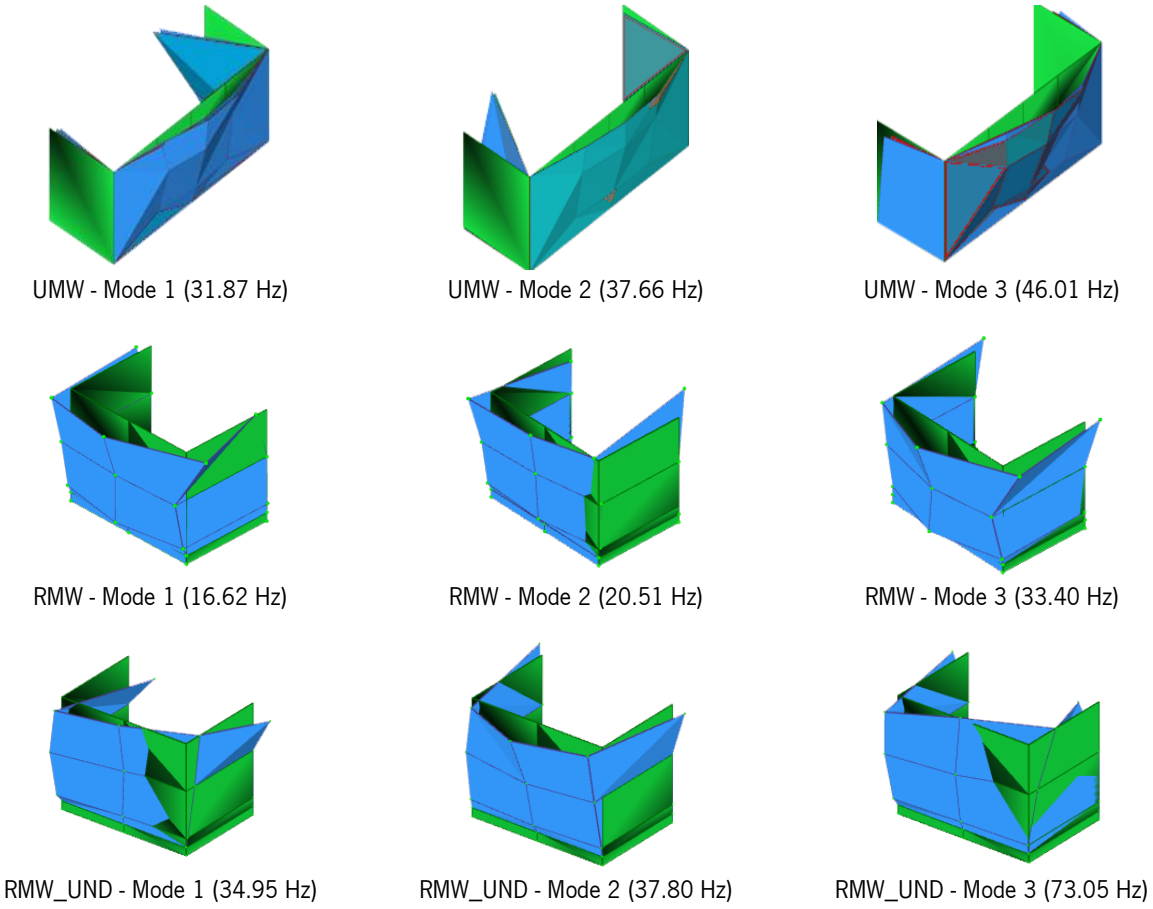


Figure 6.18 – Main mode shapes and frequency of vibration in UMW, RMW and RMW_UND before the out-of-plane airbag test.

In all the tested prototypes, the first mode consists of the out-of- plane vibration of the façade. An out of plane movement of the lateral walls characterizes the first and second mode shape, this trend being mostly visible in RMW and RNW_UND, whereas the third mode presents a combination between an out-of-plane movement of the upper part of the façade and a slightly torsional movement of the side walls.

Mode 2 frequency values in UMW and RMW_UND are closer to each other, whereas in RMW frequency values are lower overall. To this end, it must not be forgotten that RMW is already in damaged condition after being repaired, therefore it is reasonable to expect an overall reduction of stiffness and a consequently lower frequency value.

Table 6.2, Table 6.3, and Table 6.4 present a comparison of the results for the first 3 mode identified in each testing condition by means of EFDD and SSI-UPCX before the airbag test was performed. It is possible to

notice a good agreement among the natural frequencies detected, also confirmed by MAC values ranging from 0.993 to 0.996. A rather high variability in the estimation of the damping ratios emerges, likely due to the sources of uncertainty which affect it.

Table 6.2 – Dynamic identification in UMW before the airbag test: comparison between frequencies $\boldsymbol{f}$, damping ratios $\boldsymbol{\xi}$ and mode shapes in terms of MAC.

UMW	EFDD		SSI-UPCX				
	f (Hz)	ξ (%)	f (Hz)	ξ (%)	Δf (%)	Δξ (%)	MAC
MODE 1	31.87	0.70	32.77	0.78	-6.65%	10.26%	0.996
MODE 2	37.66	1.12	36.04	1.35	-4.50%	17.04%	0.993
MODE 3	46.01	2.16	44.03	4.9	-4.50%	55.92%	0.996

Table 6.3 – Dynamic identification in RMW before the airbag test: comparison between frequencies $\boldsymbol{f}$, damping ratios $\boldsymbol{\xi}$ and mode shapes in terms of MAC.

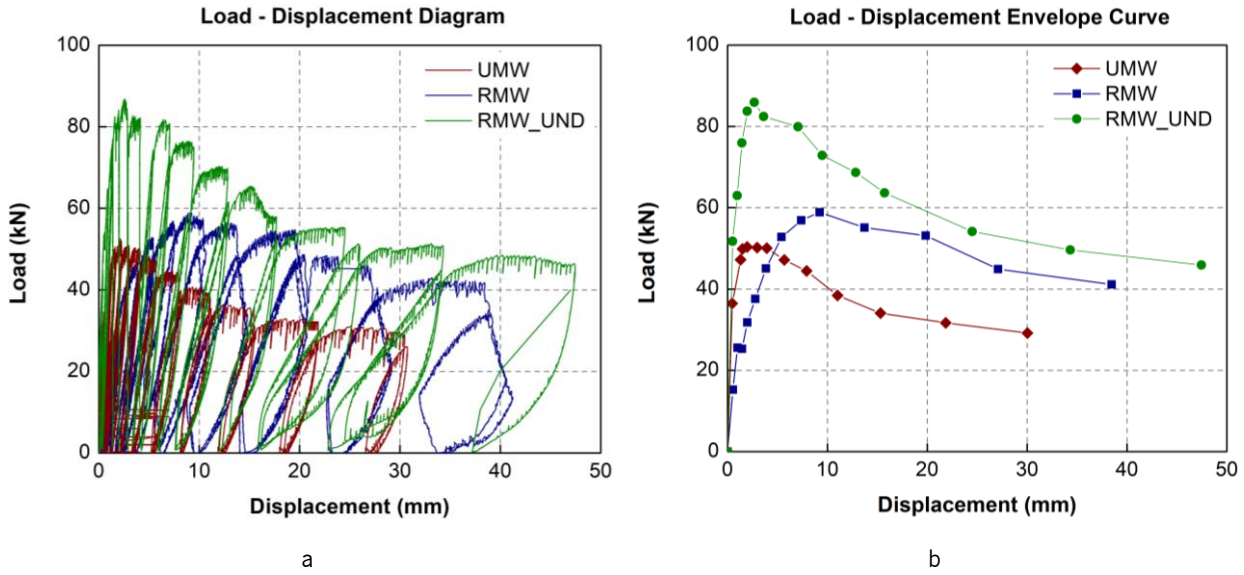
RMW	EFDD		SSI UPCX				
	f (Hz)	ξ (%)	f (Hz)	ξ (%)	Δf (%)	Δξ (%)	MAC
MODE 1	16.62	1.54	16.71	2.32	0.54%	33.62%	0.998
MODE 2	20.51	1.56	20.45	0.85	-0.29%	-83.53%	0.981
MODE 3	33.4	2.04	33.43	2.11	0.09%	3.32%	0.995

Table 6.4 – Dynamic identification in RMW before the airbag test: comparison between frequencies $\boldsymbol{f}$, damping ratios $\boldsymbol{\xi}$ and mode shapes in terms of MAC.

RMW_UND	EFDD		SSI UPCX				
	f (Hz)	ξ (%)	f (Hz)	ξ (%)	Δf (%)	Δξ (%)	MAC
MODE 1	34.95	1.50	31.85	1.305	-0.09%	-14.94%	0.997
MODE 2	37.80	2.47	37.82	2.13	0.05%	-15.96%	0.984
MODE 3	73.05	1.55	73.21	2.56	0.22%	39.45%	0.972

6.6 Experimental behaviour of the U-shaped brick walls

This section describes the out-of-plane quasi-static loading tests carried out on two reduced scale brick masonry walls. The applied force, given by the sum of the four load cells' record, is plotted in Figure 6.19a, against the displacement of the topmost measurement point in the mid span of the walls (point C1 in Figure 6.14). The corresponding envelope curves of the diagrams are reported in Figure 6.19b.



a b

Figure 6.19 – Load-displacement diagram at measurement point C1 (a); envelope curve at the same location (b).

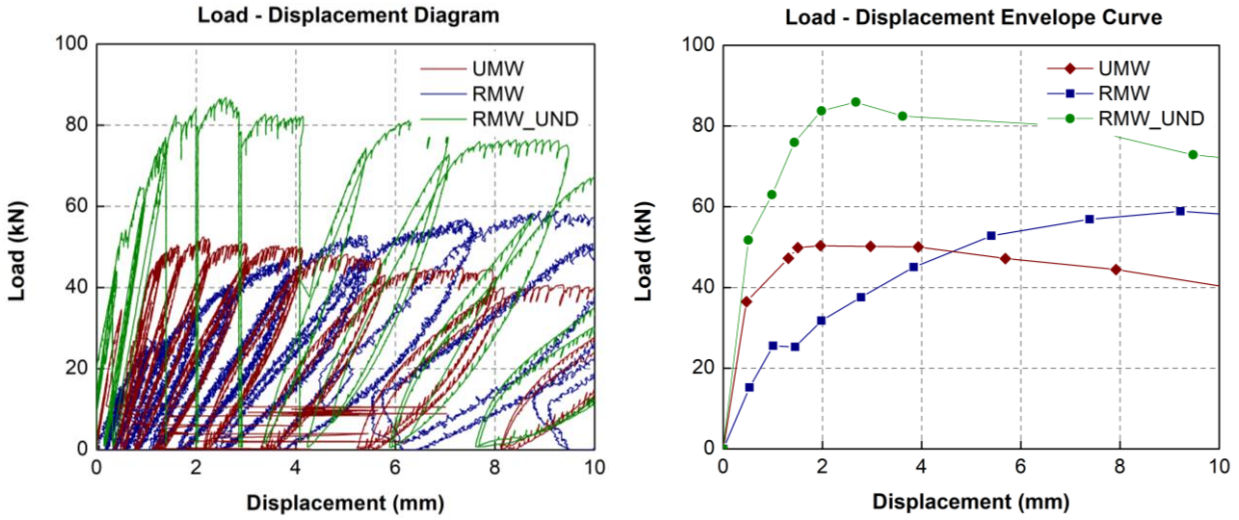
In unreinforced/undamaged configuration (UMW), the out-of-plane response is characterized by an initial linear behaviour until a displacement level equal to approximately 0.5 mm, followed by a slight stiffness loss almost until the peak load (54.39 kN) occurred after reaching a displacement level equal to 1.96 mm, when the first cracks appear (Figure 6.20).

After the peak, the load level progressively decreases, with a faster softening in the first part of the curve, followed by increasing displacement under an almost constant load, equal to about 60% of the peak (Figure 6.19).

The RMW curve displays a more ductile behaviour and more load capacity than UMW, despite its initial damaged condition. A nonlinear branch characterizes the initial stage of the test up the peak load which is approximately 8% higher than the peak load recorded in UMW (60 kN vs 54.39 kN), see Figure 6.20.

The structural performance in RMW_UND highlights a significant improvement compared to both UMW and RMW. Indeed, the load capacity is 36% and 30 % higher than UMW and RMW, respectively. The peak load

attained at the end of the linear elastic branch is 86 kN approximately. Overall, the application of the TRM solution proved to be effective both for repairing (RMW) and strengthening of the undamaged wall (RMW_UND). It is interesting to point out that the initial stiffness in UMW and RMW_UND is similar up to a load level of 40 kN approximately, hence the application of TRM resulted in an overall enhancement of the plain wall characteristics in terms of elastic behaviour and load capacity.



a b

Figure 6.20 – Load-displacement diagram up to 10 mm at measurement point C1 (a); envelope curve up to 10 mm at the same location (b).

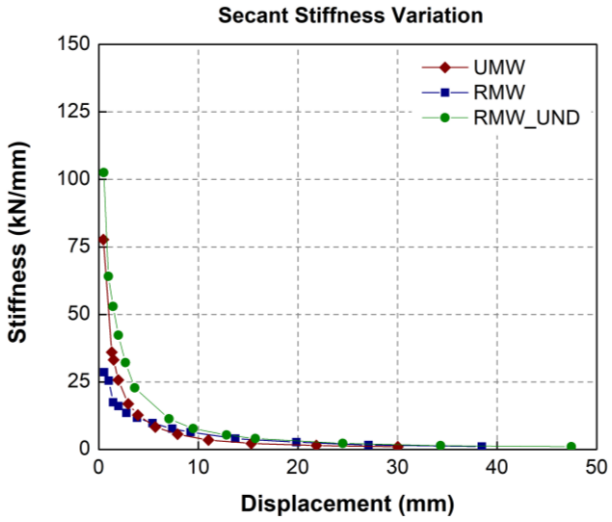


Figure 6.21 – Secant stiffness variation.

The beneficial effect related to the application of the TRM solution is visible also when comparing the graphs of the secant stiffness variation (Figure 6.21), calculated as the ratio of the maximum load to the maximum displacement at point C1 (see Figure 6.14).

As expected, the initial stiffness in RMW is lower than the stiffness value estimated for the plain wall in undamaged/unreinforced conditions (UMW) and in strengthened configuration (RMW_UND). In RMW the initial stiffness value is 25 kN/mm whereas in UMW and RMW_UND is around 75 kN/mm and 100 kN/mm respectively. When the TRM was applied to a wall in undamaged condition both peak load and initial stiffness increased notably their initial values of 36% and 25% respectively.

6.6.1 Damage patterns

The evolution of the crack pattern has been tracked and monitored during the airbag tests performed. Moreover, the data recorded by the LVTDs have been used to analyze the evolution of the displacement levels along the testing procedure. The final damage patterns for each configuration considered, namely UMW, RMW and RMW_UND are presented in Figure 6.22 and Figure 6.23. It is also worth mentioning that the convention used to identify lateral right and left walls is reported in Figure 6.10a. Moreover, no images are provided of the façade in RMW and RMW_UND since no significant damage occurred.



Figure 6.22 – Post airbag test damage pattern in UMW lateral right wall (a), façade (b), lateral left wall (c); Post airbag test damage pattern in RMW right side (c) and left side (d); Post damage pattern in RMW_UND right side (e) and left side (f).

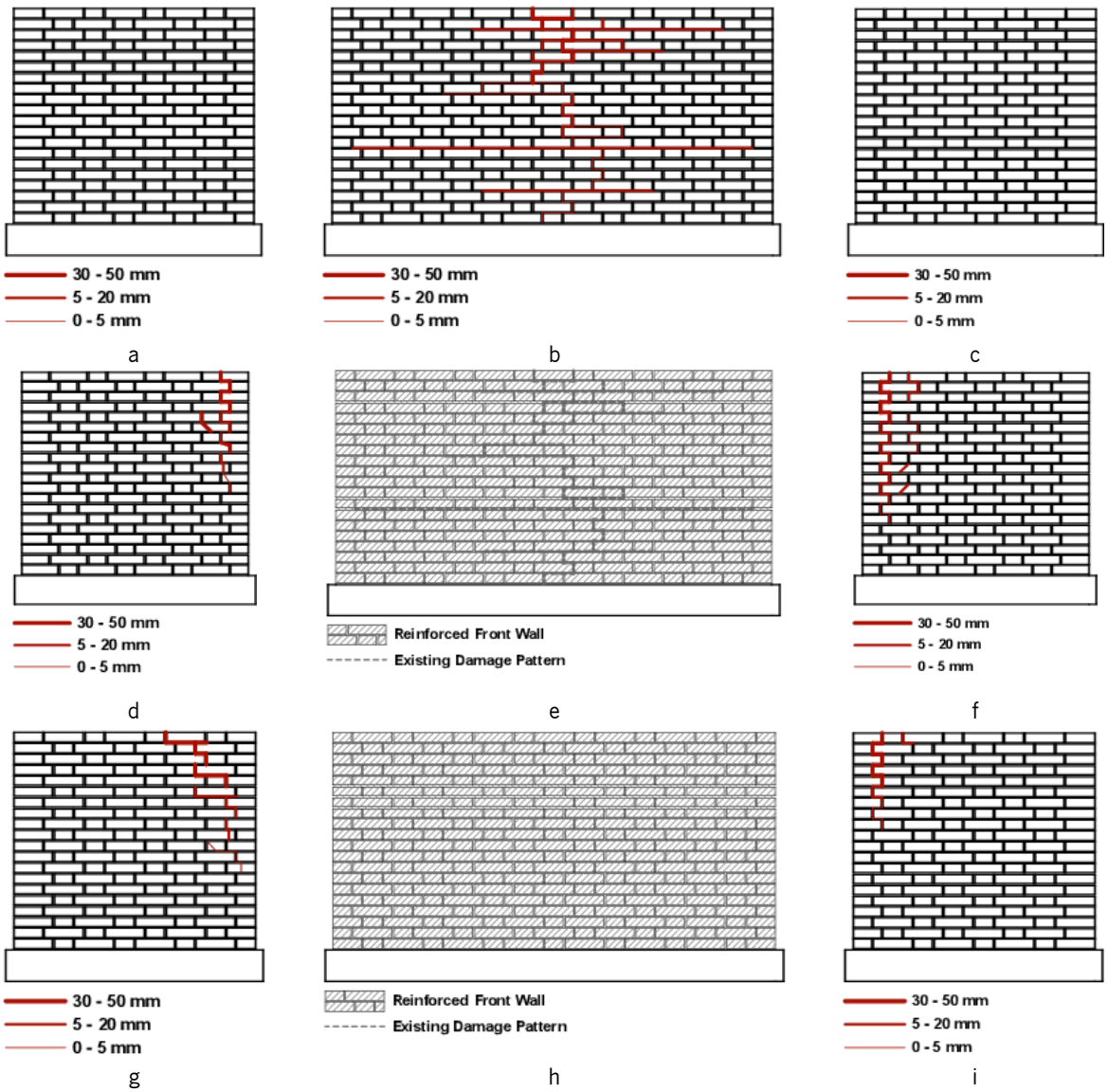


Figure 6.23 – Damage pattern in UMW right lateral wall (a), façade (b), left lateral wall (c): Damage pattern in RMW right lateral wall (d), façade (e), left lateral wall (f); Damage pattern in RMW_UND right lateral wall (g), façade (h), left lateral wall (i).

In UMW, an almost vertical crack from top to bottom in the front wall affecting the mortar joints and the interfaces between joints and bricks is clearly visible (Figure 6.23b). A horizontal crack affects a joint closer to the middle of the façade. The portion of the front wall above this crack presents evidence of sliding combined with an out-of-plane rotation. This induces cracks in the internal face of the transverse walls which, in some cases, also affect the bricks (cracks and spalling), at the connection with the front wall. Cracks on the rear surface of the front wall are mainly due to the sliding of the bricks on the bed joints and affect the unit-joint interfaces. The damage pattern is consistent with the out-of-plane displacement recorded by the

LVDTs, as clearly shown in (Figure 6.24a-b-c) and with the horizontal and vertical displacement profile shown in Figure 6.25a and Figure 6.25b respectively.

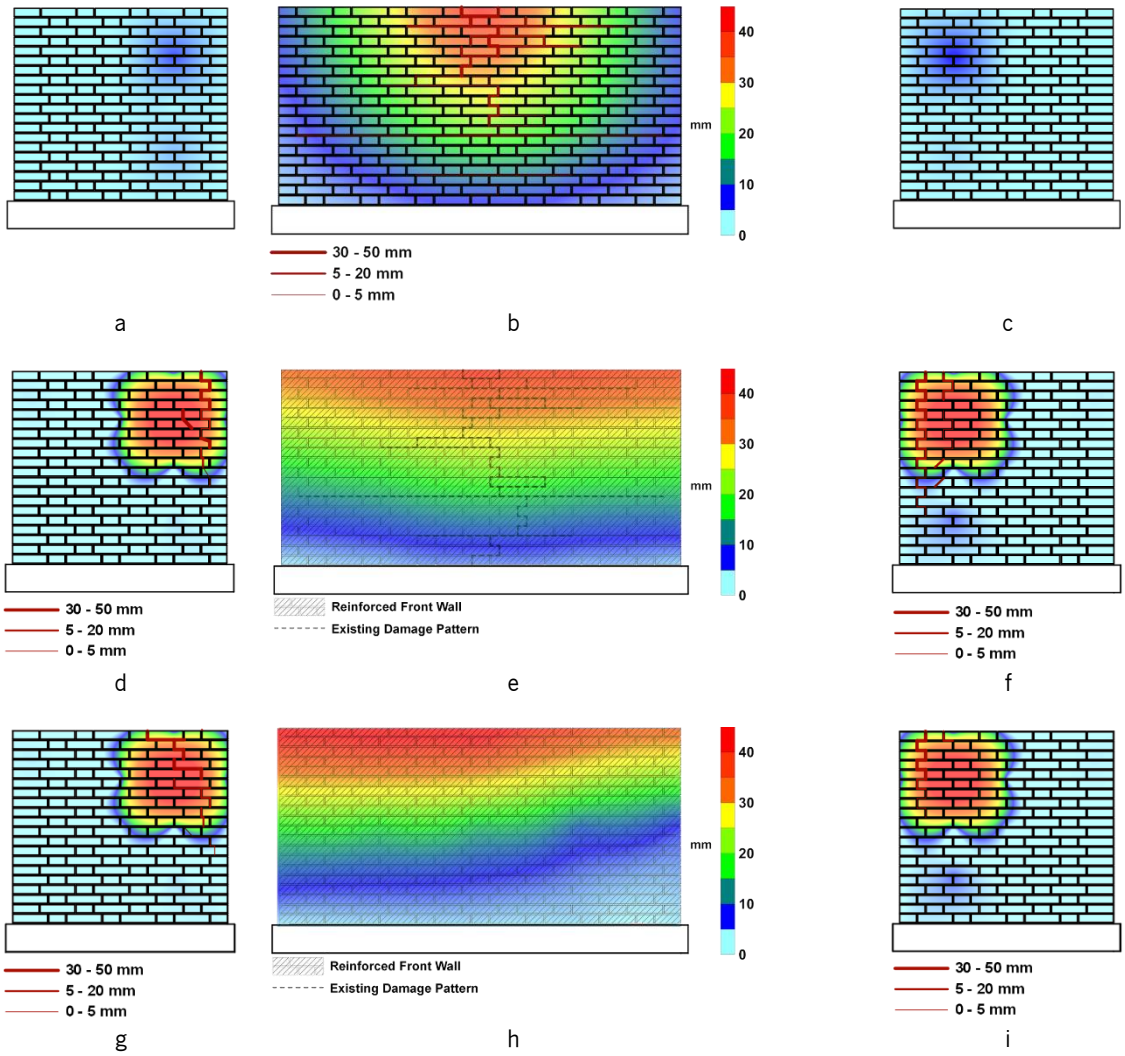


Figure 6.24 – Contour map in UMW right lateral wall (a), façade (b) left lateral wall (c); Contour map in RMW right lateral wall (d), façade (e), left lateral wall (f), Contour map in RMW_UND right lateral wall (g), façade (h), left lateral wall (i).

In RMW, cracks solely occurred in the lateral walls. The TRM reinforcement applied to the façade did not experience any sign of damage (Figure 6.22c-d). The application of the out-of-plane load to the back of the façade resulted in the detachment of the lateral walls from the façade itself, but no debonding phenomena have been observed in the interface between masonry and mortar layer of the TRM reinforcement.

In contrast to what occurred in UMW in terms of displacement concentration, RMW contour map shows a more uniform distribution in the façade, which is also due to the TRM's constraining action (Figure 6.24e).

In this case, highest displacement levels entirely affect the upper part of the façade and not exclusively its central area. It is possible to notice a slight asymmetry in the displacement distribution which is related to a rotation that occurred during the out-of-plane test. This trend is also visible in Figure 6.25a depicting the horizontal profile displacement for all the test performed.

In this regard, it worth to point out that both horizontal and vertical displacement profiles (Figure 6.25a-b) refer to the last step of the airbag test in all the considered conditions (UMW, RMW, RMW_UND. The reference acquisition points considered to define the displacement configuration refer to the LVDTs locations A1-B1-C1-D1-E1, A2-B2-C2-D2-E2 and A3-B3-C3-D3-E3 in the horizontal direction (Figure 6.14), whereas the acquisition points related to the vertical direction considers the locations A1-2-3, C1-2-3, and E1-2-3 (Figure 6.14).

Therefore for each set of points 3 profiles are shown related to UMW, RMW and RMW_UND respectively (Figure 6.25). Overall, the displacement profiles in the lower part of the façade (grey colour in Figure 6.25a) do not show significant difference between pre and post-test configuration, both in horizontal and vertical direction. On the other hand, central (blue colour in Figure 6.25a) and top horizontal displacement profiles (red colour in Figure 6.25a) provide interesting insight regarding the evolution of the airbag test and the distinct responses of the wall specimens.

More specifically, in UMW the horizontal profiles displacement do not show significant differences if lateral acquisition point data are compared to the data related to the central acquisition points, this is also due to the development of a horizontal crack extended for the whole width of the façade which resulted in a sliding movement of the upper part of the façade (Figure 6.25).

Conversely, horizontal displacement profiles in both RMW and RMW_UND highlights a difference between lateral and central displacement distribution, confirming the trend detectable from the contour maps that show a slight rotation of the wall specimens during the airbag test (Figure 6.24d-e-f and Figure 6.24g-e-h respectively).

The vertical profiles confirm the trend expected regarding the highest displacement concentration attained in the upper part of the façade. Obviously, RMW and RMW_UND displayed more dissipation capability compared to UMW, due to the presence of the TRM reinforcing solution (Figure 6.25b-d-f).

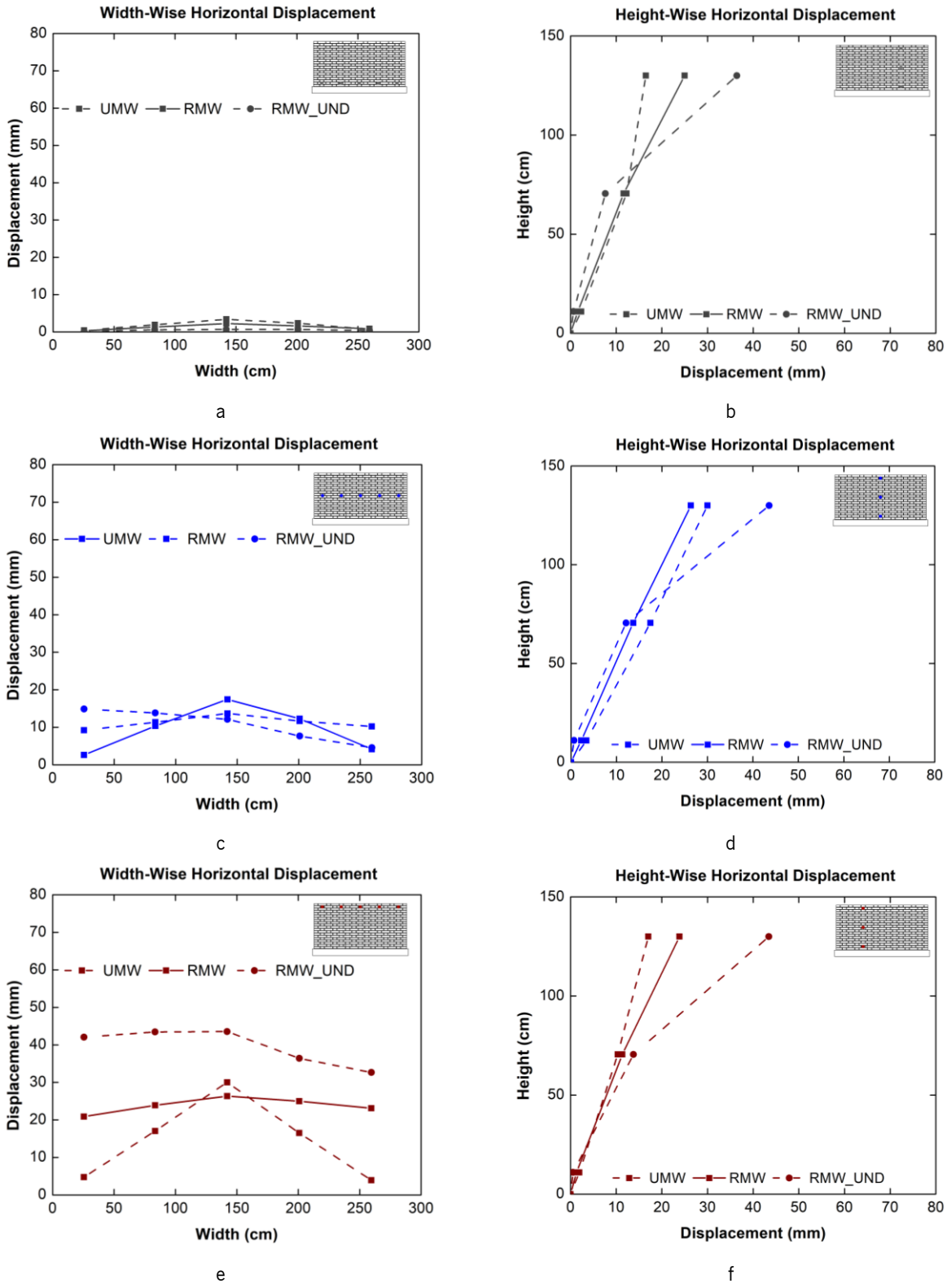
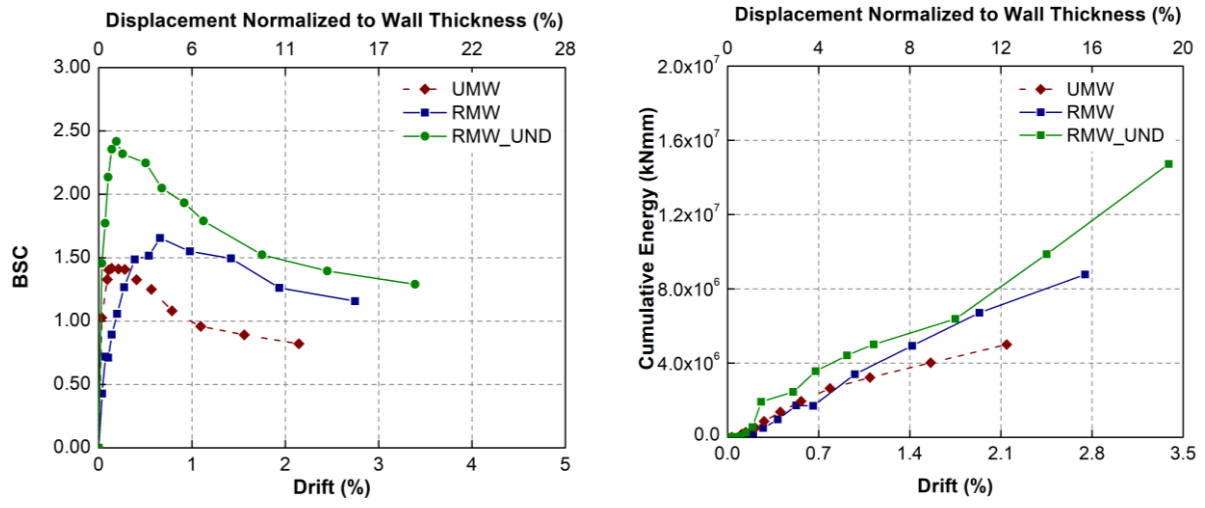


Figure 6.25 – Maximum horizontal displacement profiles façade bottom (a), middle (c), upper (e); Maximum vertical displacement profiles façade left side (b), central (d), right side (f).

RMW_UND and RMW performances are similar in terms of damage pattern. In fact, the façade does not present any significant cracks, whereas the detachment of the lateral walls is consistent with the trend highlighted in the repaired masonry wall (RMW). Similarly to what detected in RMW, the reinforced wall RMW_UND experienced a slight rotation phenomenon during the airbag test which is visible from both the contour map in Figure 6.24h and from the corresponding horizontal profile in Figure 6.25c-e.

6.6.2 Evaluation of the seismic response

The envelope curve of the base shear coefficient (BSC) – ratio of the horizontal thrust to the self-weight of the wall – is presented in Figure 6.26 as function of both drift (bottom axis) and displacement normalized to the wall thickness (top axis). In UMW, the initial stiffer behaviour of the wall leads to a 0.14% drift at the out-of-plane peak strength, which corresponds to 0.75% of the wall thickness. It is interesting to point out that the same wall in undamaged and reinforced conditions RMW_UND attained its out-of-plane peak load at a similar drift level (0.19%), which corresponds to approximately 1% of the wall thickness. As mentioned before, the application of the TRM solution resulted in an enhancement of the wall performance in terms of stiffness and peak load. Indeed, also the post peak behaviour in UMW and RMW_UND show a similar trend characterized by a decrease of 20% of the out-of-plane strength which is reached in a range between 0.60% and 0.65% drift approximately. On the other hand, RMW displayed a lower initial stiffness due to its damaged condition, which led to an out-of-plane maximum capacity (base shear coefficient equal to 1.65), attained for a drift level of 0.66% corresponding to approximately 4% of the wall thickness.



a b

Figure 6.26 – Base Shear Coefficient (a) and Energy dissipation capacity (b) of the masonry walls for each testing condition.

The positive influence of the TRM solution in the out-of-plane response of the masonry walls is further confirmed by the evolution of the hysteretic energy dissipated during the test (Figure 6.26b). Dissipated energy is represented by the area enclosed by hysteretic loops obtained from load-displacement response records in the reference LVDT (control point C1, see Figure 6.14). It is observed that for the same drift demand, the energy dissipated by RMW and RMW_UND is higher when compared to the unreinforced wall UMW. Looking at a drift level corresponding to 2%, the dissipated energy in UMW is approximately 5E6 kNmm, whereas for the same drift level the dissipated energy is 6.7E6 kNmm (25% increase) and 8.06E6 kNmm (38% increase) in RMW and RMW_UND respectively, see Figure 6.26b.

6.6.3 Limit states

Figure 6.27 provides an insight about the load and displacement corresponding to three damage levels or limit states defined by Eurocode 8 [182]. Following this approach and based on previous data of experimental campaigns on masonry buildings [101][102], the different damage limit states were defined as it follows: (1) Damage Limitation state (DM), which is associated to the point where a change of stiffness could be detected (H_{cr}, d_{cr}); (2) Severe Damage (SD) limit state, which is associated with the drift corresponding to the maximum out- of-plane strength (H_{max}, d_{Hmax}); and (3) Near collapse limit state (NC), which is associated to the lateral drift corresponding to a 20% decrease of the out-of-plane strength (H_u, d_{Hu}).

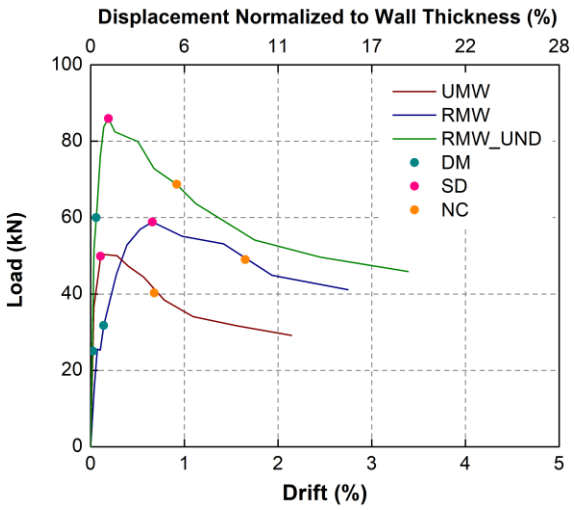


Figure 6.27 – Limit states identification in UMW, RMW and RMW_UND.

UMW and RMW_UND present a significant initial stiff behaviour, leading to very low values of lateral drift corresponding to the crack initiation (DM limit state). In RMW the initial stiffness is reduced probably due to

its initial damaged condition, in fact, the drift corresponding to DM limit state is 0.14%, which is around 90% higher than the value detected in UMW and RMW_UND, see Table 6.5.

Due to the reduced nonlinearity before the peak load, relatively low values of lateral drift corresponding to severe damage limit states (SD) are also observed. UMW and RMW_UND have a similar behaviour even if their load capacity and initial stiffness is different. Indeed, the lateral drift corresponding to the NC damage limit state is equal to 0.68% and 0.92% for UMW and RMW_UND respectively, whereas in RMW, the lateral drift related to NC damage limit state is equal to 1.65%.

Table 6.5 – Lateral drifts and corresponding limit states.

	Damage Limitation (DM)		**Severe Damage (SD)**		**Near Collapse (NC)**	
	Hcr (kN)	**dcr (%)**	**Hmax (kN)**	**dHmax (%)**	**Hu (kN)**	**du (%)**
UMW	25.03	0.023	49.88	0.107	40.28	0.68
RMW	31.77	0.14	58.86	0.66	47.09	1.65
RMW_UND	60	0.06	85.95	0.19	68.76	0.92

Even though the adopted limit states may be considered too conservative if applied to masonry walls under out- of-plane loading [183], it is possible to observe that the overall behaviour of the reinforced prototypes improved the performance of the walls in terms of the limit state corresponding to damage limitation (DM). The corresponding lateral drift increases from 0.023% (UMW) up to 0.14% and 0.06% in RMW and RMW_UND respectively, see Table 6.5. In both reinforced walls (RMW and RMW_UND), the performance levels are clearly attained for higher values of lateral resistance when compared to the plain wall (UMW).

6.6.4 Post damage dynamic identification

As mentioned in Section 6.5.2, a dynamic identification was also carried out upon completion of the test. Figure 6.28 shows the first three identified mode shapes and corresponding natural frequency of vibration. Overall, the frequency values experienced a reduction for all the testing conditions (UMW, RMW and RMW_UND).

In all the three scenarios considered the first mode shape is still characterized by an out-of-plane movement. Mode 2 and 3 in UMW appear to be similar with prevailing lateral movement in both side walls. Moreover, Mode 1 and 2 in RMW and in RMW_UND display similar trends, mainly consisting in a combination between an out-of-plane movement in the upper part of the façade, whereas Mode 3 shows an additional flexural movement.

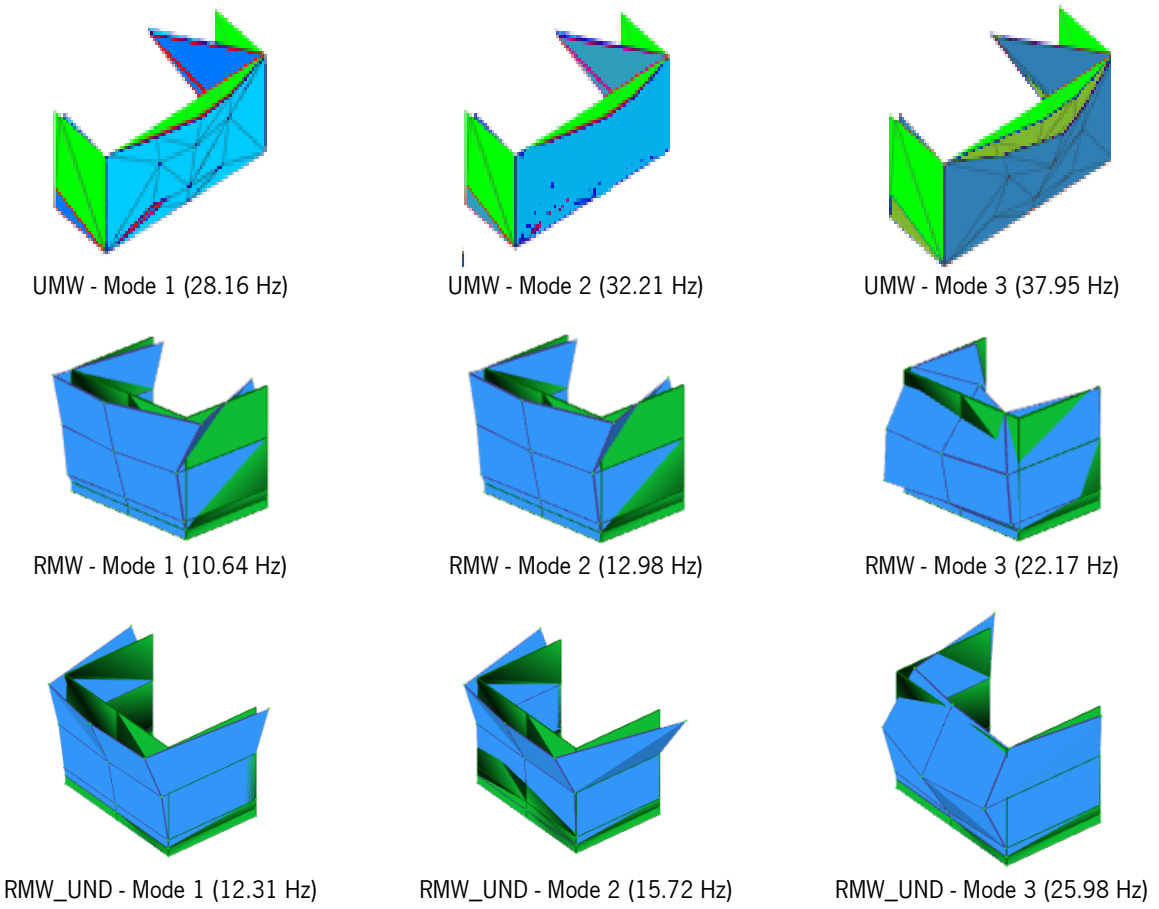


Figure 6.28 – Main mode shapes and frequency of vibration in UMW, RMW and RMW_UND after the out-of-plane airbag test.

Table 6.6, Table 6.7, and Table 6.8 present a comparison of the results for the first 3 mode identified in each testing condition by means of EFDD and SSI-UPCX after the airbag test was performed. Although a variation of the damping ratio appears, this has opposite trends for different modes and, in general, the sources of uncertainty affecting the estimation of this parameter do not allow its reliable use as damage sensitive feature[136]. The deterioration of the MAC between undamaged and damaged conditions is more evident in UMW. The comparison among the mode shapes in the three recorded configurations shows a larger modal displacement for the upper part of the front wall and suggests the feasibility of mode shape-based indicators for damage localization and quantification.

Table 6.6 – Dynamic identification in UMW after the airbag test: comparison between frequencies $\boldsymbol{f}$, damping ratios $\boldsymbol{\xi}$ and mode shapes in terms of MAC.

UMW	EFDD		SSI UPCX				
	f (Hz)	ξ (%)	f (Hz)	ξ (%)	Δf (%)	Δξ (%)	MAC
MODE 1	28.16	2.84	27.41	1.14	-2.74%	-149.12%	0.901
MODE 2	32.21	2.16	32.63	1.45	1.29%	-48.97%	0.706
MODE 3	37.95	0.53	39.25	1.58	3.31%	66.46%	0.996

Table 6.7 – Dynamic identification in RMW after the airbag test: comparison between frequencies $\boldsymbol{f}$, damping ratios $\boldsymbol{\xi}$ and mode shapes in terms of MAC.

RMW	EFDD		SSI UPCX				
	f (Hz)	ξ (%)	f (Hz)	ξ (%)	Δf (%)	Δξ (%)	MAC
MODE 1	10.64	1.28	10.63	1.49	-0.09%	14.09%	0.991
MODE 2	12.98	1.18	12.97	1.14	-0.08%	-3.33%	0.992
MODE 3	22.17	1.57	22.18	1.96	0.05%	19.90%	0.986

Table 6.8 – Dynamic identification in RMW_UND after the airbag test: comparison between frequencies $\boldsymbol{f}$, damping ratios $\boldsymbol{\xi}$ and mode shapes in terms of MAC.

RMW_UND	EFDD		SSI UPCX				
	f (Hz)	ξ (%)	f (Hz)	ξ (%)	Δf (%)	Δξ (%)	MAC
MODE 1	12.31	1.31	12.27	1.17	-0.33%	-11.97%	0.985
MODE 2	15.72	0.36	17.47	1.52	10.02%	76.45%	0.973
MODE 3	25.98	1.30	26.06	2.09	0.31%	37.80%	0.950

Looking at Table 6.9, it is possible to notice that UMW shows a difference in terms of frequency variation before and after the airbag test equal to 13%, 17% and 21% for Mode 1, Mode 2, and Mode 3 respectively (see Table 6.9).

On the other hand, RMW and RMW_UND frequency values experienced a significant reduction, which is equal to 36%, 48% and 34% in RMW for Mode1, Mode 2, and Mode 3 respectively, whereas in RMW_UND the percentage reduction between the pre airbag test and post airbag test is significantly higher, with a difference of 44% (Mode 1), 58% (Mode 2) and 64% (Mode 3) as shown in see Table 6.9.

Table 6.9 – Comparison of natural frequency variation before and after the out-of-plane airbag test.

	Pre-Airbag Out-of-Plane Test			Post Airbag Out-of-Plane Test			Percentage Variation (%)		
	Mode 1 (Hz)	Mode 2 (Hz)	Mode 3 (Hz)	Mode 1 (Hz)	Mode 2 (Hz)	Mode 3 (Hz)	Mode 1	Mode 2	Mode 3
UMW	31.87	37.66	46.01	28.16	32.21	37.95	19%	14%	18%
RMW	16.62	20.51	33.4	10.64	10.74	22.17	36%	48%	34%
RMW_UND	34.95	37.8	73.05	12.31	15.72	25.98	44%	58%	64%

6.7 Final Remarks

This chapter presents an experimental campaign on the out-of-plane characterization of two U-shaped clay brick masonry specimens and their material characterization through both destructive and non-destructive tests.

The aim of the experimental campaign is two-folded, on one hand it provides an insight into the seismic behaviour of 'placa' buildings, a traditional Portuguese mixed UMW-RC structural typology, on the other, it is intended to assess the effectiveness of the selected reinforcing solution in improving the out-of-plane performance of the tested walls.

Materials characterization allowed to estimate mortar mechanical properties (compression and flexural tests) and masonry mechanical properties (compression, diagonal compression, flexural tests and based on NDT, namely sonic tests, and dynamic identification). The cyclic seismic-cycle bending of the specimens, induced by means of an airbag exerting a horizontal thrust on the rear surface of the front wall confirmed the effectiveness of the TRM in improving the out-of-plane performance of the tested walls.

In all the tests performed, except for UMW, the recurring collapse mechanism consisted of the detachment of the lateral walls from the façade. In UMW, cracks occurred in the upper part of the façade, whereas in RMW and RMW_UND no damage was detected in the external layer of the TRM. Moreover, no debonding phenomena between brick masonry and TRM mortar occurred as well. The damage was concentrated in the lateral walls.

The application of the TRM solution to the damaged wall (RMW) resulted in an enhancement of its dissipation capacity and an improvement of its ductile behaviour, its peak load experienced approximately a 19% improvement compared to UMW (49.88 kN vs 59 kN kN) and a 31% difference compared to RMW_UND (86 vs 59 kN).

Conversely, when the TRM was applied to the undamaged wall, the beneficial effect was clear both in terms of structural capacity, with an increase of 36% (86 kN vs 49.88 kN) and 30% (86 kN vs 59 kN) of the peak load in RMW_UND compared to UMW and RMW respectively.

Overall, the results provided support the efficiency of the proposed strengthening technique as a viable and effective option applicable in different scenarios, namely to (1) prevent out-of-plane failures in existing masonry structures or (2) repair them as a consequence of seismic events.

7 Conclusions and future works

This chapter briefly summarizes the main findings of the work presented and some proposals to extend further the body of knowledge regarding the topics addressed in the document, namely the out-of-plane behaviour of masonry walls.

The document consists of six chapters that aim to analyse the out-of-plane behaviour in 2-leaf masonry walls using a comprehensive and multidisciplinary approach that encompassed all the aspects deemed crucial in providing a deeper understanding of this topic.

The initial chapter of the thesis served the purpose of identifying the areas to be analyzed throughout the thesis, based on those aspects deemed essential and significantly influential for the study of the out-of-plane behaviour in 2-leaf masonry walls.

Therefore, based on the considerations arisen from a thorough review of the literature sources, mechanical and geometrical studies have been carried out, without overlooking a critical analysis of the tools nowadays available to accurately simulate out-of-plane response in masonry structures (e.g. different numerical methods and modelling approaches).

7.1 Database of Masonry mechanical properties

Chapter 2 presents a database of mechanical properties for 2-leaf masonry walls. The data used to build the database were gathered through a literature review and later used to update, using Bayesian statistics, a set of reference values of mechanical properties proposed also by codes and standards commonly used in the building practice (e.g. Eurocode 8 and Italian Code – NTC 2018).

The main results related to this chapter are:

- Creation of a database that provides a systematic review of mechanical properties and reference values of mechanical properties for recurring masonry typologies.
- Proposal of a workflow/methodology that enables professionals involved in the field of assessment of masonry structures to update reference mechanical properties whenever new observations (e.g. experimental data) are available.

To this end, it is worth pointing out that the database can be used as it stands in its final version or further updated with new information. Data is, in fact, fully available for any user willing to update the range of mechanical properties provided, otherwise, it will be possible to use the information available as a reference to characterize existing masonry typologies similar to those presented in the database.

However, further developments can be represented by additional experimental activities aimed at the characterization of masonry typologies not exhaustively addressed in the database due to lack of information. Additionally, the methodology proposed is highly versatile, hence applicable to materials other than exclusively masonry. Therefore, further research activities could address this aspect.

7.2 Study of numerical modelling strategies comparison

Chapter 3 provides an insight regarding different modeling approaches to simulate the out-of-plane behaviour in 2-leaf stone masonry walls. The numerical methods considered are the finite element (FE) method and the distinct element (DE) method, whereas the modeling techniques selected and compared are macro and micro-modeling approaches. Results have been compared in terms of accuracy and computational effort, leading to the conclusion that both FE and DE-based micromodels proved to be effective in simulating the out-of-plane response and the consequent failure mechanisms.

However, FE micro-model analyses are characterized by a significant computational effort compared to DE micro-model analyses (7 days against 30 minutes approximately for FE-based analyses and DE-based analyses respectively). On the other hand, the FE-based macro-model approach represented a good compromise between accuracy and computational effort, suitable for practice-oriented engineering activities.

Based on the trend observed during the study proposed in Chapter 3, the work could be broadened by considering material models different from those already used, which displayed, especially in DE analyses some difficulties in capturing the post-peak behaviour (softening) in all the models considered.

Moreover, an interesting aspect highlighted in the chapter refers to the consistency of the expression used to estimate the mechanical properties used as input parameters in the numerical simulations. To this end, some expressions have been proposed in the document for the estimation of input parameters in DE models starting from FE-based macro model properties and vice versa.

This was, indeed, one of the main challenges arising from Chapter 4 whenever an estimation of input parameters in FE-based and DE-based models was required in order to compare the accuracy of these approaches in simulating the out-of-plane behaviour of the masonry walls experimentally tested and selected as a reference study.

Further studies could lead to more effective/reliable expressions, also applicable to peculiar masonry bond configurations and typologies such as drystone masonry walls which, for a series of aspects (e.g. different

interaction among masonry units compared to mortar joint walls), still represent an open challenge when it comes to accurately estimate mechanical properties.

7.3 Parametric study on reduced scale models

Chapter 4 presents the results of two parametric studies on reduced-scale 2-leaf stone masonry walls both from a mechanical and a geometrical standpoint. The reference models used in the study were calibrated in Chapter 3 and analyzed by means of different approaches to compare their effectiveness in simulating the out-of-plane behaviour of the selected case studies, namely a drystone masonry wall and a regular stone masonry wall with mortar joints. Since few information is available in the literature addressing the influence of material properties using DE-based simulations, this approach has been selected to carry out the first parametric study.

Successively, masonry bond geometrical characteristics and configuration have been analyzed. In this case, only the regular stone masonry wall has been considered as a case study because of the possibility of easily defining different bonds due to the regularity of unit arrangement replicable in a 3D CAD environment.

Different masonry bonds have been defined based on the guidelines of the Masonry Quality Index (MQI) method, a semi-empirical procedure that enables the estimation of masonry walls' mechanical properties starting from the assessment of a set of geometrical parameters (e.g. vertical/horizontal joints configuration, presence/absence of through-stones, etc.).

Additional parameters, not present in the MQI formulations, were also considered in the study, namely the corner configuration (good vs bad interlock) and the leaves configuration (perfectly overlapped vs staggered leaves).

In terms of material properties, it was possible to conclude that the elastic behaviour in both dry and mortared stone walls was mainly influenced by the normal stiffness and to a lesser extent by the shear stiffness, whereas the maximum out-plane capacity (peak load) was significantly affected by tensile strength and cohesion variation as well as friction angle variation, being the latter being more influential in drystone masonry assemblages than in mortared joint masonry walls.

Overall, the trend detected is in agreement with the formulation (Mohr-Coulomb criterion) adopted in the software used to carry out the numerical simulations (3DEC software by ITASCA). The main outcomes regarding the study on masonry bond geometrical characteristics refer to the acquisition of a deeper insight

regarding the role of parameters such as through-stones and leaves configuration which proved to have less influence than expected on the structural performance of the walls.

In order to acquire a deeper understanding of the mechanical properties influence on the structural performance of masonry walls, different or more advanced material models could be considered to carry out additional numerical sensitivity studies. To this end it must be noted that, in both FE-based and DE-based analyses, the post-peak behaviour was difficult to simulate with the material models adopted. More advanced material models may be considered to assess their capacity to capture the post-peak behaviour of masonry walls under out-of-plane load.

On the other hand, the influence of geometrical masonry bond geometric characteristics could be further analyzed by developing supporting tools for the automatic generation of 3D models in order to overcome the difficulties that occurred during the definition of masonry bond configuration carried out using CAD software with a traditional approach, namely constructions of the models based on 2D drawings defined by the user following the MQI guidelines. Some studies are already present in the literature addressing this topic, but the solutions proposed mainly refer to 1-leaf masonry panels, hence the challenge is represented by the possibility of automatically generating 2-leaf walls 3D models, having the chance to adjust parameters such as vertical/horizontal joints configuration, presence/absence of through-stones, corner configuration, leaves staggering ratio, etc.

Moreover, the use of specific generative algorithms could help to overcome the ambiguity detected and highlighted in Chapter 4, when models with partially fulfilled parameters configuration displayed better structural performance than models with fulfilled parameters.

7.4 Parametric study on full scale models

Chapter 5 background framework is represented by all the information and observations gathered from Chapter 4 and used to optimize the set of full-scale models built to carry out the parametric study both from a mechanical and a geometrical standpoint.

In Chapter 4, reduced-scale models were analyzed by means of DE-based simplified micro-models in order to assess on one hand the influence of mechanical parameters such as normal/shear stiffness, tensile strength, cohesion and friction angle.

On the other, the simplified DE micro-models were used to assess the influence of masonry bond characteristics such as vertical joints configuration (VJ), horizontal joints configuration (HJ), wall connection

(WC), corner configuration (good versus poor corner interlock), leaf configuration (staggered versus overlapped leaves) on the out-of-plane performance of stone masonry walls. The masonry bond variation based on the Masonry Quality Index (MQI) guidelines led to the definition of 108 models.

On a material level, the elastic regime was governed by normal and shear stiffness, whereas the load capacity was influenced by tensile strength, cohesion and friction angle.

From a geometrical point of view, the study on reduced-scale models made it possible to understand the reduced influence of the leave configuration and of the through-stones on the out-of-plane performance of the models considered.

Additionally, it was observed that the partially fulfilled condition (PF) in vertical/horizontal joints configuration was difficult to simulate in a 3D CAD environment. This resulted in the definition of 3D models with low MQI values (and partially fulfilled parameters) but with an overall better performance, at least in terms of load capacity, compared to models with higher MQI values.

Based on these considerations the set of full-scale models used in Chapter 5 for the geometrical parametric study on full-scale models was defined. Therefore, only perfectly overlapped leaves were considered, and the partially fulfilled condition was discarded for all the parameters.

The parametric studies conducted in Chapter 5 address the out-of-plane behaviour in 2-leaf stone masonry walls on a material level and on a geometrical level. To this end, two different numerical approaches, finite element method (FE) and distinct element method (DE), have been considered to simulate the behaviour of stone masonry walls under static-cyclic load.

From a mechanical standpoint, a set of reference parameters have been statistically studied by means of multiple linear regression in order to assess their influence on the out-of-plane performance in masonry walls associated to specific limit states.

In this case, a set of empirical expressions have been defined based on the statistical model considered. The expressions provide an estimation of the influence of the mechanical properties selected on the attainment of load and displacement level for each limit states defined. The dataset used to run the statistical analysis is based on the result of pushover analyses on FE-based macro-models.

Young modulus proved to be the most influential parameter when it comes to the assessment/estimation of displacement levels. Higher young modulus values correspond to stiffer models and reduced displacement levels attainable.

With regard to the load capacity, in addition to the Young Modulus, tensile fracture energy and tensile strength proved to be highly influential variables. In fact, an increase of these parameters corresponds to an enhancement of the load capacity.

From a geometrical standpoint, a study was conducted to assess the influence of parameters such as slenderness, height-to-span-ratio and thickness-to-span ratio on the out-of-plane performance in 2-leaf masonry walls. Additionally, a set of key parameters characterising the masonry bond configuration, namely vertical/horizontal joints configuration (VJ/HJ), presence/absence of through-stones (WC), corner configuration (CN), were also included in the study. The results of the numerical simulations carried out by means of DE-based simplified micro models were used as a starting dataset in order to run the multiple linear regression analysis.

Similarly to the study on material properties, the empirical expression obtained provided an insight regarding the influence of the selected parameters on the out-of-plane performance of the masonry typology selected (masonry walls with regularly cut stone units).

In general, the out-of-plane load capacity is strongly affected by the slenderness and, consequently, by the thickness of the walls. Higher thickness values correspond to higher peak load attained. On the other hand, wall connection parameter (WC) did not result as influential as expected. This trend was in agreement with the results obtained in the parametric study on reduced scale models (see Chapter 4). The lack of significance of WC in the out-of-plane load capacity estimation may be due to factors such as the intrinsic characteristics of the masonry typology selected (regularly cut stone masonry walls), to the modelling assumptions of the study (e.g. perfectly overlapped leaves) and to the type of load applied to simulate the out-of-lane action (static cyclic loads).

However, vertical (VJ) and horizontal (HJ) joint configuration and corner configuration proved to be highly influential on both the load capacity and the load multiplier estimation. A proper horizontal/vertical joints arrangement results in a better structural performance of the walls, hence higher out-of-plane capacity. A good masonry bond also corresponds to a higher triggering load (higher load multiplier) in the out-of-plane recurring collapse mechanisms.

To this end, it is important to point out that the analytical formulation used to calculate the load multiplier associated to the failure modes identified as a result of the numerical analyses carried out, does not explicitly take into account the contribution of the WC parameter, whereas since VJ, HJ and CN significantly affect the definition of the macro element associated to the failure of the wall, it is possible to say that an “indirect”

assessment of their influence is reflected on the analytical formulation and, consequently, on the statistical analyses conducted based also on the analytical results.

The main outcomes of this chapter can be summarized as follows:

- Identification of limit states based on the evidence resulting from the parametric study and definition of empirical expression for the assessment of the influence of the selected mechanical parameters in the attainment of load and displacement level for each limit state defined.
- Definition of empirical expressions for a deeper study and quantification of the individual influence of different geometrical parameters of the masonry bond on the out-of-plane capacity in masonry walls.
- Definition of empirical expressions for a deeper study and quantification of the individual influence of different geometrical parameters of the masonry bond on the triggering load (load multiplier) related to collapse mechanisms recurring in masonry walls under out-of-plane load.
- Definition of empirical expression to correlate input parameters used in different modeling approaches, namely macro-model, and micro-model.

Similarly to what was suggested in Chapter 4, also in this case the development of specific tools for the automatic or semi-automatic generation of masonry bonds could extend and broaden this study. Since it only addresses walls made with regularly arranged masonry units, additional masonry typologies could be considered and added to the dataset presented, overcoming also the limitations related to the ranges of values of parameters such as wall thickness, slenderness, height, and span characterising the dataset used to perform the parametric study.

Moreover, further validation studies could be carried out both from an experimental and numerical point of view to extend the scope of the present work and derive empirical expressions applicable for an expedited estimation of the out-of-plane capacity of masonry walls. Future works would focus on improving the reliability of the empirical expressions proposed by extending the dataset with further numerical and experimental analysis, and by validating the expressions with existing experimental datasets.

7.5 Experimental test on retrofitted 2-leaf brick masonry walls

Chapter 6 describes the experimental campaign carried out to assess the effectiveness of a textile-reinforced mortar (TRM) solution in preventing out-of-plane failure and in improving the performance of 2-leaf U-shaped brick masonry walls in different conditions, namely damaged and undamaged.

The cyclic seismic-cycle bending of the specimens, induced by means of an airbag exerting a horizontal thrust on the rear surface of the front wall confirmed the effectiveness of the TRM in improving the out-of-plane performance of the tested walls.

In all the tests performed, except for UMW, the recurring collapse mechanism consisted of the detachment of the lateral walls from the façade, whereas no damage was detected in the external layer of the TRM. Moreover, no debonding phenomena between brick masonry and TRM mortar occurred as well with damage patterns mainly affecting the lateral walls.

The application of the TRM solution to the damaged wall (RMW) resulted in an enhancement of its dissipation capacity and an improvement of its ductile behaviour. Conversely, when the TRM was applied to the undamaged wall, the beneficial effect was clear both in terms of structural capacity and peak load.

Overall, the proposed strengthening technique proved to be effective in enhancing the out-of-plane capacity of the tested walls. It represents a viable option in different scenarios, namely preventing out-of-plane failures in existing masonry structures or repairing masonry structures as a consequence of seismic events

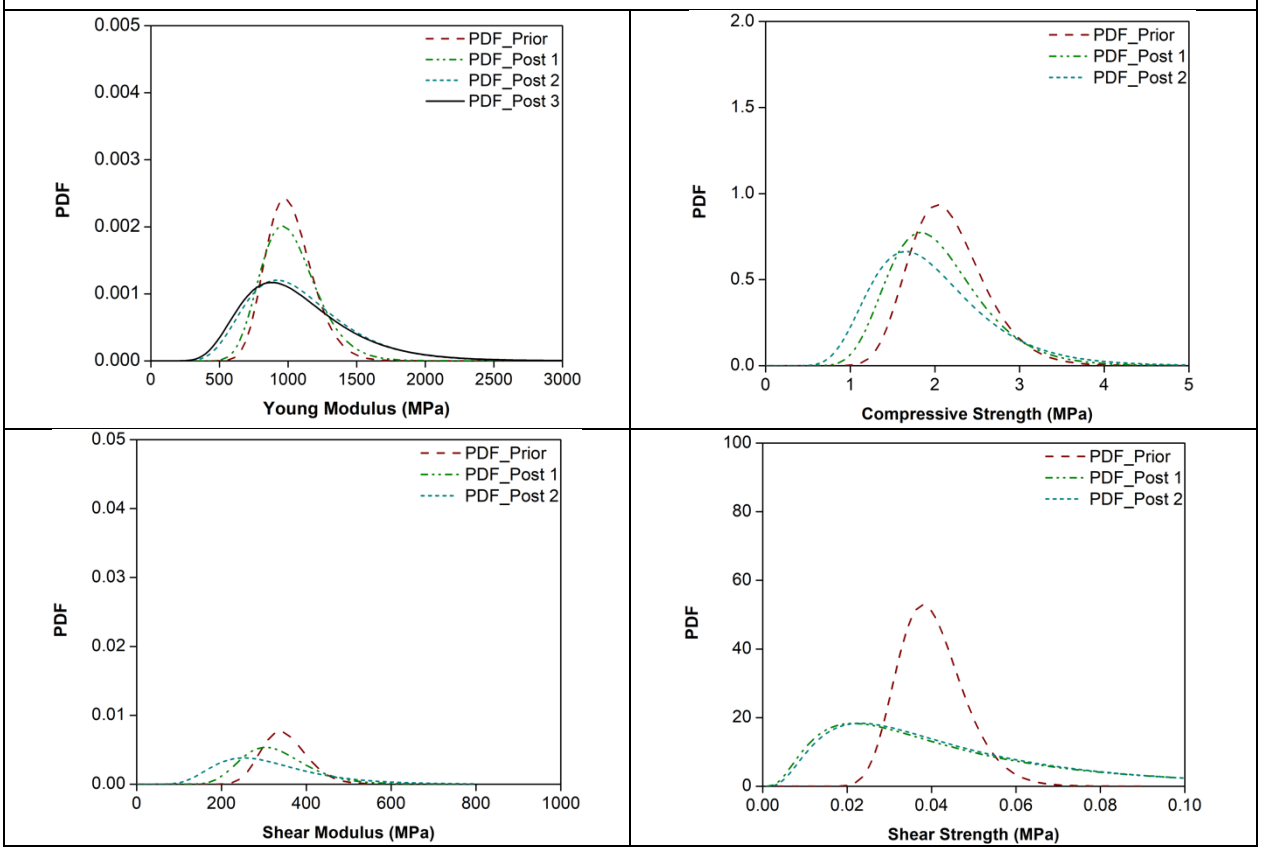
Further studies could foresee the development of TRM systems based on more advanced and innovative materials and technologies both regarding the cementitious matrix (e.g. use of recycled materials) and the embedded mesh (e.g. use of shape memory alloys).

Finally, extra numerical works could be also carried out to perform additional sensitivity studies regarding the selected strengthening solution and its performance considering aspects such as the variation of the mechanical properties of both matrix and embedded mesh. Moreover, different mesh configurations, considering, for instance, narrower or larger fiber paces, could be further analyzed using numerical simulations.

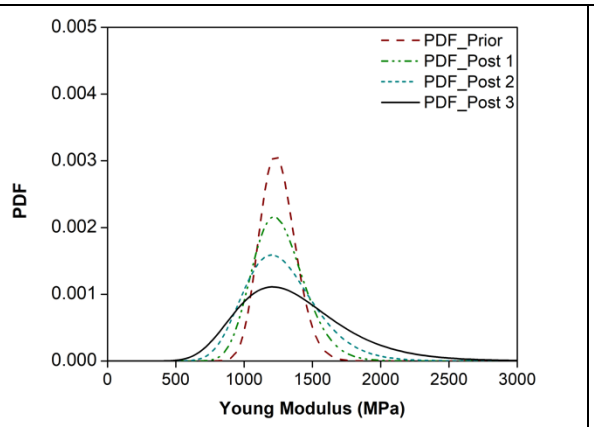
Annex 1 – Probability Density Functions (PDFs) for representative masonry typologies

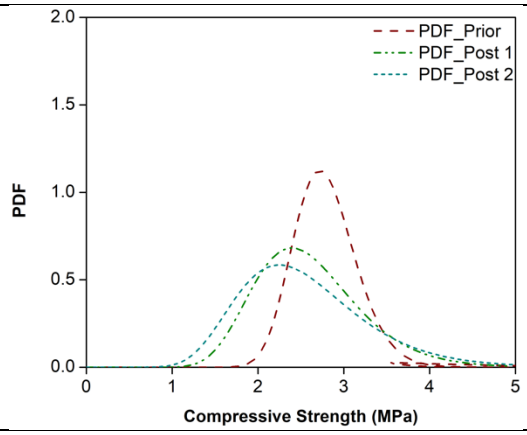
Annex 1.1 – Reference Update

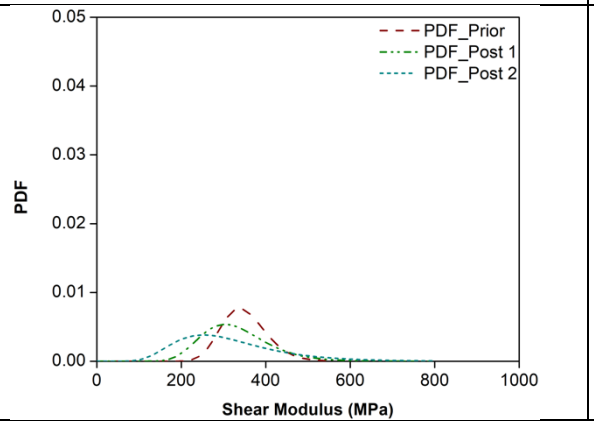
Masonry Type 1 – Reference Update

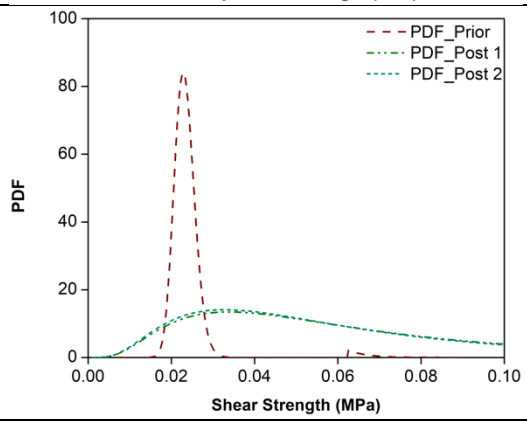


Masonry Type 2 – Reference Update

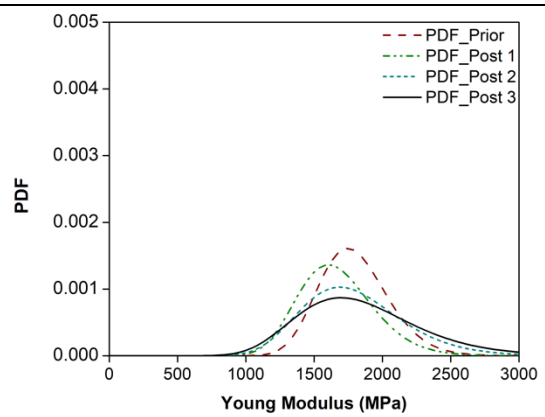


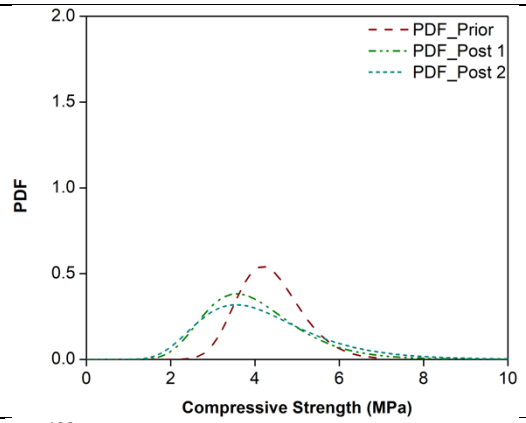


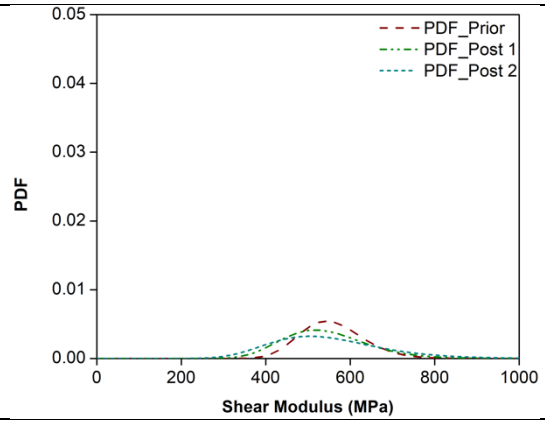


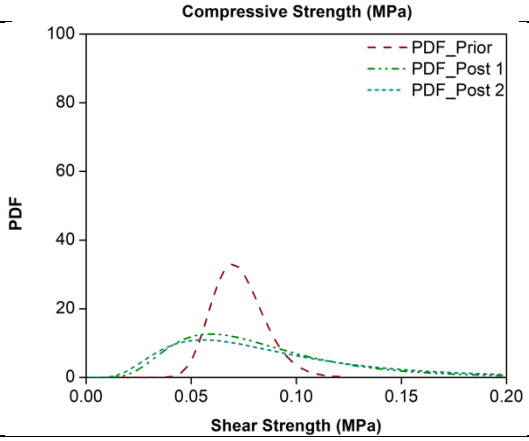


Masonry Type 3 – Reference Update

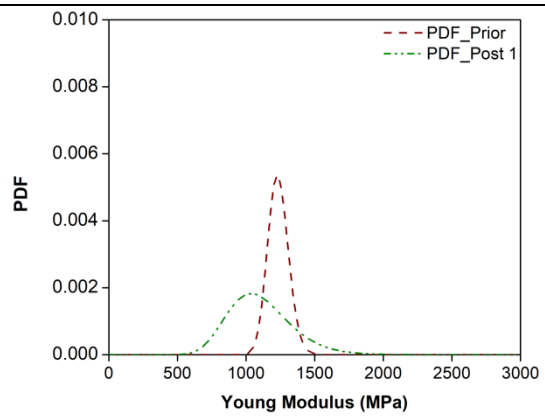


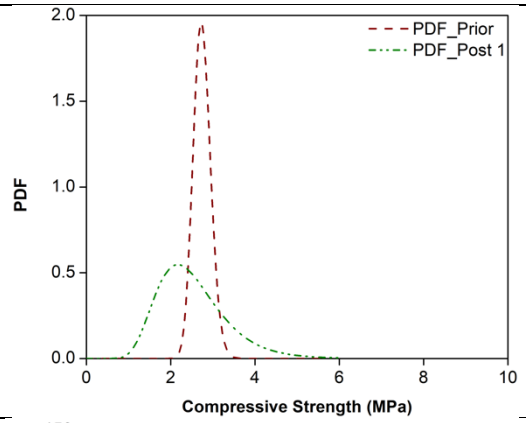


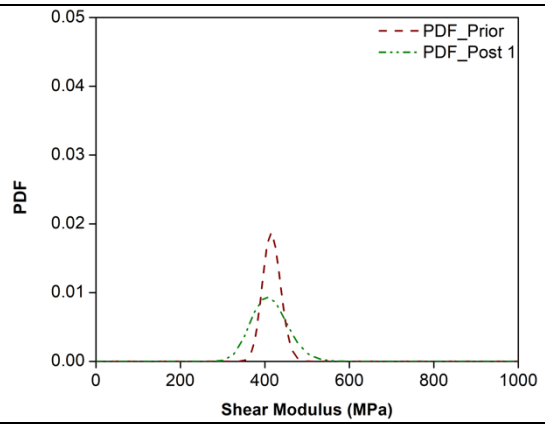


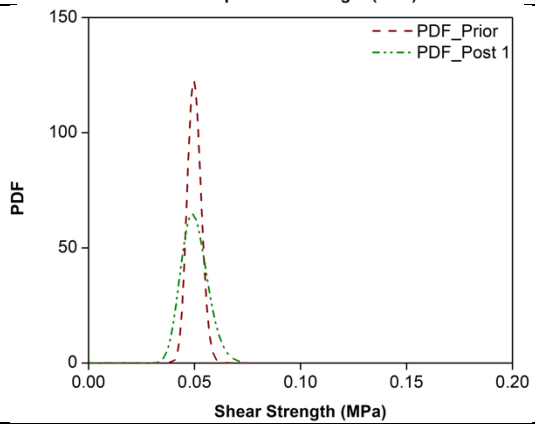


Masonry Type 4 – Reference Update

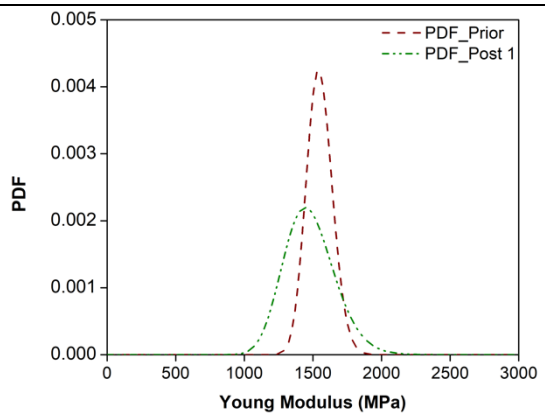


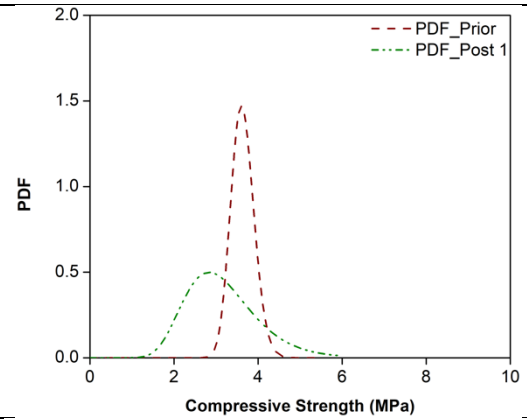


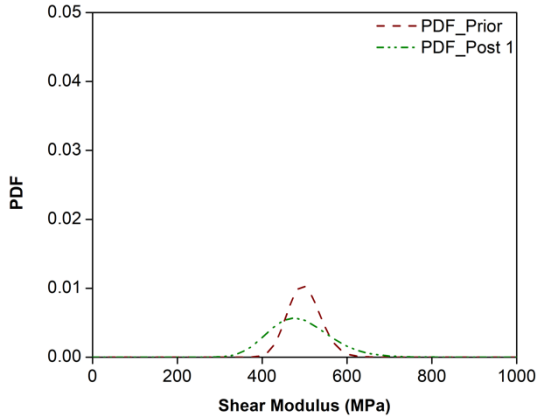


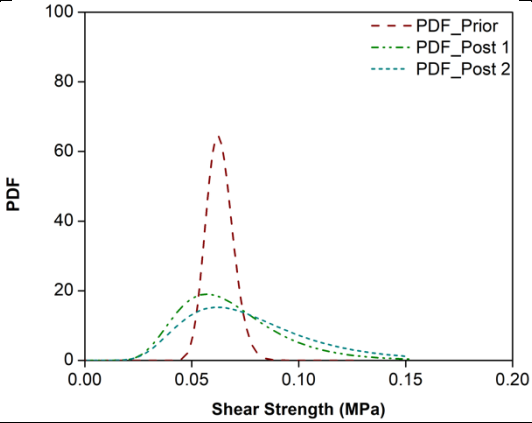


Masonry Type 5 – Reference Update

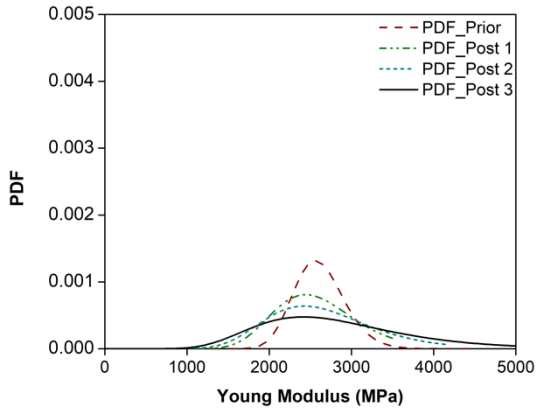


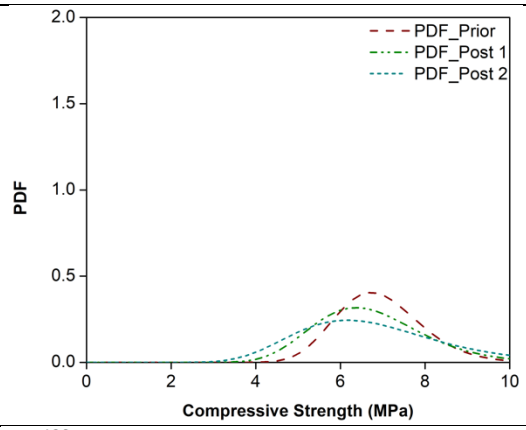


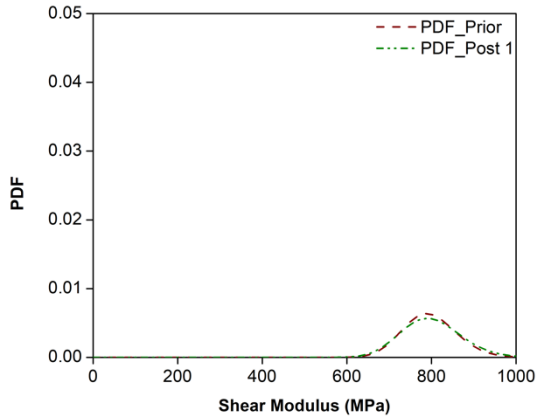


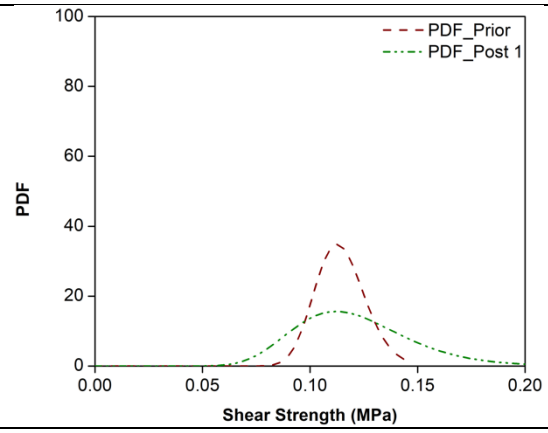


Masonry Type 6 – Reference Update





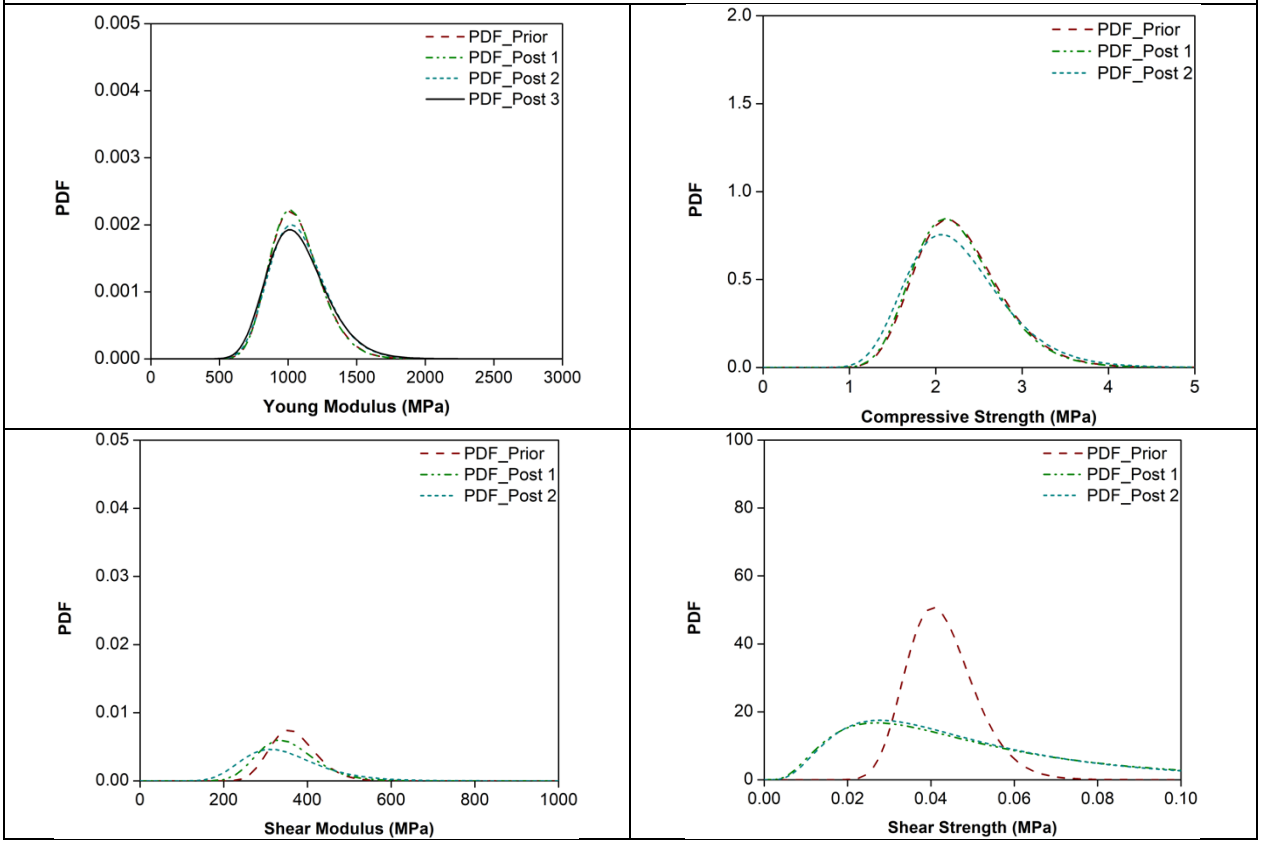




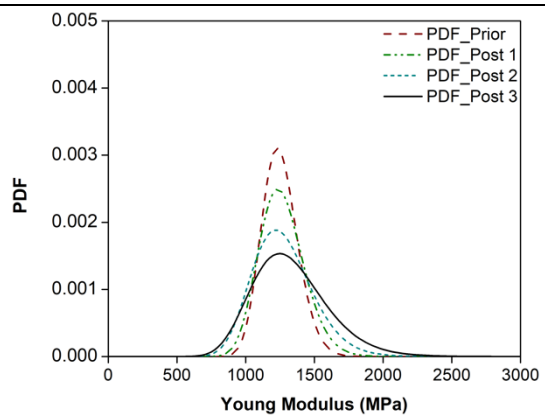
Annex 1.2 – Italian Data

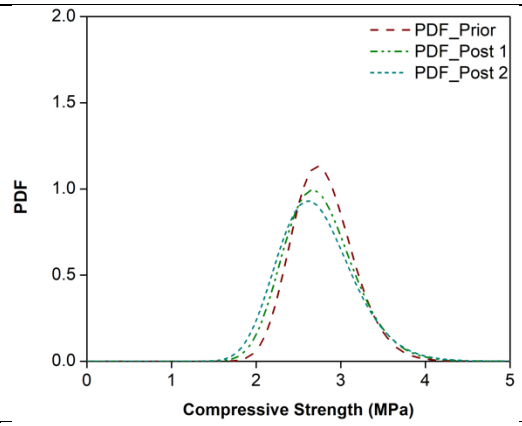
NOTE: Data related to this Masonry Type 4 and 5 refer only to experimental campaigns carried out in Italy. No other information related to different countries has been collected. Therefore, in this Annex only PDFs for Masonry Type 1, 2, 3 and 6 will be presented, being PDFs related to Masonry Type 4 and 5 the same as those previously shown.

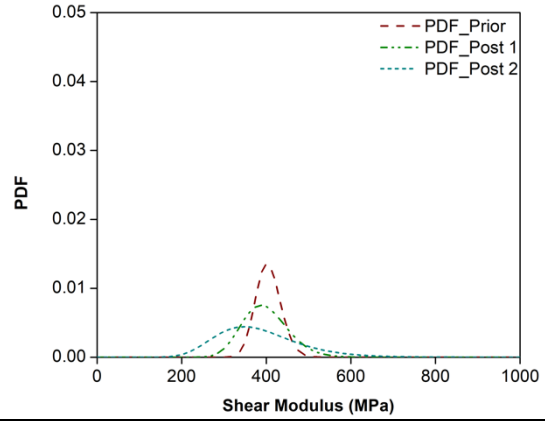
Masonry Type 1 – Italian Data

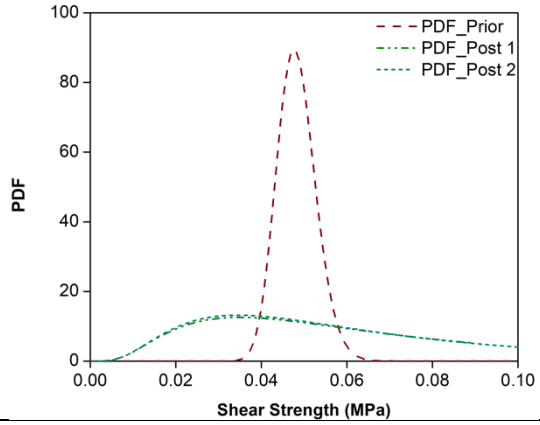


Masonry Type 2 – Italian Data

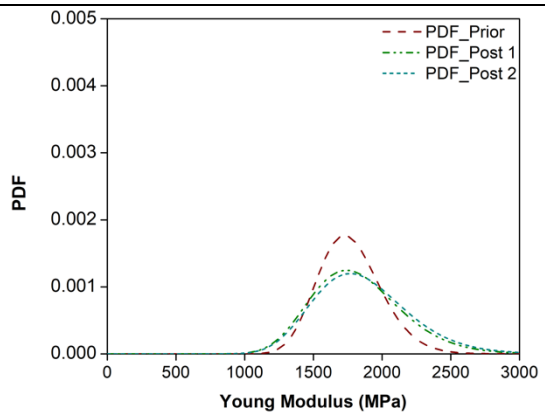


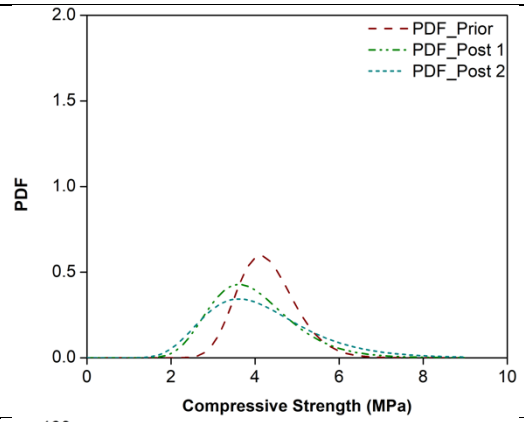


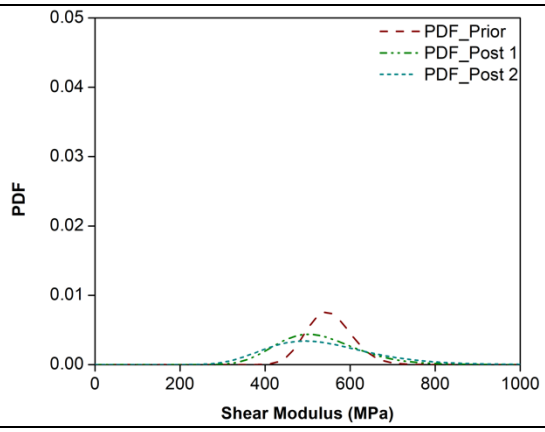


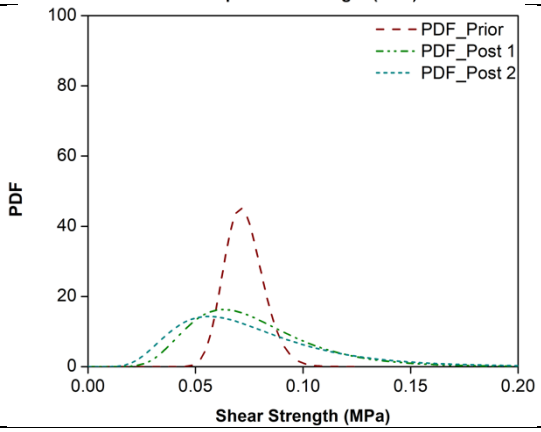


Masonry Type 3 – Italian Data

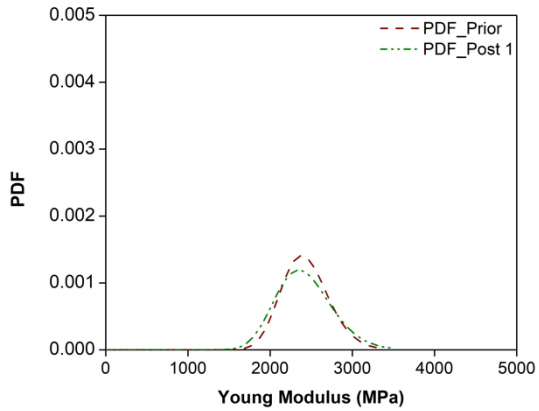


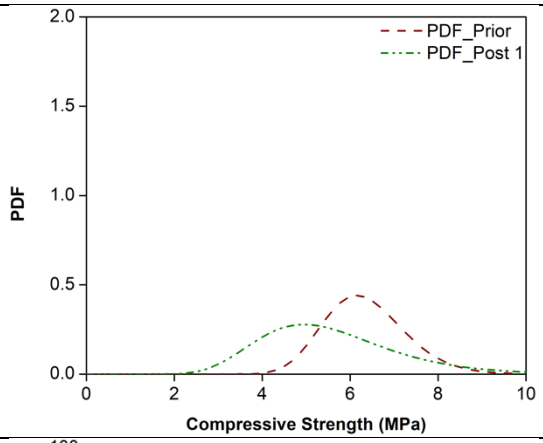


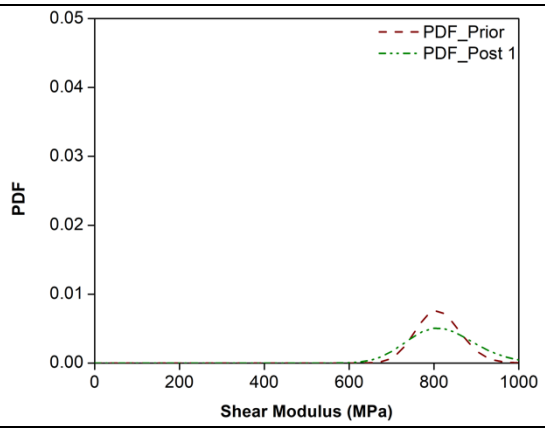


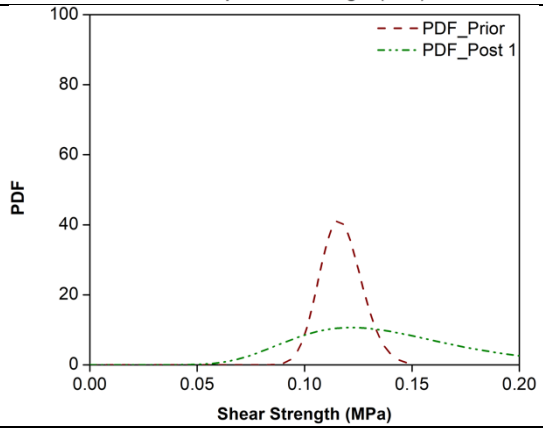


Masonry Type 6 – Italian Data







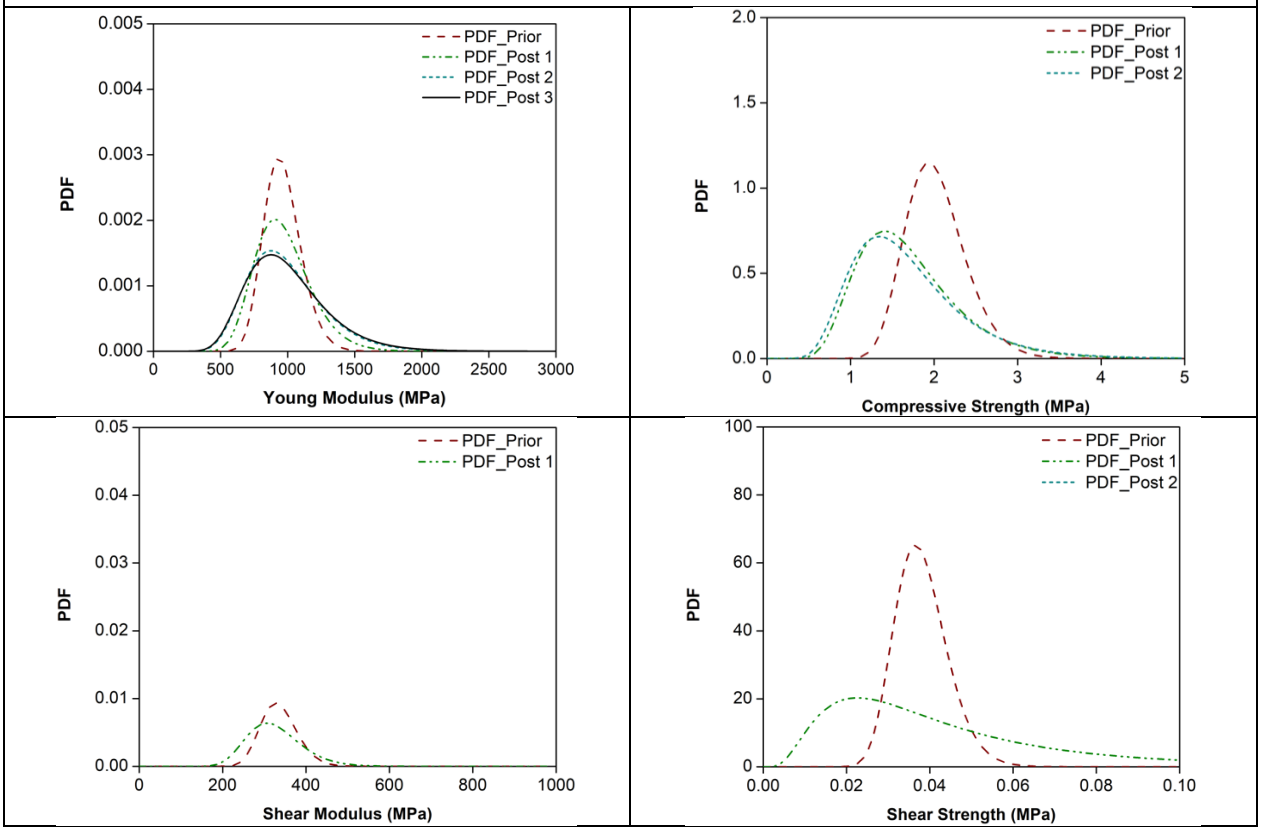


Annex 1.3 – Portuguese Data

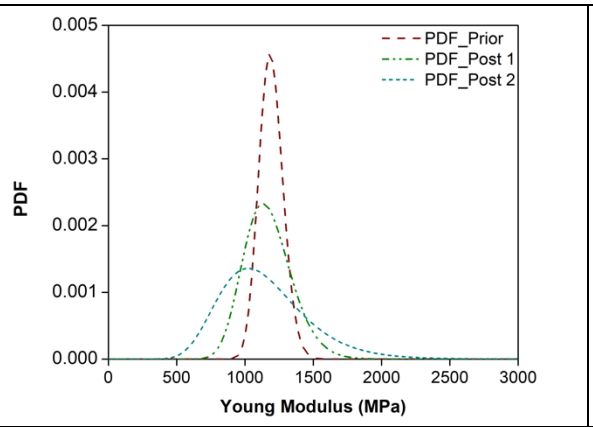
NOTE: Data related to this Masonry Type 4 and Masonry Type 5 refer only to experimental campaigns carried out in Italy. No other information related to different countries has been collected. Therefore, in this Annex only PDFs for Masonry Type 1, 2, 3 and 6 will be presented, being PDFs related to Masonry Type 4 and 5 the same as those previously shown. In Masonry Type 3, it has not been possible to update Shear Modulus and Shear Strength values because not enough data were available (the observations were deemed not representative for a reliable updating procedure).

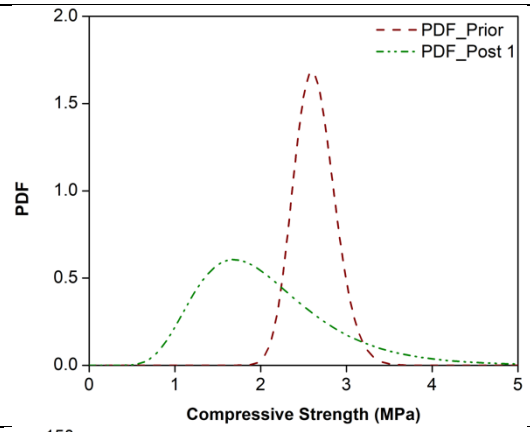
Moreover, for shear-compression tests only data related to shear strength values are available. The shear modulus value has been updated using MQI and data from diagonal-compression tests. Shear strength has been updated using MQI, shear-compression tests data and diagonal-compression tests data.

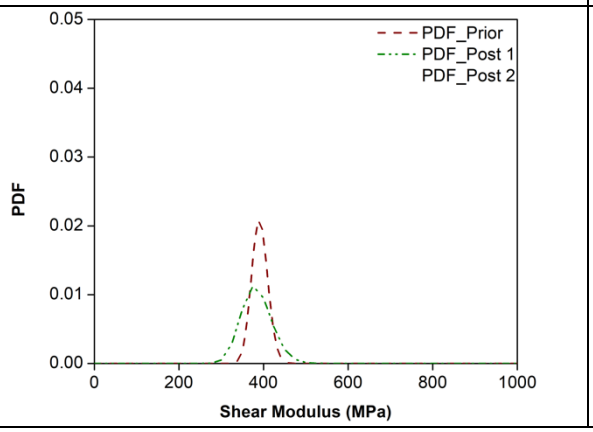
Masonry Type 1 – Portuguese Data

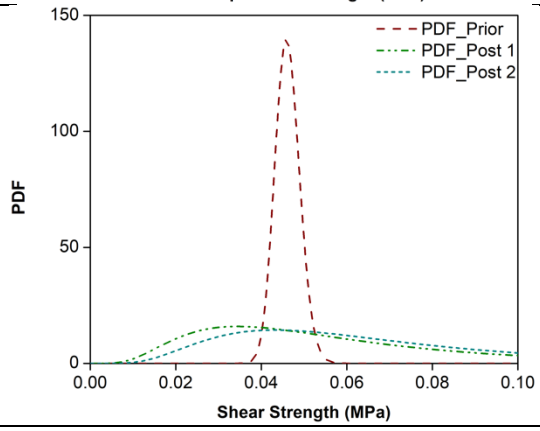


Masonry Type 2 – Portuguese Data

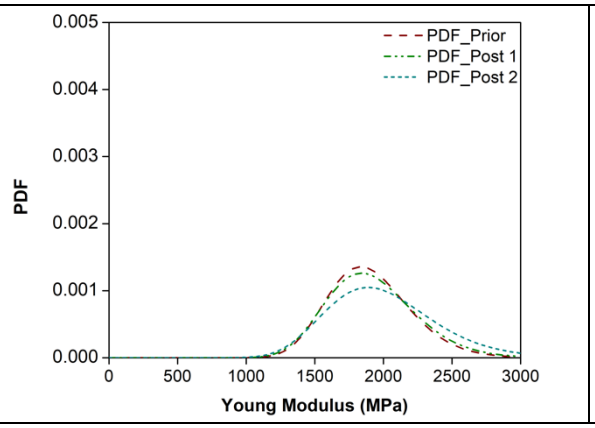


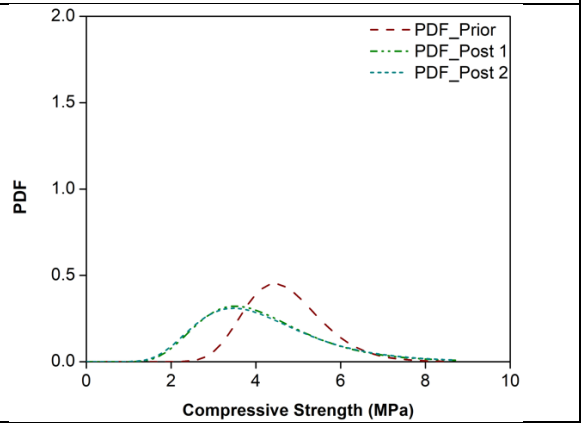




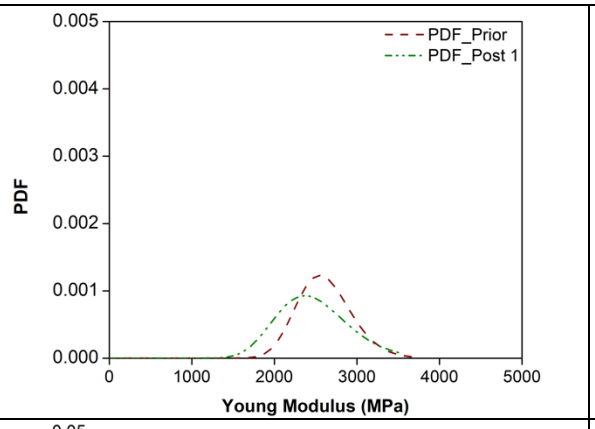


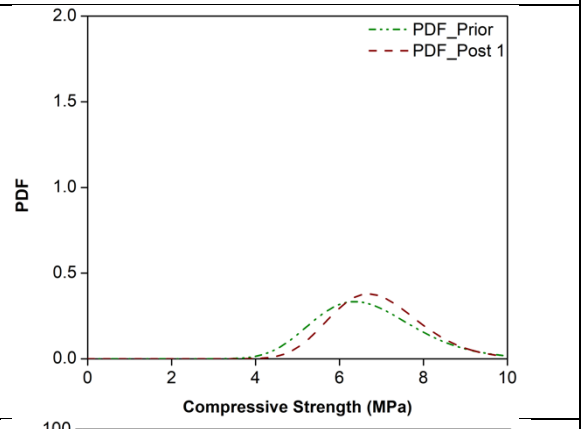
Masonry Type 3 – Portuguese Data

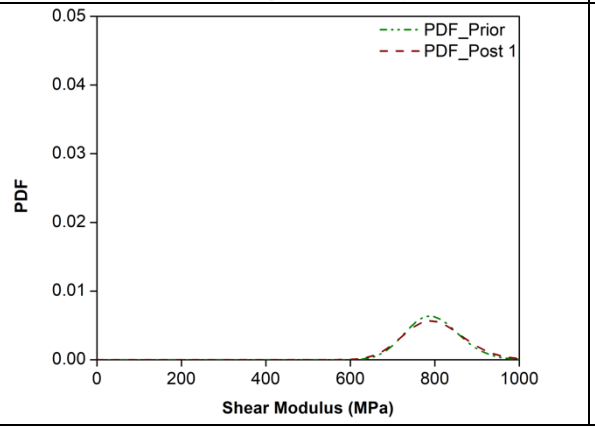


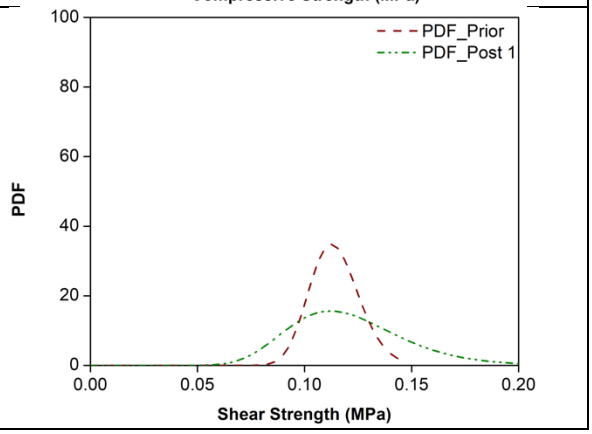


Masonry Type 6 – Portuguese Data







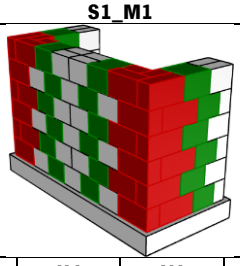
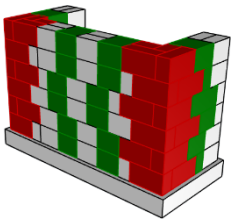
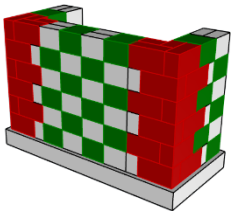
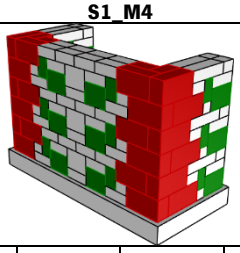
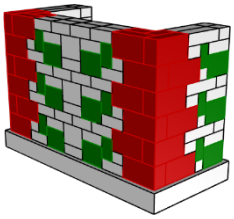
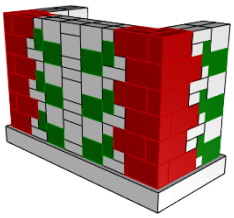
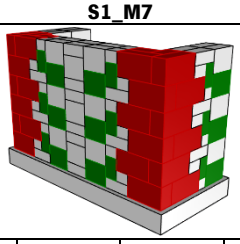
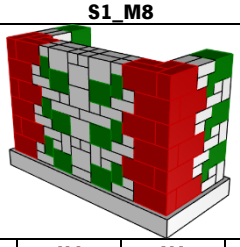
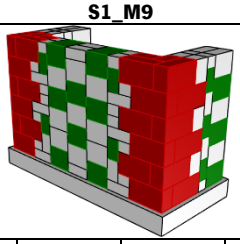
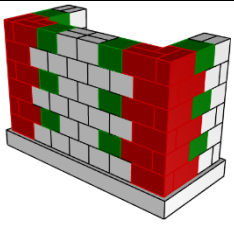
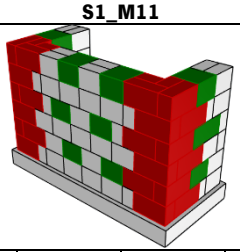
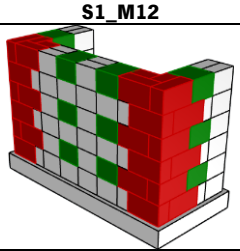


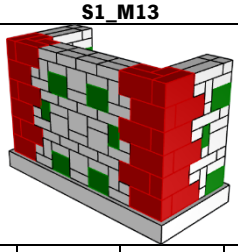
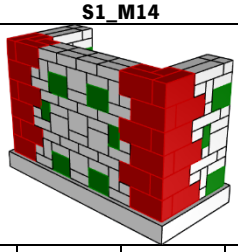
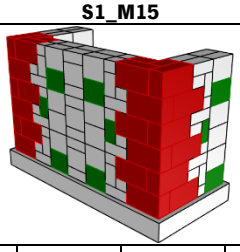
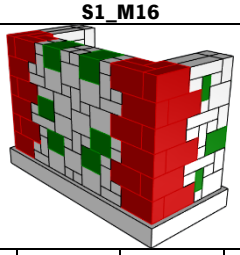
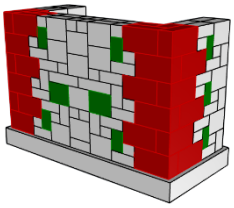
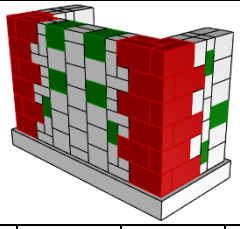
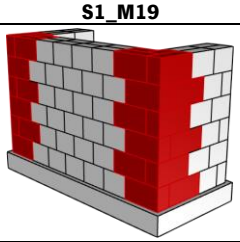
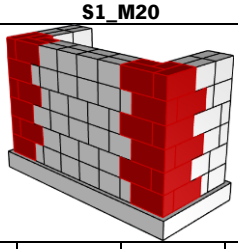
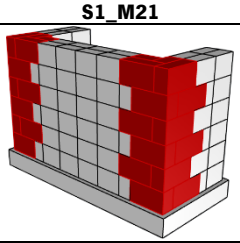
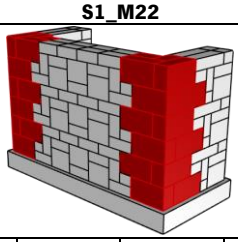
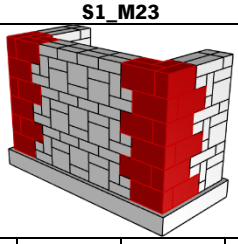
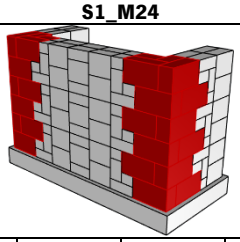
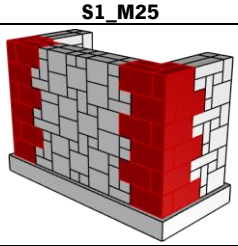
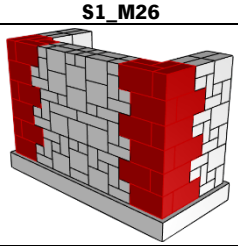
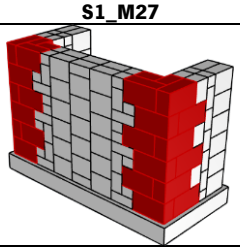
This page is intentionally left blank

Annex 2 – Geometrical parametric study on reduced scale numerical models of 2-leaf stone masonry walls

Annex 2.1 – Set 1 3D Models

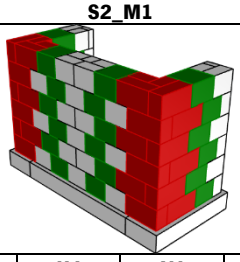
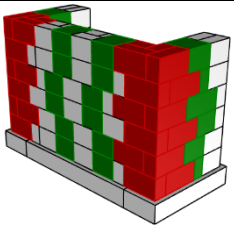
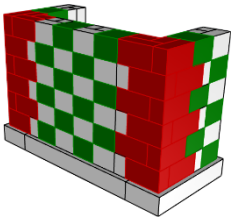
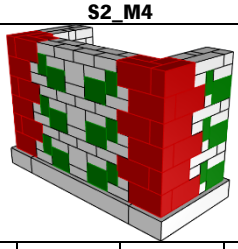
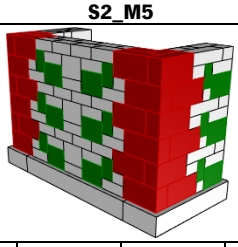
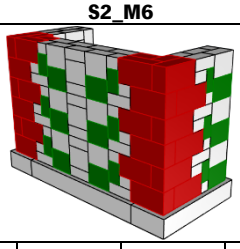
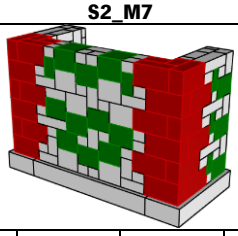
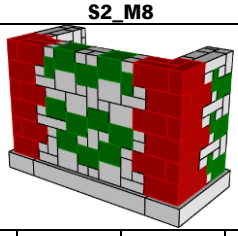
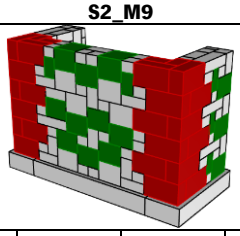
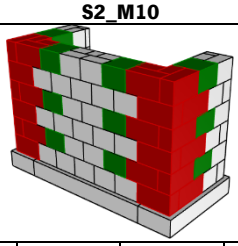
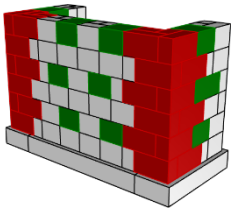
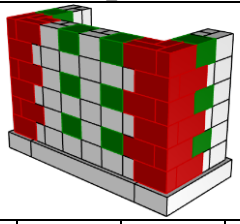
NOTE: Regular stone units are highlighted in light grey colour, corner stones are highlighted in red colour, and through-stones are highlighted in green colour.

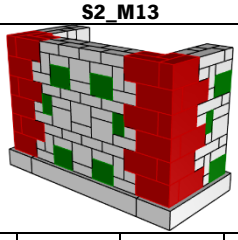
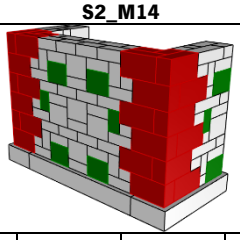
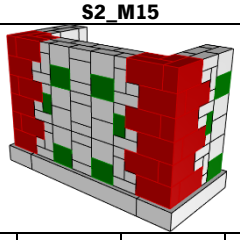
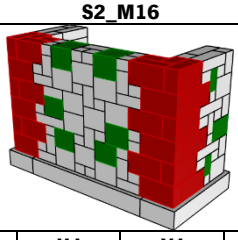
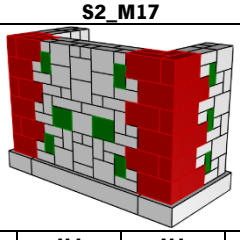
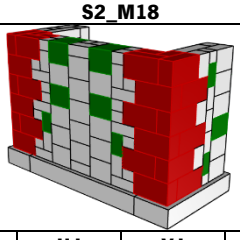
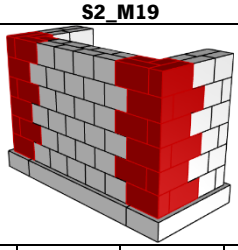
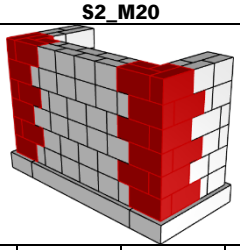
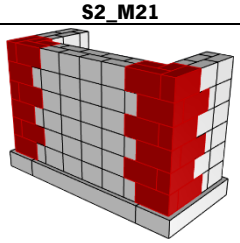
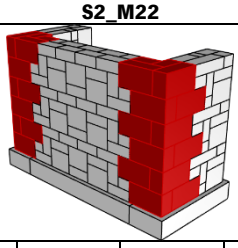
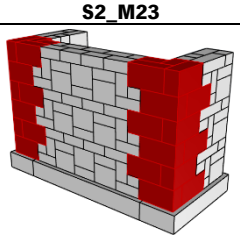
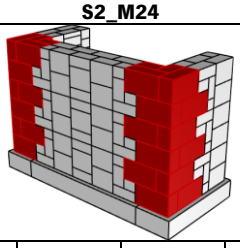
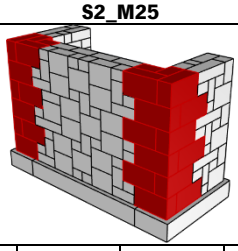
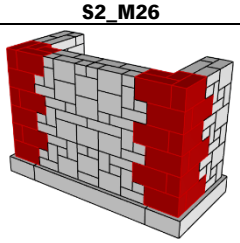
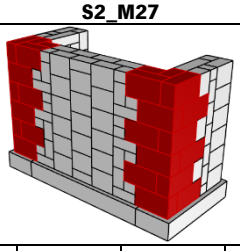
S1_M1				S1_M2				S1_M3			
											
WC	**HJ**	**VJ**	**MQI$_H$**	**WC**	**HJ**	**VJ**	**MQI$_H$**	**WC**	**HJ**	**VJ**	**MQI$_H$**
F	F	F	10	F	F	PF	9.5	F	F	NF	9
S1_M4				**S1_M5**				**S1_M6**			
											
WC	**HJ**	**VJ**	**MQI$_H$**	**WC**	**HJ**	**VJ**	**MQI$_H$**	**WC**	**HJ**	**VJ**	**MQI$_H$**
F	PF	F	9	F	PF	PF	8.5	F	PF	NF	8
S1_M7				**S1_M8**				**S1_M9**			
											
WC	**HJ**	**VJ**	**MQI$_H$**	**WC**	**HJ**	**VJ**	**MQI$_H$**	**WC**	**HJ**	**VJ**	**MQI$_H$**
F	NF	F	8	F	NF	PF	7.5	F	NF	NF	7
S1_M10				**S1_M11**				**S1_M12**			
											
WC	**HJ**	**VJ**	**MQI$_H$**	**WC**	**HJ**	**VJ**	**MQI$_H$**	**WC**	**HJ**	**VJ**	**MQI$_H$**
PF	F	F	8.5	PF	F	PF	8	PF	F	NF	7.5

S1_M13				S1_M14				S1_M15			
											
WC	**HJ**	**VJ**	**MQI$_H$**	**WC**	**HJ**	**VJ**	**MQI$_H$**	**WC**	**HJ**	**VJ**	**MQI$_H$**
PF	PF	F	7.5	PF	PF	PF	7	PF	PF	NF	6.5
S1_M16				**S1_M17**				**S1_M18**			
											
WC	**HJ**	**VJ**	**MQI$_H$**	**WC**	**HJ**	**VJ**	**MQI$_H$**	**WC**	**HJ**	**VJ**	**MQI$_H$**
PF	NF	F	6.5	PF	NF	PF	6	PF	NF	NF	5.5
S1_M19				**S1_M20**				**S1_M21**			
											
WC	**HJ**	**VJ**	**MQI$_H$**	**WC**	**HJ**	**VJ**	**MQI$_H$**	**WC**	**HJ**	**VJ**	**MQI$_H$**
NF	F	F	7	NF	F	PF	6.5	NF	F	NF	6
S1_M22				**S1_M23**				**S1_M24**			
											
WC	**HJ**	**VJ**	**MQI$_H$**	**WC**	**HJ**	**VJ**	**MQI$_H$**	**WC**	**HJ**	**VJ**	**MQI$_H$**
NF	PF	F	6	NF	PF	PF	5.5	NF	PF	NF	5
S1_M25				**S1_M26**				**S1_M27**			
											
WC	**HJ**	**VJ**	**MQI$_H$**	**WC**	**HJ**	**VJ**	**MQI$_H$**	**WC**	**HJ**	**VJ**	**MQI$_H$**
NF	NF	F	5	NF	NF	PF	4.5	NF	NF	NF	4

Annex 2.2 – Set 2 3D Models

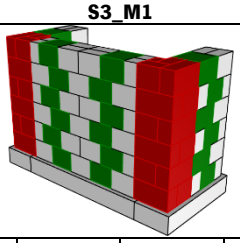
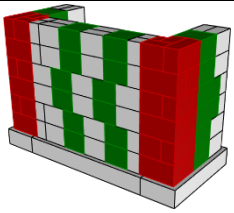
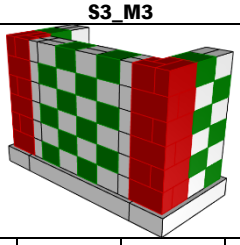
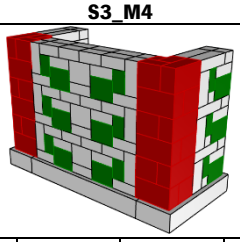
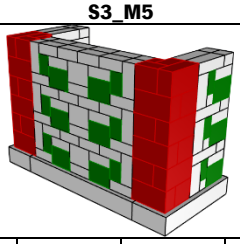
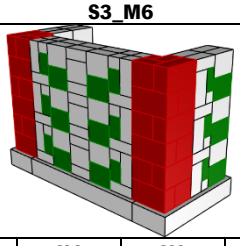
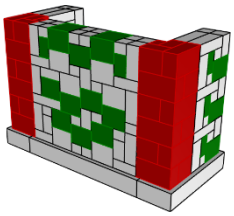
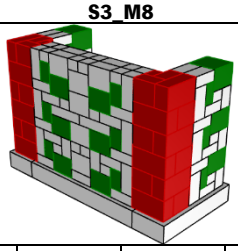
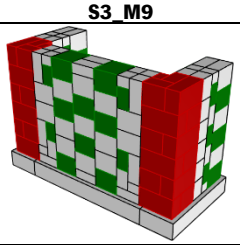
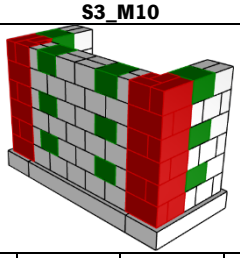
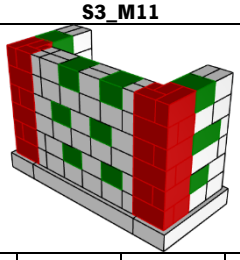
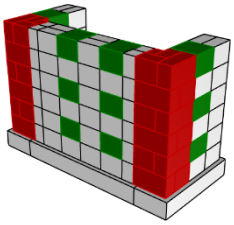
NOTE: Regular stone units are highlighted in light grey colour, corner stones are highlighted in red colour, and through-stones are highlighted in green colour.

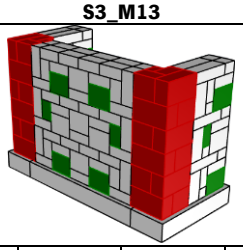
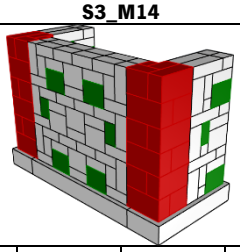
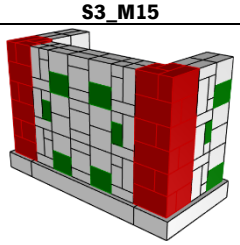
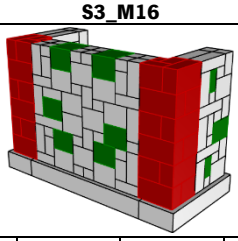
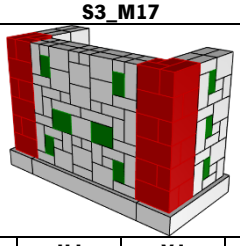
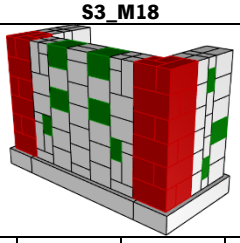
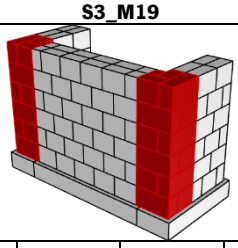
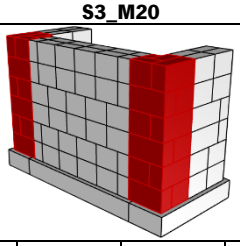
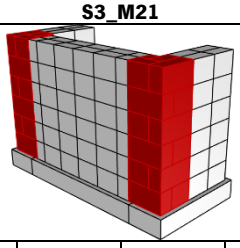
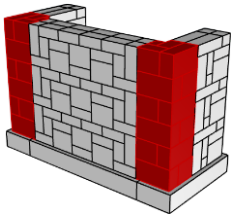
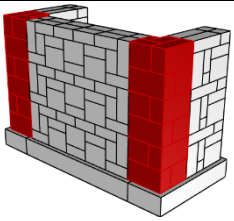
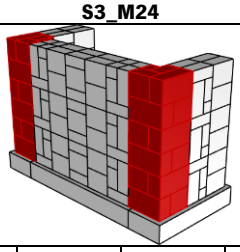
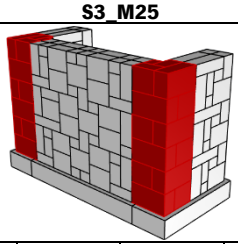
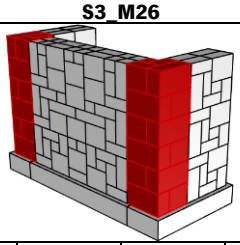
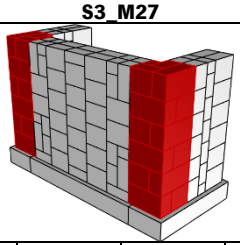
S2_M1				S2_M2				S2_M3			
											
WC	**HJ**	**VJ**	**MQI$_H$**	**WC**	**HJ**	**VJ**	**MQI$_H$**	**WC**	**HJ**	**VJ**	**MQI$_H$**
F	F	F	10	F	F	PF	9.5	F	F	NF	9
S2_M4				**S2_M5**				**S2_M6**			
											
WC	**HJ**	**VJ**	**MQI$_H$**	**WC**	**HJ**	**VJ**	**MQI$_H$**	**WC**	**HJ**	**VJ**	**MQI$_H$**
F	PF	F	9	F	PF	PF	8.5	F	PF	NF	8
S2_M7				**S2_M8**				**S2_M9**			
											
WC	**HJ**	**VJ**	**MQI$_H$**	**WC**	**HJ**	**VJ**	**MQI$_H$**	**WC**	**HJ**	**VJ**	**MQI$_H$**
F	NF	F	8	F	NF	PF	7.5	F	NF	NF	7
S2_M10				**S2_M11**				**S2_M12**			
											
WC	**HJ**	**VJ**	**MQI$_H$**	**WC**	**HJ**	**VJ**	**MQI$_H$**	**WC**	**HJ**	**VJ**	**MQI$_H$**
PF	F	F	8.5	PF	F	PF	8	PF	F	NF	7.5

S2_M13				S2_M14				S2_M15			
											
WC	**HJ**	**VJ**	**MQI$_H$**	**WC**	**HJ**	**VJ**	**MQI$_H$**	**WC**	**HJ**	**VJ**	**MQI$_H$**
PF	PF	F	7.5	PF	PF	PF	7	PF	PF	NF	6.5
S2_M16				**S2_M17**				**S2_M18**			
											
WC	**HJ**	**VJ**	**MQI$_H$**	**WC**	**HJ**	**VJ**	**MQI$_H$**	**WC**	**HJ**	**VJ**	**MQI$_H$**
PF	NF	F	6.5	PF	NF	PF	6	PF	NF	NF	5.5
S2_M19				**S2_M20**				**S2_M21**			
											
WC	**HJ**	**VJ**	**MQI$_H$**	**WC**	**HJ**	**VJ**	**MQI$_H$**	**WC**	**HJ**	**VJ**	**MQI$_H$**
NF	F	F	7	NF	F	PF	6.5	NF	F	NF	6
S2_M22				**S2_M23**				**S2_M24**			
											
WC	**HJ**	**VJ**	**MQI$_H$**	**WC**	**HJ**	**VJ**	**MQI$_H$**	**WC**	**HJ**	**VJ**	**MQI$_H$**
NF	PF	F	6	NF	PF	PF	5.5	NF	PF	NF	5
S2_M25				**S2_M26**				**S2_M27**			
											
WC	**HJ**	**VJ**	**MQI$_H$**	**WC**	**HJ**	**VJ**	**MQI$_H$**	**WC**	**HJ**	**VJ**	**MQI$_H$**
NF	NF	F	5	NF	NF	PF	4.5	NF	NF	NF	4

Annex 2.3 – Set 3 3D Models

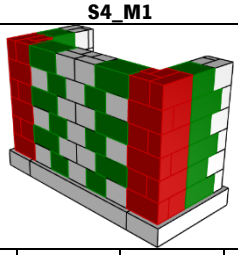
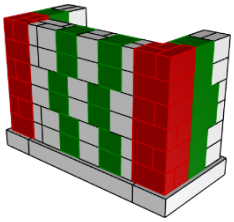
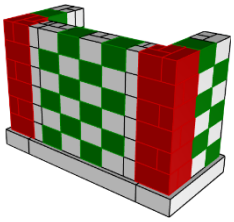
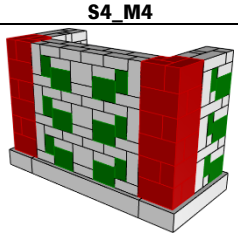
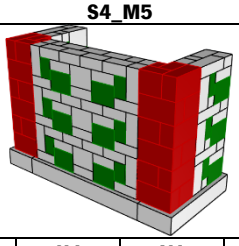
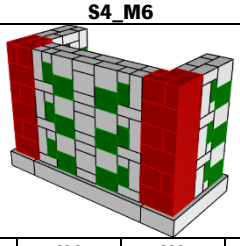
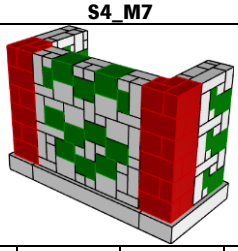
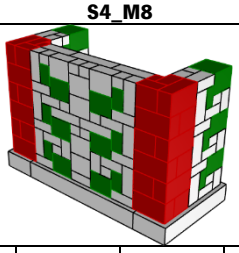
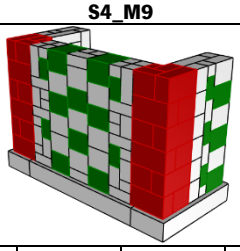
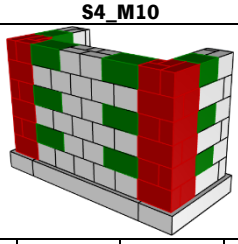
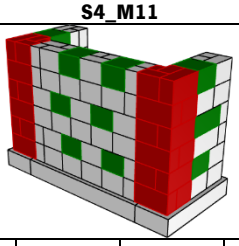
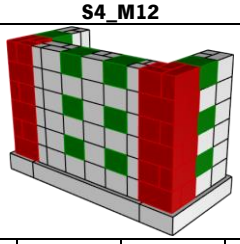
NOTE: Regular stone units are highlighted in light grey colour, corner stones are highlighted in red colour and through-stones are highlighted in green colour.

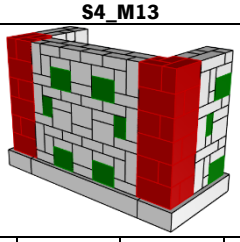
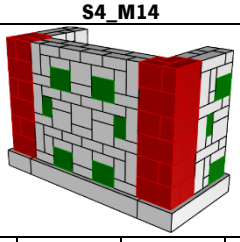
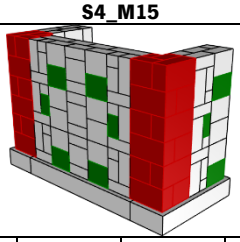
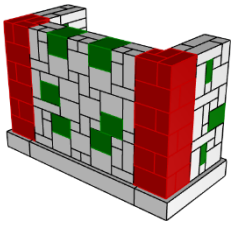
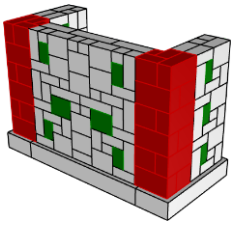
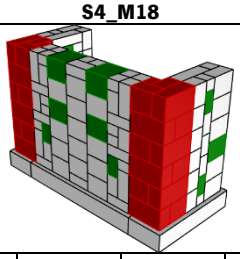
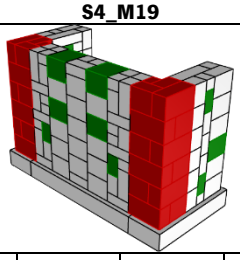
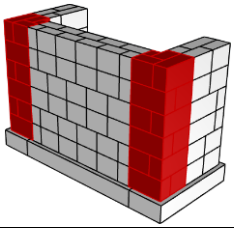
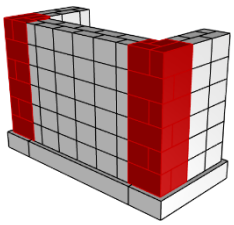
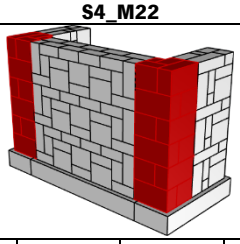
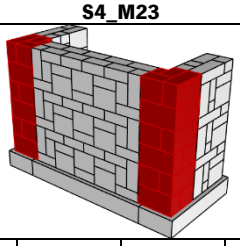
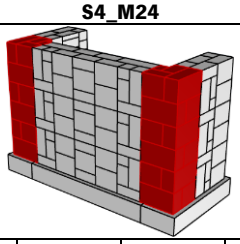
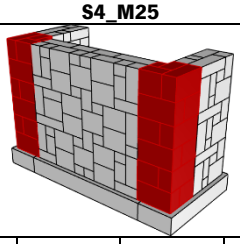
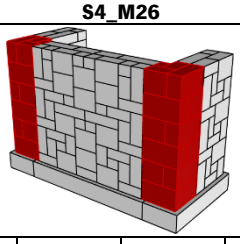
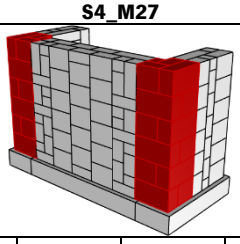
S3_M1				S3_M2				S3_M3			
											
WC	**HJ**	**VJ**	**MQI$_H$**	**WC**	**HJ**	**VJ**	**MQI$_H$**	**WC**	**HJ**	**VJ**	**MQI$_H$**
F	F	F	10	F	F	PF	9.5	F	F	NF	9
S3_M4				**S3_M5**				**S3_M6**			
											
WC	**HJ**	**VJ**	**MQI$_H$**	**WC**	**HJ**	**VJ**	**MQI$_H$**	**WC**	**HJ**	**VJ**	**MQI$_H$**
F	PF	F	9	F	PF	PF	8.5	F	PF	NF	8
S3_M7				**S3_M8**				**S3_M9**			
											
WC	**HJ**	**VJ**	**MQI$_H$**	**WC**	**HJ**	**VJ**	**MQI$_H$**	**WC**	**HJ**	**VJ**	**MQI$_H$**
F	NF	F	8	F	NF	PF	7.5	F	NF	NF	7
S3_M10				**S3_M11**				**S3_M12**			
											
WC	**HJ**	**VJ**	**MQI$_H$**	**WC**	**HJ**	**VJ**	**MQI$_H$**	**WC**	**HJ**	**VJ**	**MQI$_H$**
PF	F	F	8.5	PF	F	PF	8	PF	F	NF	7.5

S3_M13				S3_M14				S3_M15			
											
WC	**HJ**	**VJ**	**MQI$_H$**	**WC**	**HJ**	**VJ**	**MQI$_H$**	**WC**	**HJ**	**VJ**	**MQI$_H$**
PF	PF	F	7.5	PF	PF	PF	7	PF	PF	NF	6.5
S3_M16				**S3_M17**				**S3_M18**			
											
WC	**HJ**	**VJ**	**MQI$_H$**	**WC**	**HJ**	**VJ**	**MQI$_H$**	**WC**	**HJ**	**VJ**	**MQI$_H$**
PF	NF	F	6.5	PF	NF	PF	6	PF	NF	NF	5.5
S3_M19				**S3_M20**				**S3_M21**			
											
WC	**HJ**	**VJ**	**MQI$_H$**	**WC**	**HJ**	**VJ**	**MQI$_H$**	**WC**	**HJ**	**VJ**	**MQI$_H$**
NF	F	F	7	NF	F	PF	6.5	NF	F	NF	6
S3_M22				**S3_M23**				**S3_M24**			
											
WC	**HJ**	**VJ**	**MQI$_H$**	**WC**	**HJ**	**VJ**	**MQI$_H$**	**WC**	**HJ**	**VJ**	**MQI$_H$**
NF	PF	F	6	NF	PF	PF	5.5	NF	PF	NF	5
S3_M25				**S3_M26**				**S3_M27**			
											
WC	**HJ**	**VJ**	**MQI$_H$**	**WC**	**HJ**	**VJ**	**MQI$_H$**	**WC**	**HJ**	**VJ**	**MQI$_H$**
NF	NF	F	5	NF	NF	PF	4.5	NF	NF	NF	4

Annex 2.4 – Set 4 3D Models

NOTE: Regular stone units are highlighted in light grey colour, corner stones are highlighted in red colour, and through-stones are highlighted in green colour.

S4_M1				S4_M2				S4_M3			
											
WC	**HJ**	**VJ**	**MQI$_H$**	**WC**	**HJ**	**VJ**	**MQI$_H$**	**WC**	**HJ**	**VJ**	**MQI$_H$**
F	F	F	10	F	F	PF	9.5	F	F	NF	9
S4_M4				**S4_M5**				**S4_M6**			
											
WC	**HJ**	**VJ**	**MQI$_H$**	**WC**	**HJ**	**VJ**	**MQI$_H$**	**WC**	**HJ**	**VJ**	**MQI$_H$**
F	PF	F	9	F	PF	PF	8.5	F	PF	NF	8
S4_M7				**S4_M8**				**S4_M9**			
											
WC	**HJ**	**VJ**	**MQI$_H$**	**WC**	**HJ**	**VJ**	**MQI$_H$**	**WC**	**HJ**	**VJ**	**MQI$_H$**
F	NF	F	8	F	NF	PF	7.5	F	NF	NF	7
S4_M10				**S4_M11**				**S4_M12**			
											
WC	**HJ**	**VJ**	**MQI$_H$**	**WC**	**HJ**	**VJ**	**MQI$_H$**	**WC**	**HJ**	**VJ**	**MQI$_H$**
PF	F	F	8.5	PF	F	PF	8	PF	F	NF	7.5

S4_M13				S4_M14				S4_M15			
											
WC	**HJ**	**VJ**	**MQI$_H$**	**WC**	**HJ**	**VJ**	**MQI$_H$**	**WC**	**HJ**	**VJ**	**MQI$_H$**
PF	PF	F	7.5	PF	PF	PF	7	PF	PF	NF	6.5
S4_M16				**S4_M17**				**S4_M18**			
											
WC	**HJ**	**VJ**	**MQI$_H$**	**WC**	**HJ**	**VJ**	**MQI$_H$**	**WC**	**HJ**	**VJ**	**MQI$_H$**
PF	NF	F	6.5	PF	NF	PF	6	PF	NF	NF	5.5
S4_M19				**S4_M20**				**S4_M21**			
											
WC	**HJ**	**VJ**	**MQI$_H$**	**WC**	**HJ**	**VJ**	**MQI$_H$**	**WC**	**HJ**	**VJ**	**MQI$_H$**
NF	F	F	7	NF	F	PF	6.5	NF	F	NF	6
S4_M22				**S4_M23**				**S4_M24**			
											
WC	**HJ**	**VJ**	**MQI$_H$**	**WC**	**HJ**	**VJ**	**MQI$_H$**	**WC**	**HJ**	**VJ**	**MQI$_H$**
NF	PF	F	6	NF	PF	PF	5.5	NF	PF	NF	5
S4_M25				**S4_M26**				**S4_M27**			
											
WC	**HJ**	**VJ**	**MQI$_H$**	**WC**	**HJ**	**VJ**	**MQI$_H$**	**WC**	**HJ**	**VJ**	**MQI$_H$**
NF	NF	F	5	NF	NF	PF	4.5	NF	NF	NF	4

Annex 2.5 – Load Capacity comparison

2.5.1 Set 1 vs Set 2 and Set 3 vs Set 4

# MOD	MQI	Set 1	Set 2	Variation
		Load (kN)	Load (kN)	%
1	10	41.32	42.1	2%
2	9.5	30.4	30.4	0%
3	9	34.3	35.08	2%
4	9	38.98	40.9	5%
5	8.5	33.52	31.19	-7%
6	8	29.63	30.4	3%
7	8	27.06	28.7	6%
8	7.5	28.06	34.3	22%
9	7	25.72	28.06	9%
10	8.5	38.2	41.3	8%
11	8	31.96	29.62	-7%
12	7.5	35.08	39.76	13%
13	7.5	38.2	39.76	4%
14	7	33.52	31.19	-7%
15	6.5	29.62	32.74	11%
16	6.5	28.06	31.07	11%
17	6	27.06	35.64	32%
18	5.5	24.95	26.5	6%
19	7	39.24	41.65	6%
20	6.5	31.85	30.62	-4%
21	6	35.08	39.2	12%
22	6	38.2	40.43	6%
23	5.5	35.52	35.08	-1%
24	5	28.84	33.07	15%
25	5	27.28	31.85	17%
26	4.5	28	34.75	24%
27	4	24.95	30.62	23%

# MOD	MQI	Set 3	Set 4	Variation
		Load (kN)	Load (kN)	%
1	10	37.42	41.32	10%
2	9.5	29.62	31.96	8%
3	9	34.3	36.64	7%
4	9	32.97	35.64	8%
5	8.5	27.29	28.06	3%
6	8	24.95	31.19	25%
7	8	22.6	27.28	21%
8	7.5	28.84	33.52	16%
9	7	25.73	28.84	12%
10	8.5	38.2	40.42	6%
11	8	32.74	30.4	-7%
12	7.5	38.2	40.43	6%
13	7.5	32.74	39.76	21%
14	7	28.06	28.84	3%
15	6.5	24.17	31.96	32%
16	6.5	24.06	31.07	29%
17	6	26.73	27.06	1%
18	5.5	24.95	26.5	6%
19	7	38.98	42.1	8%
20	6.5	33.07	30.62	-7%
21	6	35.52	39.2	10%
22	6	31.85	41.65	31%
23	5.5	31.19	32.7	5%
24	5	23.28	30.63	32%
25	5	24.5	31.85	30%
26	4.5	28.06	32.08	14%
27	4	22.05	30.62	39%

2.5.2 Set 1 vs Set 3 and Set 2 vs Set 4

# MOD	MQI	Set 1	Set 3	Variation
		Load (kN)	Load (kN)	%
1	10	41.32	37.42	-9%
2	9.5	30.4	29.62	-3%
3	9	34.3	36.64	7%
4	9	38.98	32.97	-15%
5	8.5	33.52	27.29	-19%
6	8	29.63	24.95	-16%
7	8	27.06	22.6	-16%
8	7.5	28.06	28.84	3%
9	7	25.72	25.73	0%
10	8.5	38.2	38.2	0%
11	8	31.96	32.74	2%
12	7.5	35.08	38.2	9%
13	7.5	38.2	32.74	-14%
14	7	33.52	28.06	-16%
15	6.5	29.62	24.17	-18%
16	6.5	28.06	24.06	-14%
17	6	27.06	26.73	-1%
18	5.5	24.95	24.95	0%
19	7	39.24	38.98	-1%
20	6.5	31.85	33.07	4%
21	6	35.08	35.52	1%
22	6	38.2	31.85	-17%
23	5.5	35.52	31.19	-12%
24	5	28.84	23.28	-19%
25	5	27.28	24.5	-10%
26	4.5	28	28.06	0%
27	4	24.95	22.05	-12%

# MOD	MQI	Set 2	Set 4	Variation
		Load (kN)	Load (kN)	%
1	10	42.1	41.32	-2%
2	9.5	30.4	31.96	5%
3	9	35.08	36.64	4%
4	9	40.9	35.64	-13%
5	8.5	31.19	28.06	-10%
6	8	30.4	31.19	3%
7	8	28.7	27.28	-5%
8	7.5	34.3	33.52	-2%
9	7	28.06	28.84	3%
10	8.5	41.3	40.42	-2%
11	8	29.62	30.4	3%
12	7.5	39.76	40.43	2%
13	7.5	39.76	39.76	0%
14	7	31.19	28.84	-8%
15	6.5	32.74	31.96	-2%
16	6.5	31.07	31.07	0%
17	6	35.64	27.06	-24%
18	5.5	26.5	26.5	0%
19	7	41.65	42.1	1%
20	6.5	30.62	30.62	0%
21	6	39.2	39.2	0%
22	6	40.43	41.65	3%
23	5.5	35.08	32.7	-7%
24	5	33.07	30.63	-7%
25	5	31.85	31.85	0%
26	4.5	34.75	32.08	-8%
27	4	30.62	30.62	0%

Annex 3 – Numerical parametric study on full-scale models of 2-leaf stone masonry walls

Annex 3.1 – Table of mechanical properties for FE-based analyses

NOTE: The following table presents a set of reference mechanical properties for Masonry Type 6 (100 values) defined using a Monte Carlo simulation and a Gibbs sampling algorithm. These properties have been used to characterize the behaviour of the FE-based macro models used in the parametric study.

	Young Modulus	Compressive Strength	Tensile Strength	Compr. Fr. Energy	Ten. Fr. Energy	α	β	Ductility Index
Mod_#	E (MPa)	fc (MPa)	ft (MPa)	Gfc (N/m)	Gf1 (N/m)	E/fc	ft/fc	duc (mm)
1	3738.70	4.98	0.611	8119.26	15.54	453.54	0.042	1.824
2	1879.66	8.44	0.817	9398.56	7.06	299.11	0.095	1.114
3	3156.08	4.46	0.466	11903.90	14.29	398.27	0.057	1.386
4	2854.29	7.44	0.639	12663.90	11.72	294.81	0.046	1.227
5	2645.13	6.56	0.766	9915.99	8.44	463.90	0.052	1.764
6	3434.86	7.34	0.674	9921.63	16.72	262.00	0.059	1.330
7	3100.47	7.51	0.688	14575.05	24.12	331.93	0.073	2.522
8	2981.81	9.29	0.638	10439.25	9.50	552.69	0.046	1.411
9	4350.03	8.60	0.611	9115.35	11.75	481.97	0.060	1.563
10	3131.01	6.70	0.754	10202.82	16.45	321.68	0.057	1.778
11	6550.68	5.83	0.573	9950.71	8.75	364.18	0.048	1.452
12	2615.14	9.09	0.756	8646.42	3.89	470.46	0.063	1.949
13	2042.30	6.04	0.418	8177.49	8.42	431.27	0.064	2.183
14	5101.05	9.03	0.774	11288.42	11.81	319.87	0.052	1.453
15	3078.86	7.39	0.995	9477.59	12.47	427.86	0.116	1.932
16	3942.46	6.48	0.729	9827.70	12.67	503.68	0.063	1.500
17	2786.16	7.55	0.572	9265.25	11.79	440.00	0.063	1.222
18	2627.96	4.52	0.629	11652.64	13.76	412.14	0.041	3.182
19	2304.36	5.96	0.620	15167.68	8.35	323.51	0.059	1.035
20	2179.05	7.57	0.660	10685.26	13.08	589.57	0.064	1.592
21	2991.53	10.85	0.508	8251.18	11.58	454.29	0.081	1.964
22	3217.59	7.22	0.660	11112.99	9.89	403.21	0.067	1.248
23	2167.90	5.81	0.610	8190.94	20.28	499.43	0.047	2.364
24	3013.78	5.97	0.600	7793.07	8.31	397.19	0.034	1.559
25	3177.65	8.47	0.795	13966.03	8.87	380.40	0.066	1.402
26	3308.16	5.46	0.738	7770.38	18.00	554.32	0.042	1.321
27	5666.73	6.72	0.844	12619.86	6.24	323.43	0.059	1.135
28	3452.21	7.44	0.770	13771.57	7.22	378.21	0.070	1.547

29	4614.00	6.59	0.619	7292.61	15.15	402.63	0.067	1.110
30	3840.84	8.42	0.666	11676.39	12.04	372.42	0.046	1.394
31	3214.38	5.99	0.510	8737.01	16.69	472.80	0.044	1.756
32	2648.53	6.86	0.651	10949.06	13.20	580.77	0.046	1.136
33	3500.36	6.95	0.502	10848.08	12.24	384.72	0.055	1.849
34	2921.12	3.05	0.652	8866.78	7.09	372.56	0.049	1.880
35	4106.21	8.13	0.452	10540.24	13.80	289.16	0.059	1.494
36	2997.40	5.48	0.933	11294.21	15.91	349.79	0.090	2.324
37	4988.75	6.71	0.475	11794.45	16.16	583.39	0.059	1.260
38	3574.76	7.06	0.659	9166.75	10.66	525.44	0.050	2.061
39	2216.81	7.68	0.764	10420.98	7.50	354.20	0.082	1.235
40	3279.13	5.59	0.598	11268.09	27.28	483.05	0.047	1.582
41	2051.21	6.45	0.531	18832.48	3.36	294.50	0.055	1.678
42	2831.83	7.41	0.653	7376.01	7.47	312.27	0.078	1.258
43	3830.92	8.02	0.626	9585.37	4.44	418.02	0.045	1.729
44	1235.77	9.87	0.597	5284.60	11.81	349.41	0.045	2.144
45	2261.94	7.27	0.913	8698.22	16.45	369.07	0.066	1.341
46	3127.98	4.37	0.618	8848.22	7.87	793.83	0.062	2.362
47	2873.79	6.12	0.619	9442.22	9.31	553.57	0.064	1.665
48	3164.33	6.93	0.534	18494.20	14.27	402.65	0.059	1.701
49	1861.00	7.72	0.740	13450.47	12.00	248.75	0.055	2.217
50	3163.09	7.79	0.727	12762.21	11.75	440.05	0.094	0.741
51	2621.67	6.92	0.555	9567.69	28.40	726.74	0.061	2.120
52	1520.29	7.21	0.544	11186.81	9.98	662.71	0.071	2.126
53	3640.79	4.30	0.698	8598.45	10.29	569.01	0.064	1.650
54	3951.27	5.02	0.551	8820.56	7.01	271.39	0.043	1.913
55	4467.21	7.70	0.757	10390.56	17.96	683.83	0.046	1.594
56	1966.00	3.41	0.565	10712.73	33.72	636.20	0.053	2.145
57	1763.74	7.76	0.513	7125.57	7.42	439.84	0.065	1.673
58	1714.29	5.99	0.511	7564.88	14.08	649.44	0.045	1.487
59	2407.99	10.96	1.070	9151.56	7.46	422.98	0.053	1.455
60	4399.01	8.10	0.822	12464.47	6.47	692.43	0.033	1.409
61	5581.55	6.33	0.647	12309.51	5.40	406.53	0.079	1.331
62	3518.62	9.29	0.737	8320.50	6.78	511.73	0.042	1.774
63	3007.51	8.28	0.855	7528.09	5.76	471.46	0.052	1.641
64	2149.82	8.06	0.550	8877.63	9.48	580.67	0.047	1.607
65	2782.82	5.05	0.503	14959.85	19.76	491.59	0.053	1.732
66	2235.63	11.23	0.784	7579.00	13.54	164.28	0.041	1.210
67	2787.85	3.88	0.527	12635.63	20.52	470.89	0.033	1.417
68	3807.48	5.30	0.547	6998.97	8.65	473.01	0.039	1.505
69	4898.39	5.47	0.563	11750.51	9.42	427.64	0.056	1.317

70	6505.28	8.11	0.638	17206.29	12.33	521.20	0.047	0.958
71	3199.07	6.29	0.440	9205.34	8.79	613.84	0.059	1.563
72	2347.17	6.05	0.654	9507.24	8.35	415.61	0.045	1.441
73	2375.31	7.64	0.685	6633.73	12.85	329.11	0.056	1.378
74	2656.29	6.42	0.743	8583.70	16.48	462.60	0.055	1.815
75	1895.82	7.54	0.292	14627.10	19.49	355.66	0.056	2.065
76	3442.88	5.87	0.580	19349.01	10.51	519.53	0.058	1.890
77	2503.02	7.89	0.752	7780.97	10.28	466.87	0.068	1.568
78	4475.14	9.06	0.687	6142.73	11.45	622.10	0.069	1.580
79	2885.80	8.98	0.573	10197.08	13.66	536.73	0.043	2.342
80	2642.90	6.95	0.693	9765.79	11.57	524.62	0.053	1.821
81	1823.46	7.41	0.521	8121.26	11.84	430.00	0.042	1.711
82	1897.82	5.22	0.723	11038.12	8.62	565.76	0.034	2.904
83	3104.40	10.81	0.838	9184.24	7.57	518.82	0.071	1.317
84	3004.47	5.37	0.535	14288.33	7.91	539.78	0.041	2.607
85	4328.67	6.72	0.608	9537.60	5.08	427.14	0.045	2.148
86	2425.56	6.77	0.566	11618.70	3.05	235.77	0.063	1.652
87	2022.68	6.00	0.531	9820.57	8.93	477.15	0.068	1.420
88	3507.22	6.96	0.626	7706.01	13.04	524.78	0.049	1.545
89	3315.54	6.42	0.568	9583.47	9.43	405.09	0.050	1.485
90	3709.95	5.87	0.792	13000.63	14.38	533.52	0.047	2.059
91	3124.83	6.45	0.612	9642.91	8.64	430.65	0.044	2.002
92	3777.05	4.94	0.538	9285.43	12.58	419.64	0.053	2.012
93	2129.63	9.93	0.602	11621.68	16.67	490.50	0.042	1.906
94	2585.76	7.58	0.611	6719.39	12.10	418.21	0.095	2.377
95	2967.42	6.27	0.556	6827.37	8.57	219.54	0.075	1.700
96	3507.69	4.34	0.792	10469.64	13.07	658.19	0.037	1.252
97	2971.41	6.61	0.634	10832.23	24.44	474.55	0.042	1.723
98	2090.62	5.71	0.595	11631.11	8.15	564.99	0.038	1.982
99	1969.26	7.38	0.645	8573.96	6.16	438.31	0.041	1.311
100	2824.98	6.41	0.630	9404.08	16.54	457.39	0.044	1.422

Annex 3.2 – Limit States summary finite element macro models

Mod	Load Max	Load Detach	Load Plateau	Displ_Load Max	Displ_Detach	Displ_Load Plateau	Load Max vs Load_Detach	Load Max vs Load_Plateau	Disp_Detach vs Displ_Load Max	Displ_Plateua vs Displ_Load Max
#	kN	kN	kN	mm	mm	mm	%	%	%	%
Mod_1	287.76	123.47	82.65	0.74	0.88	1.94	-57%	-71%	-57%	62%
Mod_2	187.73	102.06	68.94	0.50	0.54	2.25	-46%	-63%	-46%	78%
Mod_3	173.42	103.52	72.59	0.85	0.94	1.95	-40%	-58%	-40%	56%
Mod_4	197.92	110.92	77.00	0.72	0.04	0.10	-44%	-61%	-44%	-614%
Mod_5	291.83	120.58	92.55	0.81	0.98	2.32	-59%	-68%	-59%	65%
Mod_6	175.76	59.34	61.08	0.88	0.04	0.12	-66%	-65%	-66%	-638%
Mod_7	193.69	100.86	66.69	0.98	1.16	4.90	-48%	-66%	-48%	80%
Mod_8	290.40	115.86	99.42	0.69	0.03	0.12	-60%	-66%	-60%	-480%
Mod_9	366.81	139.39	116.99	0.72	1.01	2.95	-62%	-68%	-62%	76%
Mod_10	294.24	120.21	83.81	0.57	0.68	1.63	-59%	-72%	-59%	65%
Mod_11	190.84	109.53	75.00	0.69	0.78	3.22	-43%	-61%	-43%	79%
Mod_12	289.77	111.73	86.61	0.74	0.93	2.24	-61%	-70%	-61%	67%
Mod_13	445.74	143.05	142.19	0.61	0.67	4.24	-68%	-68%	-68%	86%
Mod_14	299.50	113.22	106.56	1.24	1.62	3.69	-62%	-64%	-62%	66%
Mod_15	289.42	121.19	93.84	0.65	0.79	1.74	-58%	-68%	-58%	63%
Mod_16	191.93	106.56	72.70	0.85	1.19	3.33	-44%	-62%	-44%	74%
Mod_17	156.83	92.21	66.91	0.62	0.70	3.51	-41%	-57%	-41%	82%
Mod_18	171.77	94.70	67.51	1.01	1.16	4.22	-45%	-61%	-45%	76%
Mod_19	284.34	140.61	101.54	0.56	0.72	1.69	-51%	-64%	-51%	67%
Mod_20	294.52	119.77	123.92	0.68	0.81	3.88	-59%	-58%	-59%	83%
Mod_21	195.44	104.97	82.10	1.12	1.56	3.23	-46%	-58%	-46%	65%
Mod_22	285.16	112.88	95.96	0.90	1.38	5.34	-60%	-66%	-60%	83%
Mod_23	460.17	149.41	153.49	0.56	0.71	1.55	-68%	-67%	-68%	64%
Mod_24	382.13	119.47	114.64	0.87	1.16	2.99	-69%	-70%	-69%	71%
Mod_25	379.77	134.85	126.10	0.78	1.03	2.49	-64%	-67%	-64%	69%
Mod_26	376.25	117.71	116.93	0.98	1.45	3.15	-69%	-69%	-69%	69%
Mod_27	163.88	60.48	62.93	0.76	1.04	2.59	-63%	-62%	-63%	70%
Mod_28	185.85	106.78	72.94	0.75	0.94	3.72	-43%	-61%	-43%	80%
Mod_29	458.94	149.19	129.96	0.70	0.95	2.35	-67%	-72%	-67%	70%
Mod_30	176.86	96.80	69.32	0.90	1.14	5.73	-45%	-61%	-45%	84%
Mod_31	270.95	125.81	94.08	0.62	0.78	1.96	-54%	-65%	-54%	68%
Mod_32	185.92	104.23	70.92	0.69	0.88	3.82	-44%	-62%	-44%	82%
Mod_33	199.48	105.73	72.20	1.28	1.43	3.43	-47%	-64%	-47%	63%
Mod_34	274.84	120.21	86.06	0.71	0.86	2.13	-56%	-69%	-56%	67%
Mod_35	384.22	140.69	119.91	0.72	1.01	3.12	-63%	-69%	-63%	77%
Mod_36	289.68	117.93	88.50	0.56	0.70	1.78	-59%	-69%	-59%	68%

Mod_37	285.66	92.51	93.71	0.91	1.13	3.10	-68%	-67%	-68%	71%
Mod_38	192.33	117.44	79.83	0.58	0.83	2.95	-39%	-58%	-39%	80%
Mod_39	375.92	109.73	110.73	0.91	1.33	3.94	-71%	-71%	-71%	77%
Mod_40	470.67	121.07	133.03	0.54	0.70	2.72	-74%	-72%	-74%	80%
Mod_41	294.32	113.05	112.83	0.56	0.67	3.01	-62%	-62%	-62%	81%
Mod_42	289.64	120.14	120.10	0.57	0.70	4.32	-59%	-59%	-59%	87%
Mod_43	199.65	96.46	67.67	0.72	0.93	2.68	-52%	-66%	-52%	73%
Mod_44	289.48	96.68	99.02	0.74	1.18	3.11	-67%	-66%	-67%	76%
Mod_45	158.54	96.08	65.55	0.77	0.86	2.61	-39%	-59%	-39%	71%
Mod_46	356.65	121.22	93.48	0.98	2.77	13.13	-66%	-74%	-66%	93%
Mod_47	285.68	128.21	121.44	0.51	0.66	4.54	-55%	-57%	-55%	89%
Mod_48	194.05	89.62	66.89	0.67	0.87	2.14	-54%	-66%	-54%	69%
Mod_49	279.55	140.52	98.24	0.67	0.83	1.99	-50%	-65%	-50%	66%
Mod_50	291.75	118.42	104.74	0.56	0.66	2.15	-59%	-64%	-59%	74%
Mod_51	193.77	98.00	74.80	0.73	0.91	3.37	-49%	-61%	-49%	78%
Mod_52	455.50	147.69	141.36	0.65	0.83	2.23	-68%	-69%	-68%	71%
Mod_53	293.04	126.59	85.39	0.67	0.79	2.06	-57%	-71%	-57%	67%
Mod_54	285.49	93.36	94.55	0.81	0.99	2.72	-67%	-67%	-67%	70%
Mod_55	283.22	130.97	94.53	0.77	0.96	2.40	-54%	-67%	-54%	68%
Mod_56	291.51	95.68	100.85	0.73	1.18	3.56	-67%	-65%	-67%	80%
Mod_57	283.10	117.72	90.23	0.74	0.92	2.30	-58%	-68%	-58%	68%
Mod_58	193.09	112.12	74.95	0.67	0.95	2.85	-42%	-61%	-42%	77%
Mod_59	292.94	92.67	100.46	0.91	1.47	4.38	-68%	-66%	-68%	79%
Mod_60	284.20	112.99	78.62	0.68	0.83	1.99	-60%	-72%	-60%	66%
Mod_61	292.96	121.46	116.90	0.46	0.56	2.22	-59%	-60%	-59%	79%
Mod_62	377.71	127.33	114.15	0.74	1.05	2.01	-66%	-70%	-66%	63%
Mod_63	291.23	122.91	103.49	0.93	1.17	2.93	-58%	-64%	-58%	68%
Mod_64	274.45	123.36	119.67	0.95	1.17	5.71	-55%	-56%	-55%	83%
Mod_65	377.86	133.90	115.93	0.75	1.07	3.09	-65%	-69%	-65%	76%
Mod_66	187.55	88.47	64.39	0.88	1.16	3.11	-53%	-66%	-53%	72%
Mod_67	377.98	123.21	110.48	0.84	1.13	2.97	-67%	-71%	-67%	72%
Mod_68	293.02	124.60	84.68	0.69	0.83	2.05	-57%	-71%	-57%	66%
Mod_69	291.78	121.66	92.83	0.66	0.80	1.75	-58%	-68%	-58%	62%
Mod_70	288.11	125.57	87.44	0.68	0.86	2.10	-56%	-70%	-56%	68%
Mod_71	161.76	93.74	64.60	0.70	0.77	2.52	-42%	-60%	-42%	72%
Mod_72	376.34	123.51	117.33	0.65	0.96	2.65	-67%	-69%	-67%	75%
Mod_73	284.72	118.36	79.79	0.64	0.98	2.27	-58%	-72%	-58%	72%
Mod_74	284.72	118.36	104.85	0.64	0.98	4.06	-58%	-63%	-58%	84%
Mod_75	195.28	113.28	77.49	0.60	0.86	2.17	-42%	-60%	-42%	72%
Mod_76	145.38	94.55	64.52	0.94	1.04	3.08	-35%	-56%	-35%	70%
Mod_77	196.41	101.65	79.55	1.46	1.67	5.33	-48%	-59%	-48%	73%

Mod_78	375.87	124.84	109.97	0.80	1.17	3.56	-67%	-71%	-67%	78%
Mod_79	286.87	123.44	101.75	0.86	1.04	2.81	-57%	-65%	-57%	70%
Mod_80	457.18	116.31	151.19	0.70	1.21	3.52	-75%	-67%	-75%	80%
Mod_81	122.08	78.31	49.57	0.63	0.77	2.89	-36%	-59%	-36%	78%
Mod_82	376.59	116.30	119.43	0.95	1.44	3.14	-69%	-68%	-69%	70%
Mod_83	288.84	133.50	86.65	0.48	0.60	1.41	-54%	-70%	-54%	66%
Mod_84	294.00	119.30	88.63	0.58	0.69	1.55	-59%	-70%	-59%	63%
Mod_85	289.19	126.59	83.29	0.65	0.81	1.92	-56%	-71%	-56%	66%
Mod_86	300.10	117.38	103.15	1.12	1.50	4.14	-61%	-66%	-61%	73%
Mod_87	289.55	126.71	88.45	0.84	1.04	2.65	-56%	-69%	-56%	68%
Mod_88	383.15	133.23	114.57	0.70	0.96	2.43	-65%	-70%	-65%	71%
Mod_89	291.36	119.32	118.97	0.68	1.80	3.80	-59%	-59%	-59%	82%
Mod_90	286.86	118.65	102.96	0.95	1.17	2.85	-59%	-64%	-59%	67%
Mod_91	273.59	122.00	87.85	0.73	0.91	2.23	-55%	-68%	-55%	67%
Mod_92	292.07	133.22	130.84	0.53	0.66	2.55	-54%	-55%	-54%	79%
Mod_93	142.65	58.26	59.37	0.59	0.71	4.97	-59%	-58%	-59%	88%
Mod_94	291.28	115.49	81.39	0.96	1.19	2.91	-60%	-72%	-60%	67%
Mod_95	181.97	108.32	70.07	0.68	0.76	3.42	-40%	-61%	-40%	80%
Mod_96	375.13	102.28	104.34	0.98	1.33	3.57	-73%	-72%	-73%	73%
Mod_97	290.35	121.53	124.11	0.75	0.91	4.26	-58%	-57%	-58%	82%
Mod_98	287.45	120.69	129.23	0.44	0.57	3.12	-58%	-55%	-58%	86%
Mod_99	196.13	104.38	78.14	0.98	1.21	4.53	-47%	-60%	-47%	78%
Mod_100	194.09	109.89	72.43	0.65	0.92	2.75	-43%	-63%	-43%	76%
AVERAGE	278.27	114.31	94.72	0.76	0.97	3.01	-57%	-65%	-57%	54%

Annex 3.3 – Summary load levels for each limit state

	A	B	C	D	E	LS1	LS2	LS3	LS4
	E	fc	ft	Gfc	Gf1	Load	Load	Load	Load
Mod_ID	kN/m2	kN/m2	kN/m2	kN/m	kN/m	kN	kN	kN	kN
Mod_100	2429183.00	5764.37	350.88	9.01	0.01	1.88	194.09	97.05	67.93255
Mod_11	2274818.00	4700.14	270.99	8.91	0.02	1.87	190.84	95.42	66.79253
Mod_16	1848750.00	4550.73	320.11	8.54	0.02	1.85	191.93	95.97	67.17603
Mod_18	2267432.00	6434.20	244.98	12.17	0.01	1.92	171.77	85.88	60.11832
Mod_21	2192206.00	4258.64	258.36	5.90	0.01	1.87	195.44	97.72	68.40567
Mod_27	1754446.00	4237.28	469.79	6.21	0.01	1.92	163.88	81.94	57.35668
Mod_3	2033747.00	4885.78	172.30	8.05	0.02	1.88	173.42	86.71	60.69721
Mod_30	2073511.00	2993.47	239.52	5.75	0.01	1.86	176.86	88.43	61.90142
Mod_33	2485744.00	5879.34	310.60	9.33	0.01	1.92	199.48	99.74	69.81859
Mod_37	2489534.00	6401.97	356.49	9.69	0.02	1.85	285.66	142.83	99.97948
Mod_43	2318944.00	5954.93	375.69	11.92	0.01	1.86	199.65	99.83	69.87914
Mod_45	2067331.00	4511.27	185.79	8.39	0.01	1.83	158.54	79.27	55.48881
Mod_48	2400534.00	6518.86	418.23	12.01	0.01	1.81	194.05	97.03	67.91761
Mod_58	2355545.00	3754.23	318.11	3.52	0.01	2.01	193.09	96.54	67.58013
Mod_6	1677484.00	5375.86	357.03	12.75	0.01	1.82	175.76	87.88	61.51751
Mod_63	2414314.00	4660.04	433.22	7.82	0.02	1.89	291.23	145.62	101.9313
Mod_64	2406749.00	4467.99	244.93	11.87	0.02	1.97	274.45	137.23	96.05804
Mod_66	1771151.00	6184.21	471.85	14.49	0.01	2.30	187.55	93.77	65.64121
Mod_7	2156516.00	4691.80	252.82	8.86	0.01	1.94	193.69	96.84	67.79005
Mod_71	1913406.00	4278.45	249.45	5.41	0.01	1.86	161.76	80.88	56.6155
Mod_77	1700108.00	5612.90	253.92	9.70	0.02	1.90	196.41	98.20	68.74235
Mod_81	1612022.00	2967.78	156.98	4.20	0.01	1.85	122.08	61.04	42.72897
Mod_90	2388029.00	4585.01	354.33	6.06	0.02	1.85	286.86	143.43	100.4005
Mod_93	1995840.00	4674.87	194.72	10.10	0.01	1.80	142.65	71.33	49.92757
Mod_94	2338852.00	8637.34	457.14	11.29	0.02	1.87	291.28	145.64	101.9463
Mod_95	2176146.00	4319.07	273.22	7.16	0.01	1.84	181.97	90.98	63.68856
Mod_99	2087818.00	4741.98	212.80	18.17	0.02	1.85	196.13	98.06	68.64385
Mod_1	3066042.00	6509.67	402.58	9.93	0.01	1.84	287.76	143.88	100.7146
Mod_12	3046135.00	5245.22	490.51	9.53	0.01	1.83	289.77	144.88	101.4194
Mod_14	2956243.00	7476.33	558.12	11.36	0.01	1.84	299.50	149.75	104.8246
Mod_15	3480611.00	10114.78	613.38	20.08	0.01	1.89	289.42	144.71	101.2971
Mod_17	2606985.00	3547.60	175.00	5.54	0.01	2.04	156.83	78.42	54.89175
Mod_2	3082369.00	5509.50	296.55	5.71	0.01	1.99	187.73	93.86	65.70458
Mod_20	3318236.00	15724.11	1003.19	27.63	0.01	1.92	294.52	147.26	103.083
Mod_22	2523184.00	4498.78	319.41	7.58	0.02	1.95	285.16	142.58	99.8067
Mod_24	3396402.00	11912.19	1098.60	18.06	0.02	2.09	382.13	191.07	133.7461
Mod_26	3013158.00	6070.85	556.36	12.13	0.02	1.95	376.25	188.13	131.6889

Mod_28	2640587.00	3674.53	226.94	5.15	0.01	1.92	185.85	92.92	65.04576
Mod_32	2813298.00	6377.72	223.86	12.65	0.01	1.84	185.92	92.96	65.07321
Mod_34	3249407.00	6211.47	247.00	8.45	0.01	1.84	274.84	137.42	96.19408
Mod_38	2746080.00	4641.89	328.16	7.76	0.01	1.87	192.33	96.17	67.31652
Mod_39	3266824.00	10970.66	561.57	19.52	0.02	2.01	375.92	187.96	131.5715
Mod_4	2661274.00	5029.20	180.14	7.16	0.02	1.85	197.92	98.96	69.27038
Mod_44	3039713.00	6727.59	428.73	10.09	0.01	1.89	289.48	144.74	101.3189
Mod_46	2569912.00	4679.61	200.96	6.32	0.01	1.80	356.65	178.33	124.8278
Mod_49	3411781.00	6574.07	271.77	17.19	0.02	1.88	279.55	139.77	97.84154
Mod_5	2773756.00	7749.63	759.49	16.13	0.01	1.85	291.83	145.91	102.1396
Mod_51	2691369.00	3891.18	237.96	5.44	0.01	1.82	193.77	96.89	67.82032
Mod_53	3326498.00	9182.80	828.27	14.14	0.01	1.86	293.04	146.52	102.5655
Mod_54	2797173.00	7738.75	362.78	15.24	0.01	1.98	285.49	142.74	99.92014
Mod_55	2935468.00	4819.24	298.49	8.24	0.02	1.93	283.22	141.61	99.12689
Mod_56	3237693.00	7387.97	553.74	12.05	0.01	1.86	291.51	145.75	102.0282
Mod_57	3067168.00	7610.86	305.04	7.45	0.01	1.86	283.10	141.55	99.08329
Mod_59	2631961.00	7652.34	686.11	13.39	0.01	1.85	292.94	146.47	102.5276
Mod_60	3315303.00	7574.60	389.13	17.79	0.01	1.99	284.20	142.10	99.46881
Mod_68	3244136.00	10359.60	810.70	13.19	0.01	1.91	293.02	146.51	102.5574
Mod_69	3392751.00	7964.38	709.71	10.12	0.01	1.84	291.78	145.89	102.1227
Mod_70	3332840.00	7041.00	360.26	11.88	0.02	1.88	288.11	144.05	100.8373
Mod_73	3043897.00	5967.04	275.06	9.65	0.01	1.93	284.72	142.36	99.6537
Mod_75	2602250.00	6803.76	337.39	12.19	0.01	1.82	195.28	97.64	68.34956
Mod_76	2627644.00	3043.82	99.29	4.75	0.01	2.11	145.38	72.69	50.88311
Mod_79	2647498.00	6164.70	344.74	6.46	0.02	1.93	286.87	143.44	100.4058
Mod_8	3279545.00	9414.41	422.09	19.56	0.01	1.86	290.40	145.20	101.639
Mod_82	3121297.00	7964.82	579.07	9.91	0.02	1.84	376.59	188.30	131.8072
Mod_85	3480279.00	6665.23	386.23	11.56	0.02	1.87	289.19	144.59	101.2148
Mod_86	3249437.00	11845.63	816.77	14.33	0.01	1.84	300.10	150.05	105.0345
Mod_87	2685495.00	7254.73	396.56	11.28	0.02	1.90	289.55	144.78	101.3431
Mod_89	3325726.00	6942.11	596.63	9.16	0.02	1.91	291.36	145.68	101.9761
Mod_91	3144146.00	5409.90	238.95	5.65	0.02	1.92	273.59	136.80	95.75688
Mod_96	3023360.00	7251.05	515.37	8.83	0.02	1.89	375.13	187.57	131.2957
Mod_97	3025735.00	13333.66	638.04	20.25	0.02	1.84	290.35	145.18	101.6233
Mod_10	3962332.00	9582.40	542.66	14.99	0.01	1.88	294.24	147.12	102.9825
Mod_19	4034738.00	7168.00	306.96	12.05	0.02	1.88	284.34	142.17	99.51766
Mod_25	3792715.00	13462.90	592.28	24.54	0.02	1.90	379.77	189.88	132.9178
Mod_31	3691085.00	6413.99	223.70	12.60	0.02	1.85	270.95	135.47	94.83203
Mod_35	4091138.00	11343.51	749.84	18.16	0.02	1.82	384.22	192.11	134.478
Mod_36	3995653.00	7140.50	398.36	11.19	0.01	1.84	289.68	144.84	101.3867
Mod_41	4026862.00	14096.27	840.46	18.41	0.01	1.95	294.32	147.16	103.012

Mod_42	3962909.00	9651.32	591.21	16.42	0.01	1.85	289.64	144.82	101.3726
Mod_47	4433476.00	6016.86	330.46	8.58	0.01	1.86	285.68	142.84	99.98634
Mod_50	4044563.00	10947.27	753.63	13.04	0.01	1.88	291.75	145.87	102.1114
Mod_62	4001089.00	12624.15	838.74	16.93	0.01	2.14	377.71	188.86	132.1996
Mod_65	3953804.00	12308.16	505.05	25.12	0.02	1.97	377.86	188.93	132.2517
Mod_67	3534366.00	9658.41	607.91	13.44	0.02	1.83	377.98	188.99	132.2916
Mod_74	3562614.00	4728.26	313.47	9.27	0.02	2.05	284.72	142.36	99.6537
Mod_78	3685647.00	9972.88	548.34	17.26	0.01	1.84	375.87	187.93	131.5533
Mod_84	3882488.00	17075.77	872.75	18.44	0.01	1.91	294.00	147.00	102.9002
Mod_88	4186442.00	11649.18	646.93	21.76	0.02	1.87	383.15	191.57	134.1018
Mod_9	4131121.00	8928.11	374.80	18.64	0.02	1.92	366.81	183.40	128.3827
Mod_92	4247510.00	6610.28	455.15	12.21	0.01	1.95	292.07	146.03	102.224
Mod_29	5219432.00	11062.23	662.45	25.11	0.02	1.83	458.94	229.47	160.6299
Mod_61	4920814.00	11502.36	484.92	16.98	0.01	1.90	292.96	146.48	102.5369
Mod_72	4532117.00	7666.41	549.28	11.46	0.01	1.85	376.34	188.17	131.7204
Mod_80	5259008.00	11840.22	812.06	12.54	0.02	1.90	457.18	228.59	160.0118
Mod_83	4656771.00	8380.81	391.24	12.74	0.01	1.88	288.84	144.42	101.0953
Mod_98	5167242.00	9591.74	359.13	20.93	0.01	2.03	287.45	143.73	100.608
Mod_13	6077962.00	11842.61	458.20	23.25	0.02	1.90	445.74	222.87	156.0084
Mod_23	6553024.00	18955.36	723.97	26.15	0.01	1.90	460.17	230.09	161.061
Mod_40	6735010.00	12662.76	866.12	20.89	0.02	2.02	470.67	235.33	164.733
Mod_52	5673825.00	18543.89	671.54	30.51	0.02	1.92	455.50	227.75	159.4265

Annex 3.4 – Summary displacement levels for each limit state

	A	B	C	D	E	LS1	LS2	LS3	LS4
	E	fc	ft	Gfc	Gf1	Displ.	Displ.	Displ.	Displ.
Mod_ID	kN/m2	kN/m2	kN/m2	kN/m	kN/m	m	m	m	m
Mod_100	2429183.00	5764.37	350.88	9.01	0.01	5.83E-05	5.98E-04	1.14E-03	0.003
Mod_11	2274818.00	4700.14	270.99	8.91	0.02	4.46E-05	5.83E-04	1.14E-03	0.003
Mod_16	1848750.00	4550.73	320.11	8.54	0.02	3.11E-05	5.61E-04	1.14E-03	0.003
Mod_18	2267432.00	6434.20	244.98	12.17	0.01	4.59E-05	5.92E-04	1.14E-03	0.003
Mod_21	2192206.00	4258.64	258.36	5.90	0.01	1.90E-05	5.28E-04	1.14E-03	0.003
Mod_27	1754446.00	4237.28	469.79	6.21	0.01	1.38E-05	5.16E-04	1.14E-03	0.003
Mod_3	2033747.00	4885.78	172.30	8.05	0.02	4.26E-05	6.14E-04	1.14E-03	0.003
Mod_30	2073511.00	2993.47	239.52	5.75	0.01	4.31E-05	5.60E-04	1.15E-03	0.003
Mod_33	2485744.00	5879.34	310.60	9.33	0.01	6.04E-05	6.62E-04	1.14E-03	0.003
Mod_37	2489534.00	6401.97	356.49	9.69	0.02	5.25E-05	5.95E-04	1.14E-03	0.003
Mod_43	2318944.00	5954.93	375.69	11.92	0.01	4.86E-05	5.85E-04	1.13E-03	0.003
Mod_45	2067331.00	4511.27	185.79	8.39	0.01	3.85E-05	5.57E-04	1.13E-03	0.003
Mod_48	2400534.00	6518.86	418.23	12.01	0.01	2.67E-05	6.29E-04	1.12E-03	0.003
Mod_58	2355545.00	3754.23	318.11	3.52	0.01	3.61E-05	6.03E-04	1.12E-03	0.003
Mod_6	1677484.00	5375.86	357.03	12.75	0.01	2.94E-05	4.65E-04	1.12E-03	0.003
Mod_63	2414314.00	4660.04	433.22	7.82	0.02	5.58E-05	5.97E-04	1.13E-03	0.003
Mod_64	2406749.00	4467.99	244.93	11.87	0.02	5.75E-05	6.59E-04	1.12E-03	0.003
Mod_66	1771151.00	6184.21	471.85	14.49	0.01	2.59E-05	5.23E-04	1.12E-03	0.003
Mod_7	2156516.00	4691.80	252.82	8.86	0.01	4.25E-05	6.22E-04	1.13E-03	0.003
Mod_71	1913406.00	4278.45	249.45	5.41	0.01	3.28E-05	5.24E-04	1.14E-03	0.003
Mod_77	1700108.00	5612.90	253.92	9.70	0.02	7.67E-07	5.09E-04	1.15E-03	0.003
Mod_81	1612022.00	2967.78	156.98	4.20	0.01	8.50E-06	5.02E-04	1.17E-03	0.003
Mod_90	2388029.00	4585.01	354.33	6.06	0.02	5.58E-05	6.27E-04	1.18E-03	0.003
Mod_93	1995840.00	4674.87	194.72	10.10	0.01	4.02E-05	5.59E-04	1.19E-03	0.003
Mod_94	2338852.00	8637.34	457.14	11.29	0.02	5.50E-05	5.46E-04	1.20E-03	0.003
Mod_95	2176146.00	4319.07	273.22	7.16	0.01	4.09E-05	5.68E-04	1.20E-03	0.003
Mod_99	2087818.00	4741.98	212.80	18.17	0.02	4.00E-05	6.21E-04	1.21E-03	0.003
Mod_1	3066042.00	6509.67	402.58	9.93	0.01	7.55E-05	6.81E-04	1.22E-03	0.003
Mod_12	3046135.00	5245.22	490.51	9.53	0.01	5.07E-05	7.30E-04	1.22E-03	0.003
Mod_14	2956243.00	7476.33	558.12	11.36	0.01	5.84E-05	6.52E-04	1.22E-03	0.003
Mod_15	3480611.00	10114.78	613.38	20.08	0.01	9.63E-05	7.27E-04	1.22E-03	0.003
Mod_17	2606985.00	3547.60	175.00	5.54	0.01	6.29E-05	6.23E-04	1.21E-03	0.003
Mod_2	3082369.00	5509.50	296.55	5.71	0.01	8.25E-05	7.12E-04	1.22E-03	0.003
Mod_20	3318236.00	15724.11	1003.19	27.63	0.01	8.33E-05	7.21E-04	1.21E-03	0.003
Mod_22	2523184.00	4498.78	319.41	7.58	0.02	5.61E-05	5.69E-04	1.21E-03	0.003
Mod_24	3396402.00	11912.19	1098.60	18.06	0.02	8.78E-05	7.17E-04	1.21E-03	0.003
Mod_26	3013158.00	6070.85	556.36	12.13	0.02	4.95E-05	7.33E-04	1.21E-03	0.003

Mod_28	2640587.00	3674.53	226.94	5.15	0.01	4.66E-05	6.29E-04	1.21E-03	0.003
Mod_32	2813298.00	6377.72	223.86	12.65	0.01	7.16E-05	7.02E-04	1.21E-03	0.003
Mod_34	3249407.00	6211.47	247.00	8.45	0.01	8.67E-05	6.87E-04	1.22E-03	0.003
Mod_38	2746080.00	4641.89	328.16	7.76	0.01	7.01E-05	6.37E-04	1.21E-03	0.003
Mod_39	3266824.00	10970.66	561.57	19.52	0.02	8.14E-05	7.04E-04	1.21E-03	0.003
Mod_4	2661274.00	5029.20	180.14	7.16	0.02	6.13E-05	6.61E-04	1.21E-03	0.003
Mod_44	3039713.00	6727.59	428.73	10.09	0.01	7.45E-05	6.87E-04	1.22E-03	0.003
Mod_46	2569912.00	4679.61	200.96	6.32	0.01	3.30E-05	5.74E-04	1.21E-03	0.003
Mod_49	3411781.00	6574.07	271.77	17.19	0.02	7.52E-05	7.19E-04	1.22E-03	0.003
Mod_5	2773756.00	7749.63	759.49	16.13	0.01	7.01E-05	7.04E-04	1.22E-03	0.003
Mod_51	2691369.00	3891.18	237.96	5.44	0.01	6.60E-05	6.35E-04	1.22E-03	0.003
Mod_53	3326498.00	9182.80	828.27	14.14	0.01	9.16E-05	7.65E-04	1.23E-03	0.003
Mod_54	2797173.00	7738.75	362.78	15.24	0.01	6.40E-05	6.32E-04	1.23E-03	0.003
Mod_55	2935468.00	4819.24	298.49	8.24	0.02	7.14E-05	6.60E-04	1.23E-03	0.003
Mod_56	3237693.00	7387.97	553.74	12.05	0.01	8.19E-05	7.00E-04	1.22E-03	0.003
Mod_57	3067168.00	7610.86	305.04	7.45	0.01	5.15E-05	7.10E-04	1.22E-03	0.003
Mod_59	2631961.00	7652.34	686.11	13.39	0.01	4.63E-05	6.37E-04	1.22E-03	0.003
Mod_60	3315303.00	7574.60	389.13	17.79	0.01	9.02E-05	6.65E-04	1.22E-03	0.003
Mod_68	3244136.00	10359.60	810.70	13.19	0.01	8.65E-05	6.98E-04	1.23E-03	0.003
Mod_69	3392751.00	7964.38	709.71	10.12	0.01	9.40E-05	7.80E-04	1.23E-03	0.003
Mod_70	3332840.00	7041.00	360.26	11.88	0.02	8.38E-05	7.14E-04	1.22E-03	0.003
Mod_73	3043897.00	5967.04	275.06	9.65	0.01	7.55E-05	7.30E-04	1.22E-03	0.003
Mod_75	2602250.00	6803.76	337.39	12.19	0.01	5.83E-05	6.08E-04	1.22E-03	0.003
Mod_76	2627644.00	3043.82	99.29	4.75	0.01	3.52E-05	6.23E-04	1.22E-03	0.003
Mod_79	2647498.00	6164.70	344.74	6.46	0.02	4.69E-05	6.28E-04	1.23E-03	0.003
Mod_8	3279545.00	9414.41	422.09	19.56	0.01	8.88E-05	7.36E-04	1.24E-03	0.003
Mod_82	3121297.00	7964.82	579.07	9.91	0.02	8.20E-05	6.96E-04	1.25E-03	0.003
Mod_85	3480279.00	6665.23	386.23	11.56	0.02	9.73E-05	6.85E-04	1.25E-03	0.003
Mod_86	3249437.00	11845.63	816.77	14.33	0.01	8.07E-05	6.99E-04	1.26E-03	0.003
Mod_87	2685495.00	7254.73	396.56	11.28	0.02	6.22E-05	6.93E-04	1.26E-03	0.003
Mod_89	3325726.00	6942.11	596.63	9.16	0.02	8.51E-05	7.13E-04	1.28E-03	0.003
Mod_91	3144146.00	5409.90	238.95	5.65	0.02	5.43E-05	7.42E-04	1.28E-03	0.003
Mod_96	3023360.00	7251.05	515.37	8.83	0.02	6.08E-05	6.60E-04	1.29E-03	0.003
Mod_97	3025735.00	13333.66	638.04	20.25	0.02	7.94E-05	6.71E-04	1.31E-03	0.003
Mod_10	3962332.00	9582.40	542.66	14.99	0.01	1.13E-04	7.89E-04	1.32E-03	0.003
Mod_19	4034738.00	7168.00	306.96	12.05	0.02	1.18E-04	8.28E-04	1.32E-03	0.003
Mod_25	3792715.00	13462.90	592.28	24.54	0.02	1.01E-04	7.78E-04	1.32E-03	0.003
Mod_31	3691085.00	6413.99	223.70	12.60	0.02	9.95E-05	7.11E-04	1.31E-03	0.003
Mod_35	4091138.00	11343.51	749.84	18.16	0.02	1.14E-04	8.01E-04	1.31E-03	0.003
Mod_36	3995653.00	7140.50	398.36	11.19	0.01	8.59E-05	8.53E-04	1.31E-03	0.003
Mod_41	4026862.00	14096.27	840.46	18.41	0.01	9.81E-05	7.98E-04	1.31E-03	0.003

Mod_42	3962909.00	9651.32	591.21	16.42	0.01	1.14E-04	8.42E-04	1.31E-03	0.003
Mod_47	4433476.00	6016.86	330.46	8.58	0.01	1.31E-04	8.32E-04	1.31E-03	0.003
Mod_50	4044563.00	10947.27	753.63	13.04	0.01	1.18E-04	7.96E-04	1.31E-03	0.003
Mod_62	4001089.00	12624.15	838.74	16.93	0.01	1.09E-04	7.93E-04	1.32E-03	0.003
Mod_65	3953804.00	12308.16	505.05	25.12	0.02	1.09E-04	8.18E-04	1.33E-03	0.003
Mod_67	3534366.00	9658.41	607.91	13.44	0.02	9.29E-05	7.47E-04	1.33E-03	0.003
Mod_74	3562614.00	4728.26	313.47	9.27	0.02	6.98E-05	6.95E-04	1.35E-03	0.003
Mod_78	3685647.00	9972.88	548.34	17.26	0.01	8.54E-05	7.52E-04	1.36E-03	0.003
Mod_84	3882488.00	17075.77	872.75	18.44	0.01	1.11E-04	8.39E-04	1.38E-03	0.003
Mod_88	4186442.00	11649.18	646.93	21.76	0.02	1.21E-04	8.18E-04	1.40E-03	0.003
Mod_9	4131121.00	8928.11	374.80	18.64	0.02	1.21E-04	8.63E-04	1.42E-03	0.003
Mod_92	4247510.00	6610.28	455.15	12.21	0.01	1.18E-04	8.09E-04	1.45E-03	0.003
Mod_29	5219432.00	11062.23	662.45	25.11	0.02	1.56E-04	9.39E-04	1.46E-03	0.003
Mod_61	4920814.00	11502.36	484.92	16.98	0.01	1.44E-04	9.06E-04	1.46E-03	0.003
Mod_72	4532117.00	7666.41	549.28	11.46	0.01	1.06E-04	8.89E-04	1.48E-03	0.003
Mod_80	5259008.00	11840.22	812.06	12.54	0.02	1.44E-04	9.57E-04	1.50E-03	0.003
Mod_83	4656771.00	8380.81	391.24	12.74	0.01	1.40E-04	8.29E-04	1.52E-03	0.003
Mod_98	5167242.00	9591.74	359.13	20.93	0.01	1.58E-04	9.33E-04	1.56E-03	0.003
Mod_13	6077962.00	11842.61	458.20	23.25	0.02	1.94E-04	1.11E-03	1.56E-03	0.003
Mod_23	6553024.00	18955.36	723.97	26.15	0.01	2.03E-04	1.11E-03	1.57E-03	0.003
Mod_40	6735010.00	12662.76	866.12	20.89	0.02	2.12E-04	1.18E-03	1.55E-03	0.003
Mod_52	5673825.00	18543.89	671.54	30.51	0.02	1.72E-04	9.83E-04	1.42E-03	0.003

Annex 3.5 – Dataset correlation Young Modulus vs interface properties

Mod_ID (#)	E (kn/m²)	Norm. Stiff. (kN/m³)	Sh. Stiff. (kN/m³)	Tens. Strength (kn/m²)	Cohesion (kn/m²)
Mod_1	3066042.31	3700000	1850000	100	125
Mod_2	3082368.85	3800000	1900000	60	75
Mod_3	2033746.72	1900000	950000	53	66
Mod_4	2661274.35	2700000	1350000	63	79
Mod_5	2773756.12	3800000	1900000	100	125
Mod_6	1677483.93	1900000	950000	54	67
Mod_7	2156515.75	1900000	950000	60	75
Mod_8	3279545.15	3600000	1800000	100	125
Mod_9	4131120.81	4100000	2050000	160	200
Mod_10	3962332.22	4300000	2150000	100	125
Mod_11	2274818.20	2700000	1350000	60	75
Mod_12	3046135.47	3700000	1850000	100	125
Mod_13	6077962.24	6300000	3150000	225	281
Mod_14	2956243.35	2100000	1050000	100	125
Mod_15	3480610.88	4100000	2050000	100	125
Mod_16	1848749.85	1900000	950000	58	73
Mod_17	2606984.67	2400000	1200000	53	66
Mod_18	2267431.96	1328906	664453	47	59
Mod_19	4034738.46	4200000	2100000	0	0
Mod_20	3318236.35	3700000	1850000	110	138
Mod_21	2192206.23	1550000	775000	58	73
Mod_22	2523183.70	2900000	1450000	95	119
Mod_23	6553024.00	6600000	3300000	230	288
Mod_24	3396401.66	4200000	2100000	150	188
Mod_25	3792715.07	4100000	2050000	165	206
Mod_26	3013158.06	3600000	1800000	165	206
Mod_27	1754445.55	1800000	900000	50	63
Mod_28	2640587.36	2400000	1200000	56	70
Mod_29	5219431.89	6400000	3200000	230	288
Mod_30	2073510.84	1950000	975000	54	68
Mod_31	3691084.51	4350000	2175000	90	113
Mod_32	2813298.34	2800000	1400000	60	75
Mod_33	2485743.89	1400000	700000	63	79
Mod_34	3249406.80	3850000	1925000	90	113
Mod_35	4091138.21	4400000	2200000	170	213
Mod_36	3995653.38	4300000	2150000	96	120
Mod_37	2489534.49	2900000	1450000	96	119

Mod_38	2746079.51	3250000	1625000	66	83
Mod_39	3266824.16	3650000	1825000	165	206
Mod_40	6735009.97	6800000	3400000	230	288
Mod_41	4026862.44	4300000	2150000	99	123
Mod_42	3962909.24	4300000	2150000	97	121
Mod_43	2318944.45	2800000	1400000	64	80
Mod_44	3039713.05	3600000	1800000	100	125
Mod_45	2067331.03	2100000	1050000	49	61
Mod_46	2569912.47	3600000	1800000	145	181
Mod_47	4433475.78	4300000	2150000	96	119
Mod_48	2400533.61	2700000	1350000	60	75
Mod_49	3411781.37	3600000	1800000	106	132
Mod_50	4044563.46	4100000	2050000	99	123
Mod_51	2691369.03	2300000	1150000	60	75
Mod_52	5673824.75	6562500	3281250	234	293
Mod_53	3326498.12	4100000	2050000	110	138
Mod_54	2797172.57	3600000	1800000	99	123
Mod_55	2935467.54	3600000	1800000	105	131
Mod_56	3237692.66	3600000	1800000	108	135
Mod_57	3067167.92	3600000	1800000	107	133
Mod_58	2355544.53	2700000	1350000	61	76
Mod_59	2631960.99	3150000	1575000	113	141
Mod_60	3315303.30	3600000	1800000	107	133
Mod_61	4920813.61	5000000	2500000	107	133
Mod_62	4001088.50	5000000	2500000	170	213
Mod_63	2414313.79	2950000	1475000	107	133
Mod_64	2406748.95	2700000	1350000	107	133
Mod_65	3953803.71	5010000	2505000	171	214
Mod_66	1771150.89	1950000	975000	57	71
Mod_67	3534365.65	4450000	2225000	170	213
Mod_68	3244135.76	4150000	2075000	110	138
Mod_69	3392751.39	4150000	2075000	110	139
Mod_70	3332839.59	4150000	2075000	112	140
Mod_71	1913405.50	2100000	1050000	50	63
Mod_72	4532117.36	4800000	2400000	170	213
Mod_73	3043896.87	3750000	1875000	98	122
Mod_74	3562614.10	3750000	1875000	95	119
Mod_75	2602249.93	3150000	1575000	60	75
Mod_76	2627644.48	1400000	700000	42	53
Mod_77	1700108.25	1350000	675000	60	75
Mod_78	3685647.38	4650000	2325000	170	213

Mod_79	2647498.31	3200000	1600000	98	122
Mod_80	5259007.82	6000000	3000000	200	250
Mod_81	1612022.23	2100000	1050000	34	43
Mod_82	3121296.57	3700000	1850000	170	213
Mod_83	4656771.26	4700000	2350000	100	125
Mod_84	3882488.03	4550000	2275000	110	138
Mod_85	3480279.44	3800000	1900000	100	125
Mod_86	3249437.42	2300000	1150000	110	138
Mod_87	2685495.38	3250000	1625000	110	138
Mod_88	4186441.86	4900000	2450000	175	219
Mod_89	3325725.98	4150000	2075000	113	141
Mod_90	2388029.39	2362500	1181250	84	105
Mod_91	3144145.69	3650000	1825000	86	107
Mod_92	4247509.72	4350000	2175000	98	122
Mod_93	1995839.95	2100000	1050000	40	50
Mod_94	2338851.75	2950000	1475000	110	138
Mod_95	2176146.00	2000000	1000000	57	71
Mod_96	3023360.06	3600000	1800000	155	194
Mod_97	3025735.14	3600000	1800000	155	194
Mod_98	5167241.70	4950000	2475000	98	122
Mod_99	2087817.67	1950000	975000	60	75
Mod_100	2429182.52	310000	155000	60	75

Annex 3.6 – Table of interface properties for DE-based analyses

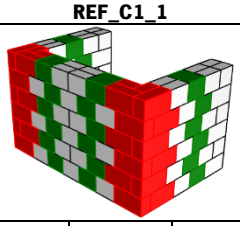
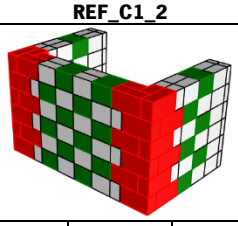
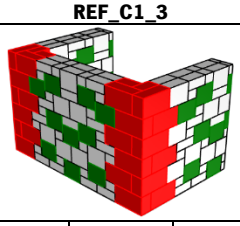
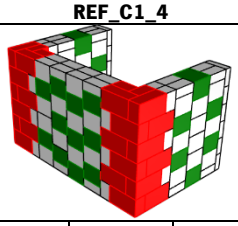
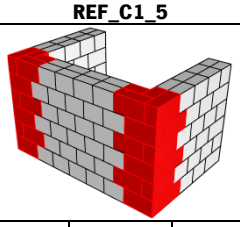
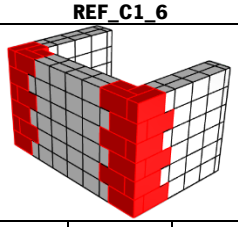
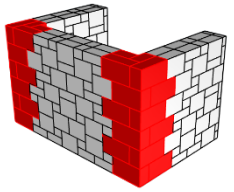
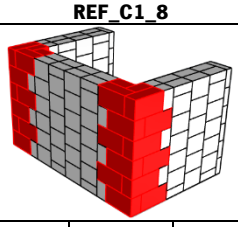
	Normal Stiffness	Shear Stiffness	Tensile Strength	Cohesion	Friction Angle	Dilatancy
Mod_#	N/m³	N/m³	N/m²	N/m²	°	°
1	3.70E+09	1.85E+09	1.00E+05	1.250E+05	33	0
2	3.80E+00	1.90E+00	6.00E+04	7.500E+04	33	0
3	1.90E+09	9.50E+08	5.30E+04	6.625E+04	33	0
4	2.70E+09	1.35E+09	6.30E+04	7.875E+04	33	0
5	3.80E+09	1.90E+09	1.00E+05	1.250E+05	33	0
6	1.90E+09	9.50E+08	5.35E+04	6.688E+04	33	0
7	1.90E+09	9.50E+08	6.00E+04	7.500E+04	33	0
8	3.60E+09	1.80E+09	1.00E+05	1.250E+05	33	0
9	4.10E+09	2.05E+09	1.60E+05	2.000E+05	33	0
10	4.30E+09	2.15E+09	1.00E+05	1.250E+05	33	0
11	2.70E+09	1.35E+09	6.00E+04	7.500E+04	33	0
12	3.70E+09	1.85E+09	1.00E+05	1.250E+05	33	0
13	6.30E+09	3.15E+09	2.25E+05	2.813E+05	33	0
14	2.10E+09	1.05E+09	1.00E+05	1.250E+05	33	0
15	4.10E+09	2.05E+09	1.00E+05	1.250E+05	33	0
16	1.90E+09	9.50E+08	5.80E+04	7.250E+04	33	0
17	2.40E+09	1.20E+09	5.30E+04	6.625E+04	33	0
18	1.33E+09	6.64E+08	4.75E+04	5.933E+04	33	0
19	4.20E+09	2.10E+09	9.70E+00	1.213E+01	33	0
20	3.70E+09	1.85E+09	1.10E+05	1.375E+05	33	0
21	1.55E+09	7.75E+08	5.80E+04	7.250E+04	33	0
22	2.90E+09	1.45E+09	9.50E+04	1.188E+05	33	0
23	6.60E+09	3.30E+09	2.30E+05	2.875E+05	33	0
24	4.20E+09	2.10E+09	1.50E+05	2.250E+05	33	0
25	4.10E+09	2.05E+09	1.65E+05	2.063E+05	33	0
26	3.60E+09	1.80E+09	1.65E+05	2.063E+05	33	0
27	1.80E+09	9.00E+08	5.00E+04	6.250E+04	33	0
28	2.40E+09	1.20E+09	5.60E+04	7.000E+04	33	0
29	6.40E+09	3.20E+09	2.30E+00	2.875E+00	33	0
30	1.95E+09	9.75E+08	5.40E+04	6.750E+04	33	0
31	4.35E+09	2.18E+09	9.00E+04	1.125E+05	33	0
32	2.80E+09	1.40E+09	6.00E+04	7.500E+04	33	0
33	1.40E+09	7.00E+08	6.30E+04	7.875E+04	33	0
34	3.85E+09	1.93E+09	9.00E+04	1.125E+05	33	0
35	4.40E+09	2.20E+09	1.70E+05	2.125E+05	33	0
36	4.30E+09	2.15E+09	9.60E+04	1.200E+05	33	0
37	2.90E+09	1.45E+09	9.55E+04	1.194E+05	33	0
38	3.25E+09	1.63E+09	6.60E+04	8.250E+04	33	0

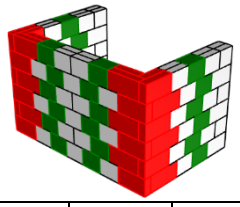
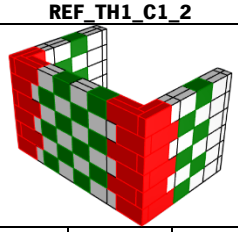
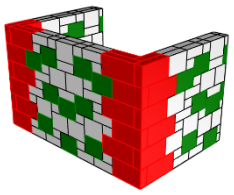
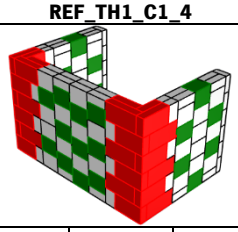
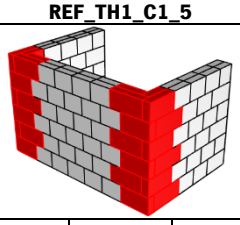
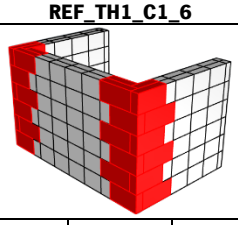
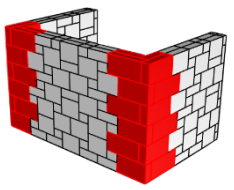
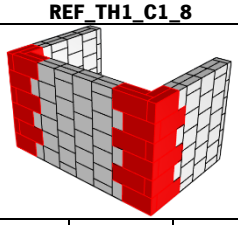
39	3.65E+09	1.83E+09	1.65E+05	2.063E+05	33	0
40	6.80E+09	3.40E+09	2.30E+05	2.875E+05	33	0
41	4.30E+09	2.15E+09	9.85E+04	1.231E+05	33	0
42	4.30E+09	2.15E+09	9.65E+04	1.206E+05	33	0
43	2.80E+09	1.40E+09	6.40E+04	8.000E+04	33	0
44	3.60E+09	1.80E+09	1.00E+05	1.250E+05	33	0
45	2.10E+00	1.05E+00	4.90E+04	6.125E+04	33	0
46	3.60E+09	1.80E+09	1.45E+05	1.813E+05	33	0
47	4.30E+09	2.15E+09	9.55E+04	1.194E+05	33	0
48	2.70E+09	1.35E+09	6.00E+04	7.500E+04	33	0
49	3.60E+09	1.80E+09	1.06E+05	1.319E+05	33	0
50	4.10E+09	2.05E+09	9.85E+04	1.231E+05	33	0
51	2.30E+09	1.15E+09	6.00E+04	7.500E+04	33	0
52	6.56E+09	3.28E+09	2.34E+05	2.930E+05	33	0
53	4.10E+09	2.05E+09	1.10E+05	1.375E+05	33	0
54	3.60E+09	1.80E+09	9.85E+04	1.231E+05	33	0
55	3.60E+09	1.80E+09	1.05E+05	1.313E+05	33	0
56	3.60E+09	1.80E+09	1.08E+05	1.350E+05	33	0
57	3.60E+09	1.80E+09	1.07E+05	1.331E+05	33	0
58	2.70E+09	1.35E+09	6.10E+04	7.625E+04	33	0
59	3.15E+09	1.58E+09	1.13E+05	1.406E+05	33	0
60	3.60E+09	1.80E+09	1.07E+05	1.331E+05	33	0
61	5.00E+09	2.50E+09	1.07E+05	1.331E+05	33	0
62	5.00E+09	2.50E+09	1.70E+05	2.125E+05	33	0
63	2.95E+09	1.48E+09	1.07E+05	1.331E+05	33	0
64	2.70E+09	1.35E+09	1.07E+05	1.331E+05	33	0
65	5.01E+09	2.51E+09	1.71E+05	2.138E+05	33	0
66	1.95E+09	9.75E+08	5.70E+04	7.125E+04	33	0
67	4.45E+09	2.23E+09	1.70E+05	2.125E+05	33	0
68	4.15E+09	2.08E+09	1.10E+05	1.375E+05	33	0
69	4.15E+09	2.08E+09	1.11E+06	1.388E+06	33	0
70	4.15E+09	2.08E+09	1.12E+05	1.400E+05	33	0
71	2.10E+09	1.05E+09	5.00E+04	6.250E+04	33	0
72	4.80E+09	2.40E+09	1.70E+05	2.125E+05	33	0
73	3.75E+09	1.88E+09	9.75E+04	1.219E+05	33	0
74	3.75E+09	1.88E+09	9.50E+04	1.188E+05	33	0
75	3.15E+09	1.58E+09	6.00E+04	7.500E+04	33	0
76	1.40E+09	7.00E+08	4.20E+04	5.250E+04	33	0
77	1.35E+09	6.75E+08	6.00E+04	7.500E+04	33	0
78	4.65E+09	2.33E+09	1.70E+05	2.125E+05	33	0
79	3.20E+09	1.60E+09	9.75E+04	1.219E+05	33	0

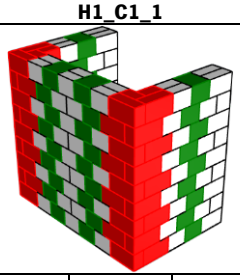
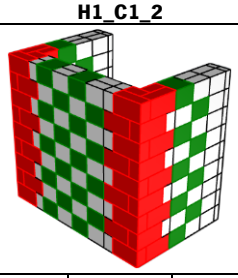
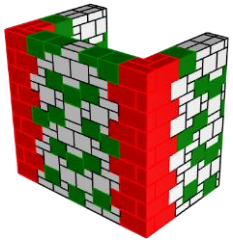
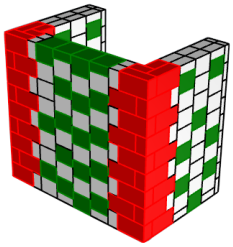
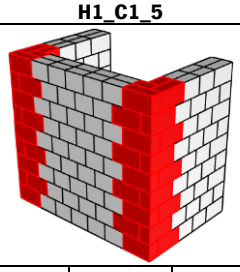
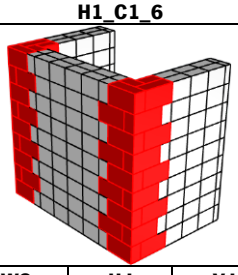
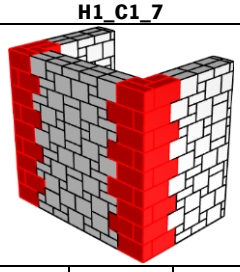
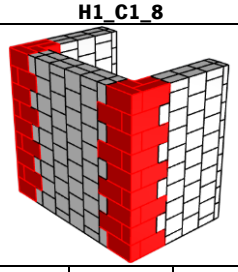
80	6.00E+09	3.00E+09	2.00E+05	2.500E+05	33	0
81	2.10E+09	1.05E+09	3.40E+04	4.250E+04	33	0
82	3.70E+09	1.85E+09	1.70E+05	2.125E+05	33	0
83	4.70E+09	2.35E+09	1.00E+05	1.250E+05	33	0
84	4.55E+09	2.28E+09	1.10E+05	1.375E+05	33	0
85	3.80E+09	1.90E+09	1.00E+05	1.250E+05	33	0
86	2.30E+00	1.15E+00	1.10E+05	1.375E+05	33	0
87	3.25E+09	1.63E+09	1.10E+05	1.375E+05	33	0
88	4.90E+09	2.45E+09	1.75E+05	2.188E+05	33	0
89	4.15E+09	2.08E+09	1.13E+05	1.413E+05	33	0
90	2.36E+09	1.18E+09	8.44E+04	1.055E+05	33	0
91	3.65E+09	1.83E+09	8.55E+04	1.069E+05	33	0
92	4.35E+10	2.18E+10	9.75E+04	1.219E+05	33	0
93	2.10E+09	1.05E+09	4.00E+04	5.000E+04	33	0
94	2.95E+09	1.48E+09	1.10E+05	1.375E+05	33	0
95	2.00E+09	1.00E+09	5.65E+04	7.063E+04	33	0
96	3.60E+09	1.80E+09	1.55E+05	1.938E+05	33	0
97	3.60E+09	1.80E+09	1.55E+05	1.938E+05	33	0
98	4.95E+09	2.48E+09	9.75E+04	1.219E+05	33	0
99	1.95E+09	9.75E+08	6.00E+04	7.500E+04	33	0
100	3.10E+08	1.55E+08	6.00E+04	7.500E+04	33	0

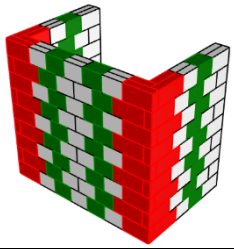
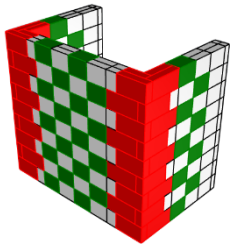
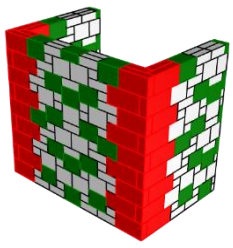
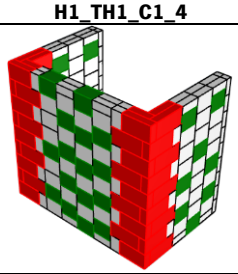
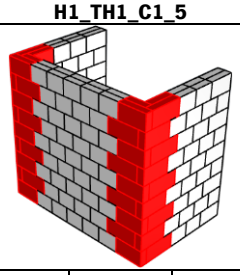
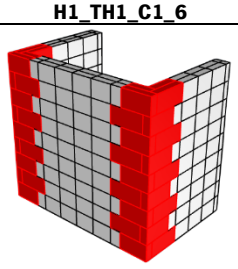
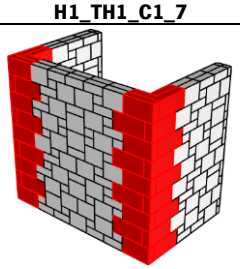
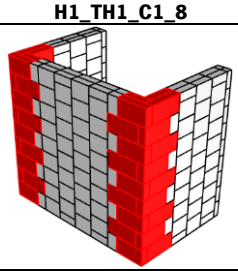
Annex 3.7 – Set 1 3D Models (good corner interlock)

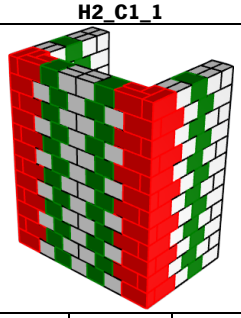
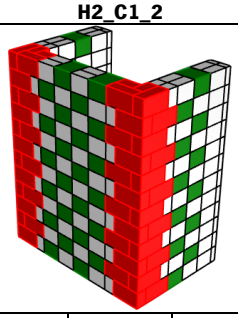
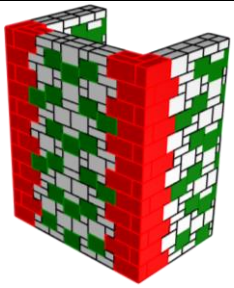
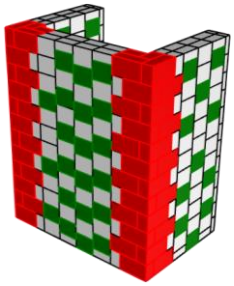
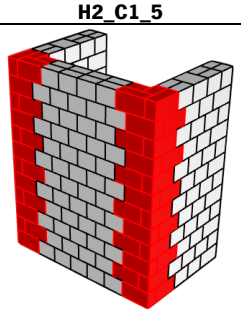
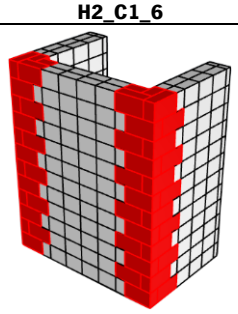
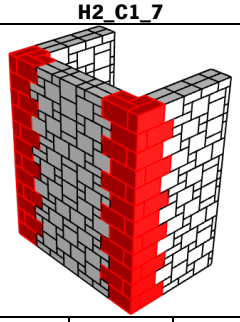
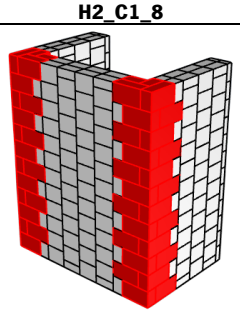
NOTE: Regular stone units are highlighted in light grey colour, corner stones are highlighted in red colour, and through-stones are highlighted in green colour.

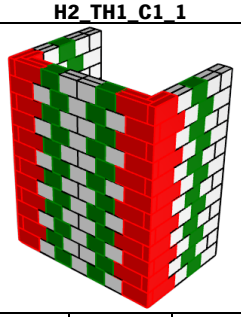
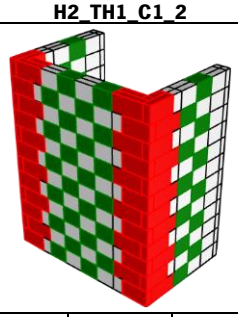
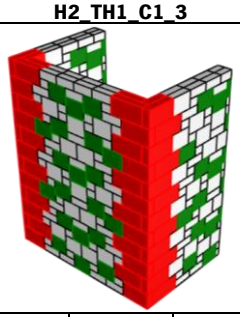
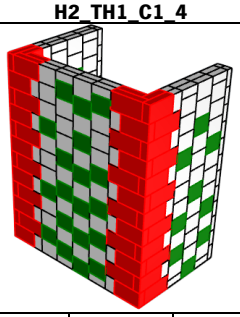
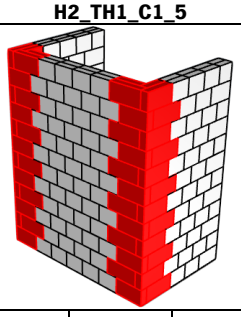
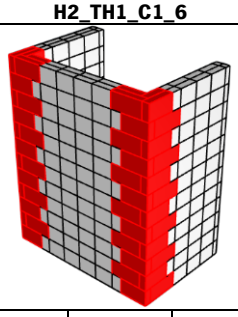
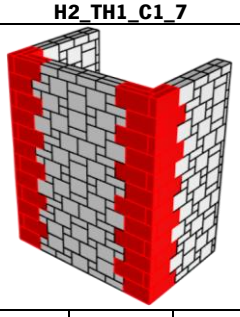
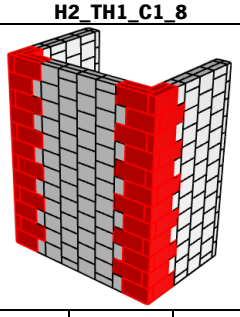
REF_C1_1			REF_C1_2			REF_C1_3			REF_C1_4		
											
WC	**HJ**	**VJ**	**WC**	**HJ**	**VJ**	**WC**	**HJ**	**VJ**	**WC**	**HJ**	**VJ**
F	F	F	F	F	NF	F	NF	F	F	NF	NF
REF_C1_5			**REF_C1_6**			**REF_C1_7**			**REF_C1_8**		
											
WC	**HJ**	**VJ**	**WC**	**HJ**	**VJ**	**WC**	**HJ**	**VJ**	**WC**	**HJ**	**VJ**
NF	F	F	NF	F	NF	NF	NF	F	NF	NF	NF

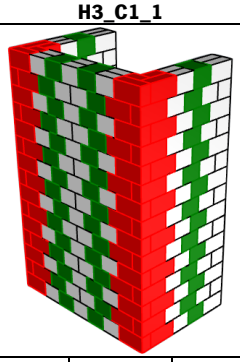
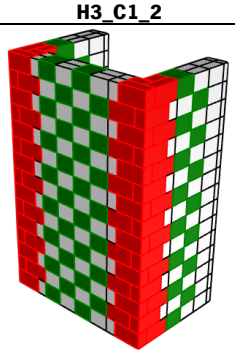
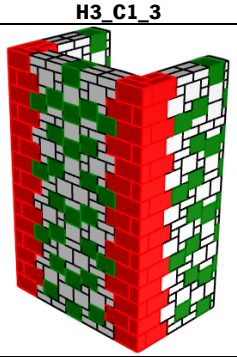
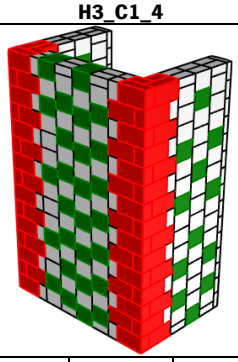
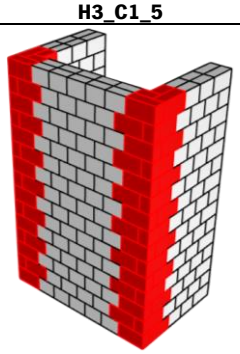
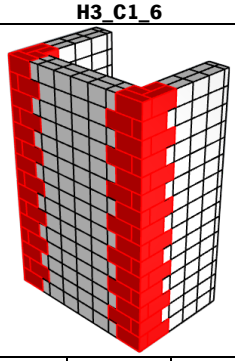
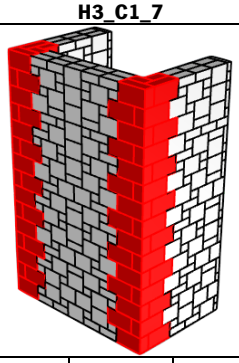
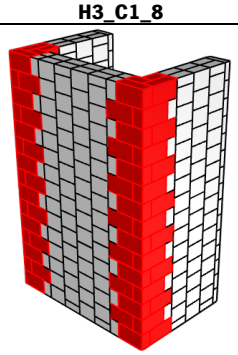
REF_TH1_C1_1			REF_TH1_C1_2			REF_TH1_C1_3			REF_TH1_C1_4		
											
WC	**HJ**	**VJ**	**WC**	**HJ**	**VJ**	**WC**	**HJ**	**VJ**	**WC**	**HJ**	**VJ**
F	F	F	F	F	NF	F	NF	F	F	NF	NF
REF_TH1_C1_5			**REF_TH1_C1_6**			**REF_TH1_C1_7**			**REF_TH1_C1_8**		
											
WC	**HJ**	**VJ**	**WC**	**HJ**	**VJ**	**WC**	**HJ**	**VJ**	**WC**	**HJ**	**VJ**
NF	F	F	NF	F	NF	NF	NF	F	NF	NF	NF

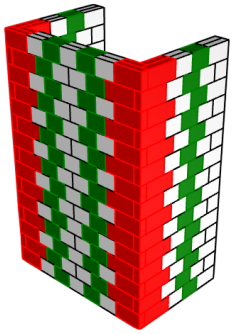
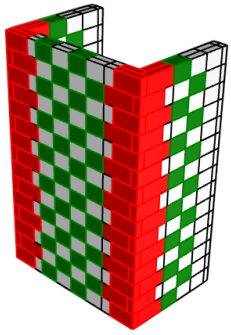
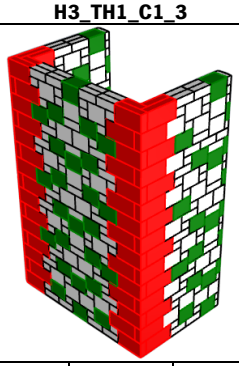
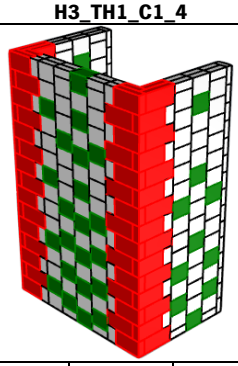
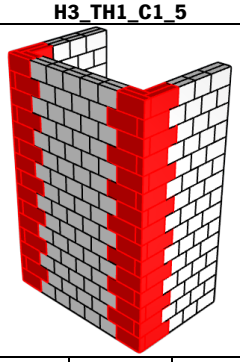
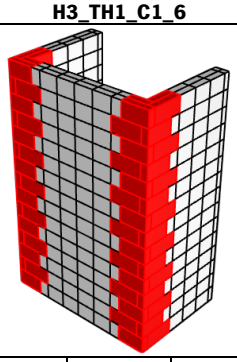
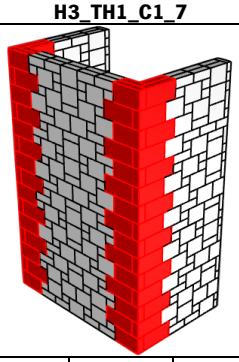
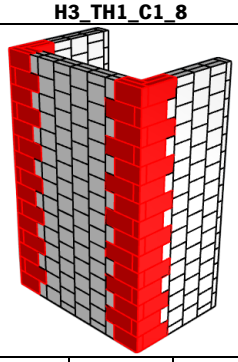
H1_C1_1			H1_C1_2			H1_C1_3			H1_C1_4		
											
WC	**HJ**	**VJ**	**WC**	**HJ**	**VJ**	**WC**	**HJ**	**VJ**	**WC**	**HJ**	**VJ**
F	F	F	F	F	NF	F	NF	F	F	NF	NF
H1_C1_5			**H1_C1_6**			**H1_C1_7**			**H1_C1_8**		
											
WC	**HJ**	**VJ**	**WC**	**HJ**	**VJ**	**WC**	**HJ**	**VJ**	**WC**	**HJ**	**VJ**
NF	F	F	NF	F	NF	NF	NF	F	NF	NF	NF

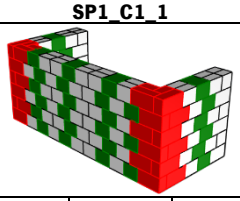
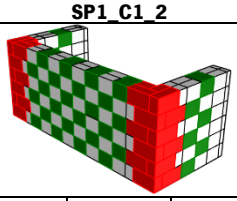
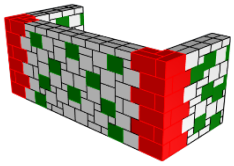
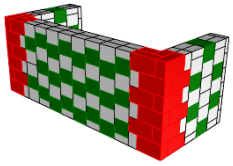
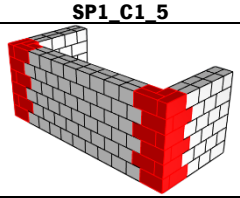
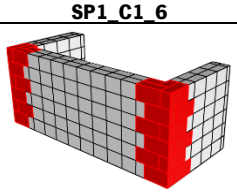
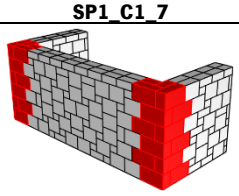
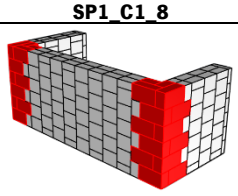
H1_TH1_C1_1			H1_TH1_C1_2			H1_TH1_C1_3			H1_TH1_C1_4		
											
WC	**HJ**	**VJ**	**WC**	**HJ**	**VJ**	**WC**	**HJ**	**VJ**	**WC**	**HJ**	**VJ**
F	F	F	F	F	NF	F	NF	F	F	NF	NF
H1_TH1_C1_5			**H1_TH1_C1_6**			**H1_TH1_C1_7**			**H1_TH1_C1_8**		
											
WC	**HJ**	**VJ**	**WC**	**HJ**	**VJ**	**WC**	**HJ**	**VJ**	**WC**	**HJ**	**VJ**
NF	F	F	NF	F	NF	NF	NF	F	NF	NF	NF

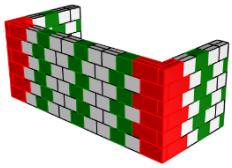
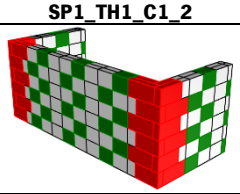
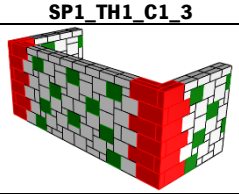
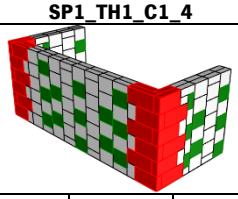
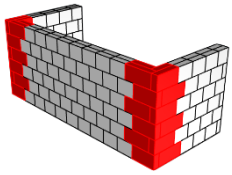
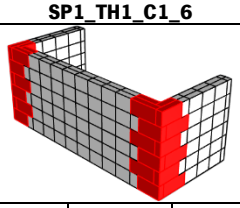
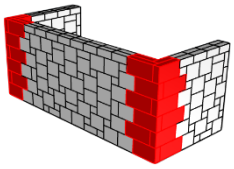
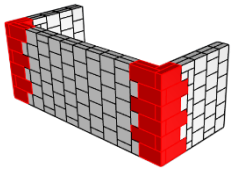
H2_C1_1			H2_C1_2			H2_C1_3			H2_C1_4		
											
WC	**HJ**	**VJ**	**WC**	**HJ**	**VJ**	**WC**	**HJ**	**VJ**	**WC**	**HJ**	**VJ**
F	F	F	F	F	NF	F	NF	F	F	NF	NF
H2_C1_5			**H2_C1_6**			**H2_C1_7**			**H2_C1_8**		
											
WC	**HJ**	**VJ**	**WC**	**HJ**	**VJ**	**WC**	**HJ**	**VJ**	**WC**	**HJ**	**VJ**
NF	F	F	NF	F	NF	NF	NF	F	NF	NF	NF

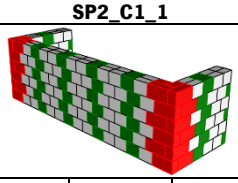
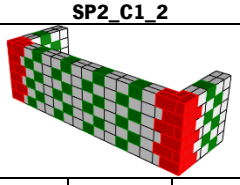
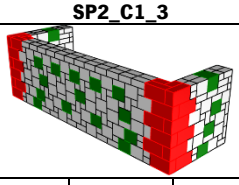
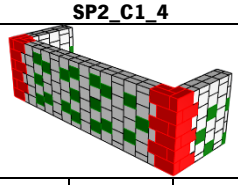
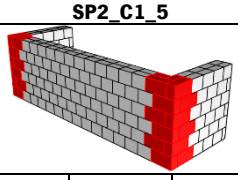
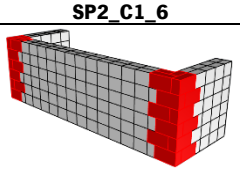
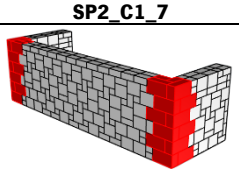
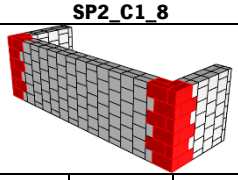
H2_TH1_C1_1			H2_TH1_C1_2			H2_TH1_C1_3			H2_TH1_C1_4		
											
WC	**HJ**	**VJ**	**WC**	**HJ**	**VJ**	**WC**	**HJ**	**VJ**	**WC**	**HJ**	**VJ**
F	F	F	F	F	NF	F	NF	F	F	NF	NF
H2_TH1_C1_5			**H2_TH1_C1_6**			**H2_TH1_C1_7**			**H2_TH1_C1_8**		
											
WC	**HJ**	**VJ**	**WC**	**HJ**	**VJ**	**WC**	**HJ**	**VJ**	**WC**	**HJ**	**VJ**
NF	F	F	NF	F	NF	NF	NF	F	NF	NF	NF

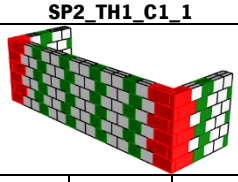
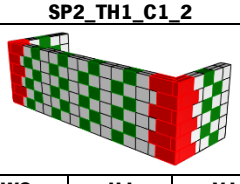
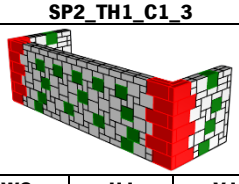
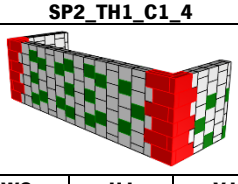
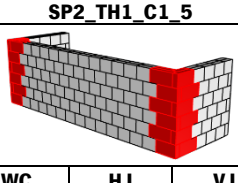
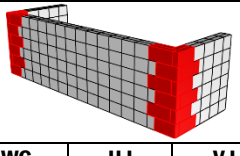
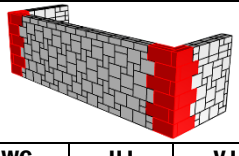
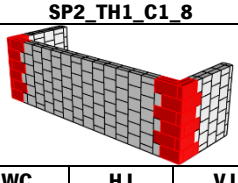
H3_C1_1			H3_C1_2			H3_C1_3			H3_C1_4		
											
WC	**HJ**	**VJ**	**WC**	**HJ**	**VJ**	**WC**	**HJ**	**VJ**	**WC**	**HJ**	**VJ**
F	F	F	F	F	NF	F	NF	F	F	NF	NF
H3_C1_5			**H3_C1_6**			**H3_C1_7**			**H3_C1_8**		
											
WC	**HJ**	**VJ**	**WC**	**HJ**	**VJ**	**WC**	**HJ**	**VJ**	**WC**	**HJ**	**VJ**
NF	F	F	NF	F	NF	NF	NF	F	NF	NF	NF

H3_TH1_C1_1			H3_TH1_C1_2			H3_TH1_C1_3			H3_TH1_C1_4		
											
WC	**HJ**	**VJ**	**WC**	**HJ**	**VJ**	**WC**	**HJ**	**VJ**	**WC**	**HJ**	**VJ**
F	F	F	F	F	NF	F	NF	F	F	NF	NF
H3_TH1_C1_5			**H3_TH1_C1_6**			**H3_TH1_C1_7**			**H3_TH1_C1_8**		
											
WC	**HJ**	**VJ**	**WC**	**HJ**	**VJ**	**WC**	**HJ**	**VJ**	**WC**	**HJ**	**VJ**
NF	F	F	NF	F	NF	NF	NF	F	NF	NF	NF

SP1_C1_1			SP1_C1_2			SP1_C1_3			SP1_C1_4		
											
WC	**HJ**	**VJ**	**WC**	**HJ**	**VJ**	**WC**	**HJ**	**VJ**	**WC**	**HJ**	**VJ**
F	F	F	F	F	NF	F	NF	F	F	NF	NF
SP1_C1_5			**SP1_C1_6**			**SP1_C1_7**			**SP1_C1_8**		
											
WC	**HJ**	**VJ**	**WC**	**HJ**	**VJ**	**WC**	**HJ**	**VJ**	**WC**	**HJ**	**VJ**
NF	F	F	NF	F	NF	NF	NF	F	NF	NF	NF

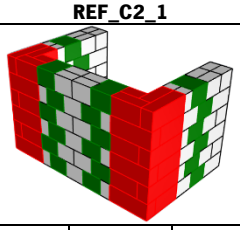
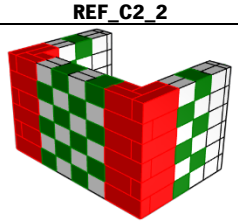
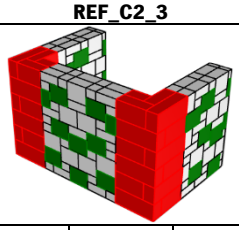
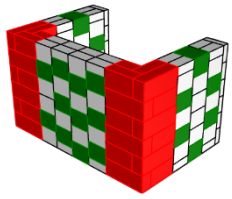
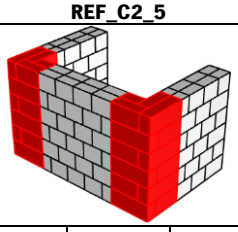
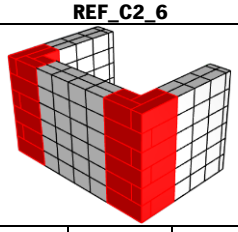
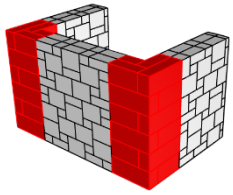
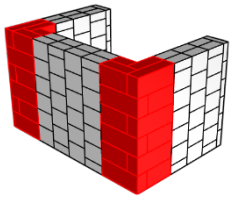
SP1_TH1_C1_1			SP1_TH1_C1_2			SP1_TH1_C1_3			SP1_TH1_C1_4		
											
WC	**HJ**	**VJ**	**WC**	**HJ**	**VJ**	**WC**	**HJ**	**VJ**	**WC**	**HJ**	**VJ**
F	F	F	F	F	NF	F	NF	F	F	NF	NF
SP1_TH1_C1_5			**SP1_TH1_C1_6**			**SP1_TH1_C1_7**			**SP1_TH1_C1_8**		
											
WC	**HJ**	**VJ**	**WC**	**HJ**	**VJ**	**WC**	**HJ**	**VJ**	**WC**	**HJ**	**VJ**
NF	F	F	NF	F	NF	NF	NF	F	NF	NF	NF

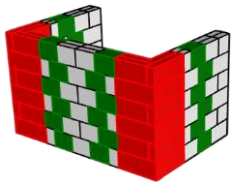
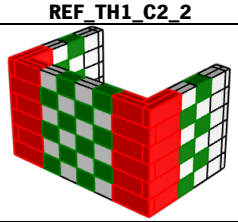
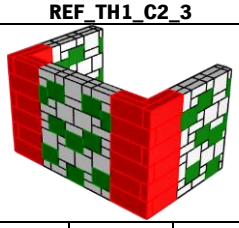
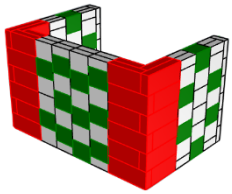
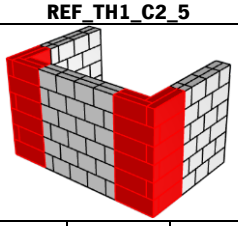
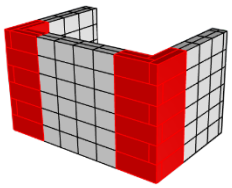
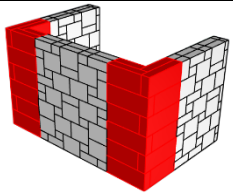
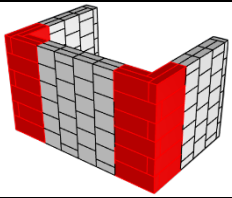
SP2_C1_1			SP2_C1_2			SP2_C1_3			SP2_C1_4		
											
WC	**HJ**	**VJ**	**WC**	**HJ**	**VJ**	**WC**	**HJ**	**VJ**	**WC**	**HJ**	**VJ**
F	F	F	F	F	NF	F	NF	F	F	NF	NF
SP2_C1_5			**SP2_C1_6**			**SP2_C1_7**			**SP2_C1_8**		
											
WC	**HJ**	**VJ**	**WC**	**HJ**	**VJ**	**WC**	**HJ**	**VJ**	**WC**	**HJ**	**VJ**
NF	F	F	NF	F	NF	NF	NF	F	NF	NF	NF

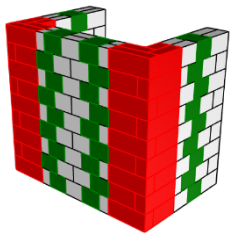
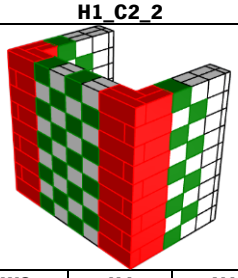
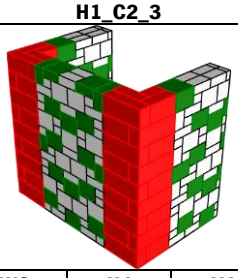
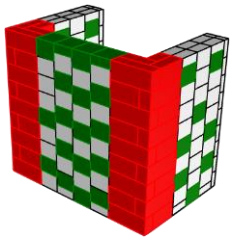
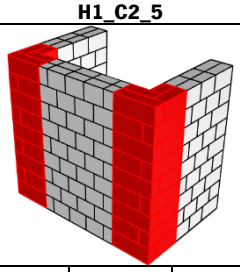
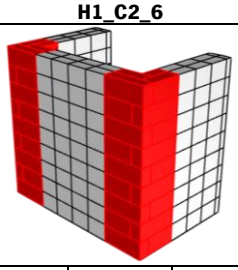
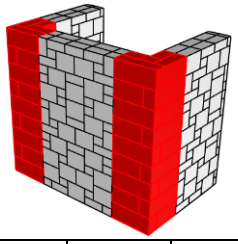
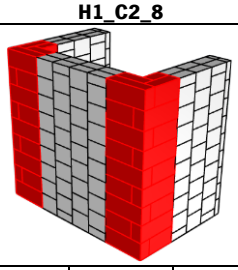
SP2_TH1_C1_1			SP2_TH1_C1_2			SP2_TH1_C1_3			SP2_TH1_C1_4		
											
WC	**HJ**	**VJ**	**WC**	**HJ**	**VJ**	**WC**	**HJ**	**VJ**	**WC**	**HJ**	**VJ**
F	F	F	F	F	NF	F	NF	F	F	NF	NF
SP2_TH1_C1_5			**SP2_TH1_C1_6**			**SP2_TH1_C1_7**			**SP2_TH1_C1_8**		
											
WC	**HJ**	**VJ**	**WC**	**HJ**	**VJ**	**WC**	**HJ**	**VJ**	**WC**	**HJ**	**VJ**
NF	F	F	NF	F	NF	NF	NF	F	NF	NF	NF

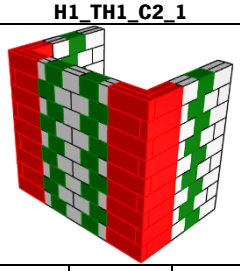
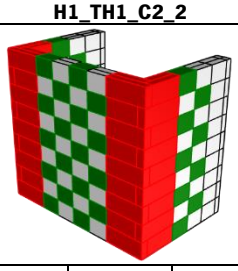
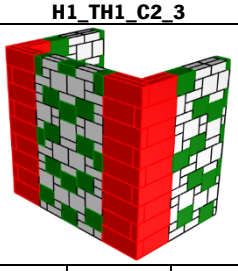
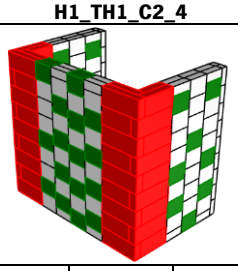
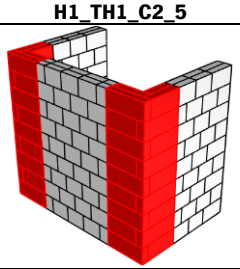
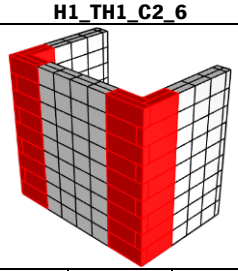
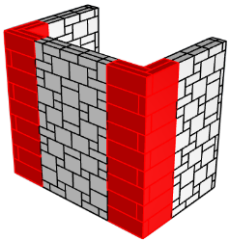
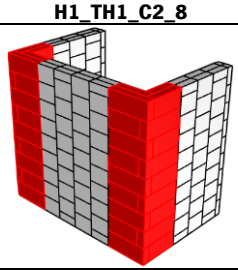
Annex 3.8 – Set 2 3D Models (ineffective corner interlock)

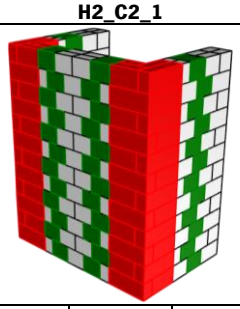
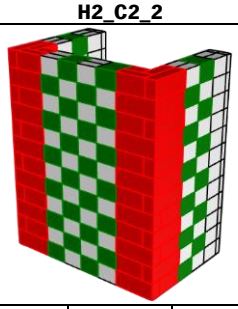
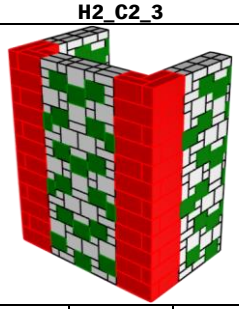
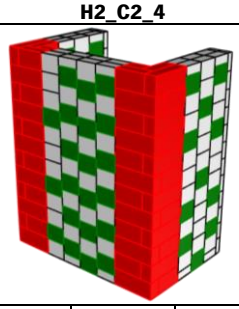
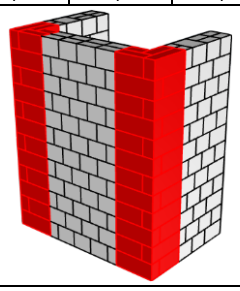
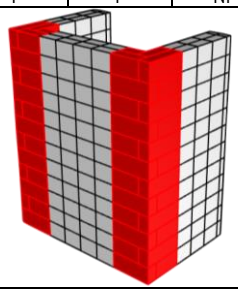
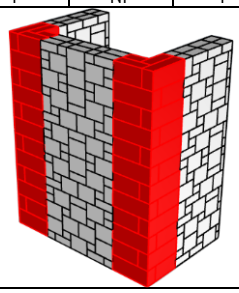
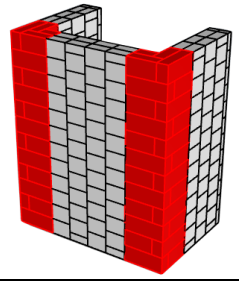
NOTE: Regular stone units are highlighted in light grey colour, corner stones are highlighted in red colour, and through-stones are highlighted in green colour.

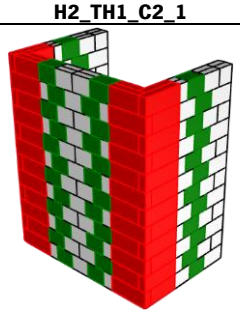
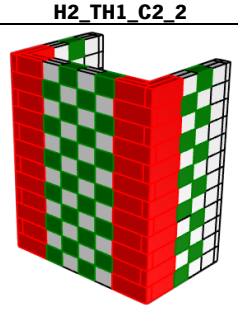
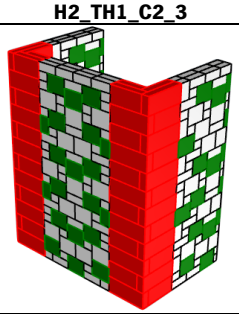
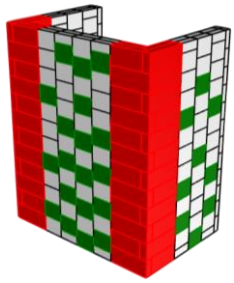
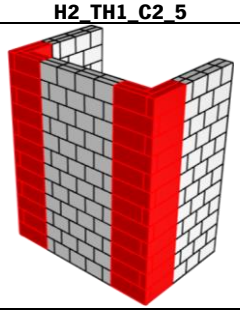
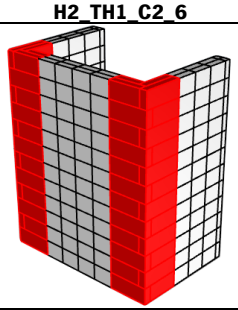
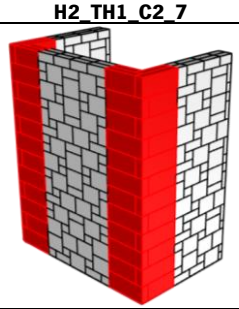
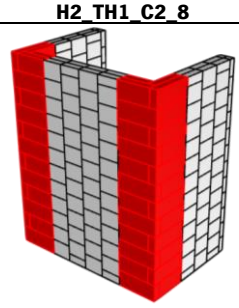
REF_C2_1			REF_C2_2			REF_C2_3			REF_C2_4		
											
WC	**HJ**	**VJ**	**WC**	**HJ**	**VJ**	**WC**	**HJ**	**VJ**	**WC**	**HJ**	**VJ**
F	F	F	F	F	NF	F	NF	F	F	NF	NF
REF_C2_5			**REF_C2_6**			**REF_C2_7**			**REF_C2_8**		
											
WC	**HJ**	**VJ**	**WC**	**HJ**	**VJ**	**WC**	**HJ**	**VJ**	**WC**	**HJ**	**VJ**
NF	F	F	NF	F	NF	NF	NF	F	NF	NF	NF

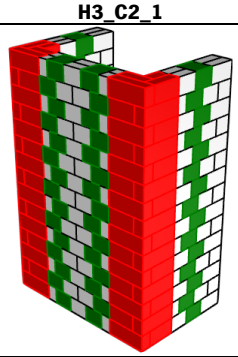
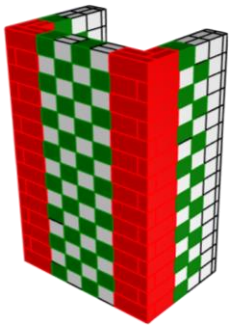
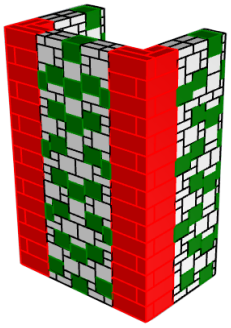
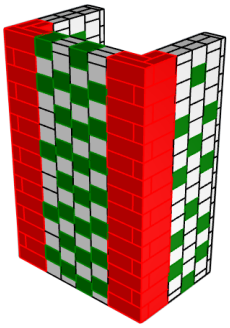
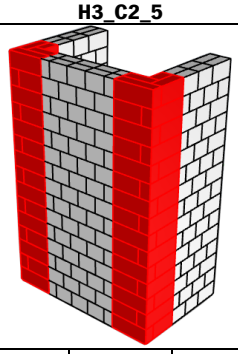
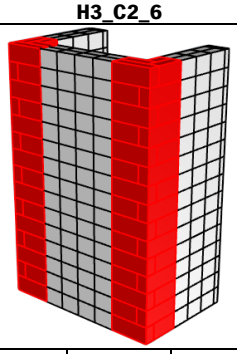
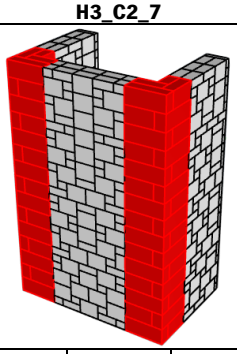
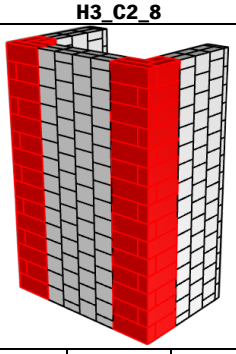
REF_TH1_C2_1			REF_TH1_C2_2			REF_TH1_C2_3			REF_TH1_C2_4		
											
WC	**HJ**	**VJ**	**WC**	**HJ**	**VJ**	**WC**	**HJ**	**VJ**	**WC**	**HJ**	**VJ**
F	F	F	F	F	NF	F	NF	F	F	NF	NF
REF_TH1_C2_5			**REF_TH1_C2_6**			**REF_TH1_C2_7**			**REF_TH1_C2_8**		
											
WC	**HJ**	**VJ**	**WC**	**HJ**	**VJ**	**WC**	**HJ**	**VJ**	**WC**	**HJ**	**VJ**
NF	F	F	NF	F	NF	NF	NF	F	NF	NF	NF

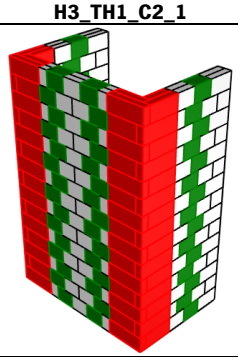
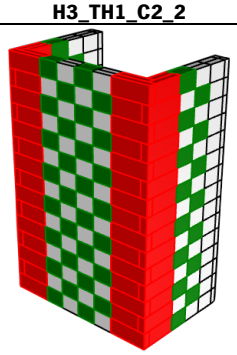
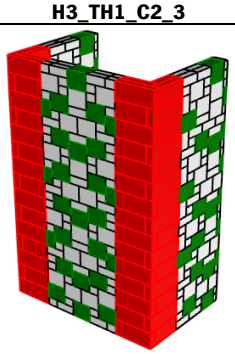
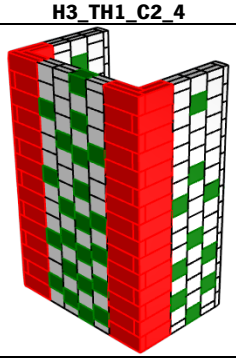
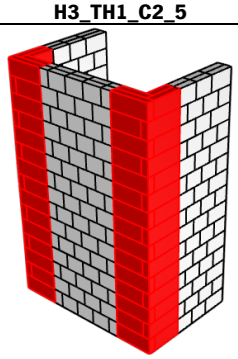
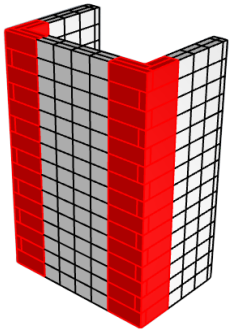
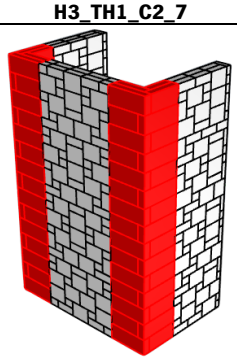
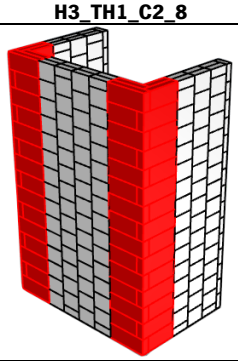
H1_C2_1			H1_C2_2			H1_C2_3			H1_C2_4		
											
WC	**HJ**	**VJ**	**WC**	**HJ**	**VJ**	**WC**	**HJ**	**VJ**	**WC**	**HJ**	**VJ**
F	F	F	F	F	NF	F	NF	F	F	NF	NF
H1_C2_5			**H1_C2_6**			**H1_C2_7**			**H1_C2_8**		
											
WC	**HJ**	**VJ**	**WC**	**HJ**	**VJ**	**WC**	**HJ**	**VJ**	**WC**	**HJ**	**VJ**
NF	F	F	NF	F	NF	NF	NF	F	NF	NF	NF

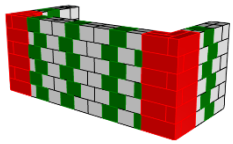
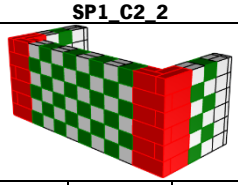
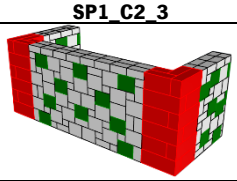
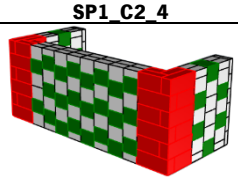
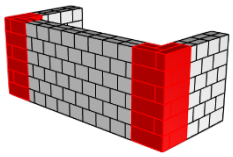
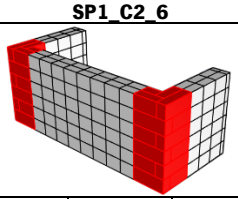
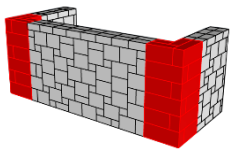
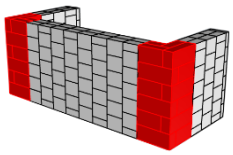
H1_TH1_C2_1			H1_TH1_C2_2			H1_TH1_C2_3			H1_TH1_C2_4		
											
WC	**HJ**	**VJ**	**WC**	**HJ**	**VJ**	**WC**	**HJ**	**VJ**	**WC**	**HJ**	**VJ**
F	F	F	F	F	NF	F	NF	F	F	NF	NF
H1_TH1_C2_5			**H1_TH1_C2_6**			**H1_TH1_C2_7**			**H1_TH1_C2_8**		
											
WC	**HJ**	**VJ**	**WC**	**HJ**	**VJ**	**WC**	**HJ**	**VJ**	**WC**	**HJ**	**VJ**
NF	F	F	NF	F	NF	NF	NF	F	NF	NF	NF

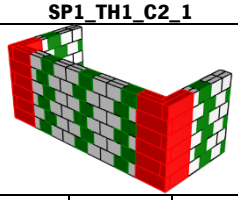
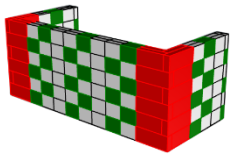
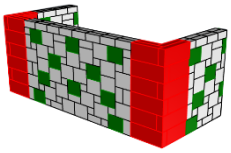
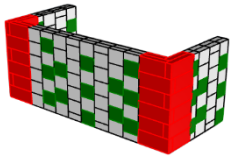
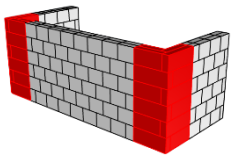
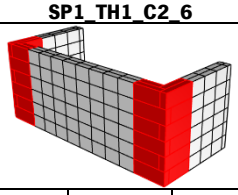
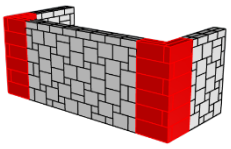
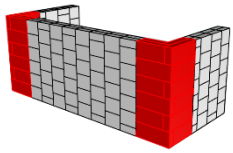
H2_C2_1			H2_C2_2			H2_C2_3			H2_C2_4		
											
WC	**HJ**	**VJ**	**WC**	**HJ**	**VJ**	**WC**	**HJ**	**VJ**	**WC**	**HJ**	**VJ**
F	F	F	F	F	NF	F	NF	F	F	NF	NF
											
H2_C2_5			**H2_C2_6**			**H2_C2_7**			**H2_C2_8**		
WC	**HJ**	**VJ**	**WC**	**HJ**	**VJ**	**WC**	**HJ**	**VJ**	**WC**	**HJ**	**VJ**
NF	F	F	NF	F	NF	NF	NF	F	NF	NF	NF

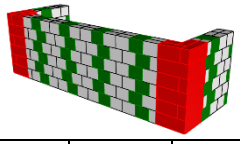
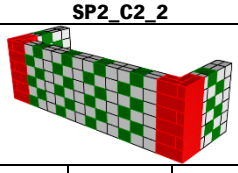
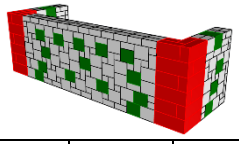
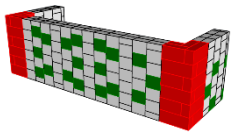
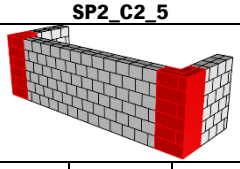
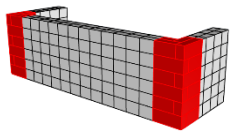
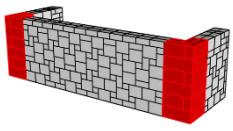
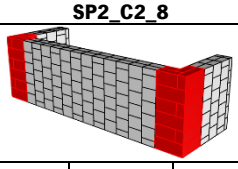
H2_TH1_C2_1			H2_TH1_C2_2			H2_TH1_C2_3			H2_TH1_C2_4		
											
WC	**HJ**	**VJ**	**WC**	**HJ**	**VJ**	**WC**	**HJ**	**VJ**	**WC**	**HJ**	**VJ**
F	F	F	F	F	NF	F	NF	F	F	NF	NF
H2_TH1_C2_5			**H2_TH1_C2_6**			**H2_TH1_C2_7**			**H2_TH1_C2_8**		
											
WC	**HJ**	**VJ**	**WC**	**HJ**	**VJ**	**WC**	**HJ**	**VJ**	**WC**	**HJ**	**VJ**
NF	F	F	NF	F	NF	NF	NF	F	NF	NF	NF

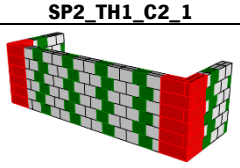
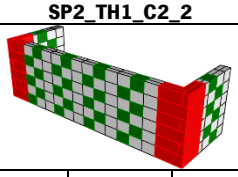
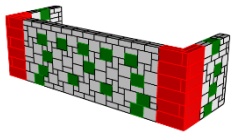
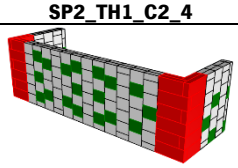
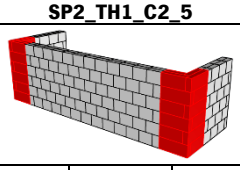
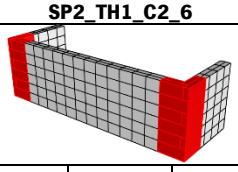
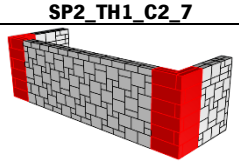
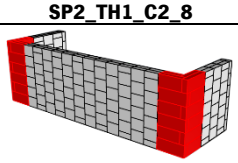
H3_C2_1			H3_C2_2			H3_C2_3			H3_C2_4		
											
WC	**HJ**	**VJ**	**WC**	**HJ**	**VJ**	**WC**	**HJ**	**VJ**	**WC**	**HJ**	**VJ**
F	F	F	F	F	NF	F	NF	F	F	NF	NF
H3_C2_5			**H3_C2_6**			**H3_C2_7**			**H3_C2_8**		
											
WC	**HJ**	**VJ**	**WC**	**HJ**	**VJ**	**WC**	**HJ**	**VJ**	**WC**	**HJ**	**VJ**
NF	F	F	NF	F	NF	NF	NF	F	NF	NF	NF

H3_TH1_C2_1			H3_TH1_C2_2			H3_TH1_C2_3			H3_TH1_C2_4		
											
WC	**HJ**	**VJ**	**WC**	**HJ**	**VJ**	**WC**	**HJ**	**VJ**	**WC**	**HJ**	**VJ**
F	F	F	F	F	NF	F	NF	F	F	NF	NF
H3_TH1_C2_5			**H3_TH1_C2_6**			**H3_TH1_C2_7**			**H3_TH1_C2_8**		
											
WC	**HJ**	**VJ**	**WC**	**HJ**	**VJ**	**WC**	**HJ**	**VJ**	**WC**	**HJ**	**VJ**
NF	F	F	NF	F	NF	NF	NF	F	NF	NF	NF

SP1_C2_1			SP1_C2_2			SP1_C2_3			SP1_C2_4		
											
WC	**HJ**	**VJ**	**WC**	**HJ**	**VJ**	**WC**	**HJ**	**VJ**	**WC**	**HJ**	**VJ**
F	F	F	F	F	NF	F	NF	F	F	NF	NF
SP1_C2_5			**SP1_C2_6**			**SP1_C2_7**			**SP1_C2_8**		
											
WC	**HJ**	**VJ**	**WC**	**HJ**	**VJ**	**WC**	**HJ**	**VJ**	**WC**	**HJ**	**VJ**
NF	F	F	NF	F	NF	NF	NF	F	NF	NF	NF

SP1_TH1_C2_1			SP1_TH1_C2_2			SP1_TH1_C2_3			SP1_TH1_C2_4		
											
WC	**HJ**	**VJ**	**WC**	**HJ**	**VJ**	**WC**	**HJ**	**VJ**	**WC**	**HJ**	**VJ**
F	F	F	F	F	NF	F	NF	F	F	NF	NF
SP1_TH1_C2_5			**SP1_TH1_C2_6**			**SP1_TH1_C2_7**			**SP1_TH1_C2_8**		
											
WC	**HJ**	**VJ**	**WC**	**HJ**	**VJ**	**WC**	**HJ**	**VJ**	**WC**	**HJ**	**VJ**
NF	F	F	NF	F	NF	NF	NF	F	NF	NF	NF

SP2_C2_1			SP2_C2_2			SP2_C2_3			SP2_C2_4		
											
WC	**HJ**	**VJ**	**WC**	**HJ**	**VJ**	**WC**	**HJ**	**VJ**	**WC**	**HJ**	**VJ**
F	F	F	F	F	NF	F	NF	F	F	NF	NF
SP2_C2_5			**SP2_C2_6**			**SP2_C2_7**			**SP2_C2_8**		
											
WC	**HJ**	**VJ**	**WC**	**HJ**	**VJ**	**WC**	**HJ**	**VJ**	**WC**	**HJ**	**VJ**
NF	F	F	NF	F	NF	NF	NF	F	NF	NF	NF

SP2_TH1_C2_1			SP2_TH1_C2_2			SP2_TH1_C2_3			SP2_TH1_C2_4		
											
WC	**HJ**	**VJ**	**WC**	**HJ**	**VJ**	**WC**	**HJ**	**VJ**	**WC**	**HJ**	**VJ**
F	F	F	F	F	NF	F	NF	F	F	NF	NF
SP2_TH1_C2_5			**SP2_TH1_C2_6**			**SP2_TH1_C2_7**			**SP2_TH1_C2_8**		
											
WC	**HJ**	**VJ**	**WC**	**HJ**	**VJ**	**WC**	**HJ**	**VJ**	**WC**	**HJ**	**VJ**
NF	F	F	NF	F	NF	NF	NF	F	NF	NF	NF

Annex 3.9 – Dataset empirical expression for the out-of-plane capacity estimation based on geometrical parameter

	A	B	C	D	E	F	G	H
MODEL_#	WC	HJ	VJ	CN	Slenderness	H/Span	Thick/Span	Max Load
REF_C1	1	1	1	1	4.5	0.6	0.13	282.03
REF_C1_2	1	1	0	1	4.5	0.6	0.13	276.13
REF_C1_3	1	0	1	1	4.5	0.6	0.13	270.28
REF_C1_4	1	0	0	1	4.5	0.6	0.13	217.4
REF_C1_5	0	1	1	1	4.5	0.6	0.13	276.16
REF_C1_6	0	1	0	1	4.5	0.6	0.13	276.16
REF_C1_7	0	0	1	1	4.5	0.6	0.13	276.16
REF_C1_8	0	0	0	1	4.5	0.6	0.13	211.5
REF_TH1_C1	1	1	1	1	6.75	0.6	0.09	192.02
REF_TH1_C1_2	1	1	0	1	6.75	0.6	0.09	175.68
REF_TH1_C1_3	1	0	1	1	6.75	0.6	0.09	171.6
REF_TH1_C1_4	1	0	0	1	6.75	0.6	0.09	134.82
REF_TH1_C1_5	0	1	1	1	6.75	0.6	0.09	171.6
REF_TH1_C1_6	0	1	0	1	6.75	0.6	0.09	171.6
REF_TH1_C1_7	0	0	1	1	6.75	0.6	0.09	167.51
REF_TH1_C1_8	0	0	0	1	6.75	0.6	0.09	134.82
REF_H1_C1	1	1	1	1	6.75	0.9	0.13	273.12
H1_C1_2	1	1	0	1	6.75	0.9	0.13	202.7
H1_C1_3	1	0	1	1	6.75	0.9	0.13	246.78
H1_C1_4	1	0	0	1	6.75	0.9	0.13	211.52
H1_C1_5	0	1	1	1	6.75	0.9	0.13	273.22
H1_C1_6	0	1	0	1	6.75	0.9	0.13	246.78
H1_C1_7	0	0	1	1	6.75	0.9	0.13	264.41
H1_C1_8	0	0	0	1	6.75	0.9	0.13	202.71
H1_TH1_C1	1	1	1	1	10.125	0.9	0.09	177.72
H1_TH1_C1_2	1	1	0	1	10.125	0.9	0.09	165.47
H1_TH1_C1_3	1	0	1	1	10.125	0.9	0.09	153.21
H1_TH1_C1_4	1	0	0	1	10.125	0.9	0.09	134.83
H1_TH1_C1_5	0	1	1	1	10.125	0.9	0.09	177.72
H1_TH1_C1_6	0	1	0	1	10.125	0.9	0.09	147.08
H1_TH1_C1_7	0	0	1	1	10.125	0.9	0.09	159.34
H1_TH1_C1_8	0	0	0	1	10.125	0.9	0.09	122.6
H2_C1	1	1	1	1	9	1.2	0.13	282.03
H2_C1_2	1	1	0	1	9	1.2	0.13	258.53
H2_C1_3	1	0	1	1	9	1.2	0.13	258.53
H2_C1_4	1	0	0	1	9	1.2	0.13	199.8

H2_C1_5	0	1	1	1	9	1.2	0.13	282.03
H2_C1_6	0	1	0	1	9	1.2	0.13	235.03
H2_C1_7	0	0	1	1	9	1.2	0.13	258.53
H2_C1_8	0	0	0	1	9	1.2	0.13	188
H2_TH1_C1	1	1	1	1	13.5	1.2	0.09	196.11
H2_TH1_C1_2	1	1	0	1	13.5	1.2	0.09	187.94
H2_TH1_C1_3	1	0	1	1	13.5	1.2	0.09	171.6
H2_TH1_C1_4	1	0	0	1	13.5	1.2	0.09	130.74
H2_TH1_C1_5	0	1	1	1	13.5	1.2	0.09	196.11
H2_TH1_C1_6	0	1	0	1	13.5	1.2	0.09	187.94
H2_TH1_C1_7	0	0	1	1	13.5	1.2	0.09	179.77
H2_TH1_C1_8	0	0	0	1	13.5	1.2	0.09	122.57
H3_C1	1	1	1	1	11.25	1.5	0.13	279.1
H3_C1_2	1	1	0	1	11.25	1.5	0.13	264.4
H3_C1_3	1	0	1	1	11.25	1.5	0.13	249.72
H3_C1_4	1	0	0	1	11.25	1.5	0.13	176.3
H3_C1_5	0	1	1	1	11.25	1.5	0.13	279.1
H3_C1_6	0	1	0	1	11.25	1.5	0.13	264.4
H3_C1_7	0	0	1	1	11.25	1.5	0.13	235.03
H3_C1_8	0	0	0	1	11.25	1.5	0.13	161.58
H3_TH1_C1	1	1	1	1	16.875	1.5	0.09	194.07
H3_TH1_C1_2	1	1	0	1	16.875	1.5	0.09	163.43
H3_TH1_C1_3	1	0	1	1	16.875	1.5	0.09	173.64
H3_TH1_C1_4	1	0	0	1	16.875	1.5	0.09	112.35
H3_TH1_C1_5	0	1	1	1	16.875	1.5	0.09	194.07
H3_TH1_C1_6	0	1	0	1	16.875	1.5	0.09	173.64
H3_TH1_C1_7	0	0	1	1	16.875	1.5	0.09	173.64
H3_TH1_C1_8	0	0	0	1	16.875	1.5	0.09	102.41
SP1_C1	1	1	1	1	4.5	0.4	0.09	277.3
SP1_C1_2	1	1	0	1	4.5	0.4	0.09	262.7
SP1_C1_3	1	0	1	1	4.5	0.4	0.09	248.11
SP1_C1_4	1	0	0	1	4.5	0.4	0.09	218.92
SP1_C1_5	0	1	1	1	4.5	0.4	0.09	248.11
SP1_C1_6	0	1	0	1	4.5	0.4	0.09	255.41
SP1_C1_7	0	0	1	1	4.5	0.4	0.09	240.82
SP1_C1_8	0	0	0	1	4.5	0.4	0.09	197.03
SP1_TH1_C1	1	1	1	1	6.75	0.4	0.06	151
SP1_TH1_C1_2	1	1	0	1	6.75	0.4	0.06	151
SP1_TH1_C1_3	1	0	1	1	6.75	0.4	0.06	145.97
SP1_TH1_C1_4	1	0	0	1	6.75	0.4	0.06	151
SP1_TH1_C1_5	0	1	1	1	6.75	0.4	0.06	151

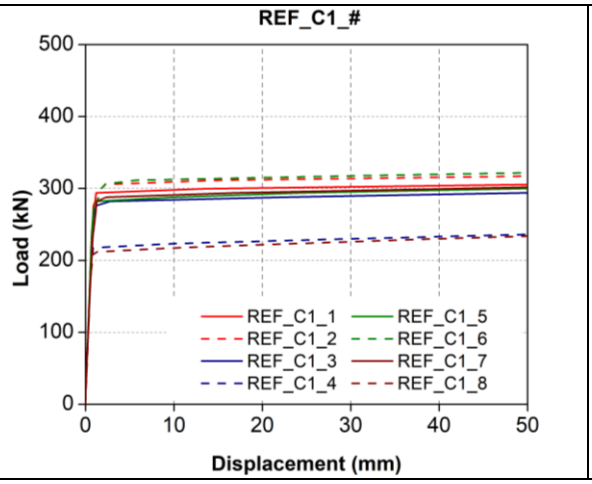
SP1_TH1_C1_6	0	1	0	1	6.75	0.4	0.06	151
SP1_TH1_C1_7	0	0	1	1	6.75	0.4	0.06	146
SP1_TH1_C1_8	0	0	0	1	6.75	0.4	0.06	146
SP2_C1	1	1	1	1	4.5	0.3	0.07	261.56
SP2_C1_2	1	1	0	1	4.5	0.3	0.07	252.85
SP2_C1_3	1	0	1	1	4.5	0.3	0.07	244.13
SP2_C1_4	1	0	0	1	4.5	0.3	0.07	191.82
SP2_C1_5	0	1	1	1	4.5	0.3	0.07	235.41
SP2_C1_6	0	1	0	1	4.5	0.3	0.07	261
SP2_C1_7	0	0	1	1	4.5	0.3	0.07	235.41
SP2_C1_8	0	0	0	1	4.5	0.3	0.07	191.82
SP2_TH1_C1	1	1	1	1	6.75	0.3	0.04	149.53
SP2_TH1_C1_2	1	1	0	1	6.75	0.3	0.04	149.53
SP2_TH1_C1_3	1	0	1	1	6.75	0.3	0.04	137.56
SP2_TH1_C1_4	1	0	0	1	6.75	0.3	0.04	131.6
SP2_TH1_C1_5	0	1	1	1	6.75	0.3	0.04	149.53
SP2_TH1_C1_6	0	1	0	1	6.75	0.3	0.04	149.53
SP2_TH1_C1_7	0	0	1	1	6.75	0.3	0.04	137.56
SP2_TH1_C1_8	0	0	0	1	6.75	0.3	0.04	131.6
REF_C2	1	1	1	0	4.5	0.6	0.13	269.7
REF_C2_2	1	1	0	0	4.5	0.6	0.13	244.72
REF_C2_3	1	0	1	0	4.5	0.6	0.13	244.72
REF_C2_4	1	0	0	0	4.5	0.6	0.13	209.76
REF_C2_5	0	1	1	0	4.5	0.6	0.13	249.72
REF_C2_6	0	1	0	0	4.5	0.6	0.13	244.72
REF_C2_7	0	0	1	0	4.5	0.6	0.13	249.72
REF_C2_8	0	0	0	0	4.5	0.6	0.13	199.78
RGW_TH1_C2	1	1	1	0	6.75	0.6	0.09	180.58
REF_TH1_C2_2	1	1	0	0	6.75	0.6	0.09	170.17
REF_TH1_C2_3	1	0	1	0	6.75	0.6	0.09	163.22
REF_TH1_C2_4	1	0	0	0	6.75	0.6	0.09	149.3
REF_TH1_C2_5	0	1	1	0	6.75	0.6	0.09	180.58
REF_TH1_C2_6	0	1	0	0	6.75	0.6	0.09	177.1
REF_TH1_C2_7	0	0	1	0	6.75	0.6	0.09	163.12
REF_TH1_C2_8	0	0	0	0	6.75	0.6	0.09	138.92
H1_C2	1	1	1	0	6.75	0.9	0.13	262.21
H1_C2_2	1	1	0	0	6.75	0.9	0.13	254.7
H1_C2_3	1	0	1	0	6.75	0.9	0.13	254.71
H1_C2_4	1	0	0	0	6.75	0.9	0.13	187.3
H1_C2_5	0	1	1	0	6.75	0.9	0.13	262.21
H1_C2_6	0	1	0	0	6.75	0.9	0.13	254.7

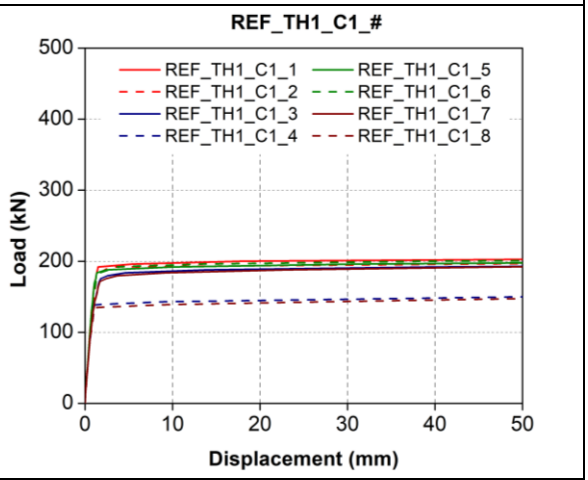
H1_C2_7	0	0	1	0	6.75	0.9	0.13	247.22
H1_C2_8	0	0	0	0	6.75	0.9	0.13	179.8
H1_TH1_C2	1	1	1	0	10.125	0.9	0.09	177.11
H1_TH1_C2_2	1	1	0	0	10.125	0.9	0.09	166.7
H1_TH1_C2_3	1	0	1	0	10.125	0.9	0.09	151.07
H1_TH1_C2_4	1	0	0	0	10.125	0.9	0.09	119.81
H1_TH1_C2_5	0	1	1	0	10.125	0.9	0.09	177.11
H1_TH1_C2_6	0	1	0	0	10.125	0.9	0.09	171.9
H1_TH1_C2_7	0	0	1	0	10.125	0.9	0.09	177.11
H1_TH1_C2_8	0	0	0	0	10.125	0.9	0.09	119.81
H2_C2	1	1	1	0	9	1.2	0.13	269.7
H2_C2_2	1	1	0	0	9	1.2	0.13	249.72
H2_C2_3	1	0	1	0	9	1.2	0.13	259.71
H2_C2_4	1	0	0	0	9	1.2	0.13	169.81
H2_C2_5	0	1	1	0	9	1.2	0.13	269.7
H2_C2_6	0	1	0	0	9	1.2	0.13	249.72
H2_C2_7	0	0	1	0	9	1.2	0.13	259.71
H2_C2_8	0	0	0	0	9	1.2	0.13	169.81
H2_TH1_C2	1	1	1	0	13.5	1.2	0.09	152.8
H2_TH1_C2_2	1	1	0	0	13.5	1.2	0.09	131.97
H2_TH1_C2_3	1	0	1	0	13.5	1.2	0.09	138.92
H2_TH1_C2_4	1	0	0	0	13.5	1.2	0.09	111.13
H2_TH1_C2_5	0	1	1	0	13.5	1.2	0.09	152.8
H2_TH1_C2_6	0	1	0	0	13.5	1.2	0.09	131.97
H2_TH1_C2_7	0	0	1	0	13.5	1.2	0.09	152.8
H2_TH1_C2_8	0	0	0	0	13.5	1.2	0.09	111.13
H3_C2	1	1	1	0	11.25	1.5	0.13	237.23
H3_C2_2	1	1	0	0	11.25	1.5	0.13	237
H3_C2_3	1	0	1	0	11.25	1.5	0.13	224.74
H3_C2_4	1	0	0	0	11.25	1.5	0.13	162.31
H3_C2_5	0	1	1	0	11.25	1.5	0.13	237.23
H3_C2_6	0	1	0	0	11.25	1.5	0.13	249
H3_C2_7	0	0	1	0	11.25	1.5	0.13	224.74
H3_C2_8	0	0	0	0	11.25	1.5	0.13	149.8
H3_TH1_C2	1	1	1	0	16.875	1.5	0.09	164.96
H3_TH1_C2_2	1	1	0	0	16.875	1.5	0.09	147.6
H3_TH1_C2_3	1	0	1	0	16.875	1.5	0.09	169.96
H3_TH1_C2_4	1	0	0	0	16.875	1.5	0.09	95.5
H3_TH1_C2_5	0	1	1	0	16.875	1.5	0.09	164.96
H3_TH1_C2_6	0	1	0	0	16.875	1.5	0.09	156.3
H3_TH1_C2_7	0	0	1	0	16.875	1.5	0.09	164.96

H3_TH1_C2_8	0	0	0	0	16.875	1.5	0.09	95.5
SP1_C2	1	1	1	0	4.5	0.4	0.09	248.11
SP1_C2_2	1	1	0	0	4.5	0.4	0.09	248.11
SP1_C2_3	1	0	1	0	4.5	0.4	0.09	241.9
SP1_C2_4	1	0	0	0	4.5	0.4	0.09	198.48
SP1_C2_5	0	1	1	0	4.5	0.4	0.09	272.92
SP1_C2_6	0	1	0	0	4.5	0.4	0.09	272.92
SP1_C2_7	0	0	1	0	4.5	0.4	0.09	241.9
SP1_C2_8	0	0	0	0	4.5	0.4	0.09	186.1
SP1_TH1_C2	1	1	1	0	6.75	0.4	0.06	145.46
SP1_TH1_C2_2	1	1	0	0	6.75	0.4	0.06	141.18
SP1_TH1_C2_3	1	0	1	0	6.75	0.4	0.06	124.07
SP1_TH1_C2_4	1	0	0	0	6.75	0.4	0.06	115.51
SP1_TH1_C2_5	0	1	1	0	6.75	0.4	0.06	145.46
SP1_TH1_C2_6	0	1	0	0	6.75	0.4	0.06	145.46
SP1_TH1_C2_7	0	0	1	0	6.75	0.4	0.06	119.79
SP1_TH1_C2_8	0	0	0	0	6.75	0.4	0.06	119.79
SP2_C2	1	1	1	0	4.5	0.3	0.07	251.98
SP2_C2_2	1	1	0	0	4.5	0.3	0.07	251.98
SP2_C2_3	1	0	1	0	4.5	0.3	0.07	237.15
SP2_C2_4	1	0	0	0	4.5	0.3	0.07	170.45
SP2_C2_5	0	1	1	0	4.5	0.3	0.07	222.33
SP2_C2_6	0	1	0	0	4.5	0.3	0.07	266.8
SP2_C2_7	0	0	1	0	4.5	0.3	0.07	214.91
SP2_C2_8	0	0	0	0	4.5	0.3	0.07	170.45
SP2_TH1_C2	1	1	1	0	6.75	0.3	0.04	116.93
SP2_TH1_C2_2	1	1	0	0	6.75	0.3	0.04	127.1
SP2_TH1_C2_3	1	0	1	0	6.75	0.3	0.04	106.76
SP2_TH1_C2_4	1	0	0	0	6.75	0.3	0.04	91.51
SP2_TH1_C2_5	0	1	1	0	6.75	0.3	0.04	116.93
SP2_TH1_C2_6	0	1	0	0	6.75	0.3	0.04	127.1
SP2_TH1_C2_7	0	0	1	0	6.75	0.3	0.04	106.8
SP2_TH1_C2_8	0	0	0	0	6.75	0.3	0.04	91.6

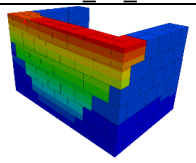
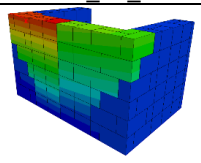
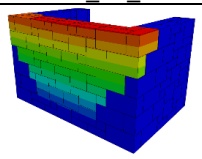
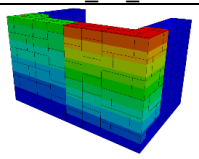
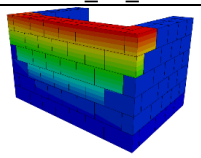
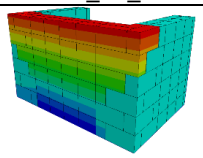
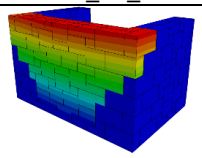
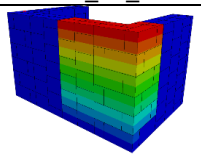
Annex 3.10 – Capacity curves and collapse mechanisms Set 1 full-scale models (C1 corner configuration)

REF SET

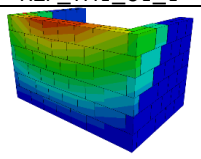
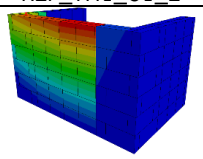
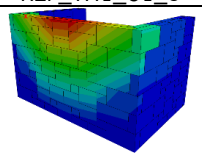
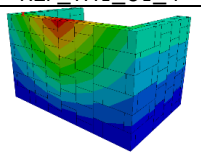
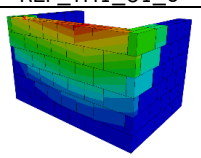
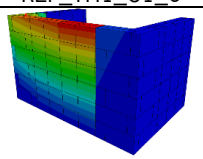
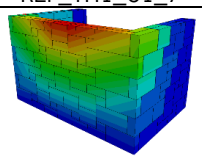
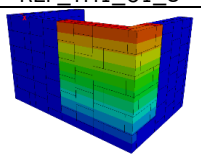




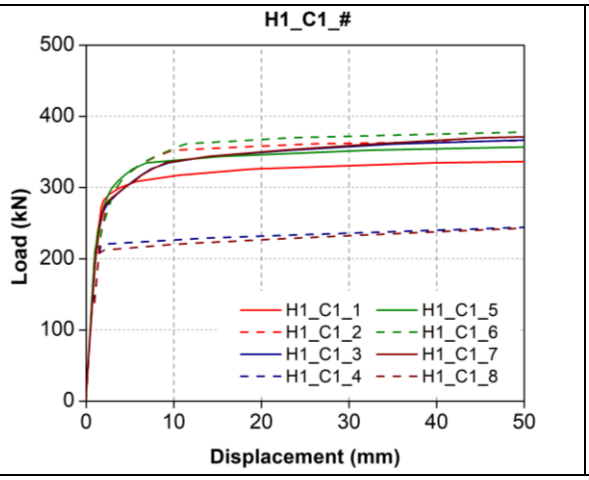
REF_C1 MODELS

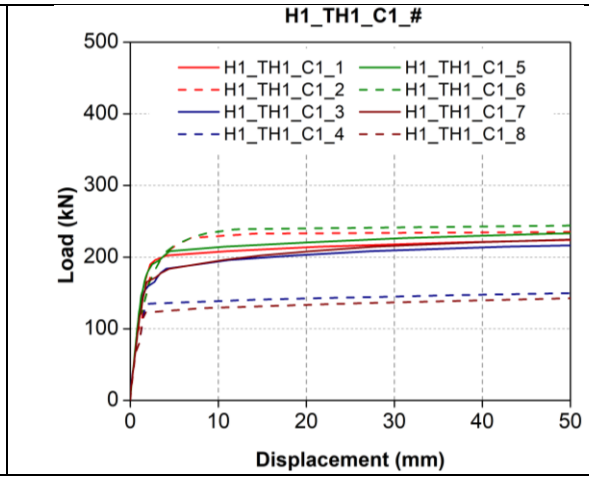
REF_C1_1	REF_C1_2	REF_C1_3	REF_C1_4
			
Failure mode - M1	Failure mode - M1	Failure mode - M1	Failure mode – M2
REF_C1_5	REF_C1_6	REF_C1_7	REF_C1_8
			
Failure mode - M1	Failure mode - M1	Failure mode - M1	Failure mode – M2

REF_TH1_C1 MODELS

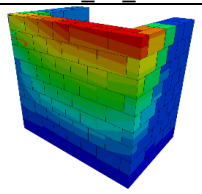
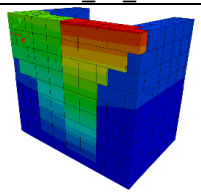
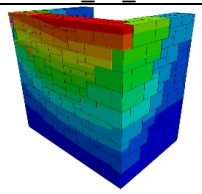
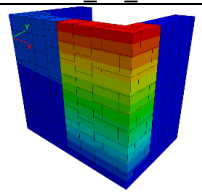
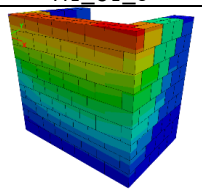
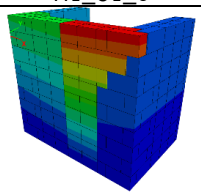
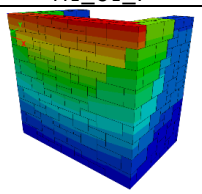
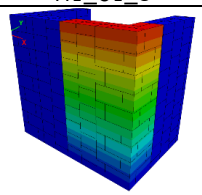
REF_TH1_C1_1	REF_TH1_C1_2	REF_TH1_C1_3	REF_TH1_C1_4
			
Failure mode - M1B	Failure mode – M2	Failure mode - M1	Failure mode - M1B
REF_TH1_C1_5	REF_TH1_C1_6	REF_TH1_C1_7	REF_TH1_C1_8
			
Failure mode - M1B	Failure mode – M2	Failure mode - M1B	Failure mode – M2

H1 SET

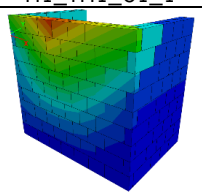
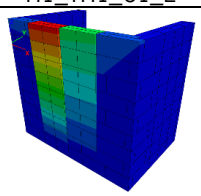
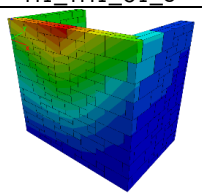
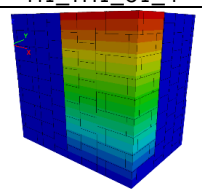
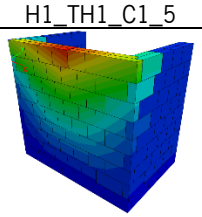
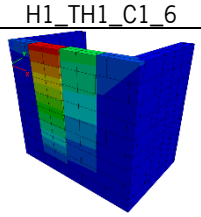
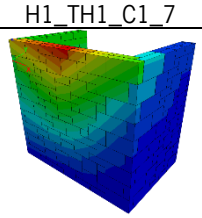
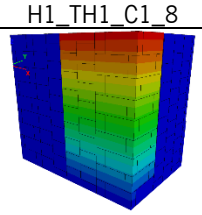




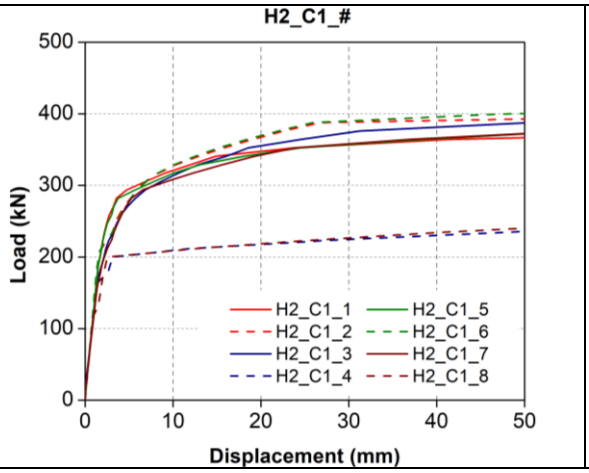
H1_C1 MODELS

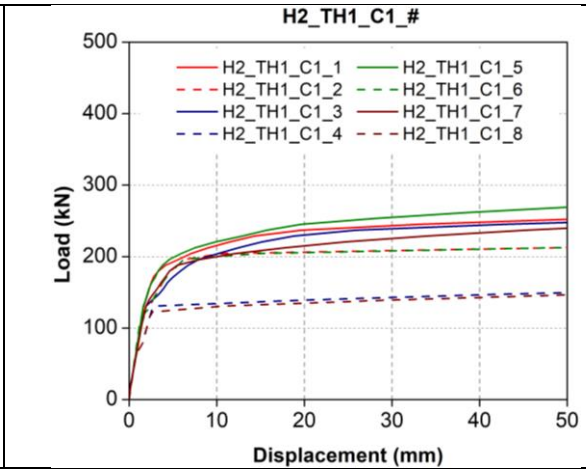
H1_C1_1	H1_C1_2	H1_C1_3	H1_C1_4
			
Failure mode - M1B	Failure mode - M1C	Failure mode - M1B	Failure mode – M2
H1_C1_5	H1_C1_6	H1_C1_7	H1_C1_8
			
Failure mode - M1B	Failure mode - M1C	Failure mode - M1B	Failure mode – M2

H1_TH1_C1 MODELS

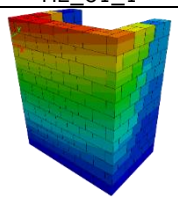
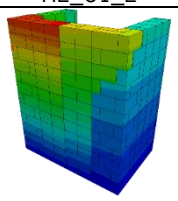
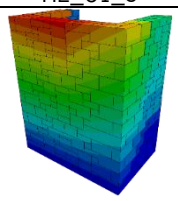
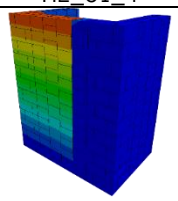
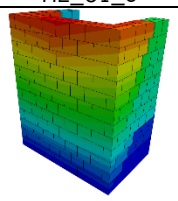
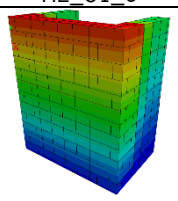
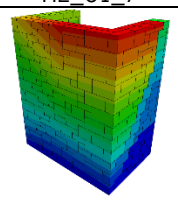
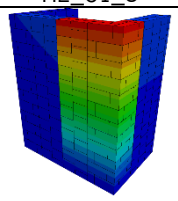
H1_TH1_C1_1	H1_TH1_C1_2	H1_TH1_C1_3	H1_TH1_C1_4
			
Failure mode - M1B	Failure mode - M1C	Failure mode - M1B	Failure mode – M2
H1_TH1_C1_5	H1_TH1_C1_6	H1_TH1_C1_7	H1_TH1_C1_8
			
Failure mode - M1B	Failure mode - M1C	Failure mode - M1B	Failure mode – M2

H2 SET

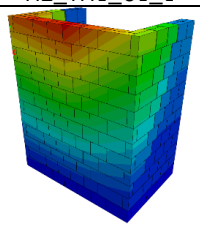
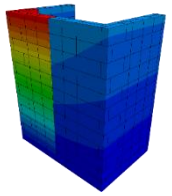
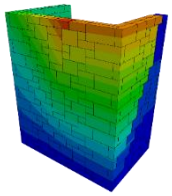
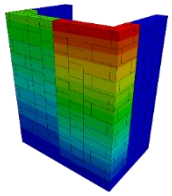
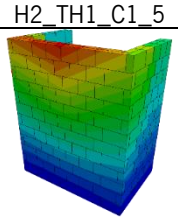
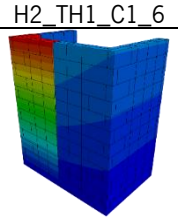
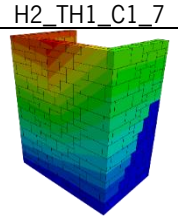
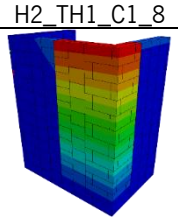




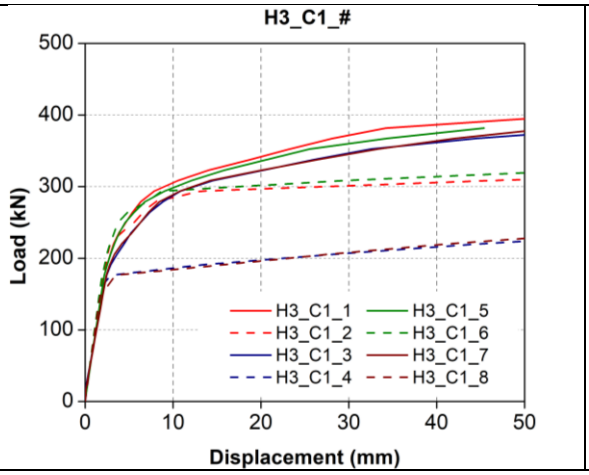
H2_C1 MODELS

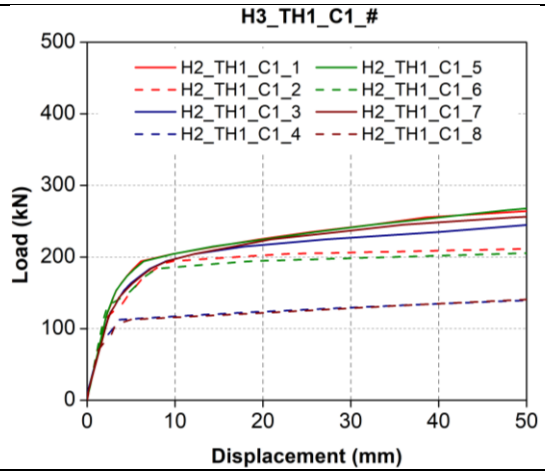
H2_C1_1	H2_C1_2	H2_C1_3	H2_C1_4
			
Failure mode - M1B	Failure mode – M2	Failure mode - M1B	Failure mode – M2
H2_C1_5	H2_C1_6	H2_C1_7	H2_C1_8
			
Failure mode - M1B	Failure mode – M2B	Failure mode - M1B	Failure mode – M2

H2_TH1_C1 MODELS

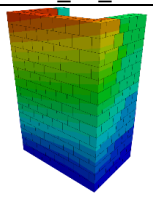
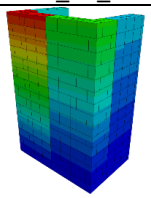
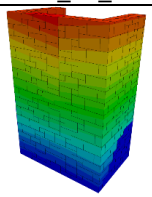
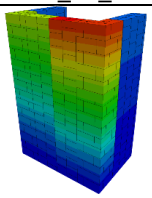
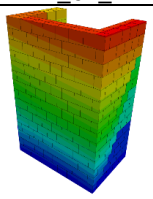
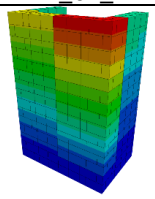
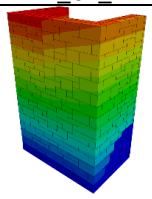
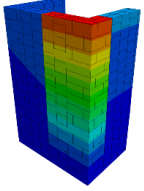
H2_TH1_C1_1	H2_TH1_C1_2	H2_TH1_C1_3	H2_TH1_C1_4
			
Failure mode - M1B	Failure mode – M2	Failure mode - M1B	Failure mode – M2
H2_TH1_C1_5	H2_TH1_C1_6	H2_TH1_C1_7	H2_TH1_C1_8
			
Failure mode - M1B	Failure mode – M2	Failure mode - M1B	Failure mode – M2

H3 SET

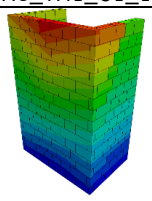
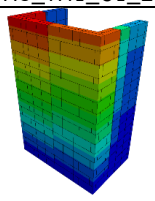
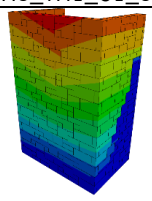
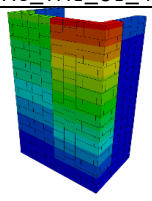
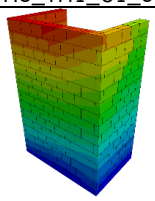
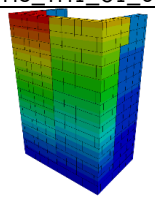
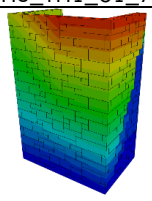
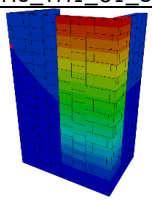




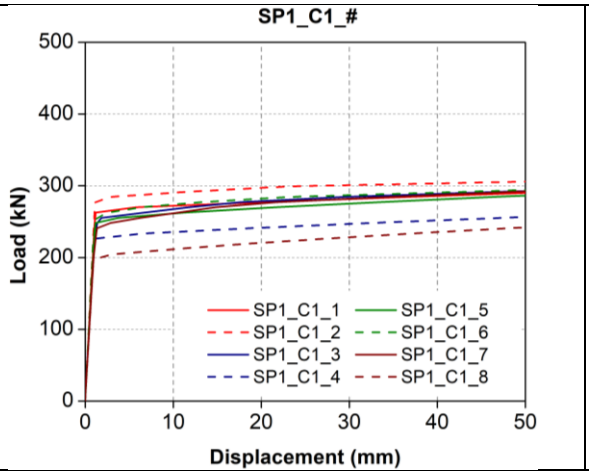
H3_C1 MODELS

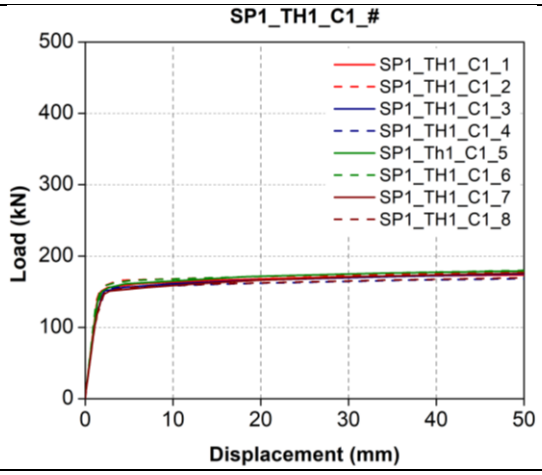
H3_C1_1	H3_C1_2	H3_C1_3	H3_C1_4
			
Failure mode - M1B	Failure mode – M2	Failure mode – M2	Failure mode – M2
H3_C1_5	H3_C1_6	H3_C1_7	H3_C1_8
			
Failure mode - M1B	Failure mode – M2	Failure mode – M1B	Failure mode – M2

H3_TH1_C1 MODELS

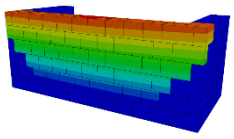
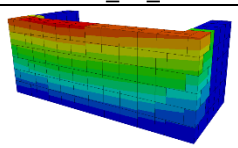
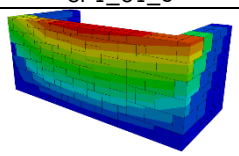
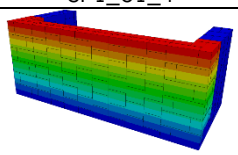
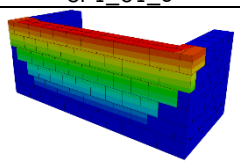
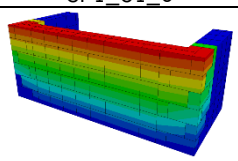
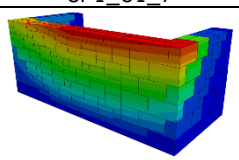
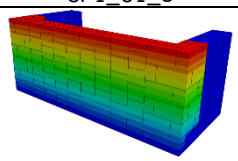
H3_TH1_C1_1	H3_TH1_C1_2	H3_TH1_C1_3	H3_TH1_C1_4
			
Failure mode - M1B	Failure mode – M2B	Failure mode - M1B	Failure mode – M2
H3_TH1_C1_5	H3_TH1_C1_6	H3_TH1_C1_7	H3_TH1_C1_8
			
Failure mode - M1B	Failure mode – M2	Failure mode - M1B	Failure mode – M2

SP1 SET

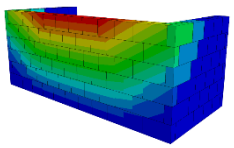
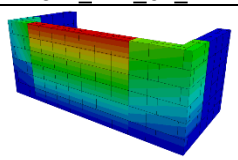
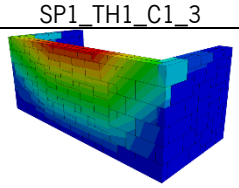
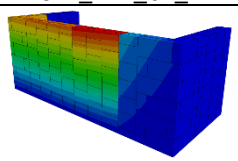
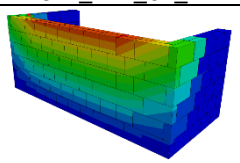
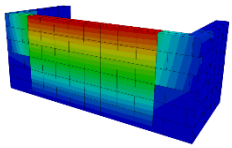
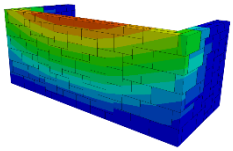
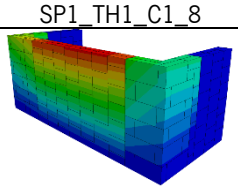




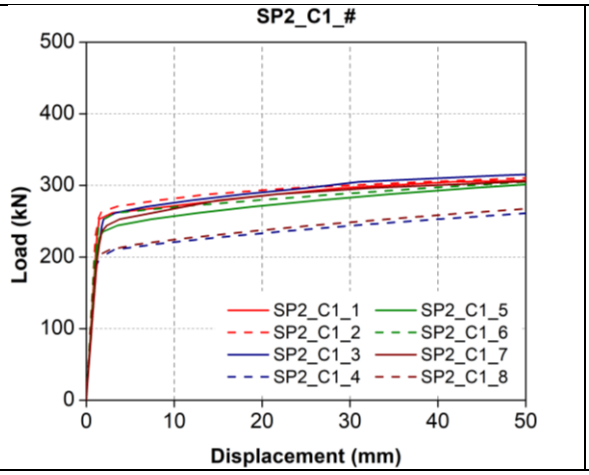
SP1_C1 MODELS

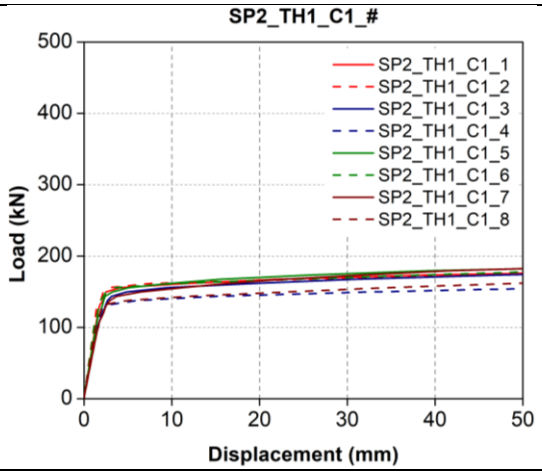
SP1_C1_1	SP1_C1_2	SP1_C1_3	SP1_C1_4
			
Failure mode - M1	Failure mode - M1B	Failure mode - M1B	Failure mode – M2B
SP1_C1_5	SP1_C1_6	SP1_C1_7	SP1_C1_8
			
Failure mode - M1	Failure mode - M1B	Failure mode - M1B	Failure mode – M2B

SP1_TH1_C1 MODELS

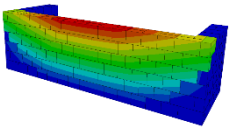
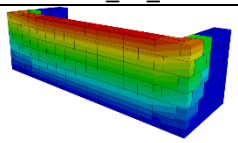
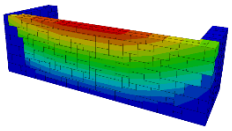
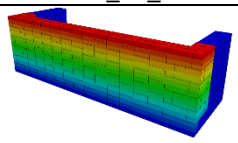
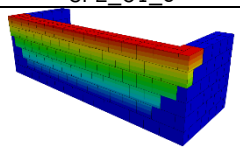
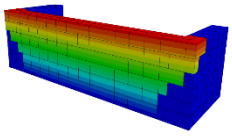
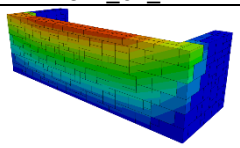
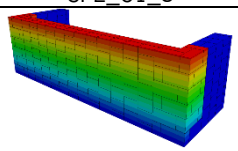
SP1_TH1_C1_1	SP1_TH1_C1_2	SP1_TH1_C1_3	SP1_TH1_C1_4
			
Failure mode - M1B	Failure mode - M1C	Failure mode - M1B	Failure mode – M2
SP1_TH1_C1_5	SP1_TH1_C1_6	SP1_TH1_C1_7	SP1_TH1_C1_8
			
Failure mode - M1B	Failure mode - M1C	Failure mode - M1B	Failure mode - M1C

SP2 SET

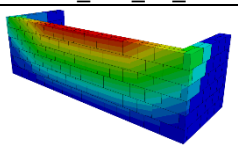
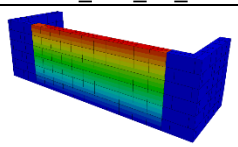
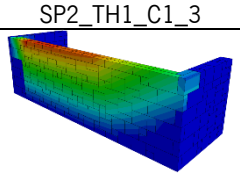
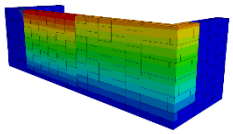
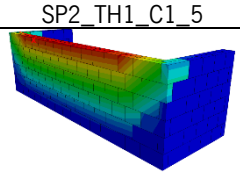
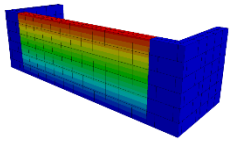
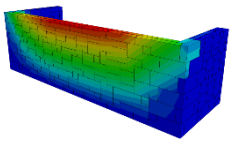
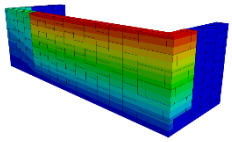




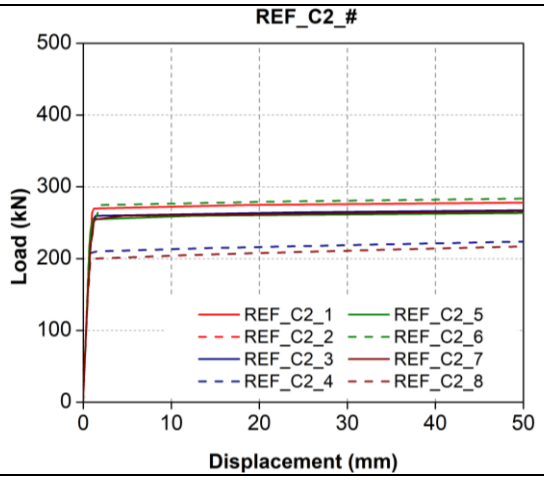
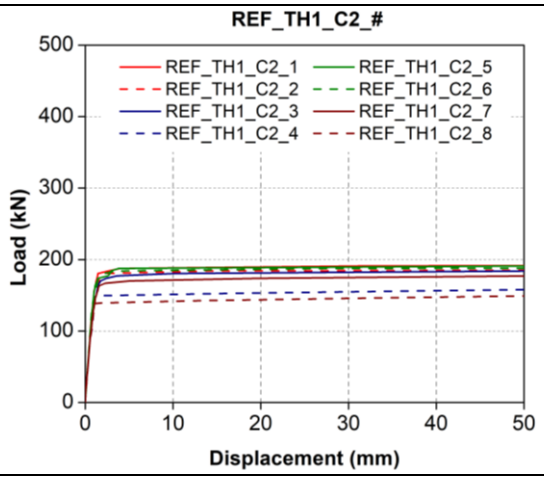
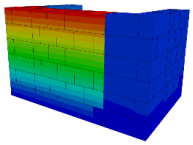
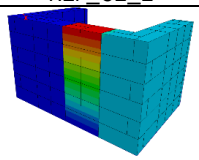
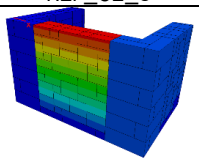
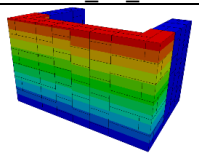
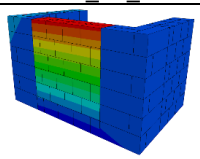
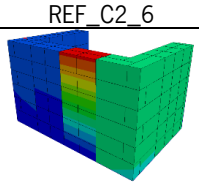
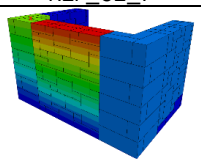
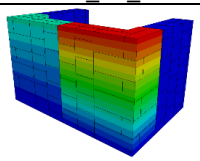
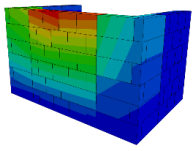
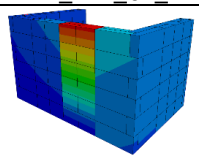
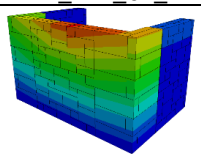
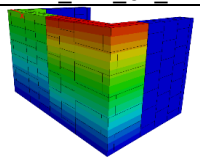
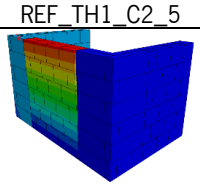
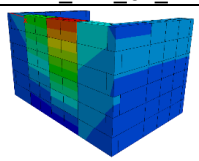
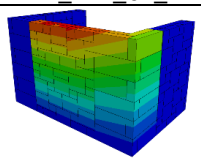
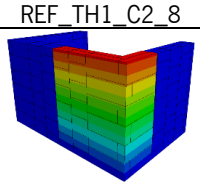
SP2_C1 MODELS

SP2_C1_1	SP2_C1_2	SP2_C1_3	SP2_C1_4
			
Failure mode - M1	Failure mode - M1B	Failure mode - M1	Failure mode – M2B
SP2_C1_5	SP2_C1_6	SP2_C1_7	SP2_C1_8
			
Failure mode - M1	Failure mode - M1	Failure mode - M1B	Failure mode – M2B

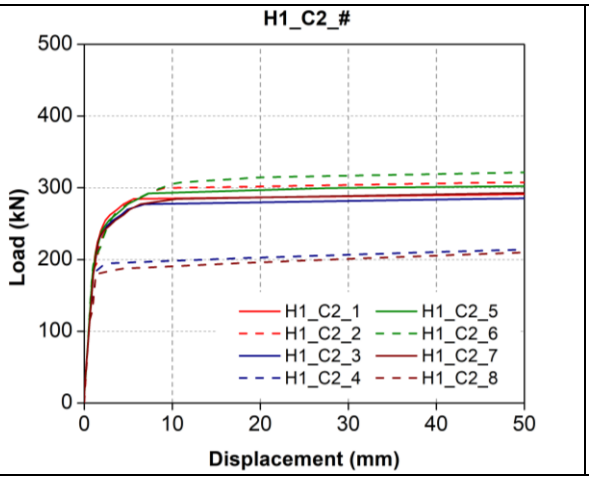
SP2_TH1_C1 MODELS

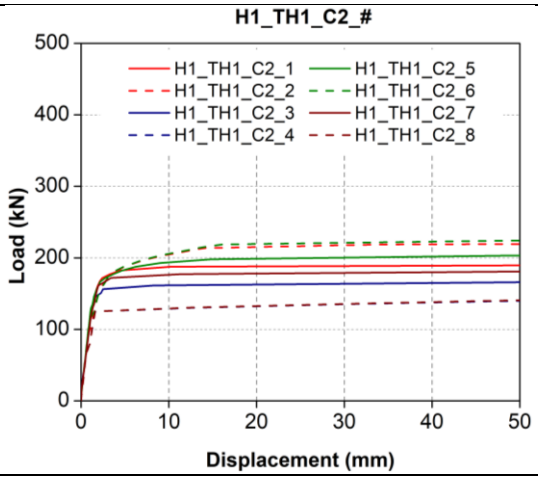
SP2_TH1_C1_1	SP2_TH1_C1_2	SP2_TH1_C1_3	SP2_TH1_C1_4
			
Failure mode - M1B	Failure mode - M1C	Failure mode - M1	Failure mode – M2
SP2_TH1_C1_5	SP2_TH1_C1_6	SP2_TH1_C1_7	SP2_TH1_C1_8
			
Failure mode - M1	Failure mode - M1C	Failure mode - M1	Failure mode – M2

Annex 3.11 – Capacity curves and collapse mechanisms Set 2 full-scale models (C2 corner configuration)

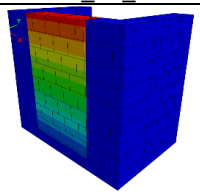
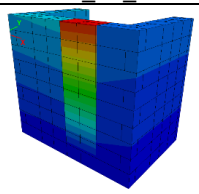
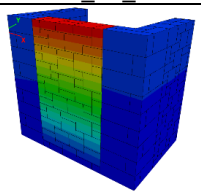
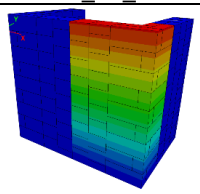
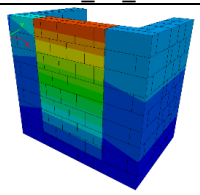
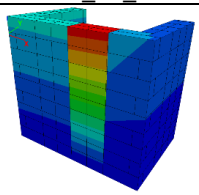
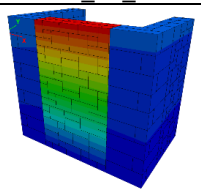
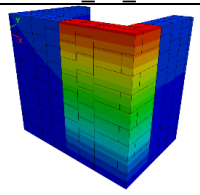
<table>
<tr><th colspan="4">REF SET</th></tr>
<tr><td colspan="2">
</td><td colspan="2">
</td></tr>
<tr><td colspan="4"></td></tr>
<tr><th colspan="4">REF_C2 MODELS</th></tr>
<tr><td>REF_C2_1</td><td>REF_C2_2</td><td>REF_C2_3</td><td>REF_C2_4</td></tr>
<tr><td>
Failure mode – M2</td><td>
Failure mode - M1C</td><td>
Failure mode - M1C</td><td>
Failure mode – M2B</td></tr>
<tr><td>REF_C2_5</td><td>REF_C2_6</td><td>REF_C2_7</td><td>REF_C2_8</td></tr>
<tr><td>
Failure mode - M1C</td><td>
Failure mode - M1C</td><td>
Failure mode - M1C</td><td>
Failure mode – M2</td></tr>
<tr><td colspan="4"></td></tr>
<tr><th colspan="4">REF_TH1_C2 MODELS</th></tr>
<tr><td>REF_TH1_C2_1</td><td>REF_TH1_C2_2</td><td>REF_TH1_C2_3</td><td>REF_TH1_C2_4</td></tr>
<tr><td>
Failure mode - M1C</td><td>
Failure mode - M1C</td><td>
Failure mode – M2B</td><td>
Failure mode – M2</td></tr>
<tr><td>REF_TH1_C2_5</td><td>REF_TH1_C2_6</td><td>REF_TH1_C2_7</td><td>REF_TH1_C2_8</td></tr>
<tr><td>
Failure mode - M1C</td><td>
Failure mode - M1C</td><td>
Failure mode – M2</td><td>
Failure mode – M2</td></tr>
</table>

H1 SET

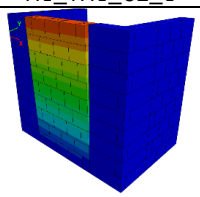
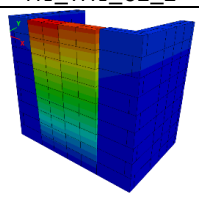
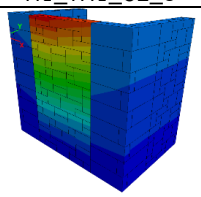
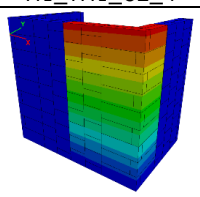
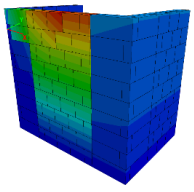
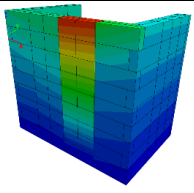
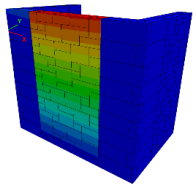
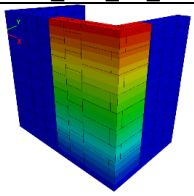




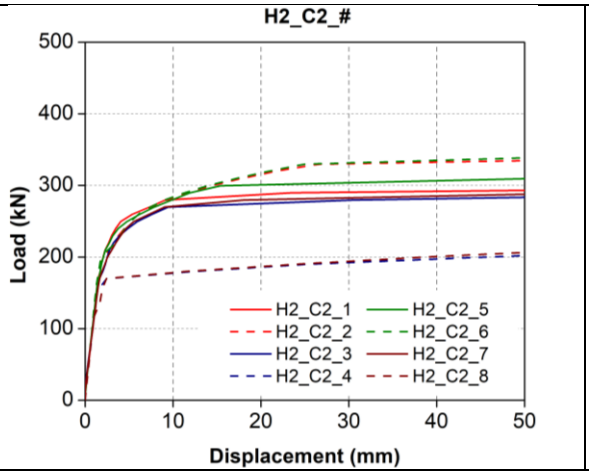
H1_C2 MODELS

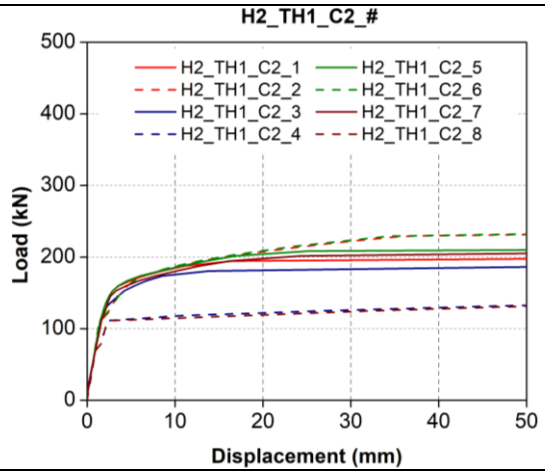
H1_C2_1	H1_C2_2	H1_C2_3	H1_C2_4
			
Failure mode - M1C	Failure mode - M1C	Failure mode - M1C	Failure mode – M2
H1_C2_5	H1_C2_6	H1_C2_7	H1_C2_8
			
Failure mode - M1C	Failure mode - M1C	Failure mode - M1C	Failure mode – M2

H1_TH1_C2 MODELS

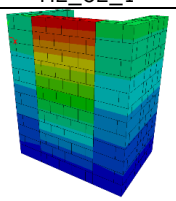
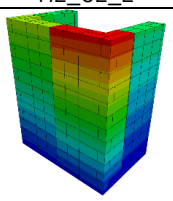
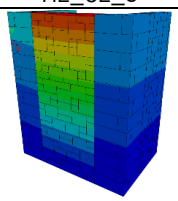
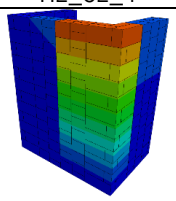
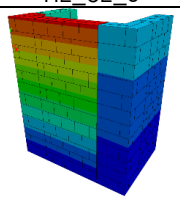
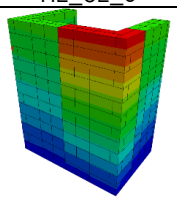
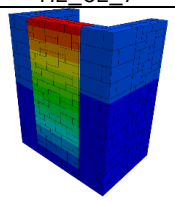
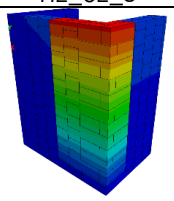
H1_TH1_C2_1	H1_TH1_C2_2	H1_TH1_C2_3	H1_TH1_C2_4
			
Failure mode - M1C	Failure mode - M1C	Failure mode - M1C	Failure mode – M2
H1_TH1_C2_5	H1_TH1_C2_6	H1_TH1_C2_7	H1_TH1_C2_8
			
Failure mode - M1C	Failure mode - M1C	Failure mode - M1C	Failure mode – M2

H2 SET

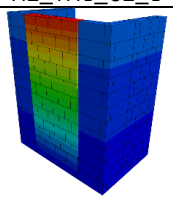
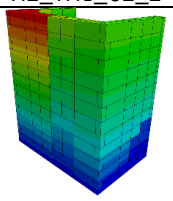
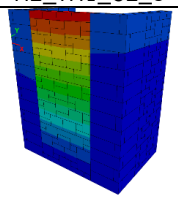
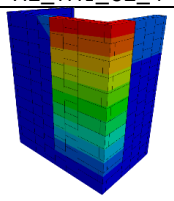
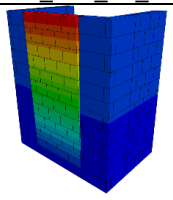
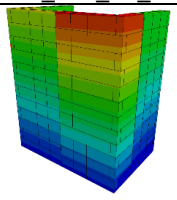
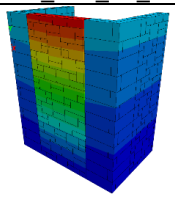
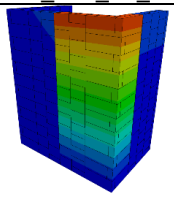




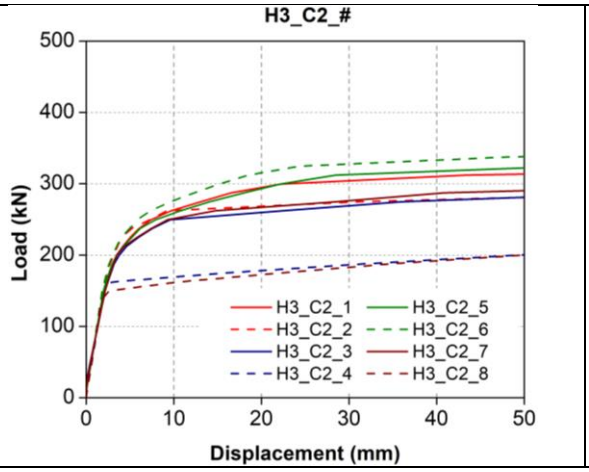
H2_C2 MODELS

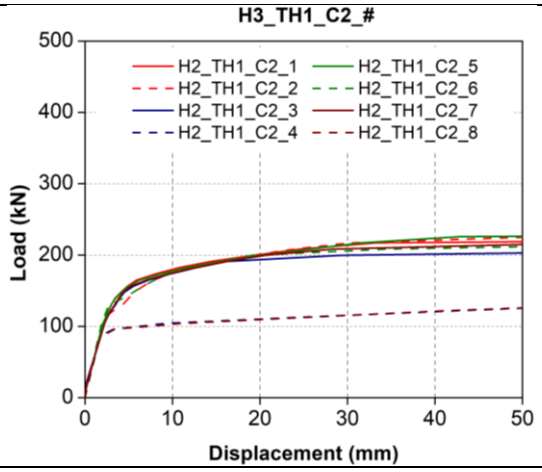
H2_C2_1	H2_C2_2	H2_C2_3	H2_C2_4
			
Failure mode - M1C	Failure mode – M2	Failure mode - M1C	Failure mode – M2
H2_C2_5	H2_C2_6	H2_C2_7	H2_C2_8
			
Failure mode – M2	Failure mode – M2	Failure mode – M1C	Failure mode – M2

H2_TH1_C2 MODELS

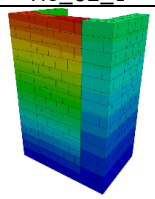
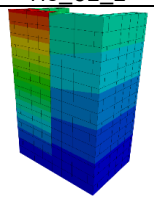
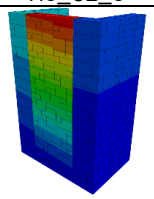
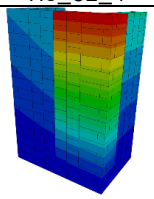
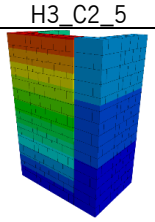
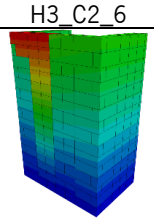
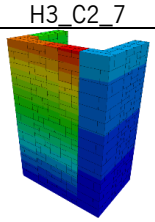
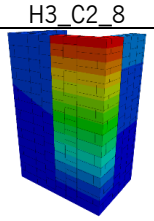
H2_TH1_C2_1	H2_TH1_C2_2	H2_TH1_C2_3	H2_TH1_C2_4
			
Failure mode - M1C	Failure mode – M2	Failure mode - M1C	Failure mode – M2
H2_TH1_C2_5	H2_TH1_C2_6	H2_TH1_C2_7	H2_TH1_C2_8
			
Failure mode - M1C	Failure mode – M2	Failure mode - M1C	Failure mode – M2

H3 SET

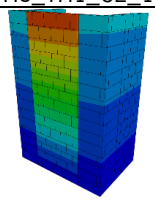
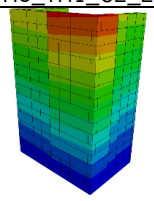
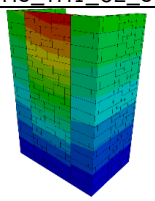
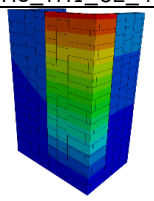
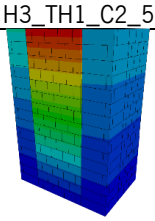
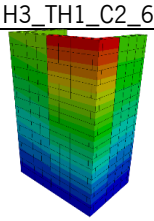
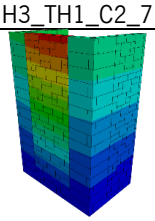
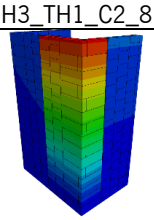




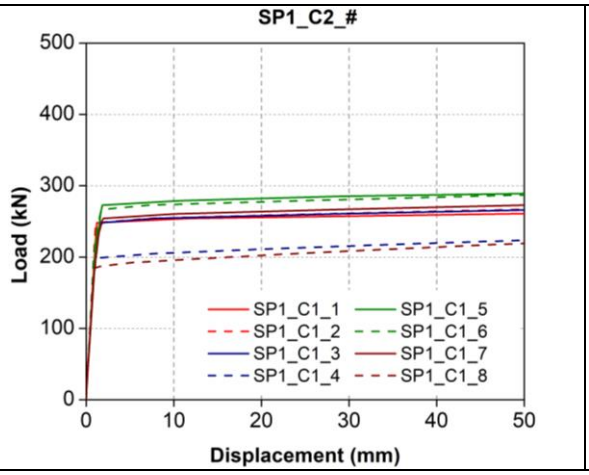
H3_C2 MODELS

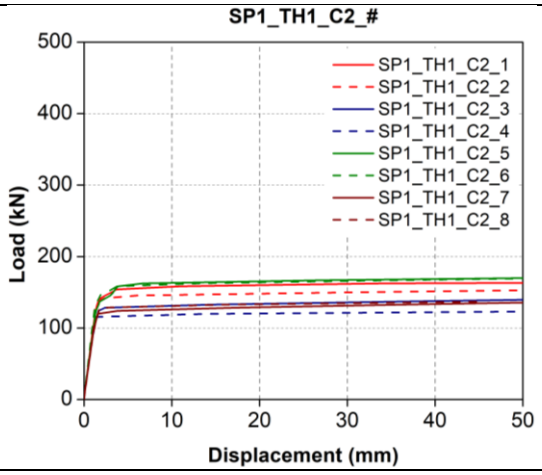
H3_C2_1	H3_C2_2	H3_C2_3	H3_C2_4
			
Failure mode – M2	Failure mode – M2	Failure mode - M1C	Failure mode – M2
H3_C2_5	H3_C2_6	H3_C2_7	H3_C2_8
			
Failure mode – M2	Failure mode – M2	Failure mode – M2	Failure mode – M2

H3_TH1_C2 MODELS

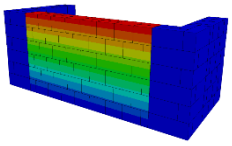
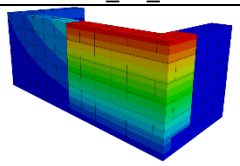
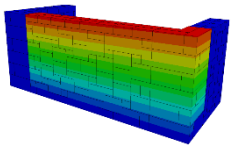
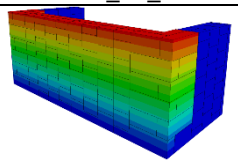
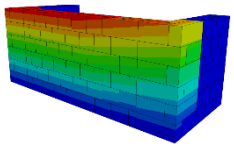
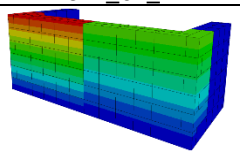
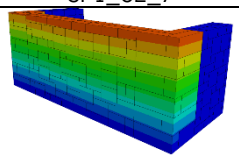
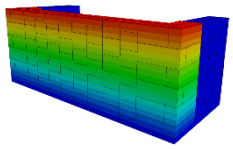
H3_TH1_C2_1	H3_TH1_C2_2	H3_TH1_C2_3	H3_TH1_C2_4
			
Failure mode - M1C	Failure mode – M2	Failure mode - M1C	Failure mode – M2
H3_TH1_C2_5	H3_TH1_C2_6	H3_TH1_C2_7	H3_TH1_C2_8
			
Failure mode - M1C	Failure mode – M2	Failure mode - M1C	Failure mode – M2

SP1 SET

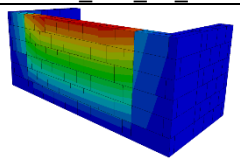
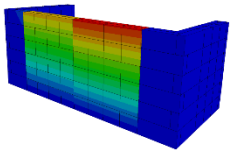
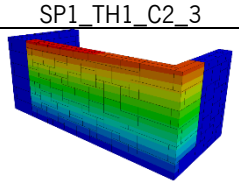
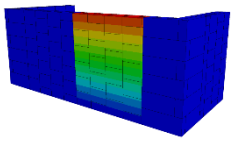
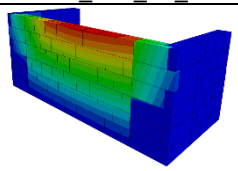
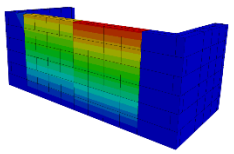
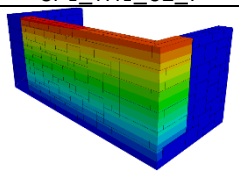
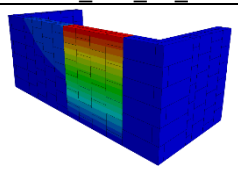




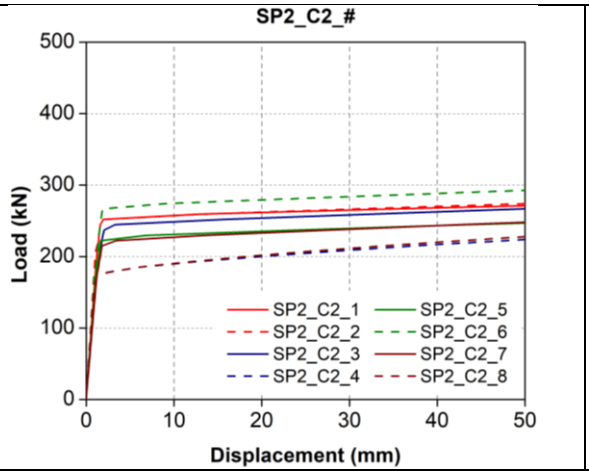
SP1_C2 MODELS

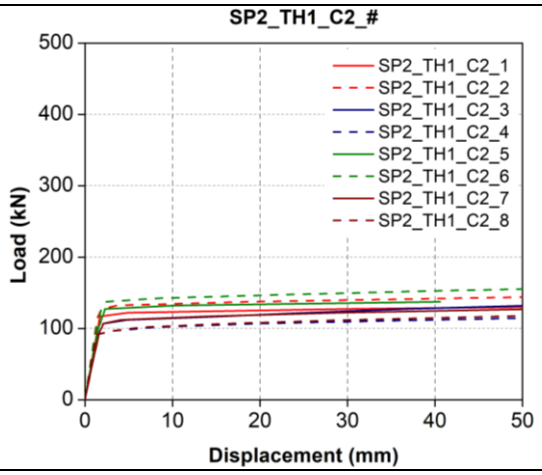
SP1_C2_1	SP1_C2_2	SP1_C2_3	SP1_C2_4
			
Failure mode - M1C	Failure mode – M2	Failure mode – M2	Failure mode – M2B
SP1_C2_5	SP1_C2_6	SP1_C2_7	SP1_C2_8
			
Failure mode – M2B	Failure mode – M2	Failure mode – M2B	Failure mode – M2B

SP1_TH1_C2 MODELS

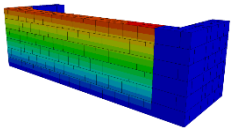
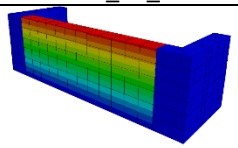
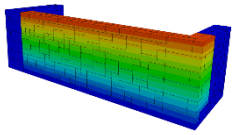
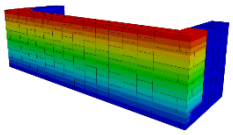
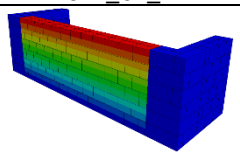
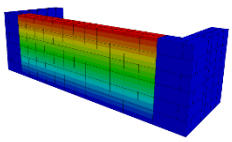
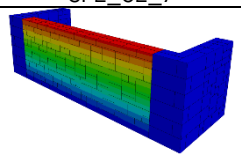
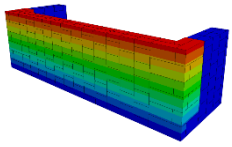
SP1_TH1_C2_1	SP1_TH1_C2_2	SP1_TH1_C2_3	SP1_TH1_C2_4
			
Failure mode - M1C	Failure mode - M1C	Failure mode – M2	Failure mode - M1C
SP1_TH1_C2_5	SP1_TH1_C2_6	SP1_TH1_C2_7	SP1_TH1_C2_8
			
Failure mode - M1C	Failure mode - M1C	Failure mode – M2	Failure mode - M1C

SP2 SET

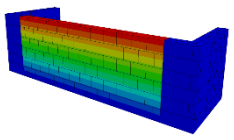
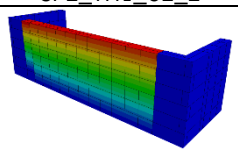
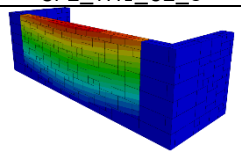
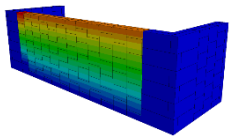
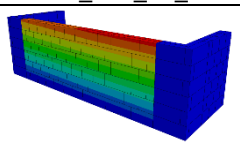
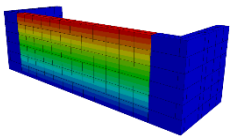
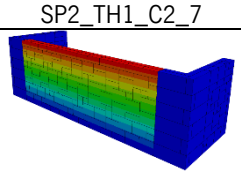
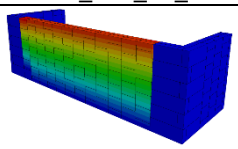




SP2_C2 MODELS

SP2_C2_1	SP2_C2_2	SP2_C2_3	SP2_C2_4
			
Failure mode – M2	Failure mode - M1C	Failure mode – M2	Failure mode – M2B
SP2_C2_5	SP2_C2_6	SP2_C2_7	SP2_C2_8
			
Failure mode - M1C	Failure mode - M1C	Failure mode - M1C	Failure mode – M2B

SP2_TH1_C2 MODELS

SP2_TH1_C2_1	SP2_TH1_C2_2	SP2_TH1_C2_3	SP2_TH1_C2_4
			
Failure mode - M1C	Failure mode - M1C	Failure mode - M1C	Failure mode - M1C
SP2_TH1_C2_5	SP2_TH1_C2_6	SP2_TH1_C2_7	SP2_TH1_C2_8
			
Failure mode - M1C	Failure mode - M1C	Failure mode - M1C	Failure mode - M1C

Annex 3.12 – Dataset empirical expression for the out-of-plane load multiplier estimation based on geometrical parameter

	A	B	C	D	E	F	G	H
MODEL_#	**WC**	**HJ**	**VJ**	**CN**	**Slenderness**	**H/Span**	**Thick/Span**	**λ**
REF_C1	1	1	1	1	4.5	0.6	0.13	0.175
REF_C1_2	1	1	0	1	4.5	0.6	0.13	0.175
REF_C1_3	1	0	1	1	4.5	0.6	0.13	0.175
REF_C1_4	1	0	0	1	4.5	0.6	0.13	0.336
REF_C1_5	0	1	1	1	4.5	0.6	0.13	0.175
REF_C1_6	0	1	0	1	4.5	0.6	0.13	0.175
REF_C1_7	0	0	1	1	4.5	0.6	0.13	0.175
REF_C1_8	0	0	0	1	4.5	0.6	0.13	0.366
REF_TH1_C1	1	1	1	1	6.75	0.6	0.09	0.244
REF_TH1_C1_2	1	1	0	1	6.75	0.6	0.09	0.102
REF_TH1_C1_3	1	0	1	1	6.75	0.6	0.09	0.244
REF_TH1_C1_4	1	0	0	1	6.75	0.6	0.09	0.157
REF_TH1_C1_5	0	1	1	1	6.75	0.6	0.09	0.244
REF_TH1_C1_6	0	1	0	1	6.75	0.6	0.09	0.102
REF_TH1_C1_7	0	0	1	1	6.75	0.6	0.09	0.244
REF_TH1_C1_8	0	0	0	1	6.75	0.6	0.09	0.157
REF_H1_C1	1	1	1	1	6.75	0.9	0.13	0.398
H1_C1_2	1	1	0	1	6.75	0.9	0.13	0.18
H1_C1_3	1	0	1	1	6.75	0.9	0.13	0.398
H1_C1_4	1	0	0	1	6.75	0.9	0.13	0.243
H1_C1_5	0	1	1	1	6.75	0.9	0.13	0.398
H1_C1_6	0	1	0	1	6.75	0.9	0.13	0.18
H1_C1_7	0	0	1	1	6.75	0.9	0.13	0.398
H1_C1_8	0	0	0	1	6.75	0.9	0.13	0.243
H1_TH1_C1	1	1	1	1	10.125	0.9	0.09	0.279
H1_TH1_C1_2	1	1	0	1	10.125	0.9	0.09	0.098
H1_TH1_C1_3	1	0	1	1	10.125	0.9	0.09	0.279
H1_TH1_C1_4	1	0	0	1	10.125	0.9	0.09	0.137
H1_TH1_C1_5	0	1	1	1	10.125	0.9	0.09	0.279
H1_TH1_C1_6	0	1	0	1	10.125	0.9	0.09	0.098
H1_TH1_C1_7	0	0	1	1	10.125	0.9	0.09	0.279
H1_TH1_C1_8	0	0	0	1	10.125	0.9	0.09	0.137
H2_C1	1	1	1	1	9	1.2	0.13	0.267
H2_C1_2	1	1	0	1	9	1.2	0.13	0.171
H2_C1_3	1	0	1	1	9	1.2	0.13	0.267
H2_C1_4	1	0	0	1	9	1.2	0.13	0.142

H2_C1_5	0	1	1	1	9	1.2	0.13	0.267
H2_C1_6	0	1	0	1	9	1.2	0.13	0.162
H2_C1_7	0	0	1	1	9	1.2	0.13	0.267
H2_C1_8	0	0	0	1	9	1.2	0.13	0.142
H2_TH1_C1	1	1	1	1	13.5	1.2	0.09	0.187
H2_TH1_C1_2	1	1	0	1	13.5	1.2	0.09	0.08
H2_TH1_C1_3	1	0	1	1	13.5	1.2	0.09	0.187
H2_TH1_C1_4	1	0	0	1	13.5	1.2	0.09	0.08
H2_TH1_C1_5	0	1	1	1	13.5	1.2	0.09	0.187
H2_TH1_C1_6	0	1	0	1	13.5	1.2	0.09	0.08
H2_TH1_C1_7	0	0	1	1	13.5	1.2	0.09	0.187
H2_TH1_C1_8	0	0	0	1	13.5	1.2	0.09	0.08
H3_C1	1	1	1	1	11.25	1.5	0.13	0.233
H3_C1_2	1	1	0	1	11.25	1.5	0.13	0.114
H3_C1_3	1	0	1	1	11.25	1.5	0.13	0.233
H3_C1_4	1	0	0	1	11.25	1.5	0.13	0.114
H3_C1_5	0	1	1	1	11.25	1.5	0.13	0.233
H3_C1_6	0	1	0	1	11.25	1.5	0.13	0.13
H3_C1_7	0	0	1	1	11.25	1.5	0.13	0.233
H3_C1_8	0	0	0	1	11.25	1.5	0.13	0.114
H3_TH1_C1	1	1	1	1	16.875	1.5	0.09	0.163
H3_TH1_C1_2	1	1	0	1	16.875	1.5	0.09	0.077
H3_TH1_C1_3	1	0	1	1	16.875	1.5	0.09	0.163
H3_TH1_C1_4	1	0	0	1	16.875	1.5	0.09	0.064
H3_TH1_C1_5	0	1	1	1	16.875	1.5	0.09	0.163
H3_TH1_C1_6	0	1	0	1	16.875	1.5	0.09	0.077
H3_TH1_C1_7	0	0	1	1	16.875	1.5	0.09	0.163
H3_TH1_C1_8	0	0	0	1	16.875	1.5	0.09	0.064
SP1_C1	1	1	1	1	4.5	0.4	0.09	0.15
SP1_C1_2	1	1	0	1	4.5	0.4	0.09	0.276
SP1_C1_3	1	0	1	1	4.5	0.4	0.09	0.382
SP1_C1_4	1	0	0	1	4.5	0.4	0.09	0.276
SP1_C1_5	0	1	1	1	4.5	0.4	0.09	0.15
SP1_C1_6	0	1	0	1	4.5	0.4	0.09	0.276
SP1_C1_7	0	0	1	1	4.5	0.4	0.09	0.382
SP1_C1_8	0	0	0	1	4.5	0.4	0.09	0.276
SP1_TH1_C1	1	1	1	1	6.75	0.4	0.06	0.253
SP1_TH1_C1_2	1	1	0	1	6.75	0.4	0.06	0.103
SP1_TH1_C1_3	1	0	1	1	6.75	0.4	0.06	0.253
SP1_TH1_C1_4	1	0	0	1	6.75	0.4	0.06	0.103
SP1_TH1_C1_5	0	1	1	1	6.75	0.4	0.06	0.253

SP1_TH1_C1_6	0	1	0	1	6.75	0.4	0.06	0.155
SP1_TH1_C1_7	0	0	1	1	6.75	0.4	0.06	0.253
SP1_TH1_C1_8	0	0	0	1	6.75	0.4	0.06	0.103
SP2_C1	1	1	1	1	4.5	0.3	0.07	0.353
SP2_C1_2	1	1	0	1	4.5	0.3	0.07	0.265
SP2_C1_3	1	0	1	1	4.5	0.3	0.07	0.353
SP2_C1_4	1	0	0	1	4.5	0.3	0.07	0.265
SP2_C1_5	0	1	1	1	4.5	0.3	0.07	0.143
SP2_C1_6	0	1	0	1	4.5	0.3	0.07	0.143
SP2_C1_7	0	0	1	1	4.5	0.3	0.07	0.353
SP2_C1_8	0	0	0	1	4.5	0.3	0.07	0.265
SP2_TH1_C1	1	1	1	1	6.75	0.3	0.04	0.228
SP2_TH1_C1_2	1	1	0	1	6.75	0.3	0.04	0.275
SP2_TH1_C1_3	1	0	1	1	6.75	0.3	0.04	0.054
SP2_TH1_C1_4	1	0	0	1	6.75	0.3	0.04	0.133
SP2_TH1_C1_5	0	1	1	1	6.75	0.3	0.04	0.228
SP2_TH1_C1_6	0	1	0	1	6.75	0.3	0.04	0.275
SP2_TH1_C1_7	0	0	1	1	6.75	0.3	0.04	0.054
SP2_TH1_C1_8	0	0	0	1	6.75	0.3	0.04	0.275
REF_C2	1	1	1	0	4.5	0.6	0.13	0.276
REF_C2_2	1	1	0	0	4.5	0.6	0.13	0.316
REF_C2_3	1	0	1	0	4.5	0.6	0.13	0.212
REF_C2_4	1	0	0	0	4.5	0.6	0.13	0.316
REF_C2_5	0	1	1	0	4.5	0.6	0.13	0.212
REF_C2_6	0	1	0	0	4.5	0.6	0.13	0.212
REF_C2_7	0	0	1	0	4.5	0.6	0.13	0.212
REF_C2_8	0	0	0	0	4.5	0.6	0.13	0.276
RGW_TH1_C2	1	1	1	0	6.75	0.6	0.09	0.102
REF_TH1_C2_2	1	1	0	0	6.75	0.6	0.09	0.102
REF_TH1_C2_3	1	0	1	0	6.75	0.6	0.09	0.186
REF_TH1_C2_4	1	0	0	0	6.75	0.6	0.09	0.186
REF_TH1_C2_5	0	1	1	0	6.75	0.6	0.09	0.102
REF_TH1_C2_6	0	1	0	0	6.75	0.6	0.09	0.102
REF_TH1_C2_7	0	0	1	0	6.75	0.6	0.09	0.154
REF_TH1_C2_8	0	0	0	0	6.75	0.6	0.09	0.154
H1_C2	1	1	1	0	6.75	0.9	0.13	0.208
H1_C2_2	1	1	0	0	6.75	0.9	0.13	0.208
H1_C2_3	1	0	1	0	6.75	0.9	0.13	0.208
H1_C2_4	1	0	0	0	6.75	0.9	0.13	0.189
H1_C2_5	0	1	1	0	6.75	0.9	0.13	0.208
H1_C2_6	0	1	0	0	6.75	0.9	0.13	0.208

H1_C2_7	0	0	1	0	6.75	0.9	0.13	0.208
H1_C2_8	0	0	0	0	6.75	0.9	0.13	0.189
H1_TH1_C2	1	1	1	0	10.125	0.9	0.09	0.098
H1_TH1_C2_2	1	1	0	0	10.125	0.9	0.09	0.098
H1_TH1_C2_3	1	0	1	0	10.125	0.9	0.09	0.098
H1_TH1_C2_4	1	0	0	0	10.125	0.9	0.09	0.104
H1_TH1_C2_5	0	1	1	0	10.125	0.9	0.09	0.098
H1_TH1_C2_6	0	1	0	0	10.125	0.9	0.09	0.098
H1_TH1_C2_7	0	0	1	0	10.125	0.9	0.09	0.098
H1_TH1_C2_8	0	0	0	0	10.125	0.9	0.09	0.104
H2_C2	1	1	1	0	9	1.2	0.13	0.207
H2_C2_2	1	1	0	0	9	1.2	0.13	0.139
H2_C2_3	1	0	1	0	9	1.2	0.13	0.207
H2_C2_4	1	0	0	0	9	1.2	0.13	0.139
H2_C2_5	0	1	1	0	9	1.2	0.13	0.136
H2_C2_6	0	1	0	0	9	1.2	0.13	0.139
H2_C2_7	0	0	1	0	9	1.2	0.13	0.207
H2_C2_8	0	0	0	0	9	1.2	0.13	0.139
H2_TH1_C2	1	1	1	0	13.5	1.2	0.09	0.097
H2_TH1_C2_2	1	1	0	0	13.5	1.2	0.09	0.078
H2_TH1_C2_3	1	0	1	0	13.5	1.2	0.09	0.097
H2_TH1_C2_4	1	0	0	0	13.5	1.2	0.09	0.078
H2_TH1_C2_5	0	1	1	0	13.5	1.2	0.09	0.097
H2_TH1_C2_6	0	1	0	0	13.5	1.2	0.09	0.078
H2_TH1_C2_7	0	0	1	0	13.5	1.2	0.09	0.097
H2_TH1_C2_8	0	0	0	0	13.5	1.2	0.09	0.078
H3_C2	1	1	1	0	11.25	1.5	0.13	0.108
H3_C2_2	1	1	0	0	11.25	1.5	0.13	0.118
H3_C2_3	1	0	1	0	11.25	1.5	0.13	0.205
H3_C2_4	1	0	0	0	11.25	1.5	0.13	0.118
H3_C2_5	0	1	1	0	11.25	1.5	0.13	0.118
H3_C2_6	0	1	0	0	11.25	1.5	0.13	0.205
H3_C2_7	0	0	1	0	11.25	1.5	0.13	0.114
H3_C2_8	0	0	0	0	11.25	1.5	0.13	0.114
H3_TH1_C2	1	1	1	0	16.875	1.5	0.09	0.096
H3_TH1_C2_2	1	1	0	0	16.875	1.5	0.09	0.068
H3_TH1_C2_3	1	0	1	0	16.875	1.5	0.09	0.096
H3_TH1_C2_4	1	0	0	0	16.875	1.5	0.09	0.064
H3_TH1_C2_5	0	1	1	0	16.875	1.5	0.09	0.096
H3_TH1_C2_6	0	1	0	0	16.875	1.5	0.09	0.064
H3_TH1_C2_7	0	0	1	0	16.875	1.5	0.09	0.096

H3_TH1_C2_8	0	0	0	0	16.875	1.5	0.09	0.064
SP1_C2	1	1	1	0	4.5	0.4	0.09	0.214
SP1_C2_2	1	1	0	0	4.5	0.4	0.09	0.268
SP1_C2_3	1	0	1	0	4.5	0.4	0.09	0.261
SP1_C2_4	1	0	0	0	4.5	0.4	0.09	0.276
SP1_C2_5	0	1	1	0	4.5	0.4	0.09	0.276
SP1_C2_6	0	1	0	0	4.5	0.4	0.09	0.276
SP1_C2_7	0	0	1	0	4.5	0.4	0.09	0.276
SP1_C2_8	0	0	0	0	4.5	0.4	0.09	0.276
SP1_TH1_C2	1	1	1	0	6.75	0.4	0.06	0.103
SP1_TH1_C2_2	1	1	0	0	6.75	0.4	0.06	0.103
SP1_TH1_C2_3	1	0	1	0	6.75	0.4	0.06	0.143
SP1_TH1_C2_4	1	0	0	0	6.75	0.4	0.06	0.103
SP1_TH1_C2_5	0	1	1	0	6.75	0.4	0.06	0.155
SP1_TH1_C2_6	0	1	0	0	6.75	0.4	0.06	0.103
SP1_TH1_C2_7	0	0	1	0	6.75	0.4	0.06	0.14
SP1_TH1_C2_8	0	0	0	0	6.75	0.4	0.06	0.103
SP2_C2	1	1	1	0	4.5	0.3	0.07	0.25
SP2_C2_2	1	1	0	0	4.5	0.3	0.07	0.215
SP2_C2_3	1	0	1	0	4.5	0.3	0.07	0.25
SP2_C2_4	1	0	0	0	4.5	0.3	0.07	0.265
SP2_C2_5	0	1	1	0	4.5	0.3	0.07	0.215
SP2_C2_6	0	1	0	0	4.5	0.3	0.07	0.215
SP2_C2_7	0	0	1	0	4.5	0.3	0.07	0.215
SP2_C2_8	0	0	0	0	4.5	0.3	0.07	0.265
SP2_TH1_C2	1	1	1	0	6.75	0.3	0.04	0.104
SP2_TH1_C2_2	1	1	0	0	6.75	0.3	0.04	0.104
SP2_TH1_C2_3	1	0	1	0	6.75	0.3	0.04	0.104
SP2_TH1_C2_4	1	0	0	0	6.75	0.3	0.04	0.104
SP2_TH1_C2_5	0	1	1	0	6.75	0.3	0.04	0.104
SP2_TH1_C2_6	0	1	0	0	6.75	0.3	0.04	0.104
SP2_TH1_C2_7	0	0	1	0	6.75	0.3	0.04	0.104
SP2_TH1_C2_8	0	0	0	0	6.75	0.3	0.04	0.104

References

[1] J. Heyman, *The Stone Skeleton*. Cambridge, United Kingdom: Cambridge University Press, 1995.

[2] A. Giuffré, *Lettura sulla meccanica delle murature storiche*. Roma: Eizioni Kappa, 1991.

[3] T. M. Ferreira, A. A. Costa, and A. Costa, "Analysis of the Out-Of-Plane Seismic Behaviour of Unreinforced Masonry: A Literature Review," *Int. J. Archit. Herit.*, vol. 9, no. 8, pp. 949–972, 2015, doi: 10.1080/15583058.2014.885996.

[4] J.-B. Rondelet, *Trattato teorico e pratico dell'arte di edificare*. Mantova, 1834.

[5] M. Tomasevic, *Earthquake Resistant Design of Masonry Buildings*. London: Imperial College Press, 1999.

[6] R. Spence, "Saving lives in earthquakes : successes and failures in seismic protection since 1960," *Bullettin Earthq. Eng.*, vol. 5, no. 2, pp. 139–251, 2007, doi: 10.1007/s10518-006-9028-8.

[7] B. Helly, "Local seismic cultures: a European research program for the protection of traditional housing stock," *Ann. Geophys.*, vol. 38, no. 5–6, p. 4, 1995, doi: 10.4401/ag-4059.

[8] D. T. G. Porphyrios, "Traditional Earthquake-Resistant Construction on a Greek Island," *J. Soc. Archit. Hist.*, vol. 30, no. 1, pp. 31–39, 1971, doi: 10.2307/988671.

[9] E. Vintzileou, "Timber-reinforced structures in Greece: 2500 BC-1900 AD," *Proc. Inst. Civ. Eng. Struct. Build.*, vol. 164, no. SB3, pp. 167–180, 2011, doi: 10.1680/stbu.9.00085.

[10] J. Ortega, G. Vasconcelos, H. Rodrigues, and M. Correia, "Local seismic cultures: The use of timber frame structures in the south of Portugal," in *Proceedings of the 2nd International Conference on Historic Earthquake-Resistant Timber Frames in the Mediterranean Region*, 2015, vol. 1, pp. 101–111, doi: 10.1007/978-3-319-39492-3_8.

[11] K.-H. Chang, *Computer-aided engineering design*. Academic Press - Elsevier, 2015.

[12] S. Cattari, S. Lagomarsino, V. Bosiljkov, and D. F. D'Ayala, "Sensitivity analysis for setting up the investigation protocol and defining proper confidence factors for masonry buildings," *Bull. Earthq. Eng.*, no. 13, pp. 129–151, 2015, doi: 10.1007/s10518-014-9648-3.

[13] European Committee for Standadization (CEN), *Eurocode 8: Design of structures for earthquake resistance - Part 3: Assessment and retrofitting of buildings*, vol. 3. Brussels: European Committee for Standadization, 2005.

[14] MIT, *Norme Tecniche per le costruzioni (NTC 2008)*. Rome: Ministero delle Infrastrutture e dei

Trasporti, 2008.

[15] A. committee on technical recommendations for Constructions, *Guide for the Probabilistic Assessment of the Seismic Safety of Existing Buildings*. Rome: National Research Council of Italy (CNR), 2014.

[16] MIT, *Norme tecniche per le costruzioni (NTC 2018)*. Rome: Ministero delle Infrastrutture e dei Trasporti (MIT), 2018.

[17] M. A. Turkman Amaral, C. D. Paulino, and P. Muller, *Computational Bayesian Statistics. An Introduction*. Cambridge, UK: Cambridge University Press, 2019.

[18] A. German, J. Carlin, H. Stern, and D. Rubin, *Bayesian Data Analysis*, Second Edi. Boca Raton (USA): Chapman & Hall/CRC, 2003.

[19] L. Held and D. Sabanés Bové, *Applied Statistical Inference - Likelihood and Bayes*. Berlin (Germany): Springer Berlin Heidelberg, 2014.

[20] J. L. Beck and L. S. Katafygiotis, "Updating models and their uncertainties: Bayesian statistical framework," *J. Eng. Mech.*, no. 124, pp. 455–461, 1998.

[21] C. Papadimitriou, J. L. Beck, and L. S. Katafygiotis, "Updating robust reliability using structural test data," *Probabilistic Eng. Mech.*, vol. 16, pp. 103–113, 2001.

[22] J. P. Conte, R. Astroza, and H. Ebrahimian, "Bayesian methods for nonlinear system identification of civil structures," *MATEC Web Conf.*, no. 24, pp. 1–7, 2015.

[23] G. Bartoli, M. Betti, and A. Vignoli, "A numerical study on seismic risk assessment of historic masonry towers: a case study in San Gimignano," *Bull. Earthq. Eng.*, vol. 14, no. 6, pp. 1475–1518, 2016, doi: 10.1007/s10518-016-9892-9.

[24] G. Bartoli, M. Betti, L. Facchini, A. M. Marra, and S. Monchetti, "Bayesian model updating of historic masonry towers through dynamic experimental data," *Procedia Eng.*, vol. 199, pp. 1258–1263, 2017, doi: 10.1016/j.proeng.2017.09.267.

[25] G. Bartoli, M. Betti, A. M. Marra, and S. Monchetti, "A Bayesian model updating framework for robust seismic fragility analysis of non-isolated historic masonry towers," *Philos. Trans. A*, 2019.

[26] P. Gardoni, A. Der Kiureghian, and K. M. Mosalam, "Probabilistic capacity models and fragility estimates for reinforced concrete columns based on experimental observations," *J. Eng. Mech.*, no. 1, pp. 1024–1038, 2002.

[27] G. Monti and S. Alessandri, "Application of Bayesian techniques to material strength evaluation and calibration of confidence factors," in *Eurocode 8: Perspective from the Italian Standpoint Workshop*,

E. Cosenza, Ed. Naples (ITA): Doppiavoce, 2009, pp. 53–65.

[28] F. Jalayer, I. Iervolino, and G. Manfredi, "Structural modeling uncertainties and their influence on seismic assessment of existing RC structures," *Struct. Saf.*, vol. 32, pp. 220–228, 2010, doi: 10.1016/j.strusafe.2010.02.004.

[29] X. Romao, R. Gonçalves, A. Costa, and R. Delgado, "Evaluation of the EC8-3 confidence factors for the characterization of concrete strength in existing structures," *Mater. Struct.*, vol. 45, no. 11, 2012, doi: 10.1617/s11527-012-9868-4.

[30] M. Tondelli, M. Rota, A. Penna, and G. Magenes, "Evaluation of uncertainties in the seismic assessment of existing masonry buildings," *J. Earthq. Eng.*, no. 16, pp. 37–64, 2012, doi: 10.1080/13632469.2012.670578.

[31] P. Croce and F. Marsili, "Bayesian strategies for the reliability assessment of heritage structures," in *Structural Studies, Repairs and Maintenance of Heritage Architecture XIV*, 2015, no. May 2016, pp. 221–232, doi: 10.2495/STR150191.

[32] G. P. Campostrini, S. Taffarel, G. Bettiol, M. R. Valluzzi, F. Da Porto, and C. Modena, "A Bayesian approach to rapid seismic vulnerability assessment at urban scale," *Int. J. Archit. Herit.*, vol. 12, no. 1, pp. 36–46, 2017, doi: 10.1080/15583058.2017.1370506.

[33] M. L. Beconcini, P. Croce, F. Marsili, M. Muzzi, and E. Rosso, "Probabilistic reliability assessment of a heritage structure under horizontal loads," *Probabilistic Eng. Mech.*, vol. 45, pp. 198–211, 2016, doi: 10.1016/j.probengmech.2016.01.001.

[34] B. Conde, P. Eguía, G. E. Stavroulakis, and E. Granada, "Parameter identification for damaged condition investigation on masonry arch bridges using a Bayesian approach," *Eng. Struct.*, vol. 172, pp. 275–284, 2018, doi: 10.1016/j.engstruct.2018.06.040.

[35] T. Miranda, A. Gomes Correia, and L. Sousa Ribeiro, "Bayesian methodology for updating geomechanical parameters and uncertainty quantification," *Int. J. Rock Mech. Min. Sci.*, vol. 46, no. 7, pp. 1144–1153, 2009, doi: 10.1016/j.ijrmms.2009.03.008.

[36] L. F. Ramos, T. Miranda, M. Mishra, F. M. Fernandes, and E. Manning, "A Bayesian approach for NDT data fusion: The Saint Torcato church case study," *Eng. Struct.*, vol. 84, pp. 120–129, 2015, doi: 10.1016/j.engstruct.2014.11.015.

[37] L. Binda, G. Cardani, and A. Saisi, "A classification of structures and masonries for the adequate choice of repair," in *International RILEM Workshop on Repair Mortars for Historic Masonry*, 2005, pp.

20–34, [Online]. Available: http://www.rilem.net/images/publis/pro067-003.pdf.

[38] MIT, *Circolare 21/01/2019*. Rom: Ministero delle Infrastrutture e dei Trasporti (MIT), 2019.

[39] M. Como, *Statics of Historic Masonry Constructions*. Rome (Italy): Springer, 2015.

[40] N. Augenti, F. Parisi, and E. Acconcia, "MADA: Online experimental database for mechanical modelling of existing masonry assemblages," 2012.

[41] A. Borri, M. Corradi, G. Castori, and A. De Maria, "A method for the analysis and classification of historic masonry," *Bull. Earthq. Eng.*, vol. 13, no. 9, pp. 2647–2665, 2015, doi: 10.1007/s10518-015-9731-4.

[42] A. Borri and A. De Maria, "Indice di Qualità Muraria (IQM): correlazione con le caratteristiche meccaniche e livelli di conoscenza," *Progett. Sismica*, vol. 6, no. 3, pp. 45–63, 2015, doi: 10.7414/PS.6.3.45-63.

[43] Vv.Aa, *Manuale delle Murature Storiche - Volume 1*. Rome: DEI - Tipografia del Genio Civile, 2011.

[44] L. F. Miranda, J. Rio, J. Miranda Guedes, and A. Costa, "Sonic Impact Method - A new technique for characterization of stone masonry walls," *Constr. Build. Mater.*, vol. 36, pp. 27–35, 2012, doi: 10.1016/j.conbuildmat.2012.04.018.

[45] L. Miranda, L. Cantini, J. Guedes, L. Binda, and A. Costa, "Applications of sonic tests to masonry elements : Influence of joints on the propagation velocity of elastic waves," *J. Mater. Civ. Eng.*, no. June, pp. 667–682, 2013, doi: 10.1061/(ASCE)MT.1943-5533.0000547.

[46] L. Binda, A. Saisi, C. Tiraboschi, S. Valle, C. Colla, and M. Forde, "Application of sonic and radar tests on the piers and walls of the Cathedral of Noto," *Constr. Build. Mater.*, vol. 17, no. 8, pp. 613–627, 2003, doi: 10.1016/S0950-0618(03)00056-4.

[47] L. Binda, M. Lualdi, and A. Saisi, "Investigation strategies for the diagnosis of historic structures: On-site tests on Avio Castle, Italy, and Pišece Castle, Slovenia," *Can. J. Civ. Eng.*, vol. 35, no. 6, pp. 555–566, 2008, doi: 10.1139/L07-143.

[48] M. R. Valluzzi, E. Cescatti, G. Cardani, L. Cantini, L. Zanzi, C. Colla, and F. Casarin, "Calibration of sonic pulse velocity tests for detection of variable conditions in masonry walls," *Constr. Build. Mater.*, vol. 192, pp. 272–286, 2018, doi: 10.1016/j.conbuildmat.2018.10.073.

[49] P. Gregorczyk and P. Lourenço, "A Review on Flat-Jack Testing," *Eng. Civ. - Univ. Minho*, no. 9, pp. 39–50, 2000.

[50] ASTM, "In-situ measurement of masonry deformability properties using flat-jack method." ASTM

Standard C 1197-91, 1991.

[51] ASTM, "In-situ compressive stress within solid unit masonry estimated using flat-jack measurements." ASTM Standard C 1196-91, 1991.

[52] RILEM, "In-situ Stress Tests based on the Flat-Jack." RILEM, Bagneux, France, 2004.

[53] L. Binda, C. Tiraboschi, and G. Baronio, "On-site investigation on the remains of the Cathedral of Noto," *Constr. Build. Mater.*, vol. 17, no. 8, pp. 543–555, 2003, doi: 10.1016/S0950-0618(03)00057-6.

[54] J. Roque Almendra and P. Lourenço, "Caracterização Mecânica de Paredes Antigas de Alvenaria. Um Caso de Estudo no Centro Histórico de Bragança," *Eng. Civ. - Univ. Minho*, no. 17, pp. 31–42, 2003.

[55] P. Croce, M. L. Beconcini, P. Formichi, P. Cioni, F. Landi, C. Mochi, F. De Lellis, E. Mariotti, and I. Serra, "Shear modulus of masonry walls: A critical review," *Procedia Struct. Integr.*, vol. 11, pp. 339–346, 2018, doi: 10.1016/j.prostr.2018.11.044.

[56] S. Moreira, "Seismic retrofit of masonry-to-timber connections in historical constructions Susana Maria Trindade Moreira Seismic retrofit of masonry-to-timber connections in historical constructions," University of Minho, Guimaraes (Portugal), 2015.

[57] G. Vasconcelos and P. B. Lourenço, "Experimental characterization of stone masonry in shear and compression," *Constr. Build. Mater.*, vol. 23, no. 11, pp. 3337–3345, 2009, doi: 10.1016/j.conbuildmat.2009.06.045.

[58] "ASTM E519-02, Standard Test Method for Diagonal Tension (Shear) in Masonry Assemblages," West Conshohocken, PA, 2002.

[59] P. F. Sheppard, "In situ test of the shear strength and deformability of an 18th century stone and brick masonry wall," in *Proceedings 7th International Brick Masonry Conference*, 1985, pp. 149–160.

[60] V. Turnsek and F. Cacovic, "Some experimental results on the strength of brick masonry walls," in *Proceedings of the 2nd International Brick Masonry Conference*, 1971, pp. 149–156.

[61] D. Montgomery and G. Runger, *Applied Statistics and Probability for Engineers*, Sixth Edit. Hoboken, New Jersey (USA): Wiley, 2014.

[62] Y. Z. Totoev and J. M. Nichols, "A Comparative Experimental Study of the Modulus of Elasticity of Bricks and Masonry," in *11th International Brick/Block Masonry Conference*, 1997, no. October, pp. 14–16.

[63] N. Makoond, L. Pelà, and C. Molins, "Dynamic elastic properties of brick masonry constituents," *Constr. Build. Mater.*, vol. 199, pp. 756–770, 2019, doi: 10.1016/j.conbuildmat.2018.12.071.

[64] N. Makoond, A. Cabané, L. Pelà, and C. Molins, "Relationship between the static and dynamic elastic modulus of brick masonry constituents," *Constr. Build. Mater.*, vol. 259, p. 120386, 2020, doi: 10.1016/j.conbuildmat.2020.120386.

[65] P. Candeias, A. Correia, A. Campos Costa, J. M. Catarino, M. Pipa, H. Cruz, E. Carvalho Cansado, and A. Costa, "General aspects of the application in Portugal of Eurocode 8 – Part 3 – Annex C (Informative) – Masonry Buildings," *Rev. Port. Eng. Estruturas*, vol. 12, no. 3, pp. 99–120, 2020.

[66] P. Roca, P. B. Lourenço, and A. Gaetani, *Historic Construction and Conservation. Materials, Systems and Damage*. New York: Routledge, 2019.

[67] C. Carocci, "Guidelines for the safety and preservation of historical centres in seismic areas," in *Historical Construcions - Possibilities of numerical and experimental techniques*, 2001, pp. 145–166.

[68] C. Casapulla, L. Argiento, A. Maione, and E. Speranza, "Upgraded formulations for the onset of local mechanisms in multi-storey masonry buildings using limit analysis," *Structures*, vol. 31, no. February, pp. 380–394, 2021, doi: 10.1016/j.istruc.2020.11.083.

[69] C. Casapulla and L. Argiento, "The comparative role of friction in local out-of-plane mechanisms of masonry buildings. Pushover analysis and experimental investigation," *Eng. Struct.*, vol. 126, pp. 158–173, 2016, doi: 10.1016/j.engstruct.2016.07.036.

[70] D. F. D'Ayala and E. Speranza, "Definition of Collapse Mechanisms and Seismic Vulnerability of Historic Masonry Buildings," *Earthq. Spectra*, vol. 19, no. 3, pp. 479–509, 2003, doi: 10.1193/1.1599896.

[71] G. Vlachakis, E. Vlachaki, and P. B. Lourenço, "Learning from failure: Damage and failure of masonry structures, after the 2017 Lesvos earthquake (Greece)," *Eng. Fail. Anal.*, vol. 117, p. 104803, 2020, doi: 10.1016/j.engfailanal.2020.104803.

[72] M. Vitruvio Pollione, *De Architectura*. Pordenone.

[73] A. M. D'Altri, V. Sarhosis, G. Milani, J. Rots, S. Cattari, S. Lagomarsino, E. Sacco, A. Tralli, G. Castellazzi, and S. de Miranda, *Modeling Strategies for the Computational Analysis of Unreinforced Masonry Structures: Review and Classification*, vol. 27, no. 4. Springer Netherlands, 2020.

[74] P. G. Asteris and A. D. Tzamtzis, "On the Use of a Regular Yield Surface for the Analysis of Unreinforced Masonry Walls," *Electron. J. Struct. Eng.*, vol. 3, pp. 23–42, 2003.

[75] P. Lourenço, "Recent advances in Masonry modelling: micromodelling and homogenisation," in *Multiscale Modeling in Solid Mechanics: Computational Approaches*, London: Imperial College Press, 2009, pp. 251–294.

[76] M. Orlando, M. Betti, and P. Spinelli, "Assessment of structural behaviour and seismic retrofitting for an Italian monumental masonry building," *J. Build. Eng.*, vol. 29, p. 101115, 2020, doi: 10.1016/j.jobe.2019.101115.

[77] M. Orlando, G. Becattini, and M. Betti, "Multilevel structural evaluation and rehabilitation design of an historic masonry fortress," *J. Build. Eng.*, vol. 63, no. PA, p. 105379, 2023, doi: 10.1016/j.jobe.2022.105379.

[78] M. Valente, G. Milani, E. Grande, and A. Formisano, "Historical masonry building aggregates: advanced numerical insight for an effective seismic assessment on two row housing compounds," *Eng. Struct.*, vol. 190, no. February, pp. 360–379, 2019, doi: 10.1016/j.engstruct.2019.04.025.

[79] A. Formisano and N. Ademovic, "An overview on seismic analysis of masonry building aggregates," *Front. Built Environ.*, vol. 8, no. August, pp. 1–14, 2022, doi: 10.3389/fbuil.2022.966281.

[80] N. Chieffo, A. Formisano, and P. B. Lourenço, "Seismic vulnerability procedures for historical masonry structural aggregates: Analysis of the historical centre of Castelpoto (South Italy)," *Structures*, vol. 48, no. January, pp. 852–866, 2023, doi: 10.1016/j.istruc.2023.01.022.

[81] C. Chácara, N. Mendes, and P. Lourenço, "Simulation of Shake Table Tests on Out-of-Plane Masonry Buildings . Part (IV): Macro and Micro FEM Based Approaches," *Int. J. Archit. Herit.*, vol. 11, no. 1, pp. 103–116, 2017, doi: 10.1080/15583058.2016.1238972.

[82] S. Sharma, L. C. Silva, F. Graziotti, G. Magenes, and G. Milani, "Modelling the experimental seismic out-of-plane two-way bending response of unreinforced periodic masonry panels using a non-linear discrete homogenized strategy," *Eng. Struct.*, vol. 242, no. June, 2021, doi: 10.1016/j.engstruct.2021.112524.

[83] P. B. Lourenco and J. Rots, "Multisurface Interface Model for analysis of Masonry Structures," *J. Eng. Mech.*, vol. 123, no. 7, pp. 660–668, 1997.

[84] K. F. Abdulla, L. S. Cunningham, and M. Gillie, "Simulating masonry wall behaviour using a simplified micro-model approach," *Eng. Struct.*, vol. 151, pp. 349–365, 2017, doi: 10.1016/j.engstruct.2017.08.021.

[85] A. M. D'Altri, S. de Miranda, G. Castellazzi, and V. Sarhosis, "A 3D detailed micro-model for the in-

plane and out-of-plane numerical analysis of masonry panels," *Comput. Struct.*, vol. 206, pp. 18–30, 2018, doi: 10.1016/j.compstruc.2018.06.007.

[86] M. F. Funari, L. C. Silva, N. Savalle, and P. B. Lourenço, "A concurrent micro/macro FE-model optimized with a limit analysis tool for the assessment of dry-joint masonry strucutres," *Int. J. Multiscale Comput. Eng.*, vol. 20, no. 5, pp. 53–64, 2022, doi: 10.1615/IntJMultCompEng.2021040212.

[87] J. V. Lemos, "Discrete element modeling of masonry structures," *Int. J. Archit. Herit.*, vol. 1, no. 2, pp. 190–213, 2007, doi: 10.1080/15583050601176868.

[88] I. N. Psycharis, A. E. Drougas, and M. E. Dasiou, "Seismic behaviour of the walls of the Parthenon: A numerical study," in *Computational Methods in Structural Dynamics and Earthquake Engineering*, 2009, pp. 265–283, doi: 10.1007/978-94-007-0053-612.

[89] V. Sarhosis, P. Asteris, T. Wang, W. Hu, and Y. Han, "On the stability of colonnade structural systems under static and dynamic loading conditions," *Bull. Earthq. Eng.*, vol. 14, no. 4, pp. 1131–1152, 2016, doi: 10.1007/s10518-016-9881-z.

[90] T. Bui, A. Limam, V. Sarhosis, and M. Hjiaj, "Discrete element modelling of the in-plane and out-of-plane behaviour of dry-joint masonry wall constructions," *Eng. Struct.*, vol. 136, pp. 277–294, 2017, doi: 10.1016/j.engstruct.2017.01.020.

[91] T. T. Bui, A. Limam, and V. Sarhosis, "Failure analysis of masonry wall panels subjected to in-plane and out-of-plane loading using the discrete element method," *Eur. J. Environ. Civ. Eng.*, vol. 25, no. 5, pp. 876–892, 2021, doi: 10.1080/19648189.2018.1552897.

[92] V. Sarhosis, S. W. Garrity, and Y. Sheng, "Influence of brick-mortar interface on the mechanical behaviour of low bond strength masonry brickwork lintels," *Eng. Struct.*, vol. 88, pp. 1–11, 2015, doi: 10.1016/j.engstruct.2014.12.014.

[93] V. Sarhosis and Y. Sheng, "Identification of material parameters for low bond strength masonry," *Eng. Struct.*, vol. 60, pp. 100–110, 2014, doi: 10.1016/j.engstruct.2013.12.013.

[94] N. Savalle, P. B. Lourenço, and G. Milani, "Joint Stiffness Influence on the First-Order Seismic Capacity of Dry-Joint Masonry Structures: Numerical DEM Investigations," *Appl. Sci.*, vol. 12, no. 4, 2022, doi: 10.3390/app12042108.

[95] A. Ferrante, E. Giordano, F. Clementi, G. Milani, and A. Formisano, "Fe vs. De modeling for the nonlinear dynamics of a historic church in central italy," *Geosciences*, vol. 11, no. 5, pp. 1–20, 2021,

doi: 10.3390/geosciences11050189.

[96] M. Schiavoni, E. Giordano, F. Roscini, and F. Clementi, "Numerical Assessment of Interacting Structural Units on the Seismic Damage: A Comparative Analysis with Different Modeling Approaches," *Appl. Sci.*, vol. 13, no. 2, 2023, doi: 10.3390/app13020972.

[97] S. Cattari, B. Calderoni, I. Caliò, G. Camata, S. de Miranda, G. Magenes, G. Milani, and A. Saetta, *Nonlinear modeling of the seismic response of masonry structures: critical review and open issues towards engineering practice*, vol. 20, no. 4. Springer Netherlands, 2022.

[98] *Displacement method Analizer. User's Manual, release 10.2*. Delft (Netherlands): DIANA FEA BV, 2017.

[99] Itasca, *Three Dimensional Distinct Element Code (3DEC), Version 7.0, Official Documentation*. Minneapolis (USA): Itasca Consulting Group, 2019.

[100] L. Martins, G. Vasconcelos, J. Ortega, P. B. Lourenço, H. Rodrigues, L. Silva, and C. Palha, "Characterization of dry stone walls to out-of-plane actions," in *10º Congresso Nacional de Mecânica Experimental*, 2016, no. October.

[101] H. Maccarini, G. Vasconcelos, H. Rodrigues, J. Ortega, and P. B. Lourenço, "Out-of-plane behaviour of stone masonry walls: Experimental and numerical analysis," *Constr. Build. Mater.*, vol. 179, pp. 430–452, 2018, doi: 10.1016/j.conbuildmat.2018.05.216.

[102] A. Murano, J. Ortega, G. Vasconcelos, and H. Rodrigues, "Influence of traditional earthquake-resistant techniques on the out-of-plane behaviour of stone masonry walls: Experimental and numerical assessment," *Eng. Struct.*, vol. 201, p. 109815, Dec. 2019, doi: 10.1016/j.engstruct.2019.109815.

[103] P. Roca, M. Cervera, G. Gariup, and L. Pelà, "Structural Analysis of Masonry Historical Constructions. Classical and Advanced Approaches," *Arch. Comput. Methods Eng.*, vol. 17, no. 3, pp. 299–325, 2010, doi: 10.1007/s11831-010-9046-1.

[104] A. Panagiotis, V. Plevris, V. Sarhosis, L. Papaloizou, A. Mohebkhah, P. Komodromos, and J. Lemos, "Numerical Modeling of Historic Masonry Structures," in *Handbook of Research on Seismic Assessment and Rehabilitation of Historic Structures*, A. Panagiotis, Ed. Hershey PA (USA): IGI Global, 2015, pp. 213–255.

[105] G. Bartoli and M. Betti, "A numerical study on seismic risk assessment of historic masonry towers: a case study in San Gimignano," *Bull. Earthq. Eng.*, 2016, doi: 10.1007/s10518-016-9892-9.

[106] M. Betti and A. Vignoli, "Numerical assessment of the static and seismic behaviour of the basilica of

Santa Maria all'Impruneta (Italy)," *Constr. Build. Mater.*, vol. 25, no. 12, pp. 4308–4324, 2011, doi: 10.1016/j.conbuildmat.2010.12.028.

[107] S. Tiberti, M. Acito, and G. Milani, "Comprehensive FE numerical insight into Finale Emilia Castle behaviour under 2012 Emilia Romagna seismic sequence: Damage causes and seismic vulnerability mitigation hypothesis," *Eng. Struct.*, vol. 117, pp. 397–421, 2016, doi: 10.1016/j.engstruct.2016.02.048.

[108] H. Maccarini, G. Vasconcelos, H. Rodrigues, J. Ortega, and P. Lourenço, "Out-of-plane behaviour of stone masonry walls: Experimental and numerical analysis," *Constr. Build. Mater.*, vol. 179, pp. 430–452, 2017, doi: 10.1016/j.cois.2017.06.009.

[109] A. Mordanova, G. de Felice, and A. Genoese, "Assessment of the stability condition of the Claudio aqueduct," 2017.

[110] S. Gonen, B. Pulatsu, E. Erdogmus, E. Karaesmen, and E. Karaesmen, "Quasi-static nonlinear seismic assessment of a fourth century A.D. Roman Aqueduct in Istanbul, Turkey," *Heritage*, vol. 4, no. 1, pp. 401–421, 2021, doi: 10.3390/heritage4010025.

[111] C. Papantonopoulos, I. N. Psycharis, D. Y. Papastamatiou, J. V. Lemos, and H. P. Mouzakis, "Numerical prediction of the earthquake response of classical columns using the distinct element method," *Earthq. Eng. Struct. Dyn.*, vol. 31, no. 9, pp. 1699–1717, 2002, doi: 10.1002/eqe.185.

[112] I. N. Psycharis, J. V. Lemos, D. Y. Papastamatiou, C. Zambas, and C. Papantonopoulos, "Numerical study of the seismic behaviour of a part of the Parthenon Pronaos," *Earthq. Eng. Struct. Dyn.*, vol. 32, no. 13, pp. 2063–2084, 2003, doi: 10.1002/eqe.315.

[113] P. B. Lourenço and A. Gaetani, *Finite Element Analysis for building assessment - Advanced Use and Practical Recommendations*. Abingdon (UK): Routledge, 2022.

[114] J. Scacco, G. Salazar, N. Bianchini, N. Mendes, C. Cullimore, and L. Jain, "Seismic assessment of the church of Carmo Convent," in *Congress on Numerical Methods in Engineering (CMN2019)*, 2019, no. July, pp. 1–16.

[115] G. E. Sincraian and J. V. Lemos, "Seismic Analysis of a Stone Masonry Aqueduct using Discrete Elements," in *8th Canadian Conference on Earthquake Engineering*, 1999, pp. 131–136.

[116] A. Drei and C. Oliveira Sousa, "The seismic behaviour of the 'Aqueduto da Amoreira' in Elvas using distinct element modelling," in *Proceedings of the 3rd International Seminar on Historical Constructions*, 2001, pp. 903–912.

[117] G. Mirabella Roberti and O. Spina, "Discrete element analysis on the Sardinian 'Nuaraghe,'" in *Proceedings of the 3rd International Seminar on Historical Constructions*, 2001, pp. 719–727.

[118] D. V. de C. Oliveira, G. Grecchi, A. McCall, J. Noh, E. Speer, and M. Tohidi, "Seismic analysis of the Roman Temple of Évora, Portugal," 2012, [Online]. Available: https://repositorium.sdum.uminho.pt/bitstream/1822/22022/1/2012_Seismic analysis of the Roman Temple of Évora%2C Portugal.pdf.

[119] G. Rouxinol and M. Morais, "Analysis of masonry arch bridges using DEM with two distinct mesh generations," 2014.

[120] J. V. Lemos, C. Oliveira Sousa, and M. Navarro, "3-D nonlinear behaviour of an obelisk subjected to the Lorca May 11, 2011 strong motion record," *Eng. Fail. Anal.*, vol. 58, pp. 212–228, 2015, doi: 10.1016/j.engfailanal.2015.09.001.

[121] B. Pulatsu, E. Erdogmus, and E. M. Bretas, "Parametric Study on Masonry Arches Using 2D Discrete-Element Modeling," *J. Archit. Eng.*, vol. 24, no. 2, 2018, doi: 10.1061/(asce)ae.1943-5568.0000305.

[122] B. Pulatsu, F. Gencer, and E. Erdogmus, "Study of the effect of construction techniques on the seismic capacity of ancient dry-joint masonry towers through DEM," *Eur. J. Environ. Civ. Eng.*, 2020, doi: 10.1080/19648189.2020.1824823.

[123] C. Oliveira Sousa, J. V. Lemos, and G. E. Sincraian, "Modelling large displacements of structures damaged by earthquake motions," *Eur. Earthq. Eng.*, vol. 16, no. 3, pp. 56–71, 2002.

[124] R. Schlegel and K. Rautenstrauch, "Failure anlysis of masonry shear walls," *Numer. Model. Discret. Mater.*, pp. 15–18, 2004.

[125] A. Alexandris, E. Protopapa, and I. Psycharis, "Collapse mechanisms of masonry buildings drived by the distinct element method," 2004.

[126] G. de Felice, "Out-of-plane fragility of historic masonry walls," in *Structural Analysis of Historical Constructions*, 2005, pp. 1143–1148.

[127] V. Sarhosis, D. V. Oliveira, J. V. Lemos, and P. B. Lourenco, "The effect of skew angle on the mechanical behaviour of masonry arches," *Mech. Res. Commun.*, vol. 61, pp. 53–59, 2014, doi: 10.1016/j.mechrescom.2014.07.008.

[128] J. P. Gomes and J. V. Lemos, "Characterization of the dynamic behaviour of a concrete arch dam by means of forced vibration tests and numerical models," *Earthq. Eng. Struct. Dyn.*, vol. 49, no. 7, pp.

679–694, 2020, doi: 10.1002/eqe.3259.

[129] J. Ortega Heras, “Reduction of the seismic vulnerability of vernacular architecture with traditional strengthening solutions,” University of Minho, 2018.

[130] J. V. Lemos, “Discrete element modelling of the seismic behaviour of stone masonry arches,” in *Proceedings of the 4th International Symposium on Computer Methods in Structural Masonry*, 1998, pp. 220–227.

[131] A. Celeste Maria, “Paredes de alvenaria do Porto - Tipificaçao e caraterizaçao experimental,” University of Porto, 2013.

[132] S. Gonen, B. Pulatsu, E. Erdogmus, P. B. Lourenço, and S. Soyoz, “Effects of spatial variability and correlation in stochastic discontinuum analysis of unreinforced masonry walls,” *Constr. Build. Mater.*, vol. 337, no. September 2021, p. 127511, 2022, doi: 10.1016/j.conbuildmat.2022.127511.

[133] S. Szabó, M. F. Funari, and P. B. Lourenço, “Masonry patterns’ influence on the damage assessment of URM walls: Current and future trends,” *Dev. Built Environ.*, vol. 13, no. January, 2023, doi: 10.1016/j.dibe.2023.100119.

[134] M. Corradi, A. Borri, E. Poverello, and G. Castori, “The use of transverse connectors as reinforcement of multi-leaf walls,” *Mater. Struct. Constr.*, vol. 50, no. 2, pp. 1–14, 2017, doi: 10.1617/s11527-016-0977-3.

[135] M. Griffith, N. Lam, and J. Wilson, “Displacement-Based Assessment of the Seismic Capacity of Unreinforced Masonry Walls in Bending,” *Aust. J. Struct. Eng.*, vol. 6, no. 2, pp. 119–132, 2006.

[136] A. Barontini, J. Scacco, L. Da Silva, G. Vasconcelos, P. B. Lourenço, and G. Milani, “Experimental quasi-static out-of-plane test of a U-shaped brick masonry wall,” *Eng. Struct.*, vol. 287, 2023.

[137] S. Petry and K. Beyer, “Testing unreinforced masonry structures at reduced scale,” in *15th World Conference on Earthquake Engineering 2012 (15WCEE)*, 2012.

[138] S. Petry and K. Beyer, “Scaling unreinforced masonry for reduced-scale seismic testing,” *Bull. Earthq. Eng.*, vol. 12, no. 6, pp. 2557–2581, 2014, doi: 10.1007/s10518-014-9605-1.

[139] ABK, “Methodology for mitigation of seismic hazards in existing unreinforced masonry buildings,” El Segundo (California), 1981.

[140] A. Giuffè, *Sicurezza e conservazione dei centri storici - Il caso Ortigia*. Bari (Italy): Laterza, 1993.

[141] O. AlShawa, G. De Felice, A. Mauro, and L. Sorrentino, “Out-of-plane seismic behaviour of rocking masonry walls,” *Earthq. Eng. Struct. Dyn.*, vol. 41, no. 5, pp. 949–968, 2011, doi: 10.1002/eqe.

[142] A. Costa, A. Arêde, A. Campos Costa, A. Penna, and A. Costa, "Out-of-plane behaviour of a full-scale stone masonry façade. Part 1: specimen and ground motion selection," *Earthq. Eng. Struct. Dyn.*, vol. 42, no. 14, pp. 2081–2095, 2013, doi: 10.1002/eqe.

[143] A. Costa, A. Arêde, A. Campos Costa, A. Penna, and A. Costa, "Out-of-plane behaviour of a full scale stone masonry façade. Part 2: shaking table tests," *Earthq. Eng. Struct. Dyn.*, vol. 42, no. 14, pp. 2097–2111, 2013, doi: 10.1002/eqe.

[144] U. Tomassetti, A. Correia, P. X. Candeias, F. Graziotti, and A. Campos Costa, "Two-way bending out-of-plane collapse of a full-scale URM building tested on a shake table," *Bull. Earthq. Eng.*, vol. 17, no. 4, pp. 2165–2198, 2018.

[145] F. Graziotti, U. Tomassetti, S. Sharma, L. Grottoli, and G. Magenes, "Experimental response of URM single leaf and cavity walls in out-of-plane two-way bending generated by seismic excitation," *Constr. Build. Mater.*, vol. 195, pp. 650–670, 2019, doi: 10.1016/j.conbuildmat.2018.10.076.

[146] T. M. Ferreira, A. Costa, A. Arêde, A. Gomes, and A. Costa, "Experimental characterization of the out-of-plane performance of regular stone masonry walls , including test setups and axial load influence," *Bull. Earthq. Eng.*, vol. 13, no. 9, pp. 1–26, 2015, doi: 10.1007/s10518-015-9742-1.

[147] M. Griffith, J. Vaculik, N. Lam, J. Wilson, and E. Lumantarna, "Cyclic testing of unreinforced masonry walls in two-way bending," *Earthq. Eng. Struct. Dyn.*, vol. 36, no. 6, pp. 801–821, 2007, doi: 10.1002/eqe.

[148] A. Costa, "Determination of mechanical properties of traditional masonry walls in dwellings of Faial Island , Azores," *Earthq. Eng. Struct. Dyn.*, vol. 31, no. 7, pp. 1361–1382, 2002, doi: 10.1002/eqe.167.

[149] G. Tumialan, N. Galati, and A. Nanni, "Field assessment of urm walls strengthened with FRP laminates," *J. Struct. Eng.*, vol. 129, no. 8, 2003.

[150] D. Dizhur, H. Derakhshan, R. Lumantarna, and J. Ingham, "In-situ out-of-plane testing of unreinforced masonry wall segment in Wintec Block F Building," in *2010 NZSEE Annual Conference*, 2010, pp. 1–8.

[151] E. Ferretti and G. Pascale, "Some of the latest active strengthening techniques for Masonry Buildings: A critical analysis," *Materials (Basel).*, vol. 12, no. 7, 2019, doi: 10.3390/ma12071151.

[152] F. da Porto, M. R. Valluzzi, M. Munari, C. Modena, A. Arede, and A. A. Costa, *Strengthening and Retrofitting of Existing Structures*, vol. 9. Singapore: Springer Nature, 2018.

[153] J. Ortega, "Reduction of the seismic vulnerability of vernacular architecture with traditional strengthening solutions," University of Minho, 2018.

[154] N. Ruggieri, G. Tampone, and R. Zinno, *Historical Earthquake-Resistant Timber Frames in the Mediterranean Area*. Springer, 2015.

[155] R. Langenbach, "From 'Opus Craticium' to the 'Chicago frame': Earthquake-resistant traditional construction," *Int. J. Archit. Herit.*, vol. 1, no. 1, pp. 19–59, 2007, doi: 10.1080/15583050601125998.

[156] ICOMOS, "International Cuncil on Monuments and Sites," *The Venice Charter*. Venice (Italy), 1964, doi: 10.3109/01443615.2011.552340.

[157] ICOMOS, "Icomos Charter- Principles for the Analysis , Conservation and Structural Restoration of Architectural Heritage," *Archit. Herit.*, pp. 3–6, 2003.

[158] ISCARSAH, "Recommendations for the analysis, conservation and structural restoration of architectural heritage," *Int. Counc. Monum. Sites*, pp. 3–6, 2003.

[159] NIKER, "Critical review of retrofitting and reinforcement techniques related to possible failure," Padova (Italy), 2013.

[160] I. Boem, "Masonry Elements Strengthened with TRM: A Review of Experimental, Design and Numerical Methods," *Buildings*, vol. 12, no. 9, 2022, doi: 10.3390/buildings12091307.

[161] N. Gattesco, I. Boem, and A. Dudine, "Diagonal compression tests on masonry walls strengthened with a GFRP mesh reinforced mortar coating," *Bull. Earthq. Eng.*, vol. 13, no. 6, pp. 1703–1726, 2015, doi: 10.1007/s10518-014-9684-z.

[162] R. Antonucci, *Restauro e recupero degli edifici a struttura muraria*. Santarcangelo di Romagna (RN): Maggioli Editore, 2012.

[163] G. Marcari, G. Manfredi, A. Prota, and M. Pecce, "In-plane shear performance of masonry panels strengthened with FRP," *Compos. Part B Eng.*, vol. 38, no. 7–8, pp. 887–901, 2007, doi: 10.1016/j.compositesb.2006.11.004.

[164] O. Iuorio and J. A. Dauda, "Retrofitting masonry walls against out-of-plane loading with timber based panels," *Appl. Sci.*, vol. 11, no. 12, 2021, doi: 10.3390/app11125443.

[165] N. Damiani, G. Guerrini, and F. Graziotti, "Design procedure for a timber-based seismic retrofit applied to masonry buildings," *Eng. Struct.*, vol. 301, no. September 2023, 2024, doi: 10.1016/j.engstruct.2023.116991.

[166] R. Desroches and B. Smith, “Shape memory alloys in seismic resistant design and retrofit: A critical review of their potential and limitations,” *J. Earthq. Eng.*, vol. 8, no. 3, pp. 415–429, 2004, doi: 10.1142/S1363246904001298.

[167] L. Janke, C. Czaderski, M. Motavalli, and J. Ruth, “Applications of shape memory alloys in civil engineering structures - Overview, limits and new ideas,” *Mater. Struct. Constr.*, vol. 38, no. 279, pp. 578–592, 2005, doi: 10.1617/14323.

[168] A. Cohades and V. Michaud, “Shape memory alloys in fibre-reinforced polymer composites,” *Adv. Ind. Eng. Polym. Res.*, vol. 1, no. 1, pp. 66–81, 2018, doi: 10.1016/j.aiepr.2018.07.001.

[169] S. M. Daghash and O. E. Ozbulut, “Characterization of superelastic shape memory alloy fiber-reinforced polymer composites under tensile cyclic loading,” *Mater. Des.*, vol. 111, pp. 504–512, 2016, doi: 10.1016/j.matdes.2016.09.034.

[170] M. Shahverdi, C. Czaderski, and M. Motavalli, “Iron-based shape memory alloys for prestressed near-surface mounted strengthening of reinforced concrete beams,” *Constr. Build. Mater.*, vol. 112, pp. 28–38, 2016, doi: 10.1016/j.conbuildmat.2016.02.174.

[171] C. Czaderski, M. Shahverdi, R. Brönnimann, C. Leinenbach, and M. Motavalli, “Feasibility of iron-based shape memory alloy strips for prestressed strengthening of concrete structures,” *Constr. Build. Mater.*, vol. 56, pp. 94–105, 2014, doi: 10.1016/j.conbuildmat.2014.01.069.

[172] M. Indirli and M. G. Castellano, “Shape memory alloy devices for the structural improvement of masonry heritage structures,” *Int. J. Archit. Herit.*, vol. 2, no. 2, pp. 93–119, 2008, doi: 10.1080/15583050701636258.

[173] A. Simões, J. Milošević, H. Meireles, R. Bento, S. Cattari, and S. Lagomarsino, “Fragility curves for old masonry building types in Lisbon,” *Bull. Earthq. Eng.*, vol. 13, no. 10, pp. 3083–3105, 2015, doi: 10.1007/s10518-015-9750-1.

[174] V. Bernardo, A. Campos Costa, P. Candeias, A. Costa, A. Marques, and A. Carvalho, “Ambient vibration testing and seismic fragility analysis of masonry building aggregates,” *Bull. Earthq. Eng.*, vol. 20, no. 10, pp. 5047–5071, 2022.

[175] V. Bernardo, P. Candeias, A. C. Costa, and A. Costa, “Análise não linear de um conjunto de edifícios em placa no bairro de Alvalade: avaliação preliminar de estabilidade e previsão dos mecanismos de colapso,” *Rev. Port. Eng. Estruturas*, pp. 97–106, 2019, [Online]. Available: http://repositorio.lnec.pt:8080/xmlui/handle/123456789/1012870.

[176] A. Barontini, J. Scacco, L. Silva, G. Vasconcelos, P. Lourenço, and G. Milani, "Experimental quasi-static out-of-plane test of a U-shaped brick masonry wall," *Eng. Struct.*, vol. 287, 2023.

[177] "EN 1015-11:2019 Methods of test for mortar for masonry Determination of flexural and compressive strength of hardened mortar." 2019.

[178] "EN 1052-1 : Methods of Test for Masonry - Part 1: Determination of Compressive Strength." 1999.

[179] "ASTM E519/E519M-21: Standard Test Method for Diagonal Tension (Shear) in Masonry Assemblages." 2021.

[180] "EN 1052-2: Methods of test for masonry Determination of flexural strength." 2017.

[181] "ARTeMIS Modal, Structural Vibration Solutions A/S, Release 4.0.0.6. –x86." SVS, Aalborg (Denmark), 2015.

[182] E. C. for Standardization, *EN 1998-3 (2005)*. 2005.

[183] D. F. D'Ayala, "Assessing the seismic vulnerability of masonry buildings," in *Handbook of Seismic Risk analysis and management of civil infrastructure systems*, K. Goda, Ed. 2013.